Electronic Thesis and Dissertation Repository

7-23-2020 9:30 AM

Fluidization Characteristics of Group C+ Particles: Fine Powder with Nanoparticle Modulation

Yandaizi Zhou, *The University of Western Ontario*

Supervisor: Zhu, Jesse, *The University of Western Ontario*
A thesis submitted in partial fulfillment of the requirements for the Doctor of Philosophy degree in Chemical and Biochemical Engineering
© Yandaizi Zhou 2020

Recommended Citation

Abstract

Geldart Group C particles become increasingly attractive in industry because of their small particle sizes and large specific surface areas. The main challenge in the flow and fluidization of Geldart Group C particles is their cohesive nature due to strong interparticle forces. The "nanoparticle modulation" technique was adopted to reduce the interparticle forces of Group C particles and thus significantly improved their flow and fluidization quality. Group C^+ particles, a new type of fine particles with drastically reduced or insignificant interparticle forces, were created using the nano-modulation technique.

Fundamental studies provided a comprehensive understanding of the fluidization quality of Group C^+ particles. Group C^+ particles exhibited revolutionary advancements in fluidization, which enabled its pseudo-particulate fluidization over a wide range of operating gas velocities, up to 200%-300% times that of bed expansion. Group C^+ particles also exhibited much higher dense phase expansion than Group A particles, indicating more gas holdup in the dense phase available for intimate gas-solid contact. Bubbling behaviors for Group C^+ particles were further fully characterized, showing that bubbles were smaller in diameter, lower in rise velocity, and had a longer residence time in the Group C^+ fluidized bed in comparison with the Geldart Group A fluidized bed. With more gas flow through the dense phase for Group C^+ particles, the correction factor Y that accounts for increased dense phase gas flow in the modified two-phase theory was correlated to characterize the division of gas flow between the two phases for Group C^+ particles, based on the experimental results. A theoretical method for predicting the dense phase voidage for Group C^+ particles was also proposed. Furthermore, Group C^+ particles were used as catalysts in a fluidized bed reactor (C-plus FBR) to evaluate the reaction performance and were compared to that using Group A particles. C-plus FBR achieved a much higher reaction conversion, up to 235% of that using Group A particles, and a higher contact efficiency, being 330% more than that for Group A particles.

In summary, Group C^+ particles exhibited extremely higher dense phase expansion, smaller bubbles and less bubble holdups, more gas flow through the dense phase, etc. enhancing the gas-solid contact and thus improving the reactor performance. Therefore, Group C^+ fluidized

bed reactor is expected to cause a significant "splash" in industrial processes, especially for gas-phase catalytic reactions.

Keywords

Fluidization, Group C particles, Nanoparticles, Dense phase expansion, Bubbling behaviors, Gas distribution, Gas-solid contact, Reactor performance, Two-phase theory, Gas effect.

Summary for Lay Audience

Fluidization is an important operation which solid particles are transferred into a fluidlike state through suspension in a gas or liquid. This unique method of contacting has some unusual characteristics, such as uniform temperature distribution, high heat/mass transfer rate, and particularly more solid surface area for gas reactant and thus better gas-solid contact efficiency, etc., making fluidized beds as the most popular reactors for multi-phase reactions, especially for gas-phase catalytic reactions.

The degree of gas-solid contact is one most important factor determining the performance of a conventional fluidized bed reactor. Geldart Group C particles which have small particle size (<45) could provide much larger surface area for gas reactant to contact and react with. The challenge of the application of Group C particles is their strong interparticle forces caused by the small particle sized which lead to poor flowability and nearly none fluidizability. Nanoparticle modulation technique can successfully reduce the interparticle forces and improve the flowability and fluidization of Group C particles. Those nano-modulated Group C particles, referred to as Group C^+ particles, exhibited good flowability and fluidization quality.

A bubbling fluidized bed contains two phases, the bubble phase and the dense phase. Bubbles go through the bed quickly with little gas-solid contact, while the dense phase provides a close gas-solid contact. The fluidized bed of Group C^+ particles showed much higher dense phase expansion, smaller bubbles and less bubble holdup, and higher gas flowrate through the dense phase than the bed of Group A particles, indicating more gas has the opportunity to contact with particles and contributing to better gas-solid contact. Furthermore, Group C^+ particles were used as catalysts in a fluidized bed reactor and exhibited much higher reaction conversion

than Group A particles as catalysts, due to the higher gas holdup in the dense phase and the larger gas-solid interfacial area. Conclusively, Group C^+ particles with superior fluidization quality and reaction performance do have huge potential in gas-phase catalytic reactions.

Co-Authorship Statement

1.

Title: Group C$^+$ Particles: Enhanced Flow and Fluidization of Fine Powders with Nano-Modulation

Authors: Yandaizi Zhou, Jesse Zhu*

All the experimental works were carried out by Yandaizi Zhou under the guidance of Prof. Jesse Zhu. All drafts and modifications of this manuscript were done by Yandaizi Zhou under the supervision of Prof. Jesse Zhu. The final version of this manuscript has been published in *Chemical Engineering Science*.

2.

Title: Group C$^+$ Particles: Extraordinary Dense Phase Expansion during Fluidization through Nano-modulation

Authors: Yandaizi Zhou, Jesse Zhu*

All the experimental works were conducted by Yandaizi Zhou under the guidance of Prof. Jesse Zhu. All drafts and modifications of this manuscript were done by Yandaizi Zhou under the supervision of Prof. Jesse Zhu. The final version of this manuscript has been published in *Chemical Engineering Science*.

3.

Title: The Effect of Gas Properties on Group C$^+$ Fluidized Bed Reactor

Authors: Yandaizi Zhou, Haoran Ding, Jesse Zhu*, Yuanyuan Shao

The experimental design was done by Yandaizi Zhou in discussion with Prof. Jesse Zhu and Prof. Yuanyuan Shao. The experimental works were carried out by Yandaizi Zhou and Haoran Ding under the guidance of Prof. Jesse Zhu. All the theoretical works were conducted by Yandaizi Zhou under the supervision of Prof. Jesse Zhu. All drafts and modifications of this

manuscript were done by Yandaizi Zhou under the close supervision of Prof. Jesse Zhu. The final version of this manuscript has been published in *Chemical Engineering Journal*.

4.

Title: Different bubble behaviors in gas-solid fluidized bed of Geldart Group A and Group C$^+$ particles

Authors: Yandaizi Zhou, Jingrui Xu, Jesse Zhu*

The experimental design was done by Yandaizi Zhou in discussion with Prof. Jesse Zhu. 70% of the experimental works were carried out by Yandaizi Zhou, and 30% were done by Jingrui Xu under the guidance of Yandaizi Zhou. All drafts and modifications of this manuscript were done by Yandaizi Zhou under the close supervision of Prof. Jesse Zhu. The final version of this manuscript was submitted to *AIChE Journal* (positive reviews received and responded).

5.

Title: On the Two-phase Theory of Group C$^+$ and Geldart Group A Particles

Authors: Yandaizi Zhou, Jesse Zhu*

All the experimental and theoretical works were conducted by Yandaizi Zhou under the guidance of Prof. Jesse Zhu. All drafts and modifications of this manuscript were done by Yandaizi Zhou under the supervision of Prof. Jesse Zhu. The final version of this manuscript has been published in *Industrial & Engineering Chemistry Research*.

6.

Title: Prediction of Dense Phase Voidage for Group C$^+$ Fluidized Bed Reactor

Authors: Yandaizi Zhou, Jesse Zhu*

All the experimental and theoretical works were conducted by Yandaizi Zhou under the guidance of Prof. Jesse Zhu. All drafts and modifications of this manuscript were done by Yandaizi Zhou under the supervision of Prof. Jesse Zhu. The final version of this manuscript has been published in *Chemical Engineering Journal*.

7.

Title: Group C$^+$ Particles: Efficiency Augmentation of Fluidized Bed Reactor through Nano-modulation

Authors: Yandaizi Zhou, Zhiwei Zhao, Jesse Zhu*, Xiaojun Bao

The experimental design was done by Yandaizi Zhou and Zhiwei Zhao in discussion with Prof. Jesse Zhu and Prof. Xiaojun Bao. The experimental works were carried out by Zhiwei Zhao and Yandaizi Zhou under the guidance of Prof. Jesse Zhu. All the theoretical works were done by Yandaizi Zhou under the supervision of Prof. Jesse Zhu. All drafts and modifications of this manuscript were done by Yandaizi Zhou under the close supervision of Prof. Jesse Zhu. The final version of this manuscript has been published in *AIChE Journal*.

8.

Title: Reaction Performance of Group C$^+$ Fluidized Bed Catalytic Reactor

Authors: Zhiwei Zhao, Yandaizi Zhou, Xiaojun Bao*, Jesse Zhu*, Haiyan Liu

The experimental design was done by Yandaizi Zhou and Zhiwei Zhao in discussion with Prof. Jesse Zhu and Prof. Xiaojun Bao. The experimental works were carried out by Yandaizi Zhou and Zhiwei Zhao under the guidance of Prof. Jesse Zhu. The theoretical works were conducted by Zhiwei Zhao and Yandaizi Zhou under the supervision of Prof. Jesse Zhu. The calculations were done by Zhiwei Zhao. The drafts were done by Zhiwei Zhao. The modifications of this manuscript were conducted by Yandaizi Zhou under the close supervision of Prof. Jesse Zhu. The final version of this manuscript was submitted to *Particuology*.

Acknowledgments

I would like to express my deep gratitude to my supervisor, Prof. Jesse Zhu, a Distinguished University Professor and Canada Research Chair in the Department of Chemical and Biochemical Engineering at Western University. At first, I am so appreciated for the opportunity Prof. Zhu provided for me to study abroad. This precious experience broadens my mind and enriches my life. In addition, I have learnt so much from Prof. Zhu far more than just the knowledge and research methods. I have become more conscious of my role in the future work, inspired by his scientific minds. Moreover, I am grateful for his guidance to my whole work and his encouragement during my study.

I want to thank Yuqi Zhang, Haoran Ding, Jingrui Xu, and Zhiwei Zhao for their contributions to the experimental works. I also wish to thank all my colleagues at the Powder Technology Research Center, Danni Bao, Zhijie Fu, Xiaowei Zhang, Zeneng Sun, who have directly or indirectly heled me on my project.

The financial support from China Scholarship Council (CSC) are gratefully acknowledged as well.

Finally, I am full of thankfulness to my parents, Gaoping Zhou and Qinxia Yan, and my older sister Yao Zhou for their support and love.

Table of Contents

List of Tables

List of Figures

List of Appendices

Chapter 1

1 General Introduction

1.1 Introduction

Particle technology is increasingly significant in industry because approximately one-half of the products and at least three-quarters of the raw materials are in the form of particles, such as pigments, fertilizers, cements, industrial chemicals, pharmaceuticals, and other goods, and the impact of particulate products to the US economy was estimated to be US$ 1 trillion [1]. Fluidization is often a preferred mode of operation for handling particles in a variety of industrial processes because particles can be brought into good contact with a fluid. Therefore, the flowability and fluidizability are important characteristics of a powder which are directly related to the handling and processing of particles.

In 1973, Geldart [2] classified particles into four groups according to their flow and fluidization behaviors. Groups B and D are much large and dense particles, while having good flowability, their fluidization is less ideal usually accompanied by larger and more dynamic bubbles. Group A particles are usually 40-100 µm in diameter with particle density of 1000-3000 kg/m^3, and exhibit easy flow and smooth fluidization. Group C particles (often referred as fine or ultrafine particles), less than 30-40 µm in diameter with particle density of 1000-3000 kg/m^3, are cohesive and are hard to flow and fluidize. On the other hand, Group C particles are being increasingly preferred by a variety of processes in industry due to their small particle size and extremely high surface area [3]. The small particle size is favorable in many applications such as pharmaceutical applications [4], powder coating [5] and food industry [6]. The high specific surface area of Group C particles attracts more attention in some physical and 1chemical processes, including surface modification [7], catalytic reactions [8] and catalyst synthesis [9]. The biggest challenge of applying Group C particles is the cohesive nature ascribed to the small particle size, which leads to poor flowability and poor fluidization and thus limits their applications. If the strong cohesiveness could be overcome or reduced, Group C particles should exhibit

better flow and fluidization than Group A, B and D particles. In consequence Group C particles could be successfully applied in industry.

Understanding the increasing importance of Group C particles in modern industries, many kinds of methods, often called fluidization aids, have been investigated to improve their flow and fluidization. The strong interparticle forces of Group C particles are predominated by van der Waals forces which are affected by the surface properties and the separation distance of particles [10]. As a result, some methods, such as gas adsorption [11] and adding coarser or finer particles [12-13], can reduce the interparticle forces intrinsically by modifying particle surface or increasing the separation distance between particles, thus improving the flow and fluidization of Group C particles. These methods are scale-independent and are relatively easy to implement. In addition, other methods, such as mechanical or acoustic vibration [14-15], mechanical stirring [16], and magnetic or electrical fields disturbance [17-18], can overcome the interparticle forces by introducing external energies, however, these methods are scale-dependent and thus have limited success.

The addition of nanoparticles, referred to as nanoparticle modulation technique [19], has been found to effectively reduce the cohesiveness and agglomeration of cohesive Group C particles and turn them into free-flowing powers [19-21]. Nanoparticles could adhere on the surfaces of Group C particles like asperities to increase the surface roughness and the separation distance, thus decreasing van der Waals forces of Group C particles [22-23]. Although some researchers [24-26] reported that nanoparticles could turn Group C particles from non-flowable to free-flowing and from non-fluidizable to fluidizable, few studies have systematically investigated the fluidization behaviors and fluidization quality of Group C particles with nanoparticles so far.

Generally, a good fluidized bed is characterized by particles uniformly suspended and fewer fluctuation with small bubbles. In addition, a good fluidized bed reactor is characterized by more gas into dense phase and fewer gas into bubble phase. One of the most important characteristics that describes the fluidization quality is the bed expansion, especially the dense phase expansion. High bed expansion generally indicates better

fluidization with more gas contained in the bed, in particular, high dense phase expansion means more gas holdup in the dense phase that gas can closely contact with particles, resulting in good gas-solid contact [27-29]. Except for the dense phase properties, bubbling behaviors also affect the fluidization quality and reactor performance of the fluidized bed, such as bubble size and rise velocity which greatly influence the gas residence time and the gas-solid contact in the fluidized bed. Ideally, bubbles in a fluidize bed reactor should be small in size, uniformly distributed throughout the bed, and have low rise velocities [29-31].

In summary, a good catalytic fluidized bed reactor is expected to provide large gas-solid interfacial area and exhibit more gas holdup in the dense phase, smaller bubbles and less bubble holdups, higher gas flow through the dense phase and less through the bubble phase. All these characteristics are closely related to particle properties. As the particle size decreases from Group D to B and further to A, particles show better fluidization quality with more homogenous fluidization, which is advantages for chemical reactors. Group C particles with controlled interparticle forces using nano-modulation technique, can provide much larger specific surface area and should exhibit even better fluidization quality than Group A particles, becoming more favorable for gas-phase catalytic reactions.

This thesis systematically studied the effects of particle size, nanoparticle concentration, and gas properties, etc. on the fluidization behaviors of Group C^+ particles, Group C particles after using nano-modulation technique, characterized by pressure drop, minimum fluidization velocity, bed expansion, dense phase voidage etc. Moreover, bubbling behaviors for Group C^+ particles were also comprehensively investigated, including bubble size distribution, rise velocity, and gas residence time. From the view of two-phase theory, the gas distribution between the bubble phase and the dense phase in the fluidized bed of Group C^+ particles was determined. A theoretical method was developed to predict the dense phase voidage for group C^+ particles, which is an important parameter for evaluating the reactor performance. Furthermore, the performance of the fluidized bed reactor using Group C^+ particles as catalysts was experimentally evaluated using the ozone decomposition reaction, and was then theoretically estimated using an industrial reaction

based on a modified two-phase model. All these investigations were compared with Group A particles to exhibit the advantages of Group C$^+$ particles.

1.2 Objectives

Despite numerous previous studies on Group C particles, most people focus more on the mobility or flowability of fine particles with the addition of nanoparticles, but do not pay much attention towards fluidization behaviors, and presume that nanoparticles just make Group C particles become Group A particles. However, the fluidization behaviors of Group C$^+$ particles should be quite different from that of Group A particles. Although some studies appeared to point to high bed voidages for these Group C particles after surface coating by nanoparticles, they focused more on the minimum fluidization velocity. Not enough attention was paid for further study of the bed voidage. In addition, few detailed studies are found about bubble behaviors of Geldart Group C particles, and almost no researches have studied the reaction performance in fluidized beds of Group C$^+$ particles until now. There exists a huge gap between the fundamental studies of fine particle fluidization and its application or potential application to chemical industries. Therefore, this study aims to address the following objectives:

(1) To systematically study the flowability and fluidizability of "Group C$^+$" particles, which are essentially Group C particles after nanoparticle modulation, and to investigate the effects of nanoparticle concentrations. Given the smooth flowability and fluidization of Group A particles, a comparative study on the flow and fluidization behaviors of Group C$^+$ particles with Group A particles is conducted to find out the similarities and differences, including angle of repose (AOR), avalanche angle (AVA), particle cohesion, pressure drop, minimum fluidization velocity, and bed expansion.

(2) To characterize the dense phase and the bubble phase for Group C$^+$ particles, including the dense phase voidage and the bubble holdup, by carrying out the bed collapse test.

The differences between Group C^+ and Group A particles were also studied.

(3) To comprehensively investigate the effects of gas types on the fluidization behaviors of Group C^+ particles, including pressure drop, minimum fluidization velocity, bed expansion, dense phase voidage, and pressure fluctuation. The relative importance of the gas viscosity and the gas density on the fluidization behaviors were theoretically and experimentally discussed.

(4) To characterize bubble behaviors for Group C^+ particles in a 2-D fluidized bed via image analysis techniques, including bubble positions, diameters, and rise velocities. Similar behaviors were also characterized in the same bed of Geldart Group A particles for comparison.

(5) To investigate the gas flow distribution between the bubble phase and the dense phase in the fluidized beds of Group C^+ and Group A particles. A modified two-phase theory with a new correlation for the value of Y was determined for Group C^+ particles, based on the experimental results of the bubble holdup and the bubble rise velocity.

(6) To propose a theoretical approach to predict the dense phase behaviors for Group C^+ particles. The dense phase voidage and the cohesion for Group C^+ particles were experimentally studied, and correlations to theoretically predict the dense phase voidage in the fluidization of Group C^+ particles were developed.

(7) To experimentally investigate the reaction performance in a fluidized bed reactor using Group C^+ particles as catalysts (C-plus fluidized bed reactor) with ozone decomposition reaction and make a comparison with that using Group A particles. The fluidization hydrodynamics of Group C^+ particles and Group A particles were also studied and compared and further correlated with their reaction performance by gas-solid contact efficiency.

(8) To theoretically compare the performance of the fluidized bed reactor using Group C^+ catalysts with the same reactor of Group A catalysts using a modified two-phase model, and to show the performance improvements Group C^+ fluidized bed reactor possesses over its counterpart. The production of maleic anhydride (MAN), as a common reaction

in industry, was adopted as an example to exhibit the reactor performance using Group C$^+$ catalysts.

1.3 Thesis structure

This thesis contains eleven chapters and follows the "Integrated-Article" format as outlined *Thesis Regulation Guide* by the Faculty of Graduate Studies of The University of Western Ontario. It is organized in the flowing structure:

Chapter 1 gives a general introduction to the background of the fine particle fluidization technology and detailed statements of the research problems, the objectives, the thesis structures, and the major contribution of the present work.

Chapter 2 provides a detailed literature review about the previous researches and the current status of the fine particle fluidization technology, and addresses the factors that influence the fluidization quality and performance of a fluidized bed reactor.

Chapter 3 provides a comprehensive understanding of the flow and fluidization quality of Group C$^+$ particles, and makes comparison with that of Group A particles. Nano-modulation leads to major enhancements to both the static and dynamic flowability of Group C$^+$ particles. Group C$^+$ particles also exhibit revolutionary advancements in fluidization, showing much higher bed expansion than Group A particles.

Chapter 4 characterizes the dense phase properties of Group C$^+$ and Group A particles using the bed collapse test, and defined a factor, maximum dense phase expansion ($E_{d,max}$), to quantify the expansion ability of the dense phase for different particles. the extraordinary dense phase expansion and the large specific surface area for Group C$^+$ particles are favorable for gas-phase catalytic reactions.

Chapter 5 investigates the effects of gas species on the fluidization properties such as minimum fluidization velocity, bed expansion, dense phase voidage, and pressure fluctuation of three typical types of Group C$^+$ particles, using five types of fluidizing gases and their combinations. Both the increase of the gas viscosity and the gas density increase

the fluidization quality, while the gas viscosity proves to play a more important role on the fluidization.

Chapter 6 fully characterizes bubbling behaviors of Group C^+ and Group A particles using bubble position, diameter, rise velocity, and residence time. Bubbles are shown to be smaller in diameter, lower in rise velocity, and have a longer residence time in the Group C^+ fluidized bed in comparison with the same bed using Geldart Group A particles, all contributing to better fluidization quality and enhanced gas-solid contact.

Chapter 7 determines the distribution of the gas flow between the bubble phase and the dense phase in the fluidized beds of Group C^+ and Group A particles. The correction factor Y that accounts for increased dense phase gas flow in the modified two-phase theory is found to be not a constant but a function of the superficial gas velocity for Group C^+ particles, and a correlation is proposed to characterize the division of gas flow between the two phases for these fine Group C^+ particles, based on the experimental results.

Chapter 8 theoretically develops a general correlation for predicting the dense phase voidage for Group C^+ particles which is a critical parameter affecting reactor performance. A new method for predicting the minimum fluidization velocity of Group C^+ particles with the consideration of the particle cohesion is also proposed. The bed voidage at minimum fluidization (ε_{mf}) and the maximum dense phase voidage ($\varepsilon_{d,max}$) are shown to correlate well with a dimensionless cohesion index (σ^*).

Chapter 9 experimentally studies the reaction performance in a fluidized bed reactor using Group C^+ particles as catalysts and makes a comparison with the reactor using Group A particles. The contact efficiency is characterized by the specific surface area of the catalysts and the bed expansion in the fluidized bed reactor.

Chapter 10 theoretically compares the performance of the partial oxidation of n-butane to maleic anhydride reaction in the fluidized bed reactor using Group C^+ and Group A catalysts using a two-phase model modified based on experimental results. Group C^+ catalytic reactor is shown to achieve a much higher n-butane conversion and MAN yield compared to Group A catalytic reactor.

Chapter 11 provides a general discussion about this work and summarizes the conclusions, and also gives some recommendations for future work.

1.4   Major contribution

The major contributions of this work are summarized as follows:

(1) The flowability and fluidization behaviors of Group C^+ particles have been fully characterized and compared with that of Group A particles. The minimum fluidization velocity is related to the particle cohesion. The bed expansion of Group C^+ particles are extremely higher than that of Group A particles, indicating better fluidization quality. Nanoparticle concentration exists an optimum value depending on the surface coverage and surface roughness, around 0.5-1% (volume fraction).

(2) The properties of the dense phase and the bubble phase have been clearly characterized using the bed collapse test. Group C^+ particles exhibit a much higher dense phase expansion and larger dense phase voidage than Group A particles, indicating more gas holdup in the dense phase so that gas could closely contact with the particles. The maximum dense phase expansion ($E_{d,max}$) is proposed to quantify the expansion ability of dense phase for different particles. The larger $E_{d,max}$ values of Group C^+ particles indicate better expansion ability of the dense phase and thus contribute to better gas-solid contact.

(3) The fluidization quality for Group C^+ particles is improved with the increase of the gas viscosity and/or the gas density. The gas viscosity proves to play a more important role on determining the fluidization quality using both theoretical and experimental methods. The dimension analysis is an effective method to correlate the fluidization quality with a number of factors including the gas viscosity and density, the particle size and cohesion, and the gas velocity.

(4) The bubbling behaviors for Group C^+ particles and Geldart Group A particles have been comprehensively characterized in a 2-D fluidized bed. Group C^+ particles exhibit smaller bubbles, more uniform bubble size distribution, lower bubble rise velocities, and longer bubble residence time than Group A particles. Applying the modified two-

phase theory and using the correction factor Y to account for increased dense phase gas flow, the Y value is found to be not a constant, but correlated with the gas velocity for Group C^+ particles. Using the new correlation for the correction factor Y, the distribution of the gas flow between the dense phase and the bubble phase in the beds of Group C^+ in comparison to Group A particles can be determined, quantifying the gas flow through the dense phase and through the bubble phase.

(5) A general expression to predict the dense phase voidage for Group C^+ particle fluidization has been theoretically developed. A new method to calculate the minimum fluidization velocity for Group C^+ particles with the consideration of the particle cohesion has been proposed. The bed voidages have been correlated well with the dimensionless cohesion index. This study is helpful to further evaluate the reaction performance of a Group C^+ fluidized bed reactor.

(6) The reactor performance of the fluidized bed using Group C^+ particles as catalyst have been experimentally studied. Group C^+ fluidized bed reactor is shown to reach much higher reaction conversion than Group A fluidized bed reactor, due to better contact efficiency. Furthermore, the reactor performances of Group C^+ and Group A fluidized bed reactors with the industrial MAN production reaction are compared using a modified two-phase model. The modelling results show a much higher conversion and yield in Group C^+ fluidized bed reactor. The Group C^+ fluidized bed reactor can bring huge advancements to industrial processes, especially for gas-phase catalytic reactions.

References

[1] Rhodes MJ, editor. Introduction to particle technology. John Wiley & Sons; 2008 Jun 9.

[2] Geldart D. Types of gas fluidization[J]. Powder Technology, 1973, 7: 285-297.

[3] Ichinose, Noboru, Yoshiharu Ozaki, and Seiichiro Kashu. Superfine particle technology[M]. Springer Science & Business Media, 2012.

[4] Shur, Jagdeep, et al. The role of fines in the modification of the fluidization and dispersion mechanism within dry powder inhaler formulations[J]. Pharmaceutical Research, 2008, 25(7): 1631-1640.

[5] Shah U, Zhang C, Zhu J. Comparison of electrostatic fine powder coating and coarse powder coating by numerical simulations. Journal of electrostatics. 2006 Jun 1;64(6):345-54.

[6] Vidal B C, Dien B S, Ting K C, et al. Influence of feedstock particle size on lignocellulose conversion—a review[J]. Applied biochemistry and biotechnology, 2011, 164(8): 1405-1421.

[7] Sanjurjo, A., Wood, B.J., Lau, K.H., Tong, G.T., Choi, D.K., Mckubre, M.C.H., Song, H.K. and Church, N. Titinium-based coating on copper by chemical vapor deposition in fluidized bed reactors[J]. Surface and Coating Technology, 1991, 49: 110-115.

[8] Yamamoto K, Imaoka T, Chun W J, et al. Size-specific catalytic activity of platinum clusters enhances oxygen reduction reactions[J]. Nature chemistry, 2009, 1(5): 397.

[9] Sathish M, Viswanathan B, Viswanath R P, et al. Synthesis, characterization, electronic structure, and photocatalytic activity of nitrogen-doped TiO2 nanocatalyst[J]. Chemistry of materials, 2005, 17(25): 6349-6353.

[10] Visser, J. An invited review - van der Waals and other cohesive forces affecting powder fluidization[J]. Powder Technol., 1989, 58: 1-10.

[11] Xie, H.-Y. The role of interparticle forces in the fluidization of fine particles[J]. Powder Technology, 1997, 94: 99-108.

[12] Dutta, A. and Dullea, L.V. A comparative evaluation of negatively and positively charged submicron particles as flow conditioners for a cohesive powder[J]. AIChE Symp. Ser., 1990, 86(276): 26-40.

[13] Zhou, T. and Li, H. Effect of adding different size particles on fluidization of cohesive particles[J]. Powder Technology, 1999, 102: 215-220.

[14] Xu, Chunbao, and Jesse Zhu. Experimental and theoretical study on the agglomeration arising from fluidization of cohesive particles—effects of mechanical vibration[J]. Chemical Engineering Science, 2005, 6 (23): 6529-6541.

[15] Chirone R, L Massimilla. Sound-assisted aeration of beds of cohesive solids[J]. Chem. Eng. Sci., 1994, 49: 1185-1194.

[16] Kuipers, N. J. M., E. J. Stamhuis, and A. A. C. M. Beenackers. Fluidization of potato starch in a stirred vibrating fluidized bed[J]. Chemical engineering science, 1996, 51(11): 2727-2732.

[17] Daniel L, Jose M V, Robert P et al. Enhanced nanofluidization by alternating electric fields[J]. Particle Technology and Fluidization, 2010, 56(1): 54-65.

[18] Nakamura, Hideya, and Satoru Watano. Fundamental particle fluidization behavior and handling of nano-particles in a rotating fluidized bed[J]. Powder Technology, 2008, 183(3): 324-332.

[19] Zhu, J. and H. Zhang. Fluidization Additives to Fine Powders. U.S. Patent 6833185. December 21, 2004.

[20] Yang J, Sliva A, Banerjee A, et al. Dry particle coating for improving the flowability of cohesive powders[J]. Powder Technology, 2005, 158(1-3): 21-33.

[21] Quintanilla M A S, Valverde J M, Castellanos A. Adhesion force between fine particles with controlled surface properties[J]. AIChE journal, 2006, 52(5): 1715-1728.

[22] Xu, Chunbao Charles, Hui Zhang, and Jesse Zhu. Improving flowability of cohesive particles by partial coating on the surfaces[J]. The Canadian Journal of Chemical Engineering, 2009, 87(3): 403-414.

[23] Chen Y, Yang J, Dave R N, et al. Fluidization of coated group C powders[J]. AIChE journal, 2008, 54(1): 104-121.

[24] Han M, Zhou Y, Zhu J. Improvement on flowability and fluidization of Group C particles after nanoparticle modification. Powder Technology. 2020 Apr 1; 365:208-214.

[25] Lauga, C., Chaouki, J., Klvana, D. and Chavarie, C. Improvement of the fluidizability of Ni/SiO2 aerogels by reducing interparticle forces[J]. Powder Technol., 1991, 65: 461-468.

[26] Zhou Q T, Qu L, Larson I, et al. Effect of mechanical dry particle coating on the improvement of powder flowability for lactose monohydrate: A model cohesive pharmaceutical powder[J]. Powder technology, 2011, 207(1-3): 414-421.

[27] Grace JR, Sun G. Influence of particle size distribution on the performance of fluidized bed reactors. The Canadian Journal of Chemical Engineering. 1991 Oct;69(5):1126-34.

[28] Abrahamsen AR, Geldart D. Behaviour of gas-fluidized beds of fine powders part II. Voidage of the dense phase in bubbling beds. Powder Technology. 1980 May 1;26(1):47-55.

[29] Abrahamsen AR, Geldart D. Behaviour of gas-fluidized beds of fine powders part I. Homogeneous expansion. Powder technology. 1980 May 1;26(1):35-46.

[30] Yates JG, Rowe PN, Cheesman DJ. Gas entry effects in fluidized bed reactors. AIChE journal. 1984 Nov;30(6):890-4.

[31] Kai T, Furusaki S. Behavior of fluidized beds of small particles at elevated temperatures. Journal of chemical engineering of Japan. 1985 Apr 20;18(2):113-8.

<div align="center">Chapter 2</div>

2   Literature Review

2.1   Geldart classification

Fluidization is often the preferred operation if a fluid phase and a particulate phase need to be in good contact for physical or chemical processes, due to its special characteristics, such as uniform gas-solid contact, uniform temperature distribution, and high mass and heat transfer rates, etc. As a result, fluidization has been extensively applied to a variety industrial processes, such as gas adsorption [1-2], production of fine particles [3-4], pharmaceutical applications [5], powder coating [6-7], coal combustion [8-9], and petroleum refining processes [10-12]. The fluidization hydrodynamics are closely related to the operating conditions and the particle properties [13-15]. The particles suitable for fluidization have the sizes ranging from sub-microns to several millimeters, however, the difficulty increases as the particle size goes to the two extremes. The behaviors of different particles fluidized by gases are classified by Geldart (1973,1973) [16-17] into four groups characterized by density difference (ρ_p-ρ_g) and mean particle size (d_p), i.e., Group A (aeratable), Group B (bubble-ready or sand-like), Group C (cohesive), and Group D (spoutable), as shown in Figure 2.1.
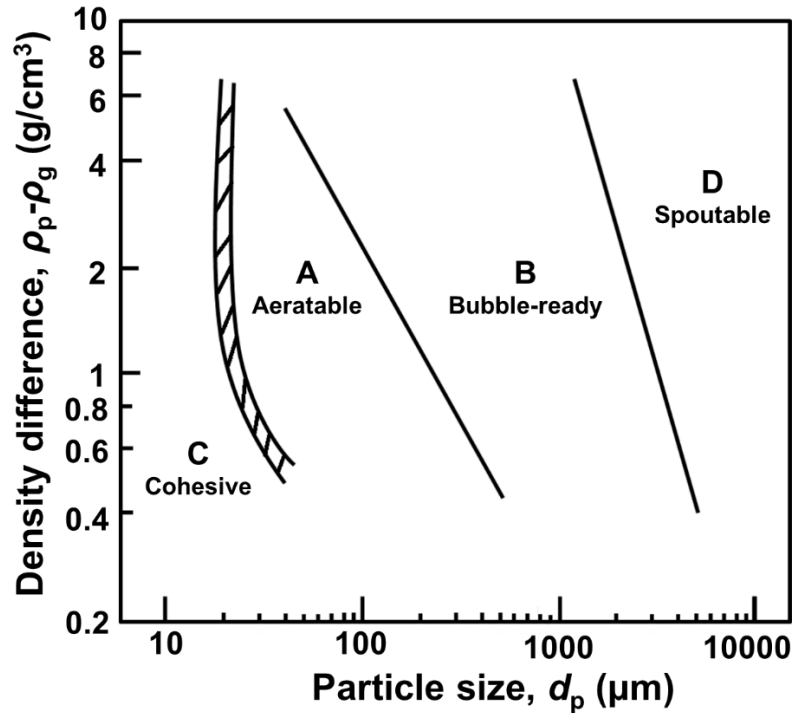
Figure 2.1: Geldart classification

Group D is the spoutable powder and confined to large and /or dense particles, which are usually in sizes of more than 1000μm. They are spoutable as the gas velocity increases. Group B is called the bubble-ready or sand-like powder usually in the mean size and density ranges 40μm < d_p < 500μm, 1400kg/m^3 < ρ_p <4000kg/m^3, sand being the most typical powder. In the fluidization of this type pf powder, bubbles start to form at or only slightly above minimum fluidization velocity. Bed expansion is small and the bed collapses very rapidly when the gas supply is cut off. Group A is the aeratable powder having a small mean size (40-100μm) and/or a low particle density (less than about 1400kg/m^3), some cracking catalysts being typical examples. The most important characteristic is that powder in Group A exhibits dense phase expansion after minimum fluidization and prior to the commencement of bubbling, that is u_{mf} < u_{mb}. The bed collapse slowly [18] when the gas supply is cut off, typically at a rate of 0.3-0.6cm/s, this being similar to the superficial velocity of the gas in the dense phase [19].

Considering the fluidization behaviors of powders in groups from D (coarse) to A (fine), the decreasing of the particle size can increase the fluidization quality. Therefore, Group C

powder having even smaller particle size (usually less than 25-40μm) is expected to show better fluidization quality. However, "normal" fluidization of such powders is extremely difficult due to their strong cohesion attributed to the small particle size. The powder lifts as a plug in small diameter tubes, or channels badly. The fluidization of such Group C powders can generally be made possible or improved by the assistance of some fluidization aids, such as the use of mechanical stirrers[20-21] or vibrators [22-25] which can break up the channels, or, the addition of finer or coarser particles [26-30] which can act as spacers and/or lubricants to reduce the cohesion and friction.

2.2   Characteristics of Group C particles

Fine Group C particles are gaining increasing importance in modern industries due to their special characteristics, such as the small particle size which helps them be applied to pharmaceutical industry and powder coating, and the large specific surface area which contributes to more significant surface phenomenon such as adsorption and chemical reactivity. However, the poor flowability and fluidizability of Group C particles hinder their applications in industrial processes, ascribed to the strong interparticle forces. In addition, the strong interparticle forces lead to the agglomeration of Group C particles, resulting in the reduction of the specific surface area.

2.2.1   Large specific surface area

A spherical particle with a radius r has a surface area S which is equal to $4\pi R^2$ and a volume V which is equal to $(4\pi/3) R^3$. The specific surface area A_p of this particle is:

$$A_p = S/V = 3/R \propto 1/R$$

If the particle is not spherical then the value of A_p will be greater, so the specific surface area A_p of a particle with a diameter of 2 μm is:

$$A_p \geq 1/10^{-4} \text{ cm}^2/\text{cm}^3$$

In other words, 1cm^3 of particles with a diameter of 2μm have a surface area of at least 1m^2. The huge size of this value may be more clearly grasped if it compared with a regular 1cm^3 cube which has a surface area of 6cm^2. Considering 1cm^3 of spherical superfine particles with diameter of 10nm, their surface area extremely increases, reaching as high as 10m^2. Evidently, Group C particles with small particle size have greatly extended

surface area which is a key for many processes, such as gas adsorption and multi-phase reactions. For example, the aerogel fine particles in the form of metal-supported simple or mixed oxides, with very high specific surface areas and porosity, could be used as catalysts for a great variety of reactions such as Fischer-Tropsch synthesis, methanol synthesis, polymerization of ethylene or propylene, deNOx reactions and hydro-treatment in HDN and HDS processes [31]. Fine particles of $Cu-Al_2O_3$ aerogel catalyst showed very high activity and selectivity in selective conversion of cyclopentadiene into cyclopentene [32]. More recently, fine residual equilibrium catalysts (less than 37μm) from a fluid catalytic cracking unit showed a higher pozzolanic activity than the coarse (74-90μm) and medium ones (44-74μm) in the process of calcium silicates hydration [33]. Because of the large specific surface area, fine particles of a small size commonly lead to a better quality of the final products in the ceramic industry and/or in the powder metallurgy [34].

2.2.2   Strong interparticle forces

Because of the small size of Group C particles, the interparticle forces increase significantly than the gravitational and drag forces. The "normal" fluidization of Group C particles is extremely difficult, not only because the interparticle forces are larger than the gravitational, but also because the drag forces which a gas can exert on these particles are not large enough for fluidization [35]. When Group C particles are subjected to fluidization, the strong interparticle forces will make the individual particles cling to each other and form agglomerates, leading to severe agglomeration, channeling, and even none fluidization. As a result, the interparticle forces are an important factor that must be considered for Group C particle fluidization.

When two particles are brought into contact, they are subject to capillary, electrostatic, and van der Waals forces [36]. Capillary forces are caused by condensed moisture on the surface of the particle, and electrostatic forces depend on the charges present in the particles. For dry fine neutral powders, these two forces are negligible compared to the van der Waals forces [36-39]. The van der Waals forces are noticeable when the particles can come sufficiently close together, that is at separation distances of the order of the size of a molecular, e.g. 0.2 to 1nm [40]. The van der Waals forces (F_{van}) between two identical spheres of radius R:

$$F_{van} = A_H R / 12Z^2$$

where A_H is the Hamaker coefficient [41] which can be directly related to the material properties [42], Z is the separation distance between the two particles.

In reality, particles are never as ideal as indicated and have sone realistic configurations [37], as shown in Figure 2.2. In cases (a) and (b), surface roughness will limit the approach of two particles and the effective separation distance will increase, thereby reducing the van der Waals forces to almost zero when the asperities are of the order of 1µm. In cases (c), (d), and (e), the intimate contact area will substantially increase the van der Waals forces. All means to increase the separation distance, for example the addition of properly chosen fines, will substantially diminish the adhesion and hence allow the fluidization of fine particles normally difficult to fluidize.
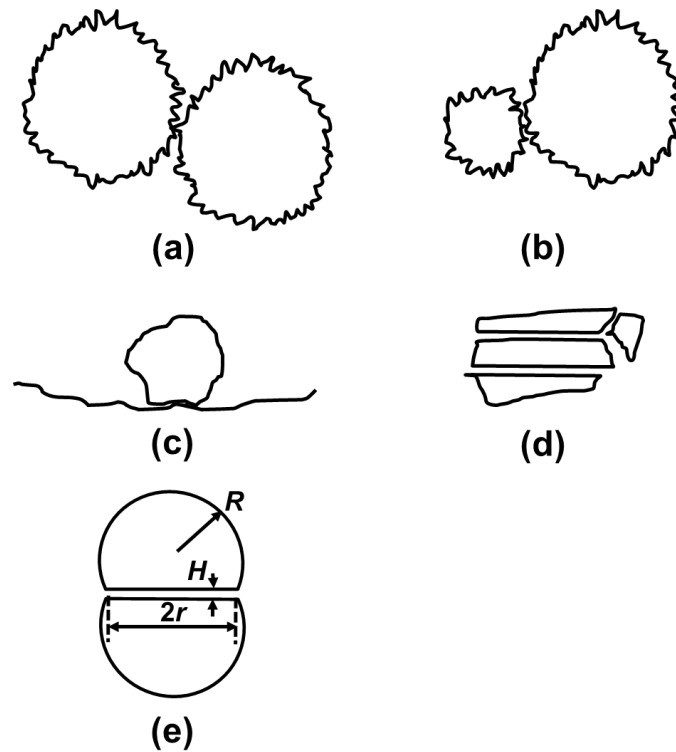
Figure 2.2: The influence of surface roughness and geometrical factors on particle interaction; (a), (b): surface roughness limiting particle approach; (c), (d): surface structures promoting close contact; (e): two idealized particles of radius *R* at a separation distance *Z* and an intimate contact area of diameter *2r*

2.2.3   Agglomeration

Because of the strong interparticle forces, cohesive Group C powders tend to agglomerate both in storage and when fluidized. The natural agglomerates, also called initial or first agglomerates, are formed from primary particles or clusters due to the cohesiveness in storage [43-44], which are generally loose in stricture and often break into smaller agglomerates or even discrete particles. The fluidized or secondary agglomerates are formed from primary particles and the natural agglomerates dur to the co-exertion of the interparticle forces and the hydrodynamic forces [43-49], which are very stable and generally show severe segregation along the fluidize bed, e.g. smaller agglomerates in upper region and larger ones in the lower region of the bed.

The properties of the agglomerates are important to decide the fluidization behaviors of cohesive particles [45-47,50-52]. Group C particles or nanometer particles with strong interparticle forces tend to form agglomerates and behave like Group A particles in fluidization, which is called agglomerating fluidization [46-47, 50, 53-56]. Many works [23,46,48,54,57-60] either measured directly or estimated the agglomerate sizes in the fluidized bed of fine Group C particles. For example, Iwadate and Horio (1998) [46] derived a mathematical model to predict an equilibrium size in agglomerating fluidized beds of Group C particles based on the balance of bed expansion force caused by bubbles and agglomerate-to-agglomerate cohesive force. Xu and Zhu (2005) [23] experimentally measured the size of the agglomerates in the fluidization of Group C particles with and without mechanical vibration, and also proposed a model for the prediction of agglomerate sizes based on the balance between the agglomerate collision energy due to cohesive forces and the energy generated by vibration.

2.3   Fluidization aids for Group C particles

Because of the small particle size and large specific surface area, Group C particles have been widely used in a variety of industries [61-65]. The most critical problems that limit the application of Group C particles are their poor flowabilty and none fluidizability ascribed to the strong interparticle forces which are mainly the van der Waals forces as discussed above. The most important parameter determining the van der Waals forces is

the separation distance between the particles. Any means to enlarge the separation distance will significantly reduce the interparticle forces and consequently increase the flowability and the fluidization of a given powder. Factors affecting the separation distance are the increase of the surface roughness and the use of spacers, e.g. the addition of fines [28-30, 66-68]. Apart from means to enlarge the separation distance, changes in surface properties also diminish the cohesive forces due to the screening effect, e.g. gas adsorption [69-70]. In addition to reduce the interparticle forces, other methods attempt to overcome the interparticle forces by introducing external energies, including mechanical or acoustic vibration [22-25,71-73], mechanical stirring [20-21], and magnetic or electrical field disturbance [74-75]. These methods to improve the fluidization quality are collectively referred to as fluidization aids.

2.3.1   The addition of finer particles

Fredrickson (1961) [76] showed that the addition of a very small amount (0.1wt%) of superfine tricalcium phosphate made cohesive starch particles fluidizable. Fried and Wheelock (1966) [77] also found that adding a small amount of submicron silica (0.5-3wt%) in flour made the flour powder less agglomerative. Dutta and Dullea (1990) [26] reported the reduction in the cohesiveness of Group C powders by mixing a small amount of nanoparticles such as alumina (29 nm) or aerosil 200 (12 nm). Xu and Zhu (2009) [78] coated nanoparticles onto the surfaces of the cohesive Group C particles and found that the partial coating on the surfaces could significantly reduce the cohesiveness and hence enhance the flowability of Group C particles. More recently, Han et al. (2019) [79] reported that nanoparticles, as flow additives, significantly improved the flowability and the fluidization quality of Group C particles, and those nano-modulated Group C particles exhibit good fluidization similar to Group A particles, achieving full fluidization with small minimum fluidization velocity.

As the van der Waals forces dominate over other interparticle forces and sharply decreased with the separation distance between two particles, the addition of finer particles reduced the van der Waals forces by acting as spacers [37,66,80] or reduced the friction by acting as lubricants [81,82]. Cheng and Yang et al. (2008) [29] proposed an adhesion force model for Group C particles coated by nanoparticles and considered that three nanoparticles

supported two Group C particles stably as shown in Figure 2.3. They found that a stable fluidization could be achieved when the surface area coverage of nanoparticles reached to 5%-90% with corresponding 0.05wt%-1.0wt% of nanoparticles, which were consistent with earlier work by Zhu and Zhang (2004) [28], stating that the weight percentage of nanoparticle additives should be at least 0.1wt% to ensure the "lubricating" effect and should be lower than 5wt%.
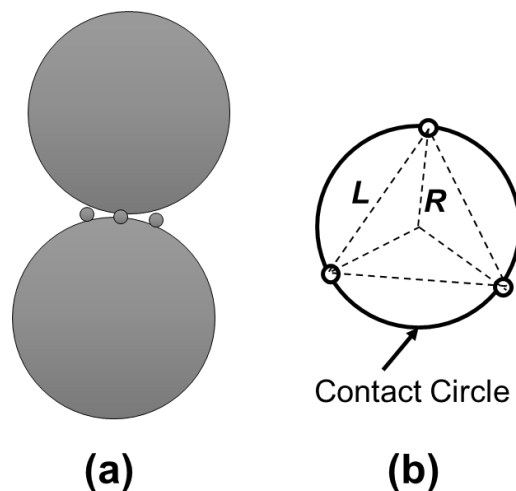
Figure 2.3: (a) Contact of two-coated cohesive particles and
(b) Location of guest particles

Xu and Zhang et al. (2009) [78] proposed two contact models based on different contacting status of the nanoparticles in relation to Group C particles to evaluate the interparticle forces: one is asperities- contact model and the other is sandwich-contact model, as shown in Figure 2.4. They found that nanoparticle surface coating could significantly reduce the cohesion forces between Group C particles, and their flowability and fluidization behaviors were effectively improved with a nanoparticle fraction of about 0.5wt%-1.0wt%.
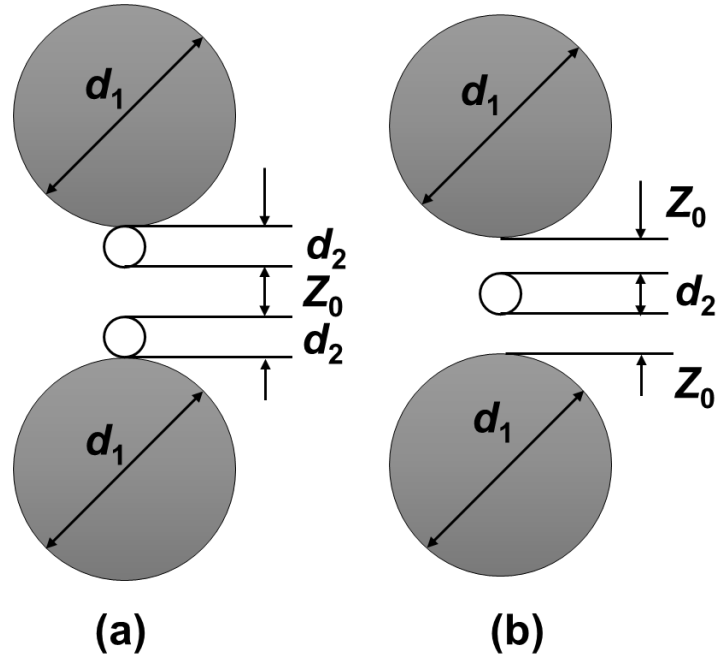
Figure 2.4: (a) The asperities-contact model and (b) The sandwich-contact model: d_1, diameter for the host Group C particles; d_2, diameter for the guest nanoparticles

2.3.2 Gas adsorption

Gas adsorption also influence the van der Waals forces of fine Group C particles through varying either the Hamaker coefficient or the separation distance between particles [37]. Piepers and Cottaar et al. (1984) [70] reported that the gas adsorption affected the cohesion between the particles and hence increased the elasticity modulus introduced by Rietema and Musters [83], resulting in the increase of bed expansion. The cohesion further increased with the gas pressure dur to the increase of the gas adsorption with pressure. The effect of gas adsorption has also been demonstrated theoretically in the works of Cottaar and Rietema (1986) [84] and Xie (1997) [85] using the Hamaker theory. More recently, Xu and Zhu (2006) [69] investigated the effect of gas adsorption on the fluidization of Group C particles on the basis of the London-van der Waals theory, and found that the interparticle forces were significantly affected by the gas adsorption and varied with the type of fluidizing gases with different London-van der Waals constants.

2.3.3 Other fluidization aids

Except for the techniques reducing the interparticle forces, other ones can overcome the interparticle forces by introducing external energies. However, these techniques are scale-dependent and hard to implement. For example, Mori (1990) [86] developed a vibro-fluidized bed to fluidize Group C powders, and found that a wide range of fine particles down to sub-micron level could be fluidized fairly well at a relatively low gas velocity. Xu and Zhu (2006) [23] found that mechanical vibration could significantly reduce the average size of agglomerates and improve the fluidization quality of cohesive Group C particles. Brekken et al. (1970a, 1970b) [87,88] reported that a mechanical stirrer was effective for breaking down channels and enabling good quality particulate fluidization in beds of cohesive powders. Zhu and Li (1996) [89] used a magnetic field to enhance the fluidization of Group C powders, and the channels and bubbles were eliminated effectively in the magnetic field. Another experimental work was reported by Lu and Li (2000) [90], showing that binary particles of $CaCO_3$ (0.37 μm) and Fe_2O_3 (0.8 μm) were well fluidized in a rotating magnetic field.

2.4 Factors affecting fluidization behaviors

Generally, particles become fluidized when an upward-flowing gas imposes a high enough drag force to overcome the downward force of gravity. For fine Group C particles, there is no question but that interparticle forces dominate the flow and fluidization behaviors over the gravity. It is the balance between the interparticle forces and the hydrodynamic forces which determine the behaviors of fine powders. The hydrodynamic forces (drag forces) are the friction forces imposed by the gas on the particles which are closely related to the operating gas velocity and gas properties. The interparticle forces are influenced by particle properties, such as particle size, the presence of fines content, and particle roughness, etc.

2.4.1 Hydrodynamic forces

It is well known that hydrodynamic forces are mainly influenced by gas properties, especially by gas viscosity in the fluidization of fine particles which is in the laminar regime. The gas viscosity has a fundamental role on the fluidization dynamics since the drag force acting on particles affects the formation of flow structures [91]. Geldart and

Abrahamsen [92] clearly demonstrated that the bubbling fluidization behaviors of Group A particles was a function of the density and viscosity of the fluidizing gas, and the dense phase voidage (ε_d) increased as gas viscosity and gas density increased. Geldart and Harnby et al. (1984) [93] showed that the bed expansion of some Group C powders was found to increase as the gas viscosity increased by using different fluidizing gases. Olowson and Almstedt (1992) [94] reported that an increase in gas density caused by an increase in pressure resulted in an increased gas momentum flux, which is a governing parameter for the hydrodynamic behavior of a fluidized bed. Xie and Geldart (1995) [95] increased the hydrodynamic forces using high viscosity gases, argon and neon, producing and increase in homogeneous expansion in the fluidization of FCC powders. Xu and Zhu (2006) [69] found that increasing the gas viscosity by using different gases or by elevating the bed temperature could improve the average bed voidage of Group C particle fluidization. Valverde et al. (2006, 2008) [91,96] investigated high viscosity gas fluidization of fine particles and concluded that increasing gas viscosity improved the uniformity of fluidization and produced a full suppression of the bubbling regime.

2.4.2 Interparticle forces

Baerns (1966) [97] investigated the effect of interparticle adhesive forces on the incipient fluidization velocity of fine particles in the size range of less than 50μm, and found that the limitations of the feasibility of fluidization depended on the ratio of a particle weight to the sum of the weight and the interparticle adhesive force. Donsi and Massimilla (1973) [98] recognized that interparticle van der Waals forces and capillary forces played an important role in the bubble-free expansion of small particles, and theoretically evaluated the interparticle forces between particles in their later work [99]. Mutsers and Rietema (1977) [83] proposed that the interparticle cohesion forces gave rise to the formation of a powder structure with a certain mechanical strength, which enabled the homogeneous fluidization of fine particles. Geldart and Wong (1984, 1985) [100,101] measured the bed expansion and the rates of de-aeration for powders showing degree of cohesiveness (Group A and C), concluding that the bed expansion in the bubble-free range and the de-aeration characteristics were different between Group A and C particles and were related to the degree of the particle cohesivity. Rietema and Piepers et al. (1990, 1993) [102,103]

reported the effect of interparticle forces on the stability of gas-fluidized beds experimentally and theoretically. More recently, Galvin and Benyahia (2014) [104] numerically investigated the effect of van der Waals forces on the fluidization od aeratable Group A particles. Oke and Lettieri et al. (2015) [105] also modelled the stable expansion of gas-fluidized beds of Group A particles (53µm and 66µm) and obtained a reasonable agreement between numerical and experimental findings, suggesting that the cohesiveness affected the homogeneous bed expansion.

Many researchers proposed that changing the cohesion of Groups A or B particles, by gas adsorption, surface coating, and the increase of temperature, could affect their fluidization behaviors [70,85,106-108]. For example, Xie (1997) [85] increased the van der Waals forces of FCC particles by gas adsorption and found that they behaved like a very cohesive power. Cui and Chaouki (2004) [109] decreased the interparticle attractive forces while increased the interparticle repulsive forces of Group A particles with increasing the temperature, and found that the fluidization behaviors of Group A particles seemed to shift from typical Geldart A toward B, consistent with the work conducted by Molerus (1982) [110], attributing the transition from Group C to A and A to B powders to the diminishing strength of van der Waals forces. Other researches illustrated that the presence of thermally induced interparticle forces in the gas-solid fluidized bed of Group A particles extended the homogeneous fluidization regime [111], and that in the bed of Group B particles increased the dense phase voidage and could alter the fluidization behaviors from Geldart Group B to A and even C with increasing the level of interparticle forces in the bed [112,113].

Particle size and particle size distribution will also influence the magnitude of the interparticle forces and thus affect fluidization behaviors. For example, a wide size distribution of Group A particles has been observed to lead to smoother fluidization and better gas-solid contacting [114]. In addition, the presence of fines (<45µm) may improve the performance of fluidized bed reactors [16,115,116]. Abrahamsen and Geldart [117] found that increasing the fine fraction (<45µm) in Group A particles would improve the fluidization, but if the fine fraction continued to increase, eventually it would change the powder into cohesive Group C particles, resulting in poor fluidization. Others, such as

Seville and Clift (1984) [118], increased interparticle forces artificially by the successive addition of small amounts of a light oil to Group B powder, thereby causing its behavior to change to that of Group A, and eventually, to Group C.

2.5   Performance of fluidized bed reactors

Gas-solid fluidized beds are widely employed in industrial operations as gas-solid contactors and chemical reactors, ranging from physical processes, such as gas adsorption, drying and mixing of particles, to chemical processes, such as catalytic cracking, combustion and biomass gasification [1,6,8,10,119-121]. The excellent mass and heat transfers have led to the success of many processes adopting fluidized beds. Gas-solid interfacial contact area is one of the most important indexes that controls the performance of a fluidized bed reactor. Generally, the conventional gas-solid fluidized bed reactors are composed of two phases, a dense or particulate phase and a bubble phase [114,122-124]. A significant increase in gas-solid interfacial contact area can be achieved by introducing more gas into the dense phase where gas is in closer contact with particles, contributing to better gas-solid contact and thus enhancing the reactor performance. As a result both the particle size and the dense phase voidage are key parameters that affect the gas-solid interfacial contact area. On the other hand, bubbling behaviors, such as bubble size and rise velocity, also greatly affect the gas-solid interfacial contact and the bubble residence time in the fluidized bed, subsequently influencing the reactor performance. In summary, the evaluation of the performance of a fluidized bed reactor depends on the dense phase characteristics, the bubble behaviors, and the gas flow distribution between the two phases.

2.5.1   Dense phase characteristics

The dense phase expansion is a critical characteristic for evaluating the fluidization quality and the reaction performance. A higher dense phase expansion or dense phase voidage (ε_d) indicates more gas holdup in the dense phase which has more opportunities to contact with particles. The dense phase expansion or the dense phase voidage can be evaluated using the bed collapse test, which was initially proposed by Rietema in 1967 [125] and now is one of the most popular methods of characterizing fluidized bed hydrodynamics. This technique is carried out by first fully fluidizing the bed, followed by suddenly shutting off

the gas supply, then tracking the bed surface level as it collapses. The bed collapse process, as shown in Figure 2.5, can be clearly divided into three stages: (1) the bubble escape stage, where the bed surface drops quickly due to gas bubbles reaching and escaping from the top of the bed; (2) the sedimentation stage, where the gas in the interstices of the dense phase in excess of εmf escapes; (3) the consolidation stage, where the fixed bed further settles to a final compacted bed. The bed collapse test is the only simple method for estimating the average dense phase voidage and bubble holdup in the bubbling fluidized bed [117,126-128].
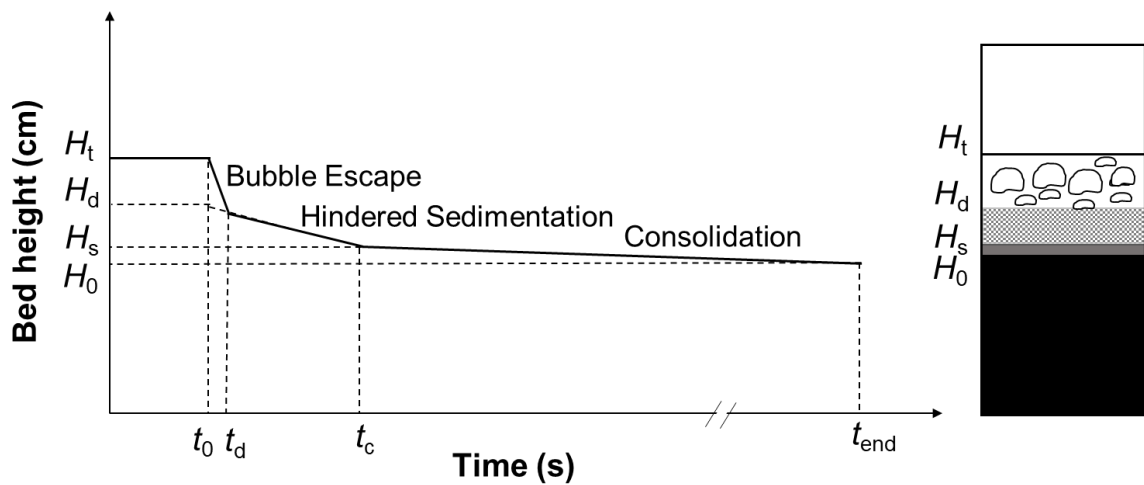
Figure 2.5: A typical bed collapse curve

Many earlier works [114,116,117,124,126,128-130] have reported that the bed expansion, especially the dense phase expansion, increased as the particle size decreased and/or the fraction of fines (<45μm) increased. For example, Geldart Group A particles show a homogeneous fluidization regime with the dense phase voidage larger than the bed voidage at minimum fluidization (ε_{mf}), different with Group B particles showing typical bubbling fluidization with $\varepsilon_d = \varepsilon_{mf}$ [124]. Abrahamsen and Geldart (1980) [128] investigated the effect of the fraction of fines less than 45μm on the dense phase voidage in the fluidization of Geldart Group A particles, showing an increase of the dense phase voidage with increasing the fraction of fines. Grace and Sun (1991) [114] found that the fines content in FCC catalysts resulted in a more expanded dense phase, smaller bubbles and an enhanced chemical conversion. Bruni and Lettieri et al. (2006) [130] divided fines into two sub-cuts

of size 0-25μm and 25-45μm and analyzed their effects on the fluidization of Group A particles. The results showed that the addition of the finer sub-cut (0-25μm) more significantly increased the dense phase expansion than the sub-cut of size 25-45μm.

2.5.2   Bubble characteristics

In general, gas bubbles rise up through a typical bubbling fluidized bed, coalesce with other bubbles, and break up intermittently, thus enhancing mass and heat transfer [131-133]. In particular, the bubbling behaviors, such as bubble size and rise velocity, greatly affect the gas residence time and the gas-solid contact, subsequently influencing reactor performance. Ideally, bubbles in a fluidize bed reactor should be small in size, uniformly distributed throughout the bed, and have low rise velocities [117,128,134-136].

Extensive studies [137-148] on bubble behaviors of typical Geldart Group A, B, and D powders (30-2600μm) have shown that bubbles are usually smaller in beds of finer particles. The smaller bubble size in the fluidized bed of finer particles generally leads to lower bubble rise velocity which is directly correlated with the bubble size [149]. Yusui and Johanson (1958) [150] were among the first researchers who studied the bubble characteristics and proposed and empirical bubble size correlation based on their experimental data using different particle types with average sizes ranging from 41 to 450μm and found that bubbles nominally smaller than about 1.3cm. Darton et al. (1977) [138] suggested a bubble size correlation based on the bubble growth pattern due to coalescence of bubbles which has become one of the most popular bubble size correlations. Since they have not considered any mechanism of bubble splitting and breakage, their model predicts a constantly increasing trend of bubble size, making this model limited to Group B and D particles. Horio and Nonaka (1987) [137] overcame this limit by introducing the concept of equilibrium bubble size which is the result of a balance between bubble coalescence and bubble splitting, decreasing the bubble size and making this model appropriate for finer Group A particles which can reach the maximum stable bubble diameter.

Werther (1984) [142] indicated that the increased fines content lead to smaller bubbles and to a higher interphase mass transfer coefficient. Grace and Sun (1991) [114] reported that

wider particle size distribution with s small fraction of fines less than 45 produced smaller bubbles in the fluidization of Group A particles. More Recently, Ma and Liu et al. (2016) [151] studied the bubbling behaviors of cohesive Geldart Group B particles, using "polymer coating" approach to introduce cohesive forces, and found that bubble fraction and bubble diameter decreased by increasing the cohesive force within a low level. Zou and Li et al (2011) [152] investigated bubble behaviors in a fluidized bed with cohesive Group C particles, and smaller bubbles were observed than that with Group A or B particles.

2.5.3 Gas flow distribution

Generally, the gas flow through a bubbling fluidized bed is divided into two portions: one makes up the bubble phase and the other goes into the dense phase or the particulate phase as interstitial gas. The relative distribution of gas flow between the bubble phase and the dense phase is a very important factor that determines the performance of a gas-solid fluidized bed reactor, because the gas flow through the dense phase is in more intimate contact with particles than that through the bubble phase, contributing to better gas-solid contacting.

The two-phase theory of gas-solid fluidization was used to evaluate the gas flow distribution through the two-phases, initially proposed by Toomy and Johnstone (1952) [153] who suggested that all gas in excess of that required for minimum fluidization would pass through the bed in the form of bubbles:

$$G_b / A = u_g - u_{mf}$$

The two-phase theory implies that the dense phase vodiage and the interstitial gas velocity in the dense phase remain almost the same as in the incipient fluidization state. However, most of the experimental evidences [154-158] have demonstrated that the original two-phase theory is only approximately true and tends to overestimate the visible bubble flow in most cases. For example, Turner (1966) [155] and Davidson and Harrison (1966) [156] suggested a factor K to account for a higher gas velocity than u_{mf} going through the dense phase:

$$G_b / A = u_g - K u_{mf}$$

with $K=1$ for the original two-phase assumption. Theory was given to predict the value of K by Lockett, Davison and Harrison in 1967 [122], and showed that $K=1+\varepsilon_b$ for a two-dimensional system, $K=1+2\varepsilon_b$ for a three-dimensional system. A number of workers [30-42] carried out experiments which allowed them to measure directly or to estimate visible bubble flow rates in freely fluidized bed. Grace and Clift (1974) [157] summarized these works and found K to vary in rang 0.7 to 27. Although the ranges of values measured for the parameter K was wide, in almost every case K was found to be well in excess of unity. Later on, in their review chapter, Clift and Grace [159] used a Y value, first proposed by Werther J (1978) [160], to account for the same effect:

$$G_b / A = Y (u_g - u_{mf})$$

where the value of the empirical parameter Y was usually less than unity which depended on the powder group, bed height, and bed diameter.

The deviation from the simple two-phase theory, that is $Y < 1$, has increasingly been found, especially for systems of Geldart Group A particles and other particles containing a high fraction of "fines" ($d_p < 45\mu m$) [114,117,124,126,128,161-165], due to the increased gas holdup and gas velocity in the dense phase than those at minimum fluidization. From 1980 onwards, an increasing number of work had studied the gas flow in the fluidized beds of fine powders (Group A), and it has become widely recognized that the dense phase voidage and the interstitial gas flow are much greater than that suggested by the original two-phase theory and the fine content played a major role in such deviation [70,108,126-128,161,166-168]. In summary, the higher interstitial gas flow through the dense phase and lower gas flow through the bubble phase for finer particles are important, especially for gas-phase catalytic reactions, contributing to better gas-solid interfacial contact.

2.6 Summary

Fluidized beds are widely used as chemical reactors and many other processing devices, especially as gas-phase catalytic reactors, which largely depend on the degree of gas-solid contact. Fine particles in small sizes can provide large gas-solid interfacial areas and thus are widely applied in these reactors as catalysts. Geldart (1973) classified particles into Groups A, B, C, and D by density difference (ρ_p-ρ_g) and mean particle size (d_p) based on their different fluidization behaviors. Group C particles with extremely small particle sizes

are deemed to non-fluidizable due to their strong interparticle forces, which lead to severe agglomeration and channeling when Group C particles are subjected to fluidization. Considering that the large specific surface areas of fine Group C particles are of increasing importance in industry, various measures referred to as fluidization aids have been developed, such as vibration and stirring by introducing external energies to overcome the interparticle forces, or gas adsorption and the addition of finer particles to intrinsically reducing the interparticle forces. The addition of finer particles such as nanoparticles is a scale-independent technique and easier to implement than other measures. Although the addition of nanoparticles has shown to significantly reduce the cohesion and increase the flowability of Group C particles, the fluidization behaviors of these nano-modulated Group C particles have not been systematically studied.

When compared with Group B particles, the fluidized beds of fine Group A particles have been shown to exhibit higher gas holdup in the dense phase, smaller bubbles, more gas flow through the dense phase and less through the bubble phase, contributing to better gas-solid contact. In addition, numerous previous studies demonstrated that the interparticle forces played an important role in bubble-free expansion in the fluidization of fine Group A particles. Introducing the interparticle forces within a low level could improve the fluidization quality for Group A and B particles, showing higher dense phase expansion and smaller bubbles. For even smaller Group C particles, there is no question but that interparticle forces dominate the flow and fluidization behaviors over the gravity. The nano-modulated Group C particles with a control of interparticle forces can provide even larger specific surface area and are expected to exhibit better fluidization quality than Group A particles, contributing to better gas-solid contact which is one of the most important indexes that controls the performance of a fluidized bed reactor. As a result, it is important and necessary to comprehensively investigate the fluidization dynamics of Group C particles with the addition of nanoparticles.

Nomenclature

A	Cross-sectional area of a fluidized bed (m^2)
A_p	Specific surface area of a particle (m^2/m^3)

A_H	Hamaker coefficient (J)
d_p	Particle size (μm)
F_{van}	Van der Waals force (N)
G_b	Gas flowrate through the bubble phase (m^3/s)
H_t	Total fluidized bed height (m)
H_d	Dense phase height (m)
H_s	Settled bed height (m)
H_0	Initial bed height (m)
R	Radius of a sphere (m)
S	Surface area of a sphere (m^2)
u_g	Superficial gas velocity (m/s)
u_{mf}	Minimum fluidization velocity (m/s)
u_{mb}	Minimum bubbling velocity (m/s)
V	Volume of a sphere (m^3)
Z	Separation distance between two particles (m)
ρ_p	Particle density (kg/m^3)
ρ_g	Gas density (kg/m^3)
ε_b	Bed voidage (-)
ε_d	Dense phase voidage (-)
ε_{mf}	Bed voidage at minimum fluidization (-)

References

[1] Karau, A., C. Benken, J. Thömmes, and M-R. Kula. "The influence of particle size distribution and operating conditions on the adsorption performance in fluidized beds." Biotechnology and bioengineering 55, no. 1 (1997): 54-64.

[2] Ammendola P, Raganati F, Chirone R. CO2 adsorption on a fine activated carbon in a sound assisted fluidized bed: Thermodynamics and kinetics. Chemical Engineering Journal. 2017. 322:302-13.

[3] Costodes VT, Lewis AE. Reactive crystallization of nickel hydroxy-carbonate in fluidized-bed reactor: fines production and column design. Chemical engineering science. 2006 Mar 1;61(5):1377-85.

[4]   Xu C, Zhu J. One-step preparation of highly dispersed metal-supported catalysts by fluidized-bed MOCVD for carbon nanotube synthesis. Nanotechnology. 2004 Oct 28;15(11):1671.

[5]   Burggraeve A, Monteyne T, Vervaet C, Remon JP, De Beer T. Process analytical tools for monitoring, understanding, and control of pharmaceutical fluidized bed granulation: a review. European journal of pharmaceutics and biopharmaceutics. 2013. 83(1):2-15.

[6]   Luo Y, Zhu J, Ma Y, and Zhang H. "Dry coating, a novel coating technology for solid pharmaceutical dosage forms." International journal of pharmaceutics 358, no. 1-2 (2008): 16-22.

[7]   Watano S, Nakamura H, Hamada K, Wakamatsu Y, Tanabe Y, Dave RN, Pfeffer R. Fine particle coating by a novel rotating fluidized bed coater. Powder Technology. 2004 Mar 30;141(3):172-6.

[8]   Lyngfelt, Anders, Bo Leckner, and Tobias Mattisson. "A fluidized-bed combustion process with inherent CO2 separation; application of chemical-looping combustion." Chemical Engineering Science 56.10 (2001): 3101-3113.

[9]   Smoot LD, Smith PJ. Coal combustion and gasification. Springer Science & Business Media; 2013 Nov 11.

[10]   Werther, Joachim. "Fluidized-bed reactors." Ullmann's encyclopedia of industrial chemistry (2000).

[11]   Jesse Zhu, Y. C. Fluidized-Bed Reactors and Applications. In Multiphase Flow Handbook; Crowe, C, Ed.; CRC Press: New York, 2005; pp 5.55-55.93.

[12]   Weerachanchai P, Horio M, Tangsathitkulchai C. Effects of gasifying conditions and bed materials on fluidized bed steam gasification of wood biomass. Bioresource Technology. 2009 Feb 1;100(3):1419-27.

[13]   Grace, John R., Bo Leckner, Jesse Zhu, and Yi Cheng. "Fluidized beds." Multiphase Flow Handbook 5 (2006): 1-93.

[14]   Bi, H. T., and J. R. Grace. "Flow regime diagrams for gas-solid fluidization and upward transport." International Journal of Multiphase Flow 21, no. 6 (1995): 1229-1236.

[15]   Yerushalmi, Joseph, and N. T. Cankurt. "Further studies of the regimes of

fluidization." Powder Technology 24, no. 2 (1979): 187-205.

[16] Geldart D. The effect of particle size and size distribution on the behaviour of gas-fluidised beds. Powder Technology. 1972 Oct 4;6(4):201-15.

[17] Geldart D. Types of gas fluidization. Powder technology. 1973 May 1;7(5):285-92.

[18] Diekman R, Forsythe WL. Laboratory prediction of flow properties of fluidized solids. Industrial & Engineering Chemistry. 1953 Jun;45(6):1174-7.

[19] Oltrogge, R.D., 1972. Correlation of the Bubble Point and Dense Phase Expansions for Small-Particle Gas-Fluidized Beds (Doctoral dissertation, Ph. D. Thesis, Univ. Michigan).

[20] Alavi S, Caussat B. Experimental study on fluidization of micronic powders. Powder technology. 2005 Sep 29;157(1-3):114-20.

[21] Kariman A, Rao VB, Farjpourlar M. Fluidization characteristics of nano particles with the assist of stirrer. Journal of Applied Physics. 2013;5:24-7.

[22] Marring E, Hoffmann AC, Janssen LP. The effect of vibration on the fluidization behaviour of some cohesive powders. Powder technology. 1994 Apr 1;79(1):1-0.

[23] Xu C, Zhu J. Experimental and theoretical study on the agglomeration arising from fluidization of cohesive particles—effects of mechanical vibration. Chemical Engineering Science. 2005 Dec 1;60(23):6529-41.

[24] Chirone R, Massimilla L, Russo S. Bubble-free fluidization of a cohesive powder in an acoustic field. Chemical Engineering Science. 1993 Jan 1;48(1):41-52.

[25] Chirone R, Massimilla L. Sound-assisted aeration of beds of cohesive solids. Chemical engineering science. 1994 Apr 1;49(8):1185-94.

[26] Dutta A, Dullea LV. A comparative evaluation of negatively and positively charged submicron particles as flow conditioners for a cohesive powder. In AIChE Symposium Series. 1990;86(276): 26-40.

[27] Ajbar A, Alhumazi K, Asif M. Improvement of the fluidizability of cohesive powders through mixing with small proportions of group A particles. The Canadian Journal of Chemical Engineering. 2005 Dec;83(6):930-43.

[28] Zhu, J. and Zhang H. Fluidization Additives to Fine Powders. U.S. Patent 6833185. December 21, 2004.

[29] Chen Y, Yang J, Dave RN, Pfeffer R. Fluidization of coated group C powders. AIChE

journal. 2008 Jan;54(1):104-21.

[30] Tomas J, Kleinschmidt S. Improvement of flowability of fine cohesive powders by flow additives. Chemical Engineering & Technology: Industrial Chemistry‑Plant Equipment‑Process Engineering‑Biotechnology. 2009 Oct;32(10):1470-83.

[31] Pajonk GM. Aerogel catalysts. Applied Catalysis. 1991 May 16;72(2):217-66.

[32] Chaouki J, Chavarie C, Klvana D, Pajonk GM. Kinetics of the selective hydrogenation of cyclopentadiene on a CuAl2O3 aerogel catalyst in an integral plug flow reactor. Applied catalysis. 1986 Feb 14;21(1):187-99.

[33] da Cunha, A. L. C., Lemos, M. S., Meth, S., Gonçalves, J. P., & Dweck, J. (2011). A study of the particle size effect on the pozzolanic activity of an equilibrium catalyst. Journal of thermal analysis and calorimetry, 106(3), 805-809.

[34] Bridgwater J. Particle technology. Chemical engineering science. 1995 Dec 1;50(24):4081-9.

[35] D. Geldart, in D. Geldart (ed.), Gas Fluidizotion Technology, Wiley, Chichester, 1986, p. 33.

[36] Krupp H. Particles adhesion theory and experiment. Advances in colloid and interface science. 1967;1:111-239.

[37] Visser J. Van der Waals and other cohesive forces affecting powder fluidization. Powder Technology. 1989 May 1;58(1):1-0.

[38] Gady B, Schleef D, Reifenberger R, Rimai D, DeMejo LP. Identification of electrostatic and van der Waals interaction forces between a micrometer-size sphere and a flat substrate. Physical Review B. 1996 Mar 15;53(12):8065.

[39] Rietema K. The dynamics of fine powders. Springer Science & Business Media; 2012 Dec 6.

[40] Israelachvili J. Interfacial forces. Journal of Vacuum Science & Technology A: Vacuum, Surfaces, and Films. 1992 Sep;10(5):2961-71.

[41] Hamaker HC. The London—van der Waals attraction between spherical particles. physica. 1937 Oct 1;4(10):1058-72.

[42] Visser J. On Hamaker constants: A comparison between Hamaker constants and Lifshitz-van der Waals constants. Advances in colloid and interface science. 1972

Dec 1;3(4):331-63.

[43] Pacek AW, Nienow AW. Fluidisation of fine and very dense hardmetal powders. Powder Technology. 1990 Feb 1;60(2):145-58.

[44] Hua B, Hu L, Li C. Process of collapse and expansion of ultrafine powder fluidization bed. J. East China Univ. Sci. Techn. 1994;20(3):290-4.

[45] Chaouki J, Chavarie C, Klvana D, Pajonk G. Effect of interparticle forces on the hydrodynamic behaviour of fluidized aerogels. Powder Technology. 1985 Jul 15;43(2):117-25.

[46] Iwadate Y, Horio M. Prediction of agglomerate sizes in bubbling fluidized beds of group C powders. Powder Technology. 1998 Dec 1;100(2-3):223-36.

[47] Wang Z, Kwauk M, Li H. Fluidization of fine particles. Chemical Engineering Science. 1998 Feb 1;53(3):377-95.

[48] Kuwagi K, Horio M. A numerical study on agglomerate formation in a fluidized bed of fine cohesive particles. Chemical Engineering Science. 2002 Nov 1;57(22-23):4737-44.

[49] Cocco R, Shaffer F, Hays R, Karri SR, Knowlton T. Particle clusters in and above fluidized beds. Powder Technology. 2010 Oct 25;203(1):3-11.

[50] Yao W, Guangsheng G, Fei W, Jun W. Fluidization and agglomerate structure of SiO2 nanoparticles. Powder Technology. 2002 Apr 8;124(1-2):152-9.

[51] Zhou T, Li H, Shinohara K. Agglomerating fluidization of group C particles: major factors of coalescence and breakup of agglomerates. Advanced Powder Technology. 2006 Jan 1;17(2):159-66.

[52] Shabanian J, Jafari R, Chaouki J. Fluidization of ultrafine powders. International review of chemical engineering. 2012 Jan;4(1):16-50.

[53] S. Morooka, K. Kusakabe, A. Kobata, Y. Kato, Fluidization state of ultrafine powders, J. Chem. Eng. Jpn. 21 (1988) 41– 46.

[54] T. Zhou, H. Li, Estimation of agglomerate size for cohesive particles during fluidization, Powder Technol. 101 (1999) 57–62.

[55] Y. Wang, F. Wei, Y. Jin, T. Luo, Agglomerate particulate fluidization and E-particles, Proceedings of the Third Joint China/USA Chemical Engineering Conference (CUChE-3), 12-006, Beijing, 2000.

[56] van Ommen JR, Valverde JM, Pfeffer R. Fluidization of nanopowders: a review. Journal of nanoparticle research. 2012 Mar 1;14(3):737.

[57] Castellanos A, Valverde JM, Quintanilla MA. Aggregation and sedimentation in gas-fluidized beds of cohesive powders. Physical Review E. 2001 Sep 24;64(4):041304.

[58] Xu C, Zhu J. Parametric study of fine particle fluidization under mechanical vibration. Powder Technology. 2006 Jan 16;161(2):135-44.

[59] Mawatari Y, Ikegami T, Tatemoto Y, Noda K. Prediction of agglomerate size for fine particles in a vibro-fluidized bed. Journal of chemical engineering of Japan. 2003;36(3):277-83.

[60] Valverde JM, Castellanos A. Effect of vibration on agglomerate particulate fluidization. AIChE journal. 2006 May;52(5):1705-14.

[61] Liu J, Shi J, He D, Zhang Q, Wu X, Liang Y, and Zhu Q. Surface active structure of ultra-fine Cu/ZrO2 catalysts used for the CO2+ H2 to methanol reaction. Applied Catalysis A: General, 2001, 218(1-2): 113-119.

[62] Dewettinck K, Huyghebaert A. Fluidized bed coating in food technology. Trends in Food Science & Technology. 1999 Apr 1;10(4-5):163-8.

[63] Minamidate Y, Yin S, Sato T. Synthesis and characterization of plate-like ceria particles for cosmetic application. Materials Chemistry and Physics. 2010 Oct 1;123(2-3):516-20.

[64] Nalinga Y, Legonda I. The effect of particles size on biogas production. Int. J. Innovative Res. Technol. Sci. 2016;4(2):9-13.

[65] Jono K, Ichikawa H, Miyamoto M, Fukumori Y. A review of particulate design for pharmaceutical powders and their production by spouted bed coating. Powder Technology. 2000 Dec 6;113(3):269-77.

[66] Zhou T, Li H. Effects of adding different size particles on fluidization of cohesive particles. Powder Technology. 1999 May 24;102(3):215-20.

[67] Chen Y, Yang J, Mujumdar A, Dave R. Fluidized bed film coating of cohesive Geldart group C powders. Powder Technology. 2009 Feb 13;189(3):466-80.

[68] Zhu X, Zhang Q, Huang C, Wang Y, Yang C, Wei F. Validation of surface coating with nanoparticles to improve the flowability of fine cohesive powders. Particuology. 2017 Feb 1;30:53-61.

[69] Xu C, Zhu JX. Effects of gas type and temperature on fine particle fluidization. China Particuology. 2006;4(03n04):114-21.

[70] Piepers HW, Cottaar EJ, Verkooijen AH, Rietema K. Effects of pressure and type of gas on particle–particle interaction and the consequences for gassolid fluidization behaviour. Powder Technology. 1984;37.

[71] Shuai W, Xiang L, Huilin L, Guodong L, Jiaxing W, Pengfei X. Simulation of cohesive particle motion in a sound-assisted fluidized bed. Powder technology. 2011 Feb 15;207(1-3):65-77.

[72] Xu C, Cheng Y, Zhu J. Fluidization of fine particles in a sound field and identification of group C/A particles using acoustic waves. Powder technology. 2006 Feb 3;161(3):227-34.

[73] Valverde JM, Castellanos A, Quintanilla MA. Effect of vibration on the stability of a gas-fluidized bed of fine powder. Physical Review E. 2001 Jul 18;64(2):021302.

[74] Lepek D, Valverde JM, Pfeffer R, Dave RN. Enhanced nanofluidization by alternating electric fields. AIChE journal. 2010 Jan;56(1):54-65.

[75] Nakamura H, Watano S. Fundamental particle fluidization behavior and handling of nano-particles in a rotating fluidized bed. Powder Technology. 2008 Apr 21;183(3):324-32.

[76] Fredrickson REC, inventor; Tate, Lyle Ingredients Americas LLC, assignee. Rendering starch fluidizable. United States patent US 3,003,894. 1961 Oct 10.

[77] Fried EM, Wheelock TD. Fluidized bed characteristics of wheat flour. InChemical Engineering Progress Symposium Series 1966 Sep (Vol. 62, No. 69, p. 117). American Institute of Chemical Engineers.

[78] Xu CC, Zhang H, Zhu J. Improving flowability of cohesive particles by partial coating on the surfaces. The Canadian Journal of Chemical Engineering. 2009 Jun;87(3):403-14.

[79] Han M, Zhou Y, Zhu J. Improvement on flowability and fluidization of Group C particles after nanoparticle modification. Powder Technology. 2019 Jul 8.

[80] Lauga C, Chaouki J, Klvana D, Chavarie C. Improvement of the fluidisability of Ni/SiO2 aerogels by reducing interparticle forces. Powder technology. 1991 Mar 1;65(1-3):461-8.

[81] Hollenbach AM, Peleg M, Rufner R. Interparticle surface affinity and the bulk properties of conditioned powders. Powder Technology. 1983 May 1;35(1):51-62.

[82] Kono HO, Huang CC, Xi M, Shaffer FD. The effect of flow conditioners on the tensile strength of cohesive powder structures. InAIChE Symposium Series: Fluidization and Fluid Particle Systems: Fundamentals and Applications 1989 (Vol. 85, No. 270, pp. 44-48).

[83] Mutsers SM, Rietema K. The effect of interparticle forces on the expansion of a homogeneous gas-fluidized bed. Powder Technology. 1977 Nov 1;18(2):239-48.

[84] Cottaar EJ, Rietema K. A theoretical study on the influence of gas adsorption on interparticle forces in powders. Journal of colloid and interface science. 1986 Jan 1;109(1):249-60.

[85] Xie HY. The role of interparticle forces in the fluidization of fine particles. Powder Technology. 1997;94(2):99-108.

[86] Mori S. Vibro-fluidization of group-c particles and its industrial application. InAIChE Symp. Ser. 1990 (Vol. 86, No. 276, pp. 88-94).

[87] Brekken RA, Lancaster EB, Wheelock TD. Fluidization of flour in a stirred aerated bed: part I. General fluidization characteristics. InChemical Engineering Progress Symposium Series 1970 (Vol. 66, No. 101, pp. 81-90).

[88] Brekken RA, Lancaster EB, Wheelock TD. Fluidization of flour in a stirred aerated bed. Part II—solid mixing and circulation. InChem. Eng. Prog. Symp. Ser. 1970 (Vol. 66, No. 101, pp. 277-284).

[89] Zhu Q, Li H. Study on magnetic fluidization of group C powders. Powder Technology. 1996 Feb 1;86(2):179-85.

[90] Lu X, Li H. Fluidization of CaCO3 and Fe2O3 particle mixtures in a transverse rotating magnetic field. Powder Technology. 2000 Jan 24;107(1-2):66-78.

[91] Valverde JM, Quintanilla MA, Castellanos A, Lepek D, Quevedo J, Dave RN, Pfeffer R. Fluidization of fine and ultrafine particles using nitrogen and neon as fluidizing gases. AIChE journal. 2008 Jan;54(1):86-103.

[92] Geldart D and Abrahamsen AR. Homogeneous fluidization of fine powders using various gases and pressures. Powder Technology. 1978;19(1):133-6.

[93] Geldart DN, Harnby N, Wong AC. Fluidization of cohesive powders. Powder

Technology. 1984 Jan 1;37(1):25-37.

[94]   Olowson PA, Almstedt AE. Hydrodynamics of a bubbling fluidized bed: influence of pressure and fluidization velocity in terms of drag force. Chemical engineering science. 1992 Feb 1;47(2):357-66.

[95]   Xie HY and Geldart D. Fluidization of FCC powders in the bubble-free regime: effect of types of gases and temperature. Powder technology. 1995;82(3):269-77.

[96]   Valverde JM, Castellanos A. High viscosity gas fluidization of fine particles: An extended window of quasihomogeneous flow. Physical Review E. 2006 Aug 8;74(2):021302.

[97]   Baerns M. Effect of interparticle adhesive forces on fluidization of fine particles. Industrial & Engineering Chemistry Fundamentals. 1966 Nov;5(4):508-16.

[98]   Donsi G, Massimilla L. Bubble-free expansion of gas-fluidized beds of fine particles. AIChE Journal. 1973 Nov;19(6):1104-10.

[99]   Massimilla L, Donsì G. Cohesive forces between particles of fluid-bed catalysts. Powder Technology. 1976 Nov 1;15(2):253-60.

[100]   Geldart D, Wong AC. Fluidization of powders showing degrees of cohesiveness—I. Bed expansion. Chemical Engineering Science. 1984 Jan 1;39(10):1481-8.

[101]   Geldart D, Wong AC. Fluidization of powders showing degrees of cohesiveness—II. Experiments on rates of de-aeration. Chemical Engineering Science. 1985 Jan 1;40(4):653-61.

[102]   Rietema K, Piepers HW. The effect of interparticle forces on the stability of gas-fluidized beds—I. Experimental evidence. Chemical Engineering Science. 1990 Jan 1;45(6):1627-39.

[103]   Rietema K, Cottaar EJ, Piepers HW. The effects of interparticle forces on the stability of gas-fluidized beds—II. Theoretical derivation of bed elasticity on the basis of van der Waals forces between powder particles. Chemical engineering science. 1993 Jan 1;48(9):1687-97.

[104]   Galvin JE, Benyahia S. The effect of cohesive forces on the fluidization of aeratable powders. AIChE Journal. 2014 Feb;60(2):473-84.

[105]   Oke O, Lettieri P, Mazzei L. An investigation on the mechanics of homogeneous expansion in gas-fluidized beds. Chemical Engineering Science. 2015 May

4;127:95-105.

[106] Godard K M and Richardson J F. The behaviour of bubble-free fluidized beds. In Institute of Chemical Engineering Symposium Series 1968; 30:126-135.

[107] Guedes de Carvalho JR, King DF, and Harrison D. Fluidization of fine particles under pressure. Fluidization. 1978:59.

[108] Barreto GF, Yates JG, and Rowe PN. The effect of pressure on the flow of gas in fluidized beds of fine particles. Chemical engineering science. 1983;38(12):1935-45.

[109] Cui H, Chaouki J. Interparticle forces in high temperature fluidization of geldart a particles. China Particuology. 2004 Jun 1;2(3):113-8.

[110] Molerus O. Interpretation of Geldart's type A, B, C and D powders by taking into account interparticle cohesion forces. Powder Technol. 1982;33(1):81–87.

[111] Girimonte R, Formisani B. The effects of thermally induced interparticle forces on the expansion and bubbling behaviour of a fluidized bed.

[112] Shabanian J, Chaouki J. Local characterization of a gas–solid fluidized bed in the presence of thermally induced interparticle forces. Chemical Engineering Science. 2014 Nov 8;119:261-73.

[113] Shabanian J, Chaouki J. Hydrodynamics of a gas–solid fluidized bed with thermally induced interparticle forces. Chemical Engineering Journal. 2015 Jan 1;259:135-52.

[114] 53. Grace JR, Sun G. Influence of particle-size distribution on the performance of fluidized-bed reactors. Can J Chem Eng. 1991;69(5): 1126–1134

[115] Pell M, Jordan SP. Effects of fines and velocity on fluid bed reactor performance. AIChE Symp Ser. 1988;84(262):68–73.

[116] Yates JG, Newton D. Fine particle effects in a fluidized-bed reactor. Chem Eng Sci. 1986;41(4):801–806

[117] Abrahamsen AR and Geldart D. Behaviour of gas-fluidized beds of fine powders part I. Homogeneous expansion. Powder technology. 1980;26(1):35-46.

[118] Seville JP, Clift R. The effect of thin liquid layers on fluidisation characteristics. Powder Technology. 1984;37(117-129).

[119] Bilbao J, Olazar M, Romero A, Arandes JM. Design and operation of a jet spouted bed reactor with continuous catalyst feed in the benzyl alcohol polymerization.

Industrial & engineering chemistry research. 1987 Jul;26(7):1297-304.

[120] Gil J, Aznar MP, Caballero MA, Francés E, Corella J. Biomass gasification in fluidized bed at pilot scale with steam− oxygen mixtures. Product distribution for very different operating conditions. Energy & Fuels. 1997 Nov 19;11(6):1109-18.

[121] Rhodes MJ, Zhou S, Hirama T, Cheng H. Effects of operating conditions on longitudinal solids mixing in a circulating fluidized bed riser. AIChE journal. 1991 Oct;37(10):1450-8.

[122] Lockett M J, Davidson J F, Harrison D. On the two-phase theory of fluidization. Chemical Engineering Science. 1967; 22(8): 1059-1066.

[123] Pyle D L, Harrison D. An experimental investigation of the two-phase theory of fluidization. Chemical Engineering Science. 1967; 22(9): 1199-1207.

[124] Dry R J, Judd M R, Shingles T. Two-phase theory and fine powders. Powder Technology. 1983; 34(2): 213-223.

[125] Rietema K. Application of mechanical stress theory to fluidization[C]//Proc. Int. Symp. on Fluidization. 1967: 154-163.

[126] Barreto G F, Yates J G, Rowe P N. The measurement of emulsion phase voidage in gas fluidized beds of fine powders. Chemical Engineering Science, 1983, 38(3): 345-350.

[127] Barreto G F, Mazza G D, Yates J G. The significance of bed collapse experiments in the characterization of fluidized beds of fine powders. Chemical engineering science, 1988, 43(11): 3037-3047.

[128] Abrahamsen A R, Geldart D. Behaviour of gas-fluidized beds of fine powders part II. Voidage of the dense phase in bubbling beds. Powder Technology, 1980, 26(1): 47-55.

[129] Lorences MJ, Patience GS, Díez FV, Coca J. Fines effects on collapsing fluidized beds. Powder technology. 2003 Apr 23;131(2-3):234-40.

[130] Bruni G, Lettieri P, Newton D, Yates J. The influence of fines size distribution on the behaviour of gas fluidized beds at high temperature. Powder technology. 2006 Apr 25;163(1-2):88-97.

[131] Oke O, Lettieri P, Salatino P, Solimene R, Mazzei L. Numerical simulations of lateral solid mixing in gas-fluidized beds. Chemical Engineering Science. 2014 Dec

16;120:117-29.

[132] Shen L, Zhang M, Xu Y. Solids mixing in fluidized beds. Powder technology. 1995 Sep 1;84(3):207-12.

[133] Kunii D, Levenspiel O. Bubbling bed model. Model for flow of gas through a fluidized bed. Industrial & Engineering Chemistry Fundamentals. 1968 Aug;7(3):446-52.

[134] Yates JG, Rowe PN, Cheesman DJ. Gas entry effects in fluidized bed reactors. AIChE journal. 1984 Nov;30(6):890-4.

[135] Yasui G, Johanson LN. Characteristics of gas pockets in fluidized beds. AIChE Journal. 1958 Dec;4(4):445-52.

[136] Kai T, Furusaki S. Behavior of fluidized beds of small particles at elevated temperatures. Journal of chemical engineering of Japan. 1985 Apr 20;18(2):113-8.

[137] Horio M, Nonaka A. A generalized bubble diameter correlation for gas-solid fluidized beds. AIChE journal. 1987 Nov;33(11):1865-72.

[138] Darton, R. C, Lanauze R. D, Davidson J. F, Harrison D. Bubble growth due to coalescence in fluidized bed. Trans. Inst. Chem. Eng. 1977, 55: 274-280.

[139] Rowe PN, Yacono CX. The bubbling behaviour of fine powders when fluidised. Chemical Engineering Science. 1976 Jan 1;31(12):1179-92.

[140] Werther J. The influence of the bed diameter on the hydrodynamics of gas fluidized beds. AIChE Meeting, Detroit, MI, 1973.

[141] Werther J. Bubble growth in large diameter fluidized beds. In Fluidization Technology; Keairns, D. L., Ed.; Hemisphere: Washington, 1976:215-235.

[142] Werther J. Hydrodynamics and mass transfer between the bubble and emulsion phases in fluidized beds for sand and cracking catalyst. In Fluidization IV; Kunii, D., Toei, R., Eds.; Engineering Foundation: New York, 1984: pp 93-101.

[143] Hilligardt K, Werther J. Local bubble gas hold-up and expansion of gas/solid fluidized beds. German chemical engineering. 1986 Aug 1;9(4):215-21.

[144] Karimipour S, Pugsley T. A critical evaluation of literature correlations for predicting bubble size and velocity in gas–solid fluidized beds. Powder Technology. 2011 Jan 10;205(1-3):1-4.

[145] Kobayashi N, Yamazaki R, Mori S. A study on the behavior of bubbles and solids in

bubbling fluidized beds. Powder Technology. 2000 Dec 6;113(3):327-44.

[146] Dry RJ, Judd MR, Shingles T. Bubble velocities in fluidized beds of fine, dense powders. Powder technology. 1984 Aug 1;39(1):69-75.

[147] Cai P, Schiavetti M, De Michele G, Grazzini GC, Miccio M. Quantitative estimation of bubble size in PFBC. Powder technology. 1994 Aug 1;80(2):99-109.

[148] Cranfield RR, Geldart D. Large particle fluidisation. Chemical Engineering Science. 1974 Apr 1;29(4):935-47.

[149] Davidson J F, Harrison D. Fluidized Particles. Cambridge University Press, Cambridge, New York, 1963.

[150] Yasui G, Johanson LN. Characteristics of gas pockets in fluidized beds. AIChE Journal. 1958 Dec;4(4):445-52.

[151] Ma J, Liu D, Chen X. Bubble behaviors of large cohesive particles in a 2D fluidized bed. Industrial & Engineering Chemistry Research. 2016 Jan 27;55(3):624-34.

[152] Zou Z, Li HZ, Zhu QS. The bubbling behavior of cohesive particles in the 2D fluidized beds. Powder technology. 2011 Sep 15;212(1):258-66.

[153] Johnstone RD and Toomey HF. Gas fluidization of solid particles. Chem. Eng. Prog. 1952, 48: 220.

[154] D.J. Nicklin, Two-phase bubble flow, Chem. Eng. Sci. 17 (1962) 693–702.

[155] J.C.R. Turner, On bubble flow in liquids and fluidized beds, Chem. Eng. Sci. 21 (1966) 971–974.

[156] J.F. Davidson, D. Harrison, The behavior of a continuously bubbling fluidized bed, Chem. Eng. Sci. 21 (1966) 731–738.

[157] J. Grace, R. Clift, On the two-phase theory of fluidization, Chem. Eng. Sci. 29 (1974) 327–334.

[158] D. Geldart, Expansion of gas fluidized beds, Ind. Eng. Chem. Res. 43 (2004) 5802–5809.

[159] Clift R and Grace JR. Continuous bubbling and slugging. In Fluidization. 1985:73-132.

[160] Werther J. Scale-up of fluidized bed reactors. Ger. Chem. Eng. 1978, 1:243.

[161] Rowe P N, Santoro L, and Yates J G. The division of gas between bubble and interstitial phases in fluidised beds of fine powders. Chemical Engineering Science,

1978, 33(1): 133-140.

[162] Baumgarten P K and Pigford R L. Density fluctuations in fluidized beds. AIChE Journal, 1960, 6(1): 115-123.

[163] Baeyens J, Geldart D, and Wu S Y. Elutriation of fines from gas fluidized beds of Geldart A-type powders—effect of adding superfines. Powder technology, 1992, 71(1): 71-80.

[164] Sun G and Grace J R. The effect of particle size distribution on the performance of a catalytic fluidized bed reactor. Chemical Engineering Science, 1990, 45(8): 2187-2194.

[165] Lanneau K P. Gas-solids contacting in fluidized beds. Trans. Inst. Chem. Eng, 1960, 38: 125-137.

[166] Yates Y G, Cheesman D J, and Sergeev Y A. Experimental observations of voidage distribution around bubbles in a fluidized bed. Chemical engineering science, 1994, 49(12): 1885-1895.

[167] Lu T, Cheng D, Wang Y, Peng C, and Li H. Characteristics of Fine-Powder Fluidized Bed. In Fluidization: Science and Technology: Conference Papers, China-Japan Symposium, Science Press, Beijing. 1982: 57.

[168] Cherntongchai P and Brandani S. A model for the interpretation of the bed collapse experiment. Powder technology, 2005, 151(1-3): 37-43.

Chapter 3

3   Group C⁺ Particles: Enhanced Flow and Fluidization of Fine Powders with Nano-Modulation

(*A version of this chapter has been published in **Chemical Engineering Science***)

*Zhou Y, Zhu J. Group C⁺ particles: Enhanced flow and fluidization of fine powders with nano-modulation. **Chemical Engineering Science**. 2019; 207:653-62.*

The main challenge in the flow and fluidization of Geldart Group C particles is their cohesive nature due to strong interparticle forces. The "nanoparticle modulation" technique is adopted to reduce the interparticle forces of Group C particles and thus significantly improve their flow and fluidization quality. Group C⁺ particles, a new type of fine particles with drastically reduced or insignificant interparticle forces, are created using the nano-modulation technique. Fundamental studies provided a comprehensive understanding of the flow and fluidization quality of Group C⁺ particles. Nano-modulation led to major enhancements to both the static and dynamic flowability of Group C⁺ particles. Moreover, Group C⁺ particles exhibited revolutionary advancements in fluidization, which enabled its pseudo-particulate fluidization over a wide range of operating gas velocities, up to 200%-300% times that of bed expansion. The high bed expansion allows more gas to be retained in the bed and provides large volumes for gas-solid interfacial contact, thus promoting chemical reactions, especially gas phase catalytic reactions.

3.1   Introduction

The flowability and fluidizability are important characteristics of powders which are directly related to the handling and processing of particles in many processes. The flow of powders dictates the quality of the products and also affects the efficiency during manufacturing. In addition, fluidization is the most important technique for handling particles in industry because of its high gas-solid contact efficiency, high mass/heat transfer rates and the ability to handle a large amount of particles continuously. In 1973, Geldart [1] classified particles into four groups according to their flow and fluidization behaviors, as shown in Figure 3.1. Group A particles are usually 40-100 µm in diameter with particle densities of 1000-3000 kg/m^3, and exhibit smooth flow and fluidization. Group B and

Group D are much larger and denser particles, while having good flowability. Their fluidization is less ideal and usually accompanied by larger and more dynamic bubbles. Group C particles (often referred as fine or ultrafine particles), less than 30-40 µm in diameter with particle density of 1000-3000 kg/m^3, are cohesive and hard to flow and fluidize. This poor flowability and fluidization quality is ascribed to their cohesiveness arising from the strong interparticle forces [2-4]. That said, Group C particles are being increasingly used over the other particles by a variety of processes in the industry due to their small particle size and extremely high surface area [5]. The small particle size is favorable in many applications such as pharmaceutical applications [6-7], powder coating [8] and the food industry [9-10]. The high specific surface area of Group C particles attracts more attention in some physical and chemical processes, including surface modification [11-13], catalytic reactions [14-15] and catalyst synthesis [16-17]. The biggest challenge of applying Group C particles is the poor flowability and poor fluidization caused by its cohesive nature, which limits their areas of application. If its strong cohesiveness could be overcome, Group C particles should exhibit better flow and fluidization than Group A, B and D particles. In conclusion Group C particles could be successfully applied in industry processes.
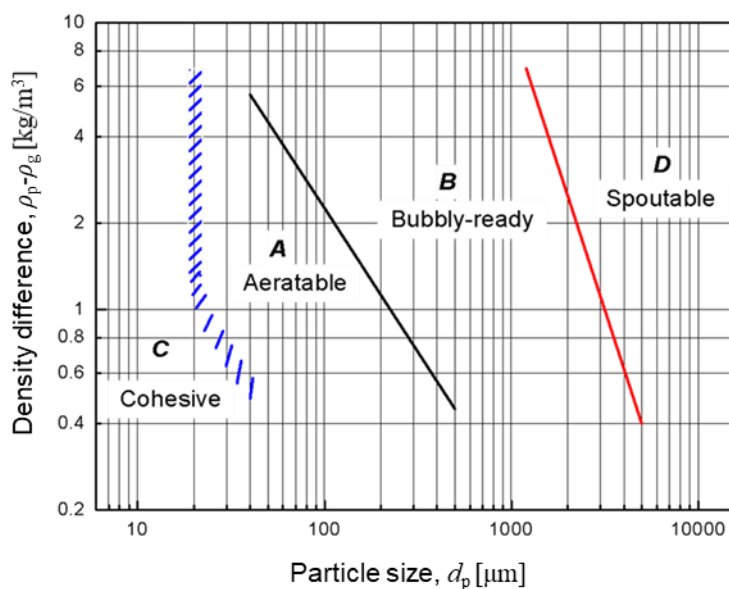
Figure 3.1: Geldart powder classification [8]

To further understand the increasing importance of Group C particles in modern industries, many methods have been investigated to improve their flow and fluidization. These methods, often called fluidization aids, may be divided into two groups in terms of the different mechanisms. One is by introducing external energies to disturb channeling and to break agglomerates, including mechanical vibration [18-19], acoustic vibration [20-21], mechanical stirring [22] and the addition of magnetic or electrical fields [23-24]. However, these methods are scale-dependent and thus have limited success. The other one is by modifying particle surface to reduce the interparticle forces intrinsically, such as gas adsorption [25-26] and adding coarser or finer particles [27-29]. These methods are scale-independent and are relatively easy to implement.

The addition of some finer particles has been found to reduce the cohesiveness and agglomeration of fine particles and turn cohesive particles into free-flowing powder [8,30-31]. In most systems with dry particles, the van der Waals force is dominant among the three major interparticle forces [27]. Xu et al. [32] found nanoparticles clinging to Group C particles as asperities and an asperities-contact model was proposed to estimate the reduction of interparticle forces. It was concluded that nanoparticles increased separation distance and decreased van der Waals between Group C particles, thus reducing the cohesiveness and improving the flowability. In addition, many other researchers [33-35] found that nanoparticles could turn Group C particles from non-flowable to free-flowing and from non-fluidizable to fluidizable. However, no researchers have studied the fluidization quality and the fluidization behaviors of Group C particles with nanoparticles so far.

Generally, a good fluidized bed is characterized by uniformly suspended particles and fewer fluctuation with small bubbles. In addition, a good fluidized bed reactor is characterized by more gas entering into the dense phase and fewer gas entering into the bubble phase. One of the most important characteristics that describes the fluidization quality is the bed expansion. High bed expansion generally indicates better fluidization with more gas contained in the bed, resulting in better gas-solid contact [36]. For fine particles, the strong interparticle forces mainly result in agglomeration and channeling during fluidization with almost little bed expansion [37]. Although the study by Xu [38]

appeared to point to high bed voidages for these Group C particles after surface coating by nanoparticles, they focused more on the minimum fluidization velocity. Not enough attention was paid for further study of the bed voidage. Similarly, most people focus more on the mobility or flowability of fine particles with the addition of nanoparticles, but do not pay much attention towards fluidization behaviors, and presume that nanoparticles just make Group C particles become Group A particles. However, our experiments showed that it is quite different between Group A particles and Group C particles with the addition of nanoparticles.

This present work looks to systematically study the flowability and fluidizability of "Group C^+" particles, which are essentially Group C particles after nanoparticle modulation, and to investigate the effects of nanoparticle concentration. Given the smooth flowability and fluidization process of Group A particles, a comparative study on the flow and fluidization behaviors of Group C^+ particles with Group A particles is conducted to find out the similarities and differences.

3.2 Experimental methodology

3.2.1 Particulate materials

The particles used in this work were glass beads (GB) and polyurethane particles (PU) with their properties listed in Table 3.1. The nanoparticles used in this experiment were SiO_2 particles with a reported size of 16 nm and a material density of 2200 kg/m^3, marketed as R972 by Evonik.

Table 3.1: Physical properties of experimental particles

Powder Name	Particle Size (µm)			Shape	Particle Density (kg/m^3)	Bulk Density (kg/m^3)	Geldart Classification
	D_{10}	D_{50}	D_{90}				
GB10	1.6	10	29	Spherical	2,500	916	C
GB39	15	39	85	Spherical	2,500	1,275	A
GB65	30	65	139	Spherical	2,500	1,254	A
PU10	2	10	30	Irregular	1,200	560	C
PU18	4	18	50	Irregular	1,200	648	C
PU36	12	36	74	Irregular	1,200	679	C
PU105	45	105	200	Irregular	1,200	720	A

3.2.2   Nanoparticle modulation

Group C particles were mixed with nanoparticles using the ultrasonic vibrating method, as detailed in the patent of Jingxu Zhu and Hui Zhang [39], where the technique was first proposed as nanoparticle modulation (nano-modulation). This is an economic method to improve the flow and fluidization of Group C particles, as the nanoparticles are cheap (around \$10/kg) and this technique is scale-independent. Group C^+ particles are nano-modulated Group C particles. SEM (S-2600N Scanning Electron Microscope, Hitachi Ltd., JP) was applied to study the surface morphology of Group C particles before and after nanoparticle modulation. In this test, five nanoparticle concentrations were used, namely 0.27%, 0.44%, 0.82%, 0.9% and 1.7% (volume fraction). Figure 3.2 shows the SEM images of Group C particles (both GB10 and PU10) before and after nanoparticle modulation. In Figure 3.2(a), GB10 virgin particles were round and possessed almost perfectly smooth surfaces. After being modulated by a small amount of nanoparticles, the surfaces of GB10+0.82% became rougher and the SiO_2 nanoparticles clung onto the GB10 particle surfaces as asperities (as shown in Figure 3.2(b)). For PU10 particles that were irregular, the surfaces were also rougher after nanoparticle modulation (as shown in Figure 3.2(c) and Figure 3.2(d)).

Figure 3.3 shows SEM images of Group C^+ particles after fluidization during the next two days. Both $GB10^+$ and $PU10^+$ particles were still clearly covered by nanoparticles, reinforcing the observation before that nanoparticles were not easily worn off during the fluidization [8].

WD 6.4 mm 5.00kv x3.0k   10µm
(a) GB10 virgin

WD 6.4 mm 5.00kv x3.0k   10µm
(b) GB10+0.82%

WD 6.4 mm 5.00kv x3.0k   10µm
(c) PU10 virgin

WD 6.4 mm 5.00kv x3.0k   10µm
(d) PU10+0.82%
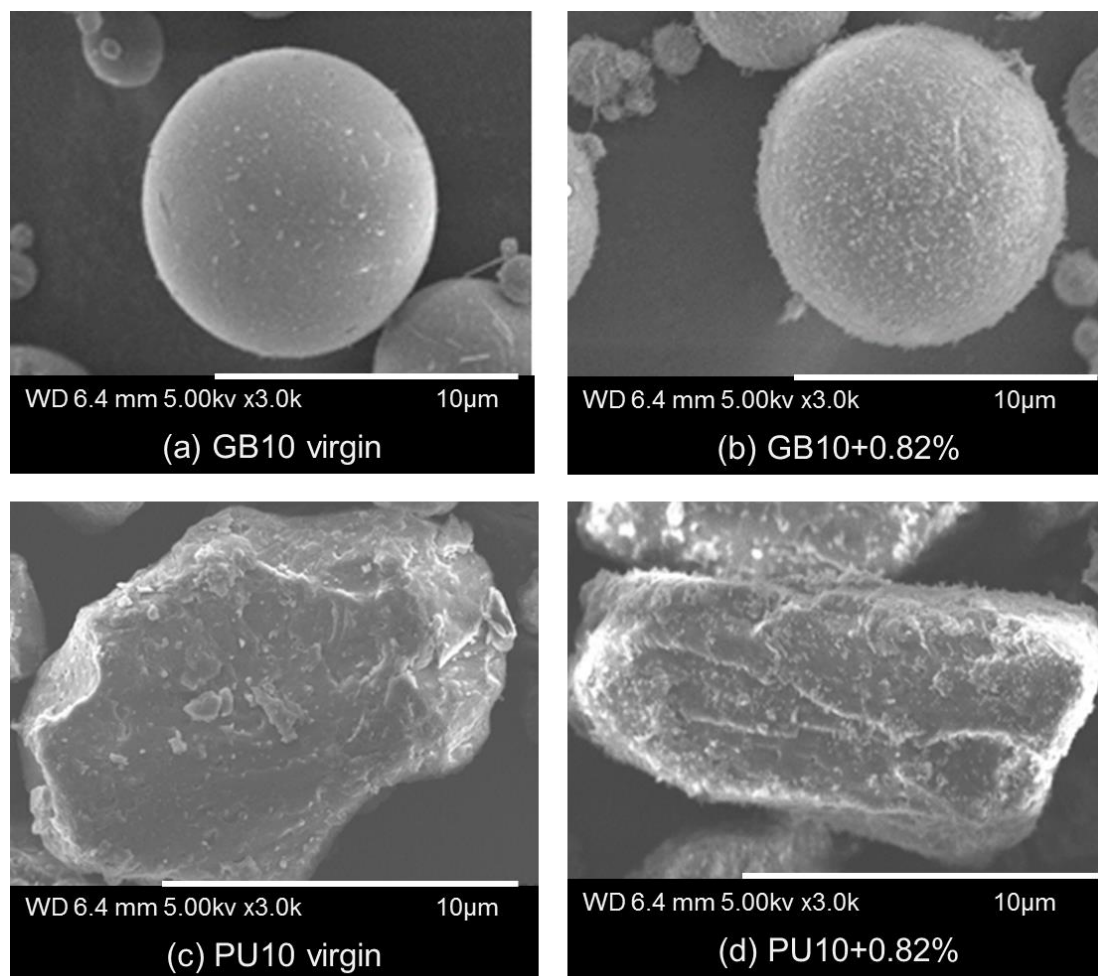
Figure 3.2: SEM images of Group C particles before and after nanoparticle modulation

WD 6.4 mm 5.00kv x3.0k   10μm   WD 6.4 mm 5.00kv x3.0k   10μm
(a) GB10+0.82%   (b) PU10+0.82%
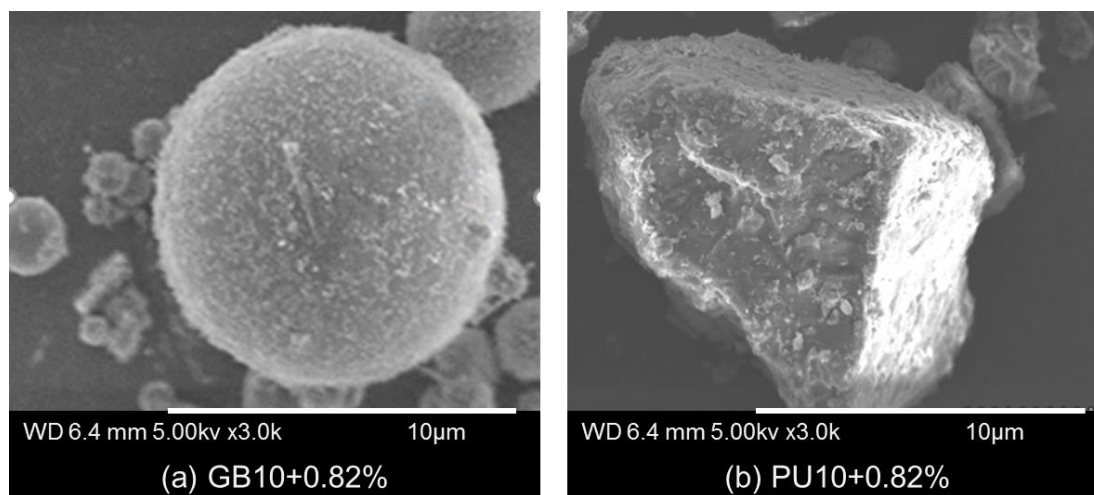
Figure 3.3: SEM images of Group C$^+$ particles after fluidization

3.2.3   Flowability tests

Particle flowability was characterized by both static and dynamic methods such as the cohesion test (FT4), angle of repose (AOR) and avalanche angle (AVA). Powder cohesion was tested by an FT4 Powder Rheometer manufactured by Freeman Technology, evaluating the static flowability of particles. A powder sample was first conditioned and pre-sheared to reach a homogenized state and then was compressed under a specified normal stress of 9 kPa. Afterwards, the powder sample was sheared under normal stresses of 7, 6, 5, 4 and 3 kPa respectively to obtain shear stresses and the yield locus was achieved to obtain the cohesion, as detailed in [40-42].

Ange of repose (AOR), the largest angle at which powders can pile up, is considered as the powder flowability under a semi-static state. It was measured using a PT-N Hosokawa Powder Characteristic Tester, following a standard test [43]. A powder sample was first loaded onto a screen with a vibrator and then the powder sample fell through the funnel to a plate at a low and constant rate by adjusting the vibration intensity. Then, the powder sample would cover the plate and pile up. The angle of repose was measured when no more powder could be accumulated on the tip of the powder heap. In general, a smaller value of AOR indicates better powder flowability, as listed in Table 3.2.

Table 3.2: Classification of powder flowability by AOR [28]

Angle of repose (AOR)	Flowability
25°< θ <30°	Very free-flowing
30°< θ <38°	Free-flowing
38°< θ <45°	Fair to passable flow
45°< θ <55°	Cohesive
55°< θ <70°	Very cohesive

Avalanche angle (AVA) is referred to as powder flowability under a dynamic state, measured using a powder analyzer (Revolution Powder Analyzer, Mercury Scientific Inc., US). A powder sample was placed into a cylindrical drum which was rotated at 0.6 rpm. The powder would collapse or avalanche when the drum was rotated a certain angle. Avalanche angle (AVA) is the maximum angle where the avalanche occurs at a low rotating speed. More details are described in literatures [44-46]. For each sample, all these measurements were repeated for two to three times and the average value was used in this work.

3.2.4   Fluidized bed

As schematically shown in Figure 3.4, the fluidization column was made of Plexiglas with 5.08 cm in I.D. and 45.7 cm in height. The compressed air flowed through PVC tubes into the wind box at two opposite positions and passed through the distributor to fluidize the particles. The distributor was a plate with 66 holes of 3 mm in diameter with an opening area ratio of 23% at the top of the wind box. Two layers of 625 mesh screen were covered on the distributor. Two pressure taps at the bottom and at the top of the fluidization column were used to measure the pressure drop of the entire bed by a slant U-tube manometer with an angle of 30°. A measuring tape was fixed outside the column for measuring bed height. Bed expansion ratio (BER) is the ratio of the total fluidized bed height (H_t) at operating conditions to the initial fixed bed height (H_0), as given by the following Equation (3.1):

$$\text{BER} = H_t / H_0 \qquad (3.1)$$

The minimum fluidization was determined by the pressure drop profile, where the pressure drop across the bed increases with superficial gas velocity in a typical fixed bed and then levels off after complete fluidization. The operating gas velocity at the interception of the fixed bed and the fluidized bed is identified as the minimum fluidization velocity. In this

paper, normalized pressure drop ($P_n = \Delta P/(W/A)$) was used and defined as the ratio of measured pressure drop (ΔP) to the particle weight per cross-sectional area (W/A).
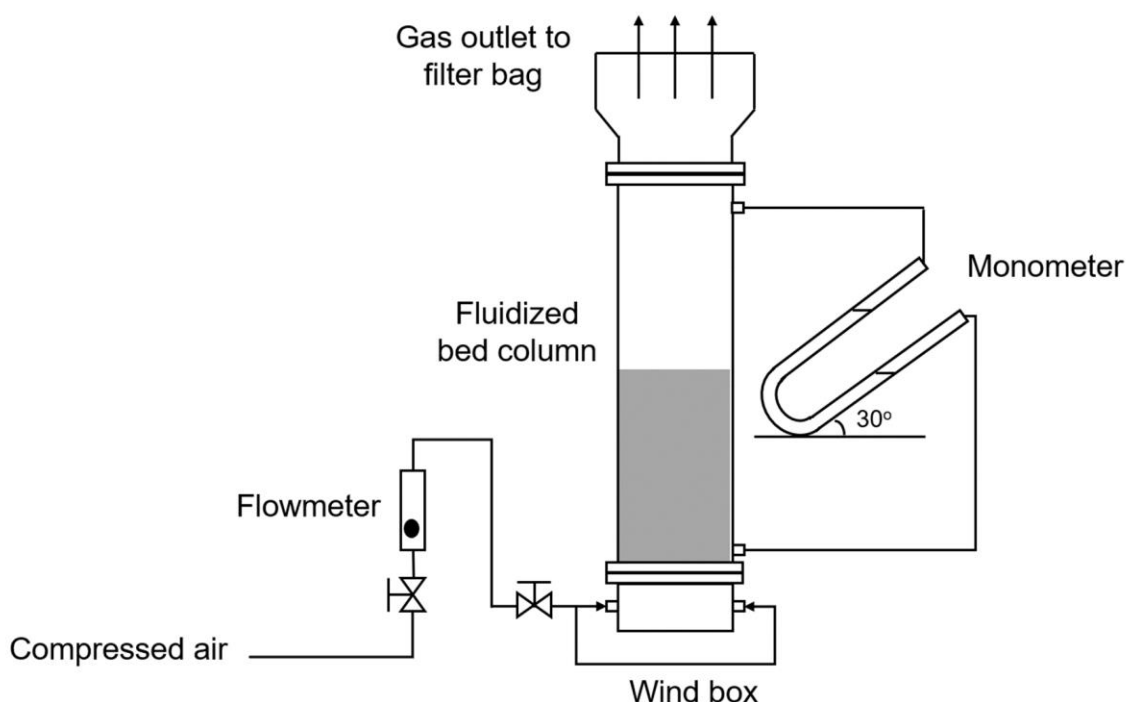
Figure 3.4: Schematic diagram of experiment setup

3.3 Results and discussion

3.3.1 Powder flowability

Powder flowability is an important index because it intrinsically affects powder behaviors in handling and processing operations in industry, such as storage, transportation, mixing and packaging [47]. Figure 3.5 shows the static (cohesion) and dynamic (AOR, AVA) powder flowability of different types of particles as a function of nanoparticle concentration. As shown in Figure 3.5(a), Group C virgin particles (GB10, PU10, 18 and 36) have strong cohesion before nanoparticle modulation, leading to poor flowability. The nanoparticle modulation could significantly reduce the cohesion of Group C particles, indicating better flowability. As the nanoparticle concentration increases, the cohesions of Group C^+ particles initially show a significant decrease and then level off or slightly

increase. As shown in Figures 3.5(b) and (c), both AOR and AVA of these Group C and Group C$^+$ particles show a similar trend in the cohesion.

Group A particles (GB39 and PU105) have much lower cohesion, smaller AOR and smaller AVA than both Group C and Group C$^+$ particles. Particularly, PU36 shows poor flowability before nanoparticle modulation, like typical Group C particles, but its cohesion, AOR and AVA are close to those of Group A particles, signifying similarly good flowability as Group A particles. In summary, Group C particles are cohesive with poor flowability, after nanoparticle modulation, Group C$^+$ particles are free-flowing and show relatively good flowability, although it is till poorer than that of Group A particles. PU36 exhibits the flow characteristics of both Group C and Group A particles, which is expected to be Group C/A particles. Moreover, the nanoparticle concentration is at an optimum value of around 0.5%-1%, consistent with previous studies by Q. Huang [48] and C.B, Xu [32].

The improvement of nanoparticles on powder flowability of Group C particles is due to the reduction of the cohesion ascribed from the interparticle forces. Nanoparticle concentration would affect the surface coverage of Group C particles and have an optimum value, at which the surface coverage may be sufficient to prevent direct contact between the two cohesive particles. As a consequence, the cohesion abruptly decreased. After that, the cohesion would become constant or even slightly increase as the surface coverage continually increases.

In another aspect, the cohesion of Group C$^+$ particles may be related to surface roughness. GB10 has higher cohesion, larger AOR and AVA than PU10 due to its surface configuration, which is spherical and much smoother than that of PU10, resulting in stronger cohesiveness and thus poorer flowability. The nanoparticles on the Group C$^+$ particles also increase the surface roughness, thus reducing the cohesion. After the optimum value, the increase of nanoparticle concentration may reduce the surface roughness to some extent, resulting in the increase of the cohesion and inducing the relatively poorer flowability.
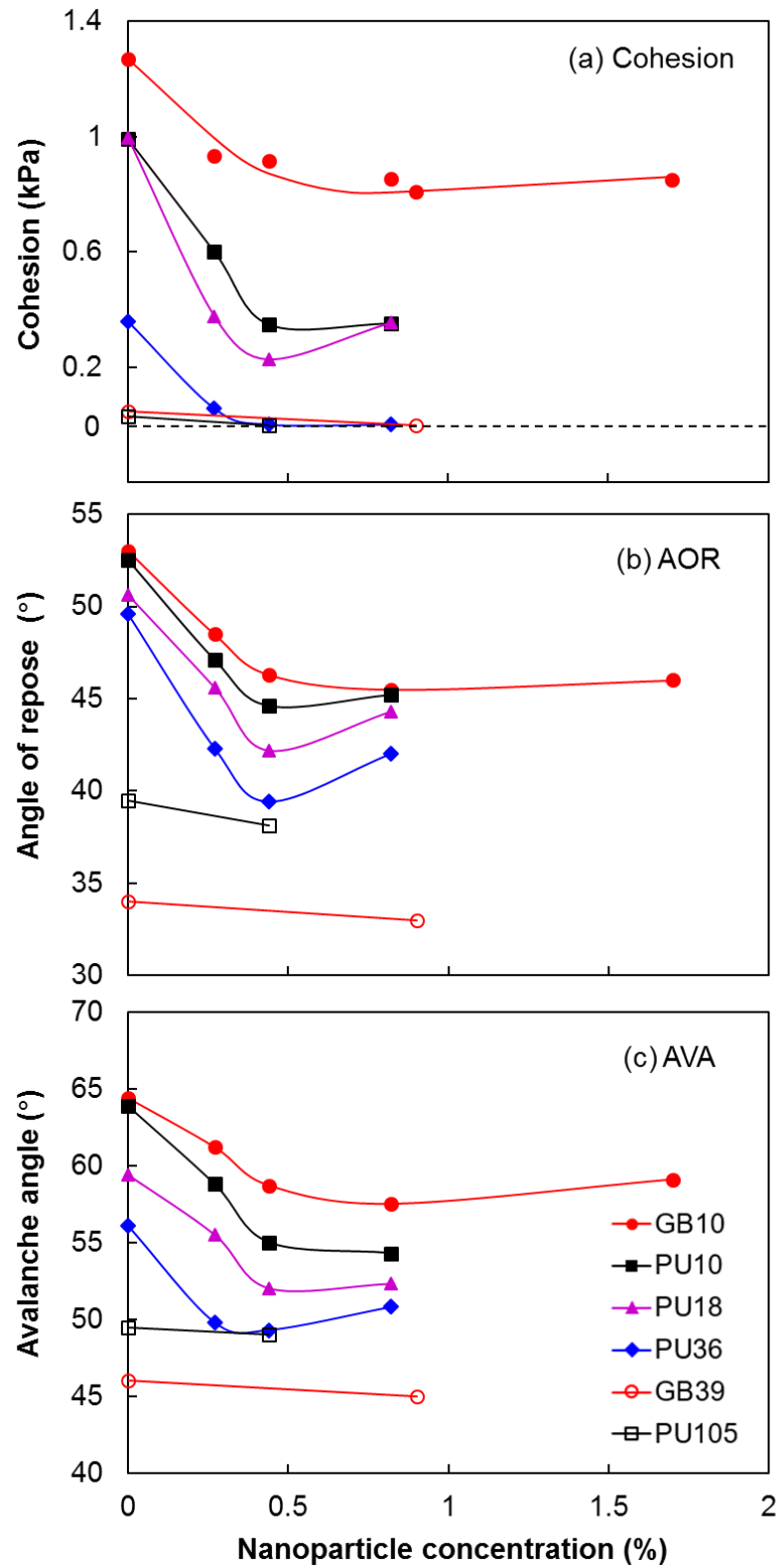
Figure 3.5: Flowability of Group C, Group C⁺ and Group A particles

3.3.2   Pressure drop

The pressure drop of the fluidized bed can be used to evaluate the fluidization quality. Generally, good fluidization is characterized by a normalized pressure drop of close to 1, signifying the whole bed is fully fluidized and all particles are suspended. Figure 3.6 shows the normalized pressure drop of Group A, Group C and Group C^+ particles. GB39 and GB65 belonging to Group A particles could fluidize well at low superficial gas velocities and achieve high normalized pressure drop of close to 1. For GB10 and PU10 belonging to Group C particles, their incipient fluidization could not be identified before nanoparticle modulation, and their normalized pressure drops are much lower due to significant channeling observed in the experiments. Gas went through the channels and most of the bed was de-fluidized, leading to the low pressure drop. After nanoparticle modulation, higher normalized pressure drops close to unity are quickly attained and incipient fluidization could be clearly identified, suggesting good fluidization of these Group C^+ particles.
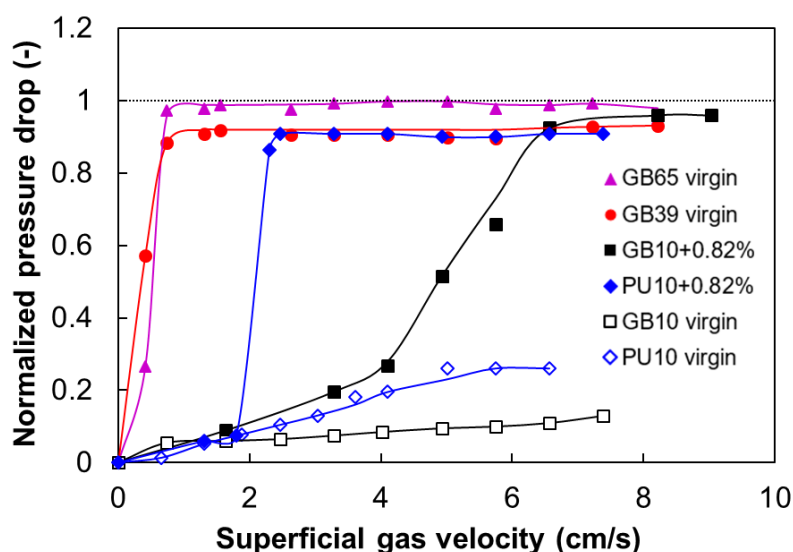
Figure 3.6: Pressure drop of Group A, Group C and Group C^+ particles

It is apparent that the normalized pressure drop will attain unity and remain in this state when all particles in the bed are fully fluidized. Figure 3.7 demonstrates the effect of nanoparticle concentrations on pressure drop of Group C^+ particles. After nanoparticle

modulation, these Group C^+ particles could be well fluidized with a normalized pressure drop of close to 1, similar to Group A particles. In addition, nanoparticle concentration has an influence on the pressure drop and incipient fluidization. This is because the nanoparticle concentration affects the cohesiveness of Group C^+ particles and further affects the fluidization behaviors.
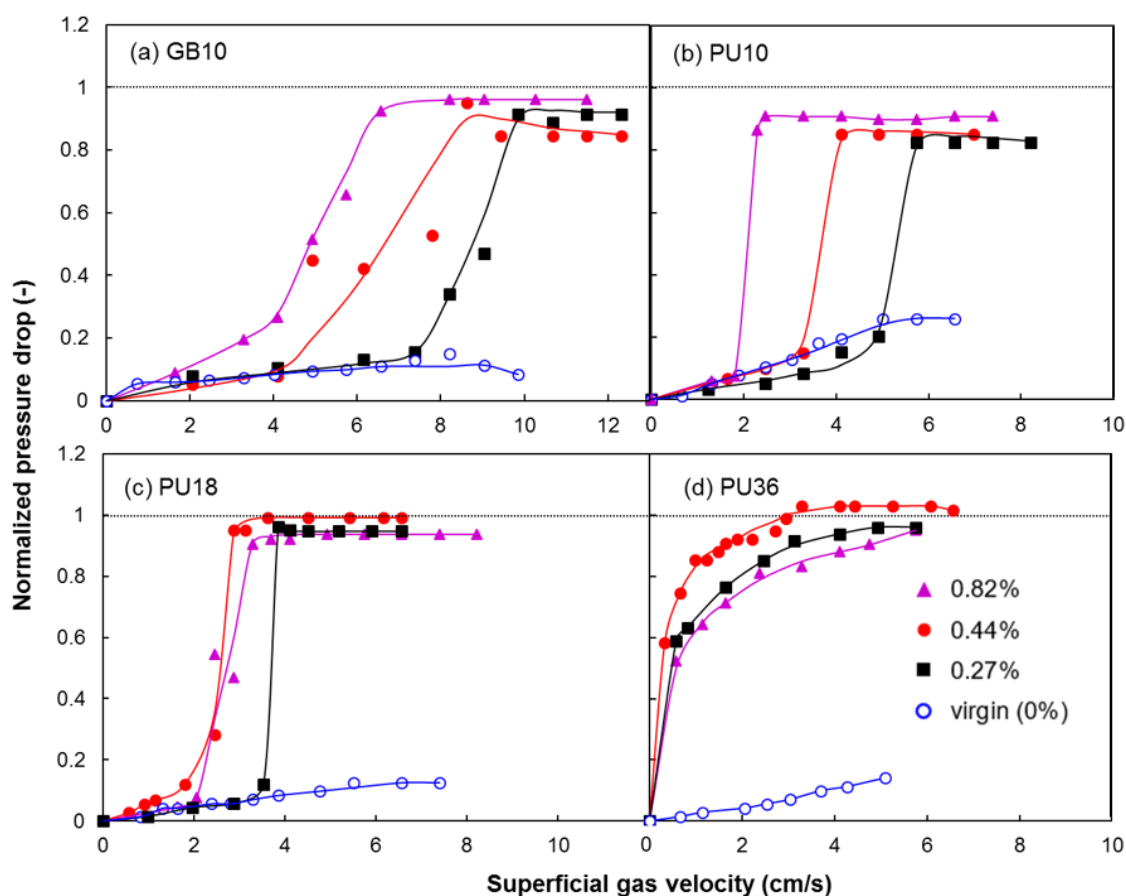
Figure 3.7: Effect of nanoparticle concentration on pressure drop of Group C^+ particles

3.3.3   Minimum fluidization velocity

Minimum fluidization velocity is an important parameter for describing the fluidizability of particles [32]. Figure 3.8 reveals the effect of nanoparticle modulation on the minimum fluidization velocities of various particles. It could be concluded that nanoparticle modulation could significantly reduce the minimum fluidization velocities of Group C^+

particles but not that of Group A particles. For example, as nanoparticle concentration increases, the minimum fluidization velocities of Group C$^+$ particles initially decrease and then show a slight increase as the nanoparticle concentration reaches a certain value of around 0.5%-1%. Nanoparticle concentration does not change the minimum fluidization velocities of Group A particles (GB39 and PU105). This phenomenon is in part because nanoparticles could reduce the cohesion of Group C particles which is negligible for Group A particles and does not play an important role in the fluidization of Group A particles.

As shown in Figure 3.7, the pressure drop of PU36 virgin particles is low and the minimum fluidization velocity could not be identified. However, after nanoparticle modulation, PU36$^+$ particles could quickly achieve a high normalized pressure drop of close to 1, indicating full fluidization. In Figure 3.8, the minimum fluidization velocities of these nano-modulated PU36 particles are almost as low as Group A particles, like GB39 and PU105, and are not affected by nanoparticle concentration. These phenomena suggest that PU36 particles may exhibit properties of both Group C and Group A particles. Intrinsically, PU36 particles are non-fluidizable, while nanoparticle modulation could help them fully fluidize with a low minimum fluidization velocity like Group A particles, signifying PU36 particles appear to be Group C/A particles.
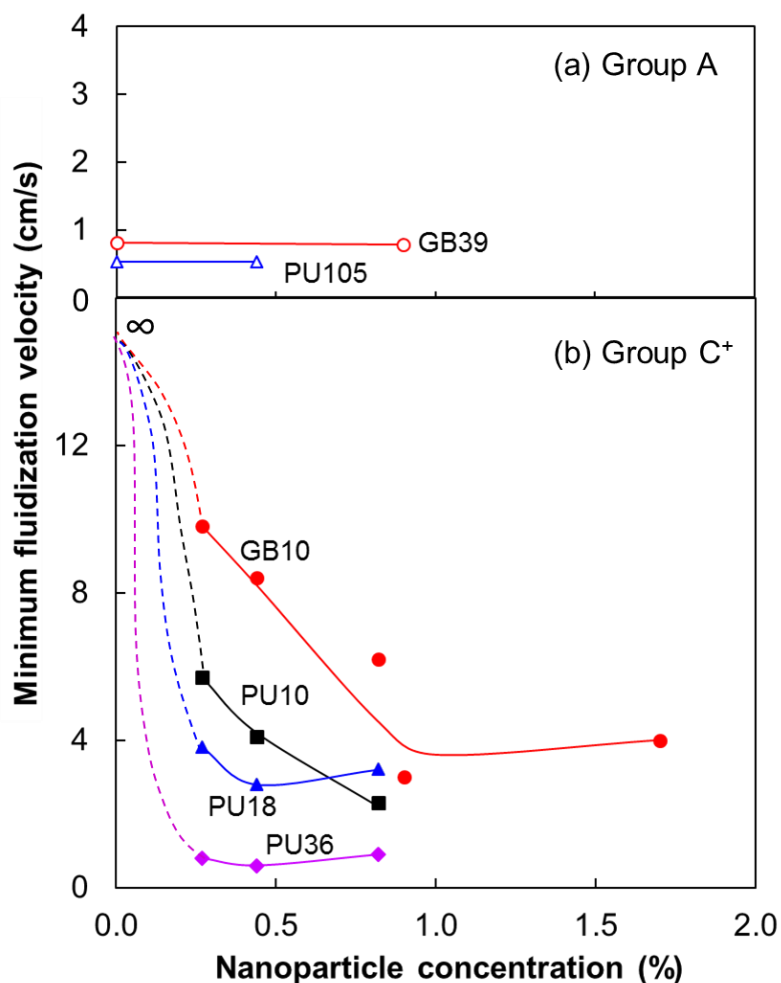
Figure 3.8: Effect of nanoparticle concentration on minimum fluidization velocity

It is evident that the minimum fluidization velocity for Group C^+ powder shows a similar trend as the cohesion in Figure 3.5 (a), indicating that fluidization behaviors are also related to powder cohesiveness. As cohesion decreases, it is expected that the minimum fluidization velocity also decreases due to the reduction in the interparticle forces. Figure 3.9 shows the relationship between the minimum fluidization velocity and the cohesion of Group C^+ particles (GB10, PU10 and PU18). For both glass beads (GB) and polyurethane particles (PU), the minimum fluidization velocity increases as the cohesion increases, demonstrating an exponential relationship. A high cohesion of the particles in the bed tends to make them agglomerate and thus increases the difficulty in incipient fluidization, since the fluidizing gas has difficulty breaking the agglomerates and is hard to uniformly suspend the particles.
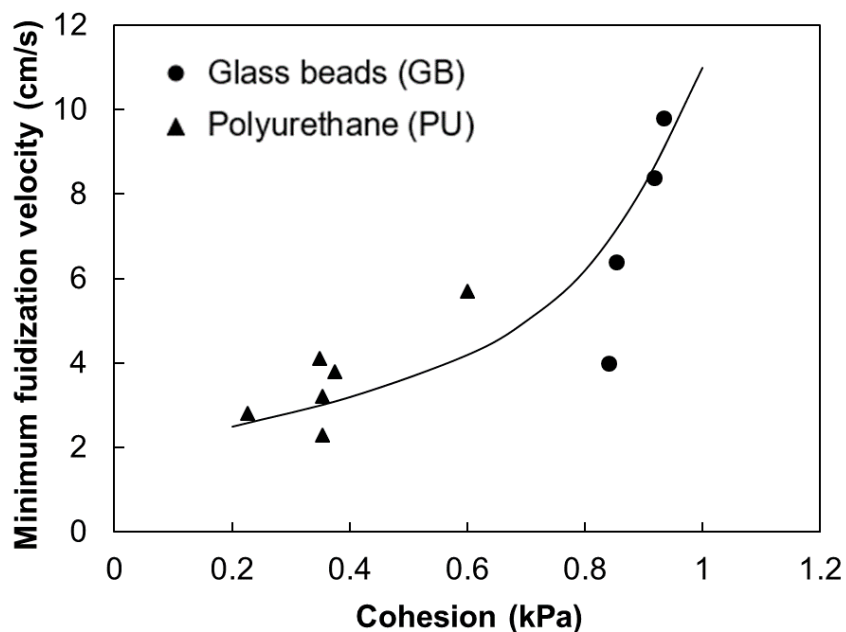
Figure 3.9: The relationship between the minimum fluidization velocity and cohesion for Group C⁺ particles

3.3.4　Bed expansion

The bed expansion ratio (BER), defined as the ratio of the fluidized bed height to the initially fixed bed height, is often employed to characterize fluidization quality. The bed expansion ratio of Group C and Group A particles before and after nanoparticle modulation are shown in Figure 3.10. The addition of nanoparticles does not exhibit an effect on the bed expansion of Group A particles. For Group C virgin particles, they present insignificant bed expansion due to de-fluidization. However, after surface modulation by nanoparticles, their beds significantly expand. For example, the bed expansion ratio of the nano-modulated GB10 and PU10 reaches as high as 2.3, which is around 180% of GB39 and PU105. Generally, a high bed expansion indicates higher gas holdup in the bed, and therefore allowing more gas to have chances make contact with particles. A large amount of gas inside the fluidized bed could provide significantly enhanced gas-solid contact. Conclusively, the Group C⁺ particles with much higher bed expansion could provide excellent gas-solid contact, which is an important characteristic for many chemical and physical processes in industry.
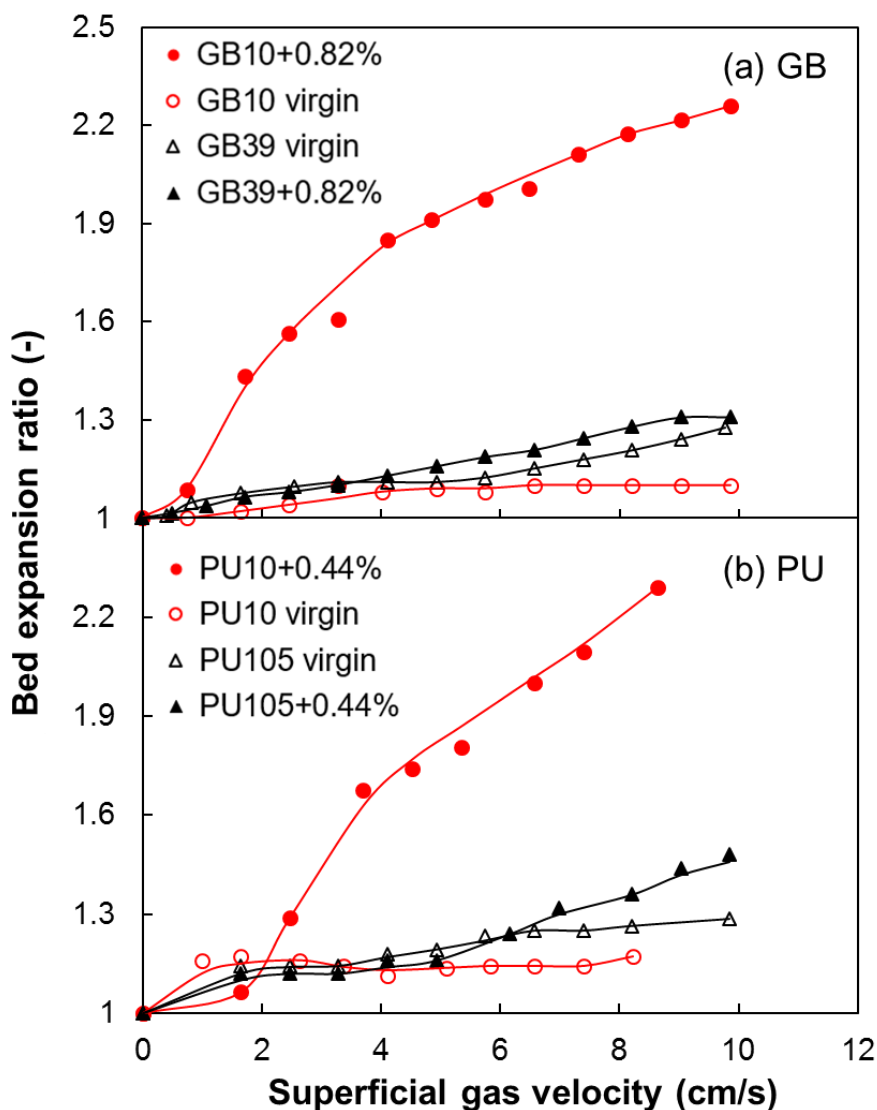
Figure 3.10: Effect of nanoparticles on bed expansion of Group C and Group A particles

Figure 3.11 illustrates the effect of nanoparticle concentration on bed expansion of Group C^+ particles. The fluidized bed of Group C^+ particles dramatically expands after nanoparticle modulation. Although the virgin Group C particles are non-fluidizable, their bed height shows a slight increase with the gas velocity. For the nano-modulated GB10 particles, the bed expansion starts later than that for Group A particles. Once the operating gas velocity reaches the minimum fluidization velocity, the bed quickly and significantly

expands. As the nanoparticle concentration increases, the bed expansion becomes higher. For nano-modulated PU10 and PU18 particles, the bed expansion ratio initially increases and then decreases with nanoparticle concentration increasing. The highest bed expansion ratio could be achieved when the nanoparticle concentration was 0.44%, consistent with the results shown in the literature [32], which reports the optimum value of nanoparticle concentration could be 0.5%-1%.

For PU36^{+} particles, they have low minimum fluidization velocities similar to Group A particles, therefore they are easy to fluidize. As a result the bed expansion starts earlier than other Group C[+] particles. In addition, the bed expansion ratio could reach 1.9, much higher than that of Group A particles which is only 1.2-1.4. It could be concluded that PU36 belongs to Group C/A powder. Both the minimum fluidization velocity and the bed expansion ratio can reflect the characteristics of Group C/A particles.
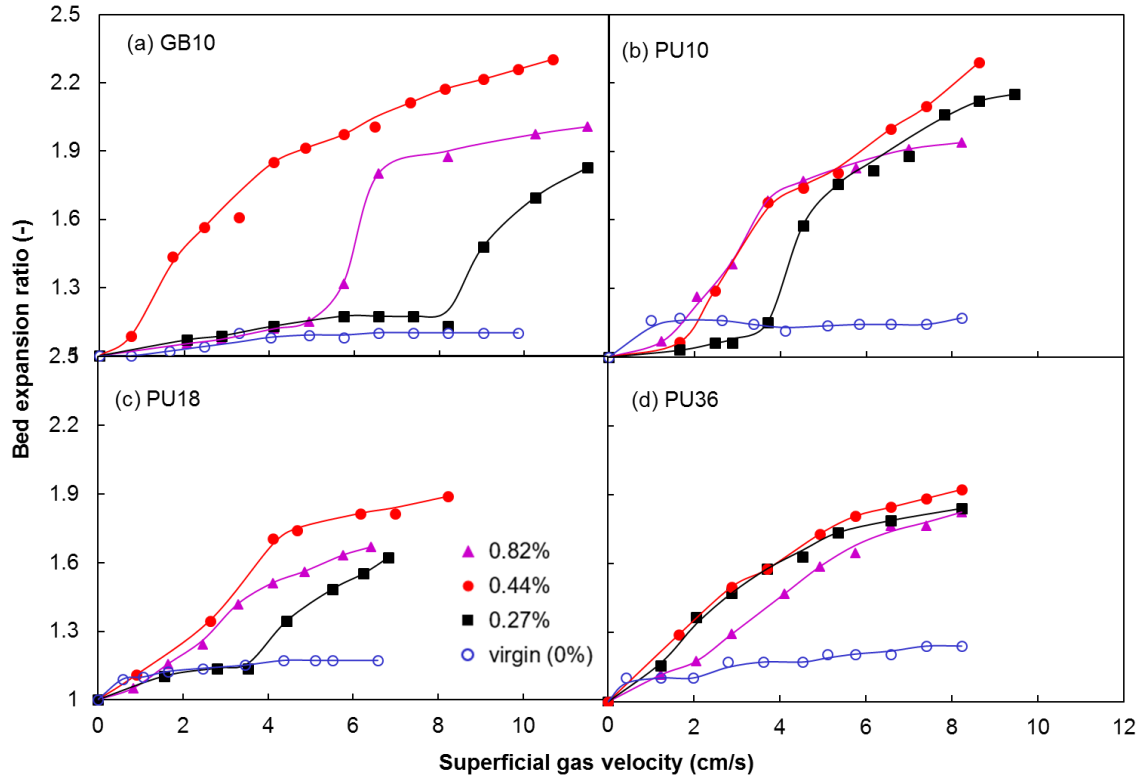
Figure 3.11: Effect of nanoparticle concentration on bed expansion of Group C⁺ particles

Figure 3.12 shows the bed voidage of Group C^+ and Group A particles. It could be found that the Group C^+ particles have much higher bed voidage than Group A particles. For example, the bed voidage of GB10+0.82% and PU10+0.44% particles after nanoparticle modulation could reach as high as 0.84 and 0.8, respectively, which are around 140% of Group A particles. Generally, a high bed voidage suggests that the fluidized bed contains more gas in it and contributes to better gas-solid contact. As a result, the fluidization of the Group C^+ particles could theoretically provide a much higher gas-solid contact efficiency than Group A particles.
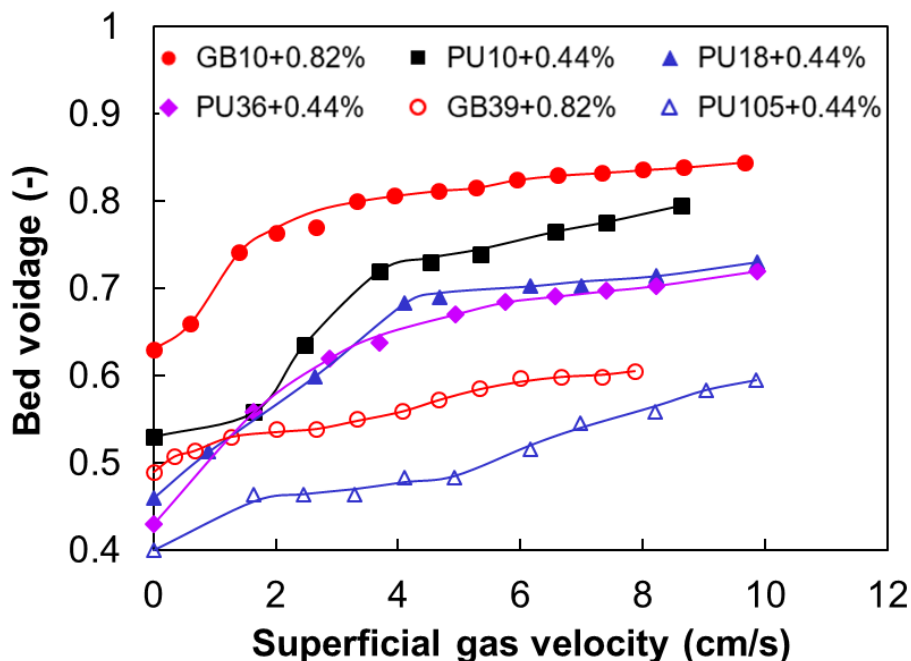
Figure 3.12: Bed voidage of Group C$^+$ And Group A$^+$ particles

3.4   General discussion

High bed expansion for Group C$^+$ particles

Group C particles with small particle size are not fluidizable because of the cohesion arising from the strong interparticle forces. However, the Group C$^+$ particles could be fluidized well and possess good fluidization quality with acceptable minimum fluidization velocity and high bed expansion over an extended range of gas velocities. As a result the small particle size of Group C$^+$ particles can provide a large specific surface area, the high bed expansion in the bed can retain more gas to contact with particles, thus significantly improving gas-solid interfacial contact which is greatly important and meaningful for chemical reactions, especially for gas-phase catalytic reactions.

The high bed expansion in the Group C$^+$ particle fluidization may be ascribed to two reasons: the small bubbles and the reduced but proper interparticle forces. The smaller particle size of Group C$^+$ particles gives rise to the reduction in the bubble diameter in the fluidized bed. Big bubbles have higher rising velocity which weaken the expansion of the

dense phase, while small bubbles with lower rising velocity have longer residence time in the bed, contributing to higher bed expansion when compared with Group A particles.

Another one is the proper interparticle forces. Although the interparticle forces between Group C^+ particles are significantly decreased by nanoparticle modulation, they are not negligible and are larger than that between Group A particles. The weakened but still existent interparticle forces could make more gas trapped in the interstices between particles, contributing to higher bed expansion. As described in many previous works [14,49-51], the addition of some fine particles (<45 microns) in Group A particle fluidization can increase the dense phase voidage and promote the capability of the fluidized bed to retain aeration gas, contributing to the stability of the bed. Supposedly, the addition of fine particles is a way to introduce the proper interparticle forces into the system, which could increase the bed voidage and improve the fluidization quality.

Optimum surface coverage for Group C^+ particles

Nanoparticle concentration clearly affects the flowability and fluidization of Group C^+ particles and has an optimum value around 0.5-1%. Intrinsically, the change in nanoparticle concentration influences the surface coverage of Group C^+ particles. It can be expected that there exists a certain value of the surface coverage that is enough to separate the fine particles and prevent the direct contact between the two fine particles, at this value the cohesion would be dramatically decreased, contributing to good flowability and fluidization quality. The surface coverage beyond this value would not result in further reduction of the cohesion. After that, the cohesion becomes constant or may even slightly increase.

Figure 3.13 shows the effect of the surface coverage for different Group C^+ particles on the cohesion and minimum fluidization velocity. To simplify the calculation, it assumes all these Group C^+ particles as spheres, nanoparticles as individual particles (Figure 3.13a) and as agglomerates (Figures 3.13b and 3.13c) on the fine particle surface. The agglomerate size is 5 times that of the individual nanoparticle size. Clearly, there is an optimum surface coverage at which the Group C^+ particles possess the smallest cohesion and the lowest minimum fluidization velocity. If considering nanoparticles as individual

ones, the optimum surface coverage is around 50%-70%, and if considering those as agglomerates, the optimum value is around 10%-20%.

Figure 3.14 shows the experimental results conducted by previous workers in our research group, Huang Qing [48] and Chunbao Xu [32]. It is evident that the smallest cohesion could be achieved at a surface coverage of 10%-20% (nanoparticles as agglomerates), and the lowest minimum fluidization velocity could be obtained at a surface coverage of 8%-12% (nanoparticles as agglomerates), consistent with our results in some degree. Figure 3.15 summarizes the optimum surface coverage for all systems conducted by us and other workers [32,48]. For most experiments, the results are close and consistent. The optimum surface coverage for Group C^+ particles should be 10%-20% (nanoparticle as agglomerates).
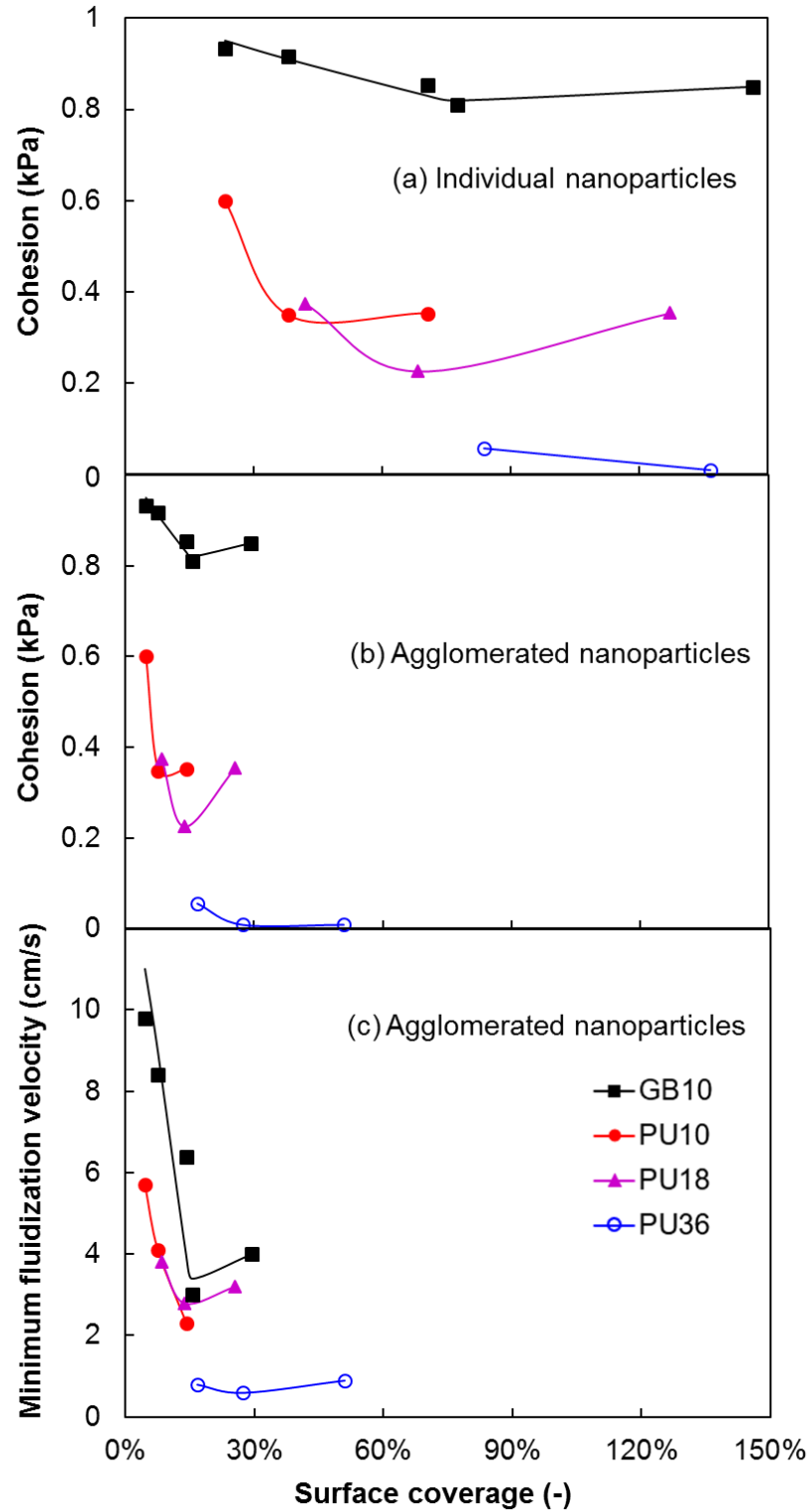
Figure 3.13: Effect of surface coverage on the cohesion and minimum fluidization velocity (data in this work)
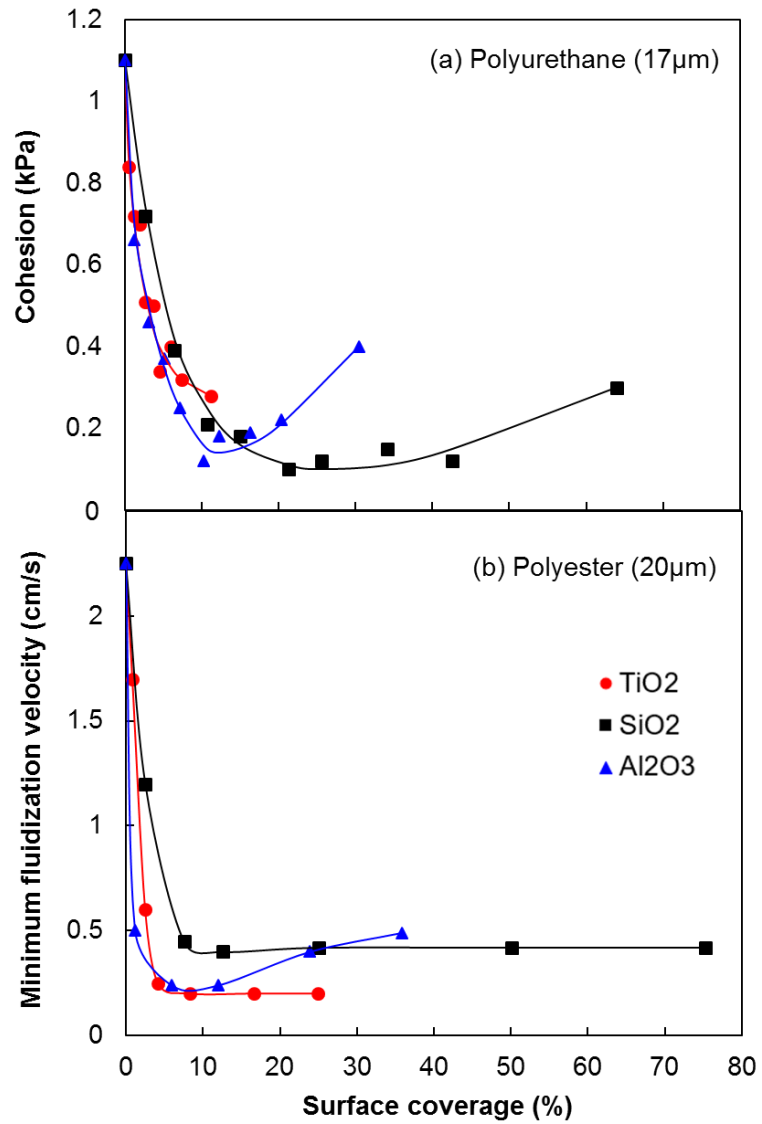
Figure 3.14: Effect of surface coverage on the cohesion and minimum fluidization velocity (data from (a) Qing Huang [48]; (b) Chunbao Xu [32], surface coverage calculated by assuming the nanoparticles as agglomerates)
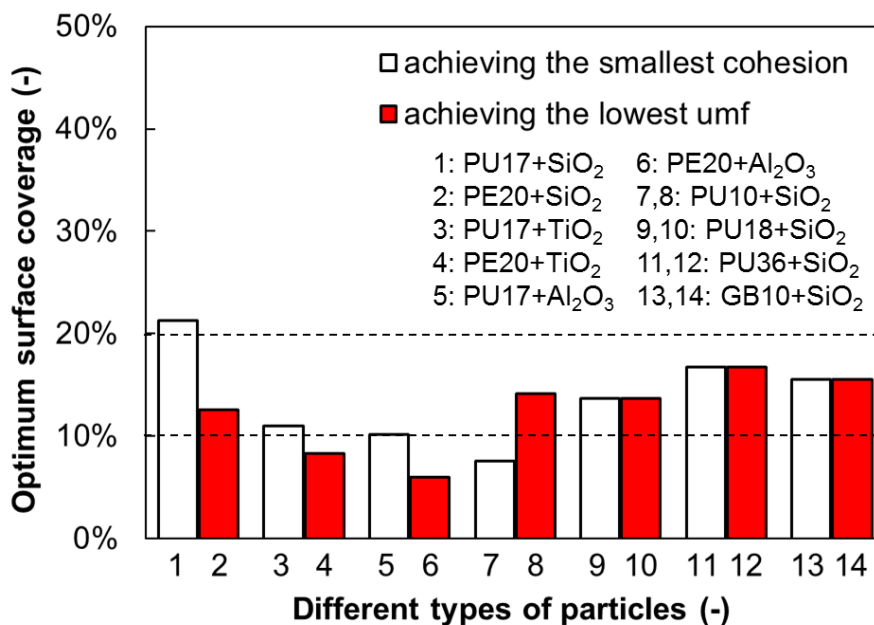
Figure 3.15: The optimum surface coverage for all systems
(1,3,5 from Qing Huang [48]; 2,4,6 from Chunbao Xu [32];
1-14 from the data in this work)

3.5 Conclusions

Group C^+ particles can be fluidized well after nanoparticle modulation. Nanoparticles as fluidization aids, do have the ability to reduce the cohesion of Group C particles and improve the fluidization quality. The minimum fluidization velocities of Group C^+ particles can be clearly identified and the values are acceptable, even if they are higher than that of Group A particles. The minimum fluidization velocity is closely related to the cohesion. A larger cohesion will result in a higher minimum fluidization velocity.

The fluidized bed of Group C^+ particles can expand to as high as 2-3 times of the fixed bed height. The bed expansion ratios (BER) for these Group C^+ particles reach as high as 2.3, around 180% of that for Group A particles. In addition, the bed voidage in the bed of the Group C^+ particles could reach as high as 0.84, around 140% of that in the bed of Group A particles. The high bed expansion and bed voidage indicate the pseudo-fluidization of Group C^+ particles. This unique and significant characteristic can retain more gas in the

bed and contribute to better gas-solid contact, which is critical and greatly meaningful for many processes in industry, especially for gas-phase catalytic reactions.

PU36 particles exhibit the characteristics of both Group C and Group A particles. They are cohesive and are not fluidizable before nanoparticle modulation. However, the nano-modulated PU36 particles possess the same low minimum fluidization velocity and low cohesion as Group A particles. Surprisingly, they exhibit a high bed expansion ratio of 1.9, around 140% of Group A particles. PU36 particles could be regarded as Group C/A particles.

Nanoparticle concentration greatly affects the fluidization quality of Group C^+ particles, and there exists an optimum nanoparticle concentration depending on the surface coverage and surface roughness. The optimum nanoparticle concentration was around 0.5-1% (volume fraction) for Group C^+ particles. Moreover, the optimum surface coverage for Group C^+ particles is around 10-20%.

Nomenclature

A	Cross-sectional area of a fluidized bed (cm^2)
d_p	Particle size (μm)
D_{10}	Percentage 10% of particles under this particle size (μm)
D_{50}	Percentage 50% of particles under this particle size (μm)
D_{90}	Percentage 90% of particles under this particle size (μm)
H_t	Total fluidized bed height (cm)
H_0	Initial bed height (cm)
ΔP	Pressure drop across the whole bed (Pa)
P_n	Normalized pressure drop (-)
W	Particle weight (N or kg m/s^2)
ρ_p	Particle density (kg/m^3)
ρ_g	Gas density (kg/m^3)
ε_b	Bed voidage (-)

Reference

[1] Geldart D. Types of gas fluidization[J]. Powder Technology, 1973, 7: 285-297.

[2] Baerns, M. Effect of interparticle adhesive forces on fluidization of fine particles[J]. Ind. & Eng. Chem. Fund., 1966, 5: 508-516.

[3] Geldart, D. The effect of particle size and size distribution on the behaviour of gas fluidized beds[J]. Powder Technol., 1972, 6: 201-209.

[4] Geldart, D. and Wong, A.C.Y. Fluidization of powders showing degrees of cohesiveness I: bed expansion[J]. Chem. Eng. Sci., 1984, 39: 1481-1488.

[5] Ichinose, Noboru, Yoshiharu Ozaki, and Seiichiro Kashu. Superfine particle technology[M]. Springer Science & Business Media, 2012.

[6] Jono, K., Ichikawa, H., Miyamoto, M. and Fukumori, Y. A review of particulate design for pharmaceutical powders and their production by spouted bed coating[J]. Powder Tech., 2000, 113: 269-277.

[7] Shur, Jagdeep, et al. The role of fines in the modification of the fluidization and dispersion mechanism within dry powder inhaler formulations[J]. Pharmaceutical Research, 2008, 25(7): 1631-1640.

[8] Zhu, J. and H. Zhang. Fluidization Additives to Fine Powders. U.S. Patent 6833185. December 21, 2004.

[9] Sanguansri P, Augustin M A. Nanoscale materials development–a food industry perspective[J]. Trends in Food Science & Technology, 2006, 17(10): 547-556.

[10] Vidal B C, Dien B S, Ting K C, et al. Influence of feedstock particle size on lignocellulose conversion—a review[J]. Applied biochemistry and biotechnology, 2011, 164(8): 1405-1421.

[11] Toda, Y. and Kato, A. Silica coating of ultrafine magnesia[J]. Ceramics International, 1989, 15(3): 161-166.

[12] Sanjurjo, A., Wood, B.J., Lau, K.H., Tong, G.T., Choi, D.K., Mckubre, M.C.H., Song, H.K. and Church, N. Titinium-based coating on copper by chemical vapor deposition in fluidized bed reactors[J]. Surface and Coating Technology, 1991, 49: 110-115.

[13] Hierso, J. C., Serp, P., Feurer, R. and Kalck, P. MOCVD of rhodium, palladium and platinum complexes on fluidized divided substrates: novel process for one-step preparation of nobel-metal catalysts[J]. Appl. Organometallic Chem., 1998, 12: 161-

172.

[14] Yates J G, Newton D. Fine particle effects in a fluidized-bed reactor[J]. Chemical engineering science, 1986, 41(4): 801-806.

[15] Yamamoto K, Imaoka T, Chun W J, et al. Size-specific catalytic activity of platinum clusters enhances oxygen reduction reactions[J]. Nature chemistry, 2009, 1(5): 397.

[16] Dai W L, Sun Q, Deng J F, et al. XPS studies of Cu/ZnO/Al2O3 ultra-fine catalysts derived by a novel gel oxalate co-precipitation for methanol synthesis by CO2+ H2[J]. Applied surface science, 2001, 177(3): 172-179.

[17] Sathish M, Viswanathan B, Viswanath R P, et al. Synthesis, characterization, electronic structure, and photocatalytic activity of nitrogen-doped TiO2 nanocatalyst[J]. Chemistry of materials, 2005, 17(25): 6349-6353.

[18] Marring, E., A. C. Hoffmann, and L. P. B. M. Janssen. The effect of vibration on the fluidization behavior of some cohesive powders[J]. Powder technology, 1994, 79(1): 1-10.

[19] Xu, Chunbao, and Jesse Zhu. Experimental and theoretical study on the agglomeration arising from fluidization of cohesive particles—effects of mechanical vibration[J]. Chemical Engineering Science, 2005, 6 (23): 6529-6541.

[20] Chirone R, L Massimilla, S Russo. Bubble-free fluidization of a cohesive powder in an acoustic field[J]. Chem. Eng. Sci., 1993, 48: 41-52.

[21] Chirone R, L Massimilla. Sound-assisted aeration of beds of cohesive solids[J]. Chem. Eng. Sci., 1994, 49: 1185-1194.

[22] Kuipers, N. J. M., E. J. Stamhuis, and A. A. C. M. Beenackers. Fluidization of potato starch in a stirred vibrating fluidized bed[J]. Chemical engineering science, 1996, 51(11): 2727-2732.

[23] Daniel L, Jose M V, Robert P et al. Enhanced nanofluidization by alternating electric fields[J]. Particle Technology and Fluidization, 2010, 56(1): 54-65.

[24] Nakamura, Hideya, and Satoru Watano. Fundamental particle fluidization behavior and handling of nano-particles in a rotating fluidized bed[J]. Powder Technology, 2008, 183(3): 324-332.

[25] Geldart, D. and Abrahamsen, A.R. Homogeneous fluidization of fine powders using various gases and pressures[J]. Powder Technol., 1978, 19: 133-136.

[26] Xie, H.-Y. The role of interparticle forces in the fluidization of fine particles[J]. Powder Technology, 1997, 94: 99-108.

[27] Visser, J. An invited review - van der Waals and other cohesive forces affecting powder fluidization[J]. Powder Technol., 1989, 58: 1-10.

[28] Dutta, A. and Dullea, L.V. A comparative evaluation of negatively and positively charged submicron particles as flow conditioners for a cohesive powder[J]. AIChE Symp. Ser., 1990, 86(276): 26-40.

[29] Zhou, T. and Li, H. Effect of adding different size particles on fluidization of cohesive particles[J]. Powder Technology, 1999, 102: 215-220.

[30] Yang J, Sliva A, Banerjee A, et al. Dry particle coating for improving the flowability of cohesive powders[J]. Powder Technology, 2005, 158(1-3): 21-33.

[31] Quintanilla M A S, Valverde J M, Castellanos A. Adhesion force between fine particles with controlled surface properties[J]. AIChE journal, 2006, 52(5): 1715-1728.

[32] Xu, Chunbao Charles, Hui Zhang, and Jesse Zhu. Improving flowability of cohesive particles by partial coating on the surfaces[J]. The Canadian Journal of Chemical Engineering, 2009, 87(3): 403-414.

[33] Chen Y, Yang J, Dave R N, et al. Fluidization of coated group C powders[J]. AIChE journal, 2008, 54(1): 104-121.

[34] Lauga, C., Chaouki, J., Klvana, D. and Chavarie, C. Improvement of the fluidizability of Ni/SiO2 aerogels by reducing interparticle forces[J]. Powder Technol., 1991, 65: 461-468.

[35] Zhou Q T, Qu L, Larson I, et al. Effect of mechanical dry particle coating on the improvement of powder flowability for lactose monohydrate: A model cohesive pharmaceutical powder[J]. Powder technology, 2011, 207(1-3): 414-421.

[36] Zhu J. Fluidization of fine powders[J]. Granular Materials: Fundamentals and Applications, 2003: 270-295.

[37] Donsì, G., Massimilla, L., Mutsers, S. M. P., Rietema, K. The effect of interparticle forces on the expansion of a homogeneous gas-fluidized bed[J]. AIChE Journal, 1973, 18(6): 239–248.

[38] Xu C, Huang Q, Zhang H, et al. Improving fluidizability of cohesive particles by

surface coating with flow conditioners[C]//The Fifth World Congress on Particle Technology Orlando, FL, United States. 2006.

[39] Zhu, J.-X. and H. Zhang. Method and Apparatus for Uniformly Dispensing Additive Particles in Fine Powders. U.S. Patent 7240861, 2007.

[40] ASTM D6128 - 06 Standard Test Method for Shear Testing of Bulk Solids Using the Jenike Shear Cell. 2006.

[41] Schwedes, J., Schulze, D. Measurement of flow properties of bulk solids[J]. Powder Technology, 1990, 61(1): 59–68.

[42] Kamath, S., Puri, V. M., Manbeck, H. B., Hogg, R. Flow properties of powders using four testers — measurement, comparison and assessment[J]. Powder Technology, 1993, 76(3): 277–289.

[43] American Society for Testing and Materials. Committee D18 on Soil and Rock. Standard Test Method for Bulk Solids Characterization by Carr Indices[M]. ASTM International, 2008.

[44] Krantz M, Zhang H, Zhu J. Characterization of powder flow: Static and dynamic testing[J]. Powder Technology, 2009, 194(3): 239-245.

[45] Hancock B C, Vukovinsky K E, Brolley B, et al. Development of a robust procedure for assessing powder flow using a commercial avalanche testing instrument[J]. Journal of pharmaceutical and biomedical analysis, 2004, 35(5): 979-990.

[46] Han M. Characterization of fine particle fluidization, Master thesis, Western University. 2015.

[47] Knowlton T M, Klinzing G E, Yang W C, et al. The importance of storage, transfer, and collection[J]. Chemical Engineering Progress;(United States), 1994, 90(4).

[48] Huang Q, Zhang H, Zhu J. Flow properties of fine powders in powder coating[J]. Particuology, 2010, 8(1): 19-27.

[49] Rowe, P.N., Santoro, L., Yates, J.G. The division of gas between bubble and interstitial phases in fluidized beds of fine powders. Chemical Engineering Science, 1978, 33: 133–140.

[50] Abrahamsen, A.R., Geldart, D. Behaviour of gas-fluidized beds of fine powders, part II. Voidage of the dense phase in bubbling beds. Powder Technology, 1980, 26: 47–55.

[51] Barreto, G.F., Yates, J.G., Rowe, P.N. The measurement of emulsion phase voidage in gas fluidized beds of fine powders. Chemical Engineering Science, 1983, 38 (3): 345–350.

Chapter 4

4 Group C$^+$ Particles: Extraordinary Dense Phase Expansion during Fluidization through Nano-modulation

Group C particles, although deemed to be difficult to fluidize because of their cohesive nature, fluidize well with high bed expansion and therefore hold more gas in the bed after nano-modulation. Using the bed collapse test, the dense phase properties of those formed Group C$^+$ and Group A particles were characterized. Group C$^+$ particles exhibited much higher dense phase expansion and larger dense phase voidage than Group A particles, indicating more gas holdup in the dense phase available for intimate gas-solid contact. Therefore, Group C$^+$ particles, with the extraordinary dense phase expansion and the large specific surface area, are significantly better for industrial processes, especially in gas-phase catalytic reactions. Maximum dense phase expansion ($E_{d,max}$) was defined as a factor for quantifying the expansion ability of the dense phase for different particles. Group C$^+$ particles with greater $E_{d,max}$ values signifies higher dense phase expansions, beneficial for gas-solid contact.

4.1 Introduction

Modern fluidization technology has been proven to be an effective way of processing particulates due to its good fluid-solid contact, higher mass and heat transfer rate and ability to handle large quantities of particles. Geldart [1] classified particles into Group A, B, C and D based on the particle size and particle density. Group B particles are bubble-ready particles which exhibit typical bubbling fluidization behaviors. Group A particles have smaller particle size, show smoother fluidization with a slight dense phase expansion, and is widely used in the fluid catalytic cracking (FCC) process [2,3]. Group C particles have an extremely high surface area and can significantly enhance many surface-based processes, such as gas-phase catalytic reactions [4-7]. That said however, the extremely small sizes of Group C particles make them cohesive and tend to form large agglomerates

due to strong interparticle forces, leading to the reduction of "valuable" surface area and difficulties in fluidization [8-11]. The cohesiveness of Group C particles limits their level of effective utilization in practical applications. Previous studies [12-14] found that nanoparticles could adhere onto the surface of Group C particles as asperities to increase the separation distance and thus reduce the van der Waals forces which predominate among interparticle forces. As a result, Group C particles after going through surface modification by nanoparticles appeared to fluidize well [14,15]. Group C$^+$ particles, which are Group C particles with nano-additives, were first proposed in Chapter 3. They exhibited a much higher total bed expansion than Group A particles, indicating better fluidization with more gas holdup and longer gas residence time in the bed, and therefore better solid-gas contact. Summarily, these works focused on the nanoparticle modification on the improvement of the flowability and fluidization behaviors for Group C particles. Seldom studies investigate the gas distribution in the dense phase and bubble phase of Group C$^+$ particle fluidization, which is more critical for gas-phase catalytic reactions.

The two-phase theory can be utilized to estimate the gas distribution in the fluidized bed. The "basic two-phase theory" originated in the work of Toomy and Johnstone [17] proposed that all gas in excess of the minimum fluidization velocity (u_{mf}) passed through the fluidized bed as bubbles ($G_B/A = u_g - u_{mf}$) while the dense phase remained at minimum fluidization ($\varepsilon_d = \varepsilon_{mf}$). The "basic two-phase theory" can describe the fluidization characteristics of Group B particles, but this theory does not apply to fine particles such as Group A particles [18-20]. A number of works [21-25] modified this "basic two-phase theory" for Group A particles and the deviation was expressed in the form: $G_B/A = u_g - ku_{mf}$, where, generally, $k>1$, indicating an increase in the interstitial gas velocity above u_{mf} and an increase in dense phase voidage above ε_{mf}. The increase in dense phase voidage means more gas is retained in the dense phase and the gas has a higher chance to interact with the solids, thus improving gas-solid contact efficiency. Group C$^+$ particles with extremely small particle sizes than Group A particles would exhibit more different characteristics than this theory expected. The performance of a fluidized bed reactor mainly depends on the degree of gas-solid contact, the solid mixing rate and the bubble size [26-28]. As a result, the dense phase expansion is a critical characteristic for evaluating the fluidization quality and the reaction performance.

Dense phase properties can be evaluated using the bed collapse test, which was initially proposed by Rietema in 1967 [29] and now is one of the most popular methods of characterizing fluidized bed hydrodynamics. This technique is carried out by first fully fluidizing the bed, followed by suddenly shutting off the gas supply, then tracking the bed surface level as it collapses. The bed collapse process, as shown in Figure 4.1, can be clearly divided into three stages: (1) the bubble escape stage, where the bed surface drops quickly due to gas bubbles reaching and escaping from the top of the bed; (2) the sedimentation stage, where the gas in the interstices of the dense phase in excess of ε_{mf} escapes; (3) the consolidation stage, where the fixed bed further settles to a final compacted bed. The bed collapse test is the only simple method for estimating the average dense phase voidage and bubble holdup in the bubbling fluidized bed [24,25,30,31].
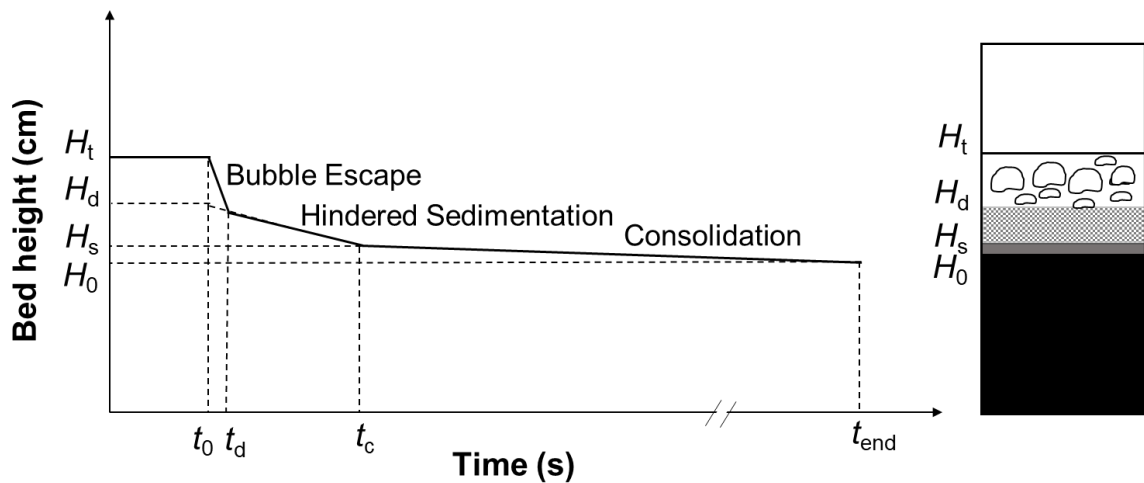
Figure 4.1: A typical bed collapse process

As previously discussed, the simple "two-phase" theory can depict the fluidization process for Group B particles but not accurately for Group A particle [32-36]. The deviation from the simple two-phase theory for Group A particles correlates strongly with the fines level (<45 µm) [30,31]. The average dense phase voidage increased as the particle size decreased and the fraction of fines (<45 µm) increased [23,37], resulting in more gas holdup in the dense phase. Following this trend, Group C^+ particles are expected to exhibit higher dense phase expansion.

In the present work, the characteristics of the dense phase and the bubble phase, including the dense phase voidage and the bubble holdup, were evaluated by carrying out the bed collapse test using Group C^+ particles, and the differences between Group C^+ and Group A particles were also studied.

4.2 Experimental

As shown in Figure 4.2, the fluidization column was made of plexiglas with a dimension of 5.08 cm (I.D.) x 45.7 cm (height). A perforated plate with an open area ratio of 23% acted as the gas distributor and was covered by two layers of filter cloth with a mesh of 625 to increase the pressure drop to provide a uniform gas distribution and prevent the particles dropping into the wind box. The pressure drop of the gas distributor accounted for around 10% or even larger of the particle weight per cross-sectional area under most operating gas velocities. The air flowed through two PVC tubes into the wind box at two opposite positions. A measuring tape fixed along the fluidization column was used to measure the bed height. The bed expansion ratio (BER) in the bed collapse tests was defined as the ratio of the fluidized bed height (H_t) to the settled bed height (H_s).

The particles used in the present experiments were glass beads (GB), fluid catalytic cracking (FCC) catalysts, polyurethane particles (PU) with their physical properties listed in Table 4.1. Glass beads and polyurethane particles are non-porous, their apparent particle densities are the material density. FCC particles are porous and the apparent density was measured and reported by Chengxiu Wang [38], based on the "wet cake" method by Abrahamsen and Geldart (1980) [30]. Both inorganic (GB and FCC) and organic (PU) particles were adopted to test the effect of the material property on the experiments. The nanoparticles used in this experiment were SiO_2 particles with a particle size of 16 nm and particle density of 2200 kg/m^3 (marketed as R972 by Evonik). Group C^+ particles were produced using the nanoparticle modulation technique by mixing a small amount of nanoparticles with Group C particles [12,39]. In the present work, three nanoparticle concentrations in volume fractions were used, namely 0.27%, 0.44%, 0.82%. Table 4.2 shows the minimum fluidization velocities (u_{mf}) of these Group C^+ particles.
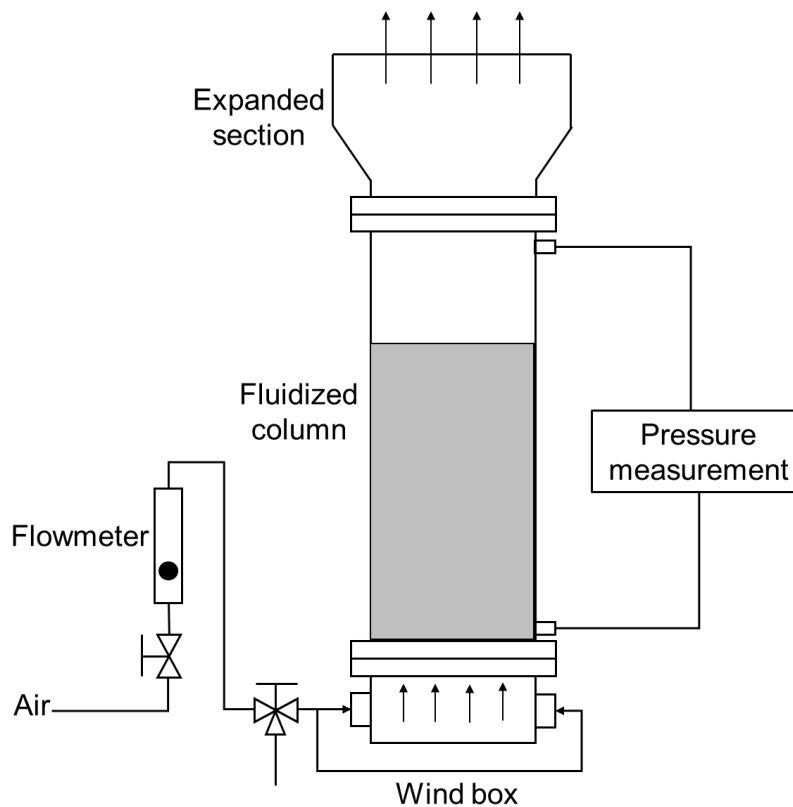
Figure 4.2: Experimental setup

Table 4.1: Physical properties of experimental particles

Powder Name	Particle Size (µm)			Sphericity	Particle Density (kg/m^3)	Compact Bulk Density[1] (kg/m^3)	Loose Bulk Density[2] (kg/m^3)
	D_{10}	D_{50}	D_{90}				
GB10	1.6	10	29	1	2500	916	788
GB39	15	39	85	1	2500	1275	1260
FCC8.5	1.5	8.5	26	0.88	1780	509	456
FCC20	4.4	20	53	0.91	1780	627	565
FCC76	20	76	139	0.98	1780	874	830
PU10	2	10	30	0.76	1200	560	498
PU18	4	18	50	0.76	1200	648	585
PU36	12	36	74	0.78	1200	679	600
PU90	23	90	205	0.77	1200	696	635

[1] Bulk density of the fixed bed before fluidization.
[2] Bulk density of the settled bed after bed collapse test.

Table 4.2: Minimum fluidization velocities of experimental particles

Powder name	Nanoparticle concentration (v%)	Minimum fluidization velocity (cm/s)	Geldart Classification
GB10	0.27	9.8	C
	0.44	8.4	
	0.82	6.4	
FCC8.5	0.27	12	C
	0.44	12.5	
	0.82	9.5	
FCC20	0.27	6	C
	0.44	6.5	
	0.82	6.5	
PU10	0.27	5.7	C
	0.44	4.1	
	0.82	2.3	
PU18	0.27	3.8	C
	0.44	2.8	
	0.82	3.2	
PU36	0.27	0.8	A/C
	0.44	0.6	
	0.82	0.9	
GB39	0	0.5	A
	0.82	0.5	
FCC76	0	0.4	A
	0.82	0.4	
PU90	0	0.6	A
	0.82	0.6	

The procedures of the bed collapse test include: (1) the bed was fully fluidized at a high superficial gas velocity; (2) the gas supply was suddenly shut off and the bed started collapsing; (3) the bed height was recorded as a function of time. The whole process was recorded using a digital camera (Canon EOS 800D), then the video was converted to RGB images second by second using Matlab. Those RGB images were cropped to obtain the region of interest and then transformed to greyscale images. To read the bed height easily and clearer, the grayscale images were converted to binary images with a threshold value of around 60 to 80 depending on different conditions. Generally, the video lasted 60 to 80 seconds and the initial 5 to 10 seconds recorded the complete fluidization state. During the fluidization state, the bed surface fluctuated and the average value was adopted as the

fluidized bed height. In bed collapse process, the bed surface was smooth and dropped as a function of the time which could be clearly read from the images. Figure 4.3 clearly shows a typical bed collapse test for GB10+0.82% at 8.2 cm/s and the process for estimating the bed height. Figure 4.4 gives schematic diagrams of the bed collapse curves of Group A and Group C^+ particles. The dense phase bed height (H_d) was identified from the bed collapse curves. Then other parameters such as the dense phase voidage (ε_d) and bubble holdup (x_b) were calculated as follows:

$$\varepsilon_d = 1 - (H_0 / H_d)(1 - \varepsilon_0) \qquad (4.1)$$

$$x_b = V_b / V_t = (H_t - H_d) / H_t \qquad (4.2)$$

where H_0 is the initial fixed bed height, H_t is the total fluidized bed height, ε_0 is the initial fixed bed voidage, V_b is the bubble volume and V_t is the total fluidized bed volume. The bed collapse tests were conducted at various superficial gas velocities, ranging from 1.2 cm/s to 13 cm/s.
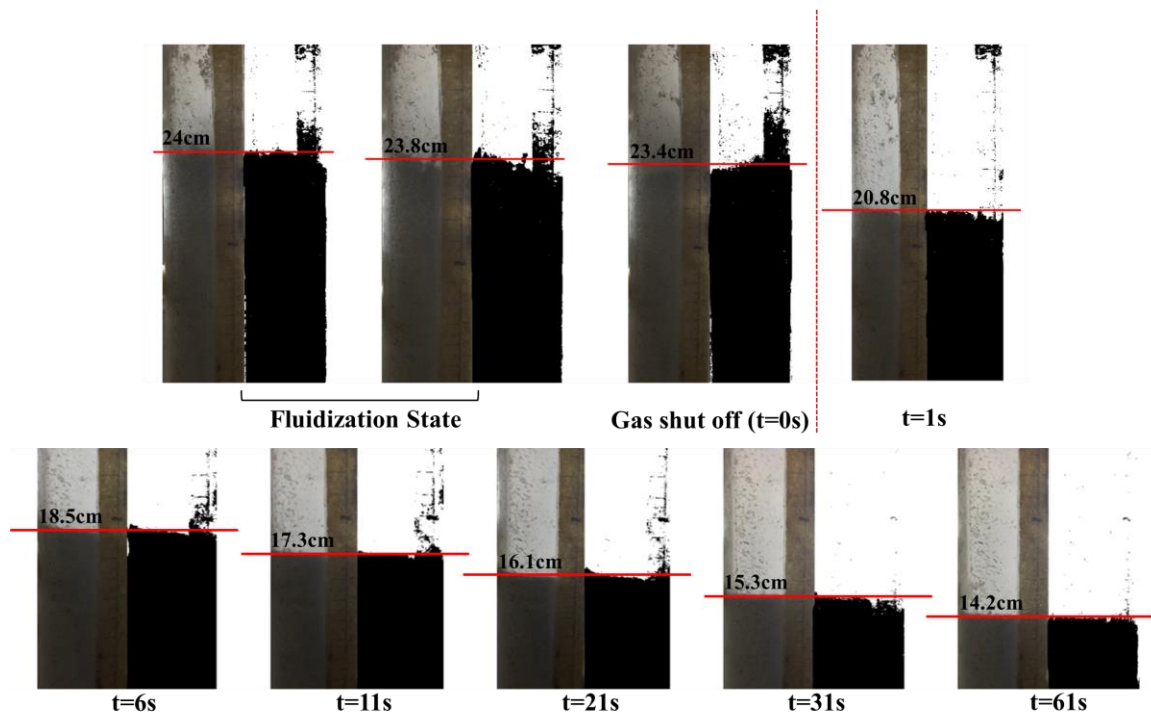
Figure 4.3: A typical bed collapse and the process for estimating the bed height (GB10+0.82% at 8.2 cm/s; left: RGB images; right: binary images)
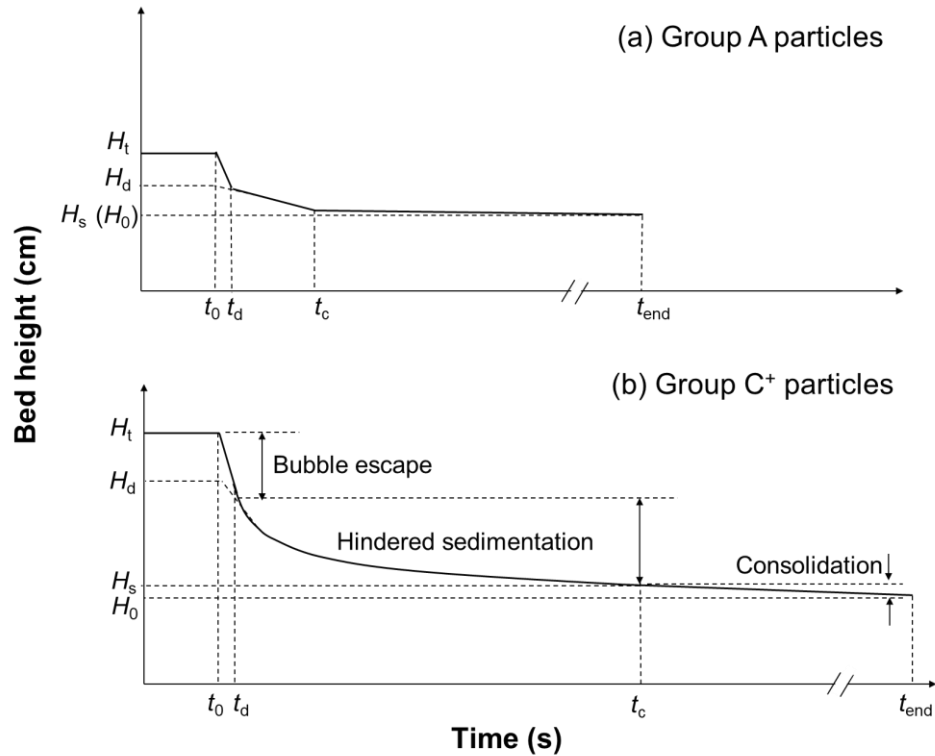
Figure 4.4: Typical bed collapse curves for Group C$^+$ and Group A particles at the same superficial gas velocity

4.3 Results and discussion

4.3.1 Results of bed collapse tests

Particle size has a significant effect on bed collapse dynamics [40-43]. As shown in Figure 4.4, the nature of the bed collapse process of Group C$^+$ particle fluidization is characteristically different. More specifically, typical bed collapse results of Group C$^+$ particles, as well as Group A particles, are presented in Figure 4.5. Group C$^+$ particles showed a much longer collapse time and much higher dense phase height when compared with Group A particles, indicating that there is more gas in the particle interstices. The bed collapse curves of Group C$^+$ particles were curved, while those of Group A particles were much more linear.

Group C$^+$ particles (GB10+, PU10+ and FCC8.5+) had much higher dense phase expansion, reaching up to around 1.6-1.7, while Group A particles (GB39, PU90 and

FCC76) showed a dense phase expansion of only around 1.15. The bed collapse time for Group C^+ particles reached up to 70s, much longer than that for Group A particles, which only lasted 2-10s. Nanoparticles had little effect on the bed collapse dynamics for Group A particles. For Group C^+ particles, for example for PU+ series, both the dense phase expansion and the collapse time increased as the particle size decreased, namely PU10+0.82% > PU18+0.82% > PU36+0.82%. Group C^+ particles with smaller particle size are more cohesive, which will help their fluidized beds hold more gas in the solid interstices and prevent the gas from escaping the bed, thus increasing the dense phase expansion and extending the bed collapse time.
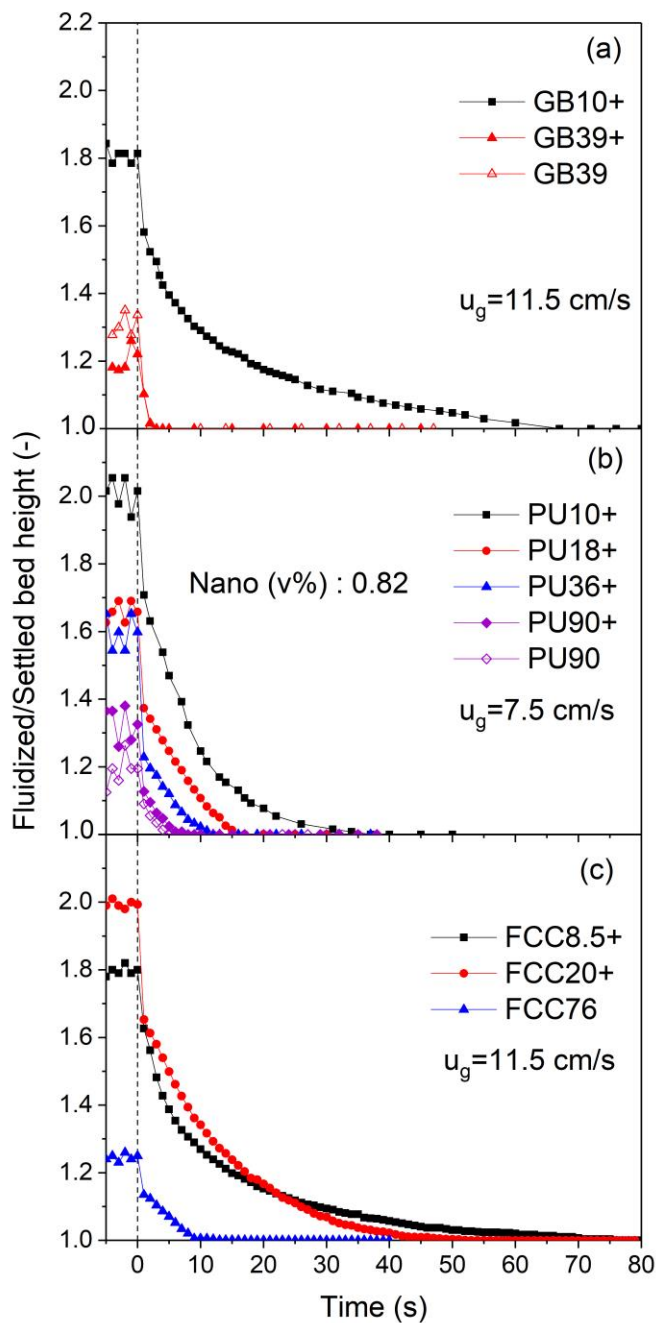
Figure 4.5: Bed collapse curves of Group C$^+$ with a nano-concentration of 0.82% and Group A particles

The effect of nanoparticle concentration on the bed collapse dynamics for Group C$^+$ particles is shown in Figure 4.6. Both the dense phase height and the bed collapse time increased with the increase of nanoparticle concentration, especially for the GB10 and FCC

8.5 series. For PU particles, the nanoparticle concentration of 0.44% (in volume) seemed to be slightly better than the other two values for improving the dense phase expansion. As a result, the optimal nanoparticle concentration would be 0.5-1%, consistent with previous results [14-16,44].
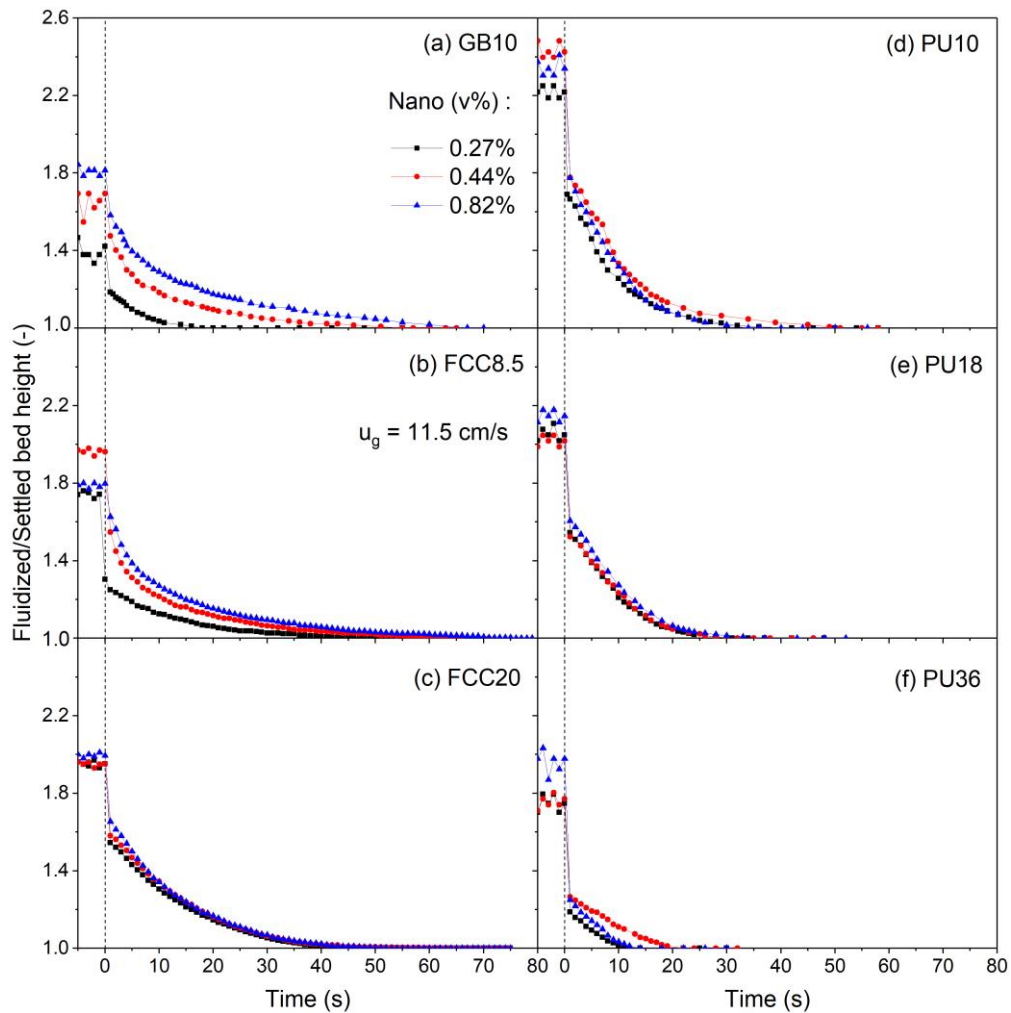
Figure 4.6: The effect of nanoparticle concentration on the bed collapse curves for Group C+ particles at 11.5 cm/s

Figure 4.7 shows the effect of superficial gas velocities on the bed collapse dynamics. Three typical Group C+ particles with nanoparticle concentration of 0.82%, GB 10+, PU10+ and FCC20+, were chosen to conduct bed collapse tests under different gas

velocities, ranging from 4.9cm/s to 11.5cm/s. As the gas velocity increased, the dense phase expanded significantly at the beginning and then showed a small and gradual increase in expansion, while the bubble phase increased more significantly. This phenomenon suggests that as the superficial gas velocity increased, more gas entered the dense phase initially which contributed to the significant increase in the dense phase expansion. After a certain superficial gas velocity, the dense phase expansion appeared to reach the maximum, where more gas tended to form bubbles and the two phases seemed to follow the normal "two-phase" theory.
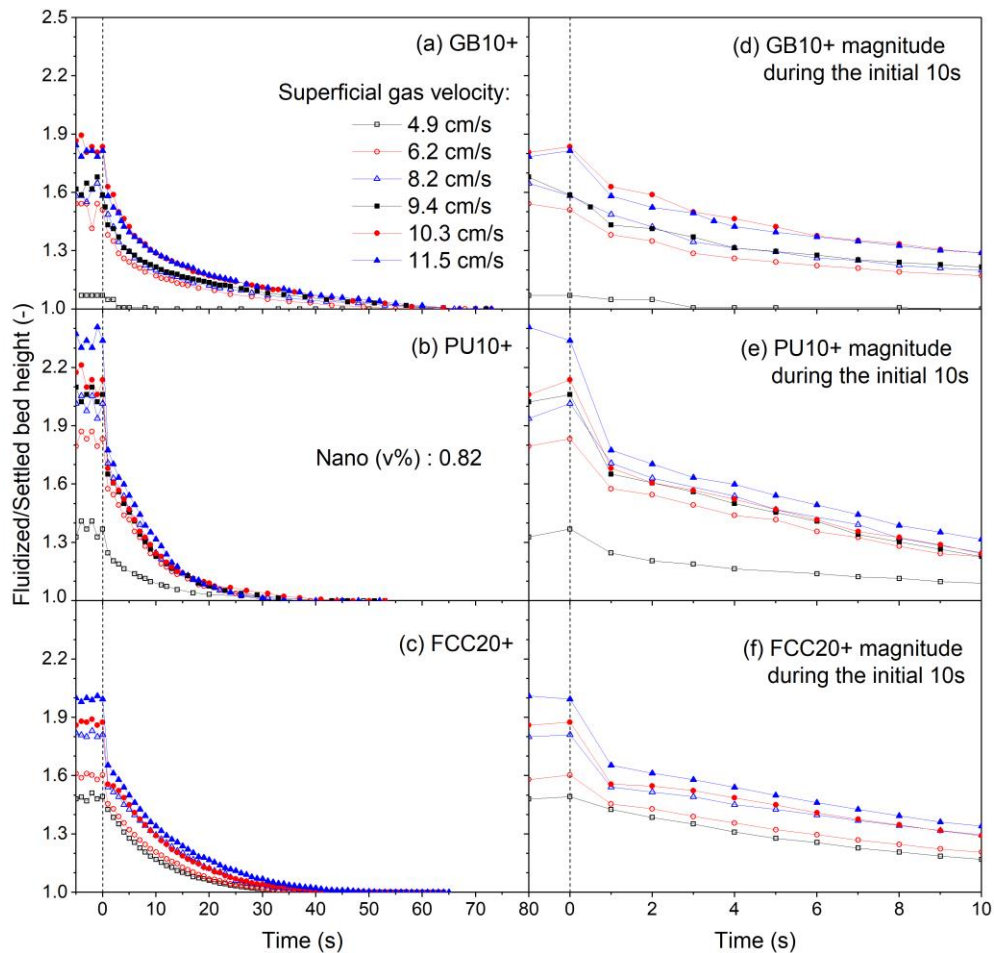
Figure 4.7: The effect of gas velocities on the bed collapse curves for Group C$^+$ particles with a nano-concentration of 0.82%

4.3.2　Two-phase separation

As depicted by the two-phase theory, the gas flowing into the fluidized bed contributes to the overall bed expansion, which can be divided into two portions: one making up the bubble phase and the other going into the dense phase. The two phases can be clearly identified from the bed collapse curves as shown in Figure 4.8. The bed height quickly dropped in the initial 1-2s due to the bubble escape. After that, a gradual and decrease of the bed height was caused by the escape of the gas in the dense phase. As a result the bubble holdup and the dense phase height could be determined.
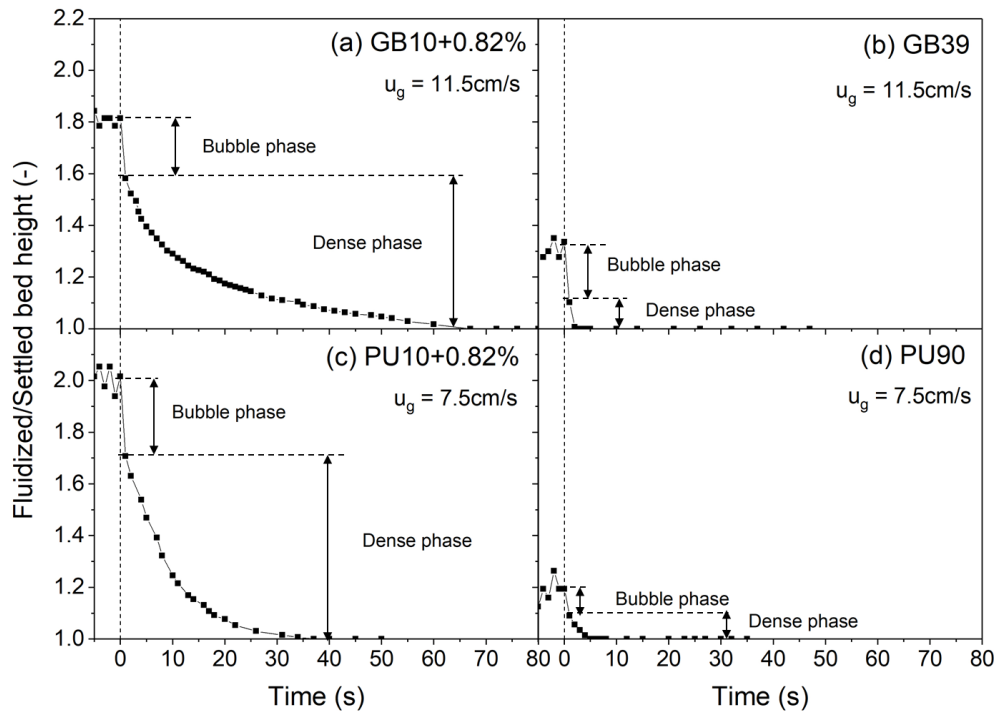
Figure 4.8: Two-phase separation identified from the bed collapse curves

The bed heights of different phases for different types of particles are shown in Figure 4.9. The fluidized bed height could be divided into three parts: the fixed bed height (H_0), the dense phase height (H_d) and the total bed height (H_t). The difference between the total bed height and the dense phase height is ascribed from bubbles. The bed heights for Group A and Group C$^+$ particles showed significant differences. Group A particles had a much lower

total bed height and much lower dense phase height than Group C$^+$ particles. For Group A particles, FCC76 had relatively higher dense phase height and less bubbles than GB39 and PU90.

Group C$^+$ particles had a high total bed height and high dense phase height. For Group C$^+$ particles, PU series had more bubble holdup than FCC and GB particles. As particle size increased, the dense phase height decreased and the bubble holdup increased. The characteristics of the two phases in Group C$^+$ particle fluidization was different from the simple "two-phase" theory which assumed that the dense phase remained at the minimum fluidization and all gas in excess of the u_{mf} passed as bubbles. As particle size decreases, the u_{mf} was expected to decrease by Ergun equation [45], and therefore the bubble holdup was expected to increase based on the simple "two-phase" theory, which was controversial due to the phenomenon observed in the fluidization of Group C$^+$ particles.
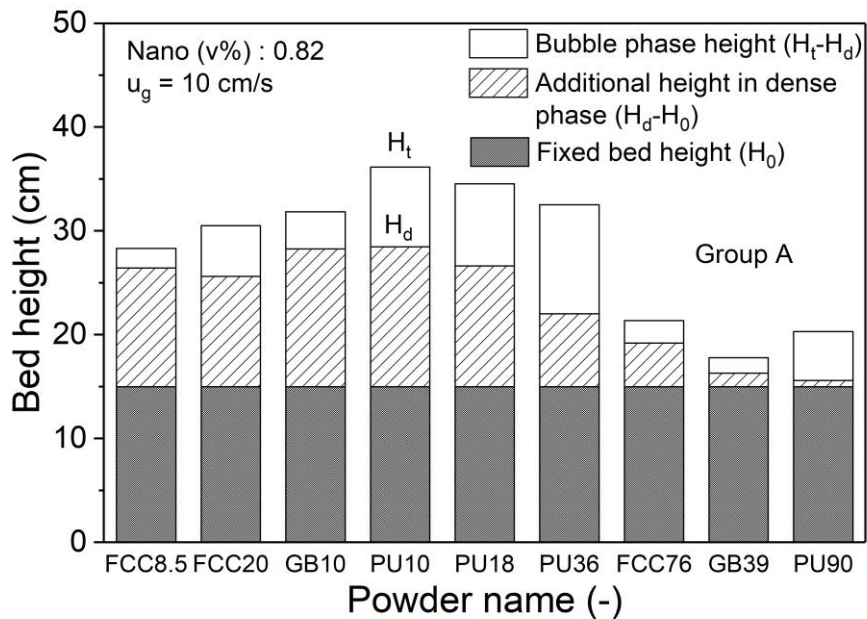
Figure 4.9: The bed heights of different phases in the fluidized bed of different particles with a nano-concentration of 0.82% at 10 cm/s

Figure 4.10 shows the total bed height and the dense phase height for Group C$^+$ and Group A particles at different gas velocities. The gas velocity had an insignificant effect on the

total bed height and the dense phase height for Group A particles, as they remained nearly constant with an increase of the gas velocity. The phenomenon in the fluidization of Group C^+ particles was completely different. As gas velocity increased, the bed for Group C^+ particles significantly expanded, much more than the fixed bed height. The dense phase showed a dramatic expansion and tended to remain stable at high gas velocities. In addition, the bubble holdup increased with the increase of gas velocity. Generally, the dense phase is where most of the gas-solid contact happens. More gas flowing to the dense phase signifies that more gas has the chance to contact with particles, thus significantly improving gas-solids contact efficiency. Group C^+ particle fluidize with a high dense phase height, indicating better gas-solid contact.
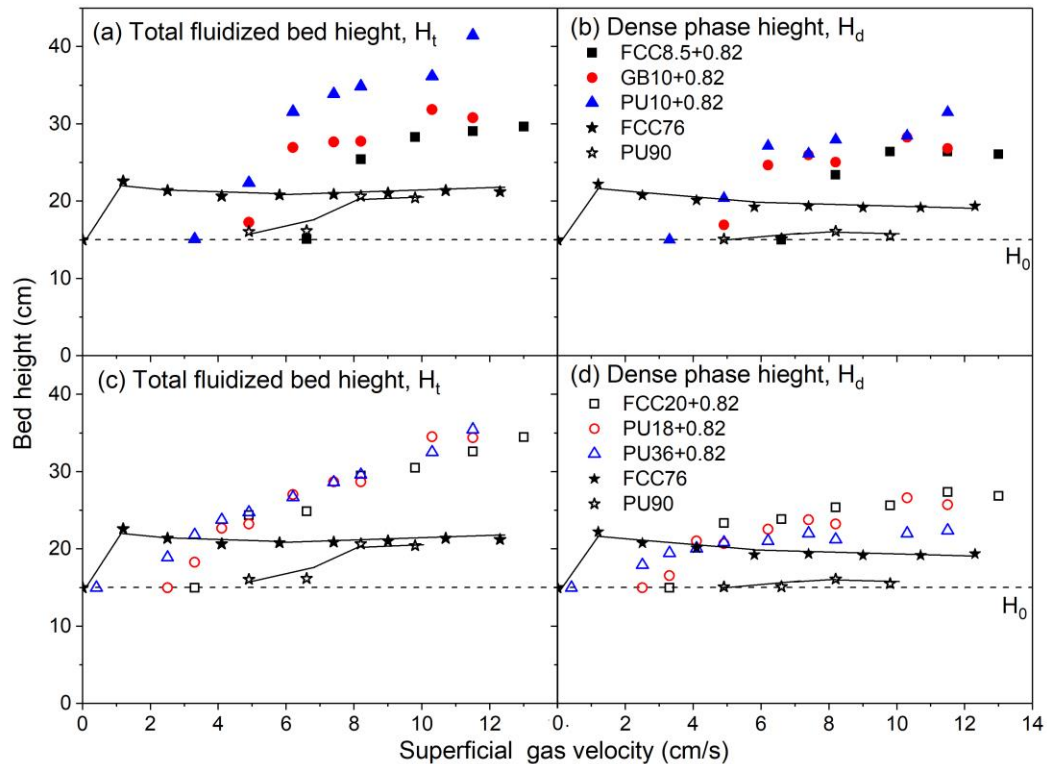
Figure 4.10: The effect of gas velocities on the bed heights in the fluidized beds of Group A and Group C^+ particles

4.3.3   Dense phase characterization

Dense phase voidage is a parameter for quantifying the gas holdup in the dense phase, which can be obtained from the bed collapse test (Equation 4.1). Figure 4.11 compares the dense phase voidage between Group C^+ and Group A particles and shows the effect of nanoparticle concentrations on that for Group C^+ particles. As shown in Figure 4.11(a), Group A particles, especially PU90, had a small dense phase voidage of around 0.45, and nanoparticles had little effect on their dense phase voidage. FCC76 showed a larger dense phase voidage, reaching up to around 0.6. Group C^+ particles possessed much larger dense phase voidage than Group A particles, reaching up to 0.85. The larger dense phase voidage indicates more gas entering the dense phase during the fluidization process, providing better gas-solid contact. As particle size increased, the dense phase voidage decreased. PU36+ had a similar dense phase voidage as FCC76, which was identified as Group A/C particles.

As shown in Figure 4.11(b), the nanoparticle concentration has a significant effect on the dense phase voidage for PU10 particles, with an optimum value of 0.44%. Nanoparticles improved the fluidization quality by adhering on the surface of Group C particles to increase the distance between the particles and thus decreasing the interparticle forces [13-15]. The nanoparticle concentration would affect the surface coverage on Group C particles. The surface coverage existed an optimum value which was enough to separate Group C particles. The excess nanoparticles would self-agglomerate and increase the cohesion of Group C^+ particles. Chapter 3 discussed the optimum nanoparticle concentration and surface coverage in details, and concluded that the optimum surface coverage was around 10%-20%. PU36 had larger particle size and smaller specific surface area, so the nanoparticle concentration of 0.27% has almost reached the optimum surface coverage. The effect of nanoparticle concentration became less significant.

In addition, the dense phase voidage for Group C^+ particles significantly increased at the beginning and then showed a plateau with increasing the gas velocity. The stable dense phase voidage after a certain gas velocity indicated that the gas velocity in excess of this value mainly led to the creation of bubbles. The initial sharp increase of the dense phase voidage may be due to the cohesion of Group C^+ particles. Although the cohesion of Group

C^+ particles was dramatically reduced, it was not negligible compared with that of Group A particles [15,16]. The appropriate cohesion could help retain more gas in the particle interstices, contributing to the soar in dense phase voidage. As more gas entered the dense phase, the separation distance between the Group C^+ particles became larger and the cohesion decreased. When it decreased to a certain value, the dense phase could no longer retain more gas and remain stable, the excess gas formed bubbles.
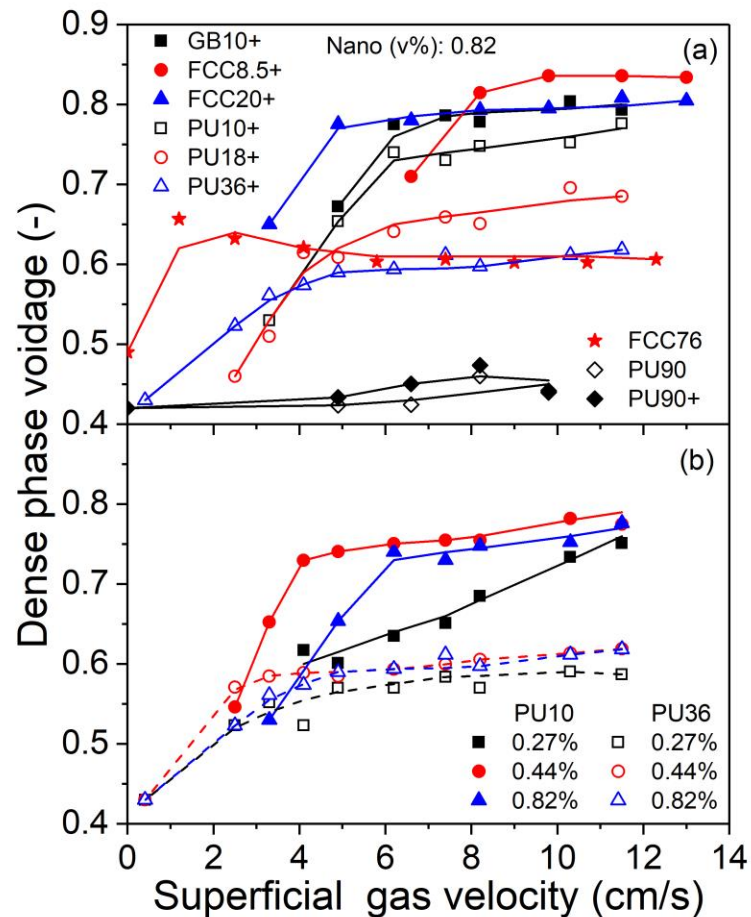
Figure 4.11: Dense phase voidage of Group A and Group C^+ particles and the effect of nanoparticle concentrations

Figure 4.12 shows the effects of nanoparticle concentrations and gas velocities on the bed heights (H_t and H_d) for Group C^+ particles. The nanoparticle concentration had a clear effect on the bed heights for GB10, FCC8.5 and PU10. As particle size increased, the effect

became less significant (for FCC20, PU18 and PU36). GB10 with a nanoparticle concentration of 0.82% showed the highest total bed height and dense phase height. For FCC8.5 and PU10, a nanoparticle concentration of 0.44% was enough to achieve a good fluidization quality with a high dense phase height. In conclusion, the high dense phase height is a unique characteristic for Group C$^+$ particle fluidization and has the potential to significantly improve the gas-solid contact. This unique characteristic is advantageous for many of the surface-based processes in the industry, especially on gas-phase catalytic reactions.
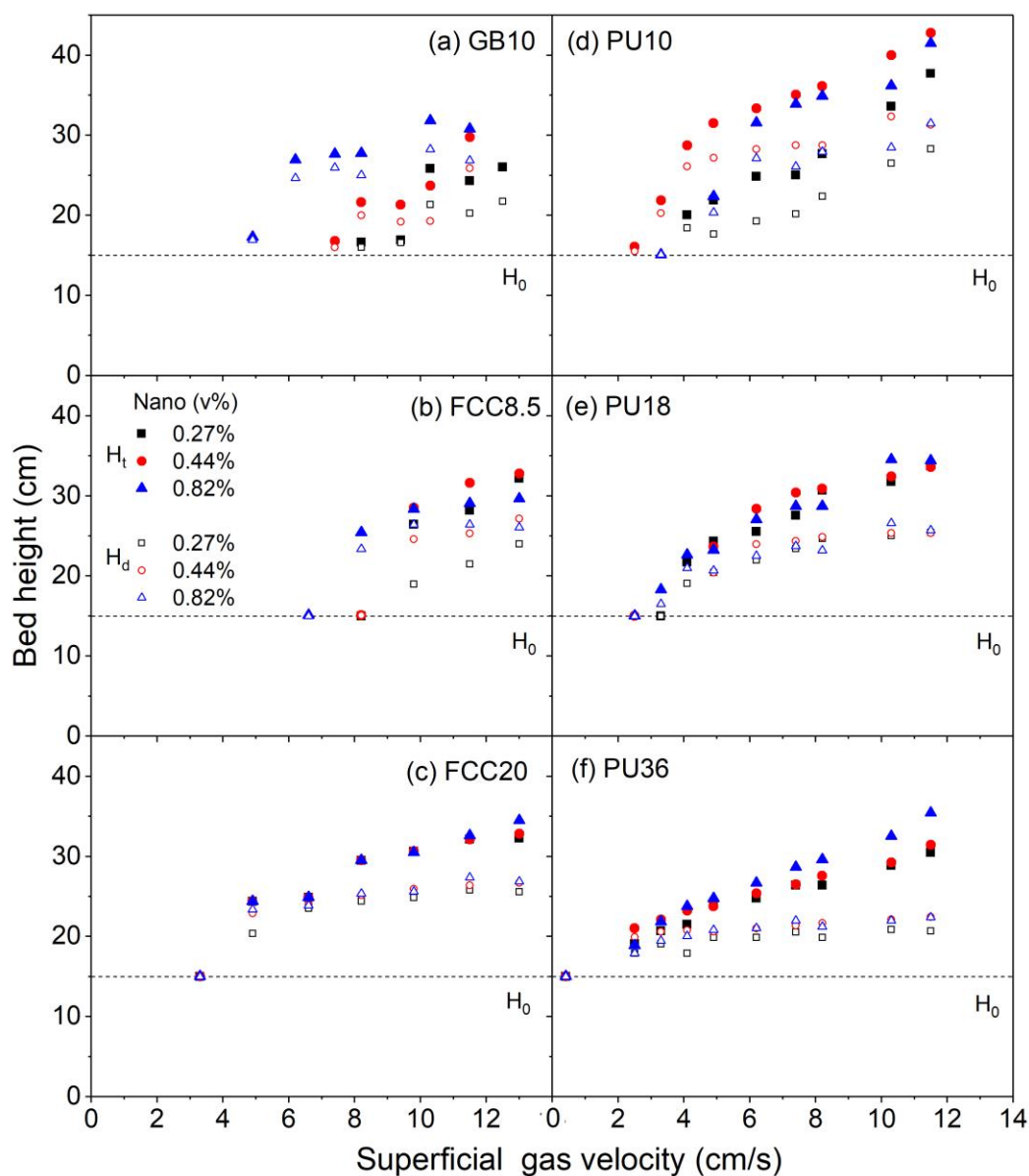
Figure 4.12: The effect of nanoparticle concentrations on the bed heights for Group C⁺ particles

4.3.4   Bubble phase characterization

It is necessary to investigate the gas holdup in the bubble phase since the gas-solid contact in the bubble phase is different from that in the dense phase. As shown in Figure 4.12, the difference between the total bed height and the dense phase height represented the bubble

phase height, which indicate the bubble holdup in the fluidized bed. The bubble phase height for Group C^+ particles increased with the increase of gas velocity and the decrease of particle size, signifying the formation of more bubbles. In addition, the nanoparticle concentration had little effect on the bubble phase height.

Figure 4.13 shows the bubble holdup in Group C^+ and Group A particle fluidization and the effect of nanoparticle concentrations. The bubble holdup increased with the increase of gas velocity for both Group A and Group C^+ particles. More specifically, the bubble holdup for Group A particles (PU90 and PU90+) had similar values as that for some types of Group C+ particles (PU10+ and PU18+). FCC76 showed similar bubble holdup as FCC8.5+ and GB10+. For Group C^+ particles, the bubble holdup evidently increased as particle size increased, following the sequence: PU36+ > PU18+ > PU10+ > FCC20+ > GB10+ > FCC8.5+. Nanoparticle concentrations had little effect on the bubble holdup in the fluidized bed of Group A particles. In terms of Group C^+ particles, the higher nanoparticle concentration could reduce the bubble holdup to some extent, especially for PU36, indicating smoother fluidization.
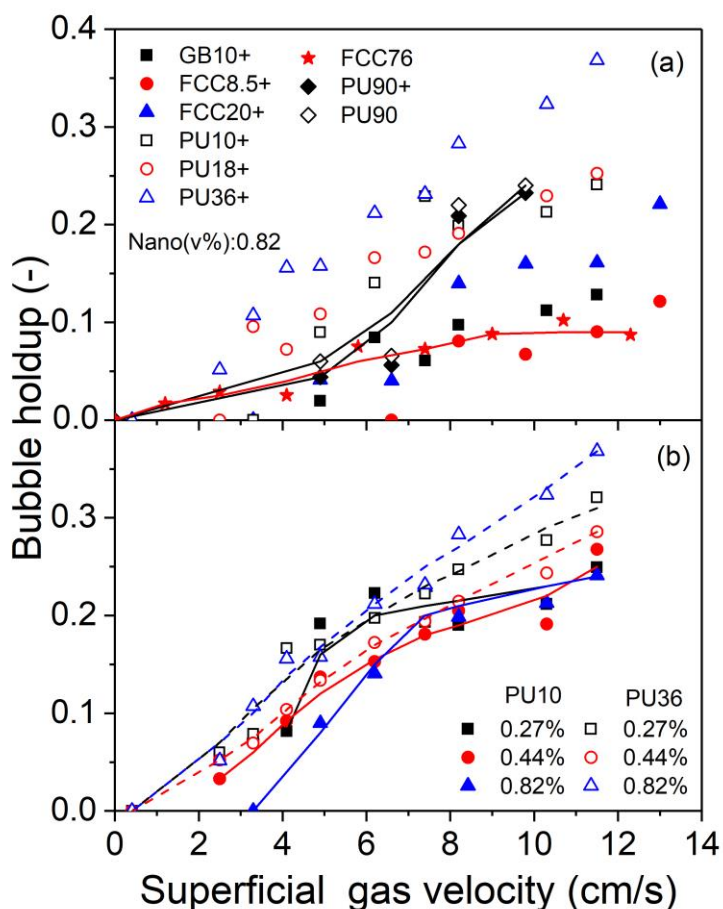
Figure 4.13: Bubble holdup of Group C⁺ and Group A particles and the effect of nanoparticle concentrations

Figure 4.14 shows the distribution of the gas entering the fluidized bed in the two phases: the bubble phase (V_b /V_0) and the dense phase (($V_d - V_0$)/ V_0), and the percentage of the additional dense phase versus the bubble phase (($V_d - V_0$)/ (V_t-V_0)). As shown in Figure 4.14(a), the percentage of the gas entering the dense phase in the fluidized bed of Group A particles was much smaller than that in the fluidized bed of Group C+ particles. More specifically, the percentage of the additional dense phase volume for PU90, PU90+ and FCC76 reached around 0.1 and 0.3, while that for FCC76 showed a trend of decrease with the increase of superficial gas velocity, indicating that Group A particles should be operated at low superficial gas velocities. For Group C⁺ particles, the percentage of the gas entering into the dense phase reached up to 1.1, and increased with the increase of the

superficial gas velocity. Group C^+ particles could be operated at high gas velocities, as it is beneficial for some catalytic reactions that need short residence time and increase the production.

As shown in Figure 4.14(b), Group A particles showed similar or even smaller percentages of bubble volume when compared with Group C^+ particles. For Group C^+ particles, PU particles exhibited a higher bubble volume than other Group C^+ and Group A particles. Although the bubble volume for Group C^+ particles was similar or even higher than that for Group A particles, the total fluidized bed volume and the dense phase volume for Group C^+ particles were much higher, signifying more gas retained in the bed and in the dense phase which contributes to better gas-solid contact.

Figure 4.14(c) illustrated the percentage of the additional dense phase volume relative to the bubble volume. For PU90 and PU90+ particles, the percentage of the gas entering the dense phase was insignificant compared to the percentage entering the bubble phase, only accounting for 0.1-0.3, and significantly decreased as gas velocity increased. Although the gas percentage entering the dense phase for FCC76 was more significant than that entering the bubble phase, the absolute value of the gas percentage entering the dense phase (Figure 4.13(a)) was small. For Group C^+ particles, the gas percentage entering the dense phase was more significant than that entering the bubble phase, especially for those with smaller particle sizes, such as FCC8.5+, FCC20+, GB10+ and PU10+. In summary, Group C^+ particles with a large gas percentage entering the dense phase during fluidization could significantly improve gas-solid contact efficiency.
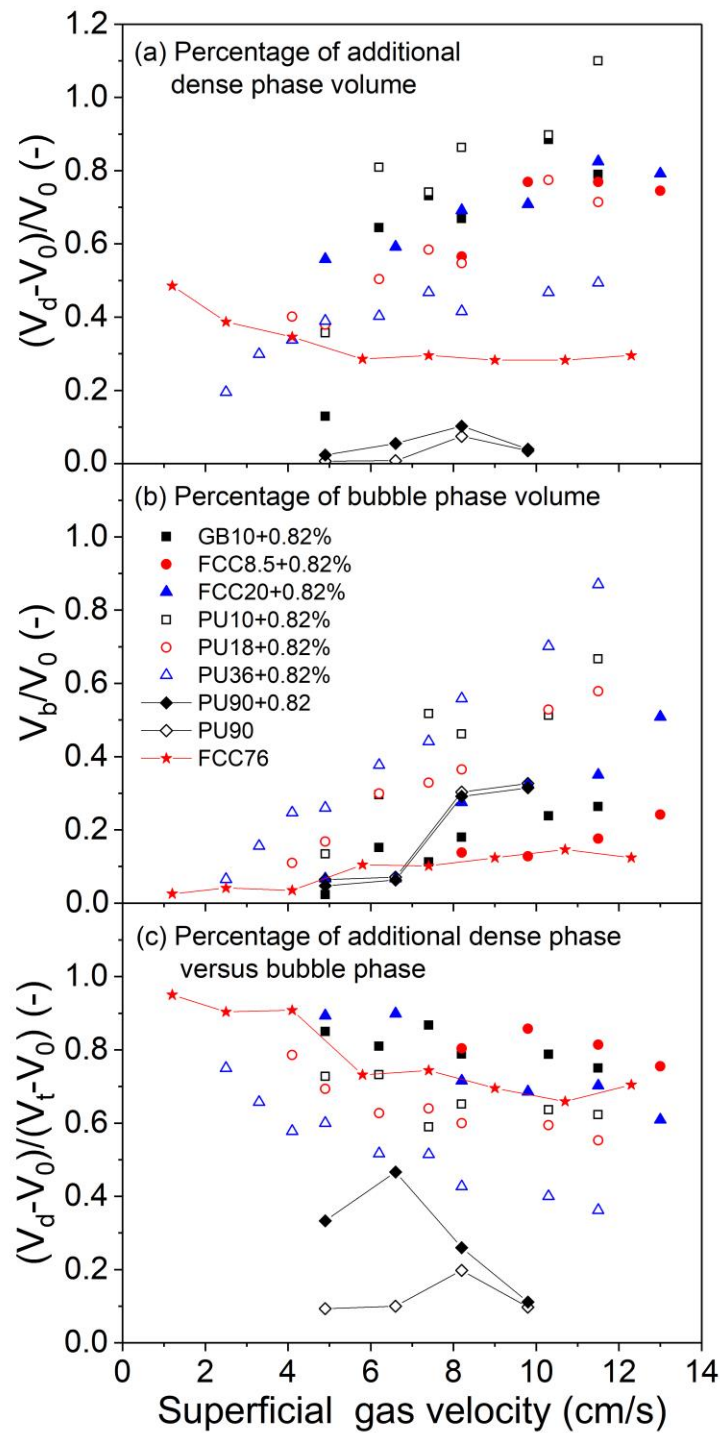
Figure 4.14: The percentage of the gas flowing into the two phases and the percentage of the additional dense phase versus the bubble phase

4.3.5　Maximum dense phase expansion

Figure 4.15 shows the additional dense phase voidage (ε_d-ε_0) for Group C$^+$ particles. The increase of the gas holdup in the dense phase for Group C$^+$ particles were higher than that for Group A particles, especially for the PU series. More specially, the additional dense phase voidage for PU10 particles reached up to 0.25 with a nanoparticle concentration of 0.44%. GB10 and FCC8.5 showed the highest values with nanoparticle concentrations of 0.82%. For FCC20, PU18 and PU36, the effect of the nanoparticle concentrations was less significant. Similar to the dense phase voidage and the dense phase height, for most particles under the operating gas velocities, the additional dense phase voidage increased initially and then remain stable with the increase of gas velocity, indicating that there is a limit for the dense phase expansion.
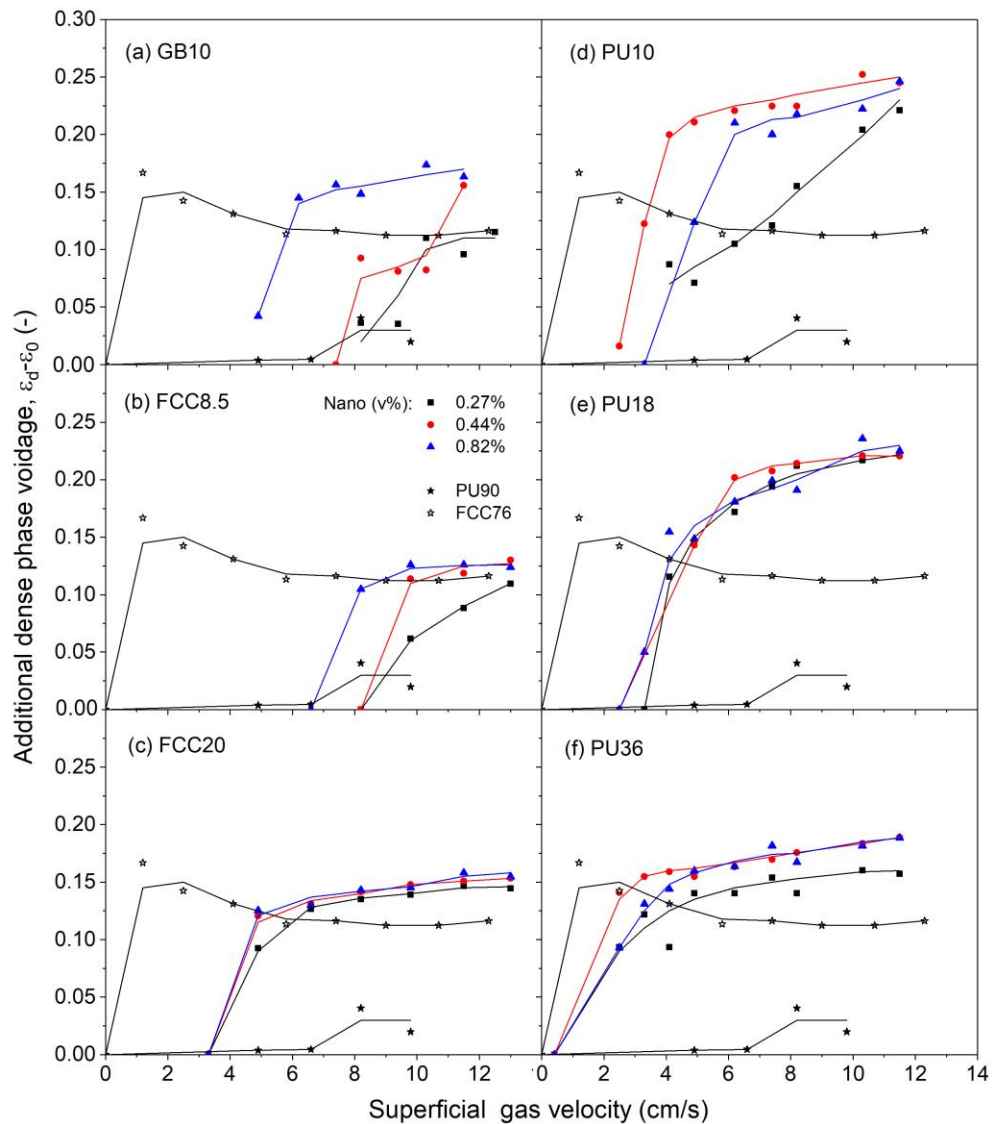
Figure 4.15: The additional dense phase voidage for Group C⁺ particles

Based on the previous results, the dense phase expansion would reach a plateau for most particles as the superficial gas velocity increased. The maximum dense phase expansion for particles of different particle sizes were diverse, which exhibit their potential to retain gas in the dense phase. The larger $E_{d,max}$ indicates a better ability to hold more gas in the dense phase, further signifying better gas-solid contact in the fluidization process. $E_{d,max}$ is calculated as the following equation:

$$E_{d,max} = \frac{H_{d,max} - H_0}{H_0} \qquad (4.3)$$

Figure 4.16 shows the effect of nanoparticle concentration on $E_{d,max}$ of Group C^+ and Group A particles (up to the highest operated gas velocity of 13cm/s). Group C^+ particles showed a much higher $E_{d,max}$ than Group A particles, indicating a stronger ability to perform dense phase expansion. The $E_{d,max}$ value increased as the particle size decreased. For Group C^+ particles, the interparticle forces have been reduced by nanoparticle modulation, which contributes to their good fluidization. When the gas velocity exceeded the minimum fluidization velocity, the bed expanded quickly and reached a high level of bed expansion [14-16]. The insignificant but not negligible interparticle forces of Group C^+ particles help to hold gas in the dense phase, resulting in a high dense phase expansion. For the particles of the same material, the smaller particle size leads to relatively stronger interparticle forces, resulting in the higher dense phase expansion and larger $E_{d,max}$. Conclusively, Group C^+ particles have a larger $E_{d,max}$ and better expansion ability of the dense phase, which can contribute to better gas-solid contact and is an important characteristic for improving gas-phase catalytic reactions.
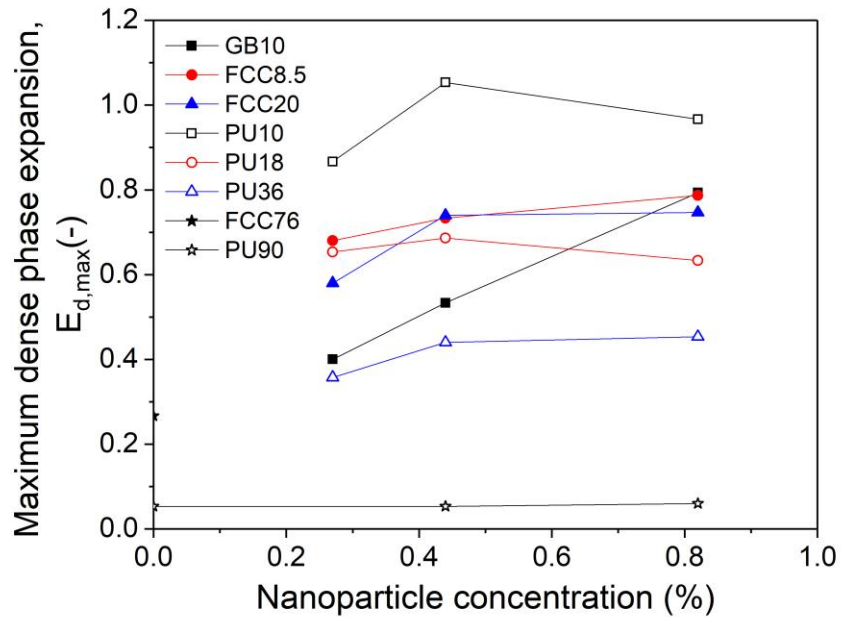
Figure 4.16: The maximum dense phase expansion for Group C⁺ and Group A particles

4.4 Conclusion

Group C^+ particles exhibited much longer bed collapse time and higher dense phase height than Group A particle. The bed collapse curves for Group C^+ particles were curved and those for Group A particles were much more linear. The properties of the dense phase and the bubble phase were clearly characterized using the bed collapse test. Group C^+ particles exhibited a much higher dense phase expansion and larger dense phase voidages than Group A particles, indicating more gas holdup in the dense phase so that gas could closely contact with the particles. The extraordinary dense phase expansion may be due to the proper interparticle forces of Group C^+ particles which could hold more gas in the particle interstices, contributing to better gas-solid contact. Although the bubble holdup for Group C^+ particles was similar or even higher than that for Group A particles, the gas percentage entering the dense phase for Group C^+ particles was much larger than that for Group A particles. In summary, Group C^+ particles with much higher gas holdup in the dense phase contributed to better fluidization quality and therefore improve the gas-solid contact.

The maximum dense phase expansion ($E_{d,max}$) was proposed to evaluate the expansion ability of dense phase for different particles. The larger $E_{d,max}$ values of Group C$^+$ particles indicated better expansion ability of the dense phase and thus contributed to better gas-solid contact. It is suggested that Group C$^+$ particle fluidization with a large specific surface area and an extremely high gas holdup in the dense phase will bring significant improvements on many surface-based processes in industry, especially on gas-phase catalytic reactions.

Nomenclature

D_{10}	Percentage 10% of particles under this particle size (μm)
D_{50}	Percentage 50% of particles under this particle size (μm)
D_{90}	Percentage 90% of particles under this particle size (μm)
H_0	Initial fixed bed height (cm)
H_s	Settled bed height (cm)
H_d	Dense phase height (cm)
H_t	Total fluidized bed height (cm)
t_0	Time when the gas shut off (s)
t_d	Time when hindered sedimentation stage starts (s)
t_c	The collapse time (s)
t_{end}	Time when the collapse process is finished
u_g	Superficial gas velocity (cm/s)
u_{mf}	Minimum fluidization velocity (cm/s)
V_0	Initial fixed bed volume (cm^3)
V_b	Bubble volume (cm^3)
V_d	Dense phase volume (cm^3)
V_t	Total fluidized bed volume (cm^3)
x_b	Bubble holdup (-)
Φ_b	The percentage of gas flowing into bubble phase (-)
Φ_d	The percentage of gas flowing into dense phase (-)
ε_0	Initial fixed bed voidage (-)

$\varepsilon_{\mathrm{mf}}$ Bed voidage at minimum fluidization (-)

ε_{d} Dense phase voidage (-)

ε_{b} Fluidized bed voidage (-)

Reference

[1] Geldart D. Types of gas fluidization. Powder technology, 1973, 7(5): 285-292.

[2] Xie HY, Geldart D. Fluidization of FCC powders in the bubble-free regime: effect of types of gases and temperature. Powder technology, 1995, 82(3):269-77.

[3] Lettieri P, Newton D, Yates JG. Homogeneous bed expansion of FCC catalysts, influence of temperature on the parameters of the Richardson–Zaki equation. Powder Technology, 2002, 123(2-3):221-31.

[4] Yates J G, Newton D. Fine particle effects in a fluidized-bed reactor. Chemical engineering science, 1986, 41(4): 801-806.

[5] Grace J R, Sun G. Influence of particle size distribution on the performance of fluidized bed reactors. The Canadian Journal of Chemical Engineering, 1991, 69(5): 1126-1134.

[6] Yamamoto K, Imaoka T, Chun WJ, Enoki O, Katoh H, Takenaga M, Sonoi A. Size-specific catalytic activity of platinum clusters enhances oxygen reduction reactions. Nature chemistry, 2009, 1(5):397.

[7] Gao X, Tang Z, Zhang H, Ji D, Lu G, Wang Z, Tan Z. Influence of particle size of ZSM-5 on the yield of propylene in fluid catalytic cracking reaction. Journal of Molecular Catalysis A: Chemical, 2010, 325(1-2): 36-39.

[8] Morooka S, Kusakabe K, Kobata A, Kato Y. Fluidization state of ultrafine powders. Journal of Chemical Engineering of Japan, 1988, 21(1):41-6.

[9] Iwadate Y, Horio M. Prediction of agglomerate sizes in bubbling fluidized beds of group C powders. Powder Technology, 1998, 100(2-3):223-36.

[10] Xu C, Zhu J. Experimental and theoretical study on the agglomeration arising from fluidization of cohesive particles—effects of mechanical vibration. Chemical Engineering Science, 2005, 60(23):6529-41.

[11] Zhou T, Li H, Shinohara K. Agglomerating fluidization of group C particles: major factors of coalescence and breakup of agglomerates. Advanced Powder Technology,

2006, 17(2):159-66.

[12] Zhu, J. and H. Zhang. Fluidization Additives to Fine Powders. U.S. Patent 6833185. December 21, 2004.

[13] Xu C, Huang Q, Zhang H, et al. Improving fluidizability of cohesive particles by surface coating with flow conditioners[C]//The Fifth World Congress on Particle Technology Orlando, FL, United States. 2006.

[14] Chen Y, Yang J, Dave R N, et al. Fluidization of coated group C powders. AIChE journal, 2008, 54(1): 104-121.

[15] Han M, Zhou Y, Zhu J. Improvement on flowability and fluidization of Group C particles after nanoparticle modification. Powder Technology, 2019 Jul 8.

[16] Zhou Y, Zhu J. Group C^+ particles: Enhanced flow and fluidization of fine powders with nano-modulation. Chemical Engineering Science, 2019, 207:653-62.

[17] R.D. Toomey, H.F. Johnstone. Gaseous fluidization of solid particles. Chem. Engng Prog., 1952, 48: 220-226.

[18] Davidson J F, Harrison D. The behaviour of a continuously bubbling fluidised bed. Chemical Engineering Science, 1966, 21(9): 731-738.

[19] Lockett M J, Davidson J F, Harrison D. On the two-phase theory of fluidisation. Chemical Engineering Science, 1967, 22(8): 1059-1066.

[20] Pyle D L, Harrison D. An experimental investigation of the two-phase theory of fluidization. Chemical Engineering Science, 1967, 22(9): 1199-1207.

[21] Grace J R, Clift R. On the two-phase theory of fluidization. Chemical Engineering Science, 1974, 29(2): 327-334.

[22] Rowe P N, Santoro L, Yates J G. The division of gas between bubble and interstitial phases in fluidised beds of fine powders. Chemical Engineering Science, 1978, 33(1): 133-140.

[23] Dry R J, Judd M R, Shingles T. Two-phase theory and fine powders. Powder Technology, 1983, 34(2): 213-223.

[24] Barreto G F, Yates J G, Rowe P N. The measurement of emulsion phase voidage in gas fluidized beds of fine powders. Chemical Engineering Science, 1983, 38(3): 345-350.

[25] Barreto G F, Mazza G D, Yates J G. The significance of bed collapse experiments in

the characterization of fluidized beds of fine powders. Chemical engineering science, 1988, 43(11): 3037-3047.

[26] Chavarie C, Grace J R. Performance analysis of a fluidized bed reactor. I. Visible flow behavior. Industrial & Engineering Chemistry Fundamentals, 1975, 14(2): 75-79.

[27] Chavarie C, Grace J R. Performance analysis of a fluidized bed reactor. II. Observed reactor behavior compared with simple two-phase models. Industrial & Engineering Chemistry Fundamentals, 1975, 14(2): 79-86.

[28] Chavarie C, Grace JR. Performance analysis of a fluidized bed reactor. III. Modification and extension of conventional two-phase models. Industrial & Engineering Chemistry Fundamentals, 1975, 14(2):86-91.

[29] Rietema K. Application of mechanical stress theory to fluidization[C]//Proc. Int. Symp. on Fluidization. 1967: 154-163.

[30] Abrahamsen A R, Geldart D. Behaviour of gas-fluidized beds of fine powders part I. Homogeneous expansion. Powder technology, 1980, 26(1): 35-46.two

[31] Abrahamsen A R, Geldart D. Behaviour of gas-fluidized beds of fine powders part II. Voidage of the dense phase in bubbling beds. Powder Technology, 1980, 26(1): 47-55.

[32] Rowe P N, Santoro L, Yates J G. The division of gas between bubble and interstitial phases in fluidised beds of fine powders. Chemical Engineering Science, 1978, 33(1): 133-140.

[33] Baumgarten P K, Pigford R L. Density fluctuations in fluidized beds. AIChE Journal, 1960, 6(1): 115-123.

[34] Dry R J, Judd M R, Shingles T. Two-phase theory and fine powders. Powder Technology, 1983, 34(2): 213-223.

[35] Barreto G F, Yates J G, Rowe P N. The measurement of emulsion phase voidage in gas fluidized beds of fine powders. Chemical Engineering Science, 1983, 38(3): 345-350.

[36] Barreto G F, Mazza G D, Yates J G. The significance of bed collapse experiments in the characterization of fluidized beds of fine powders. Chemical engineering science, 1988, 43(11): 3037-3047.

[37] Lorences M J, Patience G S, Díez F V, et al. Fines effects on collapsing fluidized beds. Powder technology, 2003, 131(2-3): 234-240.

[38] Wang, Chengxiu. High density gas-solids circulating fluidized bed riser and downer reactors. PhD thesis, Western University, Canada, 2013.

[39] Zhu, J.-X. and H. Zhang. Method and Apparatus for Uniformly Dispensing Additive Particles in Fine Powders. U.S. Patent 7240861, 2007.

[40] Geldart D, Harnby N, Wong A C. Fluidization of cohesive powders. Powder Technology, 1984, 37(1): 25-37.

[41] Gelderbloom S J, Gidaspow D, Lyczkowski R W. CFD simulations of bubbling/collapsing fluidized beds for three Geldart groups. AIChE journal, 2003, 49(4): 844-858.

[42] Geldart D, Wong A C Y. Fluidization of powders showing degrees of cohesiveness—II. Experiments on rates of de-aeration. Chemical Engineering Science, 1985, 40(4): 653-661.

[43] Lorences M J, Patience G S, Díez F V, et al. Fines effects on collapsing fluidized beds. Powder technology, 2003, 131(2-3): 234-240.

[44] Huang Q, Zhang H, Zhu J. Flow properties of fine powders in powder coating. Particuology, 2010, 8(1): 19-27.

[45] Ergun S. Fluid flow through packed columns. Chem. Eng. Prog., 1952, 48:89-94.

Chapter 5

5 The Effect of Gas Properties on Group C⁺ Fluidized Bed Reactor

The performance of a fluidized bed reactor depends mostly on the fluidization quality, which can be significantly affected by the gas properties, especially the gas viscosity and density. The effects of gas species on the fluidization properties such as minimum fluidization velocity, bed expansion, dense phase voidage, and pressure fluctuation of three typical types of Group C⁺ (nano-modulated Geldart Group C) particles, were carefully studied using five types of fluidizing gases and their combinations. With the increase of gas viscosity and density, argon possessed the lowest minimum fluidization velocity and the highest dense phase and total bed expansions, followed by air / nitrogen and helium, and trailed by hydrogen. Using two gas mixtures, the gas viscosity was singled out from the gas density and proved to play a more important role on the fluidization due to the increasing gas viscosity causing a more significant increase in the drag force on the particles. The smallest particles, 10μm glass beads, had stronger cohesion than the 17μm and 22μm larger polyurethane particles and therefore exhibited a higher minimum fluidization velocity, lower dense phase and bed expansions, and larger pressure fluctuations.

5.1 Introduction

Generally, the performance of a fluidized bed reactor is determined by the fluidization conditions. A good fluidization may be represented by a lower minimum fluidization velocity, a higher bed expansion, more gas holdup in the dense phase, and less and smaller bubbles etc. The fluidization quality can be affected by many factors, such as gas properties, powder cohesion, other operating conditions, etc. Many researches [1-5] have found that the type of fluidizing gas can significantly affect the fluidization quality, as the hydrodynamic behaviors are mainly influenced by gas viscosity and gas density. For

example, Geldart and Abrahamsen [1] have clearly demonstrated that the bubbling fluidization behaviors of Group A particles is a function of the density and viscosity of the fluidizing gas, and the dense phase voidage (ε_d) increases as gas viscosity and gas density increases.

Except for the gas properties which affect the fluidization quality by changing the hydrodynamic forces, other properties such as powder cohesion will also influence the fluidization quality. Geldart [6] classified particles into type A, B, C and D based on their particle density and particle size. As particle size decreases from Group B to A and further to C, powder cohesion becomes stronger and leads to different fluidization behaviors. Group A particles show better fluidization quality than Group B particles, displaying a more homogeneous fluidization (with smaller bubbles), which is advantageous for many reactors [6-13]. Donsi and Massimilla [14] and Rietema [15] were the first to recognize that the Van der Waals force could influence the stability of fluidization. Many researchers proposed that increasing the cohesion of Group A particles through gas adsorption could increase the bed expansion [2-3,16-18]. Abrahamsen and Geldart [7] have found that increasing the fine fraction (<45 µm) in Group A particles would also improve fluidization, but if the fine fraction continues to increase, eventually it may change the powder into cohesive Group C particles, resulting in poor fluidization.

According to Geldart classification [6], Group C particles are typically small than 30µm and are very cohesive and deemed to be non-flowable and non-fluidizable. On the other hand, Group C particles possess a high specific surface area and other special characteristics that make them uniquely attractive in the chemical industry, especially in gas-phase catalytic reactions where interfacial contact is the key. In recent years, extensive studies have focused on the fluidization of Group C particles in order to respond to industry demands [19-25]. In seeking for methods to reduce the interparticle forces, previous studies [26-30] have demonstrated that nanoparticles could reduce the cohesion of Group C particles and thus improve their flowability and fluidization quality. Chapters 3 and 4 have also shown that Group C^+ particles, which are Group C particles subjected to nanoparticle modulation with "mitigated" cohesion, exhibited much higher bed expansion and dense phase voidage when compared with Group A particles [31,32]. Thus far, few studies about

the influence of gas type on the fluidization quality of Group C^+ particles have been found. Xu and Zhu [22] investigated the effect of gas type and temperature on the fluidization of Group C particles, and found that increasing the gas viscosity by using different gases or by elevating the bed temperature could improve the average bed voidage.

Given the potentially extensive applications of the Group C^+ particles, a comprehensive investigation into the effect of gas type on the fluidization behaviors of these small particles has become necessary or even critical. A systematic study on the fluidization quality of Group C^+ particles with different types of fluidizing gas was carried out in this project. The gas effects with respect to gas viscosity and gas density on the fluidization behaviors have been discussed.

5.2   Experiments

5.2.1   Particulate materials and fluidizing gas

Three types of Group C particles, PU17, PU22 (polyurethane particles with 17μm and 22μm mean in diameter), and GB10 (glass beads with 10μm mean in diameter), were tested in the experiments, with their properties listed in Table 5.1. Figure 5.1 shows the particle size distributions of the three types of Group C particles. Different types of fluidizing gases and their key physical properties are listed in Table 5.2.

Table 5.1: Properties of particulate materials

Powder sample	Material	Particle size (μm)			Particle density kg/m^3	Bulk density kg/m^3	Shape
		D_{10}	D_{50}	D_{90}			
PU17	Polyurethane	4.7	17	40	1200	769	Irregular
PU22	Polyurethane	6.6	22	46	1200	792	Irregular
GB10	Glass beads	1.6	10	28	2500	916	Spherical
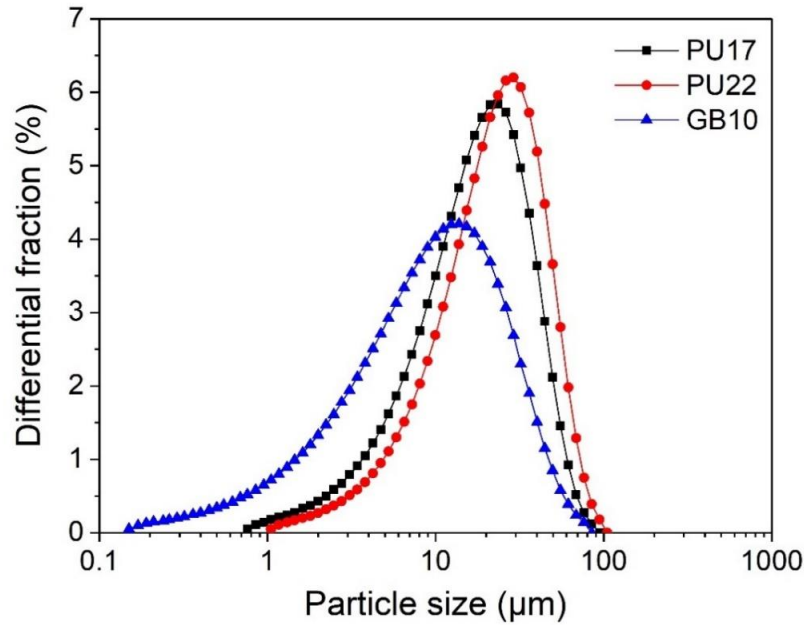
Figure 5.1: Particle size distribution

Table 5.2: Properties of fluidizing gases

Fluidizing gas	Gas viscosity (μPa s)	Gas density (kg/m^3)
Argon (Ar)	22.7	1.633
Medical air (Air)	17.9	1.29
Nitrogen (N_2)	17.8	1.25
Helium (He)	19.9	0.164
Hydrogen (H_2)	8.915	0.084

In order to investigate the relative effects of the gas viscosity and gas density on the fluidization behaviors, two types of mixed gases were used. The gas viscosity of the mixed gas is described in Equation (5.1) [33]:

$$\mu_m = \frac{y_1 \mu_1 M_1^{0.5} + y_2 \mu_2 M_2^{0.5}}{y_1 M_1^{0.5} + y_2 M_2^{0.5}} \qquad (1)$$

where μ_m is the gas viscosity of the mixed gas, y_1, y_2 are the mole fractions of the two gases, μ_1, μ_2 are the gas viscosities, and M_1, M_2 are the relative molecular weights of the two gases. The gas density of the mixed gas is described in Equation (5.2):

$$\rho_m = y_1 \rho_1 + y_2 \rho_2 \qquad (2)$$

where ρ_m is the gas density of the mixed gas and ρ_1, ρ_2 are the gas densities of the two gases.

Two types of mixed gases are obtained by mixing different volume fractions of hydrogen and argon. One mixed gas possesses the same density but a different viscosity from helium. The other has the same viscosity but a different density from the helium. Table 5.3 shows the key properties of the two mixed gases.

Table 5.3: Properties of mixed gases

Fluidizing gas	Volume fraction of H_2	Volume fraction of Ar	Gas viscosity (μPas)	Gas density (kg/m^3)
Mixed gas-1 ($\rho_{M-1} = \rho_{He}$, $\mu_{M-1} < \mu_{He}$)	0.95	0.05	11.54	0.164
Mixed gas-2 ($\rho_{M-1} > \rho_{He}$, $\mu_{M-1} = \mu_{He}$)	0.53	0.47	19.9	0.81
He	-	-	19.9	0.164

5.2.2   Nanoparticle modulation

Group C particles were modulated by nanoparticles with volume fractions of 0.27%, 0.44%, and 0.82% mixed in using the sieving method as described in a published patent by Zhu and Zhang [24,34]. The powder samples were sieved three times using an ultrasonic vibrating screen with a mesh size of 325. The nanoparticles used were SiO_2 with a reported particle size of 16 nm, marketed as AEROSIL R972 (Evonik[TM]). Figure 5.2 shows the surface morphology of GB10 and PU17 with and without nanoparticles using a SEM. After the process of nanoparticle modulation, nanoparticles adhered onto the surface of Group C particles to increase the surface roughness.
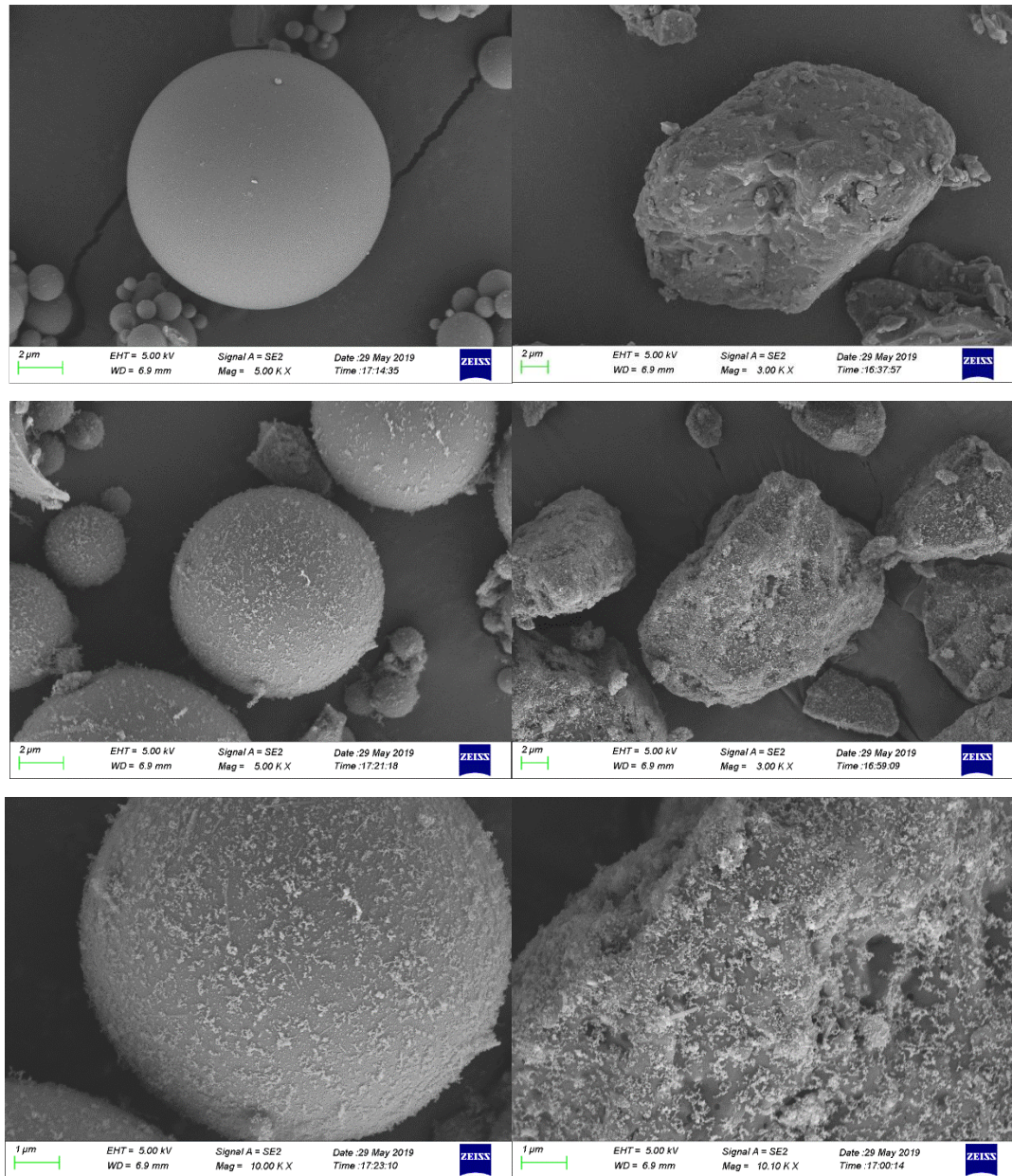
Figure 5.2: SEM images of GB10 (left) and PU17 (right) before and after nanoparticle modulation (0.82%)

5.2.3 Fluidized bed

The fluidization column was made of a plexiglas 9cm in width, 5cm in depth, and 60cm in height, as schematically shown in Figure 5.3. The distributor plate had 137 holes that were 1mm in diameter with an opening area ratio of 2.4%. Two layers of 625 mesh screen

covered the distributor plate to prevent fine particles from dropping into the wind box. The gas flowed through a PVC tube into the wind box from two opposite positions and passed through the distributor to fluidize the particles. Two pressure taps at the bottom just above the distributor and the top measured the pressure drop across the whole particle bed using a differential pressure transducer (Omega PX163 series). The pressure signals were collected by a computer using the LabVIEW DAQ program with a sampling frequency of 1000/s and a sampling time of 5s. The pressure drop across the whole particle bed was averaged from the 5000 values of the pressure signals. The bed expansion ratio (BER) is the ratio of the fluidized bed height (H_t) at operating conditions to the initial fixed bed height (H_0):

$$\text{BER} = H_t / H_0 \qquad (5.3)$$
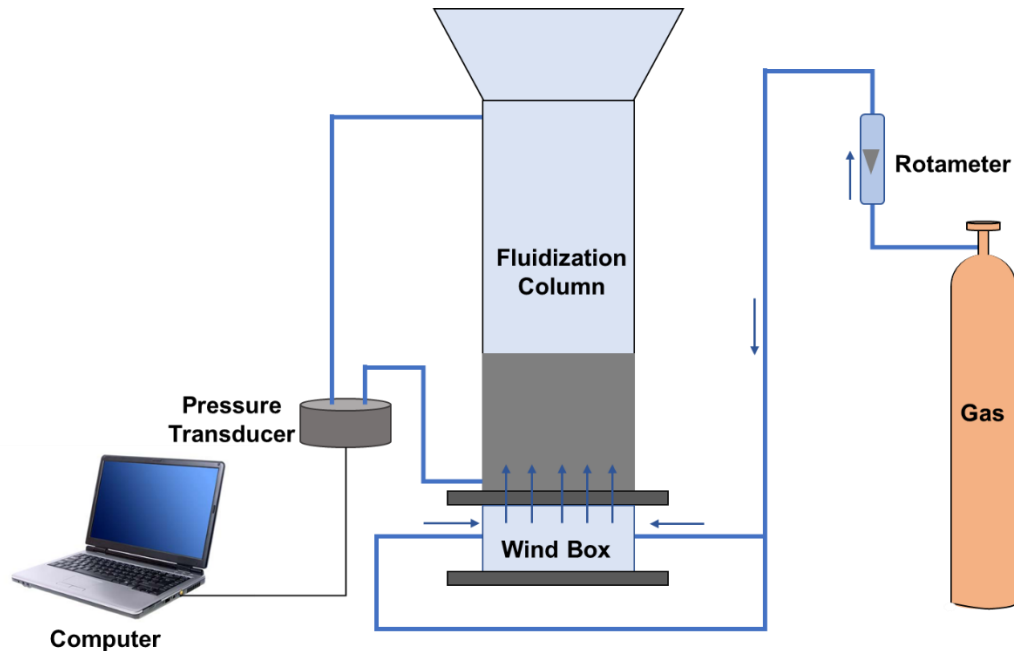
Figure 5.3: Schematic diagram of experimental apparatus

5.2.4 Bed collapse test

A bed collapse test was used to evaluate the dense phase properties. After the fluidize bed was operated at a given gas velocity and presented stable bubbling fluidization, the gas flow was suddenly cut off and the bed height decreased as the gas escaped. The bed collapse process could be divided into three stages: the bubble escape stage, the

sedimentation stage, and the consolidation stage. A typical bed collapse curve, as shown in Figure 5.4, can be used to clearly identify the dense phase and the bubble phase. The dense phase voidage (ε_d) can be calculated using the dense phase height (H_d):

$$\varepsilon_d = 1 - (H_0 / H_d)(1 - \varepsilon_0) \qquad (5.4)$$

where ε_0 is the fixed bed voidage.

The procedures of the bed collapse test included: (1) the bed was fully fluidized at 8.14cm/s; (2) the gas supply was suddenly shut off and the bed began collapsing; (3) the bed height was recorded as a function of time. The whole process was recorded using a digital camera (Canon EOS 800D), and each video was around 40-60s.
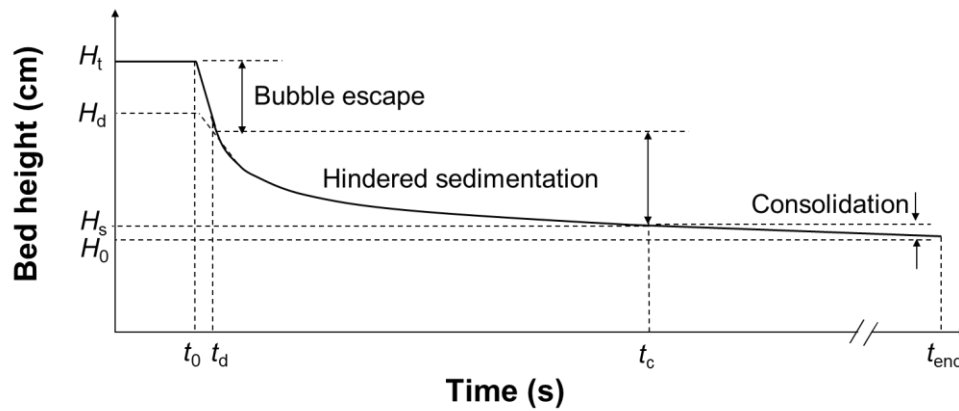
Figure 5.4: A typical bed collapse curve for Group C$^+$ particles

5.3   Results and discussion

5.3.1   The effect of gas types

Figure 5.5 shows the normalized pressure drop and the bed expansion for the three Group C$^+$ particles with a nanoparticle concentration of 0.82% using various fluidizing gases. The three types of Group C$^+$ particles could achieve complete or near-complete fluidization with almost all types of the gases tested, but the bed expansion varied greatly with the types of fluidizing gases. For example, for GB10+0.82%, when argon was used as the fluidizing gas, the bed was able to achieve a relatively high pressure drop (0.9-1), the lowest minimum fluidization velocity, and the largest bed expansion ratio, indicating the best fluidization quality. The use of hydrogen as the fluidizing gas led to the lowest pressure drop and the

lowest bed expansion however, indicating partial fluidization and the relatively poorest fluidization quality. The bed expansion ratio for GB10+0.82% in the various gases from high to low was: argon > air > nitrogen ≈ helium > hydrogen. PU17+0.82% and PU22+0.82% both exhibited higher pressure drops (close to 1) and lower minimum fluidization velocities than GB10 in all types of gases, signifying full and easy fluidization. The bed expansion ratios for PU17+0.82% and PU22+0.82% were the largest in argon and the smallest in hydrogen. Similarly, the fluidization quality for both PU17+0.82% and PU22+0.82% particles was: argon > air > helium > hydrogen.

For all types of fluidizing gases, GB10+0.82% exhibited a poorer fluidization quality when compared with PU17+0.82% and PU22+0.82%. For example, the normalized pressure drop for GB10+0.82% were mostly around to be 0.8-0.9 in the various gases, lower than those for PU particles (around 0.95-1). The highest bed expansion ratio for GB10+0.82% particles was to be around 2.0 with the application of argon, smaller than that for PU particles which could reach up to as high as 2.8. The difference in fluidization behaviors of GB particles and PU particles is mainly attributed to the particle properties: GB10 particles possess a smaller particle size, more spherical shape, and smoother surfaces were more difficult to fluidize due to the stronger cohesion.
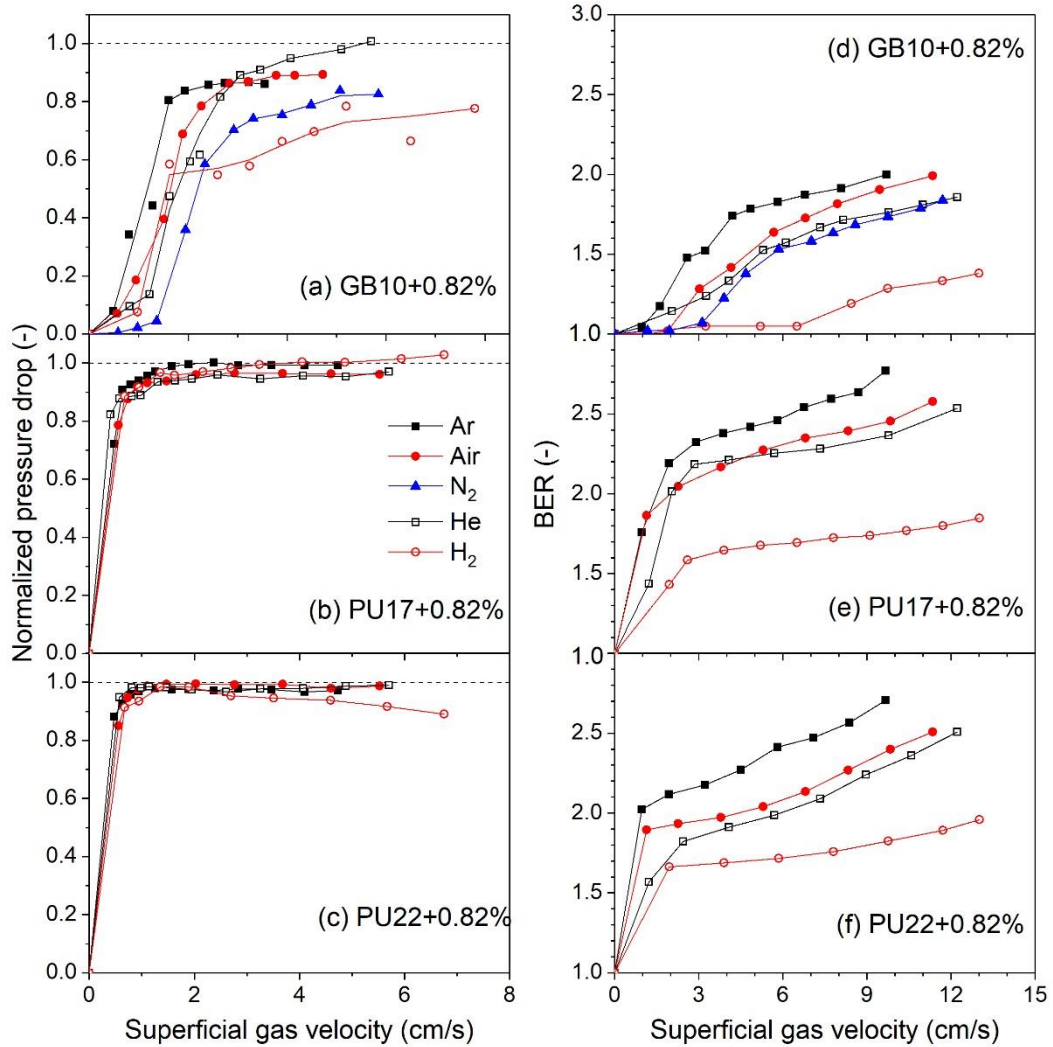
Figure 5.5: The normalized pressure drop and BER for Group C$^+$ particles in varous gases

The effect of nanoparticle concentration on the minimum fluidization velocity and the bed expansion ratio for the two types of PU particles in the various fluidizing gases is shown in Figure 5.6. Overall, the minimum fluidization velocity decreased marginally and the bed expansion increased with the increase of nanoparticle concentration. Such effect of nanoparticle addition appeared to be more evident on PU22 than on PU17, the reason of which is unclear at this moment. For both types of particles, the effect of gas types on the bed expansion was clearer and significant than that on the u_{mf}. The fluidizing gas with a

higher gas density and viscosity such as argon and air contributed to a higher bed expansion, providing an easier fluidization.
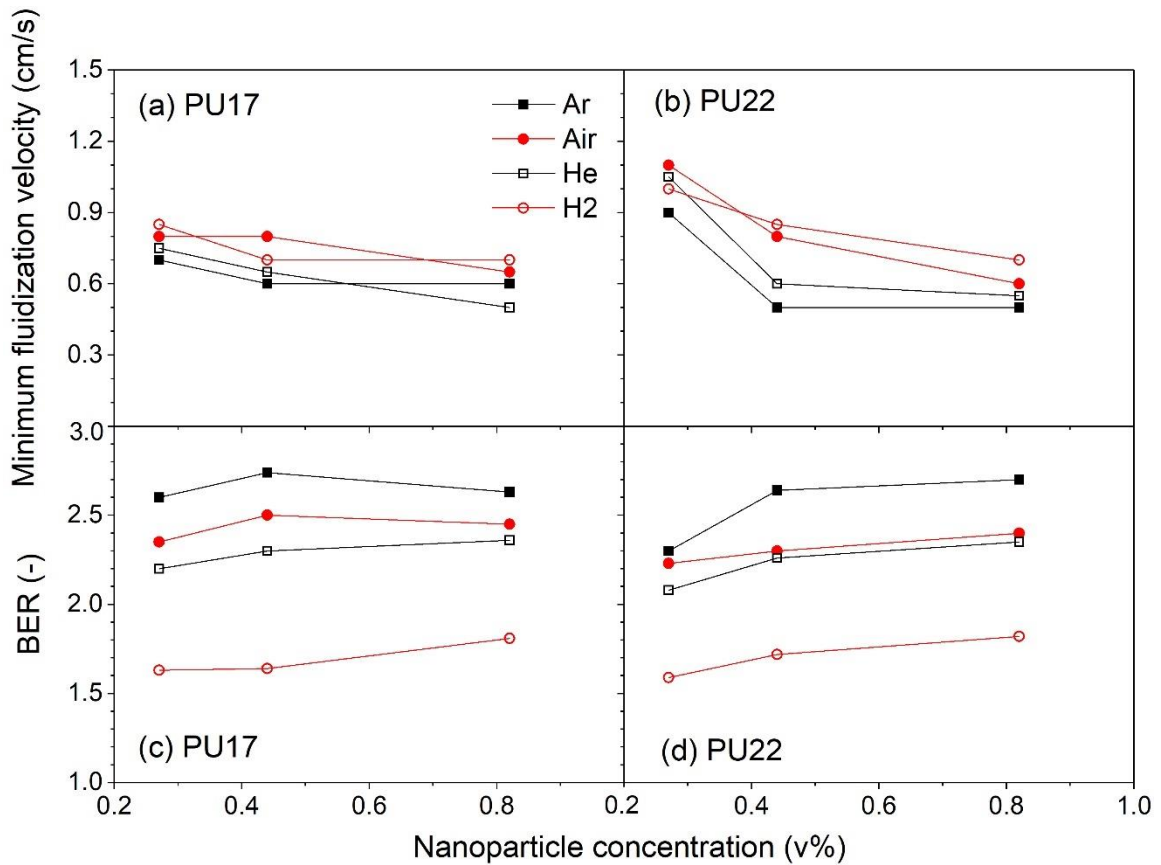
Figure 5.6: The effect of nanoparticle concentration on the u_{mf} and BER (at 10cm/s) for Group C$^+$ particles in various gases

Figure 5.7 shows the bed collapse curves and the heights of the two phases (dense phase and bubble phase) for the Group C$^+$ particles in the various fluidizing gases. Hydrogen led to the shortest collapse time (t_c), the lowest total bed height (H_t), and the lowest dense phase height (H_d). As the gas density and viscosity increased, both the total bed height and the dense phase height increased. The increase of the dense phase height revealed that more gas entered the dense phase and contacted with particles, contributing to better gas-solid contact and fluidization quality. As a result, the fluidization quality of GB10+0.82% in various gases was: argon > air > nitrogen > helium > hydrogen, similar with that of PU particles, which was: argon > air > helium > hydrogen.

In addition, Figures 5.7(e) and 5.7(f) show the effect of nanoparticle concentrations on the bed height for PU particles. The effect on PU22 was more apparent than on PU17. As the nanoparticle concentration increased, the heights of the two phases (dense and bubble) remained almost the same for PU17, while the dense phase height showed a more significant increase for PU22. The increase in the dense phase height for PU22 could improve the gas-solid contact and fluidization quality.
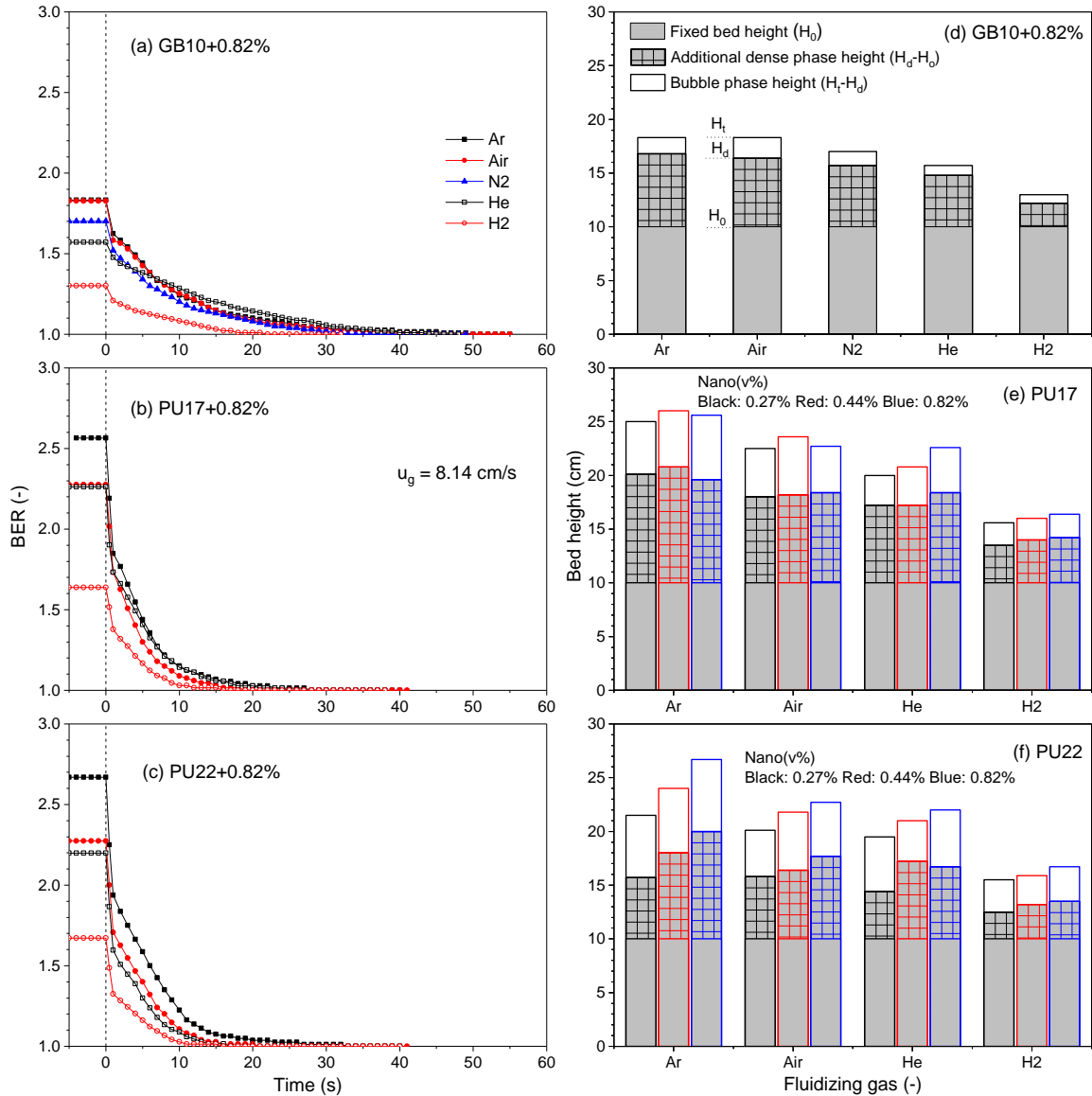
Figure 5.7: The bed collapse curves and the phase heights for Group C[+] particles using various gases

Figure 5.8 shows the dense phase voidage in the Group C⁺ fluidized beds using various fluidizing gases at 8.14 cm/s. As discussed above, good fluidization is associated with a large dense phase voidage, which gives more opportunities for gas to interact with the particles in the dense phase [32,35]. The fluidizing gas with a higher density and viscosity (argon and air) contributed to a larger dense phase voidage, such that: argon > air > (nitrogen) > helium > hydrogen. For the three types of Group C⁺ particles, their dense phase voidage decreased as: GB10 > PU17 > PU22. Particularly, GB10+0.82% showed longer collapse times, lower dense phase heights, but less bubble holdup and larger dense phase voidages in the various gases when compared with PU17+0.82% and PU22+0.82%, due to its stronger cohesion ascribed to the smaller particle size.
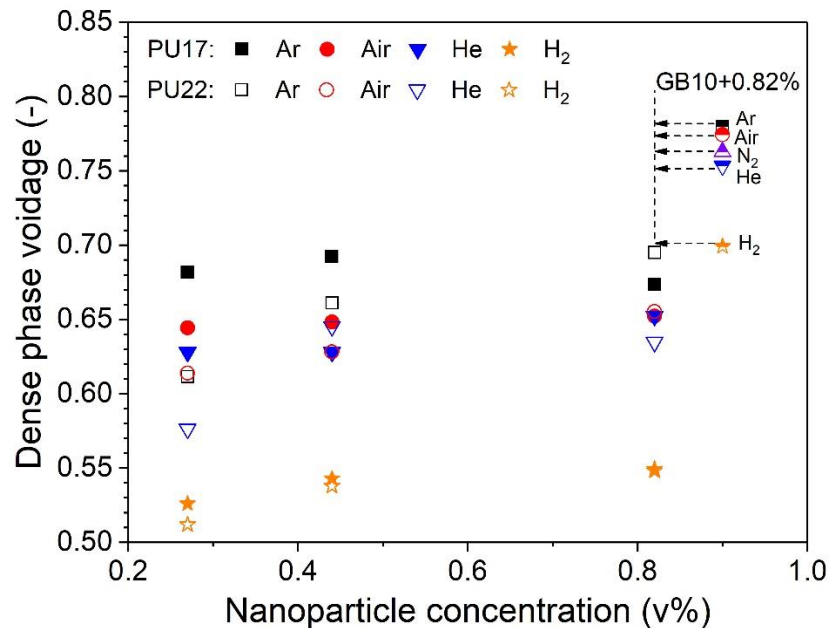
Figure 5.8: The effect of nanoparticle concentration on the dense phase voidage at 8.14 cm/s (the data points for GB10+0.82% off-set for clarity)

Combining the results of the pressure drop, the bed expansion, and the dense phase properties, the fluidization quality for the three types of Group C⁺ particles from good to poor in the various gases is: argon > air > (nitrogen) > helium > hydrogen. Evidently, the fluidization quality was improved as the gas viscosity and/or the gas density increased, as the hydrodynamic forces on particles increases with the increasing of gas viscosity and/or gas density, contributing to "fuller" fluidization and a better fluidization quality.

5.3.2 Theoretical analysis

The above results and discussion clearly demonstrated the important roles played by the viscosity and the density of fluidizing gas in the fluidization of Group C^+ particles. As the gas viscosity and /or gas density increased, so improved the fluidization quality. The extents of the influence of the viscosity and density may be analyzed theoretically:

The fluidization quality is directly related to the hydrodynamic forces exerted on the particles by an up-flowing gas stream. The total force from the gas acting on the bed, F_t, is equal to:

$$F_t = \Delta P \cdot A = \frac{\Delta P}{H} V \qquad (5.5)$$

where ΔP is the pressure drop across the whole bed, A is the cross-sectional area of the bed, H is the height of the fluidized bed, and V is the fluidized bed volume. The average drag force from the gas acting on the individual particles (assumed to be spherical and having identical size), F_D, is:

$$F_D = \frac{F_t}{N} = \frac{\pi d_p^3}{6(1-\varepsilon_b)} \frac{\Delta P}{H} \qquad (5.6)$$

where N is the number of particles, d_p is the mean particle diameter, and ε_b is the bed voidage. According to the Ergun equation [36], the pressure drop ΔP due to gas flow through a packed bed, at incipient fluidization or slightly beyond when the fluidization remains particulate [37], can be expressed as:

$$\frac{\Delta P}{H} = \frac{150(1-\varepsilon_b)^2}{\varepsilon_b^3} \frac{\mu_g u_g}{(\varphi_s d_p)^2} + \frac{1.75(1-\varepsilon_b)}{\varepsilon_b^3} \frac{\rho_g u_g^2}{\varphi_s d_p} \qquad (5.7)$$

where φ_s is the particle sphericity. The first term on the right-hand side in Equation (5.7) represents the pressure drop caused by viscous effects and is dominant at low Reynolds numbers, while the second term is due to inertial forces and is dominant at high Reynolds numbers, which is related to the gas density. If the first term is expressed by $f(\mu_g)$ and the second term by $f(\rho_g)$, the drag force F_D at or just above the incipient fluidization would equal:

$$F_D = \frac{\pi d_p^3}{6(1-\varepsilon_b)} \left[f(\mu_g) + f(\rho_g) \right] \qquad (5.8)$$

Assuming the validity of the above equation can be extended to higher gas velocities in the fine particle fluidization with smaller bubbles, it can then be used to predict the effect of gas types. The above equation clearly shows that both the viscosity and density of the fluidizing gas would positively influence the drag force, which in turn provides more dynamics to suspend the particles and therefore result in a better fluidization quality, including a higher bed expansion and higher dense phase voidage, as well as easier incipient fluidization (i.e., lower minimum fluidization velocity). This further explains, from a theoretical point of view, the effects shown in Figures 5.5-5.8.

5.3.3 The relative importance gas viscosity and density

Equation (5.8) can also illustrate the relative contributions of the two key parameters of the gas, viscosity and density on the fluidization of fine Group C^+ particles. The effects of the viscosity and the density of the fluidizing gas on the drag force may be examined with the calculation of the two functional terms. As shown in Table 5.4, the gas viscosity term is a few magnitudes larger than the density term so that the viscosity contributes much more on the drag force, and therefore has a larger effect on the fluidization quality of such small particles.

Table 5.4: The contributions of gas viscosity and gas density to the drag force

Gas type	$\dfrac{\pi d_p^3}{6(1-\varepsilon_b)}f(\mu_g)$	$\dfrac{\pi d_p^3}{6(1-\varepsilon_b)}f(\rho_g)$	F_D
Argon	1.10E-9	1.83E-12	1.11E-9
Air	9.19E-10	1.50E-12	9.20E-10
Nitrogen	9.85E-10	1.54E-12	9.86E-10
Helium	1.09E-9	2.00E-13	1.09E-10
Hydrogen	7.02E-10	1.52E-13	7.02E-10

Take spherical GB particles as an example: $d_p = 10\mu m$, $\varepsilon_0 = 0.63$, ε_b is the bed voidage at $u_g = 8cm/$

To verify the above theory, experiments were then carried out with two special gas mixtures to test the relative effects of gas viscosity and density. One gas mixture has the same density as helium but possesses a lower viscosity and the other gas mixture has the same viscosity as helium but has a higher density as given in Table 5.3. Those two gas mixtures were used as the fluidizing gases along with helium to experimentally examine the relative importance of gas viscosity and gas density. Figure 5.9 shows the fluidization behaviors of PU22+0.82% fluidized by helium and the two mixed gases. Increasing the gas

viscosity (from Mixed gas-1 to helium) and/or increasing gas density (from helium to Mixed gas-2) both led to a higher bed expansion, higher dense phase volume, and larger dense phase voidage. However, the effect of gas viscosity was much more significant to all the three indicators of fluidization quality, even though the viscosity was increased by 72% and the density is increased by 394%. In other words, gas viscosity played a more important role in determining the fluidization quality.
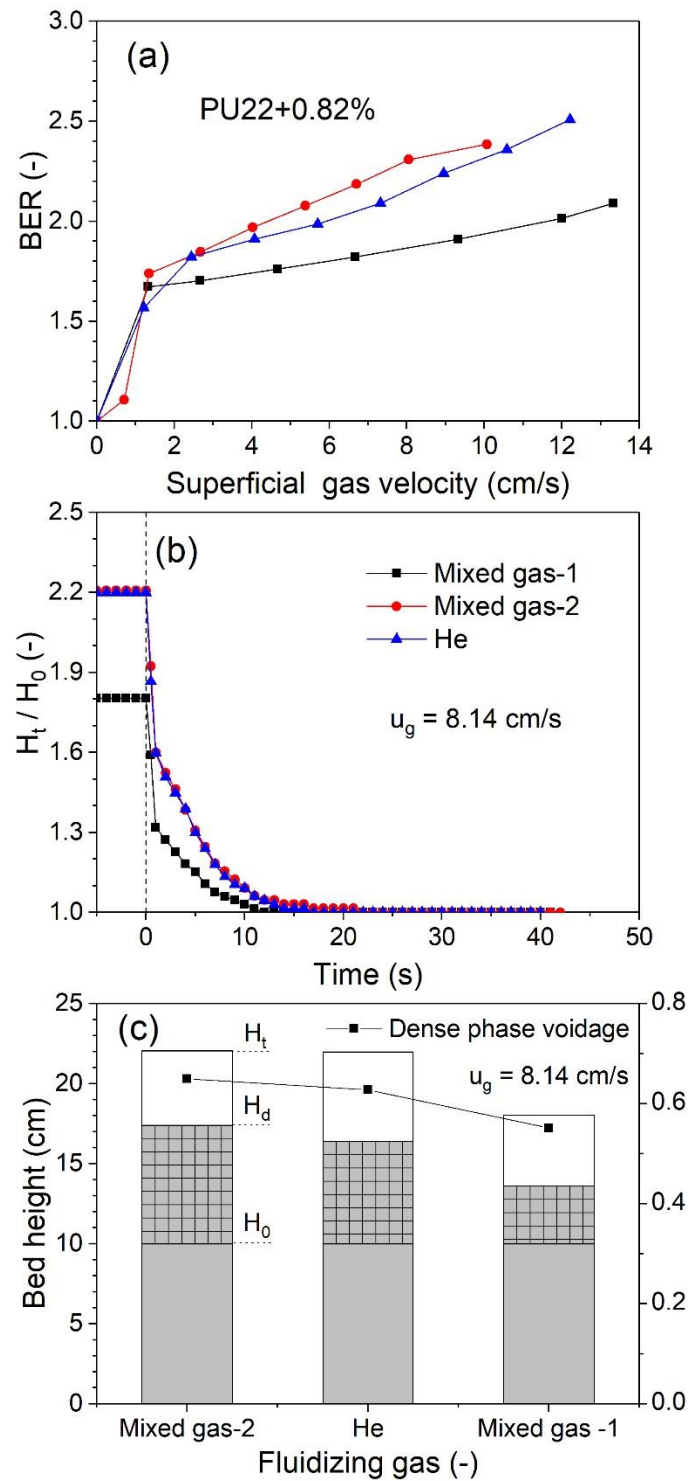
Figure 5.9: The fluidization behaviors of PU22+0.82% in helium and two types of mixed gases

5.3.4   Dimensionless groups

For smaller particles such as Group C[+] particles, the fluidization quality is not only dependent on the hydrodynamic forces, but also affected by the interparticle forces [38-40]. As have been discussed, the hydrodynamic forces are affected by the gas properties, especially the gas viscosity in the fine particle fluidization. As for the interparticle forces, earlier studies [41-44] have reported that introducing a proper level of interparticle forces could increase the dense phase expansion in Group A/B particle fluidization. Some researches illustrated that gas adsorption is a way to control the interparticle forces in fine particle fluidization, but this is significantly affected by the operating temperature and pressure [2,3,15,22], so that it does not apply to this work as the gas adsorption is negligible at a room temperature and pressure [45]. In this work, instead, the interparticle forces of Group C particles were mitigated using nanoparticle modulation. As shown in Figure 5.10, the cohesion of these Group C[+] particles studied here exhibited a reduction in cohesion after nano modulation.
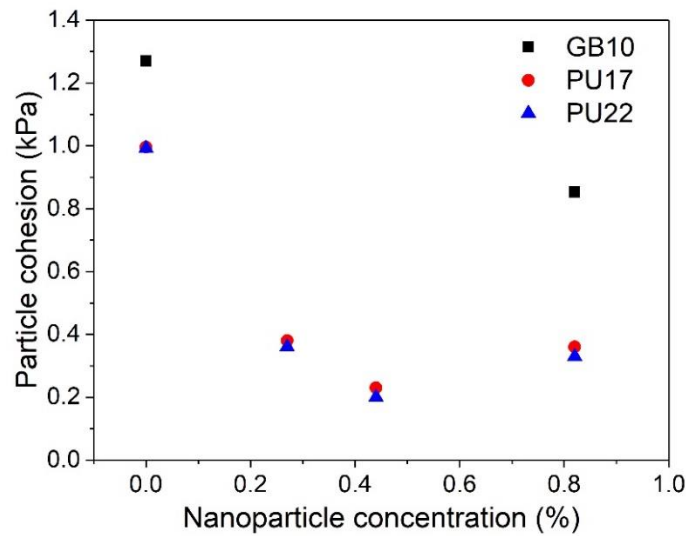
Figure 5.10: Powder cohesion of Group C particles before and after nano-modulation

Other than the gas viscosity and density, the fluidization quality is also dependent on a variety of other factors, such as the particle size and density, the particle cohesion, and the

operating gas velocity etc. In order to correlate those factors, the dimensionless groups are considered given the number of parameters involved. In 1986, John Grace [46] used dimensionless groups to describe the transitions between fluidization regimes. He found that the bed voidage could be written as $\varepsilon_b = f(\rho_g, g, \Delta\rho, \mu_g, d_p, u_g)$ for an ideal gas-solid system where spherical particles of diameter d_p and density ρ_p come in contact with a fluid of density ρ_g and viscosity μ_g in the absence of interparticle forces and wall frictions. Since this equation has seven quantities and three dimensions, Grace has written it in terms of four independent dimensionless quantities:

$$\varepsilon_b = F(\Delta\rho/\rho_g, d_p{}^*, u_g{}^*) \qquad (5.9)$$

where $\Delta\rho = \rho_p\text{-}\rho_g$, $d_p{}^* = d_p(\rho_g\Delta\rho g/\mu_g{}^2)^{1/3}$, $u_g{}^* = u_g(\rho_g{}^2/\mu_g\Delta\rho g)^{1/3}$.

The dimensionless groups $d_p{}^*$ and $u_g{}^*$ are considered as the dimensionless particle diameter and dimensionless superficial velocity respectively. Because the interparticle forces cannot be ignored for the Group C^+ particle system, the dimensionless particle diameter is modified here to consider the effect of the cohesion as particle cohesion tends to cause particle agglomeration:

$$d_p{}^{*\prime} = d_p{}^*\sigma^* \qquad \text{(with cohesion)} \qquad (5.10)$$

where σ^* is the dimensionless cohesion and σ in Pascal is the particle cohesion measured by FT4 test. Since the particle cohesion (σ) depends on the particle size and density and also affects the initial bed voidage, the dimensionless cohesion (σ^*) is a function of these parameters, that is $\sigma^* = f(d_p, \rho_p, \sigma, \varepsilon_0, g) = \dfrac{\sigma\,\varepsilon_0 d_p^2}{d_p^3 \rho_p g} = \dfrac{\sigma\varepsilon_0}{d_p\rho_p g}$.

The dense phase voidage is strongly related to the particle properties, the gas properties, and the gas velocities, so the dense phase voidage can be written as:

$$(\varepsilon_d\text{-}\varepsilon_0)/\varepsilon_0 = f(u_g{}^*/d_p{}^{*\prime}) \qquad (5.11)$$

Figure 5.11 shows the relationship between the dense phase voidage and the dimensionless groups for all types of particles in the fluidized bed with different gases at 8.14 cm/s. Evidently, $(\varepsilon_d\text{-}\varepsilon_0)/\varepsilon_0$ increases as the dimensionless ratio ($u_g{}^*/d_p{}^{*\prime}$) increases, indicating more gas holdup in the dense phase and thus a better fluidization quality. The relationship can be correlated as:

$$(\varepsilon_d\text{-}\varepsilon_0)/\varepsilon_0 = 91.22\,(u_g{}^*/d_p{}^{*\prime})^{0.6239} \qquad (5.12)$$

For a system with given particles and specified gas velocity, the fluidization quality would be further affected by the gas density, the gas viscosity, and the particle cohesion. As shown in Figure 5.11, both a decrease in the dimensionless particle diameter and an increase in dimensionless gas velocity contributed to larger dense phase voidage, consistent with the results in Chapter 4 which concluded that smaller particles with mitigated cohesion could improve the fluidization quality, especially for holding more gas in the dense phase. Conclusively, dimensional analysis is an effective tool to characterize the fluidization quality especially for Group C$^+$ fluidization.

The fitting curve shown: $Y = 91.22\, X^{0.6239}$
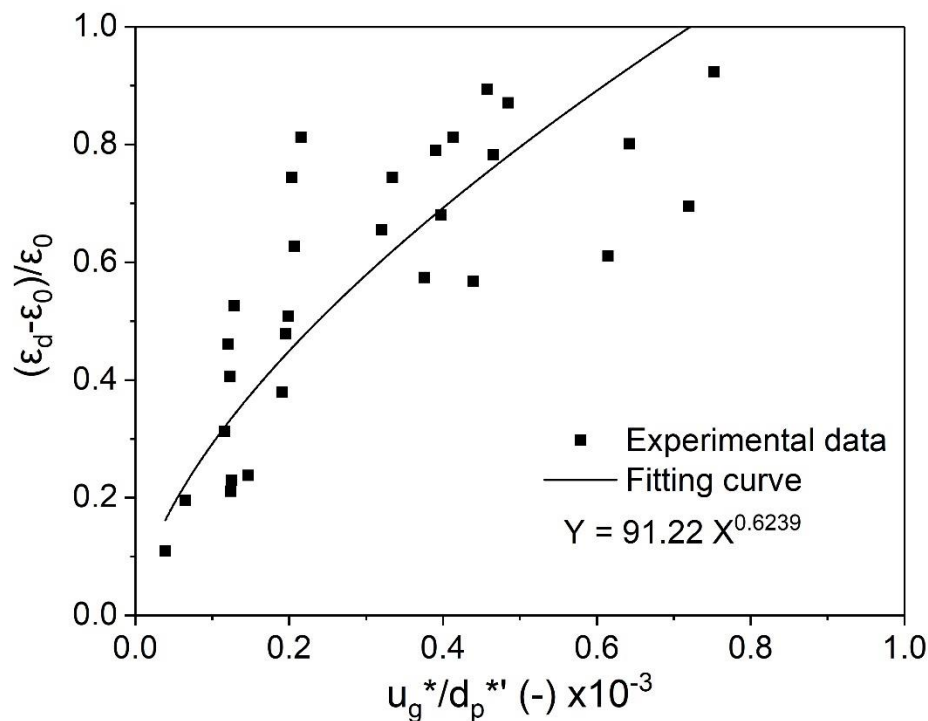
Figure 5.11: The relationship between the dimensionless groups and the dense phase voidage

Figure 5.12 shows the relative effects of the gas viscosity and density in the fluidization of PU22+0.82% based on the dimensionless groups. When the fluidizing gas was changed from helium to Mixed gas-2, the (u_g*/d_p*') was increased by 70% due to the increase of the gas density, contributing to 3% increase of the dense phase voidage. On the other hand, the (u_g*/d_p*') was decreased by 17% due to the decrease of the gas viscosity caused by the change in the fluidizing gas from mixed gas-1 to helium, resulting in a 12% decrease of

the dense phase voidage. Evidently, the gas viscosity plays a more significant role in the fluidization process.
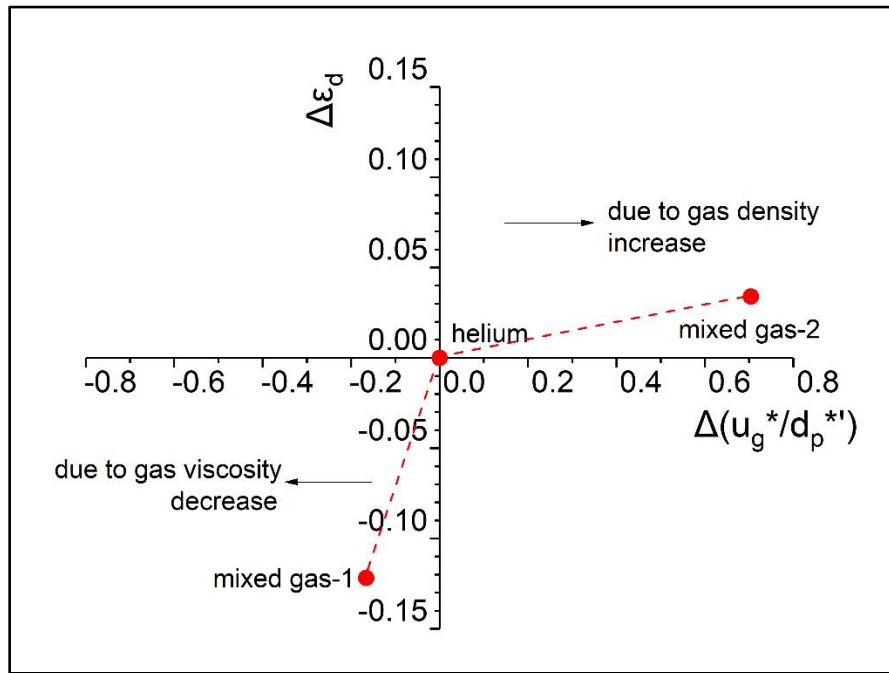
Figure 5.12: The relative importance between gas viscosity and gas density on the dense phase voidage (PU22+0.82% and u_g = 8.14cm/s)

5.3.5   Pressure fluctuations

Pressure fluctuations are usually caused by the motion of bubbles and have been typically used to reflect the fluidization quality [47-50]. The amplitude of the pressure fluctuations is related to both the bed density and the bubble size in the fluidized bed, while the major frequency of the pressure fluctuations is related the bubble frequency [47,48]. Hence, a signal with a low amplitude and high frequency in a fluidized bed usually implies the existence of small bubbles [51-53]. The pressure fluctuation was used to evaluate the fluidization quality and the pressure drop deviation (δ_P) was calculated using the following equation:

$$\delta_P = \frac{\Delta P - \overline{\Delta P}}{\overline{\Delta P}} \qquad (5.13)$$

where ΔP is the measured pressure drop across the whole bed, $\overline{\Delta P}$ is the average pressure drop across the whole bed.

Figures 5.13 and 5.14 show the pressure fluctuations in the fluidized beds of GB10+0.82% and PU22+0.82% using various fluidizing gases, respectively. For GB10+0.82%, the pressure fluctuation exhibited smaller amplitudes and higher frequencies with the application of argon, air, and nitrogen when compared with the use of helium and hydrogen, indicating the presence smaller bubbles and a superior fluidization quality. The fluidization quality of GB10+0.82% in various gases exhibited the sequence: argon > air > nitrogen > helium >hydrogen. For PU22+0.82%, the pressure fluctuations showed the same trend: the smallest amplitude as well as the highest frequency in argon and air, while the largest amplitude as well as the lowest frequency in helium and hydrogen.

PU22+0.82% showed smaller amplitudes and higher frequencies than GB10+0.82% especially in helium and hydrogen, indicating a better fluidization quality. The difference may be ascribed to the particle properties, that GB particles with smaller particle size, wider particle size distribution, and stronger cohesion lead to more difficulties and nonuniformities in fluidization.
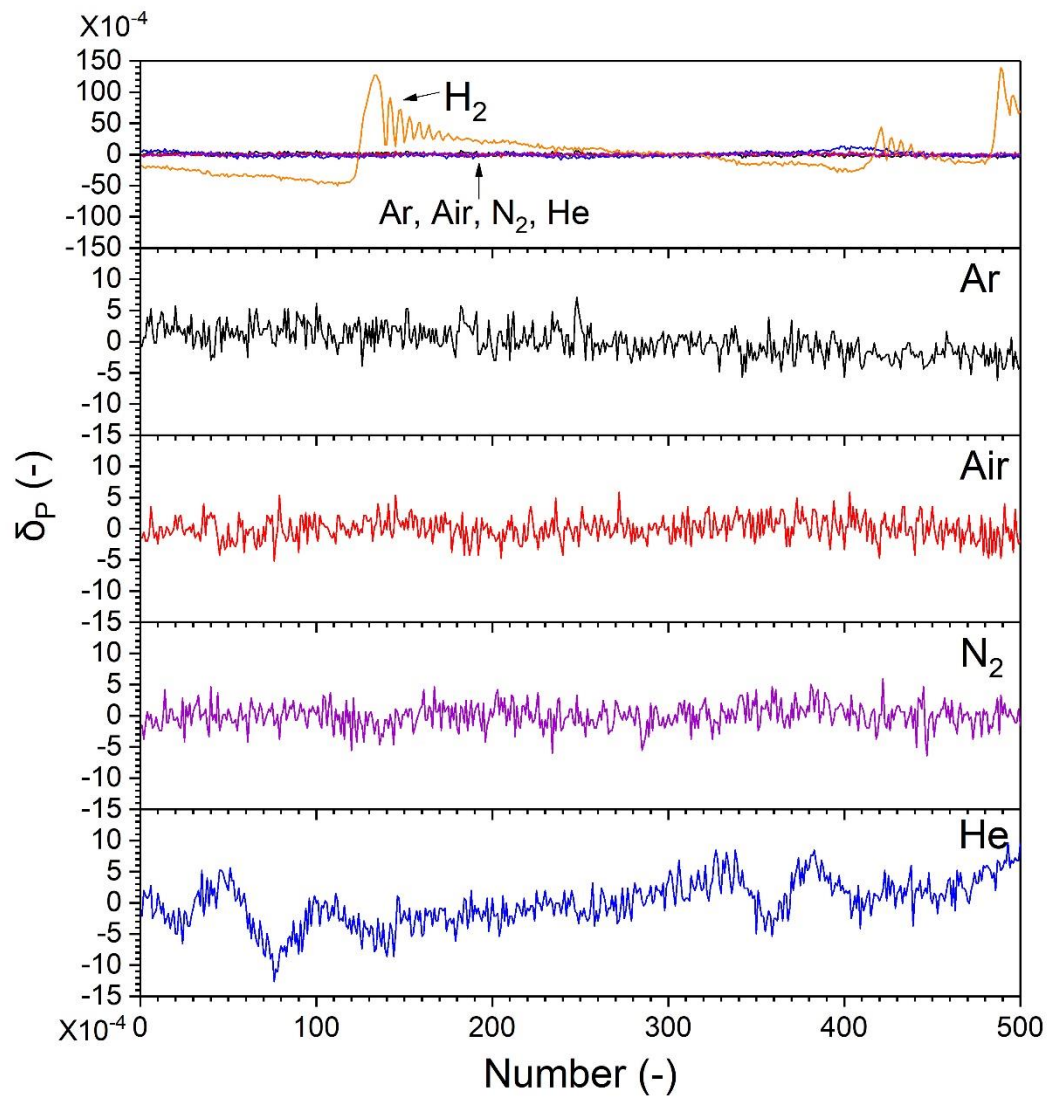
Figure 5.13: Pressure fluctuations for GB10+0.82% at 7.4 cm/s in various fluidizing gases
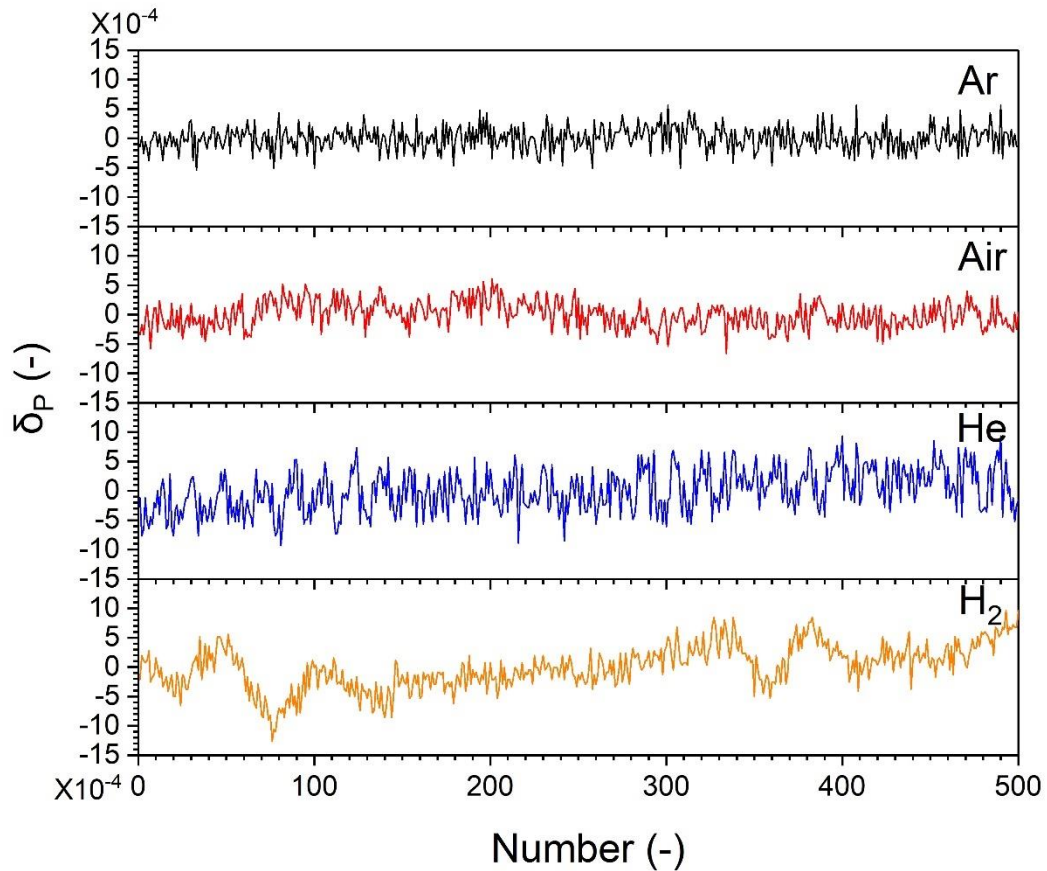
Figure 5.14: Pressure fluctuations for PU22+0.82% at 4.75 cm/s in various fluidizing gases

5.4 Summary and conclusions

The fluidization quality of Group C^+ particles using different types of gas types has been characterized by indicators such as the pressure drop, the bed expansion, the dense phase voidage, and the pressure fluctuation. Considering all these fluidization properties, the fluidization quality in various gases from good to poor exhibited: argon > air > (nitrogen) > helium > hydrogen, with the increase of the gas viscosity and/or the gas density, both of which could enhance the fluidization quality of Group C^+ particles.

Both theoretical and experimental methods were used to evaluate the relative importance of the gas viscosity and density on the fluidization quality. The effect of increasing the gas

viscosity was shown to be more significant than increasing gas density, suggesting that the gas viscosity played a more important role on determining the fluidization quality.

The dimension analysis was an effective method to correlate the fluidization quality with a number of factors such as the gas viscosity and density, the particle size and cohesion, and the gas velocity etc. A larger dense phase voidage with a smaller dimensionless particle diameter and/or higher dimensionless gas velocity provided a higher gas holdup in the dense phase and better gas-solid contact, which is the key for gas-phase catalytic reactions.

Smaller pressure fluctuation was found in argon, air and nitrogen than in helium and hydrogen as fluidizing gases, indicating smaller bubbles and a better fluidization quality. Conclusively, the fluidizing gas with high viscosity and high density could significantly improve the fluidization quality and create a smoother fluidization state.

Nomenclature

A	Cross-sectional area of the fluidized bed (cm^2)
D_{10}	Percentage 10% of particles under this particle size (μm)
D_{50}	Percentage 50% of particles under this particle size (μm)
D_{90}	Percentage 90% of particles under this particle size (μm)
d_p	Particle diameter (μm)
d_p^*	Dimensionless particle diameter (-)
$d_p^{*\prime}$	Dimensionless particle diameter with cohesion (-)
F_t	Total drag force on the bed (N)
F_D	Average drag force on an individual particle (N)
H_0	Initial fixed bed height (cm)
H_d	Dense phase height (cm)
H_t	Total fluidized bed height (cm)
$M_{1,2}$	Relative molecular weight of two gases (-)
N	Number of particles (-)
t_0	Time when the gas shut off (s)
t_d	Time when hindered sedimentation stage starts (s)

t_c	The collapse time (s)
u_g	Superficial gas velocity (cm/s)
u_g*	Dimensionless superficial gas velocity (-)
u_{mf}	Minimum fluidization velocity (cm/s)
V	Fluidized bed volume (cm^3)
$y_{1,2}$	Mole fraction of two gases (-)
$\mu_{1,2}$	Viscosity of two gases (µPa s)
μ_m	Viscosity of mixed gas (µPa s)
μ_g	Gas viscosity (µPa s)
$\rho_{1,2}$	Density of two gases (kg/m^3)
ρ_m	Density of mixed gas (kg/m^3)
ρ_g	Gas density (kg/m^3)
ρ_p	Particle density (kg/m^3)
σ	Particle cohesion (Pa)
$\sigma*$	Dimensionless particle cohesion (-)
ΔP	Pressure drop across the whole bed (Pa)
δ_p	Pressure deviation (-)
φ_s	Particle sphericity (-)
ε_0	Initial fixed bed voidage (-)
ε_d	Dense phase voidage (-)
ε_b	Fluidized bed voidage (-)

Reference

[1]   Geldart D and Abrahamsen AR. Homogeneous fluidization of fine powders using various gases and pressures. Powder Technology. 1978;19(1):133-6.

[2]   Piepers HW, Cottaar EJ, Verkooijen AH, and Rietema K. Effects of pressure and type of gas on particle-particle interaction and the consequences for gas—solid fluidization behaviour. Powder Technology. 1984;37(1):55-70.

[3]   Xie HY. The role of interparticle forces in the fluidization of fine particles. Powder Technology. 1997;94(2):99-108.

[4]   Xie HY and Geldart D. Fluidization of FCC powders in the bubble-free regime:

effect of types of gases and temperature. Powder technology. 1995;82(3):269-77.

[5]   Ye M, van der Hoef MA, and Kuipers JA. The effects of particle and gas properties on the fluidization of Geldart A particles. Chemical Engineering Science. 2005;60(16):4567-80.

[6]   Geldart D. Types of gas fluidization. Powder technology. 1973;7(5):285-92.

[7]   Abrahamsen AR and Geldart D. Behaviour of gas-fluidized beds of fine powders part I. Homogeneous expansion. Powder technology. 1980;26(1):35-46.

[8]   Cody G. Particle fluctuation velocity in gas-fluidized beds. InAPS Division of Fluid Dynamics Meeting Abstracts. 1998.

[9]   Cody GD. Particle Fluctuation Velocity in Gas Fluidized Beds-Fundamental Models Compared to Recent Experimental Data. MRS Online Proceedings Library Archive. 2000;627.

[10]   Menon N and Durian DJ. Particle motions in a gas-fluidized bed of sand. Physical Review Letters. 1997;79(18):3407.

[11]   Tsinontides SC and Jackson R. The mechanics of gas fluidized beds with an interval of stable fluidization. Journal of Fluid Mechanics. 1993; 255:237-74.

[12]   Kobayashi T, Tanaka T, Shimada N, and Kawaguchi T. DEM–CFD analysis of fluidization behavior of Geldart Group A particles using a dynamic adhesion force model. Powder technology. 2013; 248:143-52.

[13]   Cocco R, Shaffer F, Hays R, Karri SR, and Knowlton T. Particle clusters in and above fluidized beds. Powder Technology. 2010; 203(1):3-11.

[14]   Massimilla L and Donsì G. Cohesive forces between particles of fluid-bed catalysts. Powder Technology. 1976;15(2):253-60.

[15]   Rietema, K. and Musters, S.M.P. The effect of interparticle forces on the expansion of a homogeneous gas-fluidized bed. Proc. of the Int. Sym. On Fluid., Toulouse, France, 1973.

[16]   Godard K M and Richardson J F. The behaviour of bubble-free fluidized beds. In Institute of Chemical Engineering Symposium Series 1968; 30:126-135.

[17]   Guedes de Carvalho JR, King DF, and Harrison D. Fluidization of fine particles under pressure. Fluidization. 1978:59.

[18]   Barreto GF, Yates JG, and Rowe PN. The effect of pressure on the flow of gas in

fluidized beds of fine particles. Chemical engineering science. 1983;38(12):1935-45.

[19] Mori S. Vibro-fluidization of group-c particles and its industrial application. In AIChE Symp. Ser. 1990; 86(276):88-94.

[20] Xu C and Zhu J. Experimental and theoretical study on the agglomeration arising from fluidization of cohesive particles—effects of mechanical vibration. Chemical Engineering Science. 2005;60(23):6529-41.

[21] Xu C, Cheng Y and Zhu J. Fluidization of fine particles in a sound field and identification of group C/A particles using acoustic waves. Powder technology. 2006;161(3):227-34.

[22] Xu C and Zhu JX. Effects of gas type and temperature on fine particle fluidization. China Particuology. 2006; 4:114-21.

[23] Luo Y, Zhu J, Ma Y, and Zhang H. Dry coating, a novel coating technology for solid pharmaceutical dosage forms. International journal of pharmaceutics. 2008;358(1-2):16-22.

[24] Zhu J and Zhang H, inventors; University of Western Ontario, assignee. Fluidization additives to fine powders. United States patent US 6,833,185. 2004.

[25] Huang Q, Zhang H and Zhu J. Flow properties of fine powders in powder coating. Particuology. 2010;8(1):19-27.

[26] Zhou, T. and Li, H. Effect of adding different size particles on fluidization of cohesive particles. Powder Technology. 1999;102: 215-220.

[27] Yang J, Sliva A, Banerjee A, Dave RN, and Pfeffer R. Dry particle coating for improving the flowability of cohesive powders. Powder technology. 2005;158(1-3):21-33.

[28] Quintanilla M A S, Valverde J M, and Castellanos A. Adhesion force between fine particles with controlled surface properties. AIChE journal. 2006; 52(5): 1715-1728.

[29] Xu, Chunbao Charles, Hui Zhang, and Jesse Zhu. Improving flowability of cohesive particles by partial coating on the surfaces. The Canadian Journal of Chemical Engineering. 2009; 87(3): 403-414.

[30] Chen Y, Yang J, Dave RN, and Pfeffer R. Fluidization of coated group C powders. AIChE journal. 2008;54(1):104-21.

[31] Zhou Y and Zhu J. Group C+ particles: Enhanced flow and fluidization of fine

powders with nano-modulation. Chemical Engineering Science. 2019; 207:653-62.

[32] Zhou Y and Zhu J. Group C+ particles: Extraordinary dense phase expansion during fluidization through nano-modulation. Chemical Engineering Science. 2020; 214:115420.

[33] M. Asif, Volume-change of mixing at incipient fluidization of binary-solid mixtures: experimental data and predictive models, Powder Technol. 2012;217:361–368.

[34] Zhu, J. and Zhang H. Method and Apparatus for Uniformly Dispensing Additive Particles in Fine Powders. U.S. Patent 7240861, 2007.

[35] Abrahamsen AR and Geldart D. Behaviour of gas-fluidized beds of fine powders part II. Voidage of the dense phase in bubbling beds. Powder Technology. 1980; 26(1):47-55.

[36] Ergun S. Fluid flow through packed columns. Chem. Eng. Prog. 1952;48:89-94.

[37] Leva M, Shirai T, and Wen CY. Prediction of onset fluidization in beds of granular Solids. Génie chimique. 1956;75(2):33.

[38] Mutsers SM and Rietema K. The effect of interparticle forces on the expansion of a homogeneous gas-fluidized bed. Powder Technology. 1977;18(2):239-48.

[39] Raganati F, Chirone R, and Ammendola P. Effect of temperature on fluidization of Geldart's group A and C powders: role of interparticle forces. Industrial & Engineering Chemistry Research. 2017;56(44):12811-21.

[40] Lettieri P, Yates JG, and Newton D. The influence of interparticle forces on the fluidization behaviour of some industrial materials at high temperature. Powder Technology. 2000;110(1-2):117-27.

[41] Dry RJ, Judd MR, and Shingles T. Two-phase theory and fine powders. Powder Technology. 1983;34(2):213-23.

[42] Lorences MJ, Patience GS, Díez FV, and Coca J. Fines effects on collapsing fluidized beds. Powder technology. 2003;131(2-3):234-40.

[43] Grace JR and Sun G. Influence of particle size distribution on the performance of fluidized bed reactors. The Canadian Journal of Chemical Engineering. 1991;69(5):1126-34.

[44] Ma J, Liu D, and Chen X. Bubble behaviors of large cohesive particles in a 2D fluidized bed. Industrial & Engineering Chemistry Research. 2016;55(3):624-34.

[45] Cottaar EJ and Rietema K. A theoretical study on the influence of gas adsorption on interparticle forces in powders. Journal of colloid and interface science. 1986;109(1):249-60.

[46] Grace JR. Contacting modes and behaviour classification of gas—solid and other two-phase suspensions. The Canadian Journal of Chemical Engineering. 1986;64(3):353-63.

[47] Baskakov AP, Tuponogov VG, and Filippovsky NF. A study of pressure fluctuations in a bubbling fluidized bed. Powder Technology. 1986;45(2):113-7.

[48] Bi HT. A critical review of the complex pressure fluctuation phenomenon in gas–solids fluidized beds. Chemical Engineering Science. 2007;62(13):3473-93.

[49] Fan LT, Ho TC, Hiraoka SP, and Walawender WP. Pressure fluctuations in a fluidized bed. AIChE Journal. 1981;27(3):388-96.

[50] Bailie R, Fan LT, and Stewart J. Uniformity and stability of fluidized beds. Industrial & Engineering Chemistry. 1961;53(7):567-9.

[51] Kang WK, Sutherland JP, and Osberg GL. Pressure fluctuations in a fluidized bed with and without screen cylindrical packings. Industrial & Engineering Chemistry Fundamentals. 1967;6(4):499-504.

[52] Jin, Y., Yu, Z.Q., Wang, Z.W., and Cai, P. A criterion for transition from bubbling to turbulent fluidization. In: Ostergaard, K., Sorensen, A. (Eds.), Fluidization V. Engineering Foundation, New York, 1986: 289–296.

[53] Cai, P. The transition of flow regime in dense phase gas–solid fluidized bed. Ph.D. Thesis, Tsinghua University, Beijing, China, 1989.

Chapter 6

6 Different Bubble Behaviors in Gas-Solid Fluidized Bed of Geldart Group A and Group C$^+$ Particles

(A version of this chapter was submitted to AIChE Journal)

A gas-solid fluidized bed reactor composed of Geldart Group C fine powers with the addition of nano-additives (Group C$^+$) has recently been shown to have higher reaction conversion and better performance than the same reactor composed of Geldart Group A particles, due to the increased gas holdup in the dense phase and the increased gas-solid interfacial area. Based on our earlier finding that significantly smaller bubbles were also observed in such Group C$^+$ particle fluidized bed, the bubbling behavior is fully characterized in this work using bubble position, diameter, rise velocity and residence time. The results showed that bubbles were smaller in diameter, lower in rise velocity, and had a longer residence time in the Group C$^+$ fluidized bed in comparison with the same bed using Geldart Group A particles, all contributing to better fluidization quality and enhanced gas-solid contact, thus improving reaction performance.

6.1 Introduction

Gas-solid fluidized beds are widely employed in industrial operations as gas-solid contactors and chemical reactors, ranging from physical processes, such as gas adsorption, drying and mixing of particles, to chemical processes, such as catalytic cracking, combustion and biomass gasification [1-7]. The excellent mass and heat transfers have led to the success of many processes adopting fluidized beds. Generally, a good gas-solid fluidized bed reactor operated in conventional fluidization regimes is expected to provide large gas-solid contact area, small bubbles, and high rate of solids mixing. In most applications, the performance of gas-solid fluidized bed reactors mainly relies on the fluidization hydrodynamics, closely related to the particle properties and the operating conditions [8-10].

A milestone work in the field of fluidization was Geldart classification [11], which classified powders into four groups, Groups A, B, C and D, based on their fluidization

behavior in air at ambient conditions. In most fluidized bed catalytic reactors, Geldart Group A particles are most commonly used as catalysts, as they have a large specific surface area and exhibit good fluidization qualities with more homogeneous bed expansion and smaller bubbles than those for Group B particles, with the latter exhibiting typical bubbling fluidization with little bed expansion. Following this trend, smaller Geldart Group C particles with an even larger specific surface area would be expected to perform even better as catalysts than Group A particles. However, their practical applications in fluidization processes have been severely hindered due to the cohesive nature of Group C particles [12-14]. People have done many studies that looked to improve the flow and fluidization of Group C particles, such as using mechanical vibration [15,16], acoustic vibration [17,18], the addition of magnetic or electrical fields [19,20], and adding coarser or finer particles [21,22]. The addition of finer "guest" particles is more convenient and easier to implement than other methods which are scale- dependent. The added guest particles act as spacers [14] or lubricants [23] to reduce the interparticle forces or friction between the host particles, or even turn the cohesive host particles into free-flowing powders [24-26]. In particular, the addition of nanoparticles, referred to as the "nano-modulation" technique [24], can significantly reduce the cohesion of Group C particles and improve their flowability and especially the fluidization quality [27-30]. These Geldart Group C particles modified using nano-modulation, referred to as Group C^+ particles, exhibited much higher gas holdup in the dense phase than Group A particles, implying more gas is in close contact with the particles. Furthermore, reactor performance of the fluidized bed composed of Group C^+ particles was found to be significantly improved when compared with the same bed composed of Geldart Group A particles using ozone decomposition. The higher dense phase expansion and the larger surface area of catalysts contributed to the much higher reaction conversion and better gas-solid contact in the reactor of Group C^+ particles.

Another factor affecting the reactor performance is bubble size, as smaller bubbles improve gas-solid contact. Chapters 3-5 have extensively studied the hydrodynamics in a 3-D fluidized bed composed of Group C^+ particles, such as the bed expansion and the dense phase voidage, and the effects of gas properties. However, the 3-D bed did not allow us to

comprehensively study bubble behaviors. The purpose of this work is to systematically investigate the bubbling behaviors in a 2-D fluidized bed composed of Group C$^+$ particles.

In general, gas bubbles rise up through a typical bubbling fluidized bed, coalesce with other bubbles, and break up intermittently, thus enhancing mass and heat transfer [31-33]. In particular, the bubbling behaviors, such as bubble size and rise velocity, greatly affect the gas residence time and the gas-solid contact, subsequently influencing reactor performance. Ideally, bubbles in a fluidize bed reactor should be small in size, uniformly distributed throughout the bed, and have low rise velocities [36-40]. Extensive studies [34,35,41-51] on bubble behaviors of typical Geldart Group A, B, and D powders (30-2600μm) have shown that bubbles are usually smaller in beds of finer particles. However, few detailed studies are found about bubble behaviors of Geldart Group C particles, which are expected to have even smaller bubbles. Recently, Zou et al. [52] have investigated bubble behaviors in a fluidized bed with cohesive Group C particles, and smaller bubbles were observed than that with Group A or B particles. With the increased interfacial gas-solid contact area, the fluidized bed of Group C$^+$ particles are more attractive for gas-phase catalytic reactions.

In this work, bubble behaviors for Group C$^+$ particles were investigated in a 2-D fluidized bed via image analysis techniques, including bubble positions, diameters, and rise velocities. Similar behaviors were also characterized in the same bed of Geldart Group A particles for comparison.

6.2 Experimental

6.2.1 Particulate materials

Two types of Group C$^+$ particles, GB10+ and FCC8.5+, and one type of Group A particles, FCC76, were used in this project with their properties listed in Table 6.1. The materials of these particles are glass beads (GB) and fluid catalytic cracking (FCC) catalysts. The nanoparticles used in these experiments were AEROSIL R972, a type of fumed silica particles with a reported size of 16nm, a material density of 2200kg/m^3, and an approximate bulk density of 50kg/m^3. A small amount of silica particles were mixed with Group C particles using an ultrasonic vibrating method [53], referred to as nanoparticle modulation

[15]. The volume fraction of nanoparticles mixed into the Group C particles was 0.82% (mass fraction: 0.72% for GB10 and 1.01% for FCC8.5). The added nanoparticles adhered on the surface of Group C particles to increase the surface roughness, reducing the interparticle forces, as shown in Figure 6.1.
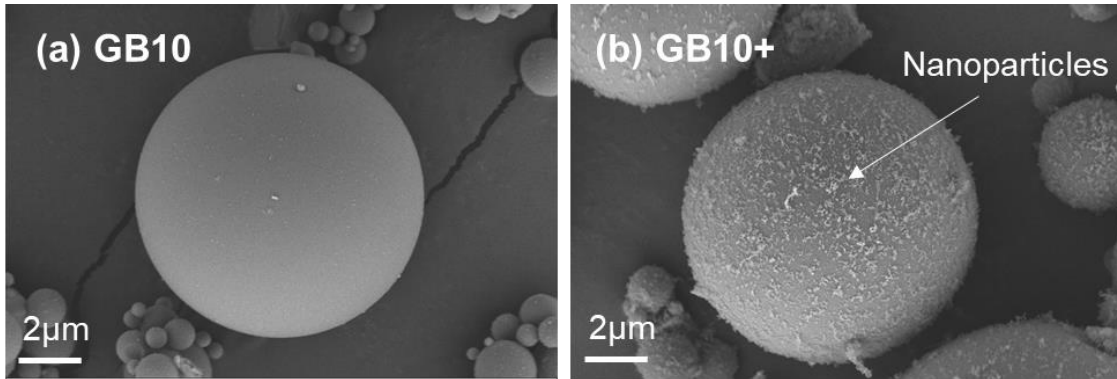
Figure 6.1: Surface morphology of Group C particles before and after nano-modulation

Table 6.1: Properties of adopted bed particles

Powder name	Material	Particle size (µm)			Particle density (kg/m^3)	Loose bulk density (kg/m^3)	Classification
		D_{10}	D_{50}	D_{90}			
GB10+	Glass beads with R972	1.6	10	29	2500	916	Group C$^+$
FCC8.5+	FCC catalysts with R972	1.5	8.5	26	1780	509	Group C$^+$
FCC76	FCC catalysts	30	76	140	1780	874	Geldart Group A

6.2.2   2-D fluidized bed reactor

The drawing of a 2-D fluidized bed is schematically shown in Figure 6.2a, the 2-D fluidization column was made of Plexiglas with a dimension of 100cm (height)×10.5cm (width)×1cm (depth), allowing direct and visible observation of bubble behaviors. A distributor plate with an opening rate of 1.4%, which was a plastic plate with 19 holes of 1mm in diameter, was placed between the fluidization column and the windbox. Three

layers of filter cloth with a 625 mesh covered the distributor plate to prevent fine particles from dropping into the wind box.

Air at ambient conditions was used as the fluidizing gas, and the flow rate was measured by a flowmeter, covering the range from 0 to 16l/min. All experiments were conducted at room temperature. The particles filled up to a bed height of 26cm (H_0) and gave a weight of 250g for GB10+, 140g for FCC8.5+, and 240g for FCC76. The minimum fluidization velocities (u_{mf}) of GB10+, FCC8.5+ and FCC76 were experimentally determined to be 6.5cm/s, 10cm/s and 0.5cm/s, respectively. The operating gas velocities reached up to 25.5cm/s.

A commercial digital camera (Canon EOS 800D) was placed in front of the bed to record the fluidization process, as shown in Figure 6.2b. Two lamps were placed at two fixed positions behind the bed to increase the contrast between the bubbles and the particles and to avoid the bright spot in the video footage. The camera viewed the whole fluidized column to allow a full field analysis of the bubble dynamics. To prevent any shading and reflections from the surrounding environment, the whole apparatus was enclosed by black boards.
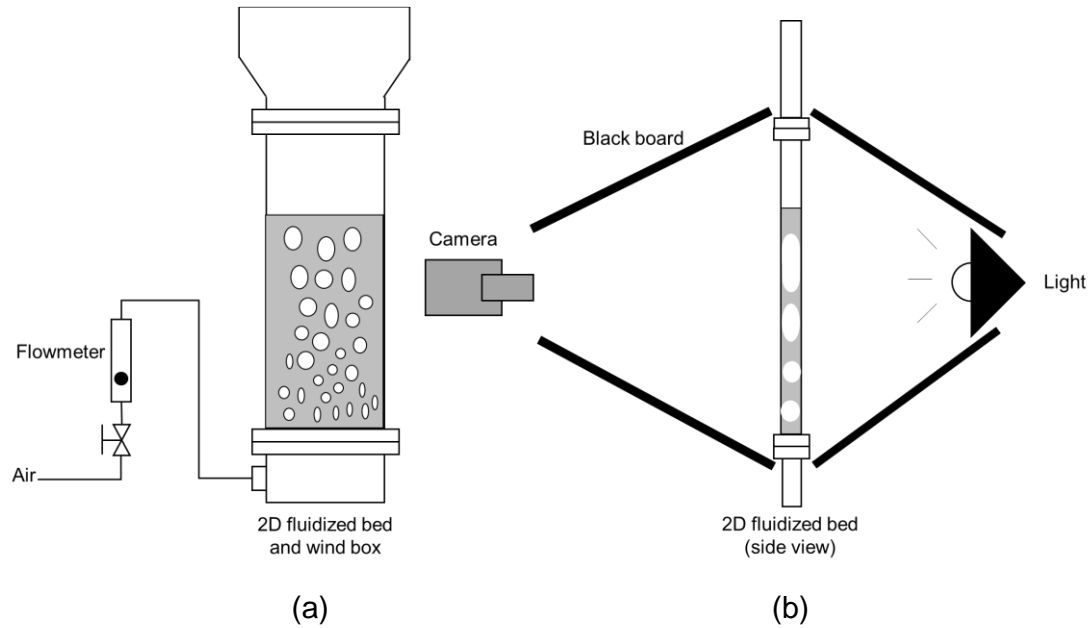
Figure 6.2: Schematic representation of experimental set-up: (a) front view; (b) side view

6.2.3 Image processing

The image processing routine was developed on Adobe Photoshop CS6 (The Adobe company) and Matlab R2018b (The MathWorks inc.). The camera recorded video clips at a frequency of 50Hz and 10s each. Each video was transferred into images frame by frame, equal to 500 pictures. The RGB images were cropped to allow for the analysis of the fluidized bed only, and were then converted into greyscale and the subsequent binary ones with a threshold value (δ) chosen using the Ostu thresholding method [54,55]. All pixels with a gray-value larger than the threshold represent the bubble phase and are coloured white; all with a smaller value represent the dense phase and made black. A threshold value of around 60 could be selected by combining the Otsu thresholding method and visual observation, good for discriminating the bubble boundaries. Figure 6.3 shows the grayscale image and the corresponding binary ones with different threshold values ranging from 50 to 70, and the threshold value within a small range has minimal influence on the bubble information.
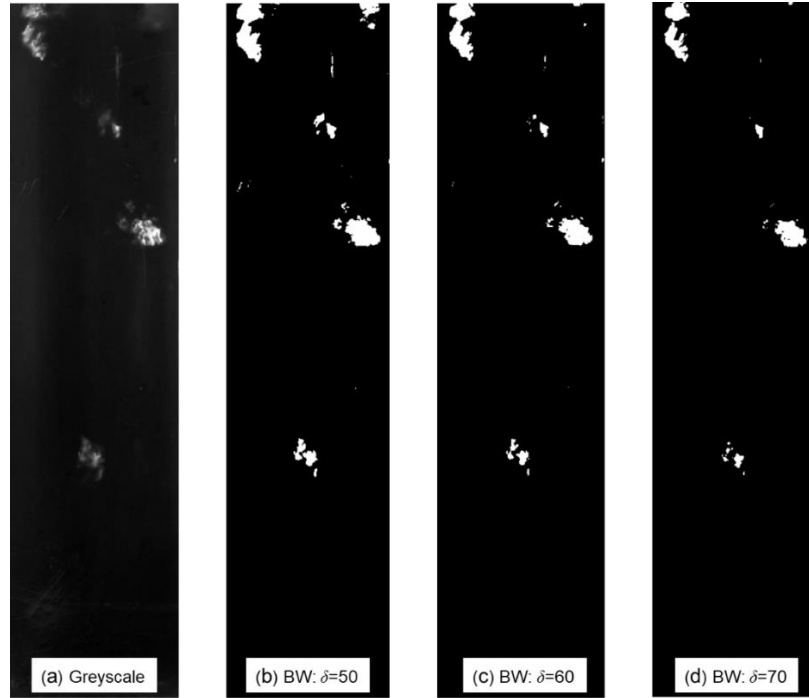
Figure 6.3: Example of a grayscale image to binary ones with different threshold values (fluidized bed of GB10+ particles at u_g-u_{mf} = 9cm/s)

6.2.4 Bubble diameter and bubble rise velocity

An area equivalent diameter (d_b) was obtained for each bubble using a function called Regionprops in Matlab, calculated as follows:

$$d_b = \sqrt{\frac{4A_b}{\pi}} \qquad (6.1)$$

where A_b is the bubble area. Frames at $\Delta t = 0.1$s were used to analyze bubble positions and diameters. Since the bed depth was 1cm, the bubbles with diameters smaller than 1cm could not be recognized accurately. However, small bubbles (<1cm) account for a large proportion of the overall population in the fluidized bed of fine particles. To make a compromise, the bubble diameter being analyzed started from 0.5cm (as shown in Appendix). D10, D50, and D90 represent the bubble diameters which comprise of 10%, 50%, and 90% of the sum of the bubble area. D50 is the medium bubble diameter.

Bubble rise velocity (u_b) was obtained by tracking several consecutive frames ($\Delta t = 0.02$s) and comparing bubble centroid positions, as illustrated in Figure 6.4. For each video, all

500 frames were analyzed, and on average, the bubble rise velocity could be tracked in 200 to 300 frames:

$$u_b = \frac{y_c(t+\Delta t) - y_c(t)}{\Delta t} \qquad (6.2)$$

The velocity was attributed to the mean vertical position according to:

$$h = \frac{y_c(t+\Delta t) - y_c(t)}{2} \qquad (6.3)$$
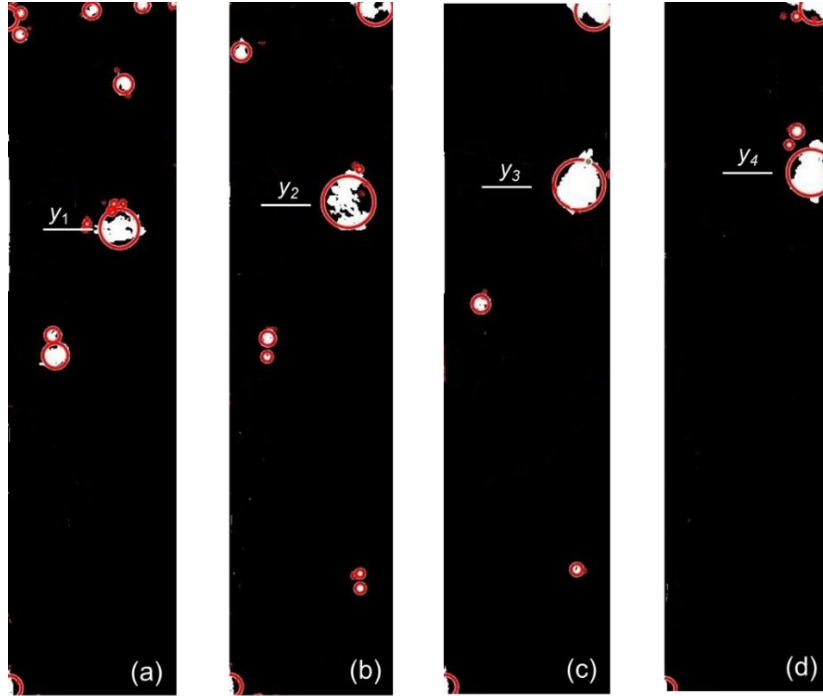
Figure 6.4: Consecutive frames with a bubble marked at different positions ($\Delta t = 0.02$s, fluidized bed of GB10+ particles at $u_g\text{-}u_{mf} = 9$cm/s)

6.3   Results and discussion

6.3.1   Bubble distribution

Figures 6.5a, b, and c illustrate fluidized beds composed of the three types of particles with $H_0 = 26$cm. It is clear that bubbles in fluidized beds composed of Group C^+ particles (FCC8.5+ and GB10+) were smaller in diameter than those observed in the same bed composed of Group A particles (FCC76). The bed of Group C^+ particles expanded more significantly than the bed of Group A particles (Figure 6.5d), as we have observed in a 3-D fluidized bed before. The smaller bubbles and higher bed expansion in the fluidized bed

composed of Group C$^+$ particles indicated more gas holdup in the dense phase which could improve gas-solid contact, and were expected to prompt a better performance of a catalytic gas-solid fluidized bed reactor. Two types of Group C$^+$ particles were tested here, with FCC 8.5+ particles have a lower density, rougher surface, lower cohesion, and are easier to be fluidized than GB10+ particles. As such, FCC8.5+ showed a higher bed expansion than GB10+.
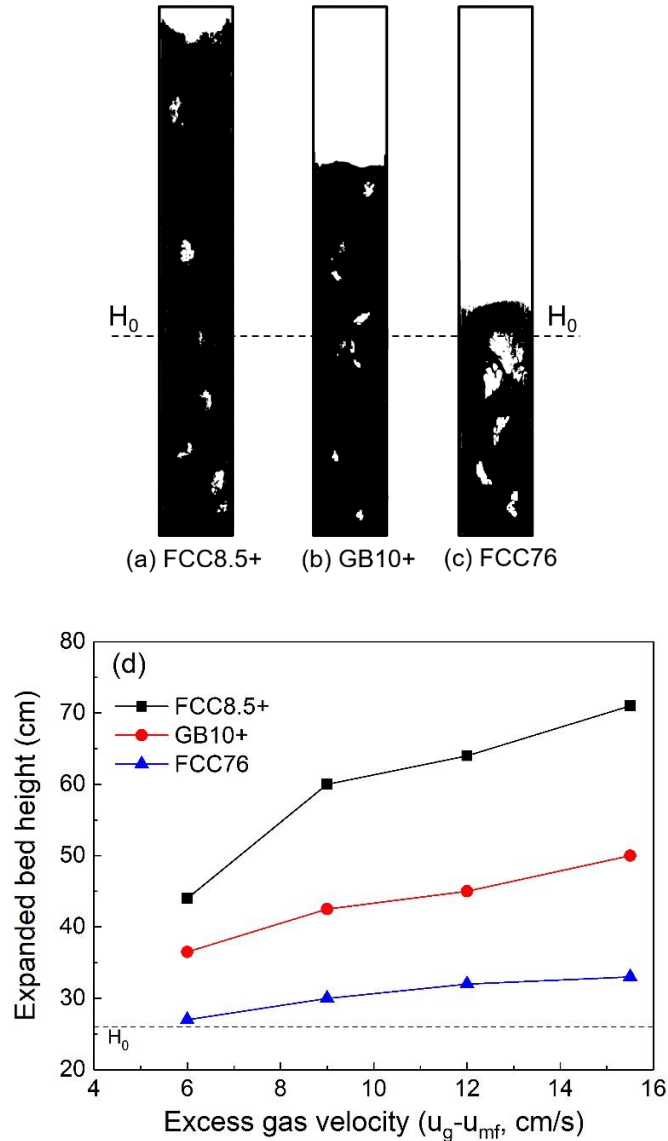
Figure 6.5: Example of fluidized beds of the three types of particles and their bed expansion at different velocities

Details on bubble positions and diameters in the fluidized bed composed of Group C^+ and Group A particles are given in Figure 6.6. Bubbles in different diameters are represented by different symbols. In the bed composed of Group C^+ particles (Figures 6.6a, b, d and e), the vast majority of bubbles (>90%-95% of the overall population) were smaller than 2cm and were uniformly dispersed throughout the bed. Bubble diameter ranging from 2 to 3cm

tended to form in the center of the fluidized bed, and the largest bubbles were less than 4cm in diameter, which occasionally appeared in the bed. In the bed composed of Group A particles (Figures 6.6c and f), bubbles were more densely populated and larger than those observed in the fluidized bed composed of Group C^+ particles. For example, the largest bubbles could reach up to 6 to 7cm in diameter at a gas velocity of 15.5cm/s (Figure 6.6f). The number of bubbles larger than 2cm in diameter was clearly greater than those in the bed of Group C^+ particles, although the bubbles smaller than 2cm in diameter accounted for 80%-85% of the overall population.
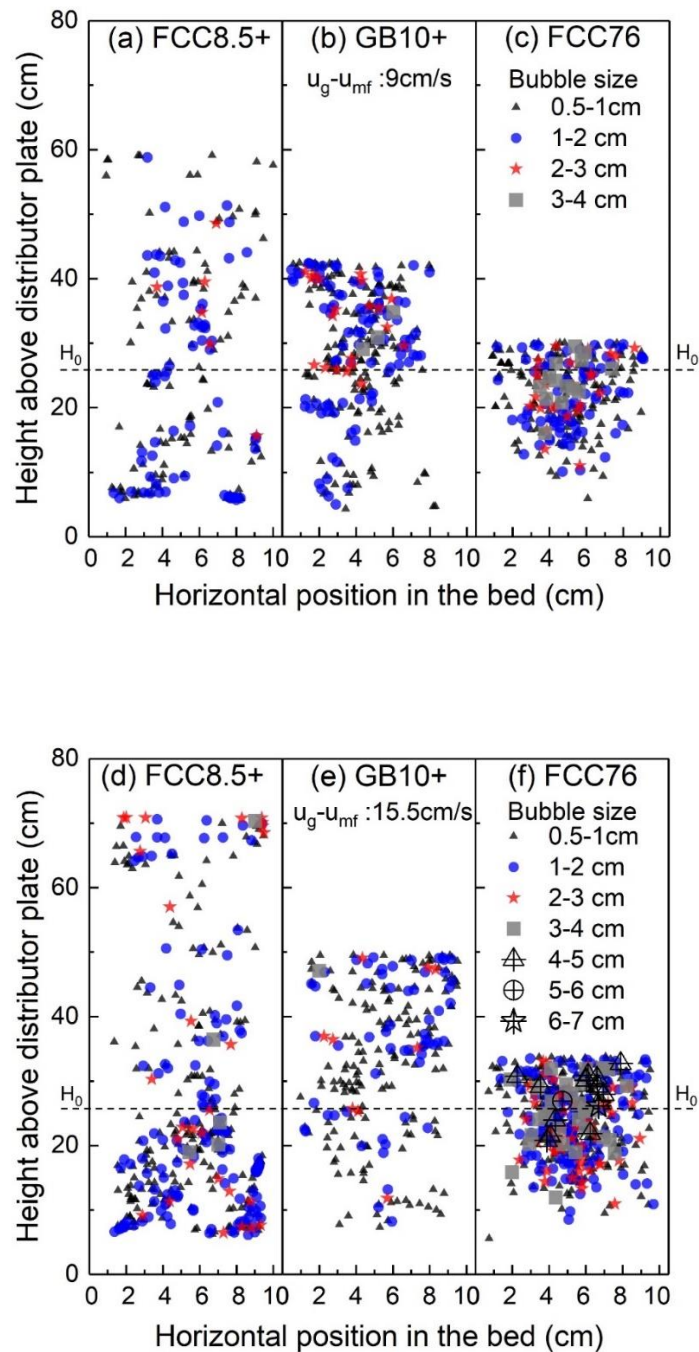
Figure 6.6: Bubble positions and diameters in fluidized beds of the three types of particles at 9cm/s and 15.5cm/s

The total number of bubbles and average bubble diameters in different sections of the fluidized bed with all three types of particles are shown in Figure 6.7. The average bubble

diameter for Group A particles was much larger than that for Group C^+ particles. The total number of bubbles for Group A particles was also larger than that in the bed of Group C^+ particles. Along the bed height from the distributor plate, the number of bubbles for Group A particles increased more significantly compared with that for Group C^+ particles. The number of bubbles also increased with increasing gas velocity, for both Group A and Group C^+ particles, as listed in Table 6.2. While the number of bubbles for Group A particles only appears to be slightly larger than that of Group C^+ particles, the number of bubbles per unit volume of the expanded bed is much larger for Group A particles than for Group C^+ particles, given the much higher bed expansion of the latter as previously shown (Figure 6.5). In addition, Group A particles exhibited widened bubble size distribution with increasing gas velocity while such was not obvious for Group C^+ particles, as shown in Figure 6.8.
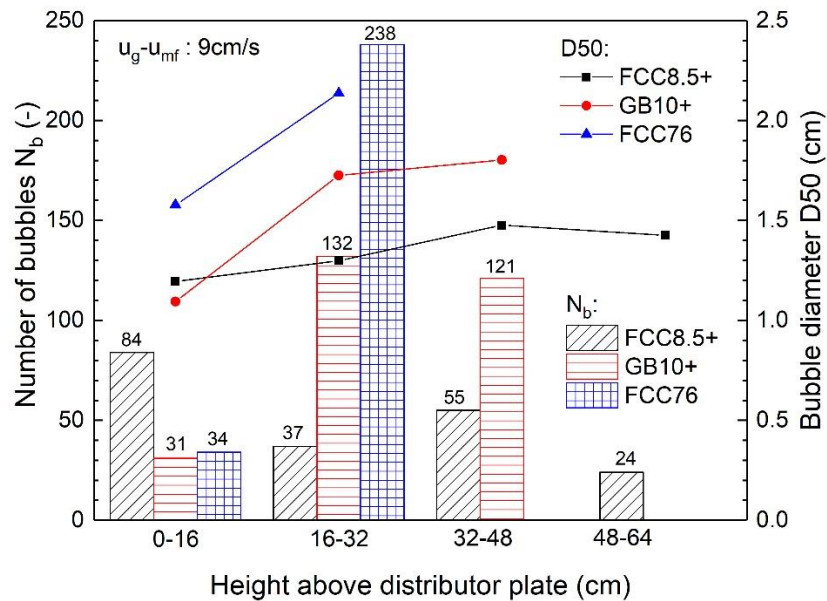
Figure 6.7: Number of bubbles and D50 in different sections of the fluidized bed composed of the three types of particles

Table 6.2: Total number and number per unit volume of bubbles

observed in the bed

u_g-u_{mf}	6 cm/s		9 cm/s		12 cm/s		15.5 cm/s	
Powder	total #	#/cm^3	total #	#/cm^3	total #	#/cm^3	total #	#/cm^3
FCC8.5+	155	0.34	200	0.33	340	0.53	408	0.57
GB10+	221	0.61	284	0.67	262	0.58	237	0.47
FCC76	174	0.64	272	0.91	368	1.12	448	1.32

number of bubbles; #/cm^3 number of bubbles per unit bed volume.
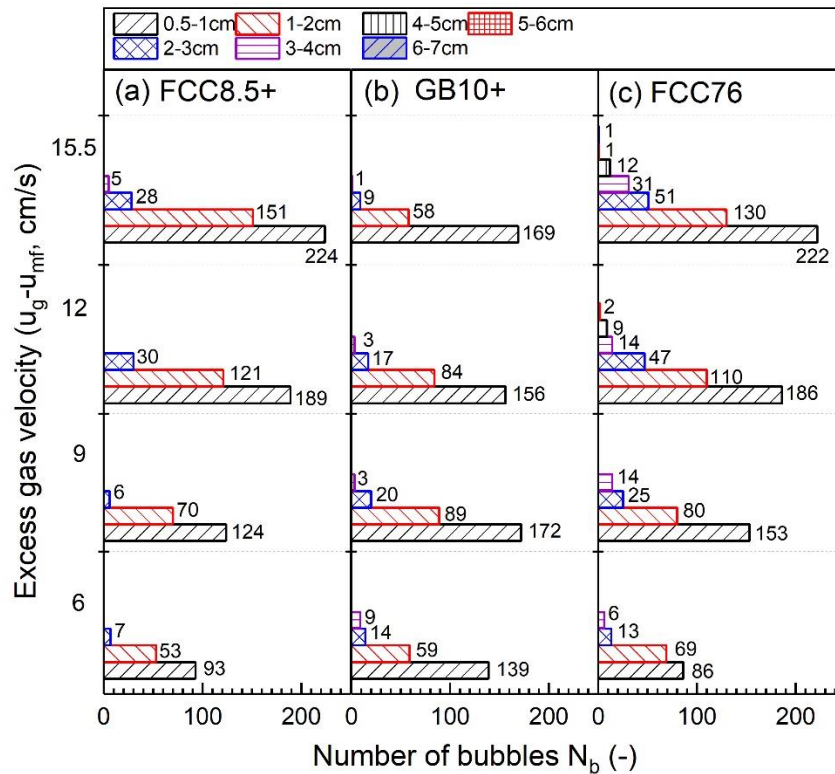
Figure 6.8: Number of bubbles with different diameters at different gas velocities

for the three types of particles

As discussed above, the bed of Group C$^+$ particles showed different characteristics from the bed of Group A particles including: (1) higher bed expansion; (2) smaller bubble diameter; (3) smaller number of bubbles. All these characteristics contribute to less gas holdup in the bubble phase and more gas holdup in the dense phase, allowing the gas to come in close contact with the particles. As a result, the quality of gas-solid contact can be

discernibly improved when switching the particulate bed from powders with a typical Geldart Group A behavior into powders with a typical Geldart Group C behavior when subjected to nano-modulation, which is attractive for gas-phase catalytic reactions.

6.3.2　Bubble diameter distribution

Figure 6.9 shows the bubble size distribution in terms of D10, D50, and D90 along the bed height, together with predicted average bubble diameters using four well-known correlations, given in Table 6.3.

Table 6.3: Correlations for the bubble diameter (SI unit)

Darton et al. [35]	$d_b = 0.54(u_g - u_{mf})^{0.4} (h + 4A_D^{0.5})^{0.8} / g^{0.2}$	(6.4)
Horio and Nonaka [34]	$\left(\frac{\sqrt{d_b}-\sqrt{d_{be}}}{\sqrt{d_{b0}}-\sqrt{d_{be}}}\right)^{1-\gamma_M/\eta} \left(\frac{\sqrt{d_b}+\sqrt{\delta}}{\sqrt{d_{b0}}+\sqrt{\delta}}\right)^{1+\gamma_M/\eta} = \exp\left(-\frac{0.3h}{D}\right)$	(6.5)
	$d_{b0} = 1.38 [(u_g - u_{mf}) A_D]^{0.4} / g^{0.2}$	(6.6)
	$d_{be} = (D/4) [-\gamma_M + (\gamma_M^2 + 4d_{bm} / D)^{0.5}]^2$	(6.7)
	$\delta = (D/4) (\gamma_M + \eta)^2$	(6.8)
	$\eta = (\gamma_M^2 + 4d_{bm} / D)^{0.5}$	(6.9)
	$\gamma_M = 2.56 \times 10^{-2} (D / g)^{0.5} / u_{mf}$	(6.10)
Cai et al. [49]	$d_b = 0.38 h^{0.8} (u_g - u_{mf})^{0.42} \exp [-0.25(u_g - u_{mf})^2 - 0.1(u_g - u_{mf})]$	(6.11)
Zou et al. [52]	$d_b = 0.21(u_g - u_{mb})^{0.49} (h + 4A_D^{0.5})^{0.48} / g^{0.2}$	(6.12)

h: height above the distributor plate; A_D: catchment area for a bubble stream at the distributor plate; D: column diameter; A_t: bed cross-sectional area;
u_{mb}: minimum bubbling velocity, substituted by u_{mf};
d_{b0}: initial bubble size; d_{bm}: maximum bubble diameter, $d_{bm} = 2.59 [(u_g - u_{mf})A_t]^{0.4} / g^{0.2}$ by Mori and Wen [56].

As shown in Figures 6.9a, and b, bubble diameters in the bed of Group C$^+$ particles changed minimally along the bed height. For both FCC8.5+ and GB10+ particles, D10 remained nearly constant with a value smaller than 1cm, indicating that small bubbles are uniformly distributed throughout the fluidized bed. D50 and D90 also hardly changed (FCC8.5+) or slightly increased (GB10+) with increasing height, but showed a decrease near the top of the bed, due to bubble splitting, while the bubble size distribution in the bed of Group C$^+$ particles was overall uniform. The bubble diameter in the bed of Group A particles (Figure 6.9c) showed a clear trend of increasing with the height, albeit a small decreasing near the top due to bubble splitting.
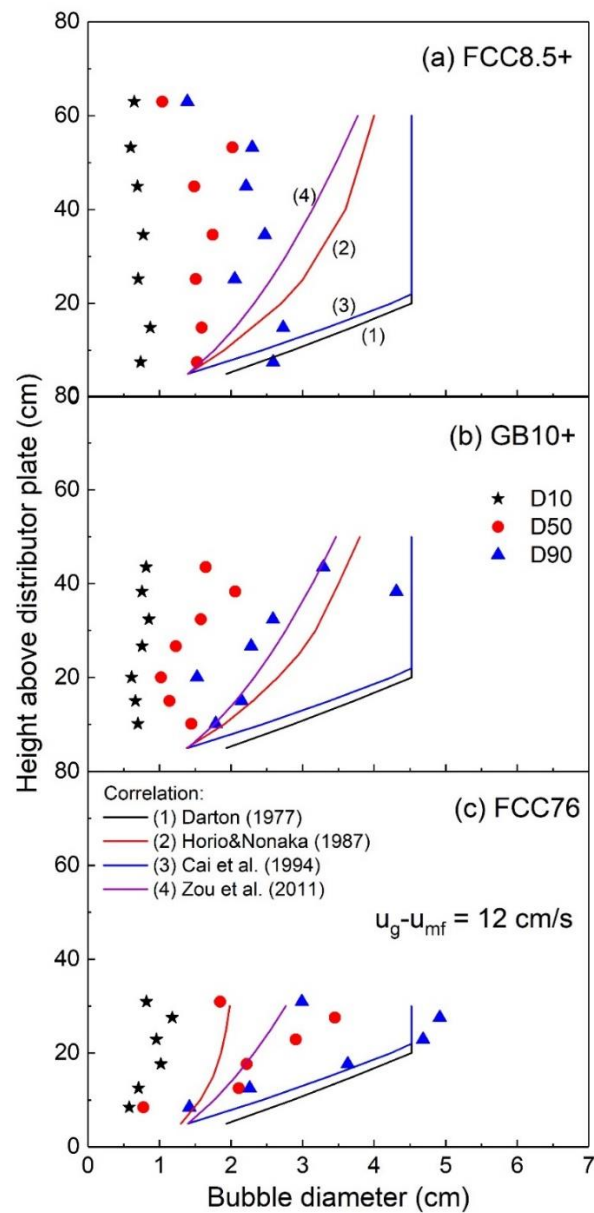
Figure 6.9: Bubble diameter distribution along the height above the distributor plate in the bed of the three types of particles

All four correlations overestimated the bubble diameter for Group C^+ particles, as they were developed based on results for larger particles. For Group A particles, the correlations of Horio and Nonaka [34] and Zou et al. [52] provided a good prediction for our experimental results. This is reasonable because the correlations established by Horio and Nonaka [34] and Zou et al [52] were developed for Group A particles (although Zou et al.

proposed this correlation for cohesive Group C particles but with agglomerates which exhibited Group A behavior).

Figure 6.10 shows the mean bubble diameters in fluidized beds of the three types of particles at different gas velocities. The mean bubble diameter for Group A particles significantly increased with the gas velocity, while that for Group C^+ particles remained nearly unchanged. As discussed before, the correlations of Horio and Nonaka [34] and Zou et al. [52] provided good predictions for Geldart Group A particles, but overestimated for Group C^+ particles. For Group A particles, the correlation of Zou et al. [52] provided a better prediction than the correlation of Horio and Nonaka [34].
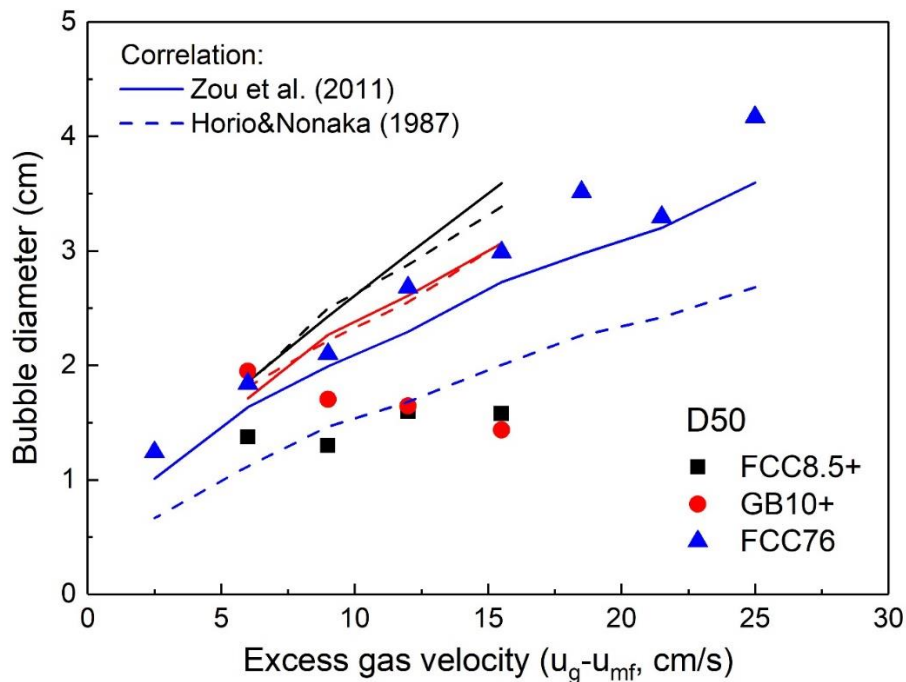
Figure 6.10: Mean bubble diameters for the three types of particles at different gas velocities: experimental results in comparison with calculated ones

Figure 6.11 shows the variations of the mean bubble diameter (D50) at the top, middle, and bottom sections of the fluidized beds with increasing gas velocity for all three types of particles. For Group A particles, the mean bubble diameter in the three sections and the

difference between the top, middle, and bottom sections both increased significantly with the gas velocity (Figure 6.11c). For Group C^+ particles, however, the bubble size distributions were uniform for FCC8.5+ and nearly uniform for GB10+, as shown in Figures 6.11a and b. That is, the mean bubble diameters remained nearly unchanged in the three sections, and showed a small change with the increase of gas velocity. The more uniform distribution of the bubble diameter for Group C^+ particles was due to the limitation of the maximum bubble diameter, which was much smaller than that in the bed of Group A particles. The smaller value of the maximum bubble diameter led to the phenomenon that bubbles quickly reached this maximum value and then remained stable as the height and/or the gas velocity increased, contributing to more uniform distribution of the bubble diameter.
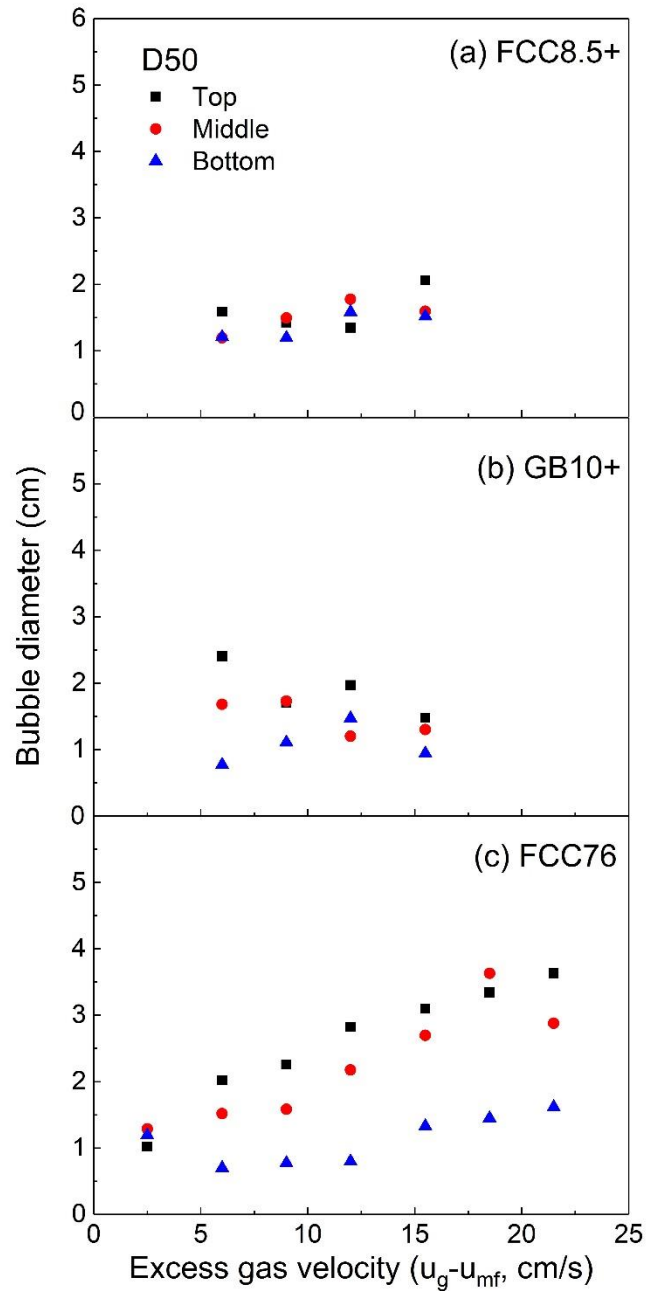
Figure 6.11: Mean bubble diameter at the top, middle, and bottom of fluidized beds of the three types of particles at different gas velocities

6.3.3　Bubble rise velocity

Bubble rise velocities are strongly dependent on the bubble size, the motion of other bubbles, the bubble distributions, and the gas flow [38,41,48]. Figures 6.12a and d show

the bubble rise velocity of each bubble in the bed of Group C^+ particles. Figures 6.12b and e depict the distribution of bubble rise velocity along the bed height at different gas velocities for two types of Group C^+ particles. Figures 6.12c and f compare the distribution of bubble rise velocity for Group C^+ and Group A particles.

For Group C^+ particles (FCC8.5+ and GB10+), a higher bubble rise velocity tended to appear at the middle and near the top of the bed, as shown in Figures 6.12a and d. For FCC8.5+, the bubble rise velocity along the bed height was fairly uniform at lower gas velocities, due to the homogeneity in the distribution of the bubble diameter, as shown in Figure 6.12b, with exception of the bubble rise velocity increasing more significantly and also becoming less uniform along the bed height at a higher gas velocity of 15.5cm/s. For GB10+, the bubble rise velocity (Figure 6.12e) also showed an increase mid-point along the bed height, but the velocity and its distribution were sensitive to the excess gas velocity, similar to the distribution of bubble diameter. For Group A particles, the bubble rise velocity was higher and less uniform than what was observed in the bed of Group C^+ particles, as shown in Figures 6.12c and f.

The distribution of the bubble rise velocity for all three types of particles was similar to the distribution of the bubble diameter in the bed, as the bubble rise velocity is mainly related to the bubble diameter. The bubble rise velocity for Group C^+ particles was lower than that for Group A particles, due to the smaller bubble diameters in the Group C^+ fluidized bed, which would contribute to a longer residence time of the bubbles.
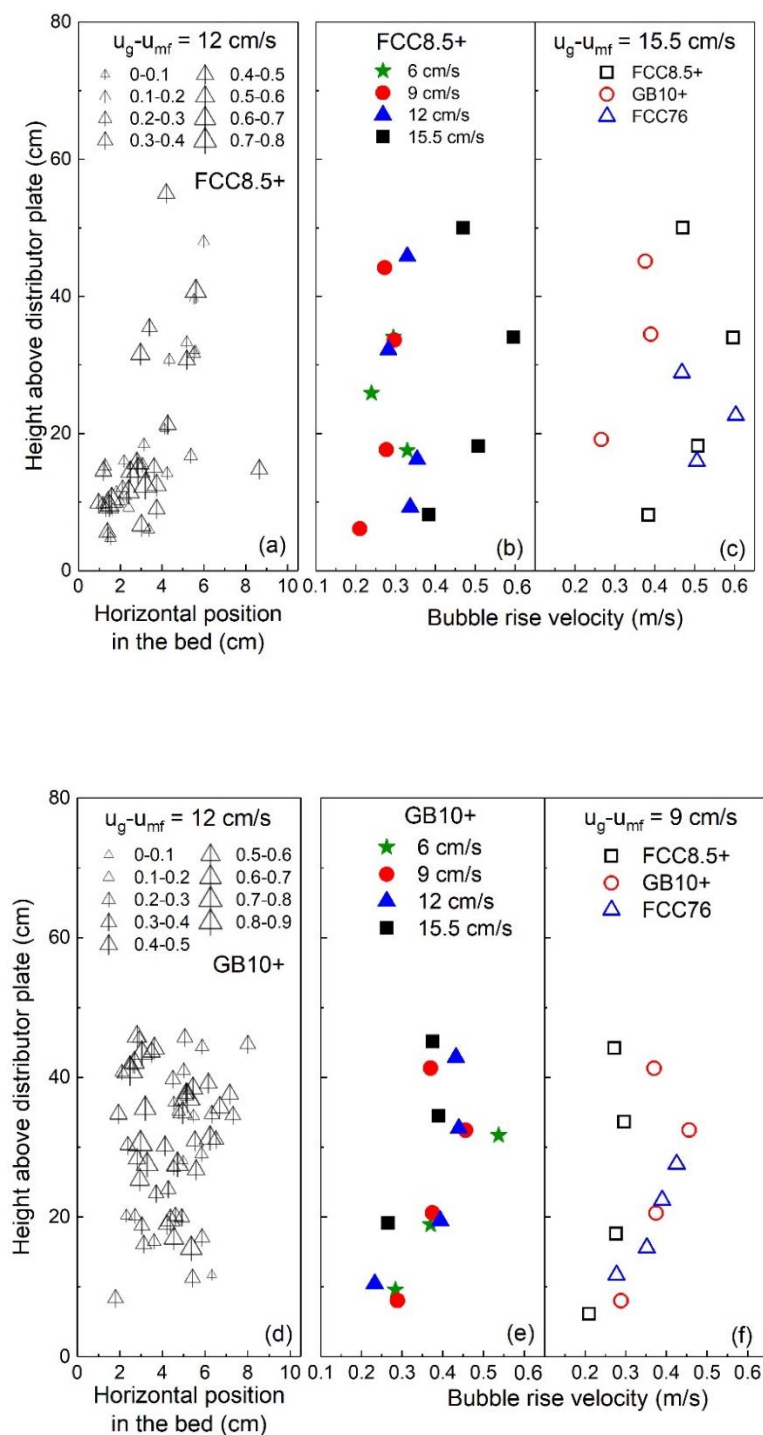
Figure 6.12: Distribution of bubble rise velocity in the fluidized bed

(a and d: rise velocity of each bubble in the bed of Group C$^+$ particles; b and e: distribution of bubble rise velocity along the height at different gas velocities; c and f: distribution of bubble rise velocity for different types of particles)

Figure 6.13 shows the relationship between bubble rise velocity and bubble diameter at different gas velocities for the three types of particles. The rise velocities of individual bubbles scattered widely around the average, but still showed a trend of increase, as shown in Figures 6.13a, b, and c. The average bubble rise velocity increased clearly with the bubble diameter, as shown in Figure 6.13d, e, f. With increasing gas velocity, FCC8.5+ (Figure 6.13d) showed an increase in the bubble rise velocity, while GB10+ (Figure 6.13e) appeared to show a small decrease, and FCC76 showed a slight increase (Figure 6.13f). It is clear, nonetheless, that the bubble rise velocity was affected by both the bubble size and the gas velocity, but the effect of the bubble size was more significant and more evident.
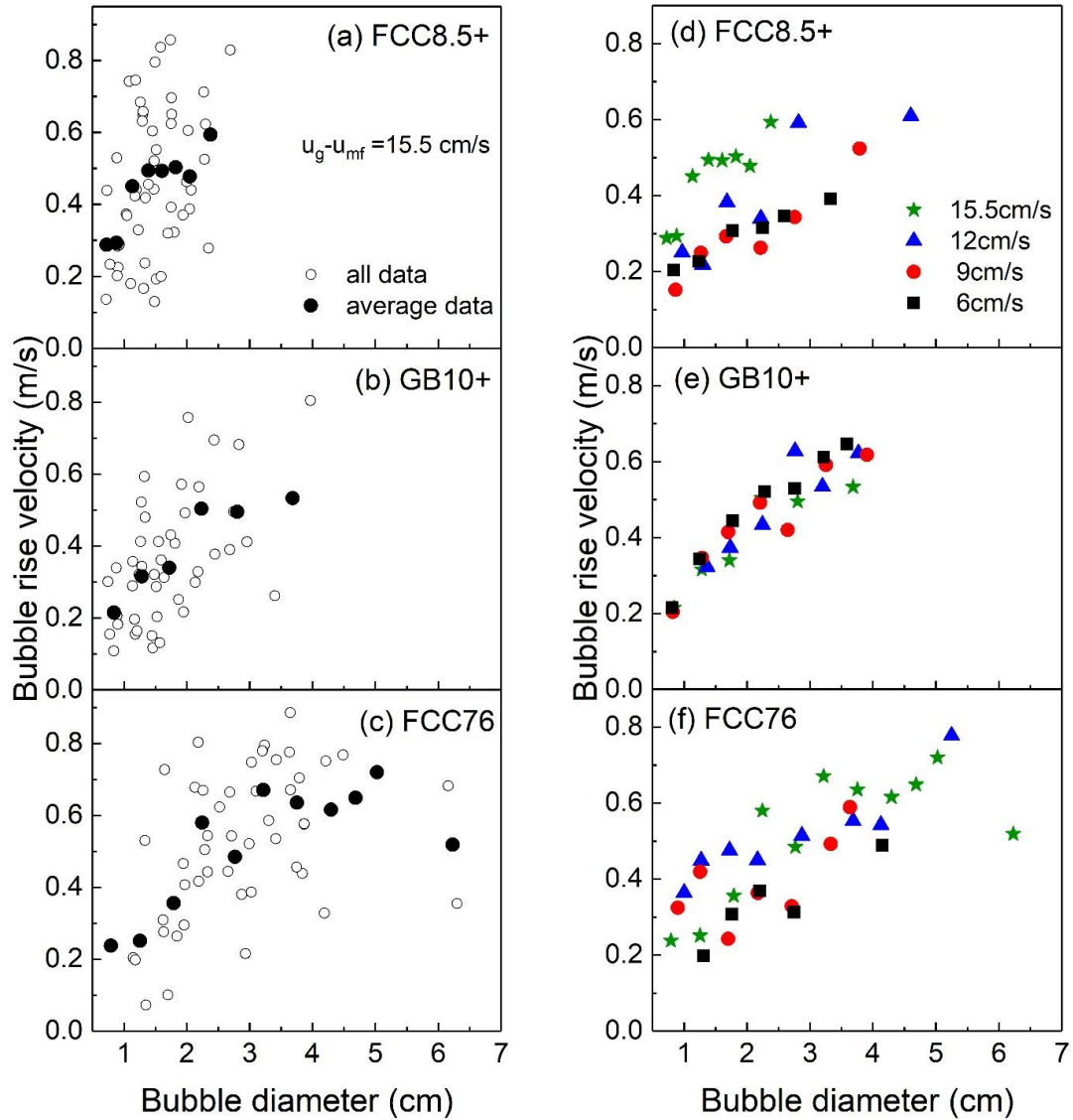
Figure 6.13: Relationship between bubble rise velocities and diameters for the three types of particles at different gas velocities
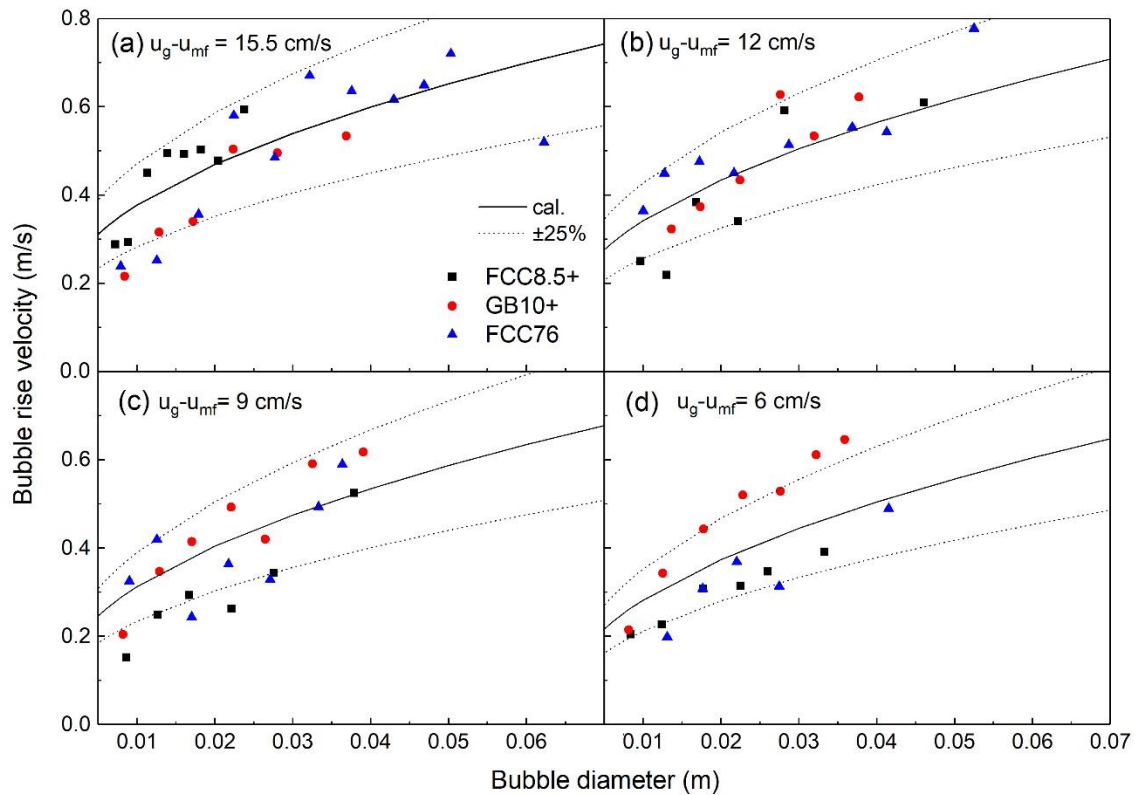
Figure 6.14: The comparison of the bubble rise velocity obtained by experiment with that by calculation

Figure 6.14 compares the rise velocity obtained by experiment with that calculated by the correlation proposed by Davidson and Harrison [57]:

$$u_b = u_g - u_{mf} + 0.711(gd_b)^{0.5} \qquad (6.13)$$

where u_g is the superficial gas velocity, u_{mf} is the minimum fluidization velocity, and d_b is the bubble diameter. Experimental values of u_{mf} and d_b were used in this calculation.

The predicted results using the Davison and Harrison equation correlated reasonably well with the experimentally measured bubble velocities, with a margin of error less than 25%, indicating that this correlation is suited for the bubble rise velocity in the fluidized bed composed of Geldart Group A and Group C$^+$ particles. Although this correlation is generally regarded to be inaccurate in predicting bubble rise velocity, by either overestimating or underestimating the value [45,58-60], the calculated results seemed to

agree well with the experimental ones in this study. This is probably because the bubble diameter and the minimum fluidization velocity used in this correlation were accurate and measured experimentally. The results proved that if the bubble diameter and the minimum fluidization velocity for Group A and Group C^+ particles were accurately determined, Equation (6.13) was accurate and could be used to predict bubble rise velocity.

6.3.4   Bubble residence time

After the bubble diameter and the bubble rise velocity have been characterized in the above sections, bubble residence time, as one of the most important parameters, was calculated to further evaluate the reactor performance. Figure 6.15 shows the bubble residence time with increasing the gas velocity for the three types of particles. The bubble residence times in beds of both types of Group C^+ particles were much longer than those in the bed of Group A particles, given the lower bubble rise velocity and higher bed expansion. As the gas velocity increased, the bubble residence time apparently reduced in the Group A fluidized bed, while that for both Group C^+ particles tended to remain nearly unchanged. This is because the increase of the bed expansion for Group A particles was not significant as that observed in the bed of Group C^+ particles with increasing the gas velocity, while the bubble rise velocity for Group A particles increased more significantly. As a result, the increase of the bed expansion with the gas velocity was not enough to "compensate" the increase in the bubble rise velocity, leading to the reduction of the bubble residence time in the bed of Group A particles.
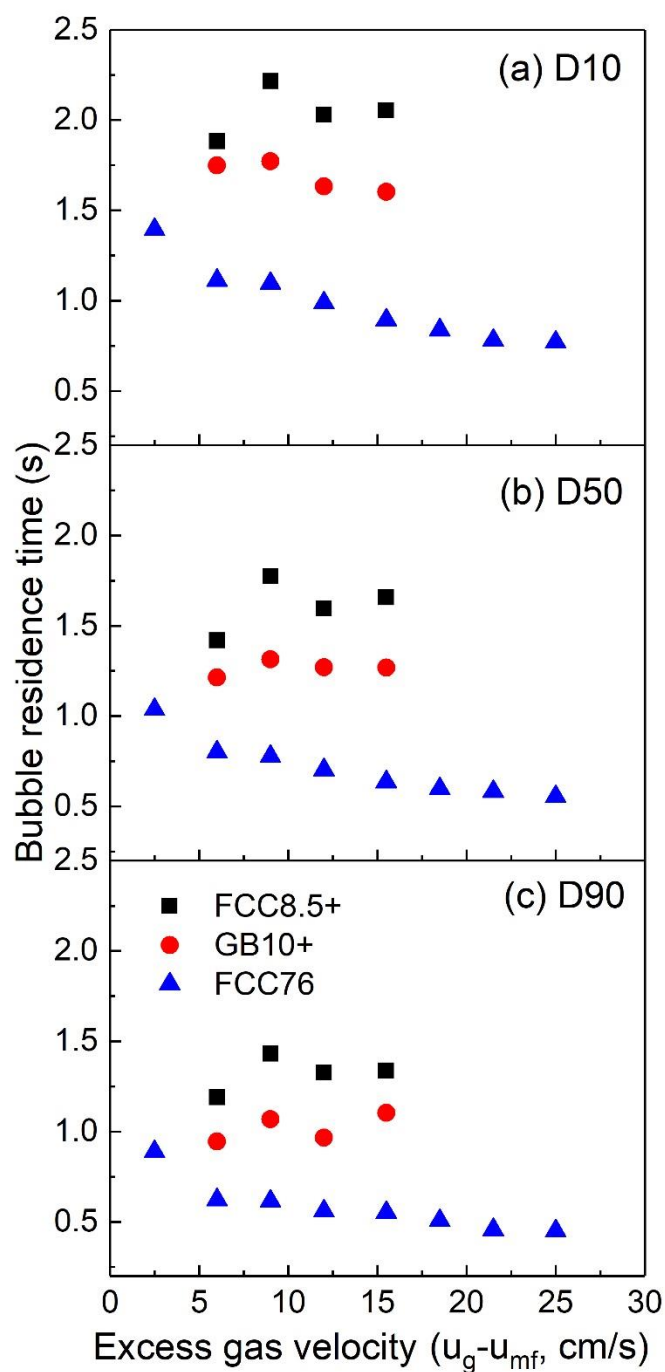
Figure 6.15: Bubble residence time in beds of the three types of particles at different gas velocities

The existence of bubbles is particularly disadvantageous for gas-phase catalytic reactions because the bypass of reactant gas in the bubble phase limits the conversion achieved in

the fluidized bed [2,61]. In fluidized beds composed of powders showing typical Geldart Group A and B behavior, the bubble diameter and subsequently the bubble rise velocity increase quickly with the gas velocity, while the increase of the bed expansion is not significant, leading to a corresponding decrease in the gas residence time and resulting in a loss of reaction conversion. In the fluidized bed of Group C$^+$ particles, the characteristics of smaller bubbles, lower bubble rise velocities, higher bed expansion, and longer bubble residence time can contribute to better gas-solid contact and improve the performance of gas-solid catalytic fluidized bed reactors. In addition, as the increase of the operating gas velocity gives rise to only a small change in bubble behaviors for Group C$^+$ particles, the reaction production is not adversely affected by the gas velocity.

6.4   General discussion

In summary, the fluidized bed of Group C$^+$ particles exhibited much a higher bed expansion, smaller bubble diameter, more uniform bubble size distribution, lower bubble rise velocity, and longer bubble residence time than the bed of Group A particles, as well as the insensitivity of those parameters to the increase of the gas velocity, contributing to a better gas-solid contact and the subsequent superior reactor performance.

The higher bed expansion and smaller bubbles in the bed of Group C$^+$ particles are mainly a result of the smaller particle size and to some extent the interparticle forces. Many earlier works [36,37,62-64] have reported that the bed expansion, especially the dense phase expansion, increased as the particle size decreased and/or the fraction of fines (<45) increased. The decrease of particle size and/or the introduction of fines are beneficial in controlling the level of interparticle forces. Chapter 3 and 4 illustrated that a proper level of cohesive interparticle forces could help to hold more gas in the fluidized bed, especially in the particle interstices, contributing to better gas-solid contact. For bubbling behaviors, it is widely recognized that bubbles are much smaller in beds of fine particles [26]. Werther [44] in 1984 indicated that the increased fines content lead to smaller bubbles and to a higher interphase mass transfer coefficient. Ma et al. [65] in 2016 demonstrated that the introduction of a cohesive force of limited magnitude in the bed of typical Geldart Group B particles could decrease the bubble diameter.

The distributions of the bubble size and rise velocity for Group C$^+$ particles were more uniform along the bed height, most likely due to the limitation of bubble growth in the bed of Group C$^+$ particles which was also ascribed from the smaller particle size and the interparticle forces. Toei et al. [66] in 1975 found that the bubble splitting frequency does not rely on the bubble diameter but does depend on the particle size. The smaller particle size and the proper level of interparticle forces for Group C$^+$ particles gave a smaller value of maximum bubble diameter which bubbles could reach more quickly, contributing to the uniform bubble distribution.

From the view of the two-phase theory, the higher bed expansion, smaller bubbles, more uniform bubble distribution, and lower bubble rise velocity for Group C$^+$ particles indicated that less gas passes through the bubble phase and more gas goes to the dense phase. As the quality of gas-solid contact is higher in the dense phase than in the bubble phase, the increasing tendency of the fluidizing gas to pass through the dense phase can help improve the performance of a catalytic gas-solid fluidized bed reactor by changing the bed material from Group A particles to Group C$^+$ particles. As a result, the bed of Group C$^+$ particles is beneficial for gas-phase catalytic reactions and is expected to enhance the reactor performance.

6.5 Conclusions

The bubble behaviors for Group C$^+$ particles and Geldart Group A particles were characterized in a 2-D bubbling fluidized bed, including the bubble distribution, diameter, rise velocity and the residence time.

Smaller bubbles ($< 2cm$) homogeneously occupied the bed for both Group C$^+$ and Group A particles, while larger bubbles tended to form in the middle of the bed. The maximum bubble diameter for Group C$^+$ particles was less than 4cm, much smaller than that in the bed of Group A particles, reaching up to 6-7cm in the range of studies. When compared with the bed of Group A particles, the bed of Group C$^+$ particles exhibited a smaller total number of bubbles, lower "density" of bubbles (number of bubbles per unit volume), more uniform bubble size distribution, lower bubble rise velocity, and longer bubble residence time.

The bubble rise velocity increased with both the bubble diameter and the gas velocity, while the effect of the bubble diameter was more significant. The correlation proposed by Davison and Harrison was suitable for predicting the bubble rise velocity in the beds of both Group A and Group C$^+$ particles.

The characteristics in the fluidized bed reactor composed of Group C$^+$ particles indicated more gas holdup in the dense phase and less gas holdup in the bubble phase, which contribute to better gas-solid contact and are attractive for gas-phase catalytic reactions.

Nomenclature

A_t	Cross-sectional area of the fluidized bed (cm^2 or m^2)
A_b	Bubble area (cm^2)
A_D	Catchment area for a bubble stream at the distributor plate (m^2)
D_{10}	Percentage 10% of particles under this particle size (cm)
D_{50}	Percentage 50% of particles under this particle size (cm)
D_{90}	Percentage 90% of particles under this particle size (cm)
D10	Percentage 10% of bubbles under this particle size (μm)
D50	Percentage 50% of bubbles under this particle size (μm)
D90	Percentage 90% of bubbles under this particle size (μm)
D	Column diameter (cm or m)
d_p	Particle diameter (μm)
d_b	Bubble diameter (cm or m)
d_{b0}	Initial bubble diameter (cm or m)
d_{bm}	Maximum bubble diameter (cm or m)
H_0	Initial fixed bed height (cm)
h	Height above the distributor plate (cm or m)
N_b	Number of bubbles (-)
u_g	Superficial gas velocity (cm/s or m/s)
u_{mf}	Minimum fluidization velocity (cm/s or m/s)
u_b	Bubble rise velocity (cm/s or m/s)
u_{mb}	Minimum bubbling velocity (cm/s or m/s)

ρ_p Particle density (kg/m^3)

δ Threshold value (-)

Reference

[1] Lyngfelt A, Leckner B, Mattisson T. A fluidized-bed combustion process with inherent CO_2 separation; application of chemical-looping combustion. Chemical Engineering Science. 2001;56(10):3101-13.

[2] Werther J. Fluidized-bed reactors. Ullmann's encyclopedia of industrial chemistry. 2000.

[3] Bilbao J, Olazar M, Romero A, Arandes JM. Design and operation of a jet spouted bed reactor with continuous catalyst feed in the benzyl alcohol polymerization. Industrial & engineering chemistry research. 1987;26(7):1297-304.

[4] Luo Y, Zhu J, Ma Y, Zhang H. Dry coating, a novel coating technology for solid pharmaceutical dosage forms. International journal of pharmaceutics. 2008;358(1-2):16-22.

[5] Gil J, Aznar MP, Caballero MA, Francés E, Corella J. Biomass gasification in fluidized bed at pilot scale with steam− oxygen mixtures. Product distribution for very different operating conditions. Energy & Fuels. 1997;11(6):1109-18.

[6] Karau A, Benken C, Thömmes J, Kula MR. The influence of particle size distribution and operating conditions on the adsorption performance in fluidized beds. Biotechnology and bioengineering. 1997;55(1):54-64.

[7] Rhodes MJ, Zhou S, Hirama T, Cheng H. Effects of operating conditions on longitudinal solids mixing in a circulating fluidized bed riser. AIChE journal. 1991;37(10):1450-8.

[8] Grace JR, Leckner B, Zhu J, Cheng Y. Fluidized beds. Multiphase Flow Handbook. 2006;5:1-93.

[9] Bi HT, Grace JR. Flow regime diagrams for gas-solid fluidization and upward transport. International Journal of Multiphase Flow. 1995;21(6):1229-36.

[10] Yerushalmi J, Cankurt NT. Further studies of the regimes of fluidization. Powder Technology. 1979;24(2):187-205.

[11] Geldart D. Types of gas fluidization. Powder technology. 1973;7(5):285-92.

[12] Geldart D, Harnby N, Wong AC. Fluidization of cohesive powders. Powder Technology. 1984;37(1):25-37.

[13] Chaouki J, Chavarie C, Klvana D, Pajonk G. Effect of interparticle forces on the hydrodynamic behaviour of fluidized aerogels. Powder Technology. 1985;43(2):117-25.

[14] Visser J. Van der Waals and other cohesive forces affecting powder fluidization. Powder Technology. 1989;58(1):1-0.

[15] Marring E, Hoffmann AC, Janssen LP. The effect of vibration on the fluidization behaviour of some cohesive powders. Powder technology. 1994;79(1):1-0.

[16] Xu C, Zhu J. Experimental and theoretical study on the agglomeration arising from fluidization of cohesive particles—effects of mechanical vibration. Chemical Engineering Science. 2005;60(23):6529-41.

[17] Chirone R, Massimilla L, Russo S. Bubble-free fluidization of a cohesive powder in an acoustic field. Chemical Engineering Science. 1993;48(1):41-52.

[18] Chirone R, Massimilla L. Sound-assisted aeration of beds of cohesive solids. Chemical engineering science. 1994;49(8):1185-94.

[19] Lepek D, Valverde JM, Pfeffer R, Dave RN. Enhanced nanofluidization by alternating electric fields. AIChE journal. 2010;56(1):54-65.

[20] Nakamura H, Watano S. Fundamental particle fluidization behavior and handling of nano-particles in a rotating fluidized bed. Powder Technology. 2008;183(3):324-32.

[21] Dutta A, Dullea LV. A comparative evaluation of negatively and positively charged submicron particles as flow conditioners for a cohesive powder. In AIChE Symposium Series. 1990;86(276): 26-40.

[22] Ajbar A, Alhumazi K, Asif M. Improvement of the fluidizability of cohesive powders through mixing with small proportions of group A particles. The Canadian Journal of Chemical Engineering. 2005;83(6):930-43.

[23] Kono HO, Huang CC, Xi M, Shaffer FD. The effect of flow conditioners on the tensile strength of cohesive powder structures. In AIChE Symposium Series: Fluidization and Fluid Particle Systems: Fundamentals and Applications 1989;85(270): 44-48.

[24] Zhu, J. and Zhang H. Fluidization Additives to Fine Powders. U.S. Patent 6833185.

2004.

[25]   Yang J, Sliva A, Banerjee A, Dave RN, Pfeffer R. Dry particle coating for improving the flowability of cohesive powders. Powder technology. 2005;158(1-3):21-33.

[26]   Quintanilla MA, Valverde JM, Castellanos A. Adhesion force between fine particles with controlled surface properties. AIChE journal. 2006;52(5):1715-28.

[27]   Millán JM. The Use of Additives to Control Powder Flow. Mechanical Properties of Fine Powder Beds. In: Fluidization of Fine Powders. Dordrecht: Springer, 2013: 99-120.

[28]   Chen Y, Yang J, Dave RN, Pfeffer R. Fluidization of coated group C powders. AIChE journal. 2008;54(1):104-21.

[29]   Xu CC, Zhang H, Zhu J. Improving flowability of cohesive particles by partial coating on the surfaces. The Canadian Journal of Chemical Engineering. 2009;87(3):403-14.

[30]   Han M, Zhou Y, Zhu J. Improvement on flowability and fluidization of Group C particles after nanoparticle modification. Powder Technology. 2020; 365:208-214.

[31]   Oke O, Lettieri P, Salatino P, Solimene R, Mazzei L. Numerical simulations of lateral solid mixing in gas-fluidized beds. Chemical Engineering Science. 2014;120:117-29.

[32]   Shen L, Zhang M, Xu Y. Solids mixing in fluidized beds. Powder technology. 1995;84(3):207-12.

[33]   Kunii D, Levenspiel O. Bubbling bed model. Model for flow of gas through a fluidized bed. Industrial & Engineering Chemistry Fundamentals. 1968;7(3):446-52.

[34]   Horio M, Nonaka A. A generalized bubble diameter correlation for gas-solid fluidized beds. AIChE journal. 1987;33(11):1865-72.

[35]   Darton, R. C, Lanauze R. D, Davidson J. F, Harrison D. Bubble growth due to coalescence in fluidized bed. Trans. Inst. Chem. Eng. 1977, 55: 274-280.

[36]   Abrahamsen AR, Geldart D. Behaviour of gas-fluidized beds of fine powders part I. Homogeneous expansion. Powder technology. 1980;26(1):35-46.

[37]   Abrahamsen AR, Geldart D. Behaviour of gas-fluidized beds of fine powders part II. Voidage of the dense phase in bubbling beds. Powder Technology. 1980;26(1):47-55.

[38]   Yates JG, Rowe PN, Cheesman DJ. Gas entry effects in fluidized bed reactors. AIChE journal. 1984;30(6):890-4.

[39]   Yasui G, Johanson LN. Characteristics of gas pockets in fluidized beds. AIChE Journal. 1958;4(4):445-52.

[40]   Kai T, Furusaki S. Behavior of fluidized beds of small particles at elevated temperatures. Journal of chemical engineering of Japan. 1985 Apr 20;18(2):113-8.

[41]   Rowe PN, Yacono CX. The bubbling behaviour of fine powders when fluidised. Chemical Engineering Science. 1976;31(12):1179-92.

[42]   Werther J. The influence of the bed diameter on the hydrodynamics of gas fluidized beds. AIChE Meeting, Detroit, MI, 1973.

[43]   Werther J. Bubble growth in large diameter fluidized beds. In Fluidization Technology; Keairns, D. L., Ed.; Hemisphere: Washington, 1976:215-235.

[44]   Werther J. Hydrodynamics and mass transfer between the bubble and emulsion phases in fluidized beds for sand and cracking catalyst. In Fluidization IV; Kunii, D., Toei, R., Eds.; Engineering Foundation: New York, 1984: pp 93-101.

[45]   Hilligardt K, Werther J. Local bubble gas hold-up and expansion of gas/solid fluidized beds. German chemical engineering. 1986;9(4):215-21.

[46]   Karimipour S, Pugsley T. A critical evaluation of literature correlations for predicting bubble size and velocity in gas–solid fluidized beds. Powder Technology. 2011;205(1-3):1-4.

[47]   Kobayashi N, Yamazaki R, Mori S. A study on the behavior of bubbles and solids in bubbling fluidized beds. Powder Technology. 2000;113(3):327-44.

[48]   Dry RJ, Judd MR, Shingles T. Bubble velocities in fluidized beds of fine, dense powders. Powder technology. 1984;39(1):69-75.

[49]   Cai P, Schiavetti M, De Michele G, Grazzini GC, Miccio M. Quantitative estimation of bubble size in PFBC. Powder technology. 1994;80(2):99-109.

[50]   Geldart D. The effect of particle size and size distribution on the behaviour of gas-fluidised beds. Powder Technology. 1972;6(4):201-15.

[51]   Cranfield RR, Geldart D. Large particle fluidisation. Chemical Engineering Science. 1974;29(4):935-47.

[52]   Zou Z, Li HZ, Zhu QS. The bubbling behavior of cohesive particles in the 2D

fluidized beds. Powder technology. 2011;212(1):258-66.

[53] Zhu, JX, Zhang H. Method and Apparatus for Uniformly Dispensing Additive Particles in Fine Powders. U.S. Patent 7240861, 2007

[54] Otsu N. A threshold selection method from gray-level histograms. IEEE transactions on systems, man, and cybernetics. 1979;9(1):62-6.

[55] Sezgin M, Sankur B. Survey over image thresholding techniques and quantitative performance evaluation. Journal of Electronic imaging. 2004;13(1):146-66.

[56] Mori S, Wen CY. Estimation of bubble diameter in gaseous fluidized beds. AIChE Journal. 1975;21(1):109-15.

[57] Davidson J F, Harrison D. Fluidized Particles. Cambridge University Press, Cambridge, New York, 1963.

[58] Busciglio A, Vella G, Micale G, Rizzuti L. Analysis of the bubbling behaviour of 2D gas solid fluidized beds: Part I. Digital image analysis technique. Chemical Engineering Journal. 2008;140(1-3):398-413.

[59] Mudde RF, Schulte HB, Van den Akker HE. Analysis of a bubbling 2-D gas-fluidized bed using image processing. Powder Technology. 1994;81(2):149-59.

[60] Shen L, Johnsson F, Leckner B. Digital image analysis of hydrodynamics two-dimensional bubbling fluidized beds. Chemical engineering science. 2004;59(13):2607-17.

[61] Knowlton TM, Karri SB, Issangya A. Scale-up of fluidized-bed hydrodynamics. Powder Technology. 2005;150(2):72-7.

[62] Dry RJ, Judd MR, Shingles T. Two-phase theory and fine powders. Powder Technology. 1983;34(2):213-23.

[63] Lorences MJ, Patience GS, Díez FV, Coca J. Fines effects on collapsing fluidized beds. Powder technology. 2003;131(2-3):234-40.

[64] Grace JR, Sun G. Influence of particle size distribution on the performance of fluidized bed reactors. The Canadian Journal of Chemical Engineering. 1991;69(5):1126-34.

[65] Ma J, Liu D, Chen X. Bubble behaviors of large cohesive particles in a 2D fluidized bed. Industrial & Engineering Chemistry Research. 2016;55(3):624-34.

[66] Toei R, Ryuichi M, Morihiro O, Katsunobu Y. Deformations and splittings of a

bubble in a two-dimensional fluidized bed. Journal of Chemical Engineering of Japan. 1975:7(6):451-455.

Chapter 7

7   On the Two-phase Theory of Group C$^+$ and Geldart Group A Particles

The relative distribution of gas flow between the bubble phase and the dense phase is a very important factor that determines the performance of a gas-solid fluidized bed reactor, because the dense phase provides a better gas-solid contact than the bubble phase. The gas flow through the dense phase was initially considered to be at minimum fluidization (the so-called two-phase theory) but was found to be higher with fine Group A particles. Using even smaller particles in this study, the fluidization of Group C$^+$ particles, Geldart Group C particles with nano-additives, exhibited lower bubble rise velocity, lower bubble holdup, and higher gas holdup in the dense phase, etc., signifying more gas flow through the dense phase and subsequently contributing to better gas-solid contact than other particles that have ever been tested, being Groups A or B. The correction factor Y that accounts for increased dense phase gas flow in the modified two-phase theory was also found to be not a constant but a function of the superficial gas velocity, and a correlation was then proposed to characterize the division of gas flow between the two phases for these fine Group C$^+$ particles, based on the experimental results. The higher dense phase gas velocity and the lower bubble phase gas velocity could improve the gas-solid contact and the reactor performance for Group C$^+$ particles.

7.1   Introduction

Fluidized beds are widely used as chemical reactors and many other processing devices. Fluidization quality is often taken into important consideration in these applications which largely depend on the degree of gas-solid contact, especially in gas-phase catalytic fluidized bed reactors. To improve the gas-solid contact, fine particles in small sizes can provide large gas-solid interfacial areas and thus are widely applied in these reactors as

catalysts [1-5]. In a conventional gas-solid fluidized bed such as a bubbling fluidized bed reactor, the division of gas flow between the dilute bubble phase and the dense particulate phase is also an important factor which determines the gas-solid contact. Generally, the gas flow through a bubbling fluidized bed is divided into two portions: one makes up the bubble phase and the other goes into the dense phase or the particulate phase as interstitial gas. The gas flow through the dense phase is in more intimate contact with particles than that through the bubble phase, contributing to better gas-solid contacting.

Numerous studies [6-14] have reported the characteristics of Geldart Group A particles [15] fluidized in three- and two-dimensional beds, showing a higher bed expansion in the fluidized beds of smaller Group A particles than in the beds of larger Group B particles. As a result, Group A particles attracted more attention and have been extensively utilized in the industry. Moreover, the gas holdup in the dense phase for Group A particles were found to increase with the fines ($d_p < 45\mu m$) content [1,3,6-7,16-17]. Following this trend, the even smaller Geldart Group C particles ($d_p < 45\mu m$) would be expected to have even higher dense phase expansion. However, they are cohesive and hard to fluidizable due to the strong interparticle forces ascribed to the small particle size [15].

Earlier studies [18-22] showed that nanoparticles can effectively reduce the interparticle forces of Group C particles and make them fully fluidize. A nano-modulation technique has been proposed by our group [21] for better integration of nanoparticles with Group C particles [23]. The nano-modulated Group C particles, referred to as Group C$^+$ particles, exhibited much higher gas holdup in the dense phase than Group A particles [24]. The bubbles in the fluidized bed of Group C$^+$ particles also exhibited smaller sizes, lower rise velocities, and longer residence times than in the bed of Group A particles [25]. All these characteristics of the two phases for Group C$^+$ particles, smaller and slower bubbles and higher dense phase gas holdup, contributed to better gas-solid contact [26]. On the other hand, the higher dense phase gas holdup for the Group C$^+$ particles clearly suggested that a much higher portion of the gas goes through the dense phase than that of minimum fluidization, as postulated by the two-phase theory. As such, to fully understand the fluidization of Group C$^+$ particles, it is important to have a comprehensive study on the gas flow division between the two phases and on the modification of the two-phase theory.

7.2   Two-phase theory

The two-phase theory of gas-solid fluidization was initially proposed by Toomy and Johnstone (1952) [27] who suggested that all gas in excess of that required for minimum fluidization would pass through the bed in the form of bubbles:

$$G_b / A = u_g - u_{mf} \qquad (7.1)$$

where A is the cross-sectional area of the bed, u_g and u_{mf} are the superficial gas velocity and the minimum fluidization velocity, respectively, and G_b is the volumetric bubble flowrate. This simple two-phase theory was questioned by Turner (1966) [28] and Davidson and Harrison (1966) [29] suggested a factor K to account for a higher gas velocity than u_{mf} going through the dense phase:

$$G_b / A = u_g - K u_{mf} \qquad (7.2)$$

with K=1 for the "simple two-phase" assumption. A number of works [30-41] measured directly or estimated indirectly the visible bubble flowrates in freely fluidized beds and came up with a range of K values. Grace and Clift [42] summarized those earlier works and found K to vary in the rang 0.7 to 27. Later on, in their review chapter, Clift and Grace [43] used a Y value, first proposed by Werther J (1978) [44], to account for the same effect:

$$G_b / A = Y (u_g - u_{mf}) \qquad (7.3)$$

where the value of the empirical parameter Y was usually less than unity which depended on the powder group, bed height, and bed diameter.

The deviation from the simple two-phase theory, that is $Y < 1$, has increasingly been found, especially for systems of Geldart Group A particles and other particles containing a high fraction of "fines" ($d_p < 45\mu m$) [1,6-11,16-17,45], due to the increased gas holdup and gas velocity in the dense phase than those at minimum fluidization. From 1980 onwards, an increasing number of work had studied the gas flow in the fluidized beds of fine powders (Group A), and it has become widely recognized that the dense phase voidage and the interstitial gas flow are much greater than that suggested by the "simple two-phase theory" and the fine content played a major role in such deviation [7-8,11-13,46-53].. With even smaller particle size, the bubbling beds of Group C$^+$ particles are expected to deviate more from the simple two-phase theory, as they exhibited even higher dense phase expansion than the beds of Group A particles.

In this project, the gas flow distribution in the fluidized beds of Group C^+ and Group A particles was investigated. A modified two-phase theory with a new correlation for the value of Y was determined for Group C^+ particles, based on the experimental results of the bubble holdup and the bubble rise velocity. The gas velocities in the two phases were also calculated.

7.3 Experimental

7.3.1 Particulate materials

Two types of Group C^+ particles (GB10+ and FCC8.5+) and one type of Group A particles (FCC76) were used in these experiments with their properties listed in Table 7.1. AEROSIL R972, a type of fumed silica nanoparticles, has a reported size of 16 nm and a particle density of 2200 kg/m^3. A volume fraction of 0.82% of the fumed silica were mixed into Group C particles by an ultrasonic vibrating method, as detailed in our earlier patent [21].

Table 7.1: Particle properties

Powder name	Material	Particle size (μm)			Particle density (kg/m^3)	Bulk density (kg/m^3)	Minimum fluidization velocity (cm/s)	Powder classification
		D_{10}	D_{50}	D_{90}				
GB10+	Glass beads with R972	1.6	10	29	2500	916	6.5	Group C^+
FCC8.5+	FCC catalysts with R972	1.5	8.5	26	1780	509	10	Group C^+
FCC76	FCC catalysts	20	76	140	1780	874	0.5	Group A

7.3.2 2-D fluidized bed

The 2-D fluidization column was made up of Plexiglas, with 100cm in height, 10.5cm in width, and 1cm in depth, as schematically shown in Figure 7.1(a). The distributor plate had 19 holes of 1 mm in diameter with an opening area ratio of 1.4%. Three layers of 625 mesh screen covered on the distributor plate to prevent fine particles dropping into the wind box. A commercial digital camera (Canon EOS 800D) was used to record the fluidization

process, and two lamps were placed behind the column at two fixed positions to increase the contrast between bubbles and particles, as shown in Figure 7.1(b). The camera viewed the whole fluidized bed to allow a full field analysis of the bubble dynamics. The whole apparatus was isolated from the external environment using black boards to shield out lights in the surrounding environment.

All experiments were conducted at room temperature and room pressure with an initial bed height of 26cm (H_o). Air at ambient conditions was used as fluidizing gas, and the flow rate was measured by a rotameter. The minimum fluidization velocities (u_{mf}) of GB10+, FCC8.5+, and FCC76, were experimentally measured to be 6.5cm/s, 10cm/s and 0.5cm/s, respectively. The operating gas velocities ranged up to 25.5 cm/s.
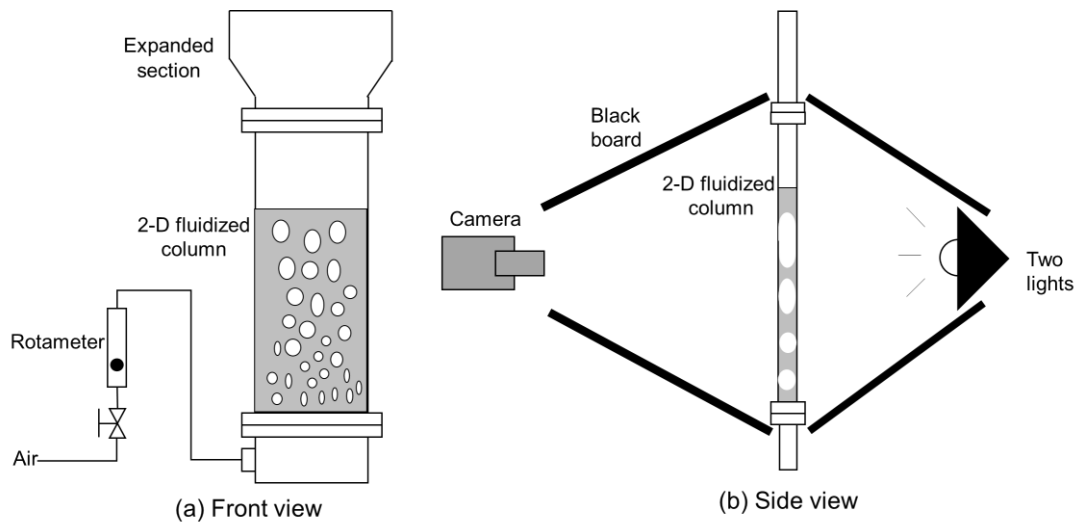
Figure 7.1: Experimental Setup and camera-lighting arrangement

7.3.3   Image processing

The camera recorded videos at a frequency of 50Hz and each video was 10s long, equal to 500 frames. The image processing routine was developed on Adobe Photoshop CS6 (The Adobe company) and Matlab R2018b (The MathWorks inc.). The whole process could be summarized as follows:

(1) Transforming Videos to RGB images frame by frame;

(2) Cropping images to allow the analysis of the fluidized bed only;

(3) Transforming RGB images to grayscale ones;

(4) Thresholding the grayscale images to binary ones;

(5) Indexing all bubbles inside the area;

(6) Filtering false bubbles and noise.

Figure 7.2 shows an example of the image processing. A threshold value of 60 was used in this project, which was found by combining visual observation and Otsu thresholding method [54]. All pixels with a gray-value larger than the threshold were indicated as bubbles and were coloured white, and all with a value smaller were dense phase and made black. Each bubble in the image was marked using a program called Regionprops in Matlab. The bubble rise velocity (u_b) could be calculated by comparing the bubble centroids in subsequent frames ($\Delta t = 0.02$s), as shown in Figure 7.3, with the following equation:

$$u_b = \frac{y_c(t+\Delta t) - y_c(t)}{\Delta t} \qquad (7.4)$$

The mean vertical position "tagged" to the bubble rise velocity was:

$$h = \frac{y_c(t+\Delta t) - y_c(t)}{2} \qquad (7.5)$$

(a) RGB image (b) Greyscale image (c) Binary image (d) Image with bubble marked
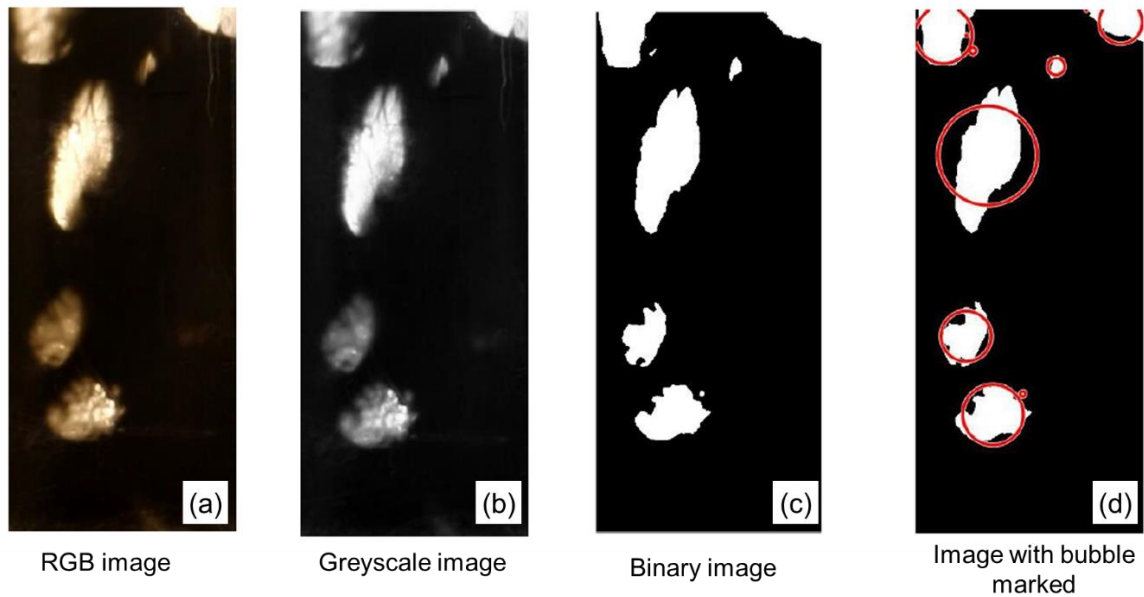
Figure 7.2: An example of image processing
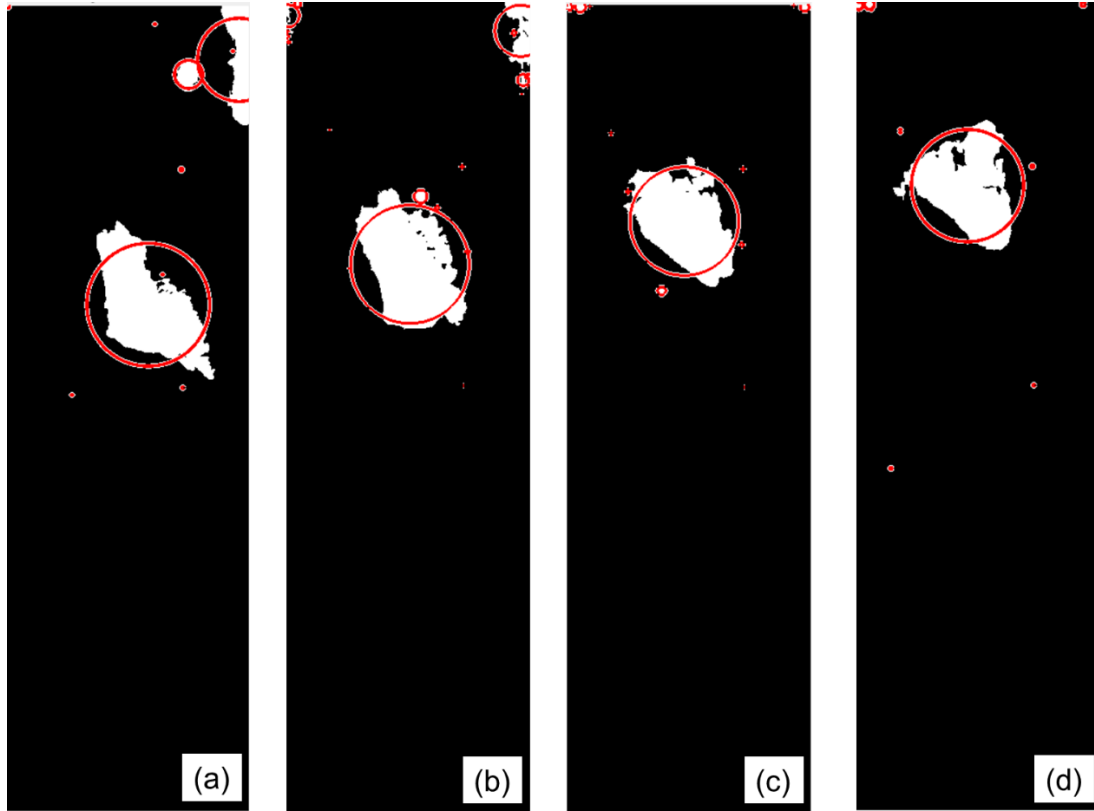
Figure 7.3: Four consecutive frames marked with the same bubble for calculating bubble rise velocity

7.3.4   Bed collapse test

The bed collapse test, initially proposed by Rietema in 1967 [55], was used to characterize properties of the bubble phase and the dense phase. It was carried out by first achieving the steady fluidization (bed height H_t) at a high gas velocity, suddenly shutting off the gas supply, then tracking the fall of the bed surface as a function of time. The typical bed collapse curves can be divided into three different stages, as shown in Figure 7.4: (1) the bubble escape stage; (2) the sedimentation stage; and (3) the consolidation stage. The bubble escape stage happened quickly and normally lasted only 1-2 seconds, followed by the sedimentation stage which yielded a linear region for Group A particles but an exponential region for Group C^+ particles [24]. The dense phase height (H_d) was obtained by extrapolating the region of the hindered sedimentation stage back to time 0 when the gas was shut off, and then the equivalent bubble phase height (H_b) was further obtained by (H_t - H_d). The bubble volume fraction (δ) was calculated by:

$$\delta = (H_t - H_d) / H_t \qquad\qquad (7.6)$$

The bed collapse tests were measured at different gas velocities ranging up to 25.5 cm/s for all three types of particles. The length of bed collapse process was much longer for Group C^+ particles than for Group A particles, giving the longer sedimentation time, as being reflected in Figure 7.4.
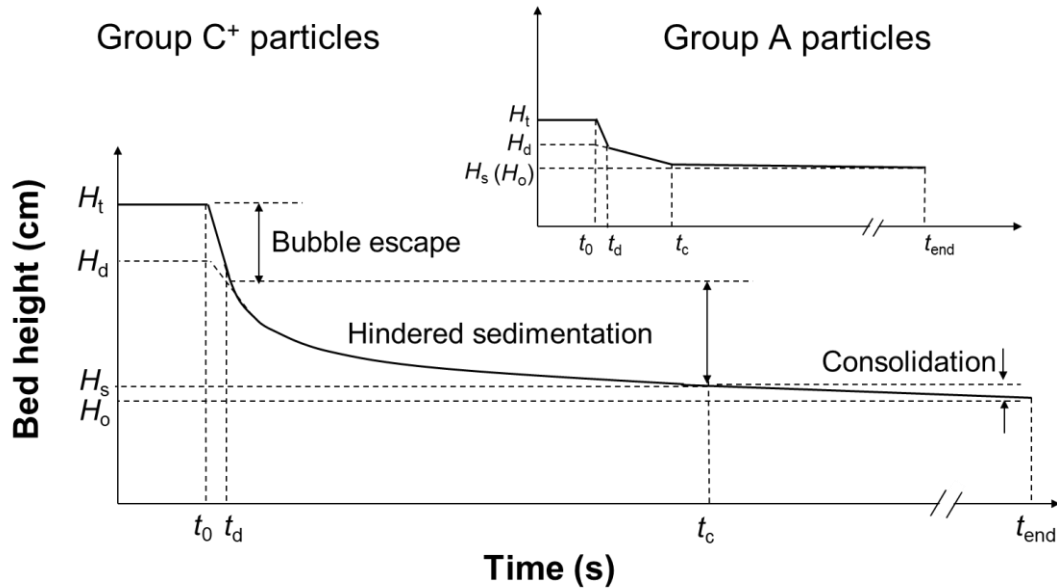
Figure 7.4: Bed collapse curves

7.4 Results and discussion

7.4.1 Bubble rise velocity distribution

The axial distributions of the bubble rise velocity for the three types of particles are shown in Figure 7.5. The bubble rise velocities of each bubbles were indicated in hollow symbols, fairly scattered because of the chaotic behaviors in the fluidized beds. The average bubble rise velocities (in solid symbols with lines) showed a clear trend with the height above the distributor plate. Among the three types of particles, the axial distribution of the bubble rise velocity in the bed of FCC8.5+ was very uniform for which the bubble rise velocity hardly changed as along the height. In the bed of $GB10^+$, the bubble rise velocity slightly increased initially and then remained constant with the increase of the height. For FCC76, the bubble rise velocity had a steeper increase with the height before it plateaued.

Evidently, the distribution of the bubble rise velocity for Group C$^+$ particles was more homogeneous than that for Group A particles.
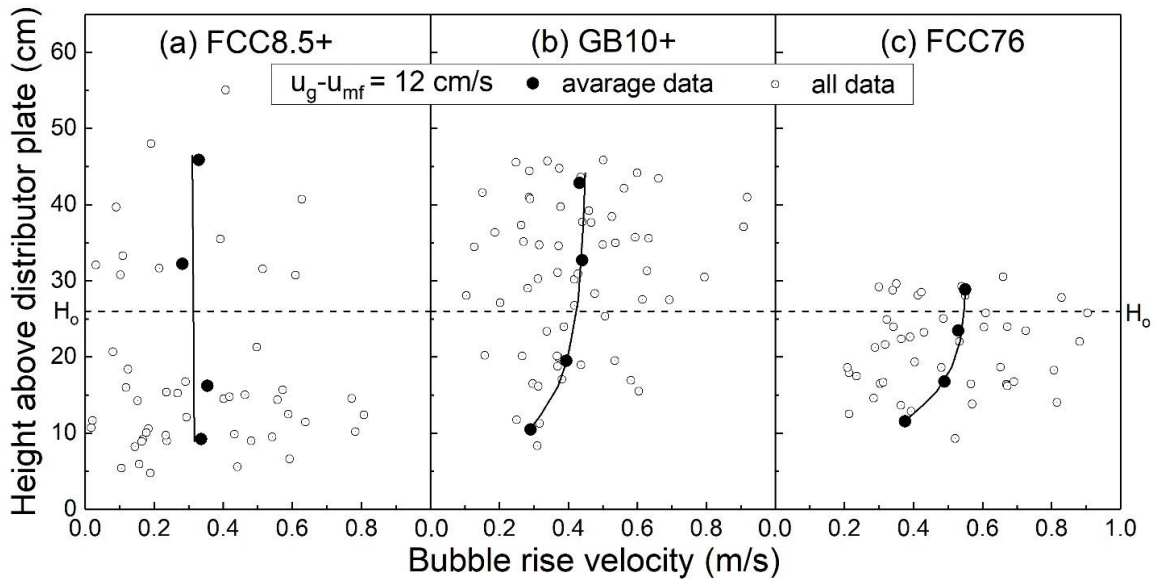
Figure 7.5: The axial distributions of the bubble rise velocity for the three type of particles

When compared with Group C$^+$ particles, Group A particles exhibited higher bubble rise velocity and lower fluidized bed height, both leading to shorter bubble residence time in the bubbling fluidized bed. The longer bubble residence time in the bed of Group C$^+$ particles would increase gas-solid contacting time, contributing to better performance for a fluidized bed reactor.

The axial distributions of the bubble rise velocity at different gas velocities for the three types of particles are shown in Figure 7.6. As the gas velocity increased, the axial distributions of the bubble rise velocity for the two C$^+$ particles did not change significantly, other than for FCC8.5$^+$ at u_g-u_{mf} of 15.5 cm/s. For example, the bubble rise velocity remained almost unchanged along the bed height with changing gas velocities, and the axial distribution of the bubble rise velocity for GB10+ became even more uniform with increasing gas velocity. For Group A particles, the axial distribution of the bubble rise velocity was less uniform than that for Group C$^+$ particles, as discussed before. The bubble

rise velocity for FCC76 obviously increased with the increase of either the bed height or the gas velocity.
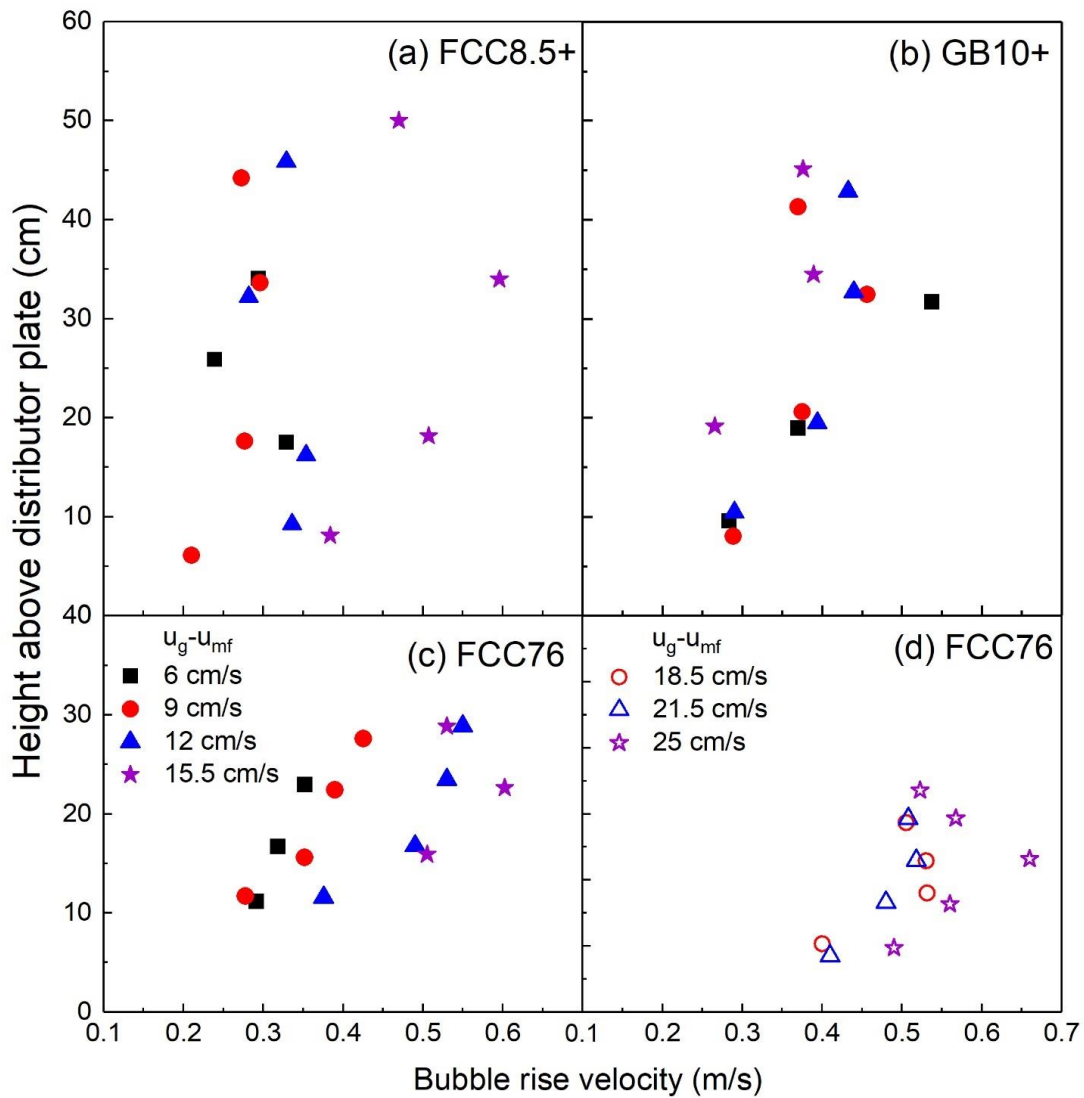
Figure 7.6: Axial distributions of the bubble rise velocity at different gas velocities for the three types of particles

In summary, the bubble rise velocity in the bed of Group C$^+$ particles was lower and did not increase significantly along the bed height, i.e., more uniformly distributed throughout the fluidized bed than that for Group A particles. The bubble rise velocity is closely related to the bubble diameter [56-58]. The lower bubble rise velocity and the more uniform axial distribution for Group C$^+$ particles were attributed to the smaller bubbles and more uniform

bubble size distribution in the bed of Group C^+ particles, as carefully discussed in Chapter 6. The smaller bubbles and lower bubble rise velocities in Group C^+ particle fluidization provided larger gas-solid interfacial area and longer time for gas-solid interaction, increasing the gas-solid contact and thus the reactor performance.

7.4.2   Gas holdup distribution

The bed collapse tests were used to identify the holdups of the two phases in the bubbling fluidized bed. As shown by the bed collapse curves for the three types of particles at different gas velocities in Figure 7.7, Group C^+ particles exhibited much higher total bed height and also extremely higher dense phase height than Group A particles with the same initial bed height of 26cm. In addition, the collapse times for Group C^+ particles were much longer than those for Group A particles, indicating the difficulty in gas escaping from the dense phase which is ascribed to the higher cohesion of Group C^+ particles.
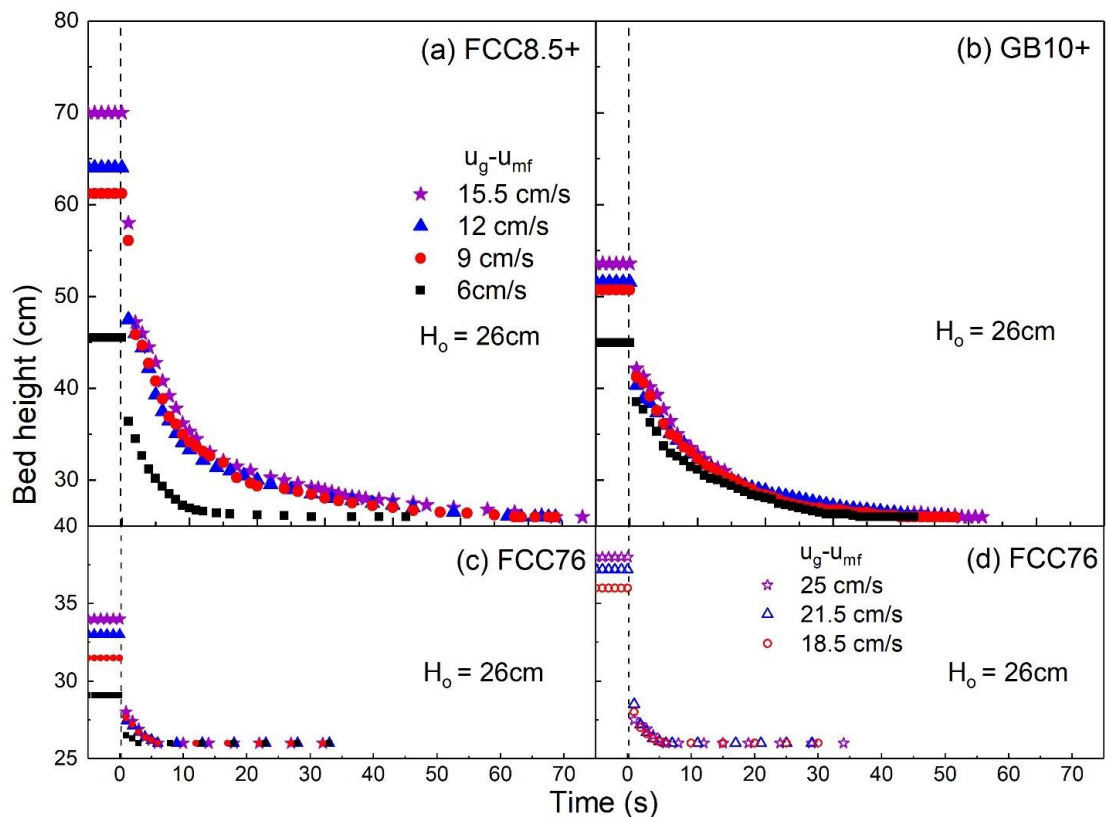
Figure 7.7: The bed collapse curves for the three types of particles at different gas velocities

The distributions of the two phases in the fluidized beds of the three types of particles at different gas velocities are shown in Figure 7.8. Both the total bed height and the dense phase height for Group C^+ particles were evidently higher than those for Group A particles. For the two Group C^+ particles, as the gas velocity increased, the gas seemed to preferentially go into the dense phase first before "filling up" the bubble phase, so that the dense phase height initially rose quickly and then remained almost unchanged, while the bubble phase height had a more steady increase. In the contrary, most gas flow in the Group A bed goes into the bubble phase with its height rising consistently as the gas velocity increased.
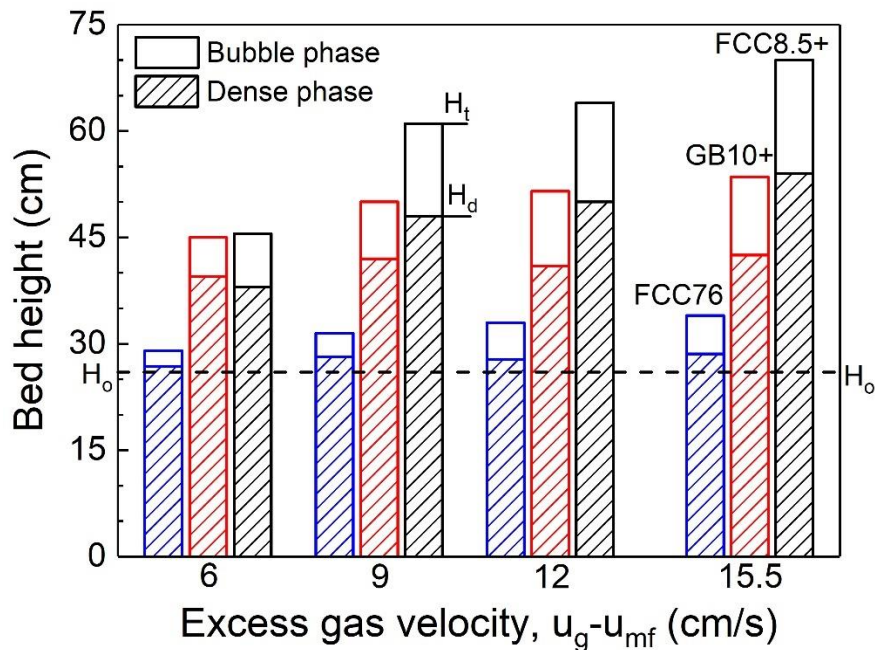
Figure 7.8: The bed height distribution for the three types of particles at different gas velocities

The gas holdups in the two phases and the extra gas holdup in the dense phase beyond fixed bed are shown in Figure 7.9, for the three types of particles with increasing gas velocity. While the bubble holdups for Group C^+ particles were slightly higher than those for Group A particles, it is the gas holdups in the dense phase (dense phase voidages) for Group C^+ particles that were significantly higher, reaching up to 87%, or 160% of those for Group A

particles. Consequently, the extra gas holdups beyond the fixed bed in the dense phase for Group C$^+$ particles were also much higher, around 4 times as those for Group A particles.
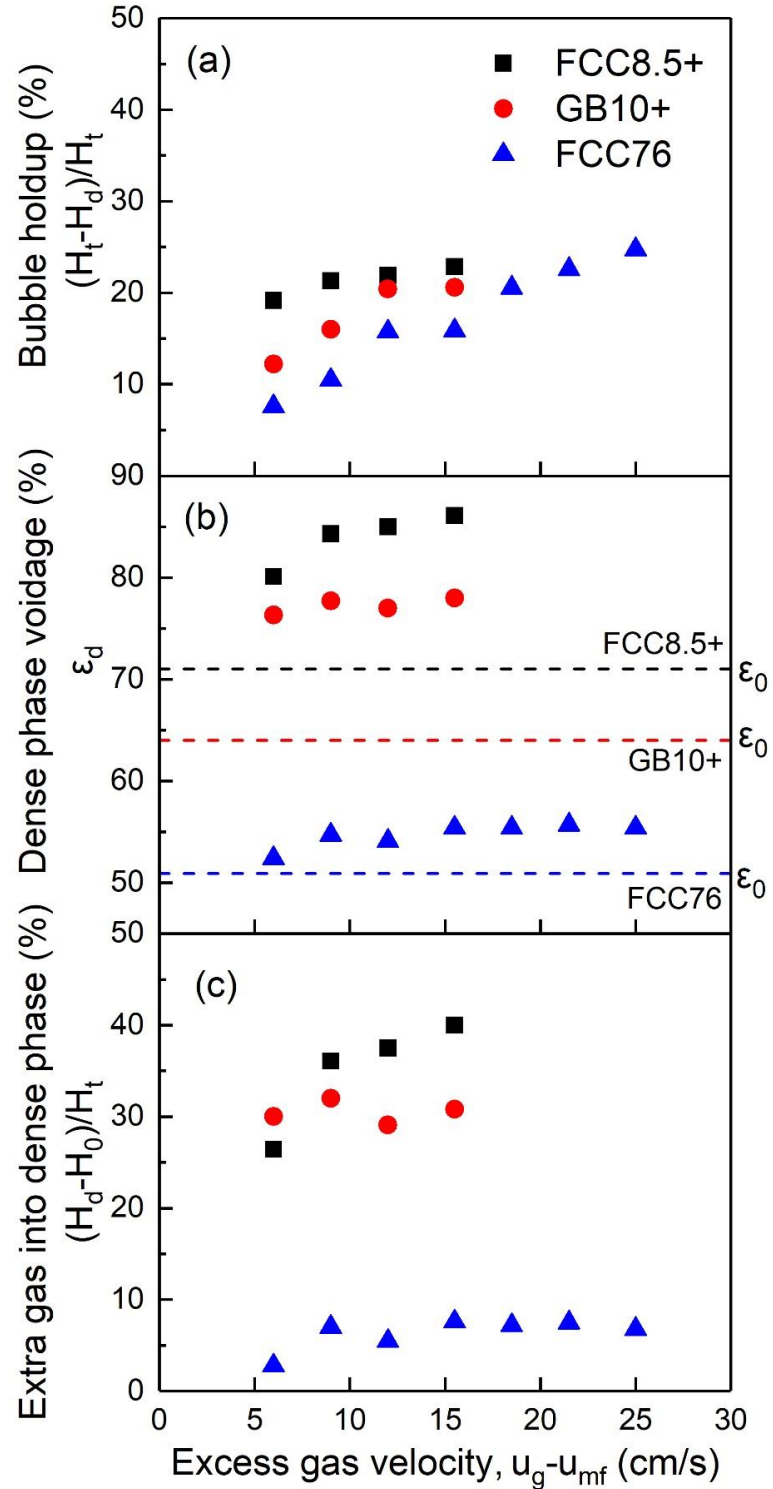
Figure 7.9: The gas holdups in the two phases for the three types of particles at different gas velocities

The extremely higher gas holdup in the dense phase for Group C$^+$ particles allowed more space for the gas stream to channel through the dense phase, providing more opportunities for better gas-solid contact. The high gas holdup in the dense phase for Group C$^+$ particles may be mainly attributed to the existence of the interparticle forces, which could help "hold" more gas in the particle interstices. Earlier workers [1,7-12,17] reported that the dense phase voidage increased with the increase of the fines (<45μm) content or the introduction of interparticle forces in Group A/B particle fluidization. Such higher gas holdup in and thus more gas flow through the dense phase, in fluidized bed reactors using Group C$^+$ particles as catalysts, would lead to better reactor performance, as have been verified in the study using ozone decomposition reaction [26].

7.4.3   Phase distribution by the two-phase theory

The concept of the two-phase theory is illustrated in Figure 7.10. The simple two-phase theory [27] suggested that the flowrate of bubbles through the fluidized bed (G_b) was equal to the excess gas flow above the minimum fluidization velocity ($G_b/A = u_g - u_{mf}$), while the dense phase remained at the minimum fluidization state ($G_d/A = u_{mf}$ and $\varepsilon_d = \varepsilon_{mf}$). This theory was later modified and a correction factor Y was introduced [44] to account for the additional gas flow through the dense phase, because the dense phase voidage for Group A particles is actually larger than the bed voidage at the minimum fluidization. The total gas flowrate (G_g) through the fluidized bed can therefore be expressed by the sum of the gas flowrate through the bubble phase (G_b) and the dense phase (G_d), as shown in the equations below:

$$G_g = G_b + G_d \qquad\qquad (7.7)$$

$$G_b = u_b\, A\, \delta = Y\,(u_g - u_{mf})\, A \qquad\qquad (7.8)$$

$$G_d = u_d\, A\,(1\text{-}\delta) = u_{di}\, A\,(1\text{-}\delta)\, \varepsilon_d = u_g\, A - Y\,(u_g - u_{mf})\, A \qquad\qquad (7.9)$$

where A is the cross-sectional area of the fluidized bed, δ and ε_d are the bubble volume fraction and the dense phase voidage found from the bed collapse test, u_b is the bubble rise velocity, u_d is the "superficial gas velocity" in the dense phase based on dense phase volume excluding the bubble phase, and u_{di} is the actual interstitial gas velocity in the dense phase. For Geldart Group A particles, the range of Y values is relatively narrow and its numerical value for Group A particles was approximately 0.8 based references [44,59-64].

(a) Fluidized bed of Group A particles

$$Y(u_g-u_{mf}) = u_b\delta \quad u_g-Y(u_g-u_{mf}) = u_d(1-\delta)$$

(b) Fluidized bed of Group C⁺ particles

$$Y(u_g-u_{mf}) = u_b\delta \quad u_g-Y(u_g-u_{mf}) = u_d(1-\delta)$$
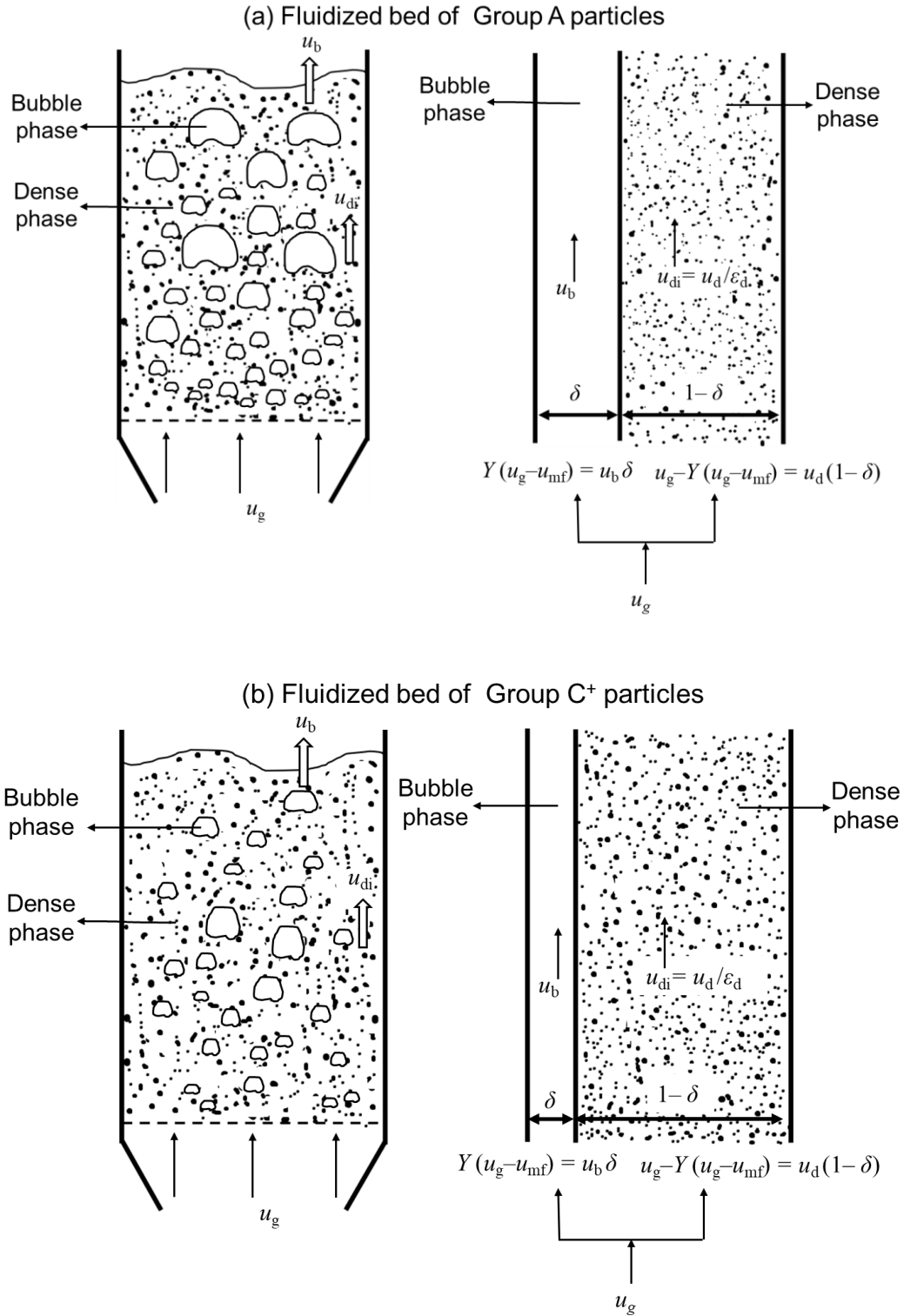
Figure 7.10: The concept of the two-phase theory

(a) Typical Group A particles and (b) Typical Group C⁺ particles

For Group C^+ particles, the gas holdup in the dense phase was considerably higher than that for Group A particles, as has been discussed. It is therefore important to study and modify the Y value for correctly predicting the division of the gas flow in the bubbling fluidized bed of Group C^+ particles. Based on the bubble volume and the bubble rise velocity obtained experimentally, the Y values can be calculated: Dividing the bed into many differential heights and the bubble volume in a given slice dz is (δA dz):

$$\delta A \, \mathrm{d}z = (A \, \mathrm{d}z) \, Y \, (u_g - u_{mf}) \, / u_b \qquad (7.10)$$

The bubble volume in the bed is:

$$\int_0^H \delta A \, \mathrm{d}z = A \, Y \left(u_g - u_{mf} \right) \int_0^H \frac{1}{u_b} \, \mathrm{d}z \qquad (7.11)$$

The Y values and the superficial gas velocities of the two phases for the three types of particles are shown in Figure 7.11(a). For Group A particles, the Y values remained relatively constant at a value of 0.7, while the Y values had a clear decreasing trend with the increase of the gas velocity for Group C^+ particles. In other words, the correction factor, Y, for the modified two-phase theory was found to be a variable of the gas velocity for Group C^+ particles.

With the Y values determined, the gas flow distribution between the two phases (G_b/A and G_d/A) could be calculated, as shown in Figures 7.11(b) and 7.11(c). For both Group C^+ and Group A particles, G_b/A was lower than u_g-u_{mf} and G_d/A was much higher than u_{mf}. As a result, the simple two-phase theory overestimated the gas flow of the bubble phase and underestimated that of the dense phase. For Group C^+ particles, G_b/A was slightly lower than that for Group A particles, but G_d/A was significantly higher than that for Group A particles, echoing the experimental observation that much more gas flows through the dense phase which contributes to better gas-solid contact.
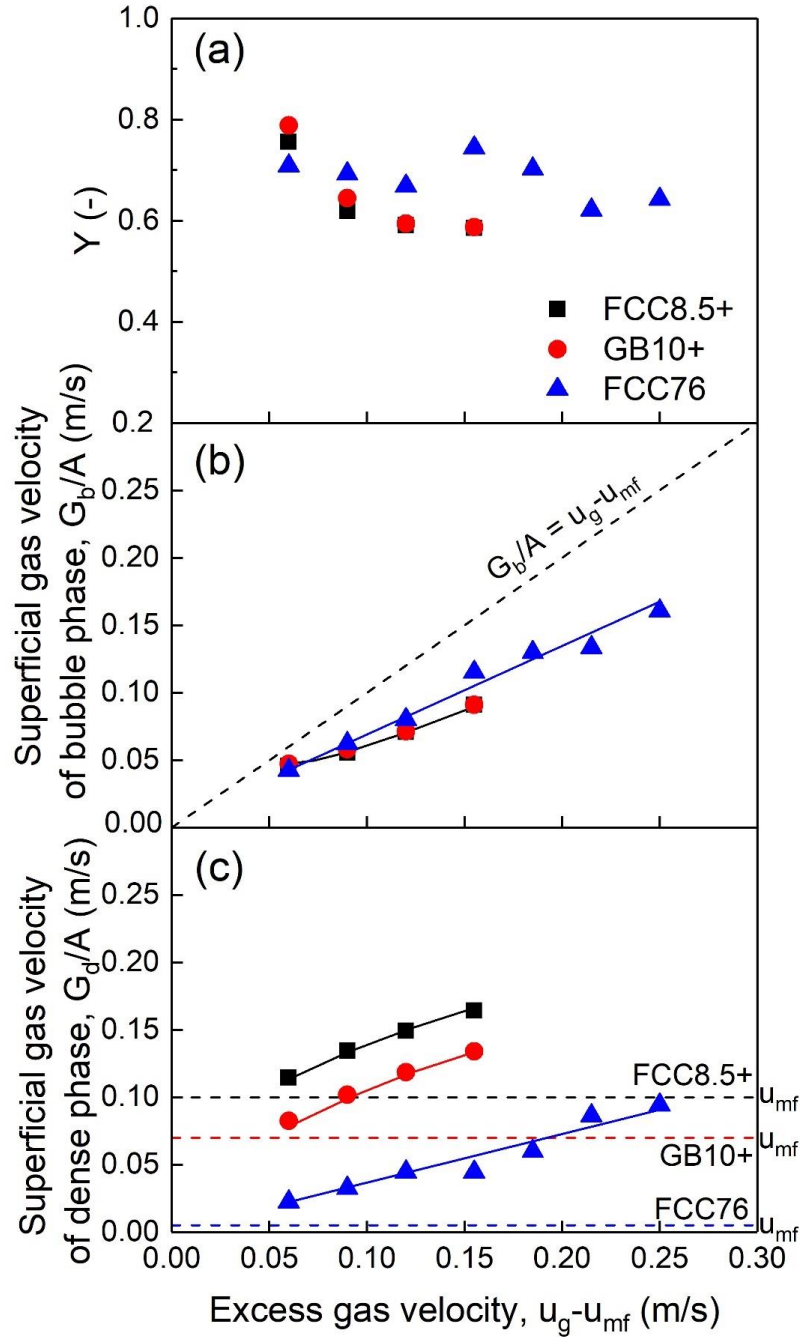
Figure 7.11: *Y* values and gas flow distributions for the three types of particles

7.4.4   Further analysis based on the modified two-phase theory

From the bubble holdup (δ) and the *Y* value obtained experimentally, one can further calculate the bubble rise velocity (u_b), the superficial gas velocity in the dense phase based on dense phase volume excluding the bubble phase (u_d), and the actual interstitial gas

velocity in the dense phase (u_{di}). To fully characterize the fluidized bed, the bubble holdup (δ) and the Y value from experiments were first correlated. As shown in Figures 7.12 and 7.13, the correlations of the bubble holdups for the three types of particles were:

$$\text{For FCC8.5+: } \delta = 0.40 \, (u_g\text{-}u_{mf}) + 0.170 \qquad (7.12)$$

$$\text{For GB10+: } \delta = 0.93 \, (u_g\text{-}u_{mf}) + 0.072 \qquad (7.13)$$

$$\text{For FCC76: } \delta = 0.90 \, (u_g\text{-}u_{mf}) + 0.030 \qquad (7.14)$$

For Group A particles, the Y values remained almost constant and were averaged at 0.7, which was slightly lower than that reported by earlier works with an approximate value of 0.8 [44,59-64], probably because the FCC76 used had a large amount of fine content ($D_{10} = 20\mu m$). For Group C$^+$ particles, the correlation of the Y value was:

$$Y = 0.33 \, (u_g\text{-}u_{mf})^{-0.30} \qquad (7.15)$$

The above correlation clearly indicated that the correction factor, Y, was a function of and decreased with the excess gas velocity. This correlation was shown to correctly predict the results of G_b/A and G_d/A well as given in Figure 7.11.
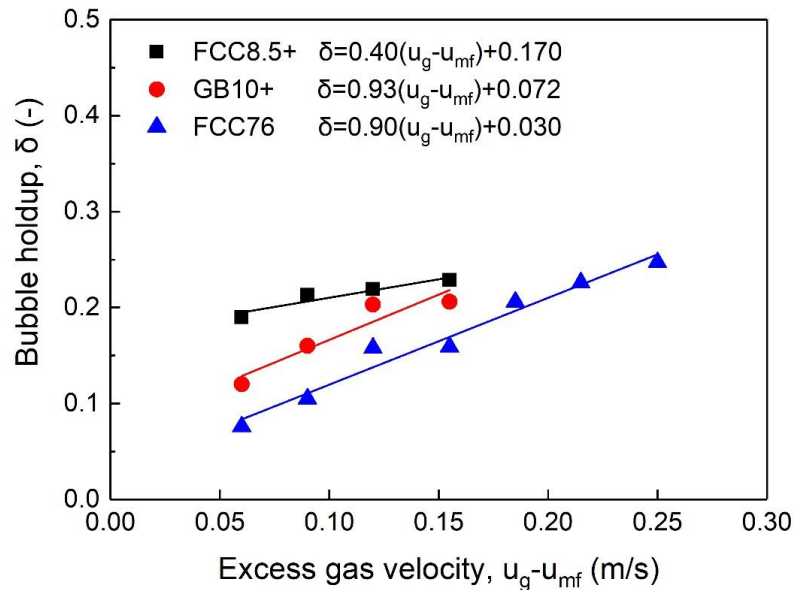
Figure 7.12: Relationships of the bubble holdup to the excess gas velocity for the three types of particles
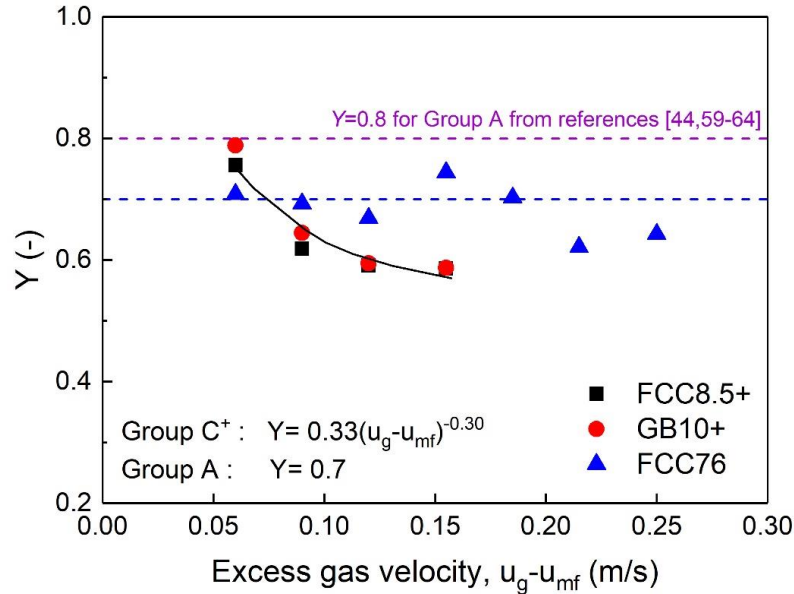
Figure 7.13: Relationships of *Y* values to the excess gas velocity for Group C$^+$ and A particles

Using the above correlations, the gas velocities of the bubble phase (u_b) and the dense phase (u_d) and the interstitial gas velocity in the dense phase (u_{di}) were obtained as shown in Figure 7.14. Group C$^+$ particles showed much lower u_b than Group A particles, indicating longer time for bubbles to interact with surrounding particles, while u_d and u_{di} for Group C$^+$ particles were much higher than for Group A particles, resulting in more gas flowing through the dense phase. More specifically, u_b for the three types of particles was: FCC76 > GB10+ > FCC8.5+, and both u_d and u_{di} for the three types of particles showed an inverse trend: FCC76 < GB10+ < FCC8.5+. The extraordinarily higher interstitial gas flow and the much lower bubble flow in the bed of Group C$^+$ particles are very favorable from a chemical reaction point of view. The grater gas flowrate of the dense phase and the lower gas flowrate of the bubble phase provided more opportunities for the gas flow to be in close contact with the particles, leading to enhanced reactor performance.
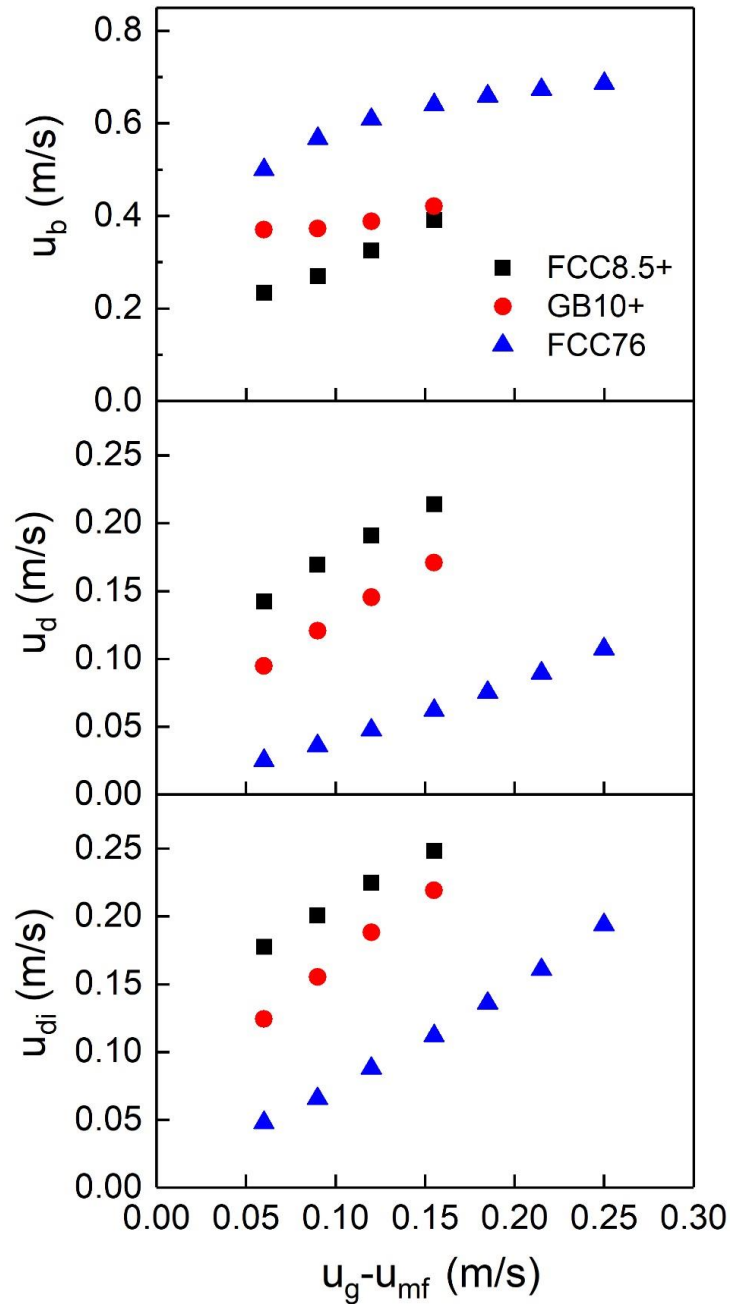
Figure 7.14: The calculated gas velocities in the two phases
for the three types of particles at different superficial gas velocities

As u_b is related to the bubble diameter (d_b), d_b can then be obtained using the correlation proposed by Davidson and Harrison [56] for predicting the bubble rise velocity:

$$u_b = (u_g - u_{mf}) + 0.71(g\ d_b)^{0.5} \qquad (7.16)$$

This correlation could then be modified with the *Y* values:

$$u_b = Y\,(u_g - u_{mf}) + 0.71(g\,d_b)^{0.5} \qquad\qquad (7.17)$$

The calculated bubble diameters using Equations (7.16) and (7.17) were compared with the experimental ones (D10, D50, and D90), as shown in Figure 7.15. D10, D50 and D90 are the mean bubble diameters at which 10%, 50% and 90% of the sum of bubbles area is comprised of bubbles with a diameter less than these values. Based on the simple two-phase theory, the calculated bubble diameters for FCC8.5+ particles were close to the value of D10, while those for GB10+ were close to the value of D50. When the modified Y correlation was applied, the calculated bubble diameters were closer to D50, the average bubble diameter, for both types of For Group C^+ particles. For the larger FCC76 particles, the calculated bubble diameters using both correlations were higher than the experimental ones, but leveled off at higher gas velocities. The modified correlation with Y could better predict the relationship between the bubble diameter and bubble rise velocity for Group C^+ particles, while overestimating the relationship for Group A particles.
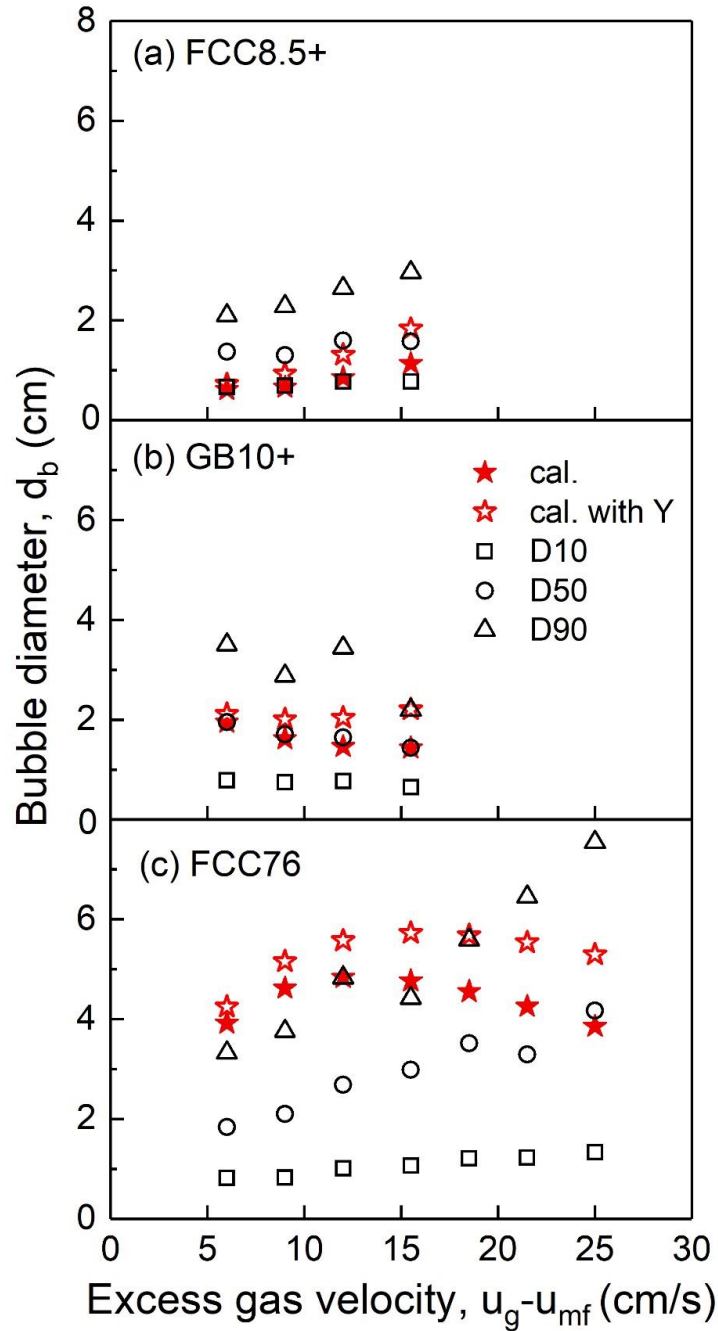
**Figure 7.15: The comparison of the calculated bubble sizes
with the experimental results**

7.5 Summary

The fluidized bed of Group C$^+$ particles was shown to have lower bubble rise velocity and
more uniform distribution of the bubble rise velocity than those in the bed of Group A

particles, corresponding to the smaller bubbles and longer bubble residence time observed in the bed. It also exhibited extraordinarily higher gas holdup in the dense phase, promoting more rigorous gas-solid contacts therein. Applying the modified two-phase theory and using the correction factor Y to account for increased dense phase gas flow, the Y value was found to be not a constant as previously suggested for Group A particles, but to decrease with the excess superficial gas velocity, for fine Group C^+ particles.

A new correlation for the correction factor, Y, was then developed in this study for Group C^+ particles. Using this new correlation (and the reported Y value for Group A particles), the distribution of the gas flow between the dense phase and the bubble phase in the beds of Group C^+ in comparison to Group A particles could be determined, quantifying the gas flow through the dense phase which was clearly higher than the minimum fluidization velocity (u_{mf}), and the gas flow through the bubble phase which was clearly lower than the excess gas velocity (u_g-u_{mf}). For Group C^+ particles, the lower gas bubble riser velocity (u_b) indicated longer time for gas bubbles to interact with the surrounding particles and the higher gas velocities through the dense phase (u_d and u_{di}) indicated more gas-solid interfacial contact through the dense phase.

Nomenclature

G_b	Volumetric flow rate into bubble phase (m^3/s, cm^3/s)
G_d	Volumetric gas flow into dense phase (m^3/s, cm^3/s)
A	Bed cross-sectional area (cm^2)
d_b	Bubble diameter (cm, m)
H_o	Initial fixed bed height (cm)
H_t	Total fluidized bed height (cm)
H_d	Dense phase height (cm)
H_b	Bubble phase height (cm)
u_g	Operating gas velocity (cm/s)
u_{mf}	Minimum fluidization velocity (cm/s)
u_b	Bubble rise velocity (cm/s, m/s)
u_{dm}	Superficial gas velocity in the dense phase (m/s, cm/s)

u_d	Gas velocity based on the dense phase without bubble volume (m/s, cm/s)
u_{di}	Interstitial gas velocity in the dense phase (m/s, cm/s)
ε_b	Fluidize bed voidage (-)
ε_d	Dense phase voidage (-)
δ	Bubble volume fraction (-)

Reference

[1] Grace J R and Sun G. Influence of particle size distribution on the performance of fluidized bed reactors. The Canadian Journal of Chemical Engineering, 1991, 69(5): 1126-1134.

[2] Liu J, Shi J, He D, Zhang Q, Wu X, Liang Y, and Zhu Q. Surface active structure of ultra-fine Cu/ZrO_2 catalysts used for the $CO_2 + H_2$ to methanol reaction. Applied Catalysis A: General, 2001, 218(1-2): 113-119.

[3] Yates J G and Newton D. Fine particle effects in a fluidized-bed reactor. Chemical engineering science, 1986, 41(4): 801-806.

[4] Zhang Y, Zhou Y, Liu J, Shao Y, and Zhu J. Performance Enhancement of Fluidized Bed Catalytic Reactors by Going to Finer Particles. Industrial & Engineering Chemistry Research. 2019, 58(43):20173-8.

[5] Li D, Zhu J, Ray M B, and Ray A K. Catalytic reaction in a circulating fluidized bed downer: ozone decomposition. Chemical engineering science. 2011, 66(20):4615-23.

[6] Abrahamsen A R and Geldart D. Behaviour of gas-fluidized beds of fine powders part I. Homogeneous expansion. Powder technology, 1980, 26(1): 35-46.

[7] Abrahamsen A R and Geldart D. Behaviour of gas-fluidized beds of fine powders part II. Voidage of the dense phase in bubbling beds. Powder Technology, 1980, 26(1): 47-55.

[8] Rowe P N, Santoro L, and Yates J G. The division of gas between bubble and interstitial phases in fluidised beds of fine powders. Chemical Engineering Science, 1978, 33(1): 133-140.

[9] Baumgarten P K and Pigford R L. Density fluctuations in fluidized beds. AIChE Journal, 1960, 6(1): 115-123.

[10] Dry R J, Judd M R, and Shingles T. Two-phase theory and fine powders. Powder Technology, 1983, 34(2): 213-223.

[11] Barreto G F, Yates J G, and Rowe P N. The measurement of emulsion phase voidage in gas fluidized beds of fine powders. Chemical Engineering Science, 1983, 38(3): 345-350.

[12] Barreto G F, Mazza G D, and Yates J G. The significance of bed collapse experiments in the characterization of fluidized beds of fine powders. Chemical engineering science, 1988, 43(11): 3037-3047.

[13] Yates Y G, Cheesman D J, and Sergeev Y A. Experimental observations of voidage distribution around bubbles in a fluidized bed. Chemical engineering science, 1994, 49(12): 1885-1895.

[14] Ye M, van der Hoef M A, and Kuipers J A M. A numerical study of fluidization behavior of Geldart A particles using a discrete particle model. Powder technology, 2004, 139(2): 129-139.

[15] Geldart D. Types of gas fluidization. Powder technology, 1973, 7(5): 285-292.

[16] Baeyens J, Geldart D, and Wu S Y. Elutriation of fines from gas fluidized beds of Geldart A-type powders—effect of adding superfines. Powder technology, 1992, 71(1): 71-80.

[17] Sun G and Grace J R. The effect of particle size distribution on the performance of a catalytic fluidized bed reactor. Chemical Engineering Science, 1990, 45(8): 2187-2194.

[18] Han M, Zhou Y, and Zhu J. Improvement on flowability and fluidization of Group C particles after nanoparticle modification. Powder Technology. 2019.

[19] Xu C, Zhang H, and Zhu J. Improving flowability of cohesive particles by partial coating on the surfaces. The Canadian Journal of Chemical Engineering, 2009, 87(3): 403-414.

[20] Xu C, Huang Q, Zhang H, and Zhu J. Improving fluidizability of cohesive particles by surface coating with flow conditioners. InThe Fifth World Congress on Particle Technology Orlando, FL, United States 2006.

[21] Zhu J and Zhang H. Fluidization additives to fine powders: U.S. Patent 6,833,185[P]. 2004-12-21.

[22] Chen Y, Yang J, Dave RN, and Pfeffer R. Fluidization of coated group C powders. AIChE journal. 2008, 54(1):104-21.

[23] Zhou Y and Zhu J. Group C+ particles: Enhanced flow and fluidization of fine powders with nano-modulation. Chemical Engineering Science. 2019, 207:653-62.

[24] Zhou Y and Zhu J. Group C+ particles: Extraordinary dense phase expansion during fluidization through nano-modulation. Chemical Engineering Science. 2020, 214:115420.

[25] Zhou Y, Xu J, and Zhu J. Different bubble behaviors in gas-solid fluidized bed of Geldart Group A and Group C+ particles. Submitted to AIChE J, 2020.

[26] Zhou Y, Zhao Z, Zhu J, and Bao X. Group C+ particles: Efficiency augmentation of fluidized bed reactor through nano-modulation. AIChE Journal. 2019: e16870.

[27] Johnstone RD and Toomey HF. Gas fluidization of solid particles. Chem. Eng. Prog. 1952, 48: 220.

[28] Turner J C R. On bubble flow in liquids and fluidised beds. Chemical Engineering Science, 1966, 21(11): 971-974.

[29] Davidson J F and Harrison D. The behaviour of a continuously bubbling fluidised bed. Chemical Engineering Science, 1966, 21(9): 731-738.

[30] Lockett M J, Davidson J F, and Harrison D. On the two-phase theory of fluidisation. Chemical Engineering Science, 1967, 22(8): 1059-1066.

[31] Pyle D L and Harrison D. An experimental investigation of the two-phase theory of fluidization. Chemical Engineering Science, 1967, 22(9): 1199-1207.

[32] Pyle D L and Harrison D. The rising velocity of bubbles in two-dimensional fluidised beds. Chemical Engineering Science, 1967, 22(4): 531-535.

[33] Geldart D. The expansion of bubbling fluidised beds. Powder Technology, 1968, 1(6): 355-368.

[34] Grace J R and Harrison D. The behaviour of freely bubbling fluidised beds. Chemical Engineering Science, 1969, 24(3): 497-508.

[35] Geldart D. The size and frequency of bubbles in two-and three-dimensional gas-fluidised beds. Powder Technology, 1970, 4(1): 41-55.

[36] McGrath L and Streatfield R E. Bubbling in shallow gas-fluidized beds of large particles. Trans. Instn. Chem. Engrs, 1971, 49(s 70).

[37] Argyriou D T, List H L, and Shinnar R. Bubble growth by coalescence in gas fluidized beds. AIChE Journal, 1971, 17(1): 122-130.

[38] Geldart D and Cranfield R. The gas fluidisation of large particles. The Chemical Engineering Journal, 1972, 3: 211-231.

[39] Werther J and Molerus O. The local structure of gas fluidized beds—I. A statistically based measuring system. International Journal of Multiphase Flow, 1973, 1(1): 103-122.

[40] Werther J and Molerus O. The local structure of gas fluidized beds—II. The spatial distribution of bubbles. International Journal of Multiphase Flow, 1973, 1(1): 123-138.

[41] Chavarie C and Grace J R. Performance analysis of a fluidized bed reactor. I. Visible flow behavior. Industrial & Engineering Chemistry Fundamentals, 1975, 14(2): 75-79.

[42] Grace J R and Clift R. On the two-phase theory of fluidization. Chemical Engineering Science, 1974, 29(2): 327-334.

[43] Clift R and Grace JR. Continuous bubbling and slugging. In Fluidization. 1985:73-132.

[44] Werther J. Scale-up of fluidized bed reactors. Ger. Chem. Eng. 1978, 1:243.

[45] Lanneau K P. Gas-solids contacting in fluidized beds. Trans. Inst. Chem. Eng, 1960, 38: 125-137.

[46] Lu T, Cheng D, Wang Y, Peng C, and Li H. Characteristics of Fine-Powder Fluidized Bed. In Fluidization: Science and Technology: Conference Papers, China-Japan Symposium, Science Press, Beijing. 1982: 57.

[47] Barreto G F, Yates J G, and Rowe P N. The effect of pressure on the flow of gas in fluidized beds of fine particles. Chemical engineering science, 1983, 38(12): 1935-1945.

[48] Piepers H W, Cottaar E J E, Verkooijen A H M, and Rietema K. Effects of pressure and type of gas on particle-particle interaction and the consequences for gas—solid fluidization behaviour. Powder Technology, 1984, 37(1): 55-70.

[49] Cherntongchai P and Brandani S. A model for the interpretation of the bed collapse experiment. Powder technology, 2005, 151(1-3): 37-43.

[50] Zimmermann S and Taghipour F. CFD modeling of the hydrodynamics and reaction kinetics of FCC fluidized-bed reactors. Industrial & engineering chemistry research, 2005, 44(26): 9818-9827.

[51] Wang J, van der Hoef M A, and Kuipers J A M. CFD study of the minimum bubbling velocity of Geldart A particles in gas-fluidized beds. Chemical Engineering Science, 2010, 65(12): 3772-3785.

[52] Chalermsinsuwan B, Gidaspow D, and Piumsomboon P. Two-and three-dimensional CFD modeling of Geldart A particles in a thin bubbling fluidized bed: Comparison of turbulence and dispersion coefficients. Chemical Engineering Journal, 2011, 171(1): 301-313.

[53] Ye M, Wang J, Van der Hoef M A, and Kuipers J A. Two-fluid modeling of Geldart A particles in gas-fluidized beds. Particuology, 2008, 6(6): 540-548.

[54] Ostu N. A threshold selection method from gray-level histograms. IEEE Transactions on Systems, Man and Cybernetics. 1979: 62-66.

[55] Rietema K. Application of mechanical stress theory to fluidization. Proc. Int. Symp. on Fluidization. 1967.

[56] Davies R M and Taylor G I. The mechanics of large bubbles rising through extended liquids and through liquids in tubes. Proceedings of the Royal Society of London. Series A. Mathematical and Physical Sciences, 1950, 200(1062): 375-390.

[57] Rippin D W T. The rise of gas bubbles in liquids. Ph. D. dissertation, 1959.

[58] Davidson J F and Harrison D. Fluidised particles. UMI Out-of-Print Books on Demand, 1990.

[59] Beyens J and Geldart D. Solids Mixing. Chapter 4 in Gas Fluidization Technology • ed, D Geldart. J Wiley&. Sons, London. 1986: pp.97- 112

[60] Hilligardt K and Werther J. Local bubble gas hold-up and expansion of gas/solid fluidized beds. German chemical engineering. 1986, 9(4):215-21.

[61] Werther J and Schoessler M. Modelling catalytic reactions in bubbling fluidized beds of fine pariticles in: Heat and mass transfer in fixed and fluidized beds (van Swaaij, W.P.M. and Afgan, H-H., eds.), Springer, Berlin, 1986: 355-370.

[62] Werther J. Scale-up modeling for fluidized bed reactors. Chemical engineering science. 1992, 47(9-11):2457-62.

[63]   Rhodes M J. Introduction to particle technology, 2nd Edition. Wiley, England 2008

[64]   Daizo K and Levenspiel O. Fluidization engineering, 2nd Edition. Butterworth-Heinemann, U.S. 1991.

Chapter 8

8 Prediction of Dense Phase Voidage for Group C⁺ Fluidized Bed Reactor

(A version of this chapter has been published in *Chemical Engineering Journal*)

Zhou Y, *Zhu J. Prediction of Dense Phase Voidage for Group C⁺ Fluidized Bed Reactor.*
Chemical Engineering Journal*. 2020 Jul 11:126217.*

Group C⁺ fluidized bed reactor exhibited better reactor performance than conventional fluidized bed reactors, due to the larger specific surface area of the catalysts and the more homogeneous fluidization, especially the extraordinary dense phase expansion which contributes to higher gas-solid contact efficiency. As a critical parameter affecting the reactor performance, the dense phase voidage (ε_d) was thoroughly characterized and general correlations for predicting ε_d were derived based on both Richardson-Zaki and Kozeny-Carman approaches. In addition, a new method for predicting the minimum fluidization velocity of Group C⁺ particles with the consideration of the particle cohesion was proposed. The bed voidage at minimum fluidization (ε_{mf}) and the maximum dense phase voidage ($\varepsilon_{d,max}$) were shown to correlate well with a dimensionless cohesion index (σ^*). All these new correlations showed good agreements with the experimental data for various types of Group C⁺ particles.

8.1 Introduction

Fluidized beds are useful contacting devices especially as industrial reactors for gas-phase catalytic and gas-solid reactions [1-5], providing high heat and mass transfer rates and large surface area for gas-solid contact. Generally, the performance of a fluidized bed is determined by many factors such as the bubble size and frequency, the minimum fluidization velocity, and the bed expansion, etc. [6-9]. For conventional fluidized bed reactors, the bed expansion is one of the critical parameters which determines the gas holdup in the bed, thus affecting the gas-solid contact and the chemical conversion [10-11]. More specifically, the bed expansion is influenced by the dense phase expansion and the bubble holdup on the basis of two-phase theory [12-14]. The degree of the dense phase

expansion, also expressed as the dense phase voidage (ε_d), quantifies the gas holdup in the dense phase which has a greater opportunity to contact with particles and thus is more beneficial for the gas-phase catalytic reactions.

As classified by Geldart [15], the fluidization quality becomes better with the decreasing of the particle size, from Group D to B and further to A particles. For example, Group A particles exhibit a homogenous expansion before the appearance of bubbles, signifying certain degree of higher dense phase expansion, while Group B particles immediately reach the bubbling regime at the minimum fluidization velocity, indicating little dense phase expansion [16-18]. Group C particles have even smaller particle size than Group A particles and are expected to show better fluidization quality, but the extremely small particle size results in strong interparticle forces and the difficulty in fluidization. Previous studies [19-28] have shown that the addition of nanoparticles can improve the flowability and fluidization quality of Group C particles. Such Group C[+] particles, providing larger specific surface area, had much higher bed expansion and larger dense phase voidage than Group A particles [28], and therefore significantly increase the reaction conversion due to the increased gas-solid interfacial contact [29-30].

It has been widely recognized that the homogeneous bed expansion before bubbling fluidization for Group A particles is ascribed to the interparticle forces [31-36]. Earlier studies [37-39] suggested that the interparticle forces could contribute to the stability of the fluidization, increase the dense phase voidage and increase the capability of the bed to retain gas. Therefore, the interparticle forces have an important effect on the fluidization hydrodynamics [40] and are helpful in maintaining the stable regime between the minimum fluidization and minimum bubbling velocities for Group A particles. There is no question but that interparticle forces play a more important role in the fluidization of Group C[+] particles, contributing to the high dense phase bed expansion and large dense phase voidage.

Considering the extremely high dense phase voidage in the fluidized bed of Group C[+] particles, it is necessary and critical to propose a theoretical approach to predict the dense phase behaviors. This work studied the dense phase voidage and the cohesion for Group

C[+] particles, and proposed equations to theoretically predict the dense phase voidage in the fluidization of Group C[+] particles.

8.2 Experimental

8.2.1 Experimental materials and apparatus

Three types of Group C particles used in the present experiments were glass beads (GB), fluid catalytic cracking (FCC) catalysts, polyurethane particles (PU) with their physical properties listed in Table 8.1. The nanoparticles used in this experiment were SiO_2 particles with a particle size of 16 nm and particle density of 2200 kg/m^3 (marketed as R972 by Evonik). Group C[+] particles were produced by mixing a small amount of nanoparticles with Group C particles [41-42]. Three nanoparticle concentrations in volume fractions were used, namely 0.27%, 0.44%, 0.82%.

Figure 8.1 schematically shows the experimental setup. The fluidization column was 5.08 cm (I.D.) x 45.7 cm (height) and was made of plexiglas. A gas distributor with an open area ratio of 2.5% was placed between the fluidized column and the wind box. Two layers of 625 mesh screen covered on the distributor to prevent fine particles dropping into the wind box. The air flowed through two PVC tubes into the wind box at two opposite positions. A measuring tape fixed along the fluidization column was used to read the bed height.

Table 8.1: Physical properties of experimental particles

Powder Name	Particle Size (µm)			Particle Density (kg/m^3)	Bulk Density[a] (kg/m^3)	ε_0[b]	Sphericity
	D_{10}	D_{50}	D_{90}				
GB10	1.6	10	29	2500	916	0.63	1
FCC8.5	1.5	8.5	26	1780	509	0.71	0.88
PU10	2	10	30	1200	560	0.53	0.76
PU18	4	18	50	1200	648	0.46	0.76
PU36	12	36	74	1200	679	0.43	0.78

[a] It is the loose bulk density (or poured density), and is measured using a Hosokawa powder tester by particles freely falling into a container with a fixed volume.
[b] Fixed bed voidage (ε_0) = 1−bulk density (ρ_b) / particle density (ρ_p).
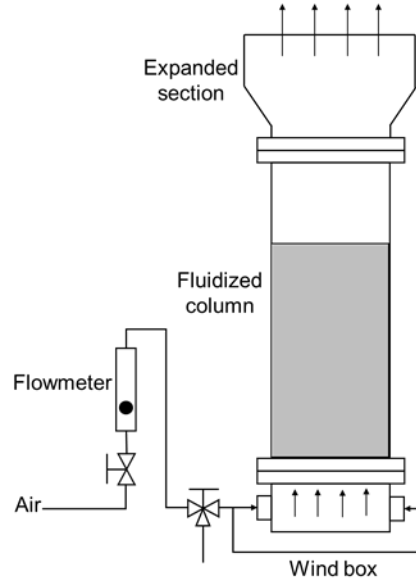
Figure 8.1: Experimental setup

8.2.2 Bed collapse test

Bed collapse test [43] was used to measure the dense phase voidage. The bed was fully fluidized at a high superficial gas velocity, and the bed height was recorded using a digital camera (Canon EOS 800D) when the gas supply was suddenly shut off. The bed height was a function of time to give a bed collapse curve as shown in Figure 8.2. The dense phase bed height (H_d) was identified from the bed collapse curves and hence the dense phase voidage (ε_d) could be calculated:

$$\varepsilon_d = 1 - (H_0 / H_d)\,(1 - \varepsilon_0) \qquad (8.1)$$

where H_0 is the initial fixed bed height, ε_0 is the initial fixed bed voidage. The bed collapse tests were conducted at various superficial gas velocities (u_g), ranging up to 13 cm/s. The superficial gas velocity in the dense phase (u_d) can be calculated as the following correlation [44]:

$$u_d = u_g - Y\,(u_g\text{-}u_{mf}) \qquad (8.2)$$

where the value of Y for Group C^+ particles is $Y = 0.33(u_g\text{-}u_{mf})^{-0.3}$, from experimental results in Chapter 7.
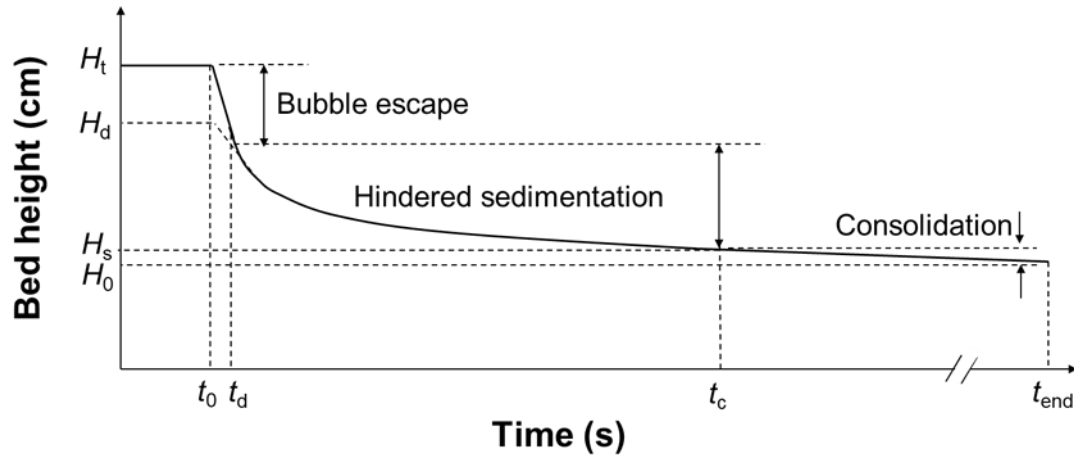
Figure 8.2: A typical bed collapse curve for Group C⁺ particles

8.2.3　FT4 cohesion test

Powder cohesion was tested following a standard process [45-46] using an FT4 Powder Rheometer manufactured by Freeman Technology, representing the degree of the interparticle forces. A powder sample was first conditioned and pre-sheared to reach a homogenized state and then was compressed under a specified normal stress of 9 kPa. Afterwards, the powder sample was sheared under normal stresses of 7, 6, 5, 4 and 3 kPa respectively to obtain shear stresses and the yield locus was achieved to obtain the cohesion, as shown in Figure 8.3. The test repeated three times and the value of the cohesion averaged for each sample, as reported in Table 8.2.
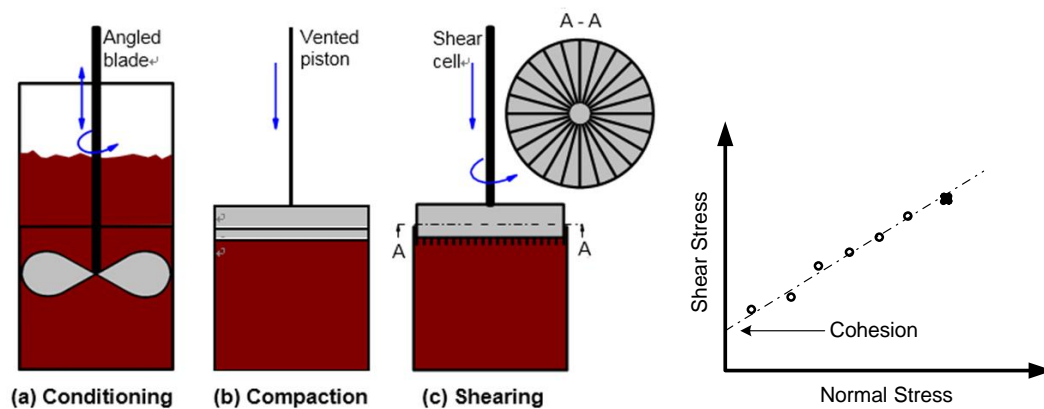
Figure 8.3: FT4 cohesion test

Table 8.2: Cohesion of experimental particles (kPa)

Cohesion	Nanoparticle volume concentration		
Powder	0.27%	0.44%	0.82%
GB10	0.933	0.917	0.853
FCC8.5	0.470	0.560	0.410
PU10	0.600	0.349	0.353
PU18	0.375	0.226	0.354
PU36	0.057	0.001	0.001

8.3   Results and discussion

8.3.1   Experimental results

The dense phase voidages for Group C$^+$ particles with the increase of the gas velocity are shown in Figures 8.4 and 8.5. When the superficial gas velocity reached and exceeded the minimum fluidization velocity (u_{mf}), the bed of Group C$^+$ particles started to fluidize and to expand significantly. As the gas velocity increased, the dense phase voidage increased and then leveled off for all types of Group C$^+$ particles, reaching a maximum value ($\varepsilon_{d,max}$, maximum dense phase voidage). For different types of Group C$^+$ particles, the dense phase voidage increased with the decrease of the particle size, because smaller particles often have stronger cohesion which may contribute to higher dense phase expansion. In addition, the nanoparticle concentration had a more significant effect on the dense phase voidage for finer Group C$^+$ particles (GB10, FCC8.5, and PU10) with stronger cohesion.

The dense phase voidage for Group C$^+$ particles reached as high as 0.84, extremely higher than that for Group A particles which is around 0.55, as more details in Chapters 3 and 4. The high dense phase voidage for Group C$^+$ particles indicated more gas holdup in the dense phase which could contribute to better gas-solid contact. Therefore, the dense phase voidage is a critical factor that affects the reactor performance for gas-phase catalytic reactions, and it is an important parameter in reactor models.
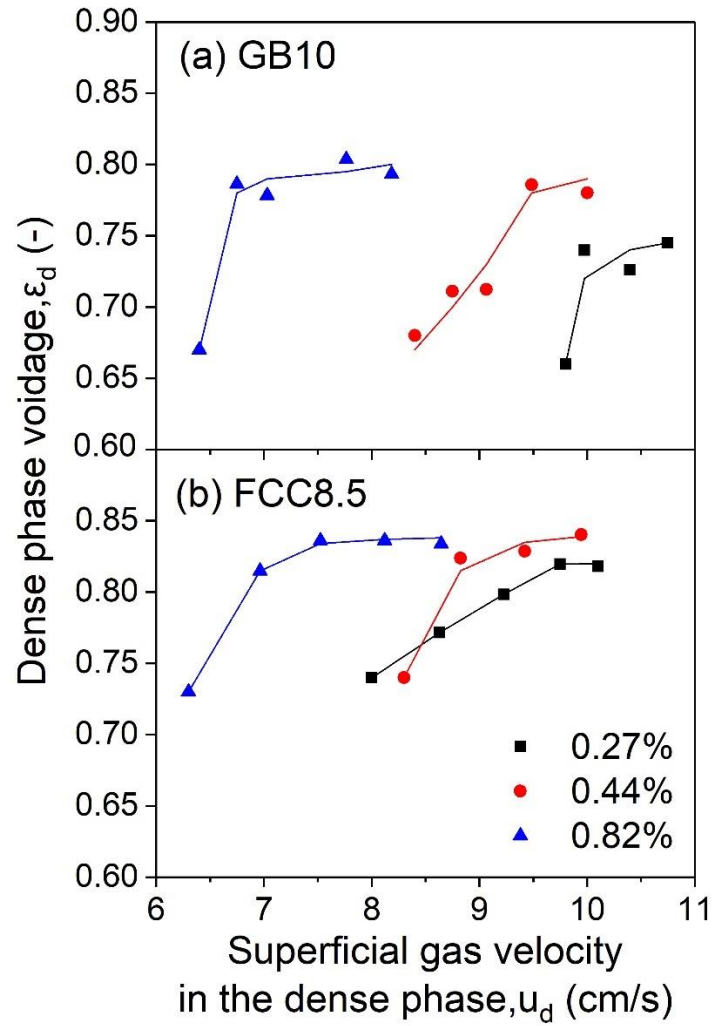
Figure 8.4: Dense phase voidages for GB10 and FCC8.5 at different gas velocities
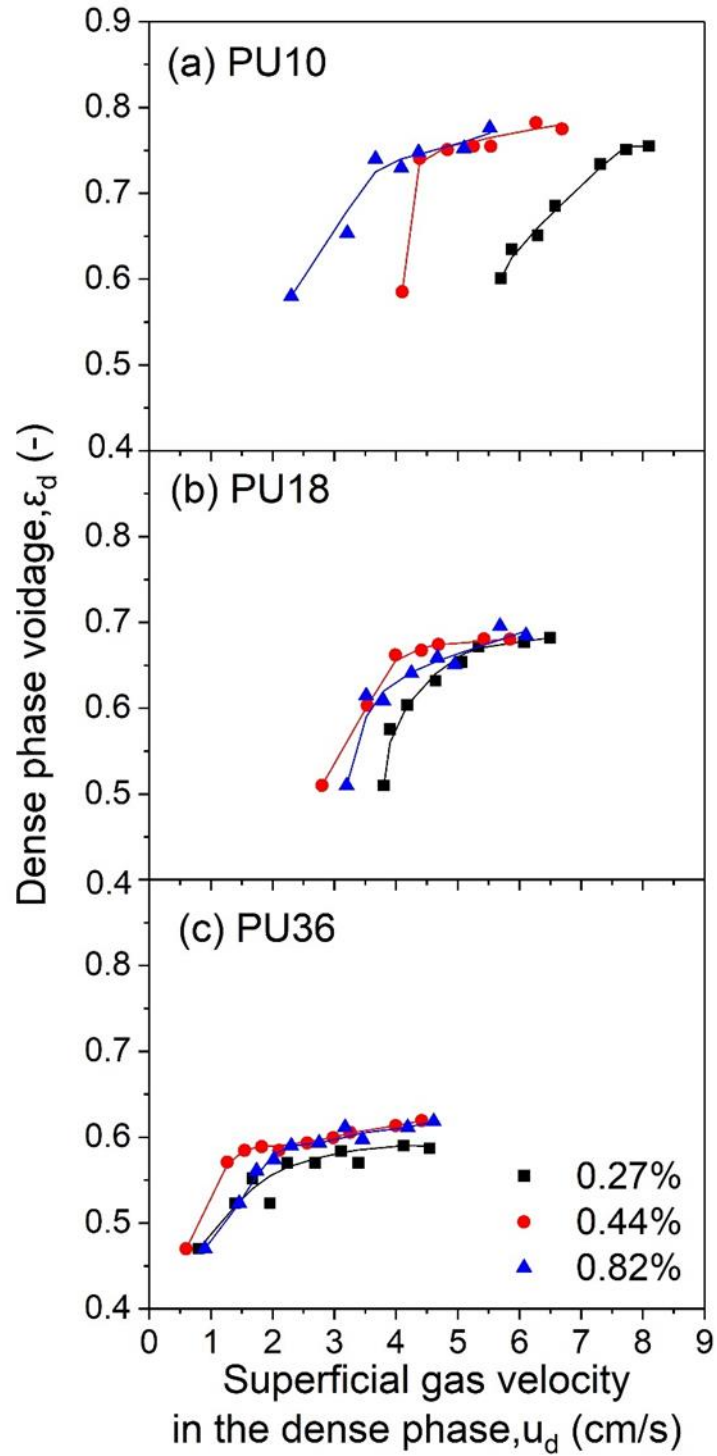
Figure 8.5: Dense phase voidages for three types of PU particles at different gas velocities

It is noted that for all types of Group C$^+$ particles, the dense phase voidage increased linearly with the gas velocity until it reached the maximum value, as specifically shown in Figure 8.6 (take PU18+0.44% as an example). The superficial gas velocity in the dense phase (u_d) when the dense phase voidage just reached its maximum was defined as the maximum dense phase expansion velocity ($u_{d,max}$). When u_d was between u_{mf} and $u_{d,max}$, the dense phase voidage (ε_d) had a linear relationship with u_d. The values of u_{mf}, $u_{d,max}$, and corresponding ε_{mf} and $\varepsilon_{d,max}$, for all types of Group C$^+$ particles are summarized in Table 8.3.
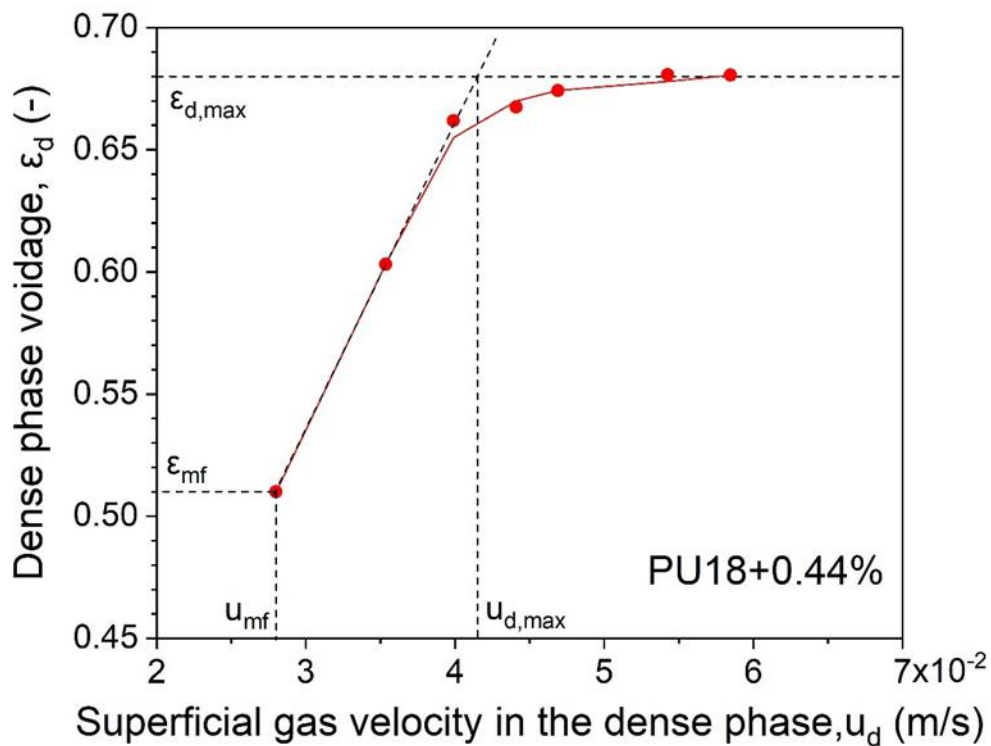
Figure 8.6: An example showing the relationship between the voidage and gas velocity

Table 8.3: Experimental values for Group C$^+$ particles of superficial gas velocity and voidage at minimum fluidization and maximum dense phase expansion conditions

Powder name	Nanoparticle concentration (v%)	u_{mf} (cm/s)	ε_{mf}	$u_{d,max}$ (cm/s)	$\varepsilon_{d,max}$
	0.27	9.8	0.66	10.0	0.75
GB10	0.44	8.4	0.67	9.5	0.78
	0.82	6.4	0.67	6.8	0.80
	0.27	8	0.74	9.8	0.82
FCC8.5	0.44	8.3	0.74	9.0	0.84
	0.82	6.3	0.73	7.1	0.84
	0.27	5.7	0.60	7.7	0.76
PU10	0.44	4.1	0.59	4.5	0.78
	0.82	2.3	0.58	4.1	0.77
	0.27	3.8	0.51	4.5	0.68
PU18	0.44	2.8	0.51	4.2	0.68
	0.82	3.2	0.51	3.9	0.69
	0.27	0.8	0.47	2.3	0.59
PU36	0.44	0.6	0.47	1.6	0.62
	0.82	0.9	0.47	2.4	0.62

When the gas velocity was between u_{mf} and $u_{d,max}$, the relationships of ε_d and u_d for all types of Group C$^+$ particles were linear, as shown in Figure 8.7. Based on the linear relationship in this region, it is feasible to correlate the dense phase voidage with the gas velocity.
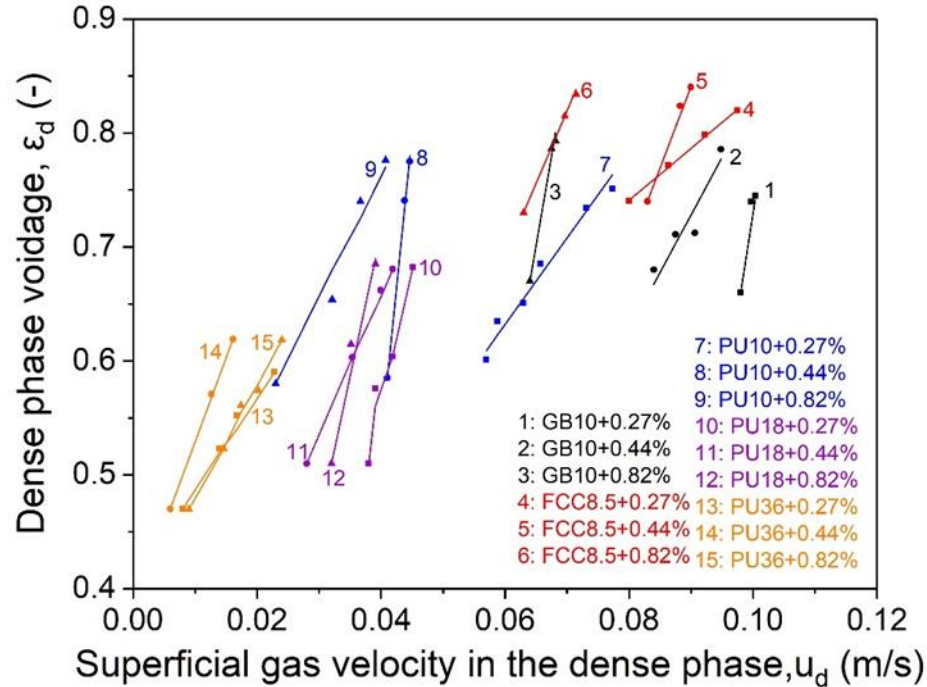
Figure 8.7: The dense phase voidages for all types of Group C⁺ particles with the increase of the gas velocity when $u_{mf} < u_d < u_{d,max}$

8.3.2   Theoretical Analysis

In conventional fluidized beds, the bed expands with the superficial fluid velocity, so that there should be a definite relationship between the bed voidage and the fluid velocity. Liquid-fluidized beds usually maintain a smooth fluidization, expanding progressively as the fluid velocity increases. This homogeneous expansion for liquid-fluidized beds has been correlated with the liquid velocity by several earlier researchers such as Ergun (1949) [47] and Richardson and Zaki (1954) [48]. Conversely, gas-fluidized beds generally exhibit heterogeneous structure with rising bubbles, making the relationship unclear. Nonetheless, aside from the bubble phase, a bubble-free dense phase does exist and displays a homogeneous expansion especially for smaller and lighter Geldart Group A particles [15,37]. For Group C⁺ particles, in our recent studies, with even smaller particle size and controlled interparticle forces, the gas-fluidized bed shows a more homogeneous fluidization with a highly expanded dense phase [26,28]. Additionally, the current study further revealed a linear relationship between the dense phase voidage and the gas velocity for Group C⁺ particles, as shown in Figure 8.7. Therefore, it is possible to correlate the

expansion of the dense phase in fluidized beds of Group C^+ particles in a similar way with the expansion in liquid-fluidized beds.

(a) Based on Richardson-Zaki approach

The Richardson-Zaki equation may be extended to correlate the dense phase expansion for Group C^+ particles with the superficial gas velocity in dense phase. The well-known Richardson-Zaki equation [48] expresses the bed voidage in liquid-solid fluidization as:

$$u_l / u_t = \varepsilon^n \qquad (8.3)$$

where u_l is the superficial liquid velocity, u_t is the terminal particle velocity, ε is the bed voidage, n is a parameter related to Reynolds number at terminal velocity ($n=4.65+20d_p/D$ when $Re_t < 0.2$). Considering the similar structure of the dense phase in the gas-solid fluidized bed with the liquid-solid fluidized bed, the Richardson-Zaki correlation may be expressed as:

$$u_d / u_{ta} = \varepsilon_d^n \qquad (8.4)$$

or in another form: $\qquad \log u_d = n \log \varepsilon_d + \log u_{ta} \qquad (8.5)$

where u_d is the superficial gas velocity in the dense phase, ε_d is the dense phase voidage, u_{ta} is the aggregated particle terminal velocity. When $\log u_d$ is plotted against $\log \varepsilon_d$, a linear relationship should be present, and n is the slope of the line.

The logarithmic plots of the superficial gas velocity in the dense phase versus the dense phase voidage for all types of Group C^+ particles are shown in Figure 8.8. Log u_d indeed showed a clearly linear relationship with log ε_d, indicating that the dense phase expansion in the fluidization of Group C^+ particles follow the Richard-Zaki Equation, and therefore have similar characteristics to those in a typical liquid-solid fluidized bed. The slopes of the straight lines varied with the types of Group C^+ particles which meant that the values of n were different for different particles.
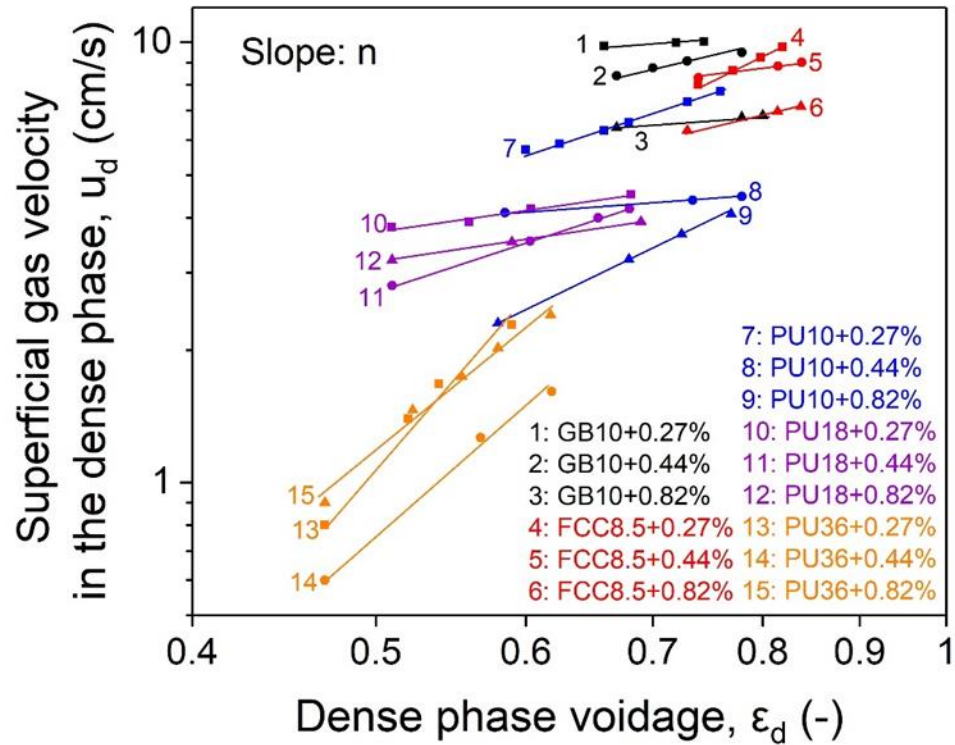
Figure 8.8: The logarithmic plots of u_d versus ε_d for all types of Group C$^+$ particles

The n values were then correlated to the particle cohesion as a key parameter for Group C$^+$ particles, as shown in Figure 8.9:

$$n = 0.47+3.56*0.013^{\sigma} \qquad (8.6)$$

The n value decreased with the increase of the particle cohesion, because higher cohesion contributed to higher dense phase voidage, which in turn gave lower n value. When the cohesion approached zero, the n value obtained via the experiments approximated to the constant $n = 4.65$ as predicted by the R-Z correlation.
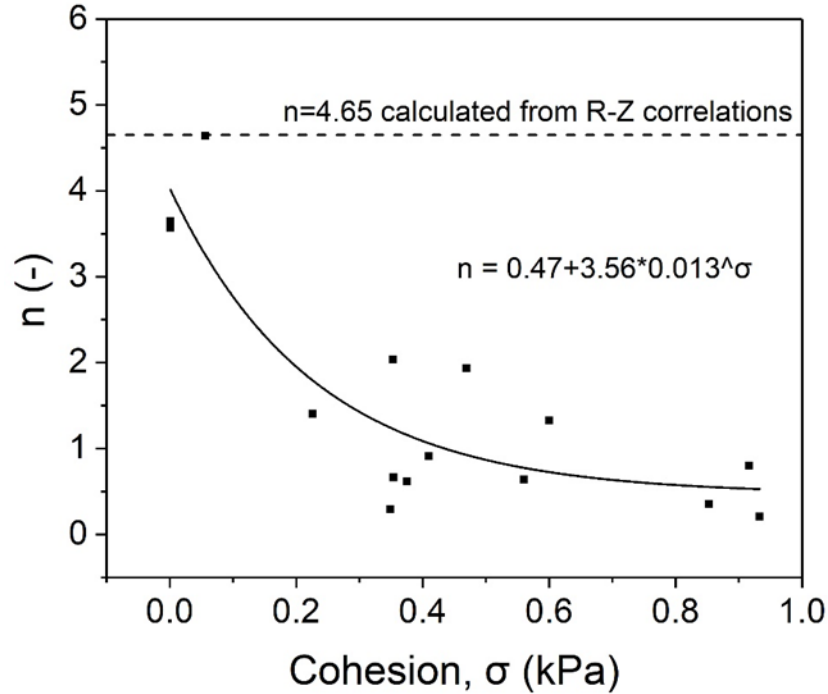
Figure 8.9: The n values plotted with the particle cohesion

With n correlated and becoming calculable, a general equation to predict the dense phase voidage could be developed: When the bed is at the minimum fluidization, Equation (8.5) can be written as:

$$\log u_{mf} = n \log \varepsilon_{mf} + \log u_{ta} \quad (8.5b)$$

Combining Equations (8.5) and (8.5b):

$$\log (u_d/u_{mf}) = n \log (\varepsilon_d/\varepsilon_{mf}) \quad (8.7)$$

or in another form: $\quad u_d/u_{mf} = (\varepsilon_d/\varepsilon_{mf})^n \quad (8.8)$

where $n=0.47+3.56*0.013^{\wedge}\sigma$ (Equation 8.6) and σ is the particle cohesion.

If the particle cohesion (σ), minimum fluidization velocity (u_{mf}), and the bed voidage at minimum fluidization (ε_{mf}) for any type of particles are known, the dense phase voidage at a given gas velocity can be calculated using Equation (8.8).

(b) Based on Kozeny-Carman approach

Ergun equation (1952) [49], was proposed to calculate the interstitial gas flow for a porous medium consisting of particles and pores between the particulate materials, built upon the

Kozeny-Carman equation [50-51] which describes laminar flow of fluid across the packed beds (viscous effect), and the Darcy-Forchheimer equation [52] which approximates the resistance due to turbulences (kinetic effect). The correlation by Ergun [49] initially provided the pressure drop across a fixed bed of particles as a function of the Reynolds number, but then extended to cover minimum fluidized bed [53] and particulate fluidized bed above the minimum fluidization [54]. Now, it is found that Group C^+ particles exhibited extremely high dense phase expansion [28], and that the dense phase expanded almost linearly with the gas velocity in between u_{mf} and $u_{d,max}$. Therefore, the dense phase expansion with homogeneous structure could be considered as particulate fluidization, and thus be predicted. As the viscous effect is dominant for fine particles with low Reynolds number, the prediction of the dense phase voidage for Group C^+ particles could be developed based only on Kozeny-Carman theory [51]:

When a fluid flow through a porous media, the pressure drop is described by the Kozeny-Carman equation [51]:

$$\frac{\Delta P}{H} = \frac{K\mu_g}{d_{sv}^2} \frac{(1-\varepsilon_b)^2}{\varepsilon_b^3} u_g \qquad (8.9)$$

where d_{sv} is the surface-volume diameter and K is Kozeny constant, which is theoretically 180 for narrow particle size distribution. If it is assumed that an expanded dense phase in the fluidized bed has the same basic structure as a packed bed, based on the Kozeny-Carman theory [51], Equation (8.9) can be rewritten as:

$$\frac{\Delta P}{H} = \frac{K_f\mu_g}{d_p^2} \frac{(1-\varepsilon_d)^2}{\varepsilon_d^3} u_d \qquad (8.10)$$

where ε_d is the dense phase bed voidage, d_p is the mean particle size, and u_d is the superficial gas velocity in the dense phase which is in the region of $u_{mf} < u_d < u_{d,max}$. In the fluidized bed, particles are free to move and the value of Kozeny constant may be different with that in the fixed bed. Therefore, K_f is proposed here as the Kozeny constant in the fluidized bed and can be determined experimentally.

When the bed is fluidized, the weight of the fluidized particles equal to the pressure drop across the bed:

$$\frac{\Delta P}{H} = (1-\varepsilon_d)(\rho_p - \rho_g)g \qquad (8.11)$$

Combing equation (8.10) and (8.11):

$$f(\varepsilon_d) = \frac{\left(\rho_p - \rho_g\right)g\bar{d}_p^{\,2}}{\mu_g}\frac{\varepsilon_d^{\,3}}{1-\varepsilon_d} = K_f u_d \qquad (8.12)$$

If this approach is valid, plotting the term on the left-hand side of Equation (12) (the "dense phase expansion function $f(\varepsilon_d)$") against the superficial gas velocity in the dense phase (u_d) should give a straight line of a slope K_f.

Take PU18+0.44% as an example, the dense phase expansion function against the u_d evidently gave a straight line of a slope K_f, as shown in Figure 8.10. The relationships between the dense phase expansion function $f(\varepsilon_d)$ and the gas velocity u_d for all types of Group C$^+$ particles are shown in Figure 8.11. For all types of Group C$^+$ particles, $f(\varepsilon_d)$ showed clearly linear relationships with u_d, but the straight lines had different slopes, indicating different values of K_f. As K_f is related to the bed voidage and the particle properties such as the particle diameter, density, and shape etc., all these factors contributing, in different degrees, to the particle cohesion (σ). Therefore, K_f was correlated to the particle cohesion in Figure 8.12, giving the following correlation:

$$K_f = 82.0\,\sigma^2 - 62.0\,\sigma + 26.6 \qquad (8.13)$$
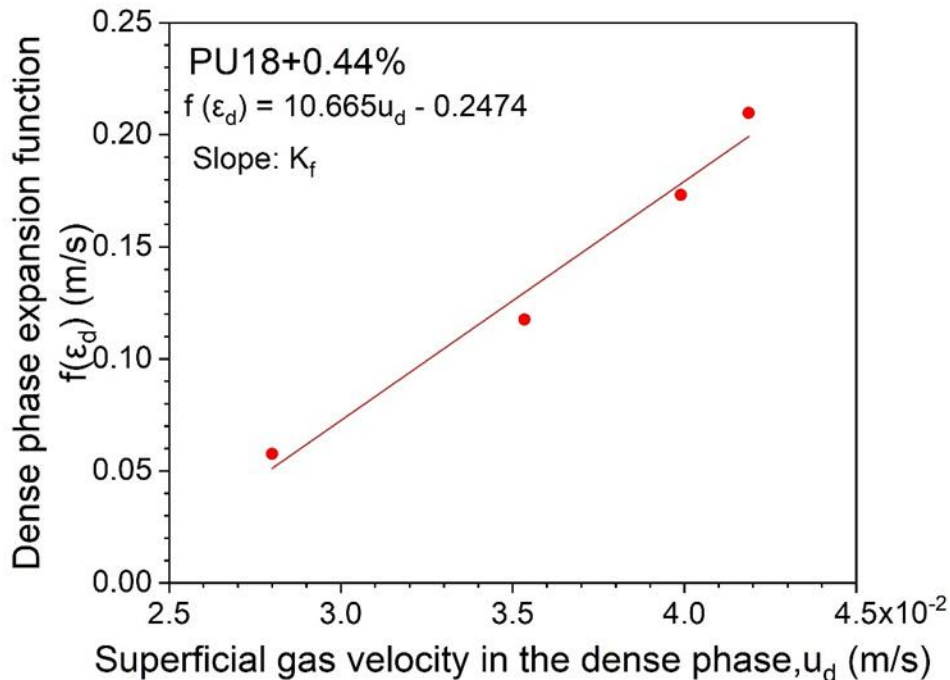
Figure 8.10: An example showing relationship between dense phase expansion function and gas velocity (PU18+0.44%)
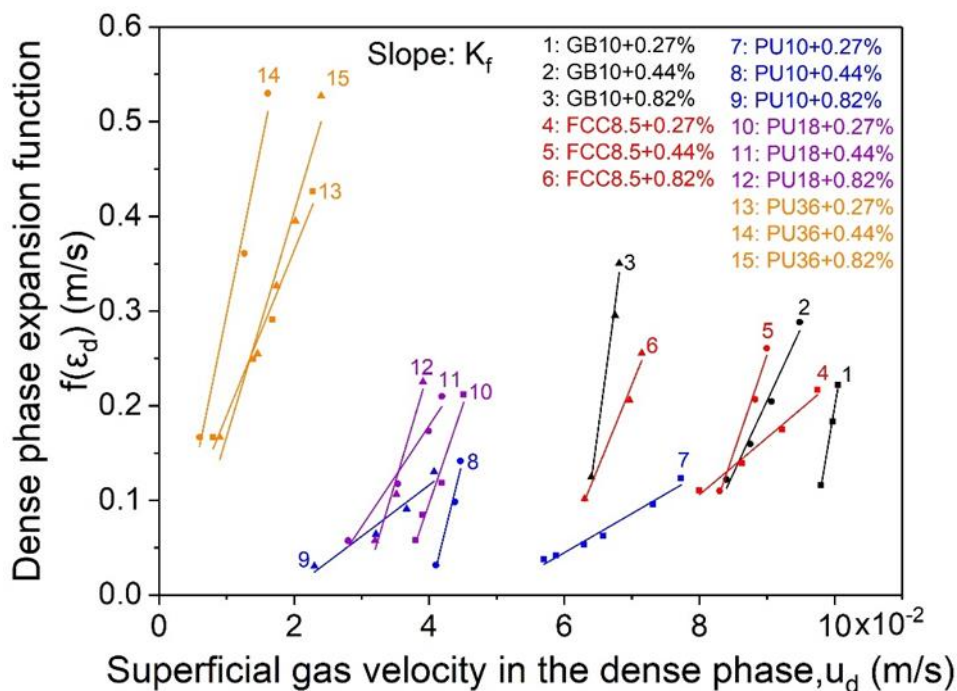
Figure 8.11: Relationship between dense phase expansion function and gas velocity for various Group C$^+$ particles
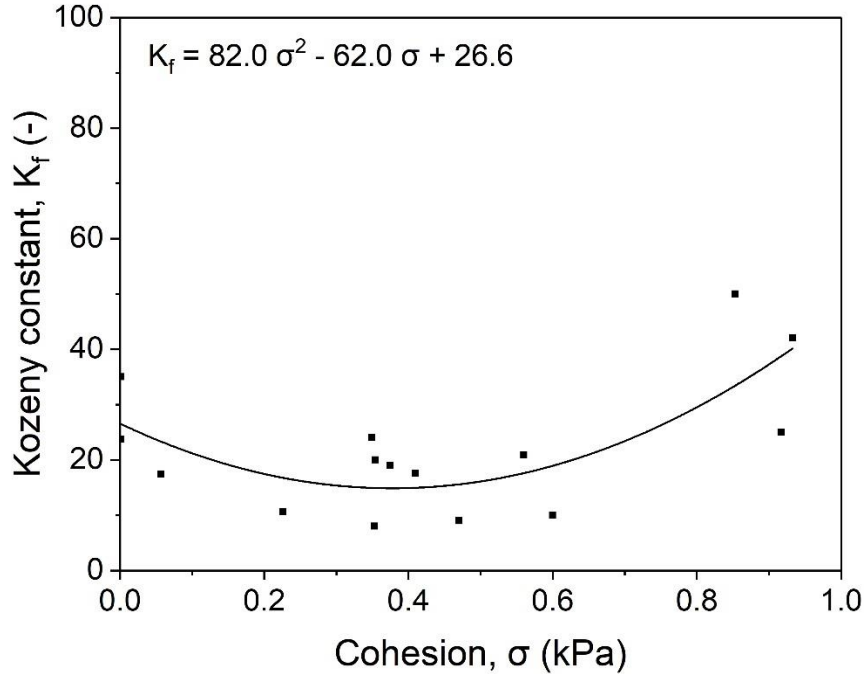
Figure 8.12: Relationship between K_f and cohesion

In summary, the relationship between the dense phase voidage and the gas velocity could be expressed by Equation (8.12) based on Kozeny-Carman theory. However, Equation (8.12) indicates that all the data should fall on the lines passing through the origin, but most lines in Figure 8.11 did not pass the origin, because the particle mobility and the "real" bed structure in the expanded bed are not the same as those in the fixed bed [37]. Therefore, within the region of $u_{mf} < u_d < u_{d,max}$, a general expression to predict the dense phase expansion for Group C$^+$ particles should be written as:

$$\frac{(\rho_p - \rho_g) g \bar{d}_p^2}{\mu_g} \frac{\varepsilon_d^3}{1 - \varepsilon_d} = K_f (u_d - u_{mf}) + \frac{(\rho_p - \rho_g) g \bar{d}_p^2}{\mu_g} \frac{\varepsilon_{mf}^3}{1 - \varepsilon_{mf}} \quad (8.14)$$

where $u_{mf} < u_d < u_{d,max}$, $\varepsilon_{mf} < \varepsilon_d < \varepsilon_{d,max}$, and $K_f = 82.0 \sigma^2 - 62.0 \sigma + 26.6$ (Equation 8.13).

If the particle cohesion (σ), minimum fluidization velocity (u_{mf}), and the bed voidage at minimum fluidization (ε_{mf}) of any types of particles are obtained, the dense phase voidage at a given gas velocity can be calculated.

8.3.3 Prediction for minimum fluidization velocity (u_{mf})

Minimum fluidization velocity is an important parameter to describe the fluidizability of particles [25] and is critical in the design and operation of a fluidized bed. Many literatures focused on the correct prediction of this parameter, such as the semi-empirical correlation proposed by Wen and Yu (1966) [53] based on the well-known Ergun equation [49], and the empirical correlation of Leva (1959) [55]. All these correlations were developed based on the data of non-cohesive particles, such as Group B particles, and were not applicable in predicting the u_{mf} of fine particles, especially of Group C$^+$ particles with a certain degree of cohesion. Here, a new method was proposed to predict the u_{mf} of Group C$^+$ particles.

For a single particle without the consideration of interparticle forces, the terminal velocity (u_t) occurs when the sum of the drag force (F_d) and the buoyancy (which is negligible in a gas-solid system) is equal to the gravity (G_p):

$$\text{Drag force } (F_d) = \text{Gravity } (G_p)$$

$$(\pi/8) \, C_D \, \rho_g \, u_t^2 \, d_p^2 = (\pi d_p^3 /6) \, (\rho_p - \rho_g) \, g \quad (8.15)$$

where the drag coefficient C_D is given by: $C_D = 24/\, Re_t$ (at low Reynolds number), and $Re_t = d_p \, u_t \, \rho_g \,/\, \mu$.

For Group C$^+$ particles with the consideration of the interparticle forces, the drag force would be equal to the sum of the gravity and the effective interparticle forces at the minimum fluidization state:

$$\text{Drag force } (F_d) = \text{Gravity } (G_p) + \text{ the effective IPFs } (\varphi) = (\pi/8) \, C_{D,mf} \, \rho_g \, u_{mf}^2 \, d_p^2 \quad (8.16)$$

$$(G_p + \varphi) \,/\, G_p = (C_{D,mf} \, u_{mf}^2) \,/\, (C_D \, u_t^2) = u_{mf} \,/u_t \quad (8.17)$$

The effective interparticle forces (φ) was related to the particle cohesion (σ), the particle diameter (d_p), and the number of contact points per particle ($n_c = 1.61 \, \varepsilon_0^{-1.48}$, proposed by Krupp in 1967 [56]):

$$\varphi = \alpha \, (\sigma d_p^2) \,/\, (1.61 \varepsilon_0^{-1.48}) \quad (8.18)$$

where α is a constant coefficient, around 0.01. More specific values for different types of particles are shown in Figure 8.13: For FCC8.5, $\alpha=0.014$; for GB10, $\alpha=0.008$; for PU10, $\alpha=0.01$; and for PU18, $\alpha=0.007$.
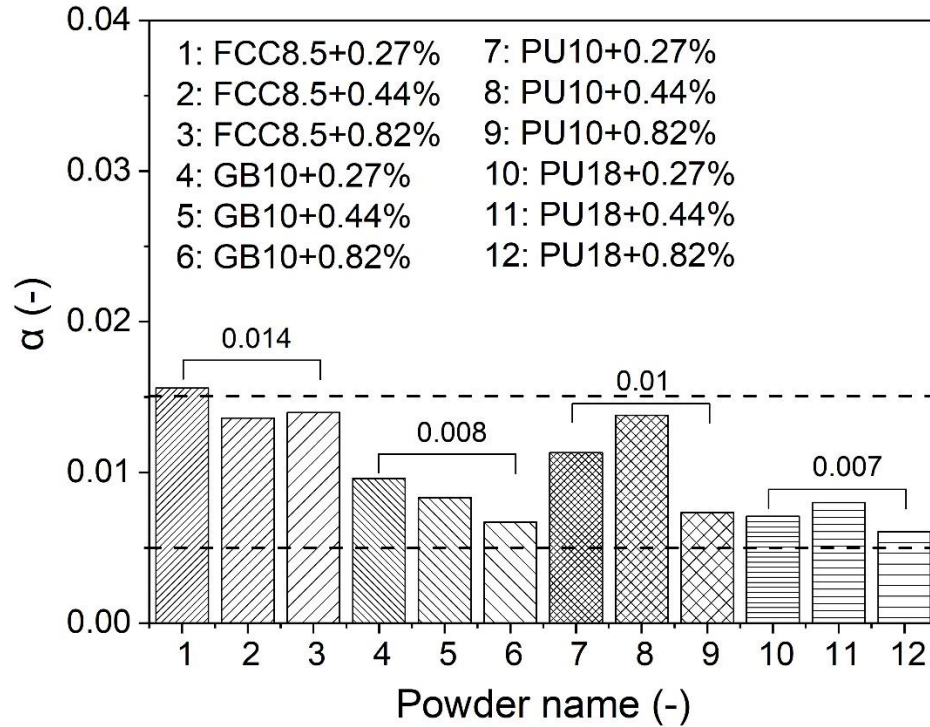
Figure 8.13: α values for various Group C$^+$ particles

Once the values of φ were determined using Equation (8.18) from the various particle properties including the particle cohesion σ, u_{mf} could be predicted by Equation (8.17b):

$$u_{mf} = u_t\,(G_p + \varphi) / G_p \qquad (8.17b)$$

Figure 8.14 compares the predicted u_{mf} with the experimental one using the method in this work, Wen and Yu equation [$u_{mf} = (\rho_p - \rho_g)g d_p / (1650\mu_g)$ for $Re_{mf} < 20$] and Lava equation [$u_{mf} = 7.169\mathrm{x}10^{-4}(\rho_p - \rho_g)^{0.94}g d_p^{1.82} / (\rho_g^{0.06}\mu_g^{0.88})$ for $Re_{mf} < 30$]. The predicted values of u_{mf} by this work were much closer to the experimental values of u_{mf} within a deviation less than 20%, except for PU36 particles with insignificant cohesion. The predicted value of u_{mf} using Wen and Yu equation [53] and Lava equation [55] were dramatically far from the experimental results. Therefore, the method proposed in this work was feasible in predicting the u_{mf} of Group C$^+$ particles with a degree of particle cohesion. On the other hand, the proposed correlation may not be applicable to particles with little or no interparticle force, such as PU36 in this study, which is a typical type of Group C/A powder but becomes a typical type of Group A particles after nano-modulation [26].
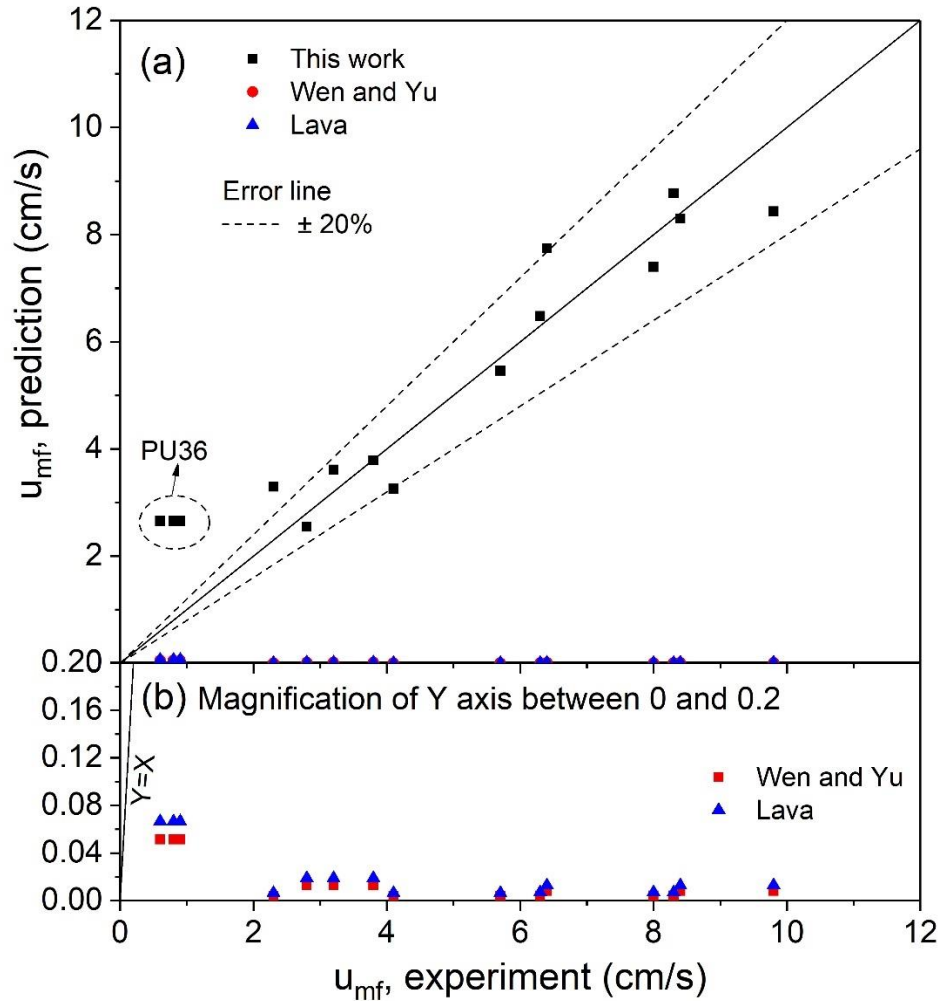
Figure 8.14: Comparison of the predicted u_{mf} with the experimental one

8.3.4 Prediction for bed voidage at minimum fluidization (ε_{mf}) and maximum dense phase voidage ($\varepsilon_{d,max}$)

The bed voidage at minimum fluidization (ε_{mf}) is an essential parameter in many correlations such as Ergun equation to predict u_{mf}. The bed voidage at minimum fluidization (ε_{mf}) was suggested to be in the range 0.40-0.45 for nearly spherical particles, increasing a bit with the decrease of the particle size [57]. In some works, ε_{mf} was assumed to be a fixed value such as 0.5 [58-59]. Other previous works [53,55,60-61] reported that the value of ε_{mf} were dependent on a variety of particle properties including particle size, shape, and material. For Group C^+ particles, the particle cohesion is normally the primary concern which affects the fluidization behaviors, and it is affected by the particle size and

density. Therefore, a dimensionless cohesion index (σ^*) was proposed here which involved the particle size (d_p), the particle density (ρ_p), the particle cohesion (σ), and the initial bed voidage (ε_0) to quantify the effect of the particle cohesion on the bed voidage, based on the concept of dimensionless groups proposed by Grace [55] which involved particle and fluid properties to describe the transition between the fluidization regimes. The dimensionless cohesion index (σ^*) was:

$$\varepsilon_{mf} = F(\sigma^*) = f(d_p, \rho_p, \sigma, \varepsilon_0, g)$$

$$\sigma^* = \frac{\sigma \varepsilon_0 d_p^2}{d_p^3 \rho_p g} = \frac{\sigma \varepsilon_0}{d_p \rho_p g} \qquad (8.19)$$

The bed voidage at minimum fluidization increased with the dimensionless cohesion index, as shown in Figure 8.15. The correlation of the bed voidage at minimum fluidization (ε_{mf}) with the dimensionless cohesion index were:

$$\varepsilon_{mf} = 9 \times 10^{-5} \, \sigma^* + 0.46 \qquad (8.20)$$

The same approach was used to correlate the maximum dense phase voidage ($\varepsilon_{d,max}$):

$$\varepsilon_{d,max} = 7 \times 10^{-5} \, \sigma^* + 0.63 \qquad (8.21)$$
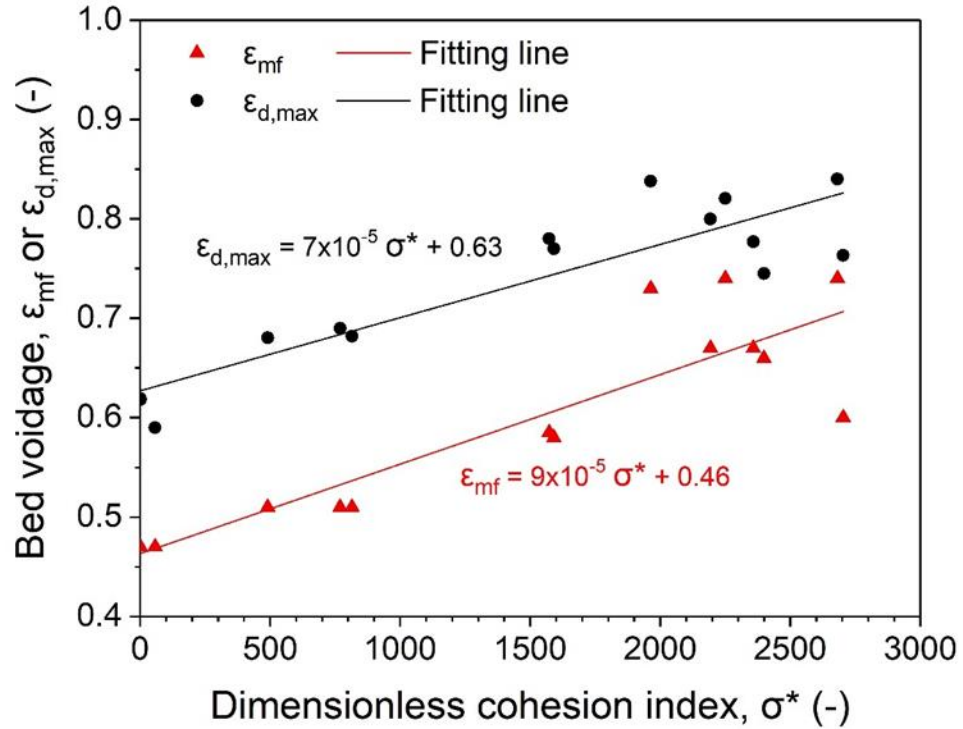
Figure 8.15: Relationship between bed voidages and dimensional cohesion index

The predicted ε_{mf} and $\varepsilon_{d,max}$ are compared with the experimental ones, as shown in Figures 8.16 and 8.17. The predicted results agreed well with the experimental ones. The deviation for ε_{mf} was less than 15% and that for $\varepsilon_{d,max}$ was less than 10%.
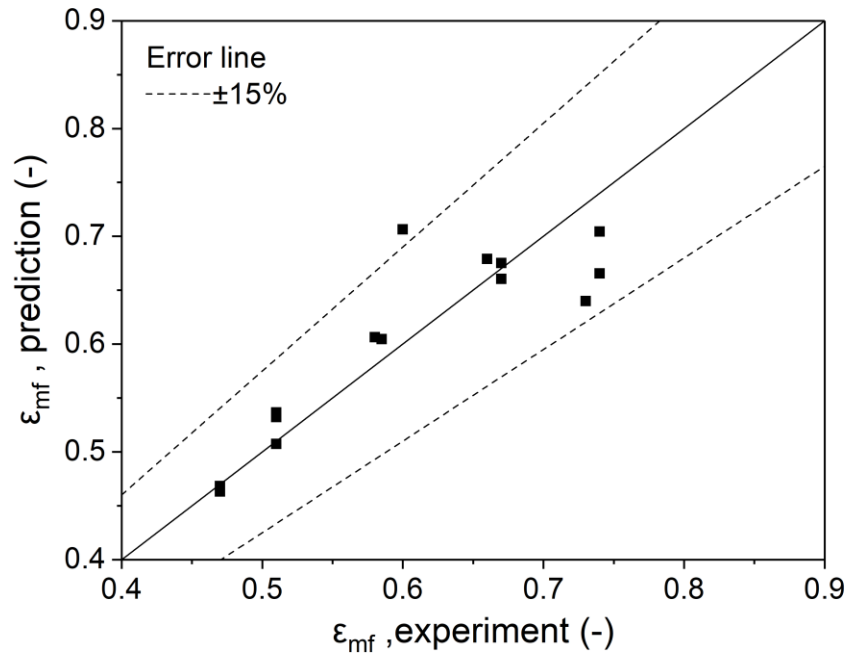
Figure 8.16: Comparison of the predicted ε_{mf} with the experimental one
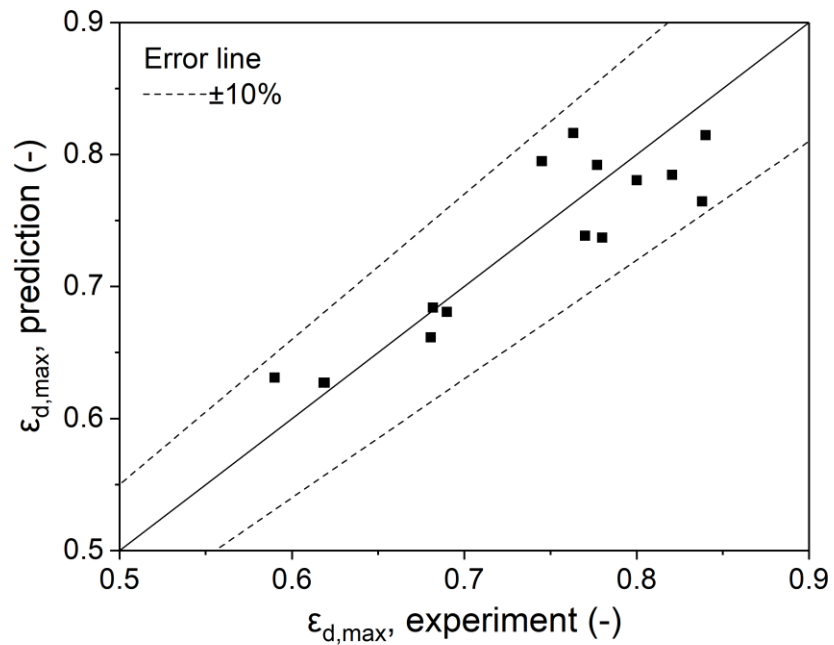
Figure 8.17: Comparison of the predicted $\varepsilon_{d,max}$ with the experimental one

8.3.5　Prediction for dense phase voidage (ε_d)

As u_{mf}, ε_{mf}, and $\varepsilon_{d,max}$ can be predicted, the dense phase voidage (ε_d) at different gas velocities can be further calculated using Equation (8.8) based on Richardson-Zaki approach or using Equation (8.14) based on Kozeny-Carman approach. In summary, the general expressions to predict the dense phase voidage for Group C$^+$ particle fluidization were:

Based on Richardson-Zaki equation: $\quad u_d/u_{mf} = (\varepsilon_d/\varepsilon_{mf})^n \quad\quad\quad\quad$ (8.8)

Based on Kozeny-Carman equation: $\dfrac{(\rho_p-\rho_g)g\bar{d}_p^2}{\mu_g}\dfrac{\varepsilon_d^3}{1-\varepsilon_d}=K_f(u_d-u_{mf})+\dfrac{(\rho_p-\rho_g)g\bar{d}_p^2}{\mu_g}\dfrac{\varepsilon_{mf}^3}{1-\varepsilon_{mf}}$ (8.14)

where $u_{mf}<u_d<u_{d,max}$, $\varepsilon_{mf}<\varepsilon_d<\varepsilon_{d,max}$,

$n=0.47+3.56*0.013^\sigma$, $K_f=82.261\sigma^2-64.054\sigma+27.265$,

$u_{mf} = u_t (G_p + \varphi)/G_p$, $\varphi = \alpha (\sigma d_p^2) / (1.61\varepsilon_0^{-1.48})$, α is a constant coefficient,

$\varepsilon_{mf} = 9\text{x}10^{-5} \sigma^* + 0.4631$, $\varepsilon_{d,max} = 7\text{x}10^{-5} \sigma^* + 0.627$, and $\sigma^* = \dfrac{\sigma\varepsilon_0}{d_p\rho_p g}$.

The predicted dense phase voidages were compared with the experimental ones in Figure 8.18 based on Richardson-Zaki approach and Figure 8.19 based on Kozeny-Carman approach. The predicted ε_d agreed well with the experimental values with deviation less than 20%, and most points were located within the deviation of 10%. As a result, it is feasible to predict the dense phase voidage for Group C$^+$ particles based on either Richardson-Zaki or Kozeny-Carman approach.

In summary, for a given type of Group C$^+$ particle, we only need to characterize the particle size (d_p), the particle density (ρ_p), the particle cohesion (σ), and the initial bed voidage (ε_0) (or the bulk density) to predict the dense phase voidage at different superficial gas velocities. The methods proposed in this work could correctly predict the dense phase voidage for Group C$^+$ particle fluidization, which is an important parameter in reactor modelling. The correct prediction of ε_d can further help to evaluate the performance of a fluidized bed reactor using Group C$^+$ particles as catalysts, and give a guidance for the design and the operation of the Group C$^+$ fluidized bed reactor.
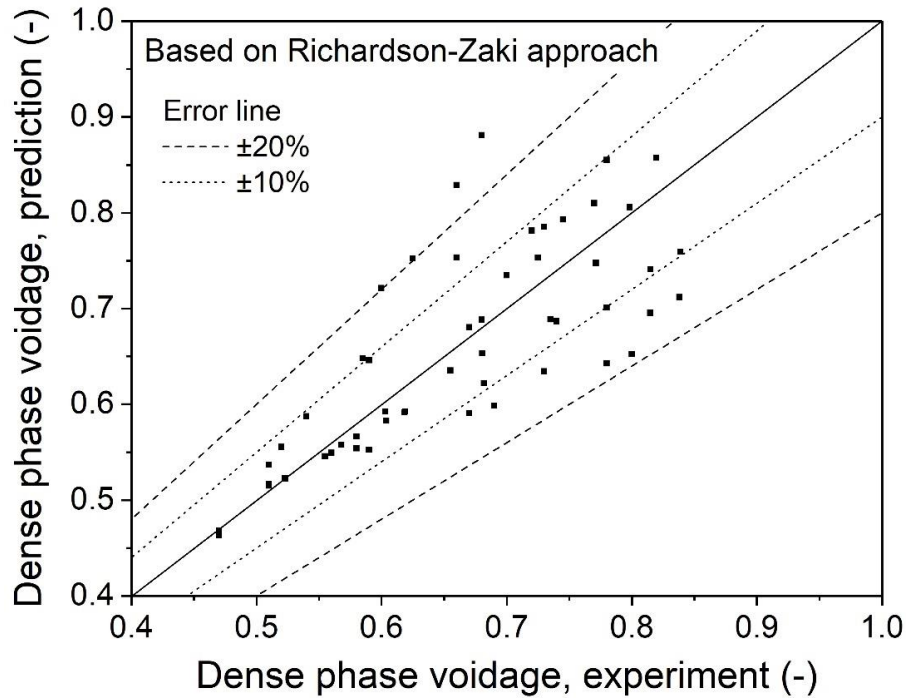
Figure 8.18: Comparison of the predicted ε_d with the experimental one based on Richardson-Zaki approach
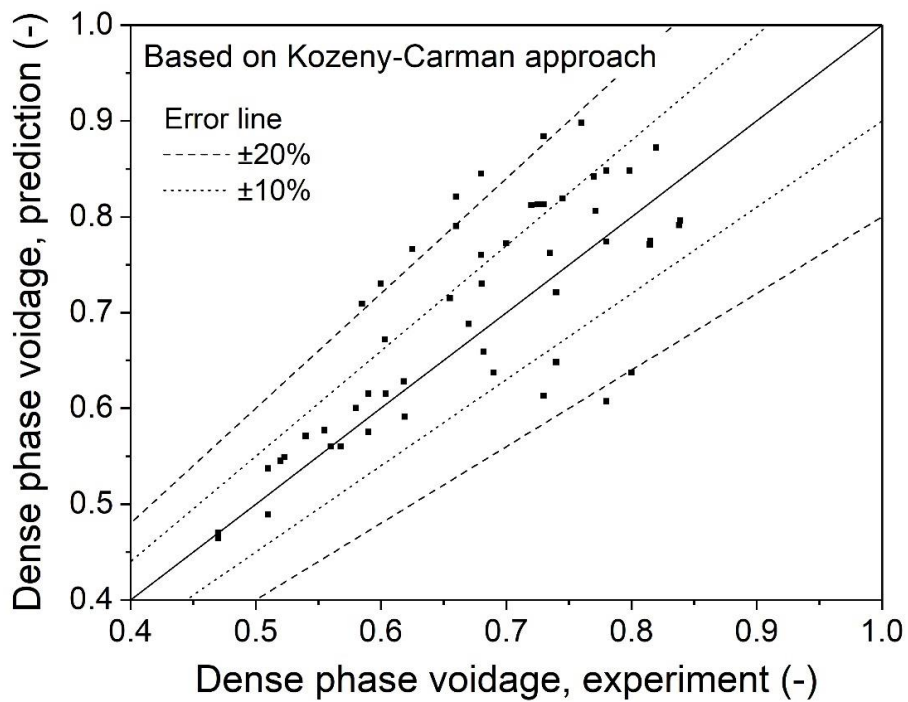
Figure 8.19: Comparison of the predicted ε_d with the experimental one based on Kozeny-Carman approach

8.4 Conclusions

The dense phase voidage (ε_d) for Group C^+ particles was found to increase linearly with the superficial gas velocity in the dense phase (u_d) when operating between the minimum fluidization velocity, u_{mf}, and the maximum dense phase expansion velocity, $u_{d,max}$, and then remained unchanged at the value of maximum dense phase voidage ($\varepsilon_{d,max}$). The dense phase in the gas-fluidized bed of Group C^+ particles showed a similar structure with the liquid-fluidized beds, leading to the possibility to make a prediction of the dense phase voidage.

General expressions to predict the dense phase voidage for Group C^+ particles were developed based on the Richardson-Zaki approach and the Kozeny-Carman approach. Both correlations predicted well the experimental results within the deviation of 20%. The correct prediction of the dense phase voidage could provide a guidance in the design and operation of the Group C^+ fluidized bed reactor.

A new method to calculate the minimum fluidization velocity for Group C^+ particles with the consideration of the particle cohesion was proposed. When compared with two commonly used correlations, the new method gave better agreement with the experimental data. Both the bed voidage at minimum fluidization (ε_{mf}) and the maximum dense phase voidage ($\varepsilon_{d,max}$) were correlated well with the dimensionless cohesion index (σ^*), indicating that the particle cohesion plays a significant role in the bed expansion for Group C^+ particles.

Nomenclature

D_{10}	Percentage 10% of particles under this particle size (µm)
D_{50}	Percentage 50% of particles under this particle size (µm)
D_{90}	Percentage 90% of particles under this particle size (µm)
D	Bed diameter (m)
d_p	Particle diameter (µm)
C_D	Drag coefficient (-)
g	Gravitational acceleration (m/s^2)

G_p	Gravity of a particle (N)
H_0	Initial fixed bed height (cm)
H_s	Settled bed height (cm)
H_d	Dense phase height (cm)
H_t	Total fluidized bed height (cm)
K	Kozeny constant (-)
K_f	Kozeny constant under fluidization (-)
n_c	Number of contact points per particle (-)
u_g	Superficial gas velocity (cm/s)
u_{mf}	Minimum fluidization velocity (cm/s)
u_d	Superficial gas velocity in the dense phase (cm/s)
$u_{d,max}$	Maximum dense phase expansion velocity (cm/s)
u_l	Superficial liquid velocity (cm/s)
u_t	Particle terminal velocity (cm/s)
u_{ta}	Aggerated particle terminal velocity (cm/s)
φ	Effective interparticle forces (N)
σ	Particle cohesion (Pa)
σ^*	Dimensionless particle cohesion index (-)
ε_0	Initial fixed bed voidage (-)
ε_{mf}	Bed voidage at minimum fluidization (-)
ε_d	Dense phase voidage (-)
$\varepsilon_{d,max}$	Maximum dense phase voidage (-)
ε_b	Fluidized bed voidage (-)
ρ_p	Particle density (kg/m^3)
ρ_g	Gas density (kg/m^3)
μ_g	Gas viscosity (pa s)

References

in a fluidized bed reactor. International journal of hydrogen energy. 2014;39(24):12586-96.

[2] Huang BS, Chen HY, Chuang KH, Yang RX, and Wey MY. Hydrogen production by biomass gasification in a fluidized-bed reactor promoted by an Fe/CaO catalyst. International journal of hydrogen energy. 2012;37(8):6511-8.

[3] Matsuda S, Hatano H, and Tsutsumi A. Ultrafine particle fluidization and its application to photocatalytic NOx treatment. Chemical Engineering Journal. 2001;82(1-3):183-8.

[4] Duan L, Sun H, Zhao C, Zhou W, and Chen X. Coal combustion characteristics on an oxy-fuel circulating fluidized bed combustor with warm flue gas recycle. Fuel. 2014; 127:47-51.

[5] Permchart W and Kouprianov VI. Emission performance and combustion efficiency of a conical fluidized-bed combustor firing various biomass fuels. Bioresource technology. 2004;92(1):83-91.

[6] Xu C and Zhu J. Parametric study of fine particle fluidization under mechanical vibration. Powder Technology. 2006;161(2):135-44.

[7] Wang Z, Kwauk M, and Li H. Fluidization of fine particles. Chemical Engineering Science. 1998;53(3):377-95.

[8] Saxena SC, Rao NS, and Tanjore VN. Diagnostic procedures for establishing the quality of fluidization of gas-solid systems. Experimental thermal and fluid science. 1993;6(1):56-73.

[9] Saxena SC and Rao NS. Pressure fluctuations in a gas fluidized bed and fluidization quality. Energy. 1990;15(6):489-97.

[10] Geldart D. Expansion of gas fluidized beds. Industrial & engineering chemistry research. 2004;43(18):5802-9.

[11] Grace JR and Sun G. Influence of particle size distribution on the performance of fluidized bed reactors. The Canadian Journal of Chemical Engineering. 1991;69(5):1126-34.

[12] Grace JR and Clift R. On the two-phase theory of fluidization. Chemical Engineering Science. 1974;29(2):327-34.

[13]   Chavarie C and Grace JR. Performance analysis of a fluidized bed reactor. I. Visible flow behavior. Industrial & Engineering Chemistry Fundamentals. 1975;14(2):75-9.

[14]   Barreto GF, Yates JG, and Rowe PN. The measurement of emulsion phase voidage in gas fluidized beds of fine powders. Chemical Engineering Science. 1983;38(3):345-50.

[15]   Geldart D. Types of gas fluidization. Powder technology. 1973;7(5):285-92.

[16]   Geldart D and Wong AC. Fluidization of powders showing degrees of cohesiveness—I. Bed expansion. Chemical Engineering Science. 1984;39(10):1481-8.

[17]   Geldart D and Wong AC. Fluidization of powders showing degrees of cohesiveness—II. Experiments on rates of de-aeration. Chemical Engineering Science. 1985;40(4):653-61.

[18]   Pyle DL and Harrison D. An experimental investigation of the two-phase theory of fluidization. Chemical Engineering Science. 1967;22(9):1199-207.

[19]   Lauga C, Chaouki J, Klvana D. and Chavarie C. Improvement of the fluidizability of Ni/SiO2 aerogels by reducing interparticle forces. Powder Technology. 1991;65:461-468.

[20]   Zhou T. and Li H. Effect of adding different size particles on fluidization of cohesive particles. Powder Technology. 1999;102:215-220.

[21]   Zhu J. Fluidization of fine powders. Granular Materials: Fundamentals and Applications. 2003:270-295.

[22]   Yang J, Sliva A, Banerjee A, Dave RN, and Pfeffer R. Dry particle coating for improving the flowability of cohesive powders. Powder technology. 2005;158(1-3):21-33.

[23]   Quintanilla M A S, Valverde J M, and Castellanos A. Adhesion force between fine particles with controlled surface properties. AIChE journal. 2006;52(5):1715-1728.

[24]   Chen Y, Yang J, Dave RN, and Pfeffer R. Fluidization of coated group C powders. AIChE journal. 2008;54(1):104-21.

[25]   Xu, C, Zhang H, and Zhu J. Improving flowability of cohesive particles by partial coating on the surfaces. The Canadian Journal of Chemical Engineering., 2009;87(3):403-414.

[26] Zhou Y and Zhu J. Group C$^+$ particles: Enhanced flow and fluidization of fine powders with nano-modulation. Chemical Engineering Science. 2019; 207:653-62.

[27] Han M, Zhou Y, and Zhu J. Improvement on flowability and fluidization of Group C particles after nanoparticle modification. Powder Technology. 2019.

[28] Zhou Y and Zhu J. Group C$^+$ particles: Extraordinary dense phase expansion during fluidization through nano-modulation. Chemical Engineering Science. 2020;214: 115420.

[29] Zhang Y, Zhou Y, Liu J, Shao Y, and Zhu J. Performance Enhancement of Fluidized Bed Catalytic Reactors by Going to Finer Particles. Industrial & Engineering Chemistry Research. 2019;58(43):20173-8.

[30] Zhou Y, Zhao Z, Zhu J, and Bao X. Group C$^+$ particles: Efficiency augmentation of fluidized bed reactor through nano-modulation. AIChE Journal. 2020;66(4):e16870.

[31] Baerns M. Effect of interparticle adhesive forces on fluidization of fine particles. Industrial & Engineering Chemistry Fundamentals. 1966;5(4):508-16.

[32] Mutsers SM and Rietema K. The effect of interparticle forces on the expansion of a homogeneous gas-fluidized bed. Powder Technology. 1977;18(2):239-48.

[33] Visser J. Van der Waals and other cohesive forces affecting powder fluidization. Powder Technology. 1989;58(1):1-0.

[34] Lettieri P, Yates JG, and Newton D. The influence of interparticle forces on the fluidization behaviour of some industrial materials at high temperature. Powder Technology. 2000;110(1-2):117-27.

[35] Rietema K and Piepers HW. The effect of interparticle forces on the stability of gas-fluidized beds—I. Experimental evidence. Chemical Engineering Science. 1990;45(6):1627-39.

[36] Rietema K, Cottaar EJ, and Piepers HW. The effects of interparticle forces on the stability of gas-fluidized beds—II. Theoretical derivation of bed elasticity on the basis of van der Waals forces between powder particles. Chemical engineering science. 1993;48(9):1687-97.

[37] Abrahamsen AR and Geldart D. Behaviour of gas-fluidized beds of fine powders part I. Homogeneous expansion. Powder technology. 1980;26(1):35-46.

[38] Abrahamsen AR and Geldart D. Behaviour of gas-fluidized beds of fine powders part II. Voidage of the dense phase in bubbling beds. Powder Technology. 1980;26(1):47-55.

[39] Bruni G, Lettieri P, and Newton D, Yates J. The influence of fines size distribution on the behaviour of gas fluidized beds at high temperature. Powder technology. 2006;163(1-2):88-97.

[40] Shabanian J and Chaouki J. Hydrodynamics of a gas–solid fluidized bed with thermally induced interparticle forces. Chemical Engineering Journal. 2015; 259:135-52.

[41] Zhu J. and Zhang H. Fluidization Additives to Fine Powders. U.S. Patent 6833185. December 21, 2004.

[42] Zhu J. and Zhang H. Method and Apparatus for Uniformly Dispensing Additive Particles in Fine Powders. U.S. Patent 7240861, 2007.

[43] Rietema K. Application of mechanical stress theory to fluidization//Proc. Int. Symp. on Fluidization. 1967: 154-163.

[44] Clift R and Grace JR. Continuous bubbling and slugging. In Fluidization. 1985:73-132.

[45] ASTM D6128 - 06 Standard Test Method for Shear Testing of Bulk Solids Using the Jenike Shear Cell. 2006.

[46] Schwedes J. and Schulze D. Measurement of flow properties of bulk solids[J]. Powder Technology, 1990, 61(1): 59–68.

[47] Ergun S and Orning AA. Fluid flow through randomly packed columns and fluidized beds. Industrial & Engineering Chemistry. 1949;41(6):1179-84.

[48] Richardson JF and Zaki WN. The sedimentation of a suspension of uniform spheres under conditions of viscous flow. Chemical Engineering Science. 1954;3(2):65-73.

[49] Ergun S. Fluid flow through packed columns. Chem. Eng. Prog. 1952; 48:89-94.

[50] Kozeny J. Ueber kapillare Leitung des Wassers im Boden. Sitzungsber Akad. Wiss., Wien. 1927;136(2a): 271-306.

[51] Carman PC. Fluid flow through granular beds. Trans. Inst. Chem. Eng. 1937; 15:150-66.

[52] Bejan A. Convection heat transfer. John wiley & sons; 2013.

[53] Wen CY and Yu YH. A generalized method for predicting the minimum fluidization velocity. AIChE Journal. 1966;12(3):610-2.

[54] Akgiray O and Saatçı AM, Water Science and Technology: Water Supply. 2001;1(2): 65–72.

[55] Leva M. Fluidization, 69, McGraw-Hill; New York, 1959.

[56] Krupp H. Particle adhesion theory and experiment. Adv. Colloid Interface Sci. 1967; 1:111–239.

[57] McCabe WE, Smith JC, and Harriott P. Unit Operations of Chemical Engineering. McGraw Hill, New York, 2001.

[58] Werther J. Scale-up modeling for fluidized bed reactors. Chemical engineering science. 1992;47(9-11):2457-62.

[59] Yates JG. Effects of temperature and pressure on gas-solid fluidization. Chemical engineering science. 1996;51(2):167-205.

[60] Wilhelm RH. Fluidization of solid particles. Chem. Eng. Prog. 1948; 44:201-18.

[61] Van Heerden C, Nobel AP, and Van Krevelen DW. Studies on fluidization. I—the critical mass velocity. Chemical Engineering Science. 1951;1(1):37-49.

Chapter 9

9 Group C⁺ Particles: Efficiency Augmentation of Fluidized Bed Reactor through Nano-modulation

(A version of this chapter has been published in *AIChE Journal*)

***Zhou Y**, Zhao Z, Zhu J, Bao X. Group C+ particles: Efficiency augmentation of fluidized bed reactor through nano-modulation. **AIChE Journal**. 2020 Apr;66(4):e16870.*

Group C⁺ particles, Group C particles after nano-modulation, with extremely large specific surface area, have been shown to exhibit extraordinarily good fluidization quality with superiorly high bed expansion, significantly increasing gas holdup in the bed. As a first attempt, Group C⁺ particles were used as catalysts in a fluidized bed reactor (C-plus FBR) to evaluate the reaction performance and were compared to that using Group A particles. C-plus FBR could achieve a much higher reaction conversion, up to 235% of that using Group A particles. The contact efficiency for Group C⁺ particles is much higher, being 330% more than that for Group A particles. The greater contact efficiency is due to both larger specific surface area and higher bed expansion, providing larger gas-solid interfacial area and longer gas residence time. Conclusively, Group C⁺ particles with superior fluidization quality and reaction performance do have huge potential in gas-phase catalytic reactions.

9.1 Introduction

Gas-solid fluidized bed reactors are used in a wide variety of industrial processes, such as combustion, gasification of biomass and fluid catalytic cracking processes [1-3]. The major advantages of the fluidized bed reactors include easy handling of a large quantity of particles, uniform temperature distribution, high heat-transfer coefficient and providing large solid-gas exchange areas in the operation of particles of small sizes [4]. Geldart Group C particles [5] with small particle sizes have attracted the attention of many researchers, because they can provide a high specific surface for gas-solid contact in the fluidized bed reactor, which is a crucial parameter for improving the reaction performance. However, Group C particles tend to form agglomerates and channeling due to their strong

interparticle forces, resulting in poor or even no fluidization at all, thus limiting their applications.

Nanoparticles as additives can remarkably reduce the cohesiveness of Group C particles and enhance their flowability [6-11]. A previous study [12] proposed a nanoparticle modulation technique, which was mixing a small amount of nanoparticles with Group C particles by ultrasonic sieving, and have found that this technique can significantly reduce the interparticle forces of Group C particles and dramatically improve their flowability and fluidization quality. Group C^+ particles, those nano-modulated Group C particles, are proven to exhibit good fluidization quality with proper minimum fluidization velocities, high bed expansion and large gas holdup in the dense phase, presumed to be pseudo-particulate fluidization at a wide range of operating gas velocities [12,13]. The good fluidization quality of Group C^+ particles may unleash their potential in industrial applications. Particularly, these unique characteristics of Group C^+ particles, especially the extremely large surface area and the large dense phase voidage, may bring superior reactor performance that other reactors cannot match in many chemical processes, especially in gas-phase catalytic reactions.

Gas-solid interfacial contact area is one of the most important indexes that controls the performance of a fluidized bed reactor. Generally, the gas-solid fluidized bed reactors are composed of two phases, a dense or particulate phase and a bubble phase [14-17]. A significant increase in gas-solid interfacial contact area can be achieved by introducing more gas into the dense phase where gas is in closer contact with particles, contributing to better gas-solid contact and thus enhancing the reactor performance. As a result both the particle size and the dense phase voidage are key parameters that affect the gas-solid interfacial contact area. As the results in the previous chapters, Group C^+ particles of smaller sizes could not only provide sufficiently large specific surface area for gas to contact their fluidization, but also exhibited large dense phase voidage, signifying there is more gas retained in the dense phase to contact with particles [13]. The large gas-solid contact area provided by the fluidization of Group C^+ particles has great possibility of enhancing the reaction performance especially of gas-phase catalytic reactions. However,

almost no researches have studied the reaction performance in fluidized beds of Group C^+ particles until now.

As a first attempt, C-plus fluidized bed reactor was proposed in this project which was the fluidized bed reactor using Group C^+ particles. The major objective of this project was to investigate the reaction performance in C-plus fluidized bed reactor with ozone decomposition reaction and make a comparison with that using Group A particles. The fluidization hydrodynamics of Group C^+ particles and Group A particles were also investigated and compared and further correlated with their reaction performance by gas-solid contact efficiency.

9.2   Experimental

9.2.1   Catalyst preparation

Ozone decomposition is a thermodynamically favored process which happens slowly at room temperature in the absence of catalysts, so catalysts are necessary for ozone decomposition at lower temperatures [18-22]. In this project, fresh FCC particles (Group A) impregnated with ferric nitrate were used as active catalysts since Fe_2O_3 is the active component for the ozone decomposition reaction [18]. Due to the high reactivity of the impregnated FCC catalysts, 10% (weight fraction) of them were added into the fresh FCC particles which do not have any reactivity for ozone decomposition to obtain a proper reactivity for the reaction. The measurement of catalyst reactivity is described in detail in Section of Reaction Characterization.

To obtain Group C^+ catalysts, both the fresh FCC particles and the impregnated FCC catalysts were crushed into Group C particles with almost the same particle size by an air classifier mill (ACM). Then the same amount of fine impregnated FCC catalysts (10%wt) were mixed with the fine fresh FCC particles to obtain a similar reactivity with Group A catalysts. After that, the Group C catalysts were modulated by nanoparticles to prepare Group C^+ catalysts. The details of the nano-modulation technique are described in literatures [23,24]. The nanoparticles used in these experiments were SiO_2 particles with a reported particle size of 16 nm and material density of 2200 kg/m^3, marketed as R972 by Evonik. Three nanoparticle concentrations were used, namely 0.27%, 0.44%, 0.82%

(volume fraction). The properties of these Group C$^+$ and Group A catalysts are listed in Table 9.1. The particle size distribution was obtained by laser diffraction measurement (Mastersizer 2000, Malvern Instruments, Worcestershire, UK) following standard test procedures. D_{10}, D_{50}, D_{90} stand for particle size distribution, for example, D_{10} is defined as a diameter where 10 vol.% of the particles of the powder is less or is equal to the diameter. Scanning electron microscopy (SEM) was used to observe the surface morphology before and after nanoparticle modulation as shown in Figure 9.1. FCC8.5 and FCC20 which were produced by ACM exhibited much rougher surfaces than FCC76. The production process significantly increased the surface roughness of FCC8.5 and FCC20. As a result the nano-modulation technique did not significantly change the surface roughness. In previous chapters, nano-modulation technique has significantly increased the surface roughness of Group C particles with smooth surfaces, and nanoparticles could be uniformly distributed on Group C particles.

Table 9.1: The properties of Group C$^+$ and Group A catalysts

Powder name	Particle size (µm)			Materials	Apparent density (kg/m^3)	Bulk density (kg/m^3)	Geldart classification	k_r (s^{-1})
	D_{10}	D_{50}	D_{90}					
FCC8.5	1.5	8.5	26	90%Fresh+10% Impregnated FCC	1780	509	C	1.32
FCC20	4.4	20	53	90%Fresh+10% Impregnated FCC	1780	627	C	1.36
FCC76	20	76	139	90%Fresh+10% Impregnated FCC	1780	874	A	1.36
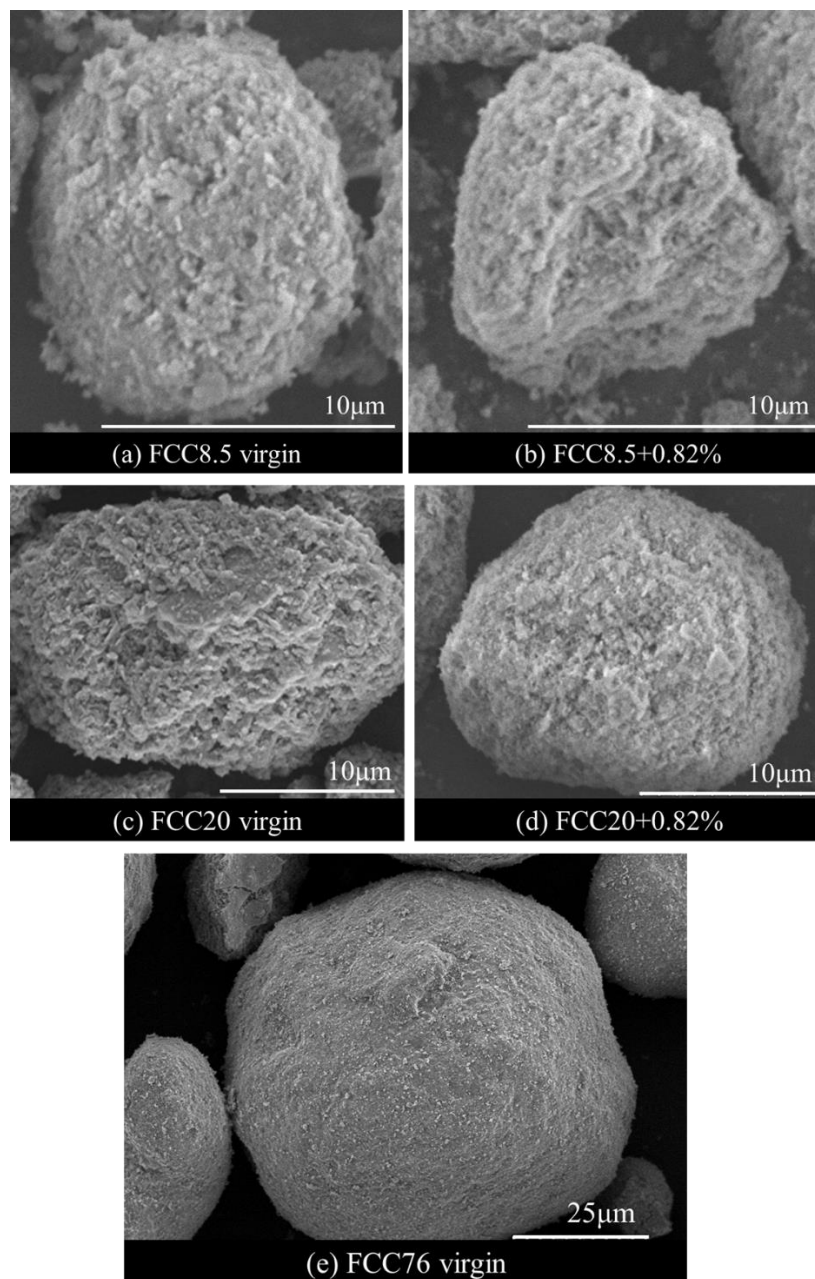
Figure 9.1: The catalyst surfaces before and after nanoparticle modulation

9.2.2 Apparatus

As shown in Figure 9.2, the fluidization reactor was made of Plexiglas with 5.08 cm in I.D. and 45.7 cm in height. An expanding section on the top of the fluidization reactor column was covered by a filter bag of 625 mesh screen, to prevent particle entrainment and to collect the extra-fine particles which were entrained. A gas distributor between the

fluidization column and the wind box below was a plastic plate with 65 holes 1 mm in diameter, with an opening area ratio of 2.5%. Two layers of 625 mesh screen were covered on the gas distributor to prevent the fine particles from dropping into the wind box. The gas reactant entered the reactor through one inlet on the wind box, another one at the opposite position was used to measure the inlet ozone concentration (C_0). Two pressure taps, one at the bottom and another near the top of the fluidized reactor column, were used to measure the pressure drop across the entire bed. One sample tap was located near the top of the column to outlet measure the ozone concentration (C_1). A measuring tape fixed on the reactor can estimate the bed height during fluidization. In this project, the first part studied the fluidization hydrodynamics of Group A, Group C and Group C^+ particles, including pressure drop (ΔP), minimum fluidization velocity (u_{mf}), bed expansion (BER) and dense phase voidage (ε_d). The second part studied the reaction conversion of the ozone decomposition reaction (X) using Group A, Group C and Group C^+ particles.
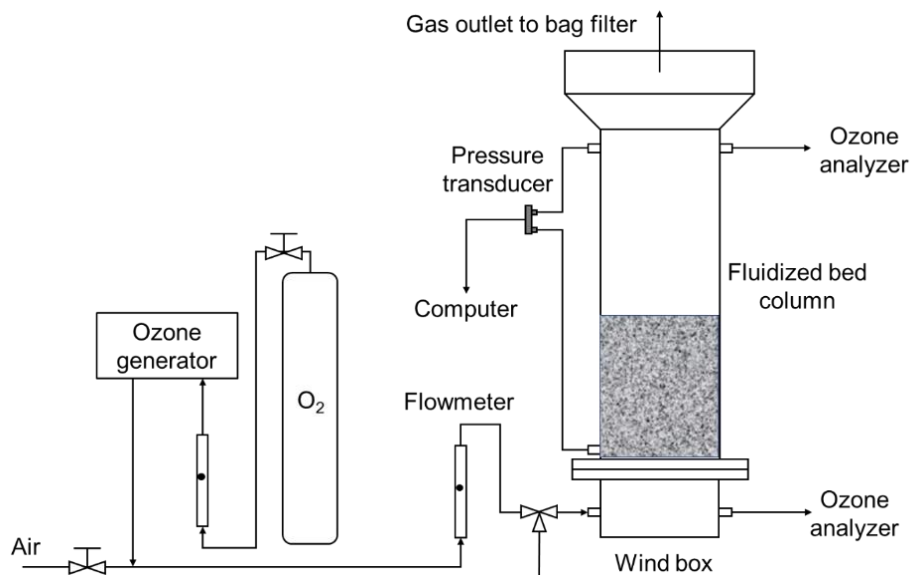
Figure 9.2: Schematic diagram of the fluidized bed and ozone testing system

9.2.3   Measurement methods

The pressure drop across the entire bed was measured using a pressure transducer (Omega PX163 series). The pressure signals are collected by a computer with the LabVIEW DAQ program. The normalized pressure drop ($\Delta P / (W/A)$) was adopted, which is defined as the

ratio of the measured pressure drops across the whole bed (ΔP) to the particle weight per cross-sectional area. When the entire bed is fluidized, the normalized pressure drop should attain unity and remain stable thereafter even if the gas velocity further increases. The bed expansion ratio was defined as the ratio of the fluidized bed height (H_t) to the initial fixed bed height (H_0). The initial bed height was 15cm. The dense phase voidage was obtained by the bed collapse test, which involved first achieving full fluidization at a high gas velocity, and then shutting off the gas supply, and recording the bed collapse process by a digital camera (Canon EOS 800D). The MATLAB software was used to transfer the video into pictures to easily and clearly obtain the bed height. The bed height was measured second by second. More details could be found in previous works [13,25,26]. Each test was repeated 3 times and the average value was used in this paper. The error deviation was around 5%. The bed height as a function of time could give a collapse curve as shown in Figure 9.3. After that, the dense phase voidage (ε_d) could be calculated by the dense phase height (H_d) obtained from the collapse curve using the following equation:

$$\varepsilon_d = 1 - \left(\frac{H_0}{H_d}\right)(1 - \varepsilon_0) \qquad (9.1)$$

where H_0 is the fixed bed height, ε_0 is the fixed bed voidage.
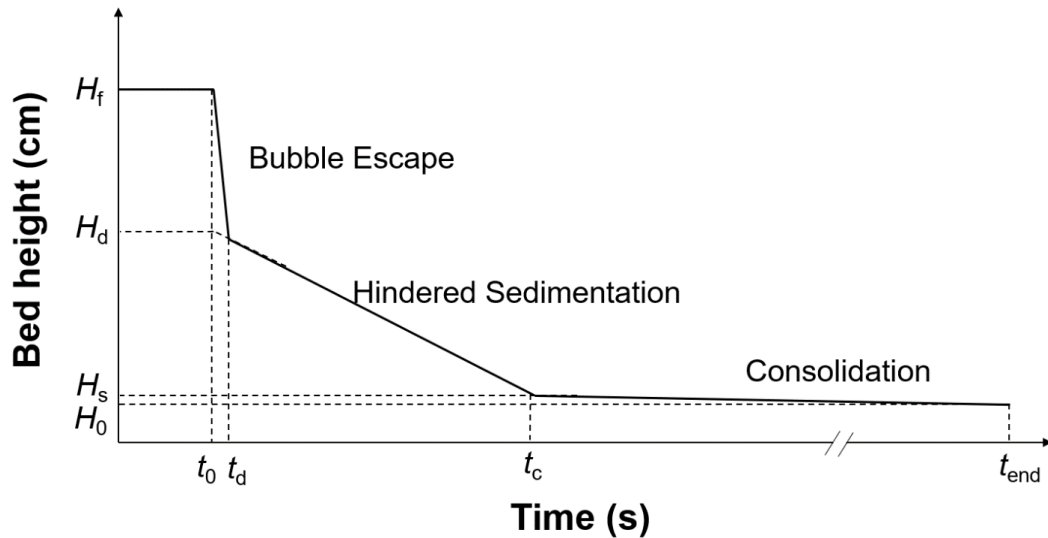
Figure 9.3: A typical bed collapse process

9.2.4   Reaction characterization

This part aimed to investigate the reaction performance of ozone decomposition in the fluidized bed reactors using Group A, Group C and Group C^+ catalysts. The weight of the catalysts loaded in the reactor was 166 g for each experiment. The fluidization gas was a mixture of the ozone and the air. An ozone generator using the corona discharge method (model AE15M, manufactured by Absolute Ozone Inc.) was used to produce ozone with a working pressure of 34−340 kPa (5−50 psig) and an oxygen flow rate of 0.1−10 standard liter per minute (SLPM). The oxygen flow rate entering into the generator was controlled by a rotameter (VWR, Catalog No: 97004-648) ranging from 0 to 10 L per minute (LPM). The ozone/oxygen mixture exiting from the ozone generator was mixed with the main fluidization air in a long flow tube before entering the fluidized bed to ensure thorough mixing. The initial ozone concentration (C_0) was set to 120−140 ppm.

An ozone analyzer (model 49i, Thermo Electron Inc.) that employs the UV photometric method was used to measure the ozone concentration, which has a measuring range of 0-200 ppm with resolutions of 0.0001 ppm for the scale of 0-10 and 0.01 ppm for the scale of 10-200 ppm. The response time of the analyzer is 4 s. The ozone concentration output was collected and displayed on a computer with a LabVIEW DAQ program. The reaction conversion test was repeated 3 times for each sample and the average value was used in this paper. The error deviation was less than 5%.

To ensure the catalyst activity during the experiments, a fixed bed reactor with 16mm I.D. and 25cm in height was used to measure the catalyst reactivity before and after each experiment. 3 grams of catalysts were loaded in the fixed bed reactor and the inlet gas flow rate operated at 4.5 cm/s. The inlet and outlet ozone concentrations were measured to calculate the reaction rate constant (k_r) using the following equation [27]:

$$k_r = \frac{F\rho_b}{m} \ln \frac{C_0}{C_1} \qquad (9.2)$$

No significant change was observed in k_r before and after several hours of reaction, therefore the reaction rate constant was assumed to the same for each experiment.

9.3   Results and discussion

9.3.1   Fluidization hydrodynamics

Pressure drop and minimum fluidization velocity

Figure 9.4 shows the normalized pressure drop of Group C (FCC8.5, FCC20) and Group A (FCC76) particles. The pressure drop could clearly reflect the fluidizability of the particles [10,27]. FCC76 could quickly achieve a high pressure drop close to 1, while FCC8.5 and FCC20 could reach the similar pressure drop only at high gas velocities. Their incipient fluidization starts much later than FCC76. Theoretically, the normalized pressure drop will attain unity when all particles in the bed are fluidized. The larger normalized pressure drop indicates more particles suspended and fluidized, signifying better fluidization.
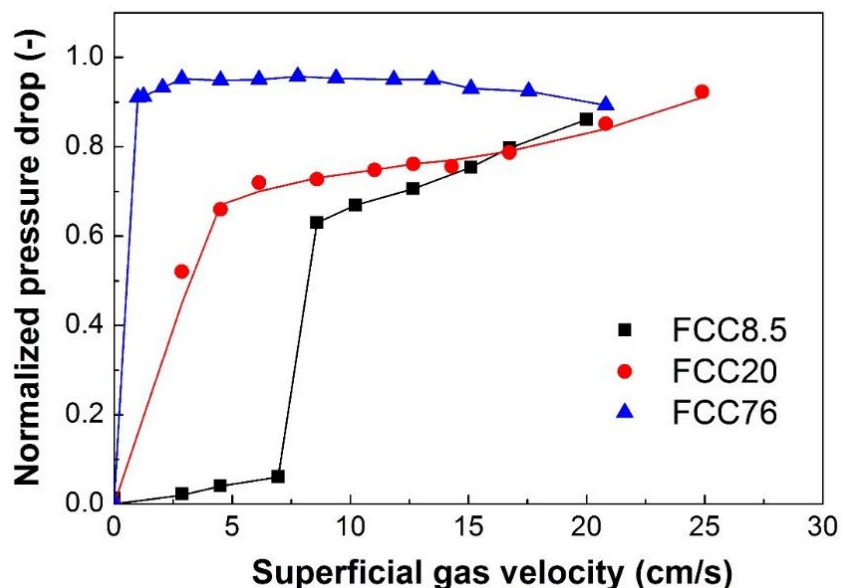
Figure 9.4: Effect of particle size on pressure drop

Figure 9.5 shows the pressure drop of Group C$^+$ particles and the effect of nanoparticle concentration on it. After nanoparticle modulation, the Group C$^+$ particles could achieve a higher pressure drop at lower gas velocities than Group C particles, indicating more particles fluidized and thus better fluidization quality. The nanoparticle concentration of

0.82% displays the highest pressure drop, which is optimum for Group C^+ particle fluidization. This result is consistent with previous studies [10,12,13,31].
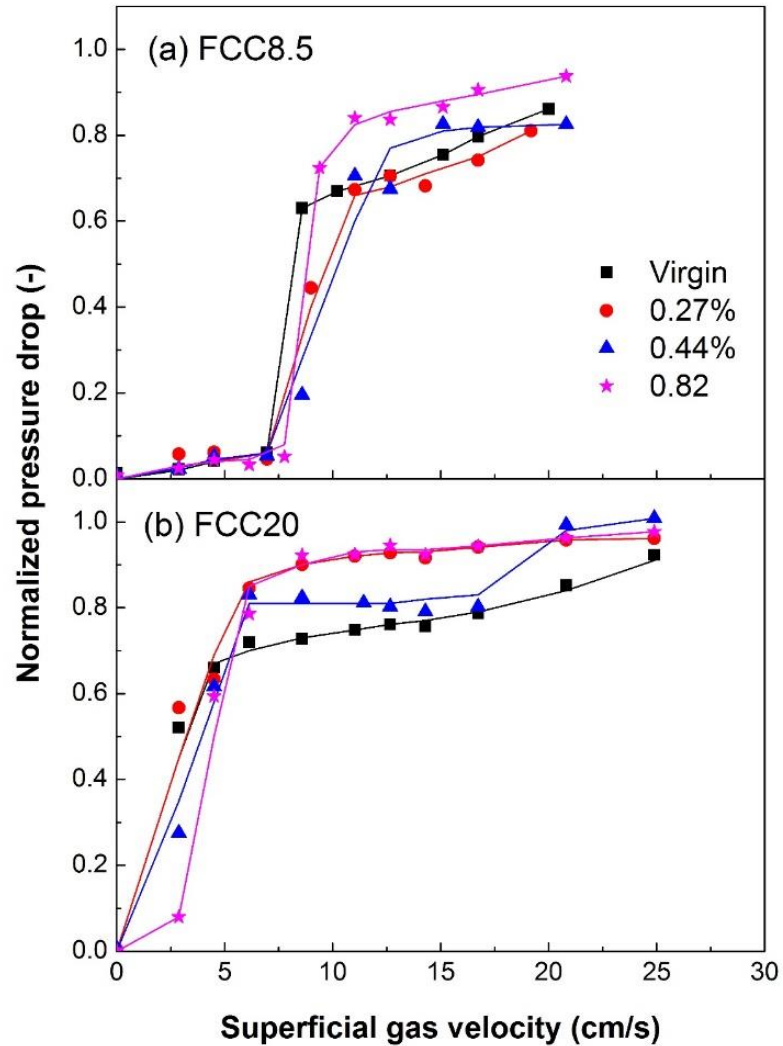
Figure 9.5: Effect of nanoparticle concentration on pressure drop

Minimum fluidization velocity is also an important parameter for describing the flowability and fluidization of the particles [10]. Figure 9.6 shows the effect of nanoparticle concentration on the minimum fluidization velocity of Group A and Group C^+ particles. The nanoparticle concentration almost has no effect on the minimum fluidization velocity for Group A particles (FCC76). For Group C^+ particles, the minimum fluidization velocities of both FCC8.5 and FCC20 increase and then decrease with nanoparticle

concentration increasing, and all of them are much higher than that of Group A particles. It is evident that the minimum fluidization velocity increases with particle size. For the three types of particles, their minimum fluidization velocities follow the sequence: FCC8.5 > FCC20 > FCC76. As demonstrated in previous studies [10,12], the minimum fluidization velocity strongly depends on powder cohesiveness. The small particles with higher cohesiveness will result in higher minimum fluidization velocity.
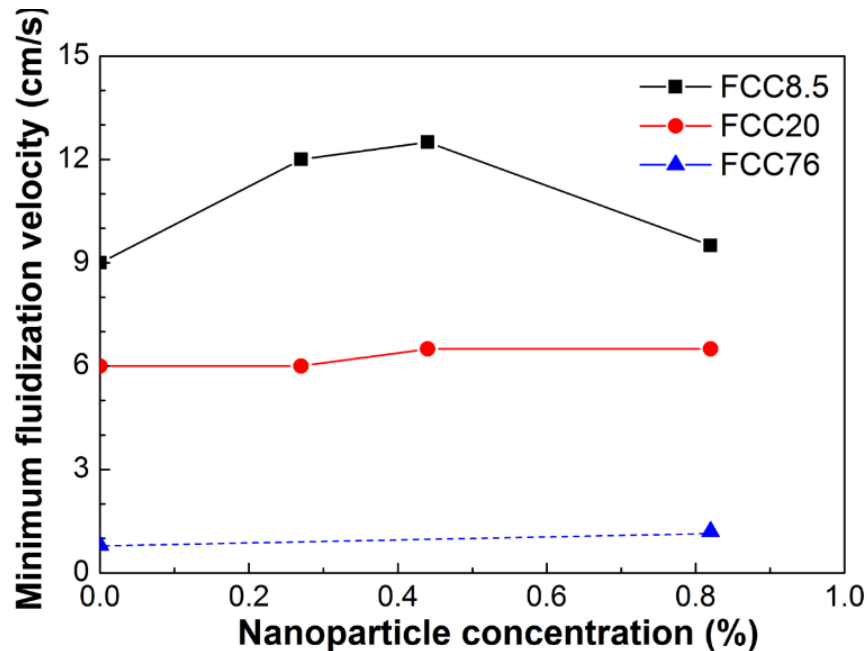
Figure 9.6: Effect of nanoparticle concentration on minimum fluidization velocity

In general, Group C particles are considered to be cohesive and non-fluidizable particles [5]. In this project, it is found that Group C particles (FCC8.5 and FCC20) are fluidizable with identifiable minimum fluidization velocity and proper pressure drop. This phenomenon may be due to the surface roughness which significantly affects the powder cohesiveness. As shown in Figures 9.1(a), (b) and (c), FCC8.5 and FCC20 particles that were produced through the crush by ACM have much rougher surfaces than the original FCC76 particles. The large surface roughness of these Group C particles significantly reduces their cohesion and makes them fluidizable. As shown in Figures 9.1 (d) and (e), nanoparticle modulation does not increase the surface roughness of these Group C particles as that in other works [10,12,28,29], so the minimum fluidization velocities for Group C

and Group C$^+$ particles do not show significant differences. It could be further speculated that Group C particles with a certain degree of surface roughness were fluidizable.

Bed expansion

Bed expansion ratio is a key parameter for evaluating the fluidization quality. A high bed expansion indicates better fluidization with more gas in the fluidized bed. The bed expansion ratios of Group C and Group A particles are displayed in Figure 9.7. Group C particles exhibit much higher bed expansion than Group A particles. In Chapter 3, the bed expansion increases as particle size decreases, while the bed expansion of FCC8.5 is lower than that of FCC20 in this project. This is because FCC8.5 is harder to fluidize than FCC20, showing higher minimum fluidization velocity and lower pressure drop which indicate more incomplete fluidization.
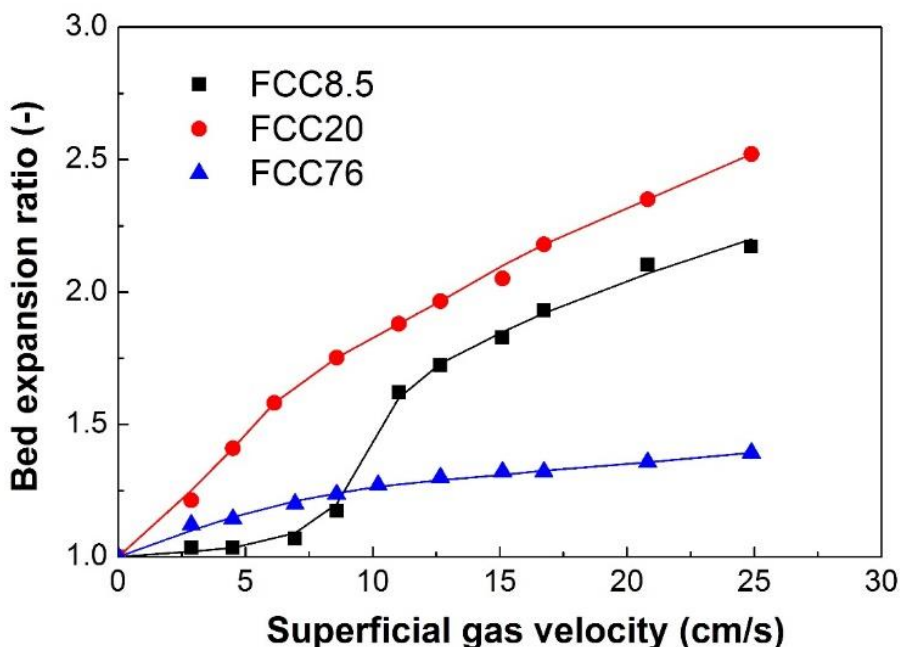
Figure 9.7: Effect of particle size on bed expansion

Figure 9.8 illustrates the effect of nanoparticle concentration on bed expansion of Group C$^+$ particles. The improvement of the nanoparticles on the bed expansion for FCC8.5 is more significant than that for FCC20. Since the fluidization of FCC8.5 particles is not as ideal as that of FCC20 particles, nanoparticles could exert more influence on the

fluidization of FCC8.5 particles. Both the beds of FCC20 with and without nanoparticles expand quickly and higher than those of FCC8.5 with and without nanoparticles due to the relatively low minimum fluidization velocities and more complete fluidization. The nanoparticle concentrations of 0.27% and 0.44% do not have much influence on the bed expansion for Group C^+ particles. Group C^+ particles with nanoparticle concentration of 0.82% show the highest bed expansion, reaching up to 2.6-2.7, which is almost 200% of Group A particles. The high bed expansion for Group C^+ particles indicates more gas holdup in the bed which could increase the opportunity for gas to make contact with particles, which is greatly favorable for gas-phase catalytic reactions.
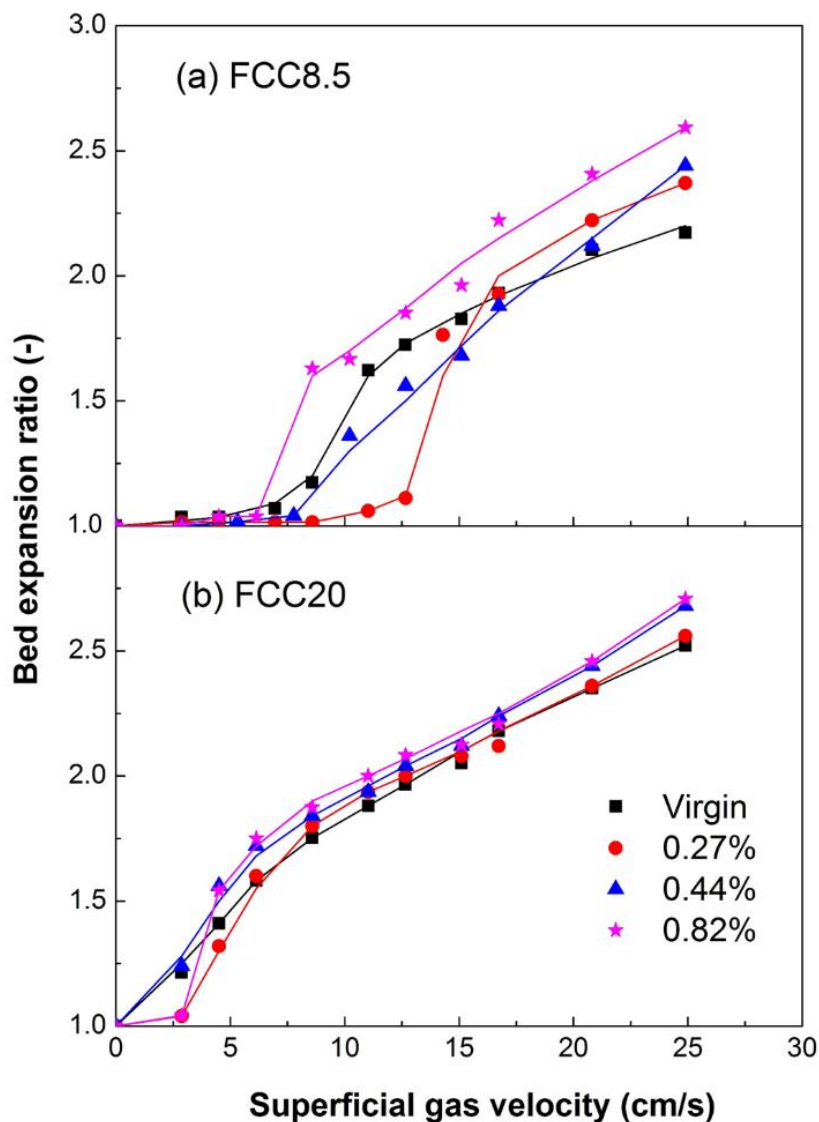
Figure 9.8: Effect of nanoparticle concentration on bed expansion

Figure 9.9 displays the effects of particle size and nanoparticle concentration on bed voidage. Group C and Group C$^+$ particles have much higher bed voidages than Group A particles. For example, the bed voidages for FCC8.5 and FCC20 after nanoparticle modulation could reach as high as 0.9 and 0.87, respectively, around 144% of that for Group A particles. The high bed voidage suggests more gas holdup in the bed which contributes to better gas-solid contact.
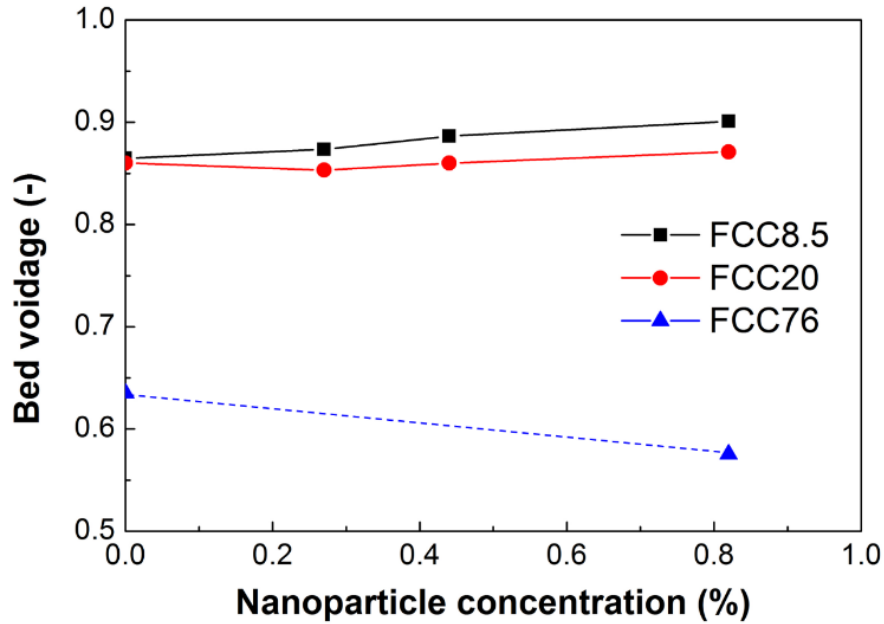
Figure 9.9: Effect of particle size and nanoparticle concentration on bed voidage

9.3.2   Gas distribution in the fluidized bed

As have been discussed, a high bed expansion indicates more gas holdup in the fluidized bed, leading to more gas possessing the opportunity to make contact with particles which would enhance the gas-solid contact. It is well accepted that dense phase is the major location where gas is in intimate contact with particles, while the bubble phase is insignificant for gas-solid contact [17,30]. To further understand the advantages of Group C^+ particle fluidization, it is vital to investigate the gas distribution in the fluidized bed and especially the dense phase properties.

Bed collapse test is widely used to identify the dense phase properties and it is considered as the easiest way to estimate the distribution of gas holdup in the fluidized bed. Figure 9.10 shows the bed collapse curves of the three types of particles under the same gas velocity of 20.8 cm/s. The gas supply shut off at at the point of $t = 0$s and the bed started to collapse. Group C^+ particles (FCC8.5+0.82% and FCC20+0.82%) exhibited much higher dense phase height (H_d) and much longer collapse time (t_c) than Group A particles (FCC76), signifying more gas holdup in the dense phase.
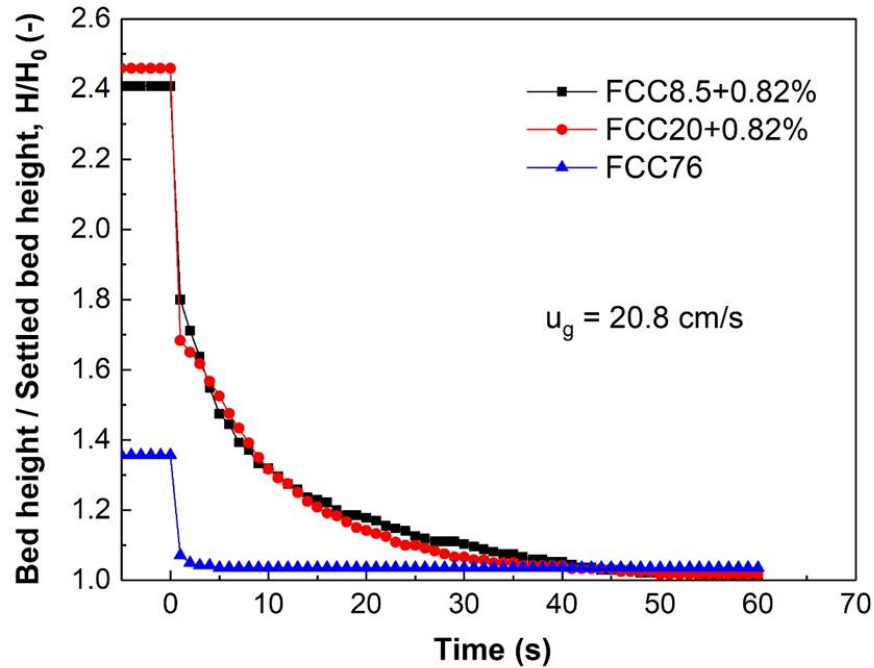
Figure 9.10: Bed collapse curves of different types of particles

Figure 9.11 illustrates the gas distribution in the beds of Group C^+ and Group A particles under different gas velocities. It is clear that Group C^+ particles have much higher bed voidages, dense phase voidages, as well as fixed bed voidages than Group A particles, which means that Group C^+ particles essentially have a greater aeration ability than Group A particles. As particle size decreases, the aeration ability increases. After fluidization, the gas flow mainly enters the dense phase in the beds of Group C^+ particles, seldom part forms bubbles. On the contrary, the gas flowing into the dense phase is negligible compared with that forming bubbles in the beds of Group A particles.
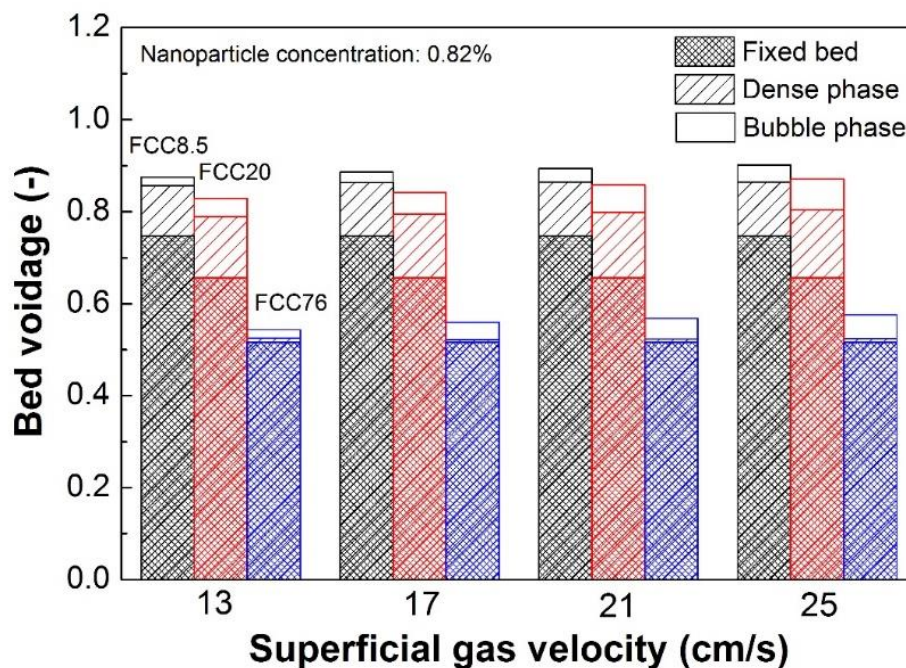
Figure 9.11: Effect of particle size and nanoparticle concentration on dense phase voidage

Figure 9.12 shows the dense phase voidage for Group C^+ and Group A particles under different gas velocities. The dense phase voidage in the beds of Group C^+ particles are dramatically larger than that in the beds of Group A particles. For example, the dense phase voidage for FCC8.5 and FCC20 particles after nanoparticle modulation could reach as high as 0.85 and 0.8, respectively, which are around 160% of that for FCC76 with a dense phase voidage of only around 0.52. The remarkably large dense phase voidages for Group C^+ particles signify the high gas holdup in the dense phase, a key advantage for improving gas-solid contact and thus enhancing reaction performance for gas-phase catalytic reactions. In addition, the nanoparticle concentration of 0.82% shows the maximum improvement on the dense phase voidage for Group C^+ particles which is higher than other ones, consistent with above results. The nanoparticle concentration does not have obvious effect on the dense phase voidage for Group A particles.
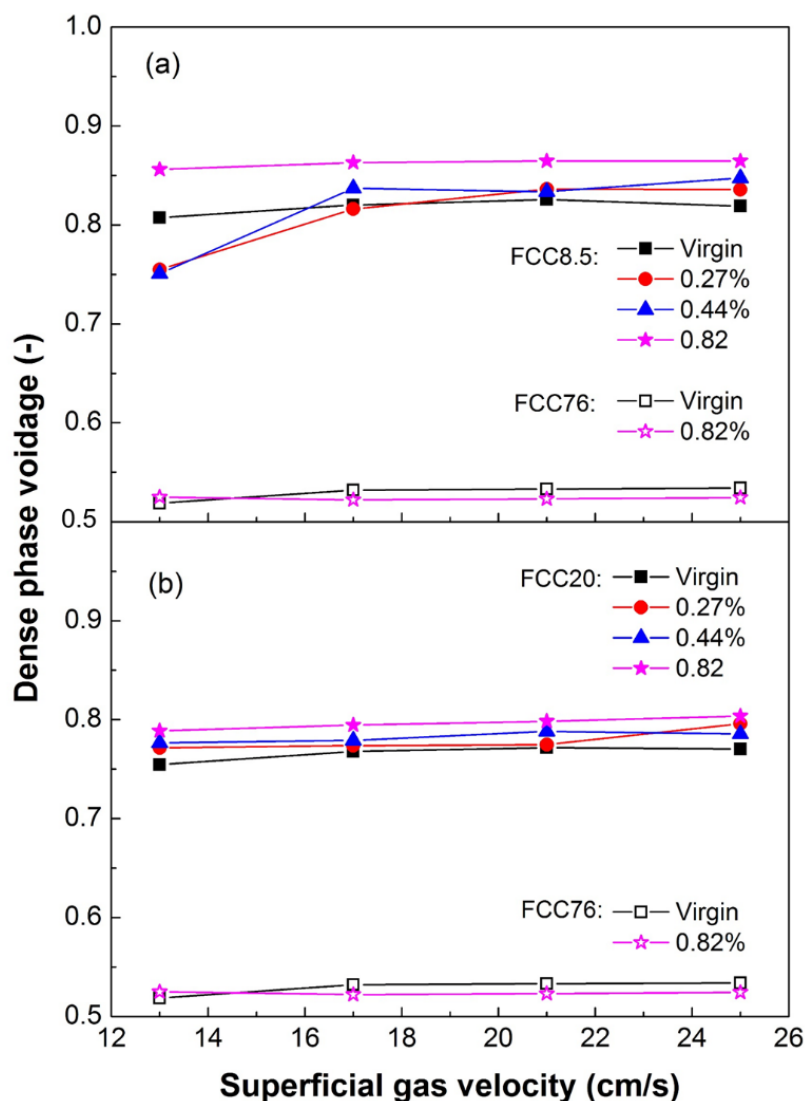
Figure 9.12: Effect of nanoparticle concentration on dense phase voidage under different gas velocities

9.3.3   Reaction conversion in fluidized bed reactor

To verify the advantages of Group C$^+$ particle fluidization, the ozone decomposition reaction, a typically first-order gas-phase catalytic reaction, was carried out in the fluidized bed reactors of Group C$^+$ and Group A particles. Figure 9.13 shows reaction conversions in the reactors of Group C$^+$ and Group A particles. Group C$^+$ particles show higher reaction conversions than Group A particles. Particularly, FCC8.5+0.82% exhibits a much higher

reaction conversion than other particles, reaching up to 63%, which is around 235% of FCC76+0.82%. The high reaction conversion in the fluidized bed reactor of FCC8.5+0.82% is due to their extremely large specific surface area and the extremely high gas holdup in the reactor. These two critical characteristics provide more spaces and more gas reactant for the reaction, contributing to higher reaction conversion.
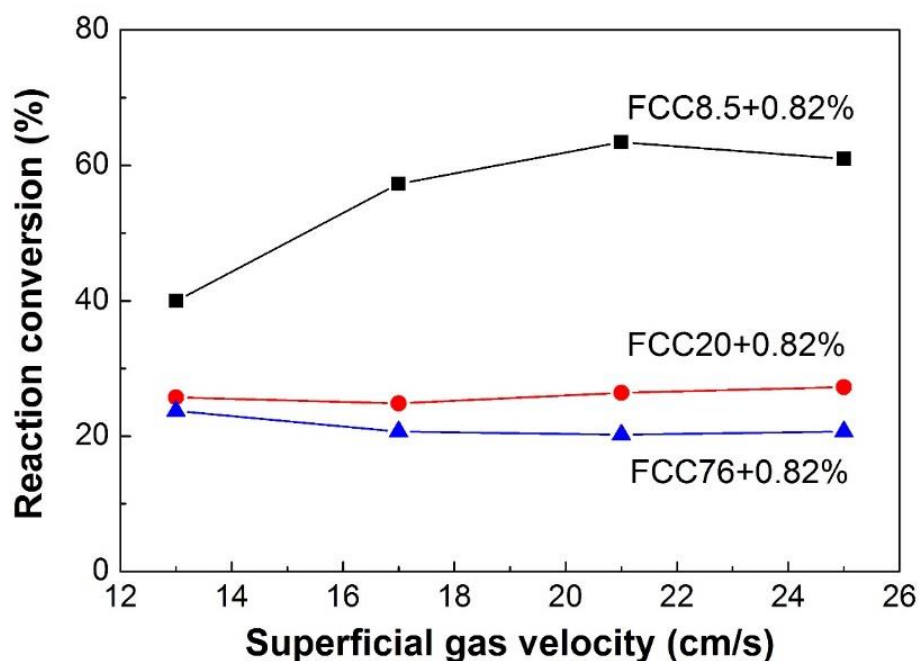
Figure 9.13: Effect of particle size on reaction conversion

As gas velocity increases, the reaction conversion for FCC8.5+0.82% initially increases and then slightly decreases. For FCC20+0.82% and FCC76+0.82%, the reaction conversions show a slight decrease with gas velocity increasing. This is because the increase of gas velocity would reduce the gas residence time in the bed and also may result in more bubble holdup, which are not good for gas-solid contacting. However, FCC8.5+0.82% particles are easier to agglomerate than the other two particles. For FCC8.5+0.82%, the increase in gas velocity may break the agglomerates to release more surfaces for gas-solid contacting, which is the major reason that improving the reaction conversion. After that, the further increase in gas velocity would reduce the gas residence time in the bed and thus decrease the reaction conversion.

Figure 9.14 shows the effect of nanoparticle concentrations on the reaction conversion in the fluidized bed reactors of Group C$^+$ and Group A particles. For the FCC8.5 series, the reaction conversion increases with nanoparticle concentration, due to the better fluidization quality with nanoparticle concentration increasing. As seen in the above results, the higher nanoparticle concentration improves fluidization quality for FCC8.5 particles, resulting in higher pressure drop, higher bed expansion and larger dense phase voidage. These boosts indicate more complete fluidization with more fine particles released and fluidized in the bed, promoting gas-solid contact and thus reaction performance. For the FCC20 series, the effect of nanoparticle concentration on the reaction conversion shows a similar trend as that on the fluidization quality. Nanoparticles do not have much effect on both fluidization quality and reaction conversion for Group A particles.
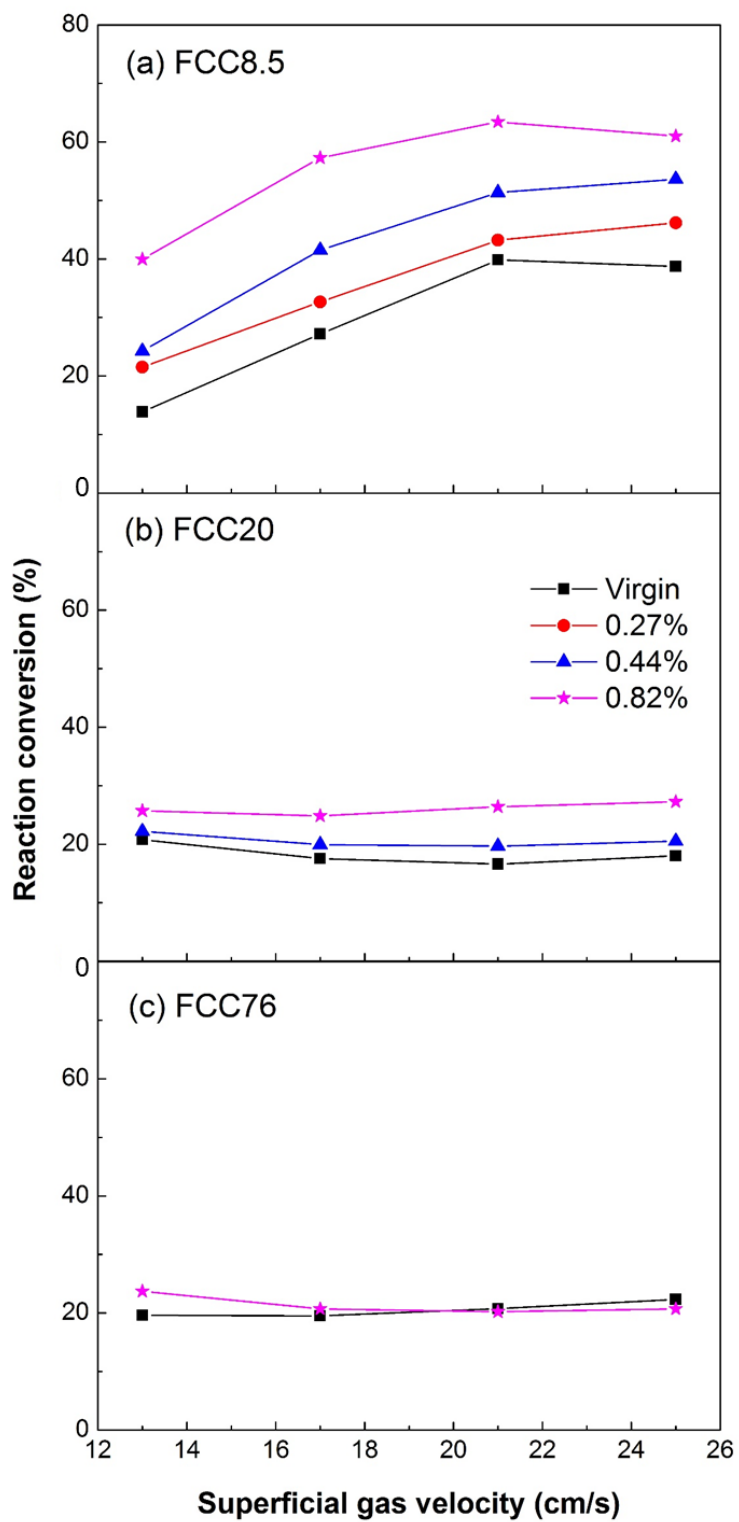
Figure 9.14: Effect of nanoparticle concentration on ozone conversion

9.3.4   Contact efficiency

As seen in the above results, the Group C$^+$ particle fluidized bed reactor with larger specific surface area and higher bed expansion significantly improves the reactor performance, showing a much higher reaction conversion than the Group A particle fluidized bed reactor. To better understand the improvement on the performance of Group C$^+$ fluidized bed reactor, contact efficiency is proposed to correlate the factors based on an ideal plug-flow reactor. For a first-order reaction, the ideal plug-flow model is [27]:

$$C_1 / C_0 = \exp\left[- k_s A_p H / u_g\right] \qquad (9.4)$$

where k_s is the reaction rate constant based on the catalyst surface, $/ [s\ (m^2/m^3)]$, which is obtained by the fixed bed reactor, equal to k_r/A_p. A_p is the specific surface area of the catalyst, m^2/m^3. H is the bed height of the catalyst in the reactor, m. u_g is the operating gas velocity, m/s.

For a fluidized bed, contact efficiency (α) is defined based on the ideal plug-flow model, where the external surface area of Group A catalysts is fully utilized and available for the gas reactant:

$$C_1 / C_0 = \exp\left[- \alpha\, k_s A_p H / u_g\right] = \exp\left[- \alpha\, k_s A_p \tau\right] \qquad (9.5)$$

where τ is the gas residence time in the bed.

It is obvious from the equation that a higher reaction conversion is due to a larger A_p and a longer τ under the same operating gas velocity and catalyst reactivity. Indeed, Group C$^+$ particle fluidization could provide a large catalyst surface area and higher bed expansion, which result in larger gas-solid interfacial contact area and longer gas residence time in the reactor, thus enhancing gas-solid contact. Therefore, Group C$^+$ particle fluidization is expected to improve the contact efficiency. In this project, the total contact efficiency of the fluidized bed reactors due to both the higher gas-solid interfacial area and longer gas residence time is defined as α_t:

$$C_1 / C_0 = \exp\left[- \alpha_t\, k_s A_p \tau_0\right] \qquad (9.6)$$

where k_s is obtained by the fixed bed reactor using Group A particles and keeps the same value in both fixed bed and fluidized bed reactors of Group C, Group C$^+$ and Group A particles, because the true catalyst reactivity is the same for the three types of catalysts. A_p is the specific surface area of Group A particles (FCC76) based on the assumption of full

utilization of the external surface area without agglomerates in the fixed bed reactor. τ_0 is the gas residence time at the fixed bed height (H_0). α_t being calculated represents the contact efficiency relative to that in the fixed bed reactor.

To specifically examine the relative contribution of the two factors, A_p and τ, another parameter α_p is defined as the contact efficiency only due to the specific surface area of catalysts, and the difference between α_t and α_p represents the contact efficiency due to the gas residence time (α_f). α_p is calculated as the following:

$$C_1 / C_0 = \exp\left[- \alpha_p k_s A_p \tau_f\right] \qquad (9.7)$$

where τ_f is the gas residence time at the total fluidized bed height (H_t) under the operating superficial gas velocities.

Figure 9.15 shows the three types of contact efficiencies in the fluidized bed reactors of Group C, Group C$^+$ and Group A particles relative to those in the fixed bed reactors. As shown in Figure 9.15, the total contact efficiencies for Group C$^+$ particles, especially for the series of FCC8.5 particles, are much higher than that for Group A particles. For Group C and Group C$^+$ particles, the contact efficiency due to the specific surface area (A_p) is slightly lower than that due to the gas residence time (τ). On the contrary, the contact efficiency due to A_p is the main factor contributing to the total contact efficiency over that due to τ. For example, FCC8.5+0.82% shows high total contact efficiency with up to 135%, among which 57% is due to the specific surface area and 77% is due to the high bed expansion which allows longer gas residence time in the bed. For FCC76, the highest total contact efficiency reaches 35%, where 27% is the contact efficiency due to A_p and 8% is due to τ. As the results in fluidization hydrodynamics, Group C$^+$ particles exhibit much higher bed expansion than Group A particles, with the highest values around 2.55 and 1.35, respectively. In consequence the effect of fluidization hydrodynamics which contribute to long gas residence time for Group C$^+$ particles is more significant than that for Group A particles on the gas-solid contact efficiency.

Nanoparticle concentration has a significant effect on the contact efficiency for Group C$^+$ particles, while its effect on that for Group A particles is not significant. All the contact efficiencies (α_t, α_f, α_p) for Group C$^+$ particles increase with nanoparticle concentration.

Nanoparticles could reduce the cohesiveness of Group C particles and thus release more surface area for gas reactant in the fluidized bed reactors. Additionally, Group C^+ particles after nanoparticle modulation display better fluidization quality with higher bed expansion, allowing more gas reactant to make contact with catalytic particles. In this project, a nanoparticle concentration of 0.82% shows the best fluidization quality and reaction performance in the fluidized bed reactor of Group C^+ particles, consistent with previous results which shows an optimum nanoparticle concentration of around 0.5-1.0% [10,12,31].
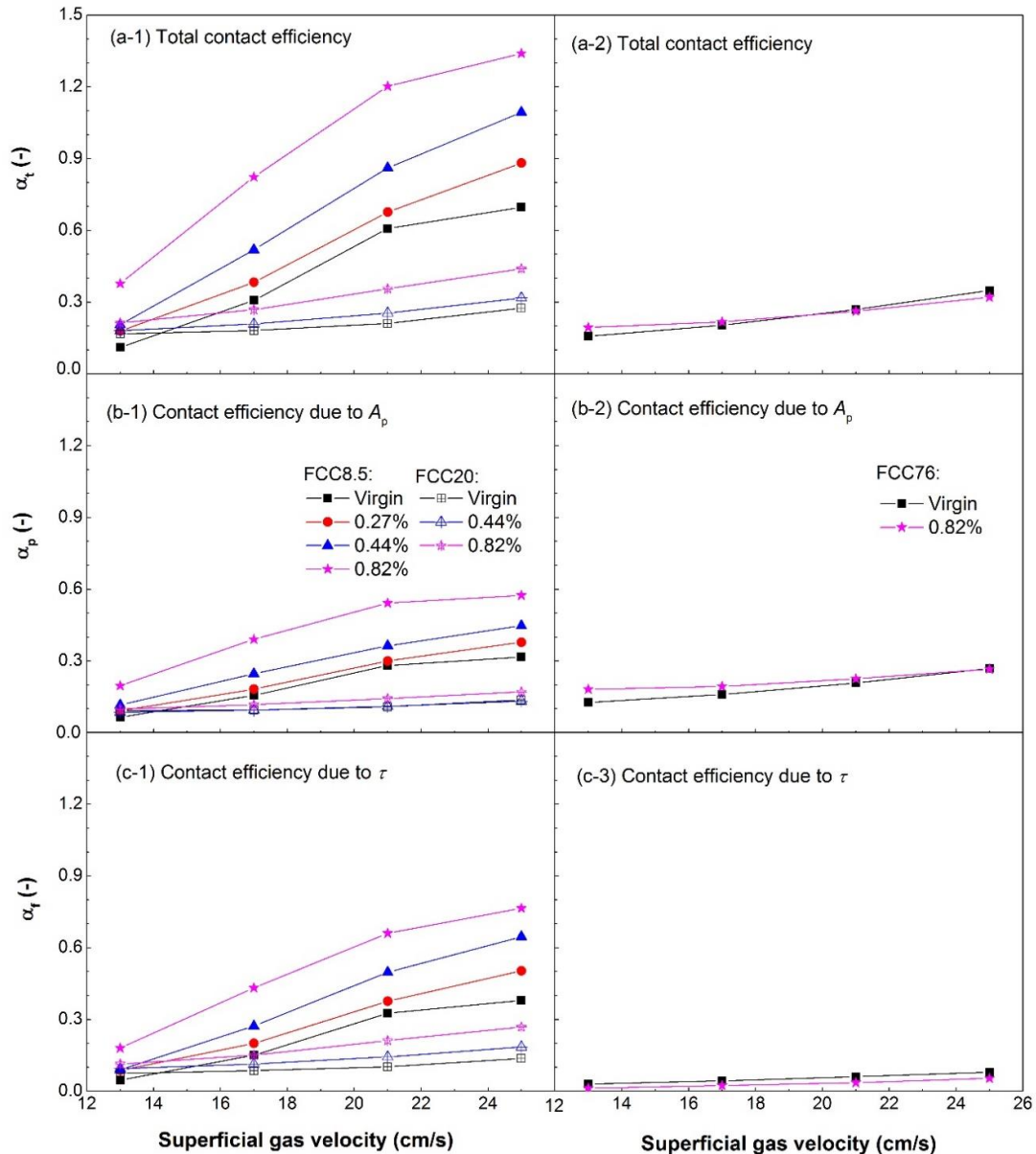
Figure 9.15: Contact efficiencies in the fluidized bed reactors of Group C, Group C⁺ and Group A particles relative to the fixed bed reactors

Figure 9.16 shows the relative contribution of α_p and α_f to the total contact efficiency in the fluidized bed reactors of Group C, Group C⁺ and Group A particles. For Group C and Group C⁺ particles, the contribution of the contact efficiency due to τ is slightly higher than that of due to A_p especially at high gas velocities, because the fluidizations of Group C and Group C⁺ particles become better and more complete with gas velocity increasing. For

Group A particles, the difference between the contribution of α_p and α_f is much more significant. The contribution of α_p is much higher than that of α_f, because Group A particle fluidization shows little bed expansion which exerts insignificant effects on improving the gas-solid contact.

The higher contact efficiencies in the fluidized bed reactors of Group C and Group C$^+$ particles than those in the fluidized bed reactors of Group A particles are ascribed from the two factors A_p and τ. To further compare the contact efficiencies for Group C and Group C$^+$ particles to Group A particles, the relative contact efficiencies are used to characterize the improvement of the fluidized bed reactors using Group C and Group C$^+$ particles over that of using Group A particles, as shown in Figure 9.17. FCC8.5 before and after nanoparticle modulation exhibit significantly higher relative contact efficiencies especially at high gas velocities. For example, the fluidized bed reactor of FCC8.5+0.82% provides the highest relative total contact efficiencies, achieving up to 330% more than that of Group A particles, of which the relative contact efficiency due to A_p could reach 150% and the relative contact efficiency due to τ could reach 180%. In addition, the higher relative contact efficiencies for FCC8.5 series due to the fluidization quality is more significant than that due to the increase of specific surface area especially at low gas velocities. For example, FCC8.5 virgin and those with low nanoparticle concentrations exhibit lower relative contact efficiency due to A_p than FCC76 particles at low gas velocities, signifying the smaller specific surface area for utilization. Although FCC8.5 particles could fluidize with high bed expansion which contributes to longer gas residence time and better gas-solid contact, the agglomeration in the fluidized bed may be more significant than those after nanoparticle modulation, reducing the available gas-solid interfacial area. For FCC20 series, the contact efficiency slightly increases than FCC76 and the gas residence time contributes more than the specific surface area.

In summary, the contact efficiency in the fluidized bed reactor of Group C$^+$ particles are much higher than that in the reactor of Group A particles, due to both the increase of the particle specific surface area and the increase of gas residence time in the bed. Nanoparticle concentration of 0.82% contributes to the most significant improvement on the reaction performance for Group C$^+$ particles.
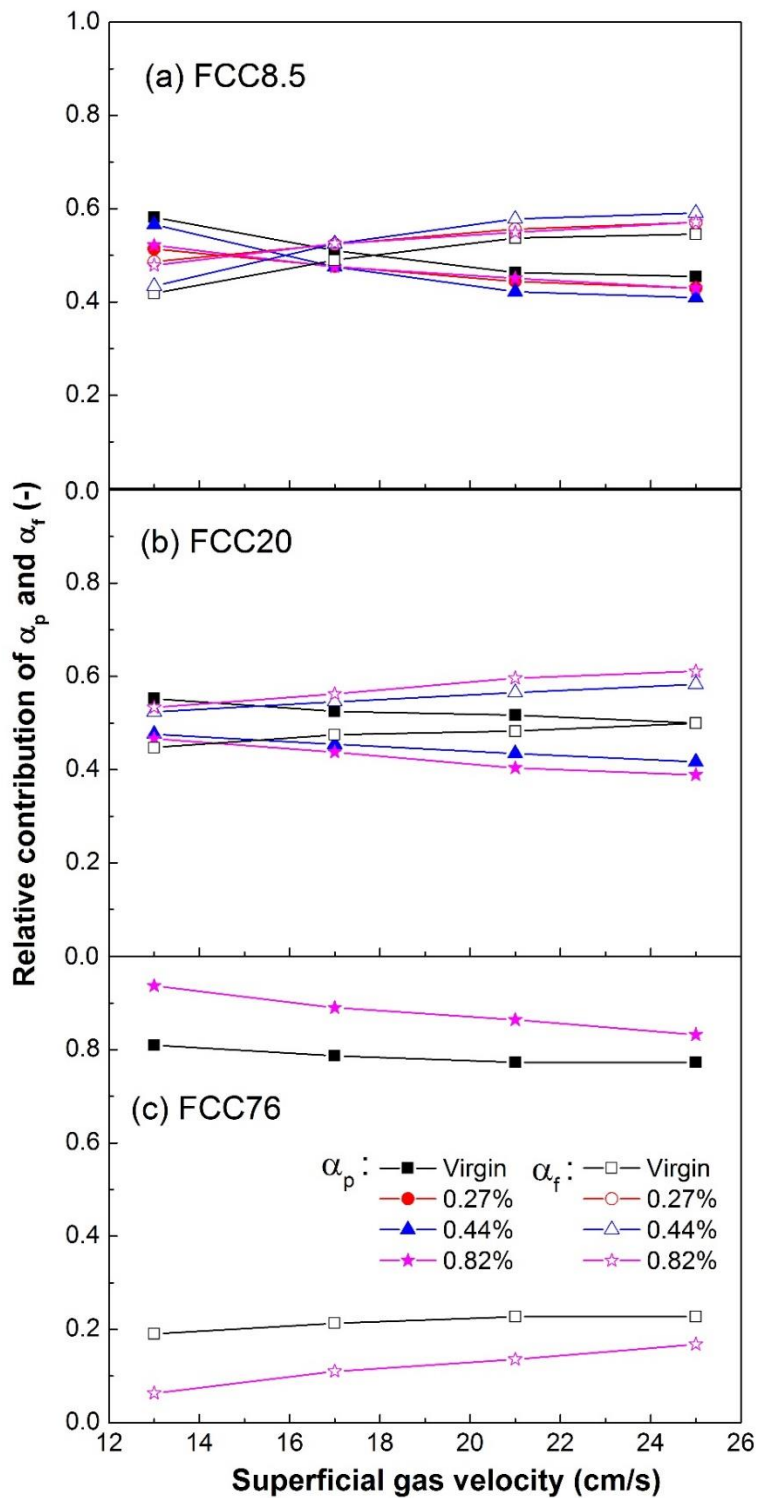
Figure 9.16: The relative contribution of contact efficiencies due to A_p and τ
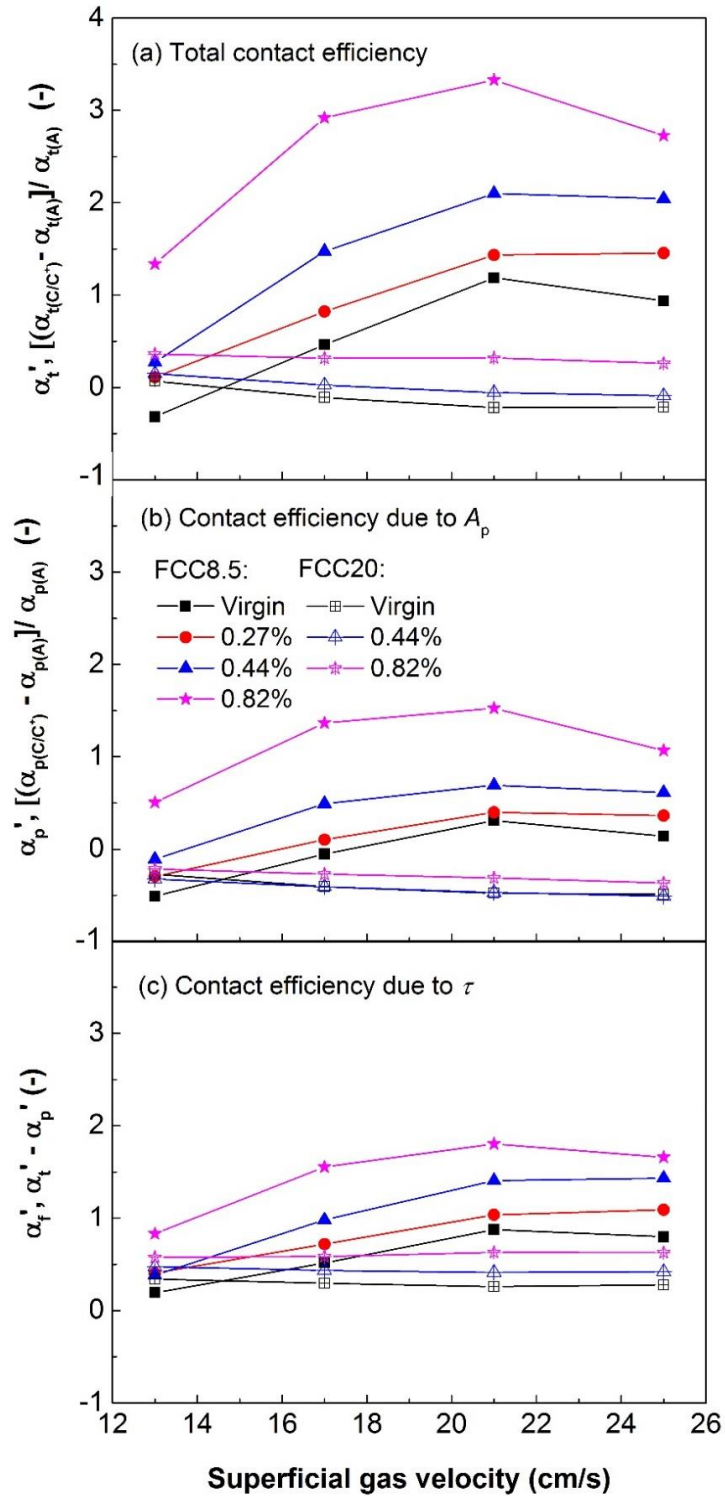
Figure 9.17: Contact efficiencies for Group C and C⁺ particles relative to Group A particles

9.4 Conclusions

The Group C^+ particles have better fluidization quality with much higher bed expansion and mcuh larger dense phase voidages when compared with Group A particles. The large dense phase voidage and the large specific surface area ascribed from the small particle size of Group C^+ particles could increase the gas holdup in the particle interstices and provide more interfacial area for gas-solid contact. These characteristics of Group C^+ particle fluidization are important for many processes, especially gas-phase catalytic reactions.

In the ozone decomposition reaction, the fluidized bed reactors using Group C^+ particles show much higher reaction conversions than those using Group A particles, reaching up to more than 2 times. The high reaction conversion in the fluidized bed reactor using Group C^+ particles confirms that Group C^+ particles with good fluidization quality could improve the reaction performance. Undoubtedly, Group C^+ particles have great potential to bring a soar in the reactor performance of gas-phase catalytic reactions.

Contact efficiency is proposed to characterize the reactor performance for Group C^+ and Group A particles. The fluidized bed reactors using Group C^+ particles contribute to much higher contact efficiency than those using Group A particles, achieving up to more than 4 times of the latter. The significant increase of the total contact efficiency is due to both the larger specific surface area and the high bed expansion in the fluidized bed, which provide larger gas-solid interfacial area and longer gas residence time in the reactors for gas-solid contact. The relative contribution of the fluidization quality for Group C^+ particles is slightly greater for their particle specific surface area.

Nanoparticle concentration do have an influence on the fluidization behaviors and the reaction performance for Group C^+ particles. Combining all the results, the optimum nanoparticle concentration would be 0.82%. With a nanoparticle concentration of 0.82%, Group C^+ particles can fluidize better and more completely with the highest pressure drop, the highest bed expansion and the largest dense phase voidage. Group C^+ particle with a nanoparticle concentration of 0.82% exhibit the best reaction performance, achieving the highest reaction conversion and the highest contact efficiency.

Nomenclature

A	Cross-sectional area of the fluidized bed (cm^2)
A_p	Specific surface area of the catalysts (m^2/m^3)
C_0	Inlet ozone concentration (ppm)
C_1	Outlet ozone concentration (ppm)
D_{10}	Particle diameter that 10% of a sample's volume is smaller than (μm)
D_{50}	Particle diameter that 50% of a sample's volume is smaller than (μm)
D_{90}	Particle diameter that 90% of a sample's volume is smaller than (μm)
F	Volumetric flowrate (l/min)
H_0	Initial fixed bed height (cm)
H_d	Dense phase height (cm)
H_t	Fluidized bed height (cm)
k_r	Reaction rate constant base on catalyst volume (s^{-1})
k_s	Reaction rate constant base on catalyst specific surface area [$s^{-1}/(m^2/m^3)$]
m	Catalyst weight in the fixed bed reactor (g)
u_g	Superficial gas velocity (cm/s)
u_{mf}	Minimum fluidization velocity (cm/s)
W	Particle weight in the fixed bed ($W = mg$, N)
X	Reaction conversion (-)
ΔP	Pressure drop across the entire bed (pa)
τ	Gas residence time in the bed (s)
ρ_b	Bulk density of particles (kg/m^3)
ε_0	Fixed bed voidage (-)
ε_d	Dense phase voidage (-)
α_t	Total contact efficiency (-)
α_p	Contact efficiency due to A_p (-)
α_f	Contact efficiency due to H (-)
α_t'	Relative total contact efficiency [$\alpha_t' = (\alpha_{t(C/C+)}-\alpha_{t(A)}) / \alpha_{t(A)}$, (-)]
α_p'	Relative contact efficiency due to A_p [$\alpha_p' = (\alpha_{p(C/C+)}-\alpha_{p(A)}) / \alpha_{p(A)}$, (-)]
α_f'	Relative contact efficiency due to τ [$\alpha_f' = \alpha_t' - \alpha_p'$, (-)]

Reference

[1]   Daizo Kunii, O. L. Fluidization Engineering (2nd edition). Washington: Butterworth-Heinemann, 1991.

[2]   Zhu J, Cheng Y. Fluidized-Bed Reactors and Applications. In: Multiphase Flow Handbook; Crowe, C, Ed. New York: CRC Press, 2005: 5.55-55.93.

[3]   van der Hoef M A, van Sint Annaland M, Kuipers J A M. Computational fluid dynamics for dense gas–solid fluidized beds: a multi-scale modeling strategy. Chemical Engineering Science. 2004; 59(22-23): 5157-5165.

[4]   Werther J. Fluidized-bed reactors. Ullmann's encyclopedia of industrial chemistry. 2000.

[5]   Geldart D. Types of gas fluidization. Powder technology. 1973; 7(5): 285-292.

[6]   Dutta A. and Dullea L V. A Comparative Evaluation of Negatively and Positively Charged Submicron Particles as Flow Conditioners for a Cohesive Powder. AIChE Symp. Ser. 1990; 86: 26-40.

[7]   Zhu, J and Zhang H. Fluidization Additives to Fine Powders. U.S. Patent 6833185. December 21, 2004.

[8]   Zhu J. Fluidization of fine powders. Granular Materials: Fundamentals and Applications. 2003; 270–295.

[9]   Yang J, Sliva A, Banerjee A, Dave R N & Pfeffer R. Dry particle coating for improving the flowability of cohesive powders. Powder Technology. 2005; 158(1-3): 21-33.

[10] Xu C B, Zhang H & Zhu J. Improving flowability of cohesive particles by partial coating on the surfaces. The Canadian Journal of Chemical Engineering. 2009; 87: 403-414.

[11] Zhou Q T, Qu L, Larson I, Stewart P J & Morton D A. Effect of mechanical dry particle coating on the improvement of powder flowability for lactose monohydrate: A model cohesive pharmaceutical powder. Powder technology. 2011; 207(1-3): 414-421.

[12] Zhou, Y. and Zhu, J. Group C$^+$ Particles: Enhanced Flow and Fluidization of Fine Powders with Nano-Modulation. Chemical Engineering Journal. 2019; 207:653-662.

[13] Han M Q. Characterization of fine particle fluidization. Master thesis, Western University, 2015.

[14] Lockett M J, Davidson J F, Harrison D. On the two-phase theory of fluidization. Chemical Engineering Science. 1967; 22(8): 1059-1066.

[15] Pyle D L, Harrison D. An experimental investigation of the two-phase theory of fluidization. Chemical Engineering Science. 1967; 22(9): 1199-1207.

[16] Dry R J, Judd M R, Shingles T. Two-phase theory and fine powders. Powder Technology. 1983; 34(2): 213-223.

[17] Grace J R, Sun G. Influence of particle size distribution on the performance of fluidized bed reactors. The Canadian Journal of Chemical Engineering. 1991; 69(5): 1126-1134.

[18] Liu J, Grace J R, Bi X. Novel multifunctional optical-fiber probe: II. High density CFB measurements. AIChE J. 2003; 49 (6):1421–1432.

[19] Cotton F A, Wilkinson G, Murillo C A, Bochmann M & Grimes R. Advanced inorganic chemistry. New York: Wiley, 1988.

[20] Wojtowicz J A. Ozone. In: Kirk-Othmer Encyclopedia of Chemical Technology. John Wiley & Sons, Inc., 2000.

[21] Lin J, Nakajima T. An AM1 study of decomposition of ozone on a Cu (110) surface, Ozone: Sci. Eng. 2002; 24 (1): 39-47.

[22] Kirschner M J. Ozone, in: Ullmann's Encyclopedia of Industrial Chemistry, Wiley-VCH Verlag GmbH & Co. KGaA, 2000

[23] Zhu J X. and Zhang H. Method and apparatus for uniformly dispensing additive particles in fine powders. U.S. Patent 7240861, July 10, 2007.

[24] Zhu J X. and Zhang H. Powder blending methods for adding fluidization additives to enhance the flowability of fine powders. U.S. Patent 7878430B2, February 1, 2011.

[25] Rietema K. Application of mechanical stress theory to fluidization. Proc. Int. Symp. on Fluidization. 1967: 154-163.

[26] Barreto G F, Mazza G D, Yates J G. The significance of bed collapse experiments in the characterization of fluidized beds of fine powders. Chemical engineering science. 1988; 43(11): 3037-3047.

[27] Davis M E, Davis R J. Fundamentals of chemical reaction engineering. Courier Corporation, 2012.

[28] Chen Y, Yang J, Dave R N & Pfeffer R. Fluidization of coated group C powders. AIChE journal. 2008; 54(1): 104-121.

[29] Zhu X, Zhang Q, Huang C, Wang Y, Yang C & Wei F. Validation of surface coating with nanoparticles to improve the flowability of fine cohesive powders. Particuology. 2017; 30: 53-61.

[30] Grace J R, Harrison D. The behaviour of freely bubbling fluidized beds. Chemical Engineering Science. 1969; 24(3): 497-508.

[31] Huang Q, Zhang H, Zhu J. Flow properties of fine powders in powder coating. Particuology. 2010; 8(1): 19-27.

Chapter 10

10   Reaction Performance of Group C⁺ Fluidized Bed Catalytic Reactor

(A version of this chapter has been submitted to *Particuology* for publication)

Often being regarded as non-fluidizable, Group C particles were proven to fluidize well with the addition of nanoparticles, showing small bubbles and high gas holdup in the dense phase during experiments. Such so-called Group C⁺ particles would provide more surface area for gas-solid contact and significantly improve the reaction performance, especially for gas-phase catalytic reactions. Based on the previous study of ozone decomposition reaction using Group C⁺ catalysts, a two-phase model was used to evaluate the reactor contact efficiency, and was further utilized to compare the performance of the partial oxidation of n-butane to maleic anhydride reaction in the fluidized bed reactor using Group C⁺ and Group A catalysts. Group C⁺ catalytic reactor is shown to achieve a much higher n-butane conversion and MAN yield compared to Group A catalytic reactor, either based on the identical catalyst quantity or based on the same gas residence time. In other words, Group C⁺ fluidized bed reactor can achieve the same reaction conversion and yield with fewer catalysts and/or smaller reactor size. Therefore, Group C⁺ fluidized bed reactor is expected to cause a significant "splash" in industrial processes, especially for gas-phase catalytic reactions.

10.1 Introduction

Given the superb ability of heat and mass transfer and ease of solids handling, fluidized-bed reactors have been applied in many chemical processes, especially in gas-phase catalytic reactions [1]. Reactor performance is mainly affected by fluidization hydrodynamics, which are related to operating conditions [2-3] and particle properties [4-6]. Geldart [7] classified particles into four groups based on their physical properties and fluidization behaviors, Groups A, B, C and D. In most reaction processes, the catalysts used in fluidized bed reactors are always Group A particles due to their good fluidization quality with more homogeneous bed expansion and large specific surface area. Group C particles have even larger specific surface area and have attracted the attention of many

researchers in recent years. However, Group C particles are more difficult to fluidize and tend to form channels and agglomerates due to their inherent cohesiveness arising from the strong interparticle forces [6-10]. In recent years, Xu et al. [11] found that the relatively strong interparticle forces of Group C particles could be reduced and Group C particles become fluidizable with the addition of nanoparticles. Zhou et al. [12,13] systematically studied the fluidization behaviors of the so-called Group C^+ particles, and revealed a much higher bed expansion and dense phase voidage than for Group A particles, indicating better fluidization quality with more gas in the fluidized bed and therefore better solid-gas contact.

In a more recent work, Zhou et al. [14] "calibrated" the reaction performance using the ozone decomposition with Group C^+ and Group A catalysts, and found that the Group C^+ fluidized bed reactor exhibited a much higher reaction conversion and better gas-solid contact than Group A fluidized bed reactor. As a result, Group C^+ fluidized bed reactor has significant advantages that can be utilized by the industry. Generally, the use of fluidized beds in chemical industries is associated with uncertainties of the scale-up and the performance. The prediction of the performance and scale-up of fluidized bed reactors become important for both research and development of new processes. Therefore, Group C^+ fluidized bed reactor, proposed as a new type of reactor, is necessary to be modeled and simulated before seeing use in chemical industries.

A large number of fluidized-bed models have been devised to describe the different regimes of fluidization, such as the Kunii-Levenspiel model [15] and the Grace model [16] for the bubbling regime, the single-phase plug-flow model [17] and the modified two-phase model [18] for the turbulent regime, and the single-region models and the two-region models for the fast fluidization regime [19]. When it comes to traditional fluidized beds, most fluidized-bed models [20-23] are based on the simple two-phase theory of fluidization, which was originally proposed by Toomey [24] and suggested that all gas in excess of that required for minimum fluidization (U_{mf}) passed through the bed as solid-free bubbles while the dense phase remained at the minimum fluidization state, meaning that the gas passes through the dense phase at the minimum fluidization velocity. However, many experiments [25,26] and theories [27,28] have shown that there are solid particles in

the bubbles, and the dense phase can hold more gas and "stay" at a higher gas velocity than the minimum fluidization velocity in the fluidized bed of fine particles [26,29].

Considering the deviation of fine particle fluidization from the simple two-phase theory, a modified two-phase model was utilized to evaluate the reactor performance based on the experiments from Zhou et al. [14], which were conducted in bubbling regime. The purpose was to compare the performance of the fluidized bed reactor using Group C^+ catalysts with the same reactor of Group A catalysts, and showed the performance improvements Group C^+ fluidized bed reactor possesses over its counterpart. The production of maleic anhydride (MAN), as a common reaction in industry, was adopted as an example to exhibit the reactor performance using Group C^+ catalysts.

10.2 A modified two-phase model

As with most multiphase reactors, the modeling of a fluidized bed is complex due to diversiform hydrodynamic behaviors. The two-phase theory is now generally accepted as the appropriate modeling approach. In the "simple two-phase model", a fluidized bed reactor consists of two phases, the bubble phase and the dense phase. All the gas in excess of U_{mf} flows through the bed as bubbles while the dense phase remains at minimum fluidization conditions. This model assumes that there are no solids in the bubbles and reactions occur only in the dense phase. In practice the reaction in the fluidized bed is more complicated than what the "simple two-phase model" assumed, as the bubbles contain a small number of particles and more gas passes through the dense phase. Therefore, the modified two-phase model takes into consideration both the reaction in the bubbles and the dense phase. In this model, the gas velocity and voidage in the dense phase were calculated based on the experimental data and were different with those at minimum fluidization conditions. The gas flowing through the dense phase is assumed as the plug-flow. The equations for this model are listed in Table 10.1. Equations 10.1 to 10.3 depict:

Consumption of reactant A in dense phase = reaction in dense phase + transfer to bubble phase

Consumption of reactant A in bubble phase = reaction in bubble phase + transfer to dense phase

Concentration of reactant A = concentration of A in the dense phase + concentration of A in the bubble phase

In Equation 10.2, γ_b represents the volume of solids dispersed in the bubble phase divided by the volume of bubbles and γ_b is 0.005 based on the observation from the experiment [30]. In this modified two-phase model, the superficial gas velocity in the dense phase is calculated from the experimental data using Equations 10.4 and 10.5. δ in Equation 10.4 is the bubble fraction, measured by the bed collapse test. The dense phase velocity (U_{dd}) was used in Equation 10.1 to calculate the mole balance for species A in the dense phase.

The correlations for various bubble properties are listed in Table 10.2. In this two-phase model, all bubbles are assumed to have a uniform size throughout the bed. The average bubble size in the whole bed ($\bar{d}_b$) is obtained by integrating d_{bz} over the whole bed. The bubble rise velocity in the fluidized bed was calculated using Equations 10.11 and 10.12. Equations for interfacial mass transfer are listed in Table 10.3. Gas interfacial coefficient between the two phases and number of transfer units (NTU) are used to quantify the interfacial mass transfer.

Table 10.1: Reaction equations for the modified two-phase model

Mole balance in the dense phase	$-(1-\delta)U_{dd}\dfrac{dC_{Ad}}{dz}=(1-\delta)(1-\varepsilon_d)R_{Ad}-\delta K_{bd}(C_{Ab}-C_{Ad})$	(10.1)
Mole balance in the bubble phase	$-\delta U_b\dfrac{dC_{Ab}}{dz}=\delta\gamma_b R_{Ab}+\delta K_{bd}(C_{Ab}-C_{Ad})$	(10.2)
Concentration of species A	$C_A=\dfrac{U_{dd}(1-\delta)}{U_g}C_{Ad}+\dfrac{U_b\delta}{U_g}C_{Ab}$	(10.3)
Dense phase velocity	$U_{dd}=\dfrac{U_g-\delta U_b}{1-\delta}=\dfrac{U_g A-G_b}{A(1-\delta)}$	(10.4)
Superficial gas velocity in dense phase	$U_{df}=(1-\delta)U_{dd}=U_g-\dfrac{G_b}{A}$	(10.5)

Table 10.2: Equations for the hydrodynamics in two-phase model

Bubble diameter [31]	$d_{bz}=0.54(U_g-U_{mf})^{0.4}(z+4\sqrt{A_D})^{0.8}g^{-0.2}$	(10.6)
Equilibrium bubble diameter [32]	$d_{be}=\left(\dfrac{D}{4}\right)[-\gamma_M+(\gamma_M^2+4d_{bm}/D)^{0.5}]^2$	(10.7)
	$\gamma_M=2.56\times10^{-2}(D/g)^{0.5}/U_{mf}$	(10.8)
Maximum bubble diameter [33]	$d_{bm}=2.59[(U_g-U_{mf})A_t]^{0.4}/g^{0.2}$	(10.9)
Average bubble diameter [34]	$\bar{d}_b=\dfrac{1}{H_f}\displaystyle\int_0^{H_f}d_{bz}\,dz$	(10.10)
Bubble velocity [20]	$U_b=U_g-U_{df}+U_{br}$	(10.11)
Single bubble velocity [20]	$U_{br}=0.71\sqrt{g\bar{d}_b}$	(10.12)

Table 10.3: Equations for interfacial mass transfer

Gas interchange coefficient between bubble and dense phase [15]	$\dfrac{1}{K_{bd}}=\dfrac{1}{K_{bc}}+\dfrac{1}{K_{cd}}$	(10.13)
	$K_{bc}=4.5\left(\dfrac{U_{dd}}{\bar{d}_b}\right)+5.85\left(\dfrac{D_g^{\frac{1}{2}}g^{\frac{1}{4}}}{\bar{d}_b^{\frac{5}{4}}}\right)$	(10.14)
	$K_{cd}=6.77\left(\dfrac{D_g\varepsilon_d U_{br}}{\bar{d}_b^{\,3}}\right)^{1/2}$	(10.15)
Number of transfer units [35]	$NTU=\dfrac{k_{bd}S_bH}{U_bV_b}=\dfrac{K_{bd}H}{U_b}$	(10.16)

10.3 Experimental results on ozone decomposition reaction

The ozone decomposition reaction is often used as the probe reaction to characterize the reactor performance, as it happens at a low reactant concentration. The reaction rate could be measured at room temperature and the analysis of the ozone concentration is quick and accurate [36-41]. As shown in literatures [36,38,40], the ozone decomposition reaction is a simple irreversible first-order catalytic reaction, given as:

$$2O_{3(g)}\rightarrow3O_{2(g)}$$
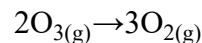
The rate of ozone decomposition reaction is $R_{O_3}=k_s\cdot A_p\cdot C_{O_3}$, where k_s is the reaction rate constant based on the specific surface area of the catalyst, which is determined by the

experimental data. Assuming the catalysts are spherical in shape, A_p is the particle surface area per unit volume, equal to $6/d_s$.

In the fluidized bed, the catalysts formed agglomerates, resulting in a reduction of the surface area which could come in contact with the gas reactant. Here, the reaction rate in the fluidized bed was set as: $R_A = k_s \cdot A_p' \cdot C_A$, where A_p' is the effective surface area of the catalyst in the fluidized bed, which was calculated based on the experimental data of the ozone decomposition reaction. Two types of particles, FCC76 belonging to the category of Group A particle and FCC8.5+0.82% (FCC8.5 with nanoparticle volume fraction of 0.82%) belonging to the category of Group C particles were selected in this project. The properties of the catalysts in the fluidized bed and the results of the ozone decomposition reaction were reported by Zhou et al. [14], as listed in Tables 10.4 and 10.5. The ozone diffusion coefficient (D_g) is 1.8×10^{-5} m^2/s [40].

Table 10.4: Properties of catalysts and fluidized bed [14]

Parameter	Value
D	5.08×10^{-2} m
A_D	5.10×10^{-5} m^2
d_s (FCC76)	76μm
d_s (FCC8.5+0.82%)	8.5μm
A_p (FCC76)	7.89×10^4 m^{-1}
A_p (FCC8.5+0.82%)	7.06×10^5 m^{-1}
ε_0 (FCC76)	0.509
ε_0 (FCC8.5+0.82%)	0.747
k_s (FCC76 and FCC8.5+0.82%)	1.72×10^{-5} m/s

Table 10.5: Experimental results of ozone decomposition reaction

Catalyst	U_{mf} (cm/s)	U_g (cm/s)	H_0 (cm)	H_f (cm)	BER (-)	ε_d (-)	δ (-)	Conversion (-)
FCC76	0.5	12.7	8.5	11.0	1.30	0.519	0.162	0.196
	0.5	16.7	8.5	11.2	1.32	0.532	0.178	0.195
	0.5	20.8	8.5	11.5	1.36	0.533	0.198	0.207
	0.5	24.9	8.5	11.8	1.39	0.534	0.217	0.223
FCC8.5+	9.8	12.7	12.5	23.1	1.85	0.856	0.130	0.400
0.82%	9.8	16.7	12.5	27.8	2.22	0.863	0.169	0.573
	9.8	20.8	12.5	30.0	2.41	0.865	0.212	0.634
	9.8	24.9	12.5	32.4	2.59	0.865	0.268	0.610

10.4 Effect of particle size on fluidization hydrodynamics

The bubble size reported by Chapter 6 was found to be small and rapidly reached the maximum stable bubble size at a bed height of 0.03m at all superficial gas velocities. Because the height of 0.03m was much lower than the total fluidized bed height, the bubble size at this height was considered to be the average bubble size for FCC8.5+0.82%. For Group A particles, the bubble size grew significantly along the bed height at given superficial gas velocities, and would reach a maximum stable bubble diameter [32] due to bubble coalescence and splitting, which may be calculated using Equation 10.7, or, due to the restriction by the reactor diameter, will considered to be 2/3 of the fluidized bed diameter (D). Figure 10.1 shows that the bubble size for Group A and Group C$^+$ particles and the possible maximum stable bubble size. Because the maximum bubble size calculated by Equation 10.7 for Group A particles was much larger, $\frac{2}{3}D$ was considered as the maximum stable bubble size. Therefore, the average bubble size throughout the bed was obtained by integrating the bubble sizes along the entire bed, including a possible section of the upper bed where the maximum bubble size has been reached. As shown in Figure 10.2, the average bubble size was much smaller for FCC8.5+0.82% than for FCC76, leading to different bubble behaviors, especially for the bubble rise velocity. The effect of capping at the maximum bubble size was shown to have a small effect only when the gas velocity was larger than 0.2m/s, as shown by the dotted line.
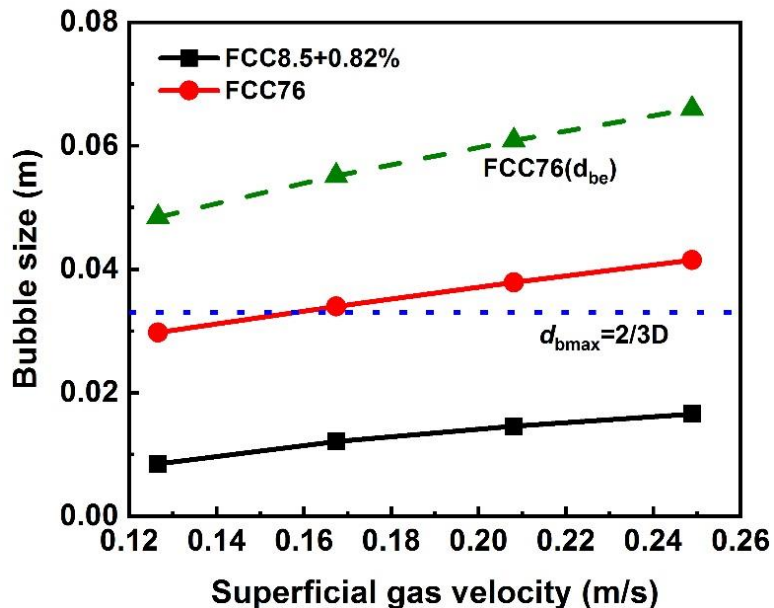
Figure 10.1: The bubble size at the top of Group C$^+$ and Group A fluidized bed reactors
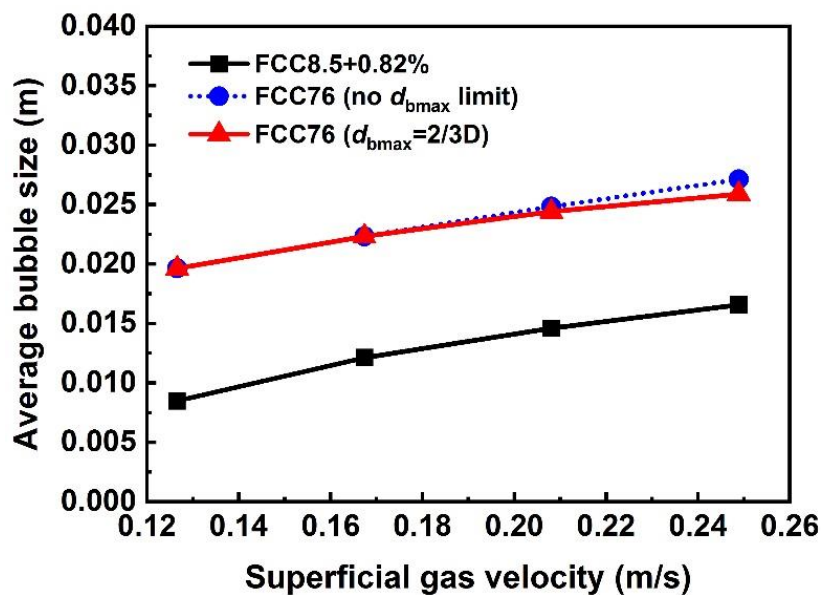
Figure 10.2: The average bubble size in Group C$^+$ and Group A fluidized bed reactors

Bubble rise velocity is closely related to the bubble diameter and the operating gas velocity. It also plays an important role in the bubble residence time of the fluidized bed reactor. The

bubble rise velocities calculated using Equation 10.11 based on the average bubble diameter and the bubble residence time are shown in Figure 10.3. Group C^+ fluidized bed reactor exhibited much lower bubble rise velocities than Group A reactor, resulting in longer bubble residence time in the bed. The smaller bubble size, lower rise velocity, and longer residence time in the Group C^+ fluidized bed reactor would contribute to better mass transfer between the bubble phase and the dense phase. For both particles, as superficial gas velocity increased, the bubble rise velocity increased and the bubble residence time decreased.
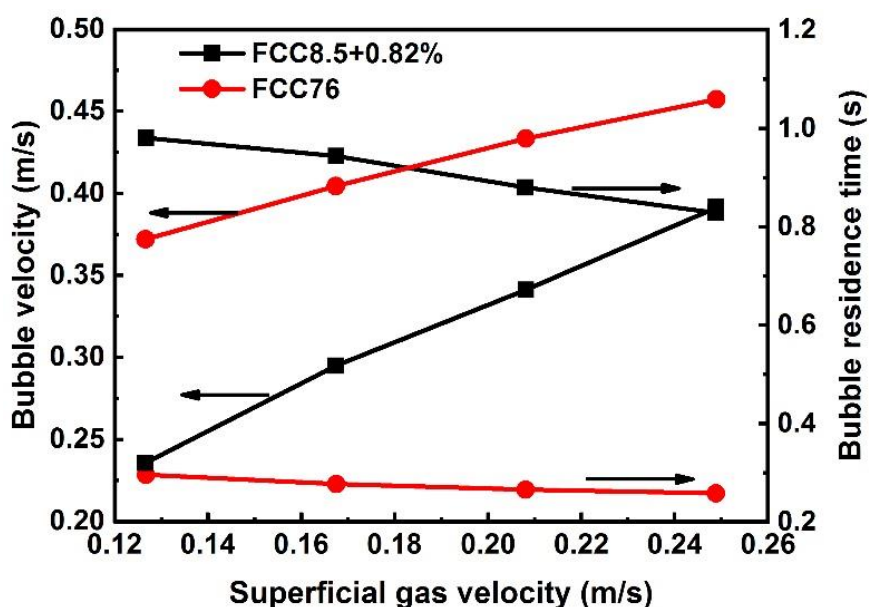
Figure 10.3: Bubble rise velocity and bubble residence time in Group C^+ and Group A fluidized bed reactors

The extend of mass transfer between the bubble phase and the dense phase can be quantified by the gas interchange coefficient, as may be calculated by Equation 10.13, or by the number of transfer units (NTU), which may be calculated using Equation 10.16.

As shown in Figure 10.4, the gas interchange coefficients in Group C^+ fluidized bed reactor were much higher than those in the Group A reactor, indicating a higher mass transfer rate. The NTU values for Group C^+ catalysts were also much higher than those for Group A catalysts, signifying that more reactants were being transferred to the dense phase, which subsequently contributes to better mass transfer. As gas velocity increased, the values of

both the gas interchange coefficient and NTU decreased, indicating that the increase of the gas velocity would produce a negative effect on the mass transfer between the bubble phase and the dense phase. The superior mass transfer showcased by the Group C^+ fluidized bed reactor supported the thinking that smaller bubbles in the bed could improve the mass transfer between the bubble phase and the dense phase, which is expected to enhance the reactor performance.
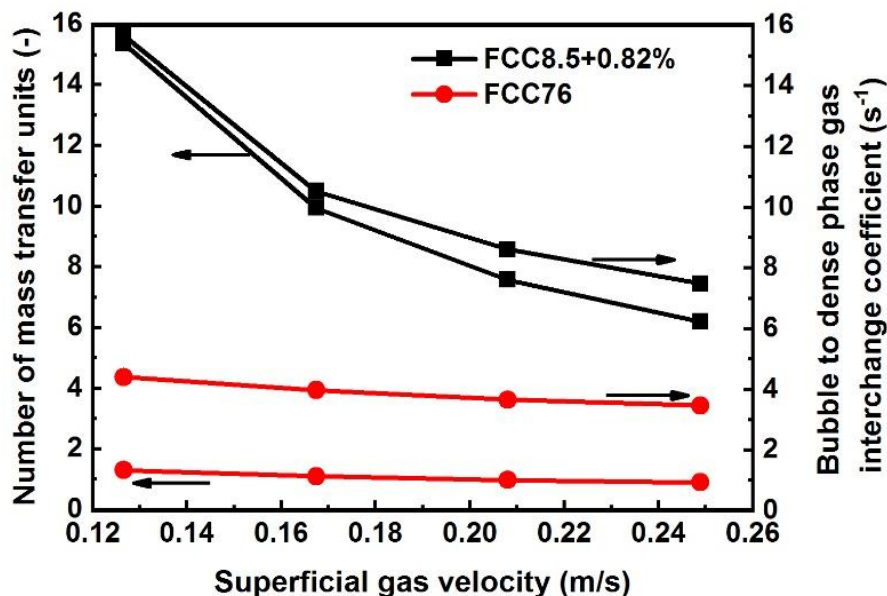
Figure 10.4: The number of mass transfer units and the bubble to dense phase gas interchange coefficient in Group C^+ and Group A fluidized bed reactors

Gas velocity (U_{dd}) and gas residence time in the dense phase for Group C^+ and Group A particles with increasing superficial gas velocity are shown in Figures 10.5 and 10.6. The reactor of FCC8.5+0.82% showed higher gas velocities in the dense phase (U_{dd}) than the reactor of FCC76, indicating that gas flowrates were higher through the dense phase. The gas residence time in the dense phase for Group C^+ particles was much longer than that for Group A particles despite the higher U_{dd}, due to the much higher bed expansion for Group C+ particles [14]. Both the higher U_{dd} and longer gas residence time contributed to more gas going through the dense phase and staying longer, causing better gas-solid contact and thus increasing the reaction conversion.
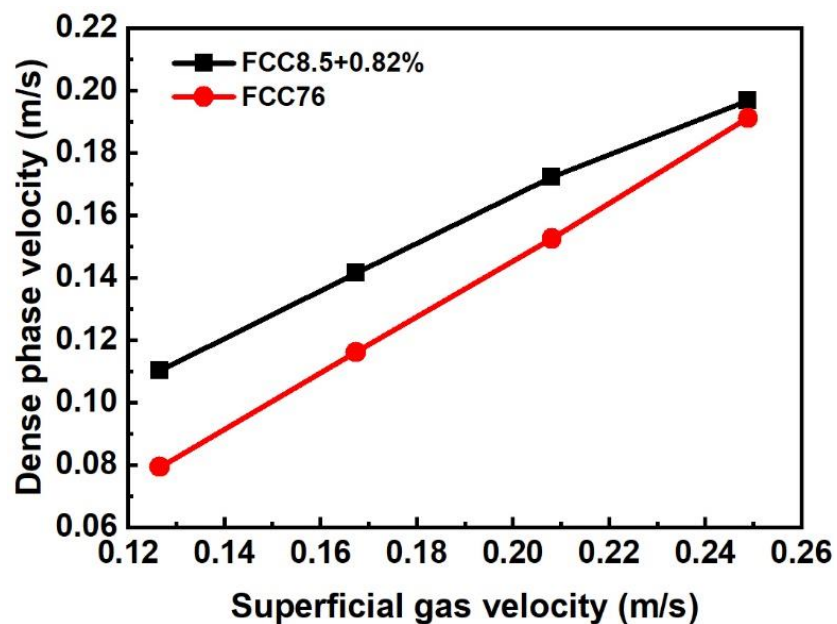
Figure 10.5: The dense phase velocity (U_{dd}) in Group C$^+$ and Group A fluidized bed reactors
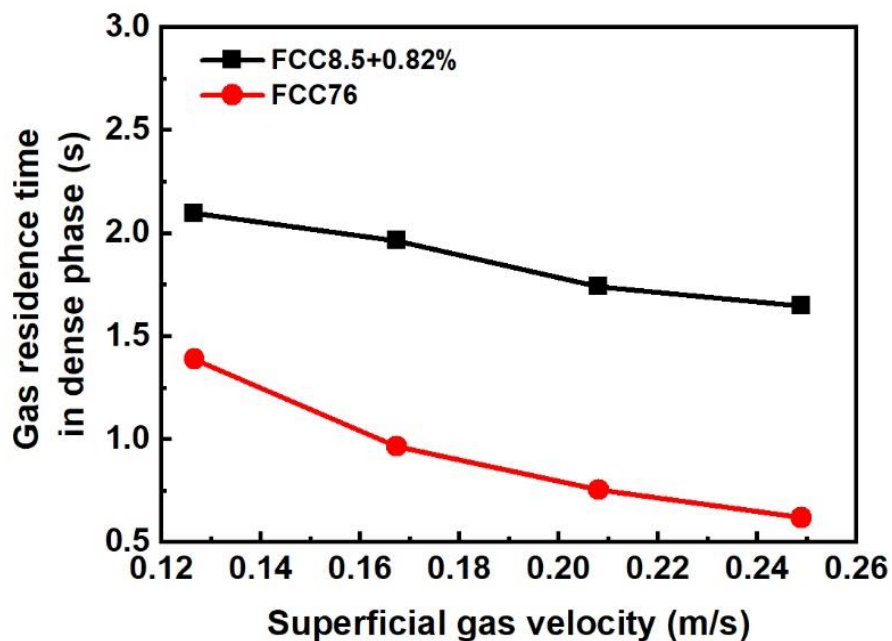
Figure 10.6: Gas residence time in the dense phase in Group C$^+$ and Group A fluidized bed reactors

10.5 Effect of particle size on reactor performance: Ozone decomposition

The fluidization hydrodynamics in the fluidized bed reactor of Group C^+ and Group A particles are summarized in Table 10.6, including the bubble and the dense phase properties and the mass transfer between the two phases. Less gas holdup in the bubble phase, more gas holdup in the dense phase, longer gas residence time in the bed, and better mass transfer between the two phases in the reactor of Group C^+ particles could enhance the gas-solid contact and contribute to a better reactor performance.

Table 10.6: Relative magnitude of the various fluidization properties for Group C^+ and Group A particles

	Group C^+ reactor	Group A reactor
Bubble diameter	↓	↑
Bubble rise velocity	↓	↑
Bubble residence time	↑	↓
Gas velocity in dense phase	↑	↓
Gas residence time in dense phase	↑	↓
Mass transfer between two phases	↑	↓

Another critical factor that affects the reactor performance is the gas-solid contact area., which is represented by the effective specific surface area. Because of the agglomeration in the fluidized bed, the surface area (A_p) of individual particles cannot be completely exposed to and come into contact with the gas reactant. The effective specific surface area (A_p') is used to present the surface area available for gas-solid contact and quantify the contact efficiency. Figure 10.7 shows the various effective specific surface areas and those deduced from the experiments. As shown, the effective surface area of FCC8.5+0.82% was much larger than that of FCC76 in the fluidized bed reactor based on the same quantity of catalyst particles. The larger effective surface area of the catalysts could provide a larger interfacial area for gas-solid contact, resulting in higher contact efficiency. However, the effective surface area of FCC8.2+0.82% was still much smaller than the surface area without agglomeration (A_p), due to the significant agglomeration in the fluidized bed of Group C^+ particles. As the increase in the gas velocity reduced the agglomeration in the fluidized bed of Group C^+ particles, the effective surface area of FCC8.5+0.82% went close

to A_p, while that for FCC76 could reach A_p, indicating that the surfaces of all the individual particles were released to the gas reactant.

Experimentally obtained effective surface areas were correlated with the superficial gas velocities for the purpose of modelling the fluidized bed reactor, expressed as follows:

Group C$^+$ (FCC8.5+0.82%): $A_p' = -1.34\text{x}10^7 U_g^2 + 7.84\text{x}10^6 U_g - 6.42\text{x}10^5$ (10.17)

Group A (FCC76): $A_p' = 1.24\text{x}10^6 U_g^2 - 1.64\text{x}10^4 U_g + 2.28\text{x}10^4$ (10.18)
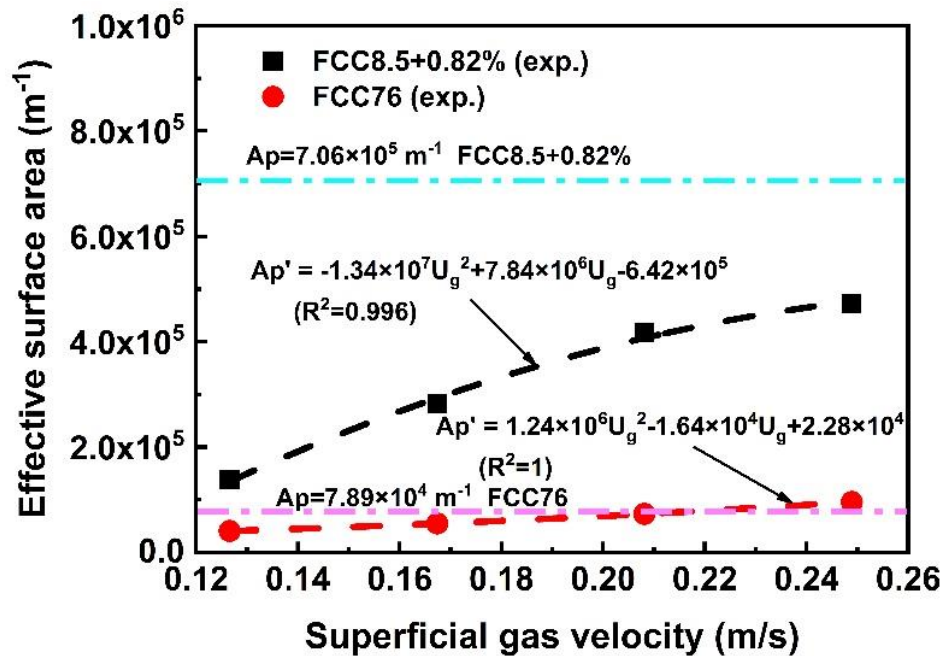
Figure 10.7: The effective surface area of catalyst in Group C$^+$ and Group A fluidized bed reactors

Aside from the effective specific surface area, the fluidization hydrodynamics such as the bubble fraction and the bed expansion are also required for the reactor model. The bubble fraction and the bed expansion ratio (BER) for FCC8.5+0.82% and FCC76 are obtained from the previous chapter 9, as shown in Figures 10.8 and 10.9, predicted by the following correlations:

Bubble fraction (δ):

Group C$^+$ (FCC8.5+0.82%): $\delta = 2.556 U_g^2 + 0.161 U_g + 0.069$ (10.19)

Group A (FCC76): $\delta = 0.451 U_g^2 + 0.285 U_g + 0.119$ (10.20)

Bed expansion ratio (BER):

Group C$^+$ (FCC8.5+0.82%): BER = $415.73U_g^3 - 262.73U_g^2 + 59.188U_g - 2.276$ (10.21)

Group A (FCC76): BER = $-74.253U_g^3 - 43.327U_g^2 - 7.403U_g + 1.693$ (10.22)

The fluidized bed height could be obtained using $H_f = H_o \times$ BER when the initial bed height is fixed. The dense phase voidage could be calculated from the following equation:

$$\varepsilon_d = 1 - \frac{1-\varepsilon_o}{(1-\delta)\cdot BER}$$ (10.23)

where ε_0 is fixed bed voidage.
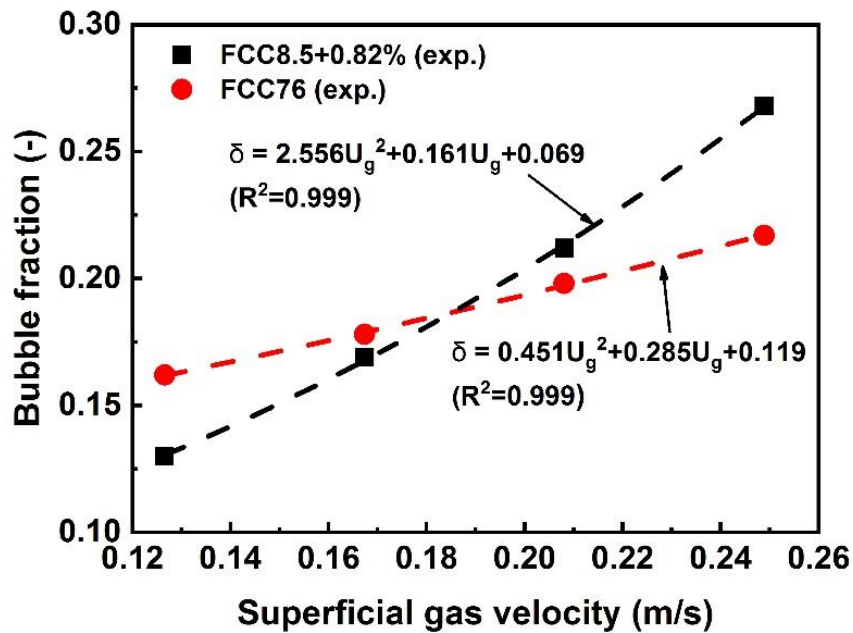
Figure 10.8: The bubble fraction in Group C$^+$ and Group A fluidized bed reactors
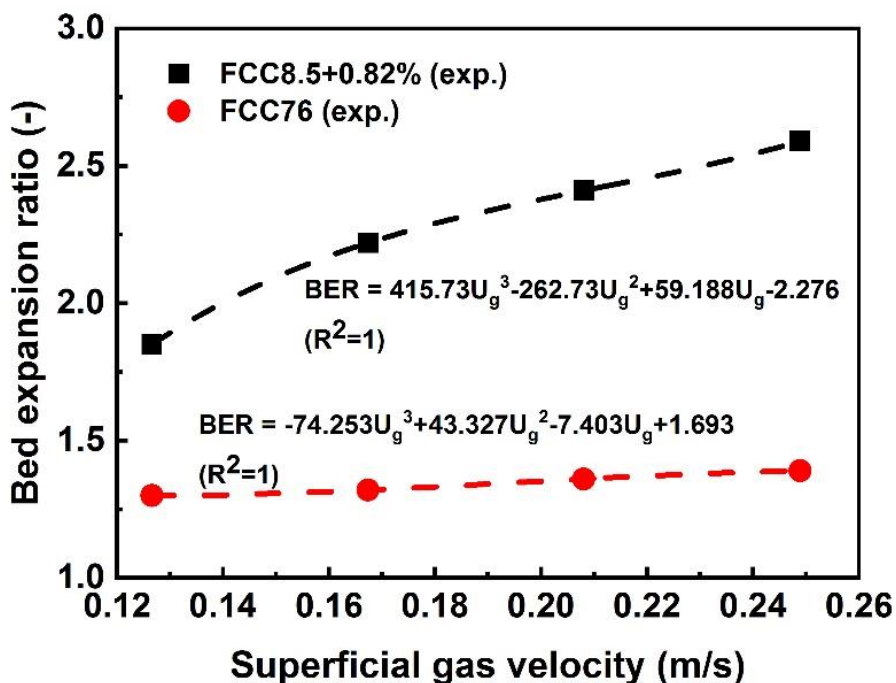
Figure 10.9: The bed expansion ratio in Group C$^+$ and Group A fluidized bed reactors

With these correlations above, the reaction conversion of the ozone decomposition reaction could be calculated using the modified two-phase model, as shown in Figure 10.10. The calculated results were consistent with the experimental ones, validating this modified model and suggesting that this model was acceptable and could be used to predict the reactor performance under the operating conditions in this work.
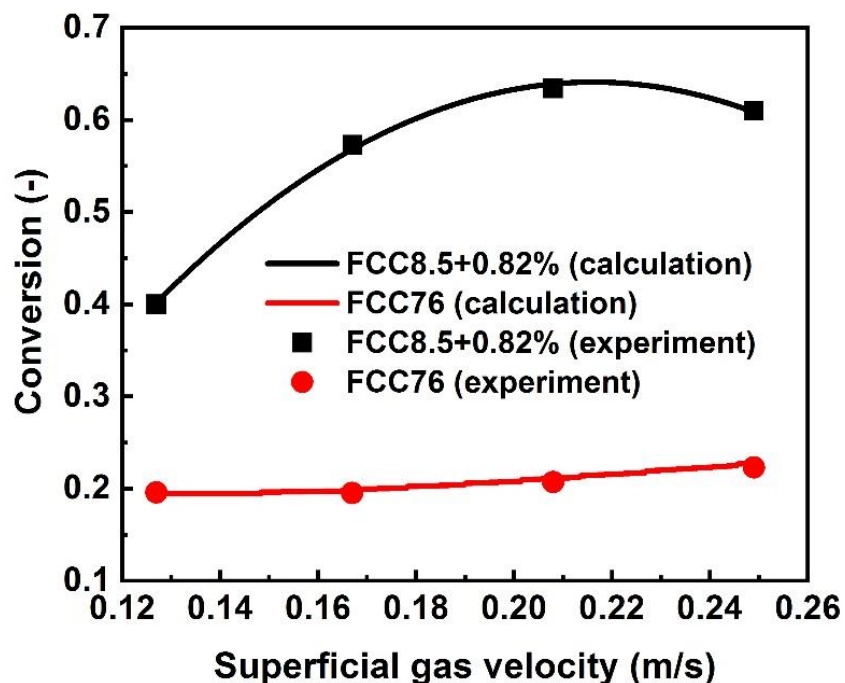
Figure 10.10: Calculated and experimental results of ozone decomposition

10.6 Effect of particle size on reactor performance: Maleic anhydride production

Industrial interest in the selective oxidation of n-butane to maleic anhydride (MAN) on vanadium-phosphorus oxides (VPO) has increased rapidly. The production of MAN is considered as the example reaction in this work for comparing the performance of Group C^+ and Group A fluidized bed reactors. The complete reaction pathway involves both serial and parallel reactions as follows:
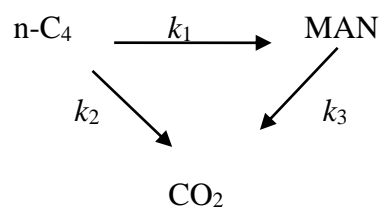
The detailed reactions are:

$$n\text{-}C_4H_{10}+3.5O_2 \rightarrow MAN+4H_2O$$
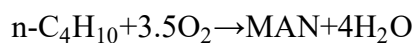
$$r_1 = \frac{k_1 A_p K_B C_B C_O^\alpha}{1 + K_B C_B} \tag{10.24}$$

$$\text{n-}C_4H_{10} + 6.5O_2 \rightarrow 4CO_2 + 5H_2O$$

$$r_2 = k_2 A_p C_O^\beta \tag{10.25}$$

$$\text{MAN} + 3O_2 \rightarrow 4CO_2 + H_2O$$
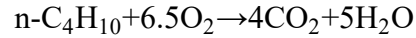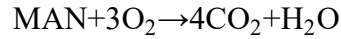
$$r_3 = k_3 A_p C_{MAN} \left(\frac{C_O^\theta}{C_B^\sigma} \right) \tag{10.26}$$

The overall reaction rates for all the species in the MAN production are listed in Table 10.7. The kinetic parameters of these reactions were obtained from the work by Centi et al. [43], as summarized in Table 10.8, and were not much different at various reaction temperatures. The reaction temperatures ranged from 300 to 340C, and were assumed to have no influence on the fluidization hydrodynamics. The particle size and physical properties of the VPO catalyst are close to the properties of FCC76 used in Chapter 9, without the consideration of Catalyst deactivation. The feed concentrations of n-butane in air was 5 mol%. The conversion $X = (C_{B0} - C_B)/C_{B0}$, selectivity $S = C_{MAN}/(C_{B0} - C_B)$, and yield of the MAN production $Y = C_{MAN}/C_{B0}$ were predicted using the modified two-phase model which has been validated by the ozone decomposition reaction.

Table 10.7: Overall reaction rates for partial oxidation of n-butane

A	R_A
n-butane	$r_1 + r_2$
MAN	$-r_1 + r_3$
CO_2	$-4r_2 - 4r_3$
O_2	$3.5r_1 + 6.5r_2 + 3 r_3$

Table 10.8: Kinetic parameters*

Temperature (C)	k_1 $(\text{mol}^{1-\alpha}L^{\alpha-1}\cdot m/s)$	k_2 $(\text{mol}^{1-\beta}L^{\beta-1}\cdot m/s)$	k_3 $(\text{mol}^{\sigma-\theta}L^{\theta-\sigma}\cdot m/s)$
300	7.57×10^{-9}	4.51×10^{-9}	9.92×10^{-10}
320	1.04×10^{-8}	9.84×10^{-9}	1.49×10^{-9}
340	1.40×10^{-8}	2.04×10^{-8}	2.18×10^{-9}

*$K_B = 2616$; $\alpha = \beta = 0.2298$; $\theta = 0.6345$; $\sigma = 1.151$.

The n-butane conversion, MAN yield and MAN selectivity observed in the fluidized bed reactors using FCC8.5+0.82% and FCC76 at different reaction temperatures are shown in

Figure 10.11. FCC8.5+0.82% showed a much higher conversion and MAN yield than FCC76 at the same temperature, indicating a better reactor performance. As the gas velocity increased, the n-butane conversion and MAN yield both increased significantly for FCC8.5+0.82%, while those for FCC76 remained stable or showed a slight increase. The selectivities for the two particle sizes were similar and also remained nearly unchanged by the gas velocity, due to the change of either the particle size or the gas velocity did not affect the kinetics based on the specific surface area (k_1, k_2, and k_3). The significant increase of the conversion and yield for FCC8.5+0.82% was due to the better fluidization quality and the larger effective surface area of catalysts. For FCC8.5+0.82%, the higher bed expansion with more gas holdup in the bed and the larger surface area of catalysts with more surfaces available for gas reactant contributed to the increase of the conversion and yield. As the temperature increased, the n-butane conversion and the MAN yield increased for both particle sizes, while the MAN selectivity decreased. This is because all the reaction kinetics increased with the temperature, leading to a higher reaction conversion, while the kinetics (k_2, k_3) of the side reactions increased more significantly than that of the main reaction (k_1), leading to more side productions thus decreasing the selectivity.

The mass transfers between the bubble phase and the dense phase for FCC8.5+0.82% and FCC76 are shown in Figure 10.12. The bed of FCC8.5+0.82% displyed better mass transfer than the bed of FCC76. For both particles, the values of NTU decreased as the gas velocity increased, mainly due to the higher gas velocity and shorter gas residence time in the bed.

The reactor performance is mainly affected by two factors: the gas-solid contact efficiency and the mass transfer between the two phases. The larger gas-solid interfacial area in Group C^+ fluidized bed reactor is ascribed from the larger surface area of catalysts, more gas holdup in the dense phase, and higher gas flowrate through the dense phase. The better mass transfer between the two phases for Group C^+ catalysts is due to smaller bubbles, longer bubble residence time, and less bubble holdup. All these characteristics of the Group C^+ fluidized bed reactor improve the gas-solid contact efficiency and enhance the reactor performance.

With increasing gas velocity, the interfacial contact area increased, positive on the reaction conversion, while the mass transfer decreased, negative on the reaction conversion. Therefore, with the increase of gas velocity, the reaction conversion in the reactor with Group C^+ particles increased and then remain stable or slightly decreased. This phenomenon indicated that the effect of the interfacial contact area played a more important role at lower gas velocities, while the effect of the mass transfer between the two phases became more significant at higher gas velocities.
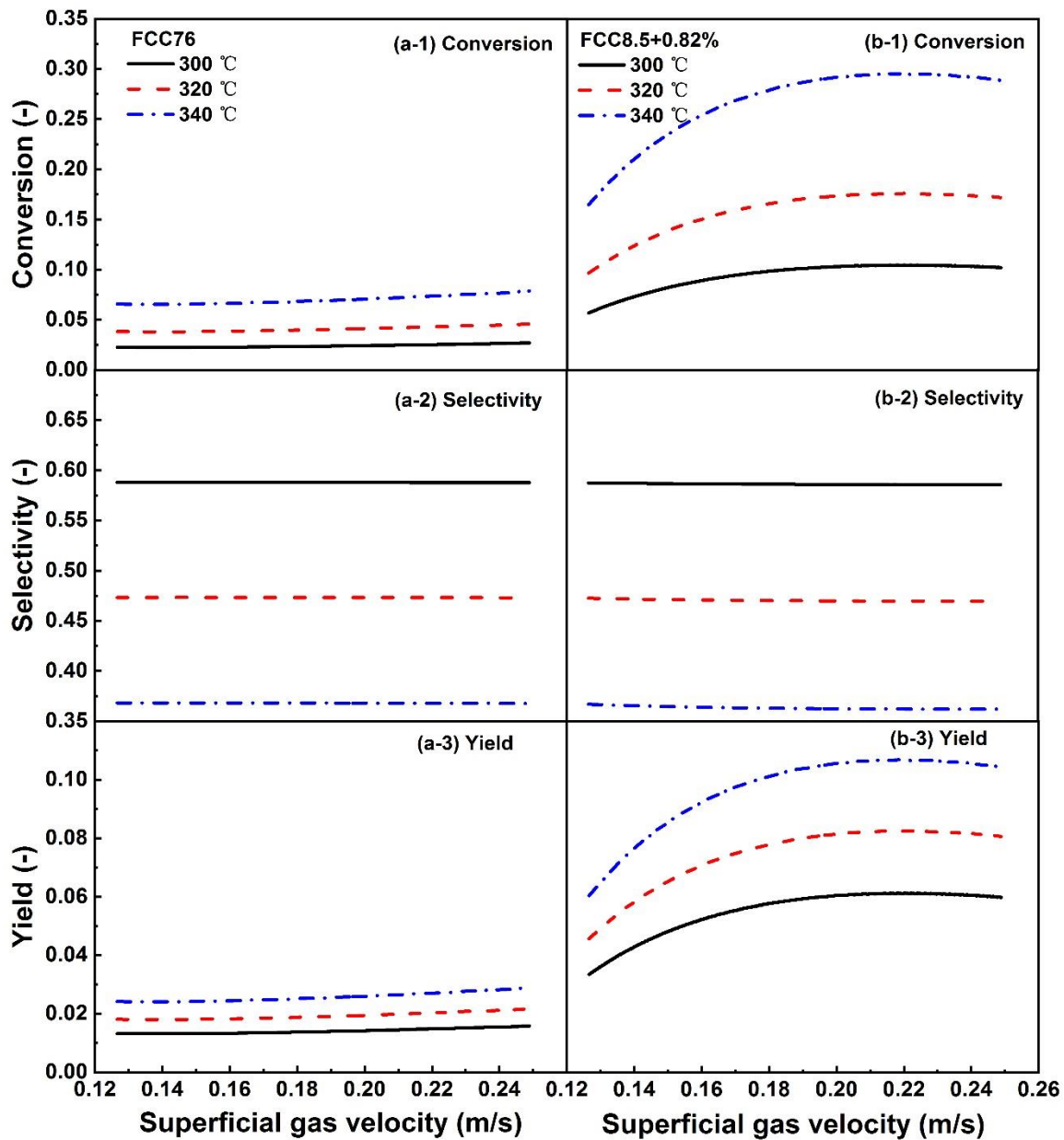
Figure 10.11: Prediction of partial oxidation of n-butane in Group C$^+$ and Group A

fluidized bed reactors:

(a) FCC76; (b) FCC8.5+0.82%;

(1) n-butane conversion; (2) MAN selectivity; (3) MAN yield
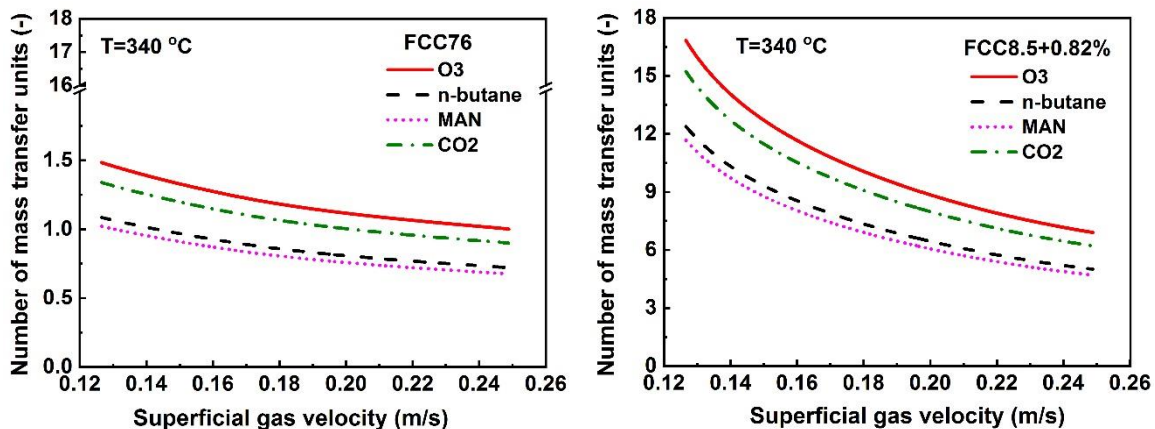
Figure 10.12: The number of mass transfer units with the superficial gas velocities at T=340 C

10.7 Effect of scale up of the fluidized bed reactor

The scale up of the fluidized bed reactor is further studied in this section, because it can act as a guide for industrial applications. The effects of scale up are investigated in three aspects: reactor diameter (D), gas distributor (A_D), and the initial bed height (H_0). The parameters of the scale-up are listed in Table 10.9a, and their effects are listed in Table 10.9b.

Table 10.9a: Scale-up parameters of the fluidized bed reactor

Name	H_0 (m)	H_f (m)	Weight of catalyst (kg)	A_D (m^2)	D (m)
F1	0.25	-	0.43 (FCC76) 0.25 (FCC8.5+0.82%)	5.01×10^{-5}	0.05
F2	0.25	-	43 (FCC76) 25 (FCC8.5+0.82%)	5.01×10^{-5}	0.50
F3	0.25	-	0.43 (FCC76) 0.25 (FCC8.5+0.82%)	5.01×10^{-4}	0.05
F4	0.25	-	43 (FCC76) 25 (FCC8.5+0.82%)	5.01×10^{-4}	0.50
F5	0.50	-	0.86 (FCC76) 0.50 (FCC8.5+0.82%)	5.01×10^{-5}	0.05
F6	0.50	-	86 (FCC76) 50 (FCC8.5+0.82%)	5.01×10^{-5}	0.50
F7	0.50	-	0.86 (FCC76) 0.50 (FCC8.5+0.82%)	5.01×10^{-4}	0.05
F8	0.50	-	86 (FCC76) 50 (FCC8.5+0.82%)	5.01×10^{-4}	0.50
F9	-	0.8	-	5.01×10^{-5}	0.50

Table 10.9b: Depiction of effects of scale-up parameters

Effects of parameters	Groups
Reactor diameter (D)	F1 and F2; F3 and F4; F5and F6; F7 and F8
Gas distributor (A_D)	F1 and F3; F2 and F4 F5 and F5; F6 and F8
Initial bed height (H_0)	F1 and F5; F2 and F6 F3 and F7; F4 and F8

The effect of the scale-up on the reactor performance was shown in Figure 10.13. The reactor diameter (D) and the gas distributor (A_D) would affect mainly the bubble diameters and thus influence the fluidization hydrodynamics. For FCC8.5+0.85%, the reactor diameter had no effect the bubble diameter, as the bubble diameter remained constant at the bed height of 0.03m and was only related to A_D and the superficial gas velocity. As A_D increased, the bubble diameter increased but not significantly. As a result, the n-butane conversion, MAN selectivity, and MAN yield showed minimal change (Figure 10.13a). For FCC76, the bubble diameter was related to both A_D and D. The increase of A_D and D resulted in the increase of the bubble diameter, the subsequent increase of the bubble rise

velocity, and the decrease of the gas residence time, leading to lower conversion, selectivity, and yield (Figures 10.13b and c). The effect of the reactor diameter on the bubble diameter was more significant than the effect of A_D.

The change of the initial bed height would mainly affect the gas residence time in the fluidized bed reactor. For both FCC8.5+0.82% and FCC76, the increase of the initial bed height (H_0) contributed to a longer gas residence time in the bed, thus increasing the conversion and the yield. Regarding the selectivity, the longer gas residence time would make more MAN further convert to CO_2, which decreased the selectivity. Overall, combining the conversion, selectivity and yield, the reactor performance was improved with the increase of the initial bed height. Based on the same gas residence time, there for a smaller quantity of Group C^+ catalysts, Group C^+ fluidized bed reactor could reach an even higher conversion and yield than Group A fluidized bed reactor, mainly due to the larger effective specific surface area and the higher bed expansion. Conclusively, using Group C^+ particles as catalysts could remarkably improve the reactor performance and increase the profits in industrial processes.
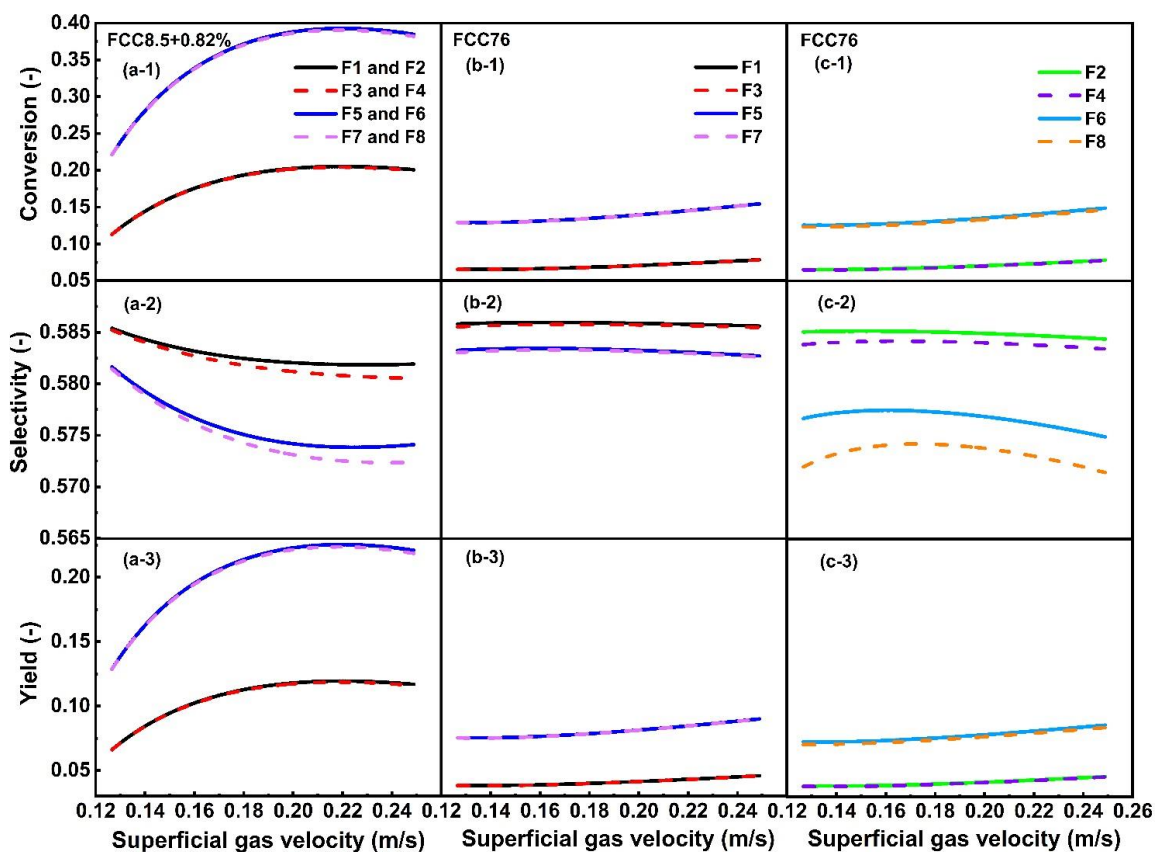
Figure 10.13: Effect of scale-up parameters on the performance of Group C⁺ and Group A fluidized bed reactors:

(1) n-butane conversion; (2) MAN selectivity; (3) MAN yield

Under the condition that the total fluidized bed height is the same in the reactor of both FCC8.5+0.82% and FCC76 (F9 in Table 10.9a), the results are shown in Figure 10.14. FCC8.5+0.82% exhibited much higher conversion, selectivity and yield than FCC76, thus boosting the reactor performance. As gas velocity increased, the conversion and the yield for FCC8.5+0.82% increased and then decreased, resulting in optimal reactor performance. With the increase of the gas velocity, the increased effective surface area had a positive effect on the reactor performance, while the decreased NTU produced a negative effect. As a result, the fluidized bed reactor using FCC8.5+0.82% created an optimal operating condition and reactor performance.
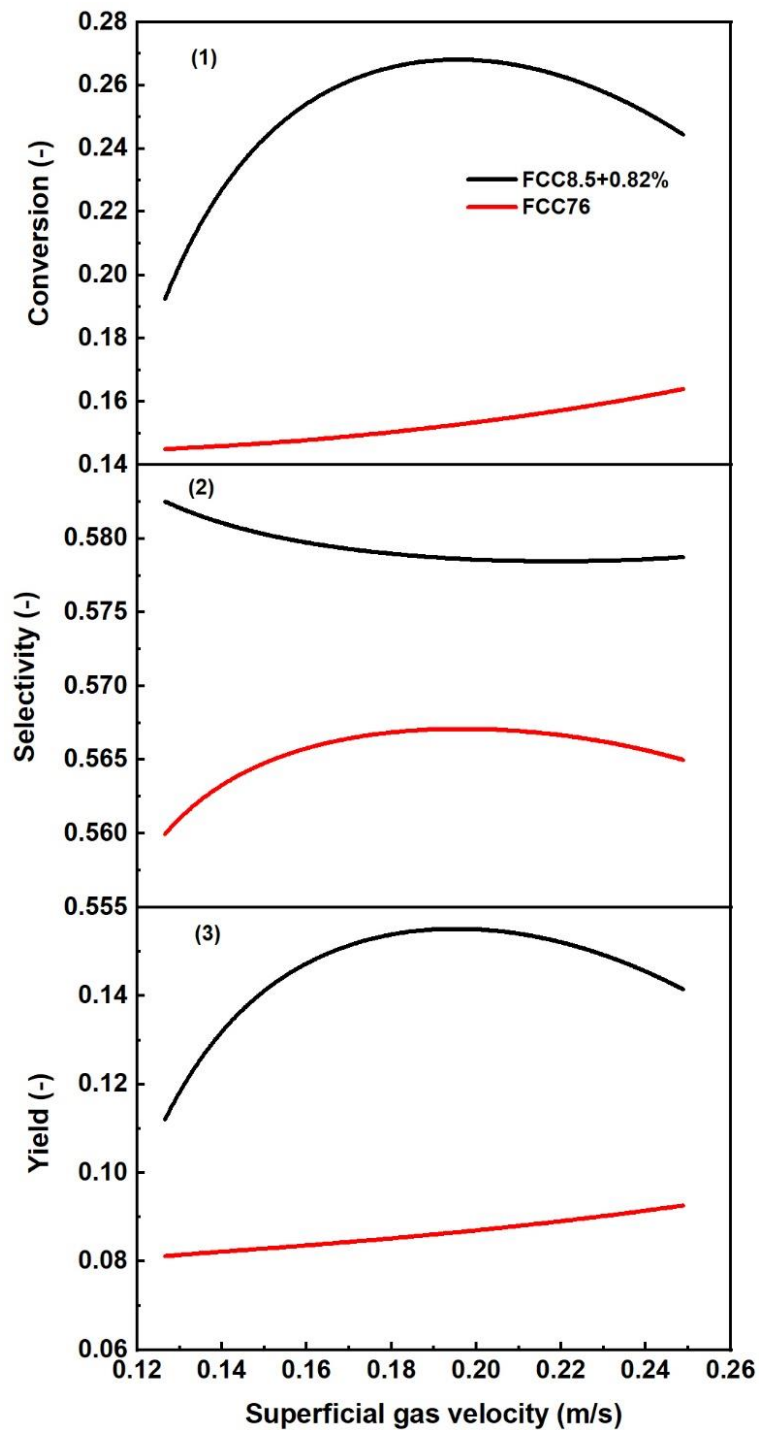
Figure 10.14: The reactor performance of Group C$^+$ and Group A fluidized bed reactors under the same fluidized bed height:

(1) n-butane conversion; (2) MAN selectivity; (3) MAN yield.

Under the same reaction conversion, the fluidized bed heights, the gas residence times and the catalyst weights that were required in the reactors of both FCC8.5+0.82% and FCC76 are shown in Figure 10.15. The fluidized bed height and the gas residence time required for FCC8.5+0.82% were 67% of that required for FCC76, which were needed to achieve the same reaction conversion. Additionally, the catalyst weight of FCC8.5+0.82% was only 20% of that of FCC76. The lower fluidized bed height, shorter gas residence time, and much lower catalyst weight of FCC8.5+0.82% could significantly reduce costs in industrial processes and thus increase profits earned.
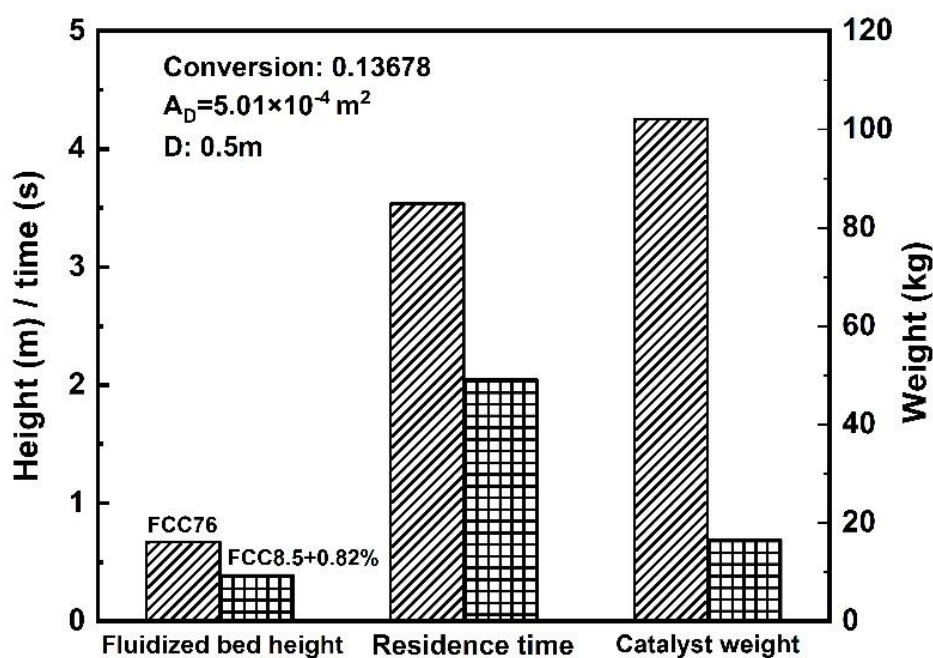
Figure 10.15: Comparison of Group C⁺ and Group A fluidized bed reactors under the same n-butane conversion

Considering that the industrial MAN reactor is operated in a turbulent regime, the comparison of the reactor performance in the bubbling regime (this work) with that in the turbulent regime [35] was investigated and shown in Figure 10.16. Mostoufi et al. [35] calculated the reaction conversion, the selectivity, and the yield of MAN production in a fluidized bed reactor using Group A catalysts (FCC75) at 0.9m/s in the turbulent regime. The catalyst activity, the reaction temperature, and the gas residence time used in this work and the work by Mostoufi et al. [35] are identical. As shown in Figure 10.16, the conversion

and the yield in the Group C$^+$ fluidized bed reactor (in this work) were higher than those calculated using the DTP and STP model in the work by Mostoufi et al. [35]. The selectivity was similar in the two works. Although the Group C$^+$ fluidized bed reactor was operated in the bubbling regime, its performance was superior to that of the MAN reactor using Group A catalysts which was operated in the turbulent regime. It is expected that the Group C$^+$ fluidized bed reactor could achieve an even better performance in the turbulent fluidization regime, which usually occurs in the industrial MAN reactor.
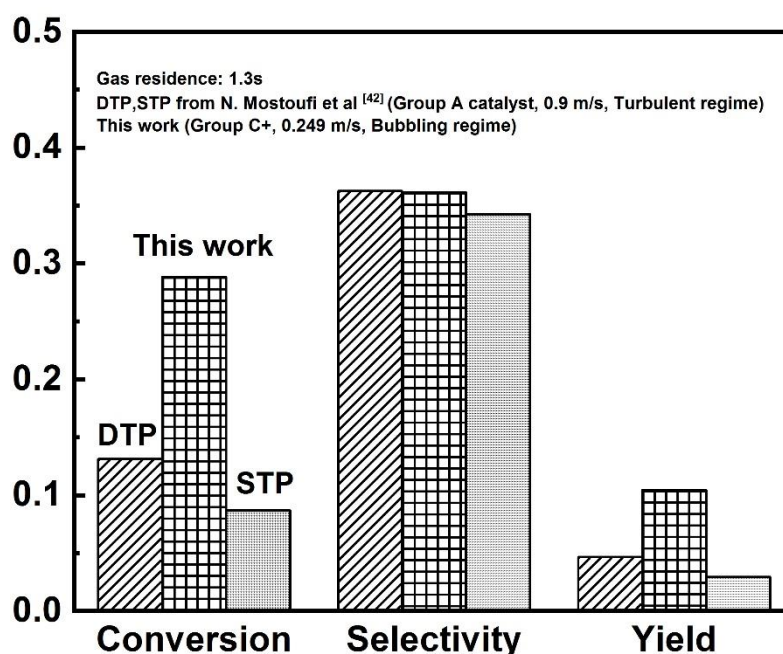
Figure 10.16: Comparison of the reactor performance in bubbling regime in this work with that in turbulent regime in the work by Mostoufi et al [35].

10.8 Conclusions

The Group C$^+$ fluidized bed reactor possessed a smaller bubble size, lower bubble rise velocity, and a longer gas residence time than the Group A fluidized bed reactor. The effective surface area in the Group C$^+$ fluidized bed reactor was much larger than that of the Group A fluidized bed reactor, meaning that more catalyst surface could come into contact with the the gas reactant and the catalyst utilization has been significantly improved.

The reactor performances of Group C$^+$ and Group A fluidized bed reactors were compared using a modified two-phase model. The fluidized bed reactor using FCC8.5+0.82% exhibited a much higher conversion, higher MAN yield, and the same selectivity when compared with that of using FCC76. The increase of superficial gas velocity significantly increased the reactor performance of FCC8.5+0.82%, but had less of an effect for FCC76.

The effect of scale-up was considered in three aspects, the bed diameter (D), the gas distributor (A_D), and the initial bed height (H_0). The increase of A_D increased the bubble diameter for both FCC8.5+0.82% and FCC76, reducing the reactor performance. The increase of bed diameter had no effect on the bubble behaviors for FCC8.5+0.82%, but could significantly increase the bubble diameter for FCC76, leading to poorer reactor performance. The increase of H_0 remarkably improve the reactor performance for both FCC8.5+0.82% and FCC76 due to the longer gas residence time in the fluidized bed. When compared with the industrial turbulent MAN reactor, the Group C$^+$ bubbling fluidized bed reactor performed even better. Conclusively, the Group C$^+$ fluidized bed catalytic reactor could bring huge advancements to industrial processes, especially for gas-phase catalytic reactions.

Nomenclature

A_D	Reflect area of single hole in the distributor, m^2
A_t	Bed cross-sectional area, m^2
A_p	Specific surface area, m^{-1}
$A_p{'}$	Effective reaction specific surface area, m^{-1}
C_A	Concentration of species A, mol/L
D	Fluidized bed diameter, m
D_g	Gas diffusion coefficient, m^2/s
d_{bz}	Bubble size at the height of z, m
d_{be}	Equilibrium bubble diameter, m
d_{bm}	Maximum bubble diameter from total coalescence of bubbles, m
d_{bmax}	Maximum bubble diameter, equal to 2/3 fluidized bed diameter, m
$\bar{d}_b$	Average bubble diameter, m

d_s	Solid diameter, m
g	Acceleration due to gravity, m/s^2
G_b	Bubble flowrate, m^3/s
H_f	Fluidized bed height, m
k_1	Rate constant for MAN formation, mol$^{1-\alpha}$L$^{\alpha-1}\cdot$m/s
k_2	Rate constant for CO$_2$ formation, mol$^{1-\beta}$L$^{\beta-1}\cdot$m/s
k_3	Rate constant for maleic anhydride decomposition, mol$^{\sigma-\theta}$ L$^{\theta-\sigma}\cdot$m/s
k_{bd}	Bubble to dense mass transfer coefficient, m/s
k_s	Rate constant based on specific surface area, m/s
K_{bd}	Bubble to dense phase gas interchange coefficient, s^{-1}
K_{bc}	Bubble to cloud phase gas interchange coefficient, s^{-1}
K_{cd}	Cloud to dense phase gas interchange coefficient, s^{-1}
K_B	Equilibrium constant in Centi et al. [43] kinetics, L/mol
NTU	Number of mass transfer units [35]
r_1	Rate of MAN formation, mol/(L·s)
r_2	Rate of CO$_2$ formation, mol/(L·s)
r_3	Rate of MAN decomposition, mol/(L·s)
R_A	Overall reaction rate of species A, mol/(L·s)
S	MAN selectivity
S_b	Bubble surface area, m^2
t_s	Bubble residence time, s
t_d	Gas residence time in dense phase, s
U_{br}	Single bubble velocity, m/s
U_g	Superficial gas velocity, m/s
U_b	Bubble velocity, m/s
U_{dd}	Dense phase velocity, m/s
U_{df}	Superficial gas velocity in dense phase, m/s
U_{mf}	Minimum fluidization velocity, m/s
V_b	Bubble volume, m^3
X	n-butane conversion
Y	MAN yield

z	Distance above the distributor, m

Greek Notation

α, β, θ, σ	Exponents in Centi et al. [43] rate expressions
δ	Bubble fraction in fluidized bed
ε_o	Fixed bed voidage
ε_d	Dense phase voidage
γ_b	Volume of solids in bubble phase divided by the volume of bubbles, m^3 of solid/m^3 of gas
ρ_s	Solid density, kg/m^3
γ_M	Parameter from Mori and Wen correlation [33]

Subscripts

0	Inlet
B	n-butane
b	Bubble
c	Cloud phase
d	Dense phase
MAN	Maleic anhydride
mf	Minimum fluidization
O	Oxygen
s	Solid

10.9 References

[1]   Grace JR, Leckner B, Zhu J, Cheng Y. Fluidized beds, In: Crowe, CT, editor. *Multiphase Flow Handbook*. New York, 2006: 5-1.

[2]   Xiong Q, Aramideh S, Kong SC. Modeling effects of operating conditions on biomass fast pyrolysis in bubbling fluidized bed reactors. *Energ Fuel*. 2013; 27: 5948-5956.

[3]   Almuttahar A, Taghipour F. Computational fluid dynamics of a circulating fluidized bed under various fluidization conditions. *Chem Eng Sci*. 2008; 63:1696-1709.

[4]   Saayman J, Ellis N, Nicol W. Fluidization of high-density particles: The influence of fines on reactor performance. *Powder Technol*. 2013; 245: 48-55.

[5]   Sun G, Grace JR. The effect of particle size distribution on the performance of a catalytic fluidized bed reactor. *Chem Eng Sci*. 1990; 45: 2187-2194.

[6]   Geldart D. The effect of particle size and size distribution on the behavior of gas fluidized beds. *Powder Technol*. 1972; 6: 201-209.

[7]   Geldart D. Types of gas fluidization. *Powder Technol*. 1973; 7: 285-292.

[8]   Sugihara K, Ono S. Galvanomagnetic properties of graphite at low temperature. *J Phys Soc Japan*. 1966; 21: 631-637.

[9]   Baerns M. Effect of interparticle adhesive forces on fluidization of fine particles. *Ind Eng Chem Res*. 1966; 5: 508-516.

[10]   Geldart D, Wong ACY. Fluidization of powders showing degrees of cohesiveness-I: Bed expansion. *Chem Eng Sci*. 1984: 39:1481-1488.

[11]   Xu CC, Zhang H, Zhu J. Improving flowability of cohesive particles by partial coating on the surfaces. *Can J Chem Eng*. 2009; 87: 403–414.

[12]   Zhou Y, Zhu J. Group C$^+$ particles: Enhanced flow and fluidization of fine powders with nano-modulation. *Chem Eng Sci*. 2019; 207: 653-662.

[13]   Zhou Y, Zhu J. Group C$^+$ particles: Extraordinary dense phase expansion during fluidization through nano-modulation. *Chem Eng Sci*. 2020; 214:115420.

[14]   Zhou Y, Zhao Z, Zhu J, Bao X. Group C$^+$ particles: Efficiency augmentation of fluidized bed reactor through nano-modulation. *AIChE J*. 2019; e16870.

[15]   Kunii D, Levenspiel O. *Fluidization Engineering*, 2nd ed. Boston: Butterworth-Heinemann, 1991.

[16]   Grace JR. Generalized models for isothermal fluidized bed reactors. *Recent Advances in the Engineering Analysis of Chemically Reacting Systems*. Doraiswamy LK, ed., Wiley, New Delhi, 1984: pp 237-255.

[17]   Fane AG, Wen CY. Fluidized bed reactors. *Handbook of Multiphase System*. Hetsroni G, ed., Hemisphere Publishing, Washington DC, 1982: pp 104-151.

[18]   Foka M, Chaouki J, Guy C, Klvana D. Gas phase hydrodynamics of a gas-solid turbulent fluidized bed reactor. *Chem Eng Sci*. 1996; 51:713-723.

[19] Grace JR, Lim KS. Reactor modeling for high-velocity fluidized beds. *Circulating Fluidized Beds*. Grace JR, Avidan AA, Knowlton TM, eds, Chapman and Hall, London, 1997:pp 504-524.

[20] Davidson JF, Harrison D. *Fluidized Particles*. Cambridge University Press, New York, 1963.

[21] Werther J. Mathematical modeling of fluidized bed reactors. *Int Chem Eng*. 1980; 20: 310-315.

[22] Theologos KN, Markatos NC. Modelling of flow and heat transfer in fluidized catalytic cracking riser-type reactors. *Chem Eng Res Des*. 1992; 70: 239-245.

[23] Partridge BA, Rowe PN. Chemical reaction in a bubbling gas-fluidized bed. *Chem Eng Res Des*. 1966; 44: 335-348.

[24] Toomey RD. Gaseous fluidization of solid particles. *Chem Eng Progr*. 1952; 48: 220-226.

[25] Aoyagi M, Kunii D. Importance of dispersed solids in bubbles for exothermic reactions in fluidized beds. *Chem Eng Commun*. 1974; 1:191-197.

[26] Chaouki J, Gonzalez A, Guy C, Klvana D. Two-phase model for a catalytic turbulent fluidized-bed reactor: Application to ethylene synthesis. *Chem Eng Sci*. 1999; 54:2039-2045.

[27] Batchelor GK, Nitsche JM. Expulsion of particles from a buoyant blob in a fluidized bed. *J Fluid Mech*. 1994; 278: 63-81.

[28] Gilbertson MA, Yates JG. The motion of particles near a bubble in a gas-fluidized bed. *J Fluid Mech*. 1996; 323:377-385.

[29] Abrahamson AR, Geldart D. Behaviour of gas-fluidized beds of fine powders: part II. Voidage of the dense phase in bubbling beds. *Powder Technol*. 1980; 26:47-55.

[30] Kunii D, Levenspiel O. Fluidized reactor models. 1. For bubbling beds of fine, intermediate, and large particles. 2. For the lean phase: freeboard and fast fluidization. *Ind Eng Chem Res*. 1990; 29:1226-1234.

[31] Darton RC, LaNauze RD, Davidson JF, Harrison D. Bubble growth due to coalescence in fluidized beds. *Trans Am Inst Chem Eng*. 1977; 55: 274-280.

[32] Horio M, Nonaka AA. generalized bubble diameter correlation for gas-solid fluidized beds. *AIChE J*. 1987; 33:1865-1872.

[33] Mori S, Wen CY. Estimation of bubble diameter in gaseous fluidized beds. *AIChE J*. 1975; 21:109-115.

[34] Cai P, Schiavetti MG, Michele D, Grazzini GC, Miccio M. Quantitative estimation of bubble size in PFBC. *Powder Technol*. 1994; 80: 99-109.

[35] Mostoufi N, Cui H, Chaouki J. A comparison of two- and single-phase models for fluidized-bed reactors. *Ind Eng Chem Res*. 2001; 40:5526-5532.

[36] Frye CG, Lake WC, Eckstrom HC. Gas-solid contacting with ozone decomposition reaction. *AIChE J*. 1958; 4:403-408.

[37] Van Swaaij WPM, Zuiderweg FJ. Investigation of ozone decomposition in fluidized beds on the basis of a two-phase model. *Proceeding of the European Symposium on Chemical Reaction Engineering*. Amsterdam: Elsevier, 1972: B9-B25.

[38] Orcutt JC, Davidson JF, Pigford RL. Reaction time distributions in fluidized catalytic reactors. *Chem Eng Prog Symp Ser*. 1962; 58:1-15.

[39] Hovmand S, Freedman W, Davidson JF. Chemical reaction in a pilot-scale fluidized bed. *Trans Am Inst Chem Eng*. 1971; 49:149-162.

[40] Fryer C, Potter OE. Experimental investigation of models for fluidized bed catalytic reactors. *AIChE J*. 1976; 22:38-47.

[41] Ouyang S, Lin J, Potter OE. Ozone decomposition in a 0.254 m diameter circulating fluidized bed reactor. *Powder Technol*. 1993; 74:73-78.

[42] Zhou Y, Xu J, Zhu J. Bubble behaviors in Group C$^+$ and Group A fluidized reactors. *submitted to AIChE J*.

[43] Centi G, Fornasari G, Trifiro F. *n*-Butane oxidation to maleic anhydride on vanadium phosphorous oxides: Kinetic analysis with a tubular flow stacked-pellet reactor. *Ind Eng Chem Prod Res Dev*. 1985; 24:32-37.

Chapter 11

11 General Discussion

Fine particles are gaining increasing importance in a variety of industrial processes due to their small particle size and large specific surface area. Fluidization is often the preferred mode of powder operations because of its many advantages over the fixed bed operation, such as good gas-solid contact, uniform temperature distribution, and high mass and heat transfer rates, etc. However, the fluidization of fine particles, especially Geldart Group C particles, is very difficult due to the strong interparticle forces. Therefore, Geldart Group C particles are often considered as non-fluidizable. In this present work, a nano-modulation technique developed for our group's research on ultrafine particle coating technology was used to effectively reduce or eliminate the interparticle forces of Group C particles and made them free-flowable and fluidizable. The term of "Group C$^+$" particles was first proposed as a new type of powders.

In this present work, the effects of the nanoparticle concentrations, the particle size, and the gas properties on the fluidization hydrodynamics of Group C$^+$ particles were systematically investigated, including the minimum fluidization velocity, bed expansion, dense phase properties, and bubble behaviors. Moreover, the performance of the fluidized bed reactor using Group C$^+$ particles as catalysts was also experimentally studied using ozone decomposition reaction, and modelled based on the two-phase theory and further applied to the industrial reaction (MAN production).

The most important contribution in this work was the great fluidization quality of Group C$^+$ particles, showing extraordinary bed expansion, especially the extremely high dense phase expansion, during fluidization. The large specific surface area and more gas holdup in the fluidized bed of Group C$^+$ particles then contributed to good gas-solid interfacial contact and thus enhanced reactor performance. Based on our experimental findings, the high dense phase expansion or the large dense phase voidage is one critical characteristic in the fluidization of Group C$^+$ particles. Therefore, it is necessary to find out the reason contributing to the good fluidization quality of Group C$^+$ particles.

Fluidization happens when the drag forces on the particles by the fluid overcome the gravitational forces, however, the interparticle forces are predominant over the gravitational forces for fine particles and govern the fluidization behaviors. As a result, for fine particles especially Group C particles, fluidization is a balance between the drag force and the interparticle forces. Although the interparticle forces of Group C$^+$ particles have been effectively reduced and are much lower than that of Group C particles, for some finer Group C$^+$ particles, they are still significant when compared with larger particles such as Group A particles. Therefore, it is necessary to consider the interparticle forces as well as the drag force when investigating the fluidization behaviors of Group C$^+$ particles.

11.1 The consideration of particle cohesion

The particle cohesion is a key parameter reflecting the degree of the interparticle forces for Group C$^+$ particles, which is affected by particle properties such as the particle size and density, etc. A dimensionless cohesion index (σ^*) was proposed in this work which involved the particle size (d_p), the particle density (ρ_p), the particle cohesion (σ), and the initial bed voidage (ε_0) to quantify the effect of the particle cohesion on the fluidization behaviors. The dimensionless cohesion index was in the form of:

$$\sigma^* = (\sigma\varepsilon_0 d_p{}^2) / (d_p{}^3\rho_p g) = (\sigma\varepsilon_0) / (d_p\rho_p g) \quad (11.1)$$

where σ is the particle cohesion (pa) which can be obtained by FT4 test, and ε_0 is the initial bed voidage which can be calculated using the particle apparent density (ρ_p) and bulk density (ρ_b).

The dimensionless cohesion index, in fact, is the ratio of the particle cohesion to the particle gravity. Therefore, it is an index that reflects the relative significance of the cohesion effect over the gravity effect on the fluidization behaviors of Group C$^+$ particles. The physical meaning of the dimensionless cohesion index is described as:

$$\text{Dimensionless cohesion index} = \text{Cohesion effect/ Gravity effect}$$

The larger dimensionless cohesion index indicated more significant effect of the particle cohesion than the particle gravity. The effect of the dimensionless cohesion index on the fluidization behaviors of Group C$^+$ particles including the minimum fluidization velocity, the bed voidage, and the dense phase voidage were shown in Figures 11.1. The minimum

fluidization velocity for Group C$^+$ particles increased with the increase of the dimensionless cohesion index, as shown in Figure 11.1a. The minimum fluidization velocity increased more significantly when the dimensionless cohesion index was larger. This is reasonable because most Geldart Group C particles are non-fluidizable due to strong cohesion, and their minimum fluidization velocity can be considered as infinite.

In addition to the minimum fluidization velocity, the fluidized bed voidage is another important parameter in the fluidization and needs to be characterized. The effect of the dimensionless cohesion index on the bed voidage for Group C$^+$ particles is shown in Figure 11.1b. The bed voidage for Group C$^+$ particles increased with the increase of the dimensionless cohesion index, indicating that the particle cohesion has a positive effect on the bed expansion.

The dense phase voidage is a more important parameter to characterize the fluidization quality, because the large dense phase voidage indicates more gas holdup in the dense phase and contributes to better gas-solid contact. The maximum dense phase voidage for Group C$^+$ particles also increased with the increase of the dimensionless cohesion index, as shown in Figure 11.1c.
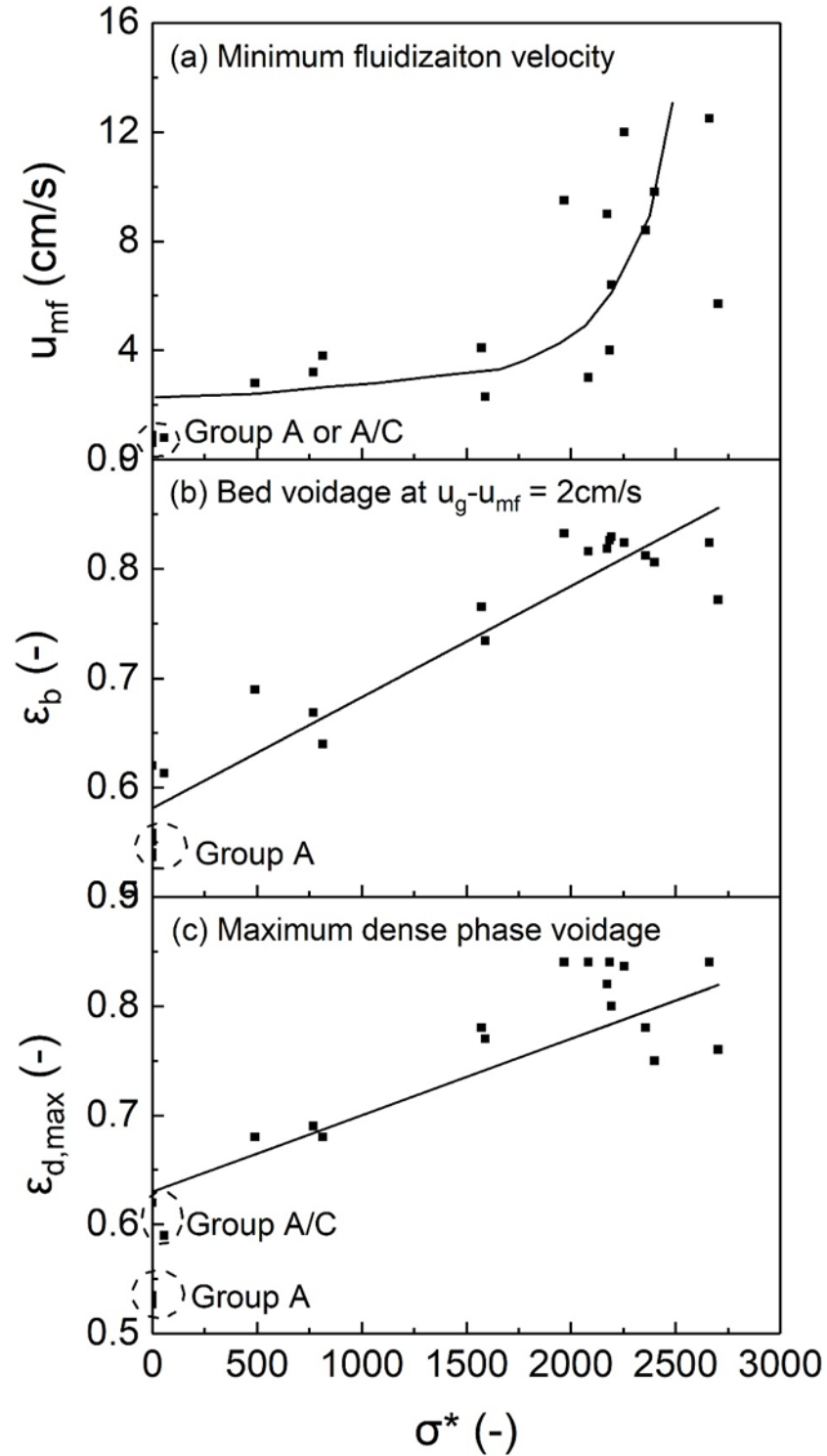
Figure 11.1: The effect of the dimensionless cohesion index on the fluidization behaviors for Group C⁺ particles

In summary, the particle cohesion did play a significant role in determining the fluidization quality for Group C^+ particles. Geldart Group C particles with too strong particle cohesion cannot fluidize with almost infinite u_{mf}, while Group C^+ particles with reduced cohesion had the minimum fluidization velocity. Although the particle cohesion resulted in higher u_{mf}, more importantly, it contributed to higher bed expansion and larger dense phase voidage. Therefore, a controlled particle cohesion of Group C^+ particles is important and can improve the fluidization quality. Additionally, for Group A or Group A/C particles, the cohesion effect was insignificant and the gravity effect would be predominant in the fluidization, so that it is not suitable to use the dimensionless cohesion index when evaluating their fluidization behaviors.

11.2 The consideration of drag force

Another important factor affecting the fluidization behaviors is the drag force exerted on the particles by the fluid which is affected by the fluid properties such as the fluid density and viscosity. In viscous fluid dynamics, the Archimedes number (Ar) is used to determine the fluid motion and is the ratio of gravitational forces to viscous forces, in the form of:

$$Ar = d_p^3 \rho_g (\rho_p - \rho_g) g / \mu_g^2 = \text{Gravitational forces / Viscous forces} \qquad (11.2)$$

For Group C^+ particles, as the cohesion effect is more significant than the gravity effect and viscous forces are the main drag forces, the revised Archimedes number (Ar^*) with the consideration of the cohesion effect could be defined as:

$$Ar^* = \text{Particle cohesion / Viscus forces} = Ar \; \sigma^* = \sigma d_p^2 \rho_g \varepsilon_0 / \mu_g^2 \qquad (11.3)$$

where $\rho_p - \rho_g \approx \rho_p$ for gas-solid fluidized beds, ρ_g is the gas density, and μ_g is the gas viscosity.

The revised Archimedes number (Ar^*) can describe the relative significance between the cohesion forces of the particles and the drag forces exerted on the particles by the fluidizing gas. The larger Ar^* indicates more significant particle cohesion and the smaller Ar^* indicates more significant drag forces. The effect of the revised Archimedes number on the fluidization behaviors of Group C^+ particles using different fluidizing gases is shown in Figures 11.2. The minimum fluidization velocity for Group C^+ particles increased with the increase of the revised Archimedes number, as shown in Figure 11.2a, due to the more significant cohesion forces than the drag force on the particles as Ar^* increased. Lower u_{mf}

could be achieved when the particle cohesion was lower or the fluidizing gas with higher viscosity was used.

In addition to the minimum fluidization velocity, the effect of Ar^* on the bed voidage and the maximum dense phase voidage were insignificant, as shown in Figures 11.2b and 2c. As have been discussed, the particle cohesion had a positive effect on both bed voidage and maximum dense phase voidage. The increase of the drag force due to higher gas viscosity would also contribute to larger bed voidage and larger maximum dense phase voidage. As a result, the higher particle cohesion resulting in a larger Ar^* increased the voidage, and the higher gas viscosity resulting in a smaller Ar^* also increased the voidage in the fluidized bed. Combining the two factors, Ar^* number did not affect the voidage in the fluidized bed significantly.
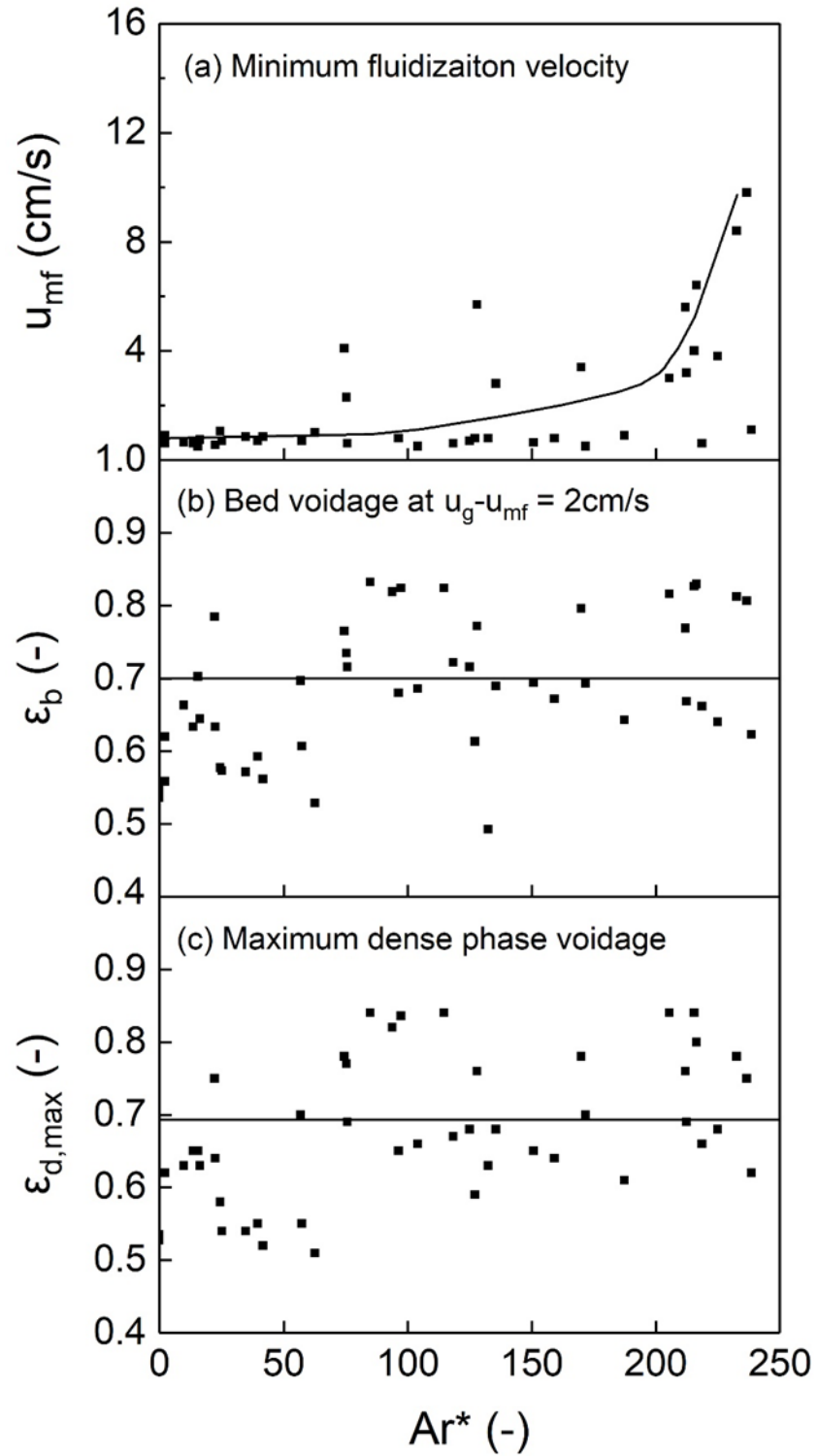
Figure 11.2: The effect of the revised Archimedes number on the fluidization behaviors for Group C$^+$ particles

In summary, the fluidization behaviors of Group C^+ particles were significantly affected by the particle cohesion. The dimensionless cohesion index can be used to effectively evaluate the fluidization quality for Group C^+ particles. The revised Archimedes number considered the balance between the particle cohesion and the drag forces exerted on the particles by the fluidizing gas. Both the increase of the particle cohesion and the drag forces could contribute to better fluidization quality for Group C^+ particles, showing larger bed voidage and larger maximum dense phase voidage.

Chapter 12

12   Conclusions and Recommendations

12.1 Conclusions

Group C^+ particles can be fluidized well after nanoparticle modulation. Nanoparticles as fluidization aids, do have the ability to reduce the cohesion of Group C particles and improve the fluidization quality. Nanoparticle concentration greatly affects the fluidization quality of Group C^+ particles, and there exists an optimum nanoparticle concentration depending on the surface coverage and surface roughness. The optimum nanoparticle concentration was around 0.5-1% (volume fraction) for Group C^+ particles.

The minimum fluidization velocities of Group C^+ particles can be clearly identified and the values are acceptable, even if they are higher than that of Group A particles. The fluidized bed of Group C^+ particles can expand as high as 2-3 times of the fixed bed height. The bed expansion for Group C^+ particles is around 180% of that for Group A particles. The high bed expansion can retain more gas in the bed and contribute to better gas-solid contact.

Group C^+ particles exhibit much longer bed collapse time and higher dense phase height than Group A particle. The bed collapse curves for Group C^+ particles are curved and those for Group A particles are much more linear. Group C^+ particles exhibit a much higher dense phase expansion and larger dense phase voidages than Group A particles, indicating more gas holdup in the dense phase so that gas can closely contact with the particles.

The fluidization quality of Group C^+ particles is closely related to the gas properties. The fluidization quality in various gases from good to poor exhibits: argon > air > (nitrogen) > helium > hydrogen, with the increase of the gas viscosity and/or the gas density, both of which can enhance the fluidization quality of Group C^+ particles. Both theoretical and experimental methods are used to evaluate the relative importance of the gas viscosity and density on the fluidization quality. The effect of increasing the gas viscosity is shown to be more significant than increasing gas density, suggesting that the gas viscosity plays a more important role on determining the fluidization quality.

The bubble behaviors for Group C$^+$ particles and Geldart Group A particles are fully characterized in a 2-D bubbling fluidized bed, including the bubble distribution, diameter, rise velocity and the residence time. Smaller bubbles (< 2cm) homogeneously occupy the bed for both Group C$^+$ and Group A particles, while larger bubbles tend to form in the middle of the bed. The maximum bubble diameter for Group C$^+$ particles is less than 4cm, much smaller than that in the bed of Group A particles, reaching up to 6-7cm in the range of studies. When compared with the bed of Group A particles, the bed of Group C$^+$ particles exhibits a smaller total number of bubbles, lower "density" of bubbles (number of bubbles per unit volume), more uniform bubble size distribution, lower bubble rise velocity, and longer bubble residence time.

Based on the fluidization characteristics for Group C$^+$ particles showing smaller bubbles, lower bubble rise velocity, less bubble holdup, and extraordinarily higher gas holdup in the dense phase, the two-phase theory for Group C$^+$ particles is re-viewed. Applying the modified two-phase theory and using the correction factor Y to account for increased dense phase gas flow, the Y value is found to be not a constant as previously suggested for Group A particles, but to decrease with the excess superficial gas velocity, for fine Group C$^+$ particles. A new correlation for the correction factor, Y, is then developed in this study for Group C$^+$ particles. Using this new correlation (and the reported Y value for Group A particles), the distribution of the gas flow between the dense phase and the bubble phase in the beds of Group C$^+$ in comparison to Group A particles can be determined, quantifying the gas flow through the dense phase which is clearly higher than the minimum fluidization velocity (u_{mf}), and the gas flow through the bubble phase which is clearly lower than the excess gas velocity (u_g-u_{mf}).

The most unique and important characteristic for Group C$^+$ particles is the extremely high dense phase voidage, which is also a critical parameter for evaluating the gas-solid contact. The dense phase voidage (ε_d) for Group C$^+$ particles is found to increase linearly with the superficial gas velocity in the dense phase (u_d) when operating between the minimum fluidization velocity, u_{mf}, and the maximum dense phase expansion velocity, $u_{d,max}$, and then remains unchanged at the value of maximum dense phase voidage ($\varepsilon_{d,max}$). Considering the similar structure of the dense phase with the liquid-fluidized beds, general

expressions to predict the dense phase voidage for Group C$^+$ particles are developed based on the Richardson-Zaki approach and the Kozeny-Carman approach. Both correlations predict well with the experimental results within the deviation of 20%. The correct prediction of the dense phase voidage can provide a guidance in the design and operation of the Group C$^+$ fluidized bed reactor. In addition, a new method to calculate the minimum fluidization velocity for Group C$^+$ particles with the consideration of the particle cohesion is proposed. Both the bed voidage at minimum fluidization (ε_{mf}) and the maximum dense phase voidage ($\varepsilon_{d,max}$) are correlated well with the dimensionless cohesion index (σ^*), indicating that the particle cohesion plays a significant role in the bed expansion for Group C$^+$ particles.

The good fluidization quality of Group C$^+$ particles contributes to good gas-solid contact, which is a key factor determining the reactor performance especially for gas-phase catalytic reactions. Therefore, Group C$^+$ particles are further used as catalysts in a gas-solid catalytic fluidized bed reactor to evaluate the performance using the ozone decomposition reaction. The fluidized bed reactor using Group C$^+$ particles shows much higher reaction conversions and much higher contact efficiency than the bed using Group A particles. The significant increase of the contact efficiency for Group C$^+$ catalysts is due to both the larger specific surface area and the higher bed expansion in the fluidized bed, which provide larger gas-solid interfacial area and more gas reactants for gas-solid contact. The high reaction conversion in the fluidized bed reactor using Group C$^+$ particles confirms that Group C$^+$ particles with good fluidization quality improve the reaction performance. Group C$^+$ particles have great potential to bring a soar in the reactor performance of gas-phase catalytic reactions.

The production of maleic anhydride (MAN), as a common reaction in industry, is adopted as an example to exhibit the reactor performance using Group C$^+$ catalysts. The reactor performances of Group C$^+$ and Group A fluidized bed reactors are theoretically compared using a modified two-phase model. The fluidized bed reactor using Group C$^+$ catalysts exhibits a much higher conversion, higher MAN yield, and the same selectivity when compared with that of using Group A catalysts. The effect of scale-up is also considered in three aspects, the bed diameter (D), the gas distributor (A_D), and the initial bed height (H_0).

The increase of A_D increases the bubble diameter for both catalysts, reducing the reactor performance. The increase of bed diameter almost has no effect on the bubble behaviors for Group C^+ catalysts, but significantly increases the bubble diameter for Group A catalysts, leading to poorer reactor performance for Group A catalysts. The increase of H_0 remarkably improves the reactor performance for both Group C^+ and Group A catalysts due to the longer gas residence time in the fluidized bed. When compared with the industrial turbulent MAN reactor, the Group C^+ bubbling fluidized bed reactor performs even better. Conclusively, the Group C^+ fluidized bed catalytic reactor could bring huge advancements to industrial processes, especially for gas-phase catalytic reactions.

A dimensionless cohesion index (σ^*) which involves the particle cohesion, size, and density is proposed to quantify the relative importance of the cohesion effect to the gravity effect for Group C^+ particles. For Group C^+ particles, the cohesion effect predominates over the gravity effect and determines the fluidization behaviors. The larger dimensionless cohesion index leads to higher u_{mf}, larger bed voidage, and larger dense phase voidage. Therefore, the good fluidization quality of Group C^+ particles is ascribed to their particle cohesion. Although the nano-modulation technique has reduced the particle cohesion of Group C particles, that of some Group C^+ particles cannot be neglected when compared with other larger particles. The controlled particle cohesion contributes to higher bed expansion and larger dense phase voidage in the fluidized bed of Group C^+ particles.

12.2 Recommendations

Comprehensive studies have been carried out in the present work on the fundamentals for Group C^+ particle fluidization (including the effects of nanoparticle concentration, particle size and gas properties on u_{mf}, bed expansion, and dense phase properties), the two-phase characterization (including the bubble behaviors, the modification of the corrector Y in two-phase theory, the prediction of dense phase voidage), and the evaluation of reactor performance using Group C^+ particles as catalysts. Nevertheless, further investigations on these subjects are necessary and recommendations are brought into attention here for more researches on fine particle fluidization technology.

- Interparticle forces play an important role in fine particle fluidization, and Van der

Waals forces are predominant over other forces. Group C^+ particles with controlled interparticle forces exhibit good fluidization. It is necessary to quantify the interparticle forces of Group C^+ particles and their effects on the fluidization quality.

- Nanoparticles adhered on the surfaces of Group C particles to increase the separation distance and surface roughness, thus reducing the interparticle forces. As a result, the separation distance and the surface roughness are key factors for evaluating the interparticle forces for Group C^+ particles. However, the surface roughness and the separation distance of Group C^+ particles cannot be measured. Further works need to characterize the surface properties as well as the separation distance to quantify the interparticle forces of Group C^+ particles.

- Group C^+ particles exhibit smaller bubbles than Group A particles in the fluidized bed. Theoretical explanation needs to be proposed, and the prediction of the bubble diameter for Group C^+ particles also needs to be developed.

- Based on the full characterization of the fluidization behaviors of Group C^+ particles, a reactor model for predicting the reaction conversion in the Group C^+ fluidized bed reactor needs to be further developed.

- The present work comprehensively investigated the bubbling behaviors of Group C^+ particles. Other fluidization regimes such as the turbulent regime need to be further determined and characterized.

- In terms of the scale-up of Group C^+ fluidized bed reactors, problems such as the recycle of the extra-fine particles, the stability of the nanoparticles, etc. need to be considered.

Appendices

Appendix A: Data repeatability and error analysis

Basic fluidization behaviors

Fluidization experiments for each type of particles including the measure of the pressure drop and the bed expansion were repeated at least three times and the average data were used. When measuring the pressure drop across the entire bed, the pressure transducer was used and the measure frequency was 1000 data points per second and the measure time was 5s. The pressure drop at one gas velocity was obtained by averaging 5000 data points. Take GB10+0.82% R972 as an example, Figure A1 shows the normalized pressure drop across the entire bed for 1 time. Each point was the average of 5000 signals obtained from the transducer, with the deviation less than 0.25%, as shown in Figure A2. Figure A3 shows the error bars for the pressure drop curved measured for 6 times. Figure A4 shows the error bars for minimum fluidization velocity (for 6 times). For the bed expansion ratio, the bed surface fluctuated, so the bed height at a given superficial gas velocity was measured for 10 times and the average was used with the deviation less than 2.5% (the black points in Figure A5). The bed expansion test was conducted for 6 times and the average bed expansion ratio with error bars was shown in Figure A5 (red line).
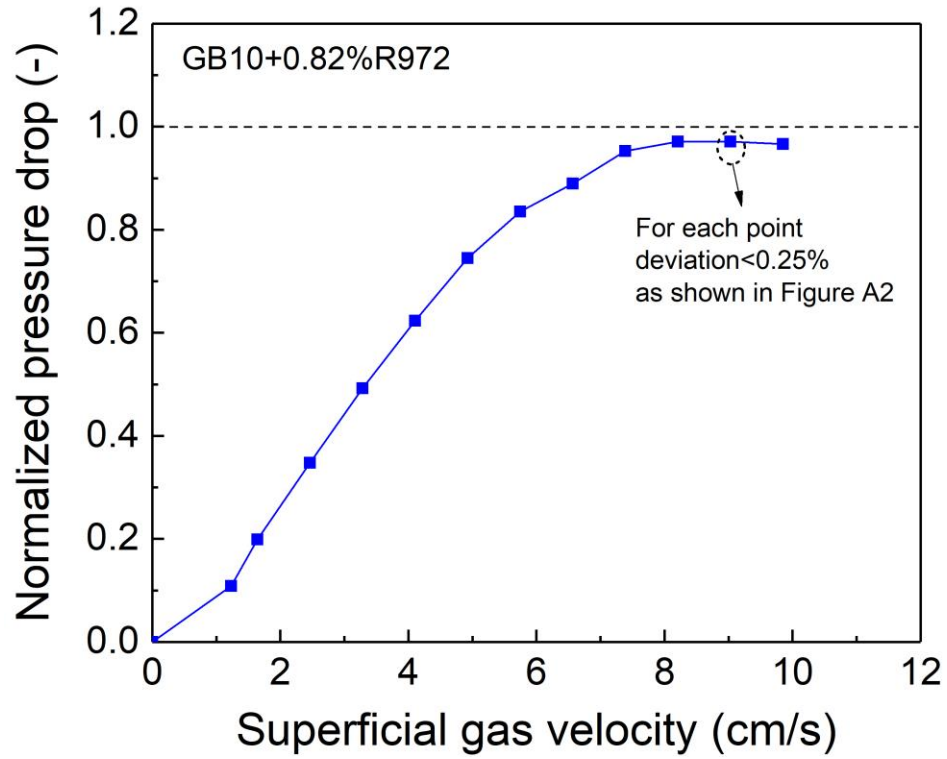
Figure A1: The normalized pressure drop curve for one sample
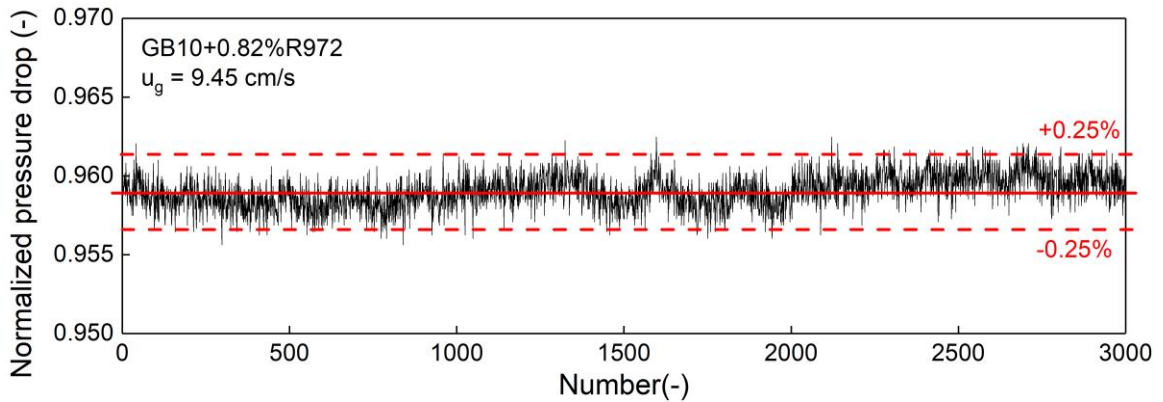
Figure A2: The fluctuation of one point at u_g = 9.45cm/s of the pressure drop curve
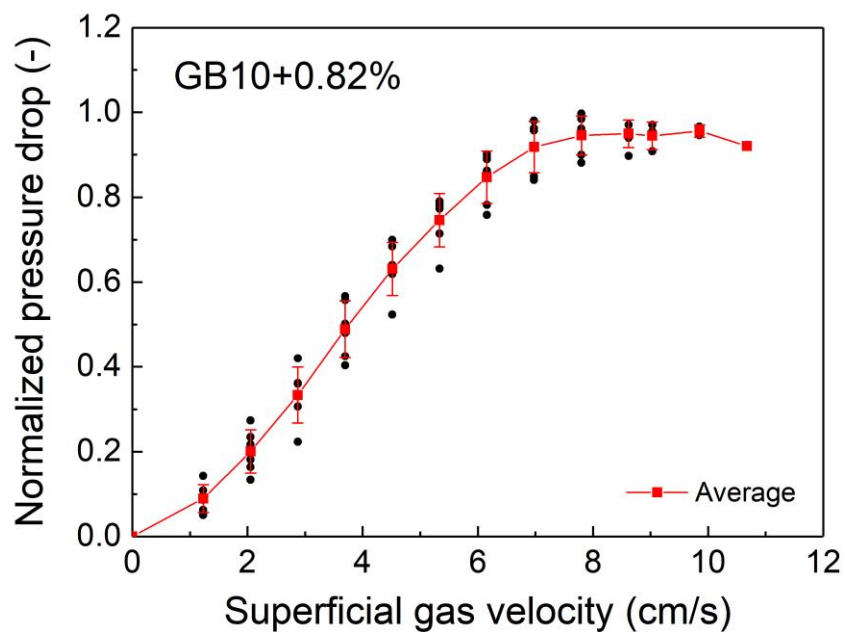
Figure A3: The average pressure drop curve for 6 times
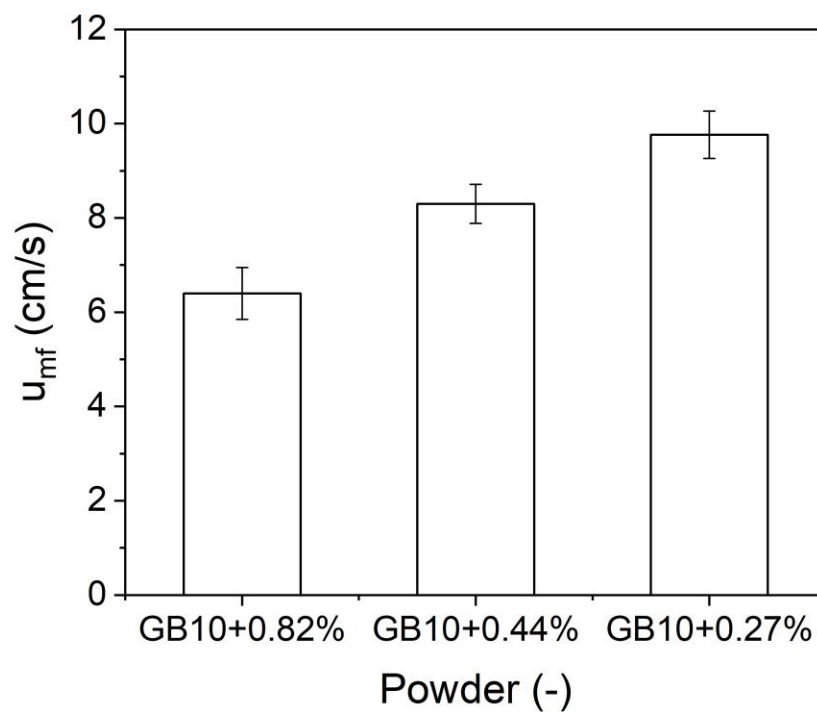
Figure A4: The average minimum fluidization velocity for 6 times

317
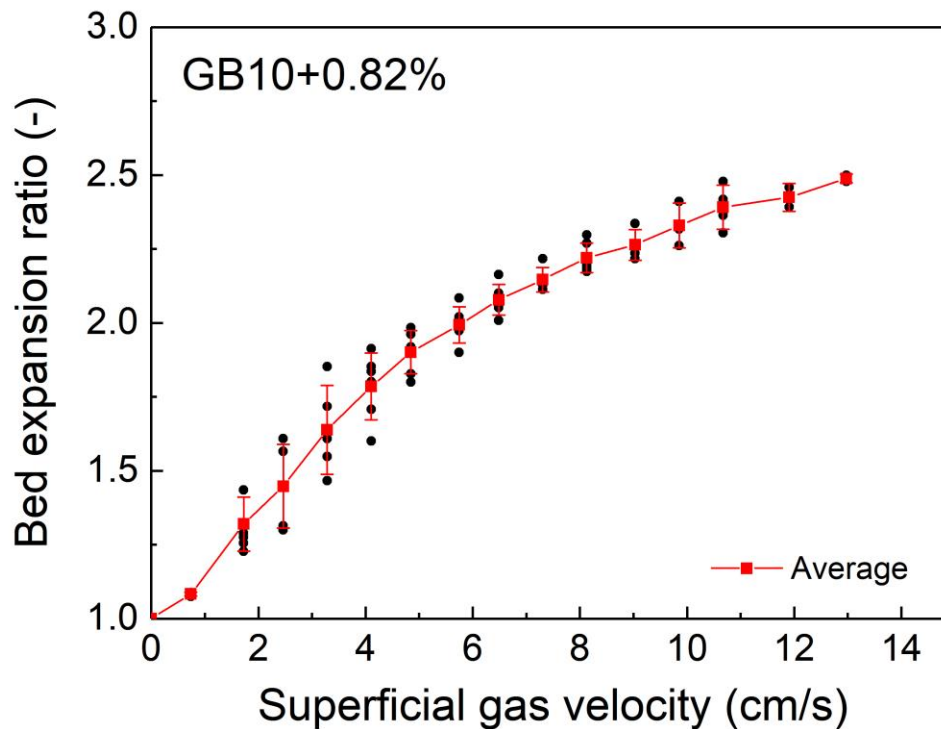
Figure A5: The average bed expansion ratio for 6 times

Bubble diameters

200 to 400 bubbles were collected at a given gas velocity for each sample, and the average bubble diameter was calculated. Figure A6 shows the bubble diameter spread for FCC8.5+ at different velocities; Figure A7 shows the bubble diameter spread for GB10+ at different velocities; and Figure A8 shows the bubble diameter spread for FCC76 at different velocities. For Group C^+ particles, most bubbles were smaller than 2cm and were distributed along the entire fluidized bed. The largest bubbles were smaller than 4cm and occasionally appeared in the bed.
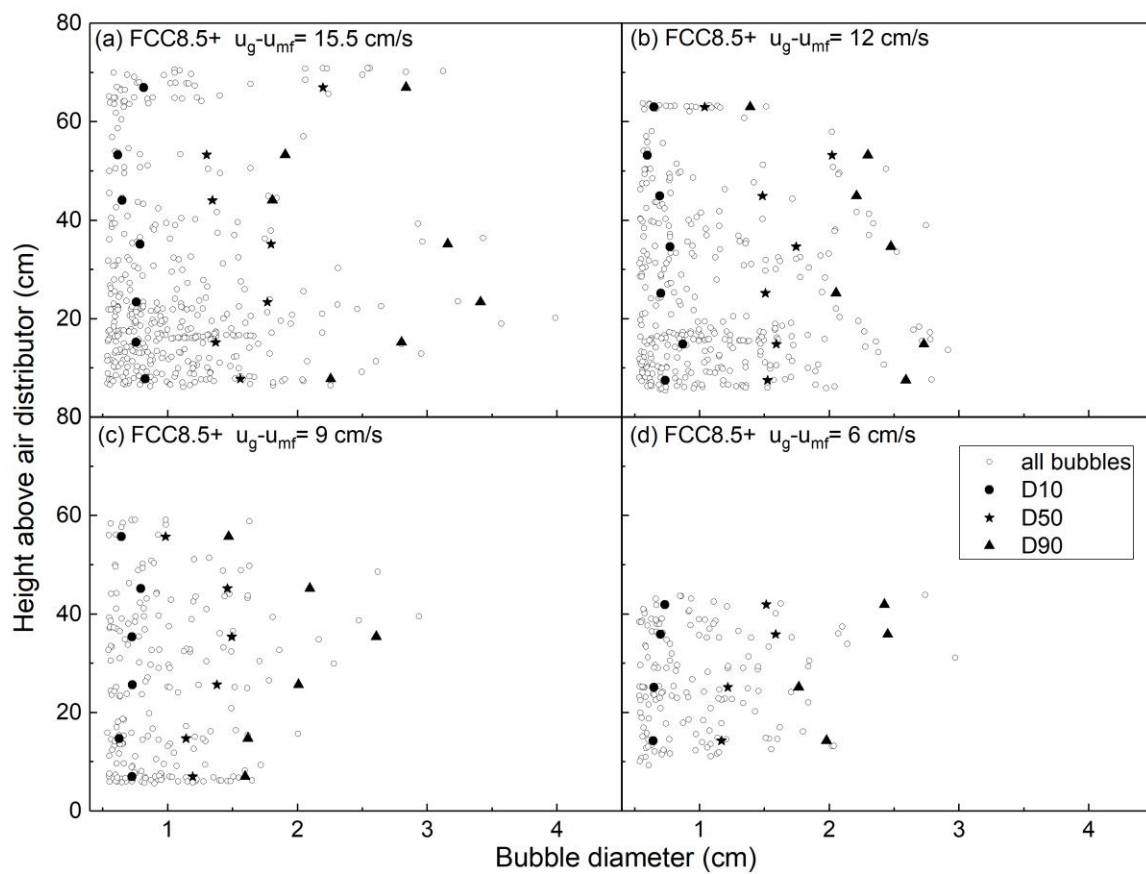
Figure A6: The bubble diameter spread and the average values for FCC8.5+
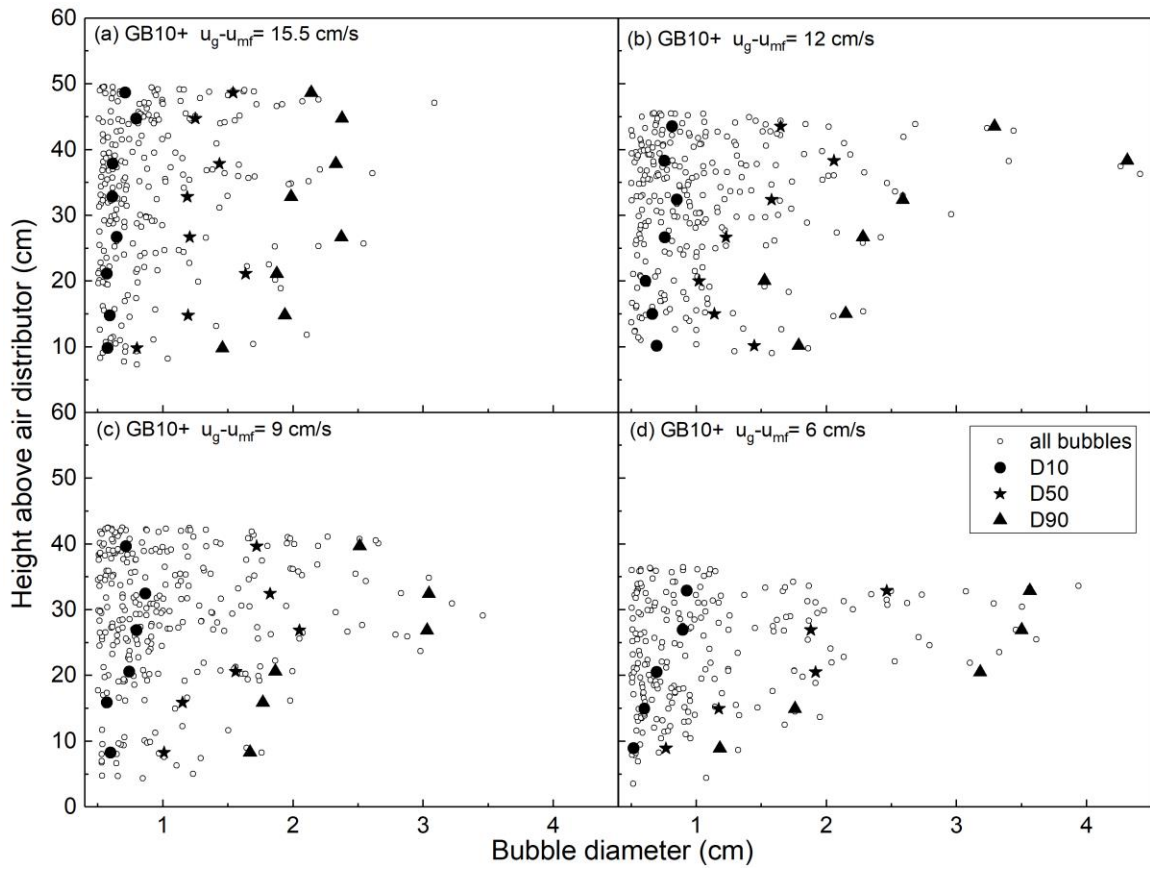
Figure A7: The bubble diameter spread and the average values for GB10+
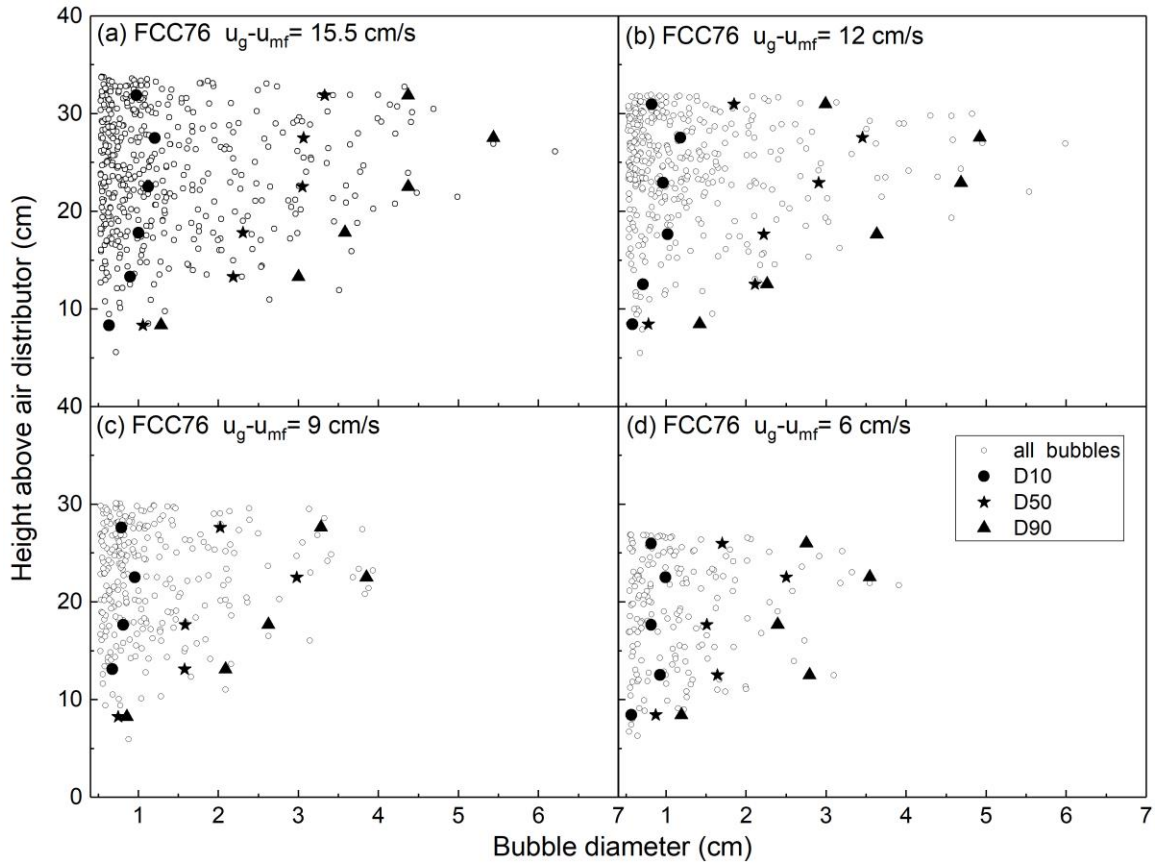
Figure A8: The bubble diameter spread and the average values for FCC76

Appendix B: Image processing

The image processing routine was developed on Adobe Photoshop CS6 (The Adobe company) and Matlab R2018b (The MathWorks inc.). It is able to collect all data relative to bubble position and bubble size. The camera recorded videos at a frequency of 50Hz and each video was 10s, equal to 500 frames. The video was transferred into images frame by frame, equal to 500 pictures. Each picture consists of 1080 x 1920 pixels and is in the Red, Green and Blue (RGB) format. Then the images were cropped to allow the analysis of the fluidized bed only, excluding all surroundings. To simplify the analysis process, the cropped RGB images were converted into greyscale ones. Each pixel in the grayscale images has a value ranging from 0 to 255 expressing a so-called grey-value, which indicates brightness. Gray-value 0 means the pixel is black and gray-value 255 means white. The image processing routine can be summarized as follows:

(1) Transforming of Videos to RGB images frame by frame;

(2) Cropping of images to allow the analysis of the fluidized bed only;

(3) Transforming of RGB images to grayscale ones;

(4) Thresholding of the grayscale images to obtain binary images;

(5) Indexing of all bubbles inside the area;

(6) Filtering false bubbles and noise.

1. Threshold value

The critical step is to discriminate the bubbles from the dense phase. This is done by choosing a threshold value to transform the grayscale images to binary ones, suitable for objective identification. In binary pictures, all pixels with a gray-value larger than the threshold are indicated as object pixels and are coloured white, represented by 1; all with a value smaller are background and made black, represented by 0. This can be accomplished by the following expression, relating the pixel coordinates $l(x,y)$ of the grayscale image to the pixel coordinates $g(x,y)$ of the binary image for a given threshold δ:

$$g(x,y) = \begin{cases} 1 & \text{when } l(x,y) \geq \delta; \\ 0 & \text{when } l(x,y) \leq \delta \end{cases} \tag{B1}$$

In the binary images, all pixels equal 1 are identified ad bubble phase pixels, while the others are identified as dense phase. One of the crucial step in image processing is to choose a proper threshold value, which has an impact one the detection of bubble boundaries. The threshold is found automatically using so-called Ostu thresholding method, named after Nobuyuki Ostu [1,2]. This algorithm assumes that the greyscale image contains two classes of pixels following bi-modal histogram, that are foreground pixels (bubbles in the images) and background pixels (dense phase in the images), it then calculates the optimum threshold separating the two classes so that their within-class variance is minimal or their between-class variance is maximal. The within-class (σ_w^2) variance is defined as a weighted sum of variances of the two classes:

$$\sigma_w^2(\delta) = \omega_0(\delta) \, \sigma_0^2(\delta) + \omega_1(\delta) \, \sigma_1^2(\delta) \qquad (B2)$$

where weights ω_0 and ω_1 are the probabilities of the two classes separated by a threshold δ, σ_0^2 and σ_0^2 are variances of the two classes. The class probability $\omega_{0,1}(\delta)$ is calculated from the L bins of the histogram:

$$\omega_0(\delta) = \sum_{i=0}^{\delta-1} p(i) \quad (B3)$$

$$\omega_1(\delta) = \sum_{i=\delta}^{L-1} p(i) \quad (B4)$$

where $p(i)$ is the probability of each grey value. Ostu shows that minimizing the within-class variance is the same as maximizing the between-class variance (σ_b^2), which is far quicker to calculate and more appropriate for implementations in Matlab:

$$\sigma_b^2(\delta) = \sigma^2 - \sigma_\omega^2 = \omega_0 \, (\mu_0 \text{-} \mu_T)^2 + \omega_1 \, (\mu_0 \text{-} \mu_T)^2 = \omega_0(\delta) \, \omega_1(\delta) \left[\mu_0(\delta) - \mu_1(\delta) \right]^2 \qquad (B5)$$

The between-class variance is expressed in terms of class probabilities ω and class means μ. While the class mean $\mu_{0,1,T}(\delta)$ is :

$$\mu_0(\delta) = \frac{\sum_{i=0}^{\delta-1} ip(i)}{\omega_0(\delta)} \qquad (B6)$$

$$\mu_1(\delta) = \frac{\sum_{i=\delta}^{L-1} ip(i)}{\omega_1(\delta)} \qquad (B7)$$

$$\mu_T = \sum_{i=0}^{L-1} ip(i) \qquad (B8)$$

The following relations can be easily verified:

$$\omega_0\mu_0 + \omega_1\mu_1 = \mu_T \quad (B9)$$

$$\omega_0 + \omega_1 = 1 \qquad (B10)$$

As shown in Figure B1, Figure C1(a) is an RGB image, Figure B1(b) is a typical greyscale image, while the its grey level distribution is shown in Figure B1(c) (the different frames of the same run or different experimental runs give similar histograms), Figure B1(d) is the binary image after thresholding and Figure B1(e) is the binary image with bubbles marked. A threshold value of 60 can be obtained by combining the Otsu thresholding method and visual observation, which is good for discriminating the bubble boundaries and removing noise.

RGB image · Greyscale image · Binary image · Image with bubble marked
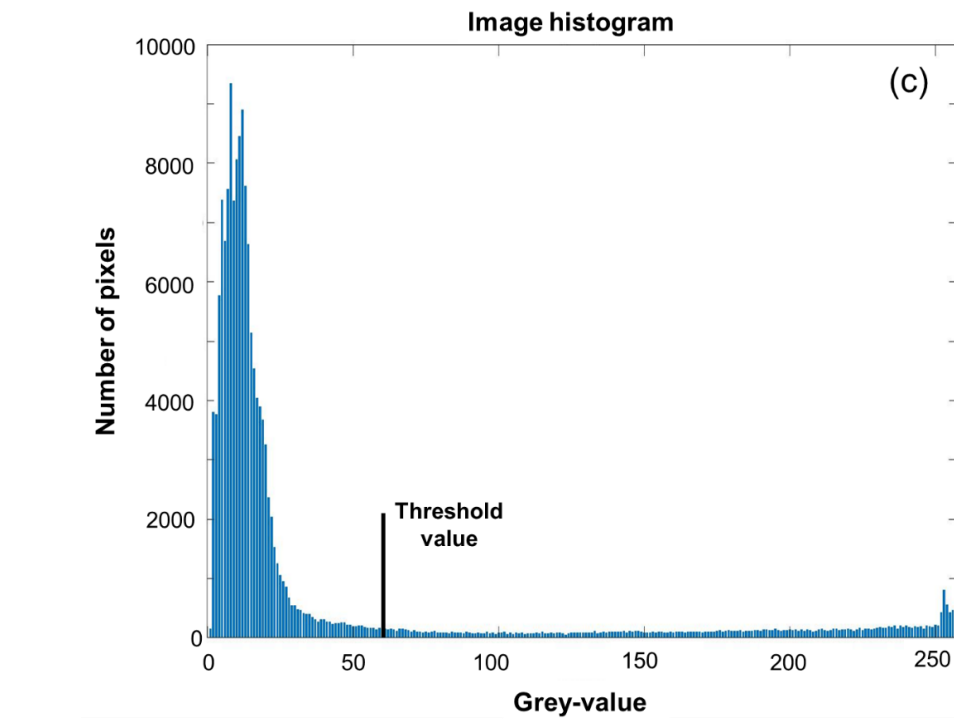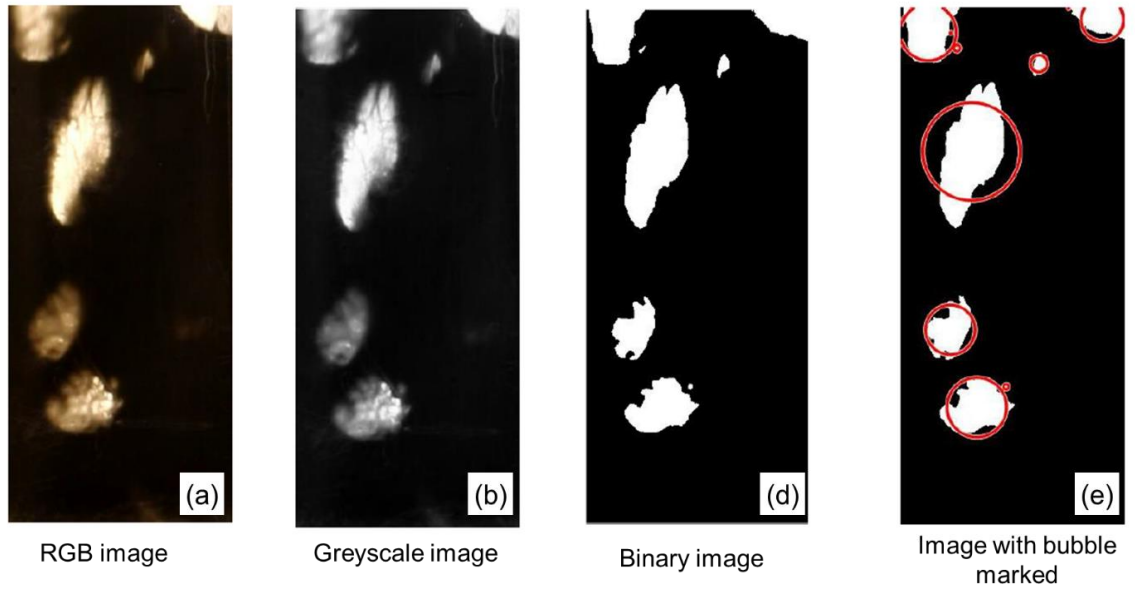
Figure B1: Example of image analysis: (a) original image; (b) greyscale image; (c) image histogram; (d) binary image; (e) image with bubble marked

2. Bubble diameter and bubble rise velocity

The area of a bubble (A_b) is the number of pixels forming this bubble, and each bubble is marked with a circle which has the same area by a function called Regionprops in Matlab. The bubble centroid is the circle centroid, which is used to identify the bubble position in the bed. Bubble area is calculated as follows:

$$A_b = \sum b(x_j, y_j) = \iint b(x,y) \, dx \, dy \qquad (B11)$$

Bubble centroid coordinates can be computed as follows:

$$x_c = \iint x \, b(x,y) \, dx \, dy \, / \, A_b \qquad (B12)$$

$$y_c = \iint y \, b(x,y) \, dx \, dy \, / \, A_b \qquad (B13)$$

where the integrals are extended to the area occupied by analyzed bubbles.

Equivalent bubble diameter (d_b) is calculated as follows:

$$d_b = \sqrt{\frac{4A_b}{\pi}} \quad (B13)$$

Every video was 500 frames, and was transformed into 500 pictures. 100 pictures were selected evenly among the 500 pictures and were analyzed to identify bubble positions and bubble diameter. D10, D50 and D90 were the mean bubble diameter at which 10%, 50% and 90% of the sum of bubbles area is comprised of bubbles with a diameter less than these values. For the purpose of calculating bubble rise velocity, several consecutive frames must be compared. The bubble rise velocity can be found by comparing bubble centroid positions in subsequent frames. Figure B2 shows 4 consecutive frames where one bubble was marked in different positions (with $\Delta t = 0.02s$). Since the number of bubbles in the fluidized bed of Group C^+ and Group A particles was not large, it is reasonable to track each bubble by observation. All bubbles in 500 frames that could be tracked by observation were used to calculate the bubble rise velocity (u_b):

$$u_b = \frac{y_c(t+\Delta t) - y_c(t)}{\Delta t} \qquad (B14)$$

The velocity was attributed to the mean vertical position according to:

$$h = \frac{y_c(t+\Delta t) - y_c(t)}{2} \qquad (B15)$$
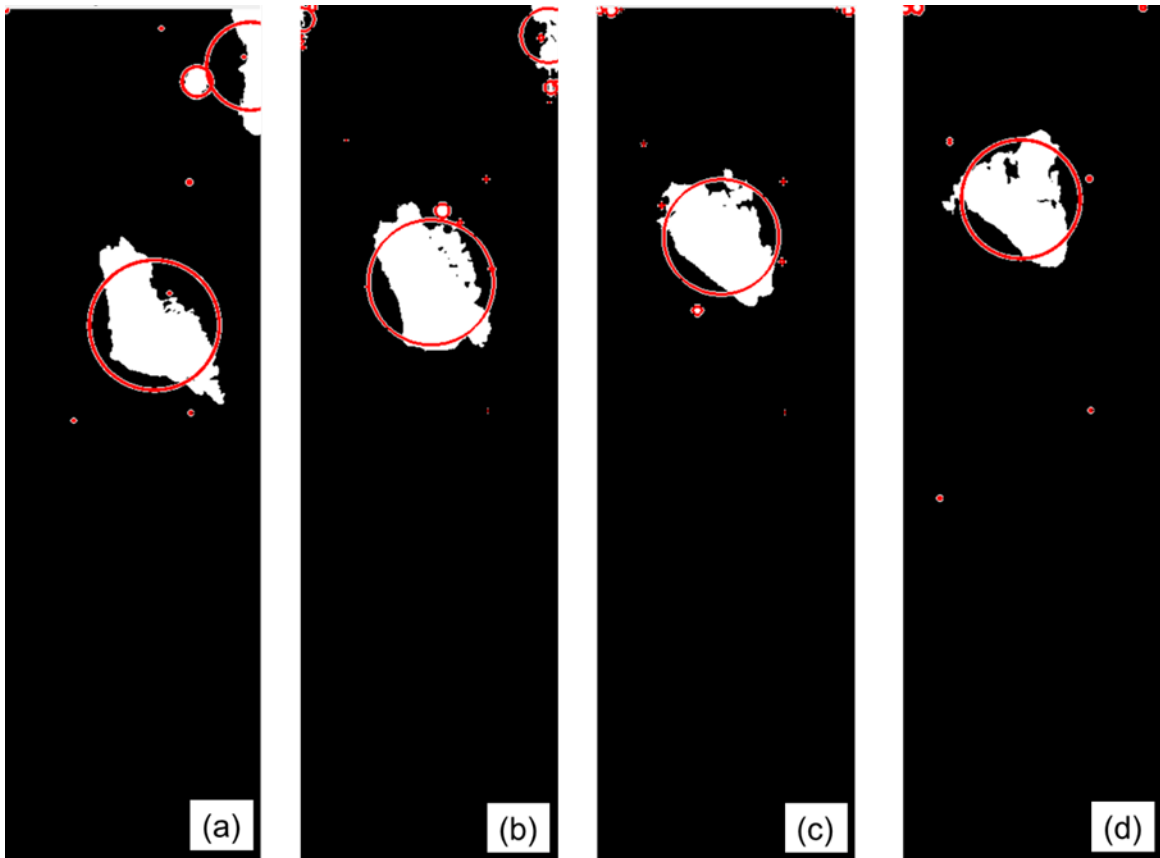
Figure B2: Four consecutive frames (with $\Delta t = 0.02$s) with one bubble marked in different positions

3. Bubble diameters smaller than 1cm

Figure B3 shows the distribution of bubbles in different diameters in the fluidized bed composed of FCC8.5+ particles at u_g-u_{mf} = 9cm/s. In the fluidized bed of fine particles, bubbles smaller than 1cm in diameter accounted for a large proportion of the overall population. Those small bubbles were fairly uniformly distributed throughout the fluidized bed. Although the 2-D fluidized bed was 1cm in depth, smaller bubbles were still visible as much more lights penetrated through those areas than the dense phase. It is not advisable to ignore all the small bubbles in the fluidized bed, but the bubbles that are too small in size would result in a decrease in accuracy of the results., Plus, the identified objects smaller than 0.2cm in diameter were close to the level of noises. Therefore, the lower cut-off size for the analysis of bubbles in the fluidized bed were chosen as 0.5cm.
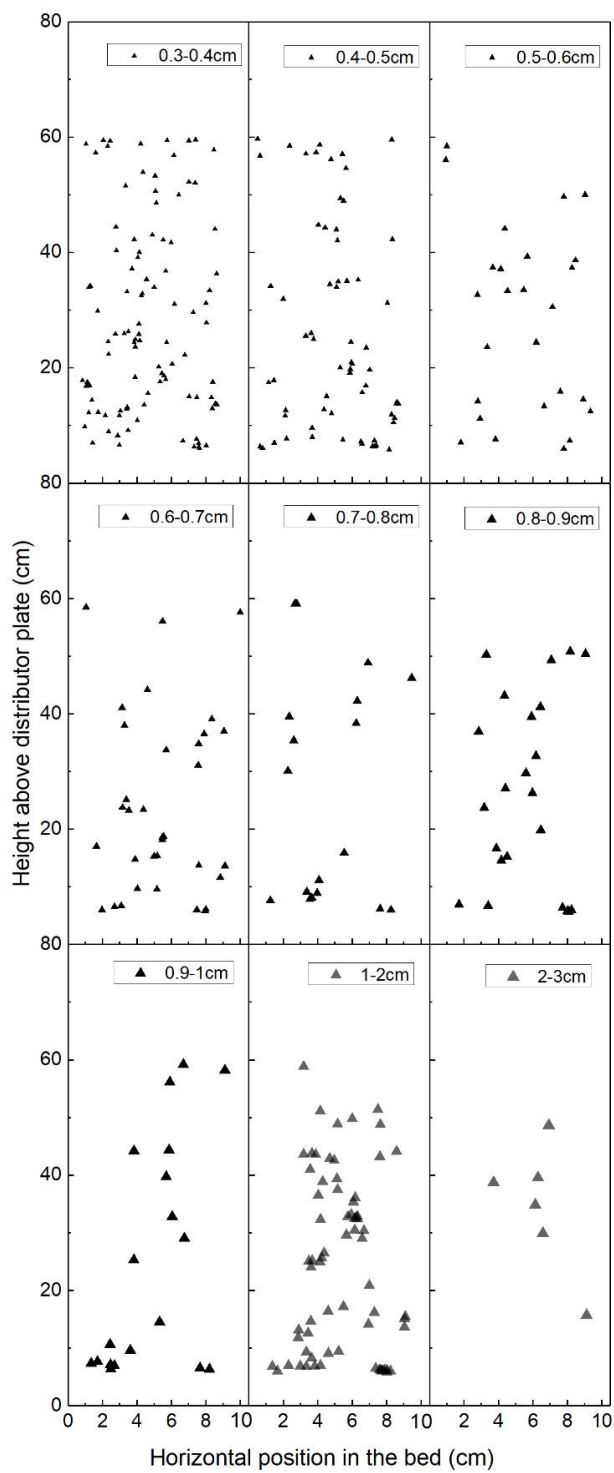
Figure B3: Distribution of bubbles in different diameters staring from 0.3cm (the fluidized bed of FCC8.5+, u_g-u_{mf} = 9cm/s)

References

[1] Ostu, Nobuyuki. A threshold selection method from gray-level histograms. IEEE Transactions on Systems, Man and Cybernetics 9.1 (1979): 62-66.

[2] Sezgin, Mehmet, and Bülent Sankur. Survey over image thresholding techniques and quantitative performance evaluation. Journal of Electronic imaging 13.1 (2004): 146-166.

Appendix C: Measurement of ozone decomposition

The ozone decomposition reaction system consists of five components: ozone generation, ozone sampling, ozone measurement, the fluidized bed and a fixed bed reactor. The fixed bed reactor (16 mm i.d.) was used to monitor the catalyst reactivity before and after experiments, keeping the catalyst reactivity constant.

1. Ozone generation

The ozone/oxygen mixture existing from the ozone generator (Model AE15M, manufactured by Absolute Ozone Inc.) was mixed with air and then entered the fluidized bed. The inlet ozone concentration (C_0) was set to 120-140 ppm. The ozone generator was preheated for 1 h before each experiment. To make sure the data reliable, it is necessary to keep the inlet ozone concentration stable. C_0 usually remained stable after running 5 minutes and kept constant during each experimental run, with fluctuations within the range of $\pm1.5\%$, as shown in Figure C1. Figure C2 shows the fixed bed reactor and the ozone generation.
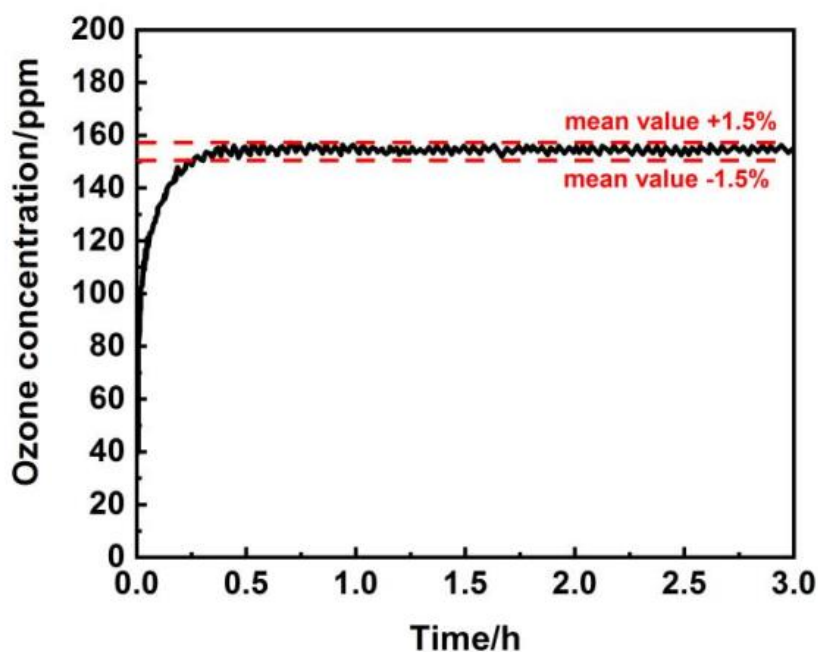
Figure C1: Stability of the inlet ozone concentration with time
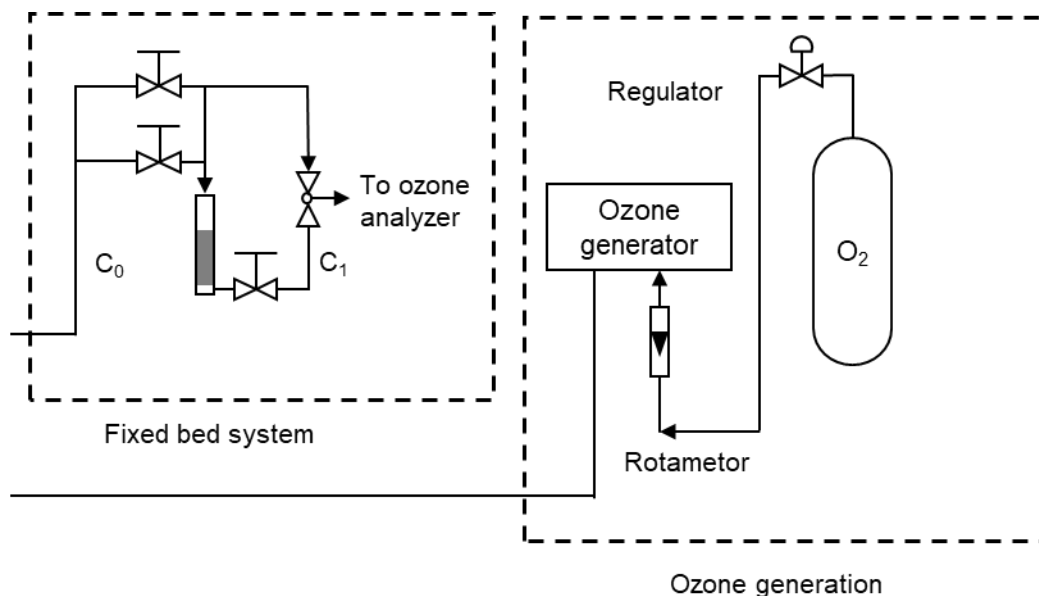
Figure C2: Ozone generation system

2. Ozone sampling

To reduce ozone losses during sampling, brass tubes (6mm o.d. and 0.36 mm wall thickness) which are a kind of ozone-inert materials were used as ozone sampling probes. The tubes were mounted with type 316 stainless steel porous disks (pore size 2μm, 6mm diameter, and 1.6mm thickness) to completely stop FCC particles in the fluidized bed from entering the ozone measurement system. A type 304 stainless steel wire mesh with pore size of 30.5μm was made in a hemispherical shape and loosely covered on the tip of the brass tube. This dome-shaped top cover can mitigate the accumulation of particles near the sampling probe tip and accurate measurement of ozone concentration. Figure C3 shows the ozone sampling system. The velocity of sucking in gas sample was 1.5L/min, which was low and would not affect the gas flow in the fluidized bed.
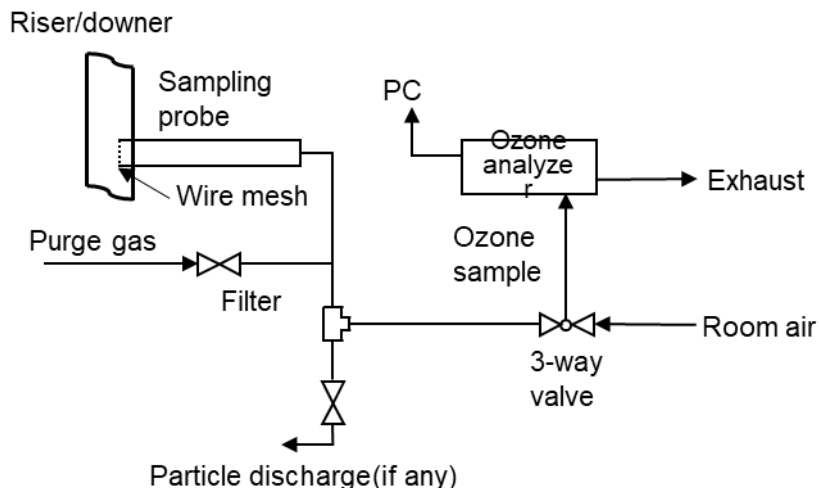
Figure C3: Ozone sampling system

3. Ozone measurement

Ozone concentration was detected using Model 49i UV ozone analyzer manufactured by Thermo Electron Inc. (Ohio, USA). It is a dual-cell photometer, having both sample and reference air flowing at the same time. Each cell has a length of 37.84 cm and an inner diameter of 0.91 cm, with the internal surfaces coated with polyvinylidine fluoride (PVDF) to ensure that ozone undergoes no decomposition upon exposure to the internal surface of the cells. The UV light source used in ozone photometers is 253.7 nm from a low-pressure Hg discharge lamp. The light intensities in the sample air and the sample-free air are used to calculate ozone concentration according to the Beer-Lamber law:

$$C = (10^6 \times \frac{P_0 T}{P T_0}) \frac{1}{\sigma l} \ln(\frac{I_0}{I}) \qquad \text{(D1)}$$

where I_0 is the intensity of the light beam with no ozone present (cd), I is the intensity of the light beam after passing through the sample (cd), l is the length path through the sample (cm), C is the molar fraction of ozone in the sample (ppm), σ is the specific absorption coefficient of ozone at wavelength 253.7nm,308cm^{-1}, P is the pressure (mmHg), P_0 is the standard pressure (760mmHg), T is the temperature (K), and T_0 is the standard temperature (273.15K).

Figure C4 shows the schematic diagram of the TEI 49i ozone analyzer. The air sample is pulled through the analyzer by an air pump at the exit of the analyzer. Ozone concentration

of the air is measured in the cells using UV radiation. The solenoid valves operating under computer control allow sample gas to pass through Cell A and reference gas (with ozone depleted in an ozone scrubber) through Cell B, or vice versa, depending upon which cycle the instrument is performing. The analyzer monitors temperature (accuracy $\pm$ 0.2°C), pressure (accuracy $\pm$ 0.3 mmHg) and flow rates of the sample air in the cells.
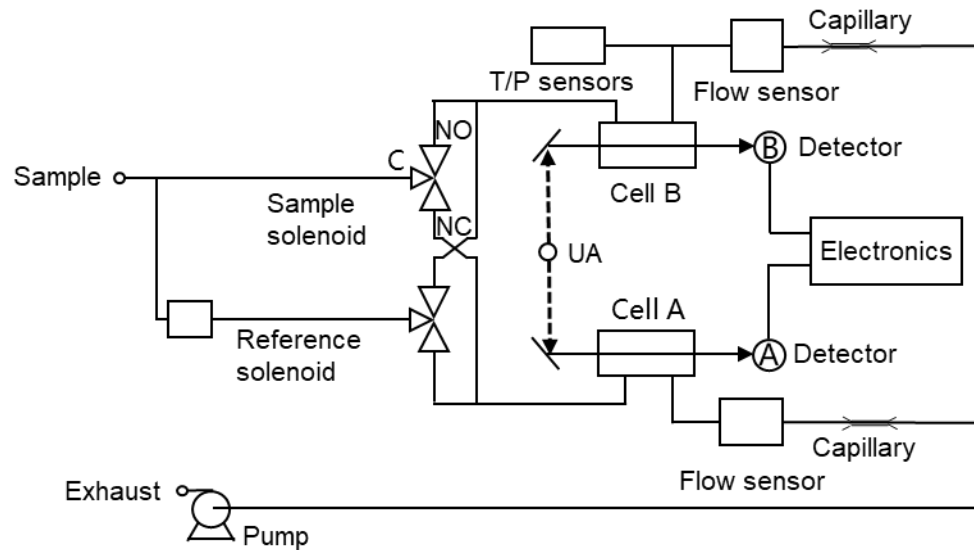
Figure C4: Ozone analyzer

Before each ozone sampling and measurement cycle, the 3-way valve before the ozone analyzer was switched to the room-air side to protect the ozone analyzer from the high pressure (791 kPa) air flow. After sampling and measurement, the valve was switched to the high-pressure-air side to blow away any particles accumulated on its tip and purge the sampling probe. Each test repeated 3 times and the average value was used.

Appendix D: Preparation of catalysts for ozone decomposition

Spent fluid catalytic cracking (FCC) particles are activated as the catalyst for ozone decomposition by being impregnated with ferric nitrate solution at room temperature. The impregnation process is shown in Figure D1.
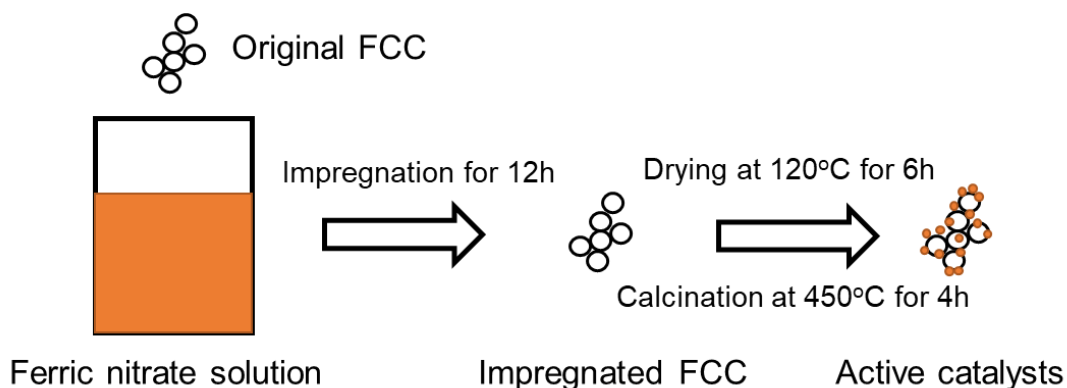
Figure D1: Particle activation process

FCC particles are impregnated with a 41% $Fe(NO_3)_3$ solution for about 12 hours and thereafter the wet particles are dried at 120°C for 6hrs in the oven followed by calcination at 450°C for 4hrs. After calcination, iron nitrate is decomposed to iron oxide as the active component loaded on the particles. After breaking up the agglomerates formed during calcination using a ball mill, the resulting particles are sifted using a sieve with pore size 250μm. Scanning electron microscopy (SEM) images of the SFCC particles at 500 magnifications shown in Figure D2 suggest that, particles before and after impregnation are similar in size distribution [1]. Table D1 shows the active component concentration of FCC particles after impregnation. The impregnated FCC particles of three different sizes have the similar active component concentration.
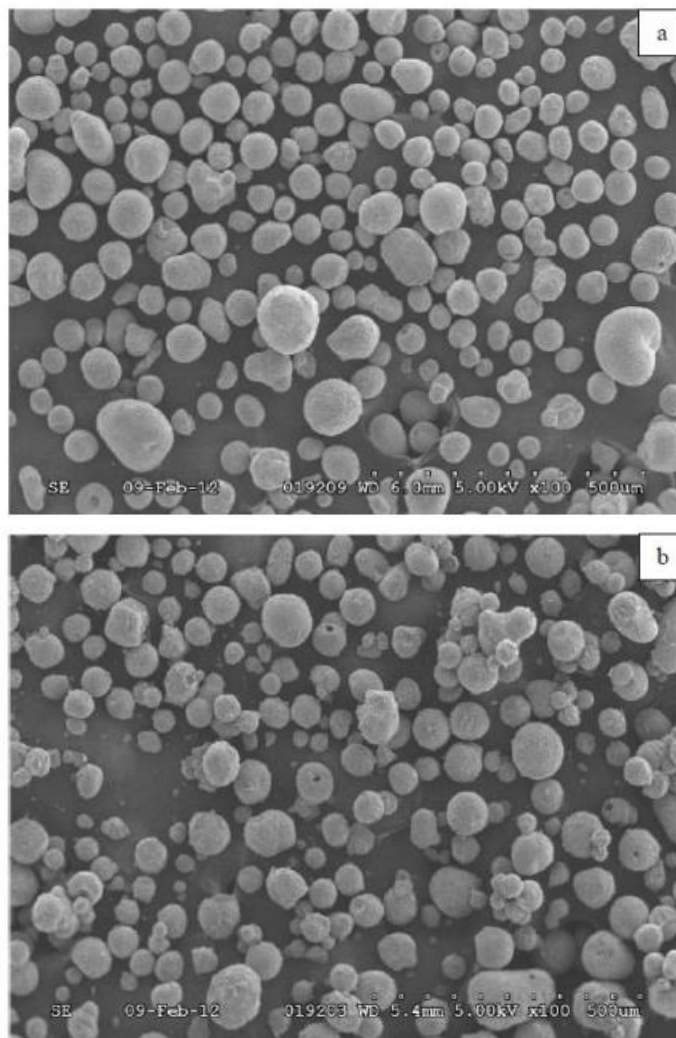
Figure D2: (a) Original FCC particles; (b) Impregnated FCC particles

The activated and non-activated particles are sieved into different particle sizes (Group C and Group A particles) and mixed together to control the overall activity of the particles. Chemical activity of the catalysts used in the experiments is measured before and after each run in the small fixed bed reactor (16mm I.D. and 25cm in height). For each measurement, 3g catalysts are loaded into the fixed bed reactor, and the inlet (C_0) and outlet (C_1) ozone concentrations are measured to calculate the chemical activity (k_r) using the equation:

$$k_r = (F\rho_b/m) \ln (C_0/C_1) \qquad \text{(E1)}$$

where F is the gas flowrate, and ρ_b is the bulk density of particles. Table D2 shows the physical properties and chemical reactivities of different catalysts.

Table D1: The active component concentration of impregnated FCC particles

Impregnated Catalysts	Analyte	Compound formula	Concentration
FCC8.5	Fe	Fe_2O_3	7.86%
FCC20	Fe	Fe_2O_3	7.75%
FCC76	Fe	Fe_2O_3	9.28%

Table D2: Properties of impregnated FCC catalysts

Catalysts	D_{50} (μm)	ρ_p (kg/m^3)	ρ_b (kg/m^3)	k_r (s^{-1})	Classification
FCC8.5	8.5	1780	509	1.32	Group C
FCC20	20	1780	627	1.36	Group C
FCC76	76	1780	874	1.36	Group A
FCC32	32	1780	921	1.50	Fine Group A
FCC100	100	1780	953	1.76	Group A

The internal porosity and pore size distribution was measured using N_2 adsorption/desorption measurements (Quanta Autosorb-iQ). The total pore volumes of FCC8.5+0.82% and FCC76 are 0.250 cm3/g and 0.254 cm3/g separately, and the results of pore size distribution show in Figure D3.
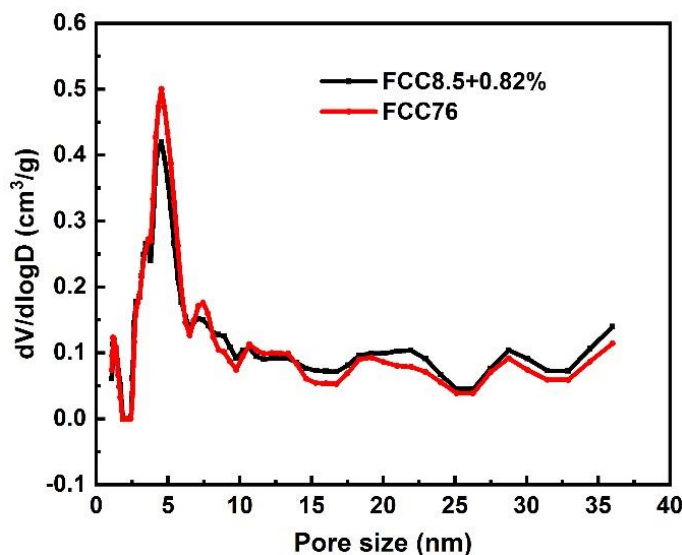
Figure D3: Pore size distribution curves of FCC8.5+0.82% and FCC76

Reference

[1]   Wang, Chengxiu. High density gas-solids circulating fluidized bed riser and downer reactors. Ph.D thesis. Western University, London, Canada, 2013.

Appendix E: SEM images for different types of Group C⁺ particle
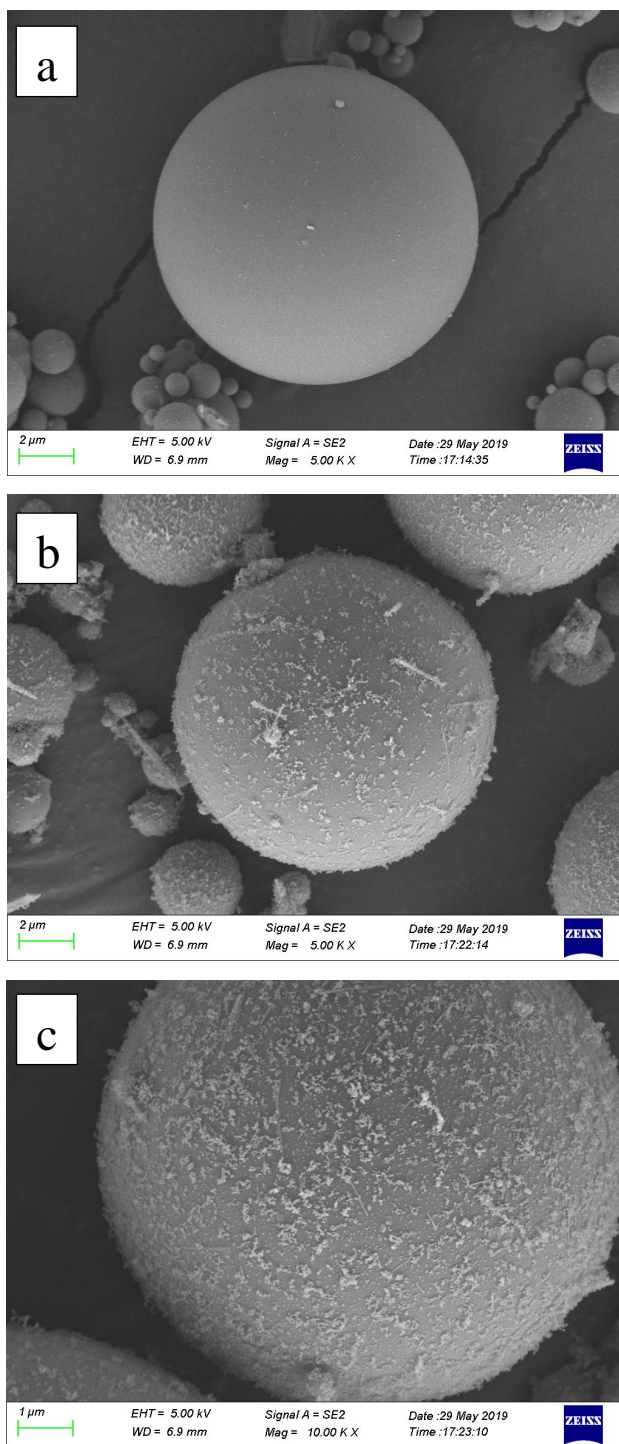
Figure E1: (a) GB10 virgin (x5K); (b) GB10+0.82% R972 (x5K); (c) GB10+0.82%R972 (x10K)
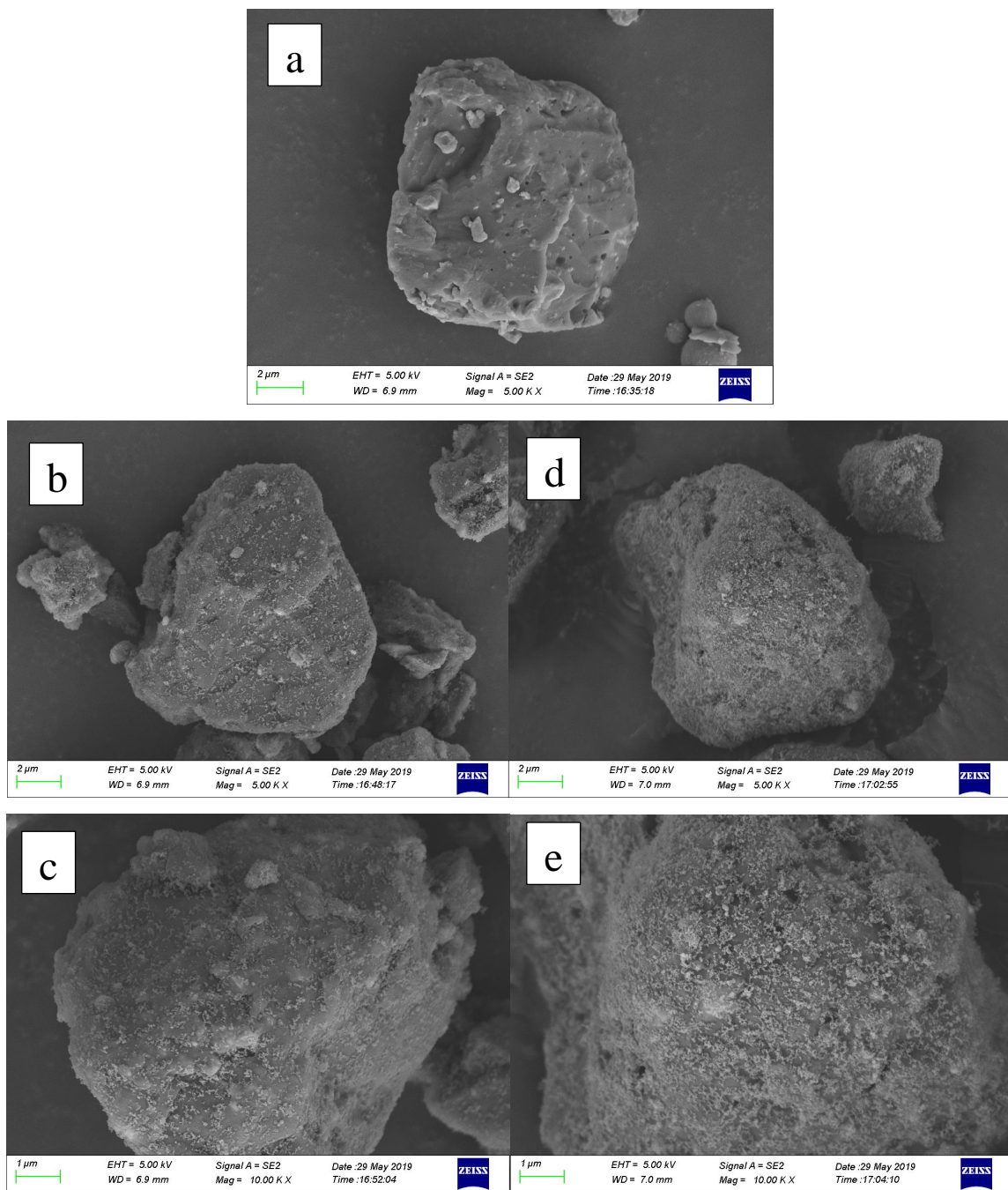
Figure E2: (a) PU10 virgin (x5K); (b) PU10+0.44% R972 (x5K); (c) PU10+0.44%R972 (x10K); (d) PU10+0.82% R972 (x5K); PU10+0.82% R972 (x10K)
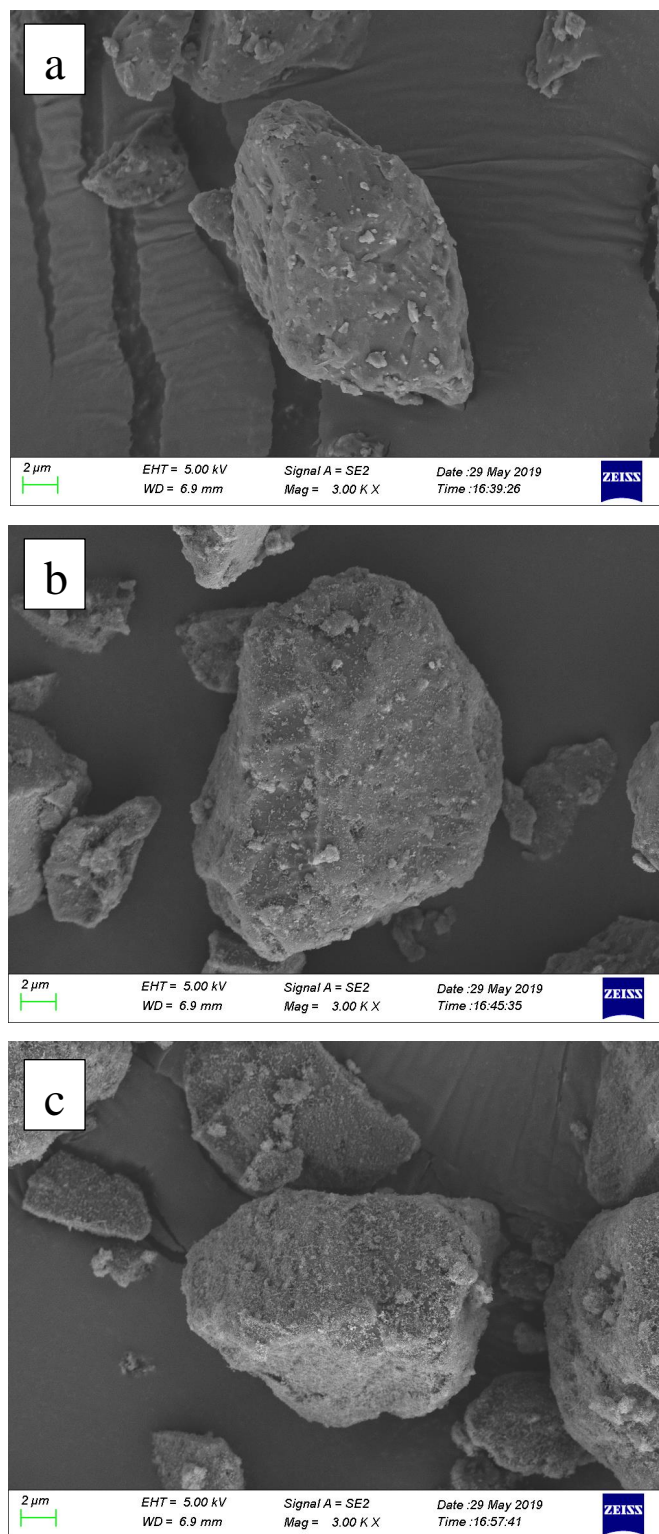
Figure E3: (a) PU18 virgin (x3K); (b) PU10+0.44% R972 (x3K); (c) PU10+0.44%R972 (x3K)
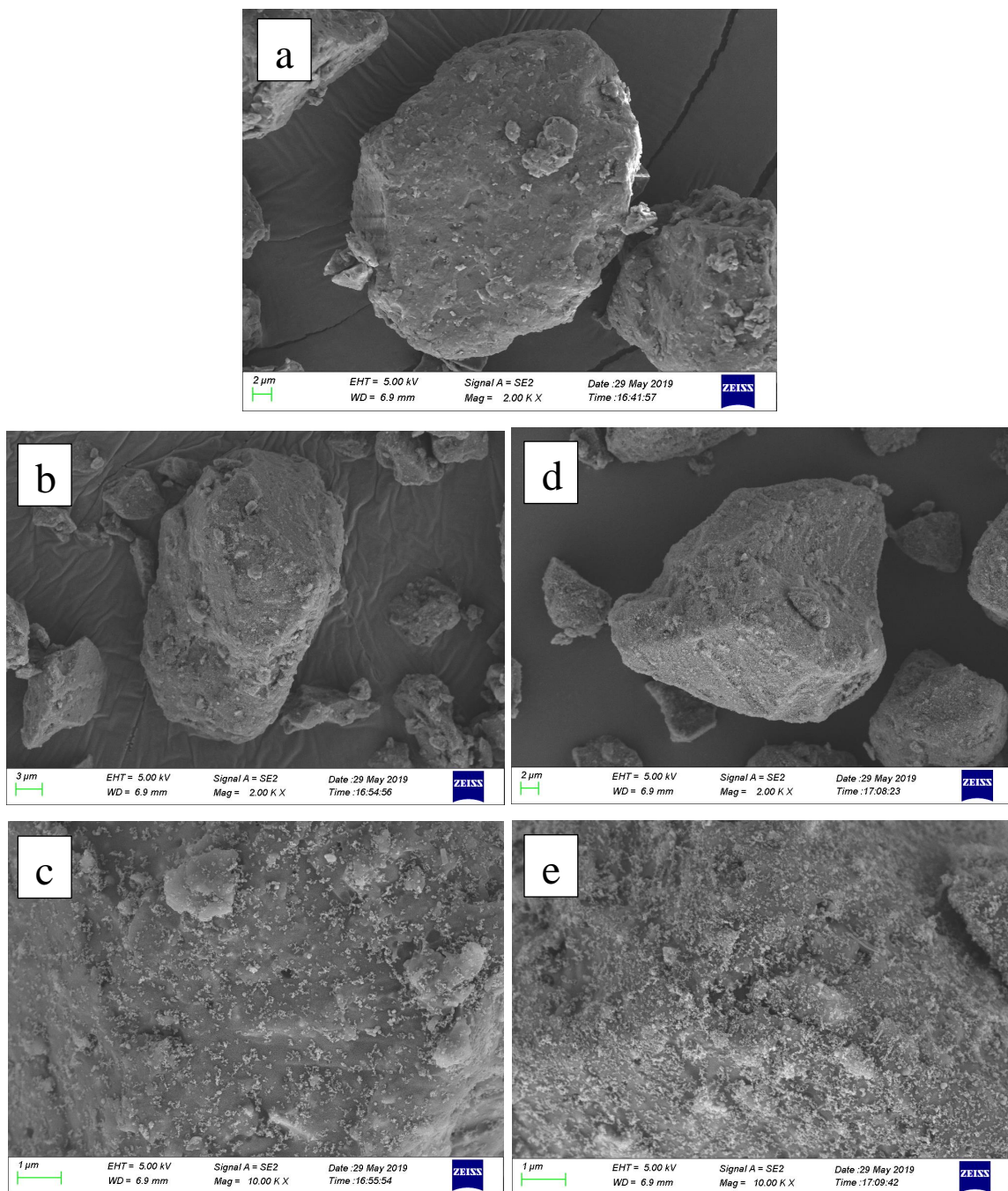
Figure E4: (a) PU36 virgin (x2K); (b) PU36+0.44% R972 (x2K); (c) PU36+0.44%R972 (x10K); (b) PU36+0.82% R972 (x2K); (c) PU36+0.82%R972 (x10K)
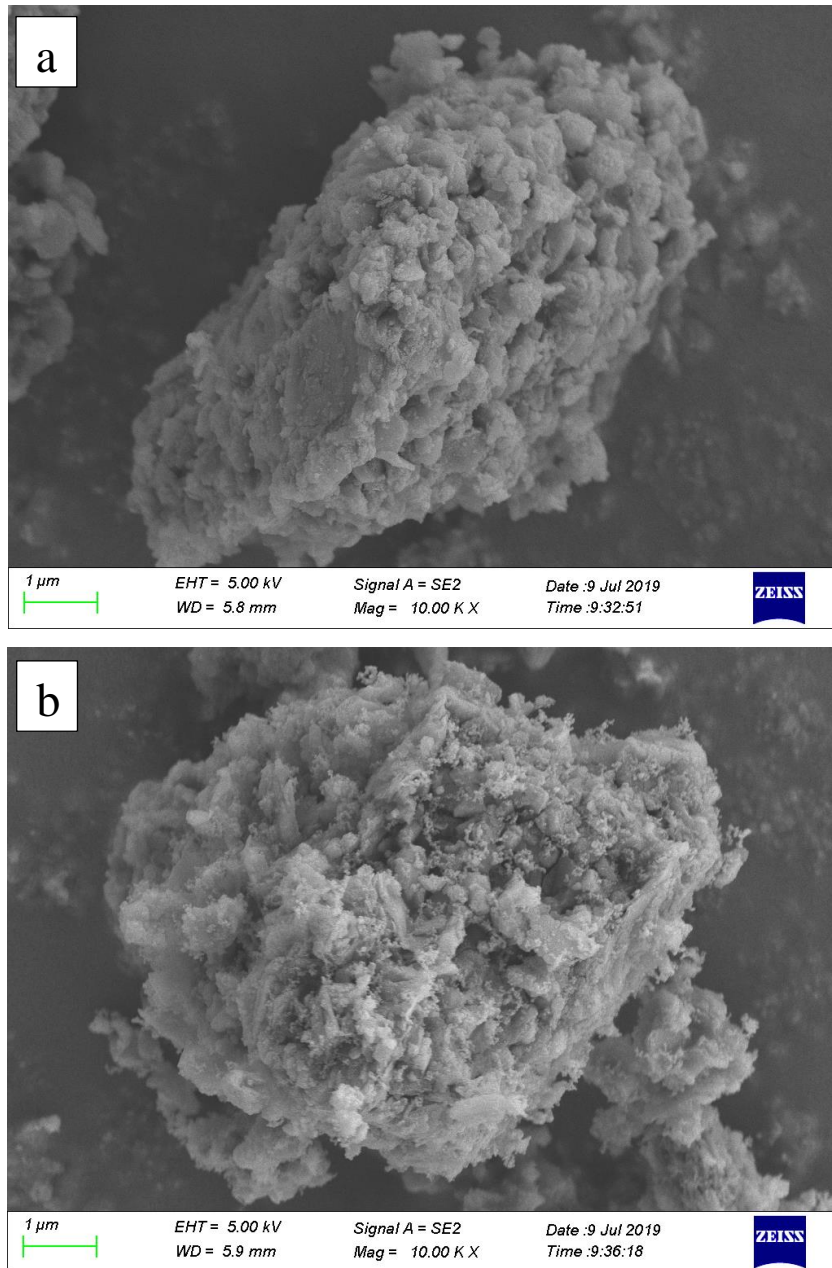
Figure E5: (a) FCC8.5 virgin (x10K); (b) FCC8.5+0.82% R972 (x10K)
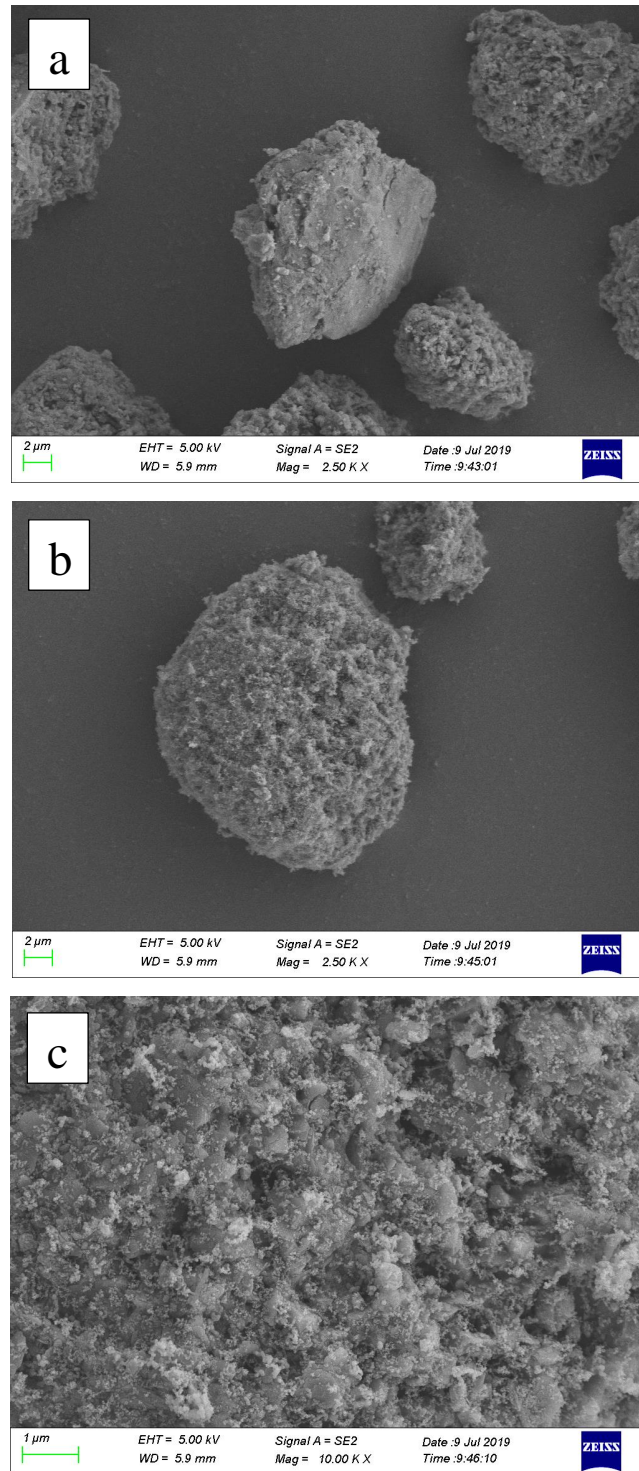
Figure E6: (a) FCC20 virgin (x2.5K); (b) FCC20+0.82% R972 (x2.5K); (c) FCC20+0.82% R972 (x10K)
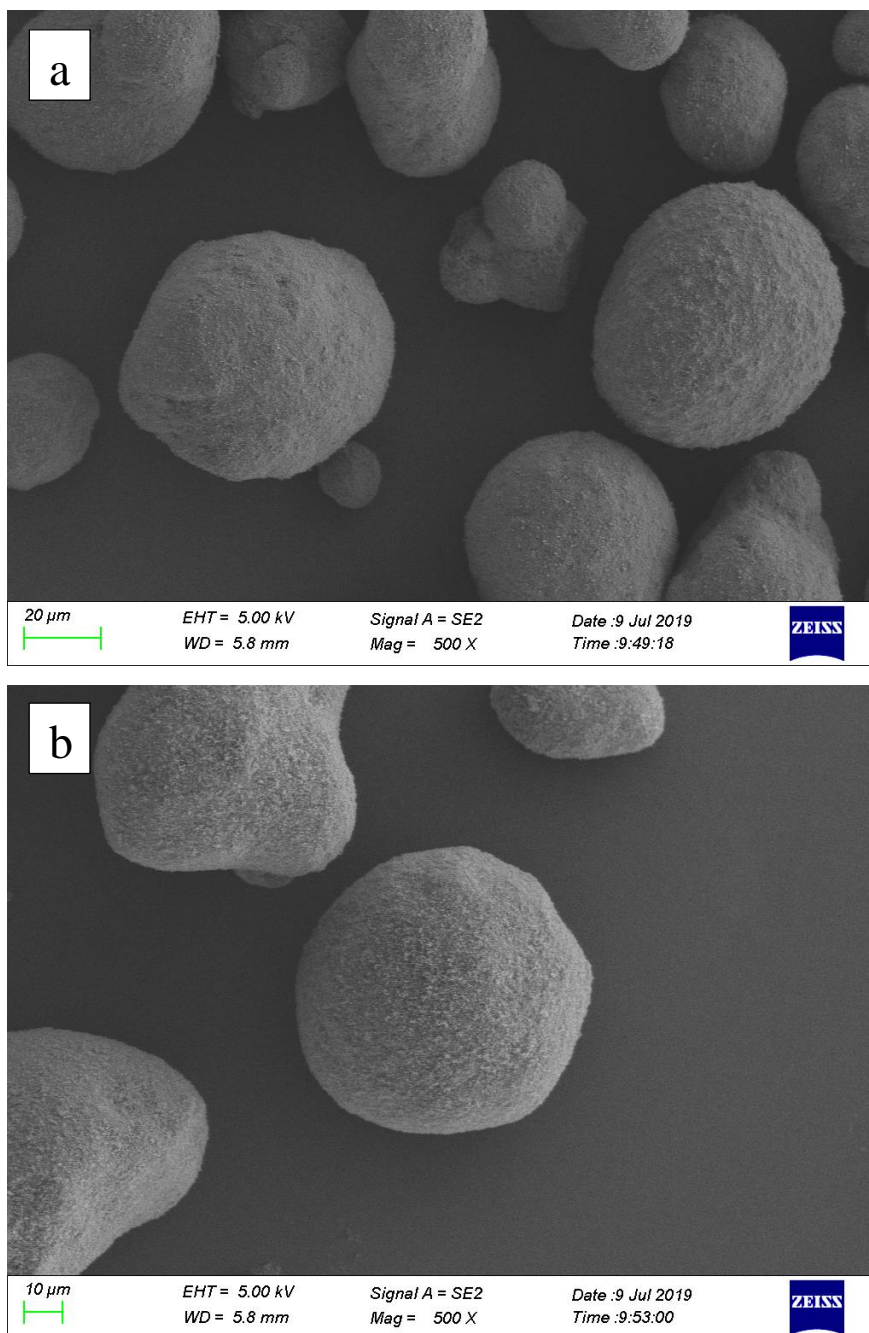
Figure E7: (a) FCC76 virgin (x500); (b) FCC76+0.82% R972 (x500)

Appendix F: Raw data

Flowability

Powder	Nano% (v)	AOR (°)	AVA (°)	Cohesion (kPa)
GB10	0	53.0	64.4	1.27
	0.27	48.5	61.2	0.93
	0.44	46.3	58.7	0.92
	0.82	45.5	57.5	0.85
	1.7	46.0	59.1	0.85
PU10	0	52.5	63.9	0.99
	0.27	47.1	58.8	0.60
	0.44	44.6	55.0	0.35
	0.82	45.2	54.3	0.35
PU18	0	50.6	59.4	1.00
	0.27	45.6	55.5	0.38
	0.44	42.2	52.0	0.23
	0.82	44.3	52.3	0.35
PU36	0	49.6	56.1	0.36
	0.27	42.3	49.8	0.06
	0.44	39.4	49.3	0.001
	0.82	42.0	50.8	0.001
FCC8.5	0	49.8	53.4	0.45
	0.27	51.6	51.8	0.47
	0.44	50.8	51.8	0.56
	0.82	51.5	52.8	0.41
FCC20	0	39.0	54.8	0.00
	0.27	41.5	58.1	0.09
	0.44	42.5	59.7	0.00
	0.82	44.4	60.6	0.00
GB39	0	34.0	46.0	0.05
	0.9	33.0	45.0	0.00
PU105	0	39.5	49.5	0.03
	0.9	38.1	49.0	0.00

Raw data for chapter 3

Normalized pressure drop across the whole bed

GB10		GB10+0.27%		GB10+0.44%		GB10+0.82%	
u_g (cm/s)	ΔP (-)	u_g (cm/s)	ΔP (-)	u_g (cm/s)	ΔP (-)	u_g (cm/s)	ΔP (-)
9.8	0.08	12.3	0.91	12.3	0.85	11.5	0.96
9.0	0.11	11.5	0.91	11.5	0.85	10.3	0.96
8.2	0.11	10.7	0.89	10.7	0.85	9.0	0.96
7.4	0.11	9.9	0.91	9.4	0.85	8.2	0.96
6.6	0.11	9.0	0.47	8.6	0.95	6.6	0.92
5.7	0.10	8.2	0.34	7.8	0.53	5.7	0.66
4.9	0.09	7.4	0.16	6.2	0.42	4.9	0.52
4.0	0.08	6.2	0.13	4.9	0.45	4.1	0.27
2.5	0.06	4.1	0.10	4.1	0.08	3.3	0.20
1.6	0.06	2.1	0.08	2.1	0.05	1.6	0.09
0	0	0	0	0	0	0	0

PU10		PU10+0.27%		PU10+0.44%		PU10+0.82%	
u_g (cm/s)	ΔP (-)	u_g (cm/s)	ΔP (-)	u_g (cm/s)	ΔP (-)	u_g (cm/s)	ΔP (-)
6.6	0.26	8.2	0.83	7.0	0.85	7.4	0.91
5.7	0.26	7.4	0.83	5.7	0.85	6.6	0.91
5.0	0.26	6.6	0.83	4.9	0.85	5.7	0.89
4.1	0.20	5.7	0.83	4.1	0.85	4.9	0.89
3.6	0.18	4.9	0.20	3.3	0.15	4.1	0.91
3.0	0.13	4.1	0.15	2.5	0.1	3.3	0.91
2.5	0.10	3.3	0.08	1.6	0.07	2.5	0.91
1.9	0.08	2.5	0.05	0	0	2.3	0.86
1.3	0.05	1.2	0.03			1.8	0.07
0.7	0.01	0	0			1.3	0.06
0	0					0	0

PU18		PU18+0.27%		PU18+0.44%		PU18+0.82%	
u_g (cm/s)	ΔP (-)	u_g (cm/s)	ΔP (-)	u_g (cm/s)	ΔP (-)	u_g (cm/s)	ΔP (-)
7.4	0.13	6.6	0.95	6.6	0.99	8.2	0.94
6.6	0.13	5.9	0.95	6.2	0.99	7.4	0.94
5.5	0.13	5.2	0.95	5.4	0.99	6.6	0.94
4.8	0.10	4.5	0.95	4.5	0.99	5.7	0.94
3.9	0.08	4.1	0.95	3.6	0.99	4.9	0.94
3.3	0.07	3.9	0.96	3.1	0.95	4.1	0.92
2.8	0.06	3.5	0.09	2.9	0.95	3.7	0.92
2.4	0.06	2.9	0.06	2.5	0.28	3.3	0.91
1.6	0.04	2.0	0.04	1.8	0.12	2.9	0.47
1.3	0.04	1.0	0.01	0.9	0.05	2.5	0.54
0.8	0.01	0	0	0.6	0.03	1.6	0.04
0	0			0	0	0	0

PU36		PU36+0.27%		PU36+0.44%		PU36+0.82%	
u_g (cm/s)	ΔP (-)	u_g (cm/s)	ΔP (-)	u_g (cm/s)	ΔP (-)	u_g (cm/s)	ΔP (-)
5.1	0.14	5.7	0.96	6.6	1.02	5.7	0.95
4.3	0.11	4.9	0.96	6.1	1.03	4.8	0.90
3.7	0.10	4.1	0.94	5.3	1.03	4.1	0.88
3.0	0.07	3.1	0.92	4.4	1.03	3.3	0.83
2.5	0.06	2.5	0.85	3.3	1.03	2.4	0.81
2.1	0.04	1.6	0.76	2.7	0.95	1.6	0.71
1.1	0.03	0.8	0.63	2.2	0.92	1.1	0.64
0.7	0.01	0.6	0.59	1.6	0.91	0.6	0.52
0	0	0	0	1.2	0.85	0	0
				0.7	0.74		
				0	0		

GB39		GB65	
u_g (cm/s)	ΔP (-)	u_g (cm/s)	ΔP (-)
8.2	0.93	8.2	0.95
7.2	0.93	7.2	0.99
6.6	0.93	6.6	0.99
5.7	0.90	5.7	0.98
5.0	0.90	5.0	1.00
4.1	0.91	4.1	1.00
3.3	0.91	3.3	0.99
2.6	0.91	2.6	0.97
1.6	0.92	1.6	0.99
1.3	0.91	1.3	0.98
0.7	0.88	0.7	0.97
0.4	0.57	0.4	0.26
0	0	0	0

Minimum fluidization velocity

Powder	Nano% (v)	u_{mf} (cm/s)
GB10	0	-
	0.27	9.8
	0.44	8.4
	0.82	6.2
	0.9	3
	1.7	4
PU10	0	-
	0.27	5.7
	0.44	4.1
	0.82	2.3
PU18	0	-
	0.27	3.8
	0.44	2.8
	0.82	3.2
PU36	0	-
	0.27	0.8
	0.44	0.6
	0.82	0.9
GB39	0	0.8
	0.9	0.8
PU105	0	0.5
	0.44	0.5

Bed expansion ratio

GB10		GB10+0.27%		GB10+0.44%		GB10+0.82%	
u_g (cm/s)	BER (-)	u_g (cm/s)	BER (-)	u_g (cm/s)	BER (-)	u_g (cm/s)	BER (-)
0.0	1.00	0.0	1.00	0.0	1.00	0.0	1.00
0.7	1.00	2.1	1.07	2.1	1.05	0.7	1.09
1.6	1.02	2.9	1.09	2.9	1.07	1.7	1.43
2.5	1.04	4.1	1.13	4.1	1.12	2.5	1.57
3.3	1.10	5.7	1.17	4.9	1.15	3.3	1.61
4.0	1.08	6.6	1.17	5.7	1.32	4.1	1.85
4.9	1.09	7.4	1.17	6.6	1.80	4.8	1.91
5.7	1.08	8.2	1.13	8.2	1.88	5.7	1.97
6.6	1.10	9.0	1.48	10.3	1.97	6.5	2.01
7.4	1.10	10.3	1.70	11.5	2.01	7.3	2.11
8.2	1.10	11.5	1.83			8.1	2.17
9.0	1.10					9.0	2.22
9.9	1.10					9.9	2.26
						10.7	2.30

PU10		PU10+0.27%		PU10+0.44%		PU10+0.82%	
u_g (cm/s)	BER (-)	u_g (cm/s)	BER (-)	u_g (cm/s)	BER (-)	u_g (cm/s)	BER (-)
0.0	1.00	0.0	1.00	0.0	1.00	0.0	1.00
1.0	1.16	1.6	1.03	1.6	1.06	1.2	1.07
1.6	1.17	2.5	1.06	2.5	1.29	2.1	1.26
2.6	1.16	2.9	1.06	3.7	1.68	2.9	1.40
3.4	1.14	3.7	1.15	4.5	1.74	3.7	1.69
4.1	1.11	4.5	1.58	5.3	1.81	4.5	1.77
5.1	1.14	5.3	1.76	6.6	2.00	5.8	1.83
5.8	1.14	6.2	1.82	7.4	2.10	7.0	1.91
6.6	1.14	7.0	1.88	8.6	2.29	8.2	1.94
7.4	1.14	7.8	2.06				
8.2	1.17	8.6	2.12				
		9.5	2.15				

PU18		PU18+0.27%		PU18+0.44%		PU18+0.82%	
u_g (cm/s)	BER (-)	u_g (cm/s)	BER (-)	u_g (cm/s)	BER (-)	u_g (cm/s)	BER (-)
0.0	1.00	0.0	1.00	0.0	1.00	0.0	1.00
0.6	1.09	1.6	1.10	0.9	1.11	0.8	1.05
1.1	1.09	2.8	1.14	2.6	1.35	1.6	1.16
1.6	1.12	3.5	1.14	4.1	1.70	2.5	1.24
2.5	1.14	4.4	1.34	4.7	1.74	3.3	1.42
3.5	1.15	5.5	1.48	6.2	1.81	4.1	1.51
4.4	1.17	6.2	1.55	7.0	1.81	4.9	1.56
5.1	1.17	6.8	1.62	8.2	1.89	5.8	1.63
5.5	1.17			9.9	2.00	6.4	1.67
6.6	1.17						

PU36		PU36+0.27%		PU36+0.44%		PU36+0.82%	
u_g (cm/s)	BER (-)	u_g (cm/s)	BER (-)	u_g (cm/s)	BER (-)	u_g (cm/s)	BER (-)
0.0	1.00	0.0	1.00	0.0	1.00	0.0	1.00
0.4	1.10	1.2	1.16	1.6	1.29	1.2	1.12
1.2	1.10	2.1	1.37	2.9	1.50	2.1	1.18
2.0	1.10	2.9	1.47	3.7	1.58	2.9	1.29
2.8	1.17	3.7	1.58	4.9	1.73	4.1	1.47
3.6	1.17	4.5	1.63	5.8	1.81	4.9	1.59
4.5	1.17	5.3	1.74	6.6	1.85	5.8	1.65
5.1	1.21	6.6	1.79	7.4	1.88	6.6	1.76
5.8	1.21	8.2	1.84	8.2	1.92	7.4	1.76
6.6	1.21			9.9	2.04	8.2	1.82
7.4	1.24						
8.2	1.24						

GB39		GB39+0.82%		PU105		PU105+0.44%	
u_g (cm/s)	BER (-)	u_g (cm/s)	BER (-)	u_g (cm/s)	BER (-)	u_g (cm/s)	BER (-)
9.8	1.28	9.9	1.31	9.9	1.29	9.9	1.48
9.0	1.24	9.0	1.31	8.2	1.26	9.0	1.44
8.2	1.21	8.2	1.28	7.4	1.25	8.2	1.36
7.4	1.18	7.4	1.24	6.6	1.25	7.0	1.32
6.6	1.15	6.6	1.21	5.7	1.24	6.2	1.24
5.7	1.12	5.7	1.19	4.9	1.19	4.9	1.16
4.9	1.11	4.9	1.16	4.1	1.18	4.1	1.16
4.1	1.11	4.1	1.13	3.3	1.14	3.3	1.12
3.3	1.11	3.3	1.10	2.5	1.14	2.5	1.12
2.5	1.10	2.5	1.08	1.6	1.14	1.6	1.12
1.6	1.08	1.7	1.06	0	1.00	0	1.00
0.8	1.05	1.1	1.04				
0.4	1.01	0.5	1.01				
0	1.00	0.0	1.00				

Bed voidage

GB10+0.82%		PU10+0.44%		PU18+0.44%		PU36+0.44%	
u_g (cm/s)	ε_b (-)	u_g (cm/s)	ε_b (-)	u_g (cm/s)	ε_b (-)	u_g (cm/s)	ε_b (-)
0.0	0.63	0.0	0.53	0.0	0.46	0.0	0.43
0.6	0.66	1.6	0.56	0.9	0.51	1.6	0.56
1.4	0.74	2.5	0.64	2.6	0.60	2.9	0.62
2.0	0.76	3.7	0.72	4.1	0.68	3.7	0.64
2.7	0.77	4.5	0.73	4.7	0.69	4.9	0.67
3.3	0.80	5.3	0.74	6.2	0.70	5.8	0.68
3.9	0.81	6.6	0.77	7.0	0.70	6.6	0.69
4.7	0.81	7.4	0.78	8.2	0.71	7.4	0.70
5.3	0.82	8.6	0.79	9.9	0.73	8.2	0.70
5.9	0.82					9.9	0.72
6.6	0.83						
7.3	0.83						
8.0	0.84						
8.7	0.84						
9.7	0.85						

GB39+0.82%		PU105+0.44%	
u_g (cm/s)	ε_b (-)	u_g (cm/s)	ε_b (-)
0.0	0.49	0.0	0.40
0.3	0.51	1.6	0.46
0.7	0.51	2.5	0.46
1.3	0.53	3.3	0.46
2.0	0.54	4.1	0.48
2.7	0.54	4.9	0.48
3.3	0.55	6.2	0.52
4.1	0.56	7.0	0.55
4.7	0.57	8.2	0.56
5.3	0.59	9.0	0.58
6.0	0.60	9.9	0.59
6.7	0.60		
7.3	0.60		
7.9	0.61		

Raw data for chapter 4

Bed collapse test ($H_0 = 15cm$)

GB10+0.27%				GB10+0.44%				GB10+0.82%			
u_g (cm/s)	H_t (cm)	H_d (cm)	ε_d (-)	u_g (cm/s)	H_t (cm)	H_d (cm)	ε_d (-)	u_g (cm/s)	H_t (cm)	H_d (cm)	ε_d (-)
12.5	26.0	21.8	0.75	11.5	29.7	25.9	0.79	11.5	30.8	26.8	0.79
11.5	24.3	20.2	0.73	10.3	23.7	19.3	0.71	10.3	31.8	28.3	0.80
10.3	25.8	21.3	0.74	9.4	21.3	19.2	0.71	8.2	27.7	25.0	0.78
9.4	16.9	16.6	0.67	8.2	21.6	20.0	0.72	7.4	27.6	26.0	0.79
8.2	16.6	16.0	0.67	7.4	16.8	16.0	0.63	6.2	26.9	24.7	0.77
								4.9	17.3	16.9	0.67

PU10+0.27%				PU10+0.44%				PU10+0.82%			
u_g (cm/s)	H_t (cm)	H_d (cm)	ε_d (-)	u_g (cm/s)	H_t (cm)	H_d (cm)	ε_d (-)	u_g (cm/s)	H_t (cm)	H_d (cm)	ε_d (-)
11.5	37.7	28.3	0.75	11.5	42.8	31.3	0.77	11.5	41.5	31.5	0.78
10.3	33.6	26.5	0.73	10.3	40.0	32.3	0.78	10.3	36.2	28.5	0.75
8.2	27.6	22.4	0.69	8.2	36.1	28.7	0.75	8.2	34.9	27.9	0.75
7.4	25.0	20.2	0.65	7.4	35.1	28.7	0.75	7.4	33.9	26.1	0.73
6.2	24.8	19.3	0.63	6.2	33.4	28.3	0.75	6.2	31.6	27.1	0.74
4.9	21.9	17.7	0.60	4.9	31.5	27.2	0.74	4.9	22.4	20.4	0.65
4.1	20.0	18.4	0.62	4.1	28.7	26.1	0.73	3.3	15.1	15.1	0.53
				3.3	21.9	20.3	0.65				
				2.5	16.1	15.5	0.55				

PU18+0.27%				PU18+0.44%				PU18+0.82%			
u_g (cm/s)	H_t (cm)	H_d (cm)	ε_d (-)	u_g (cm/s)	H_t (cm)	H_d (cm)	ε_d (-)	u_g (cm/s)	H_t (cm)	H_d (cm)	ε_d (-)
11.5	33.8	25.5	0.68	11.5	33.6	25.4	0.68	11.5	34.4	25.7	0.69
10.3	31.8	25.1	0.68	10.3	32.4	25.4	0.68	10.3	34.5	26.6	0.70
8.2	30.7	24.7	0.67	8.2	30.9	24.9	0.67	8.2	28.7	23.2	0.65
7.4	27.6	23.4	0.65	7.4	30.4	24.4	0.67	7.4	28.7	23.8	0.66
6.2	25.5	22.0	0.63	6.2	28.4	24.0	0.66	6.2	27.0	22.6	0.64
4.9	24.3	20.4	0.60	4.9	23.7	20.4	0.60	4.9	23.2	20.7	0.61
4.1	21.7	19.1	0.58	2.5	15	15	0.46	4.1	22.7	21.0	0.61
3.3	15	15	0.46					3.3	18.3	16.5	0.51
								2.5	15	15	0.46

PU36+0.27%				PU36+0.44%				PU36+0.82%			
u_g	H_t	H_d	ε_d	u_g	H_t	H_d	ε_d	u_g	H_t	H_d	ε_d
(cm/s)	(cm)	(cm)	(-)	(cm/s)	(cm)	(cm)	(-)	(cm/s)	(cm)	(cm)	(-)
11.5	30.5	20.7	0.59	11.5	31.4	22.4	0.62	11.5	35.5	22.4	0.62
10.3	28.9	20.9	0.59	10.3	29.2	22.1	0.61	10.3	32.5	22.0	0.61
8.2	26.4	19.9	0.57	8.2	27.6	21.7	0.61	8.2	29.6	21.2	0.60
7.4	26.4	20.5	0.58	7.4	26.5	21.4	0.60	7.4	28.6	22.0	0.61
6.2	27.8	19.9	0.57	6.2	25.4	21.0	0.59	6.2	26.7	21.0	0.59
4.9	24.0	19.9	0.57	4.9	23.8	20.6	0.58	4.9	24.7	20.8	0.59
4.1	21.5	17.9	0.52	4.1	23.2	20.8	0.59	4.1	23.8	20.1	0.57
3.3	20.7	19.1	0.55	3.3	22.1	20.6	0.58	3.3	21.8	19.5	0.56
2.5	19.1	17.9	0.52	2.5	21.0	19.9	0.57	2.5	18.9	17.9	0.52
0.41	15	15	0.43	0.41	15	15	0.43	0.41	15	15	0.43

FCC8.5+0.27%				FCC8.5+0.44%				FCC8.5+0.82%			
u_g	H_t	H_d	ε_d	u_g	H_t	H_d	ε_d	u_g	H_t	H_d	ε_d
(cm/s)	(cm)	(cm)	(-)	(cm/s)	(cm)	(cm)	(-)	(cm/s)	(cm)	(cm)	(-)
13	32.2	24.0	0.82	13	32.8	27.1	0.84	13	29.7	26.1	0.83
11.5	28.2	21.5	0.80	11.5	31.6	25.3	0.83	11.5	29.0	26.4	0.84
9.8	26.5	19.0	0.77	9.8	28.5	24.6	0.82	9.8	28.2	26.4	0.84
8.2	15	15	0.71	8.2	15.1	15.1	0.71	8.2	25.4	23.4	0.81
								6.6	15.1	15	0.71

FCC76				PU90			
u_g	H_t	H_d	ε_d	u_g	H_t	H_d	ε_d
(cm/s)	(cm)	(cm)	(-)	(cm/s)	(cm)	(cm)	(-)
12.3	21.2	19.4	0.61	9.8	20.4	15.5	0.44
10.7	21.4	19.2	0.60	8.2	20.7	16.1	0.46
9	21.0	19.2	0.60	6.6	16.2	15.1	0.42
7.4	20.9	19.4	0.61	4.9	16.1	15.1	0.42
5.8	20.8	19.2	0.60	0	15	15	0.42
4.1	20.7	20.1	0.62				
2.5	21.4	20.8	0.63				
1.2	22.6	22.2	0.66				
0	15	15	0.49				

Raw data for chapter 5

Normalized pressure drop across the whole bed

GB10+0.82%									
Ar		Air		N$_2$		He		H$_2$	
u$_g$ (cm/s)	ΔP (-)	u$_g$ (cm/s)	ΔP (-)	u$_g$ (cm/s)	ΔP (-)	u$_g$ (cm/s)	ΔP (-)	u$_g$ (cm/s)	ΔP (-)
7.1	0.86	9.5	0.89	11.7	0.83	11.4	1.00	15.6	0.78
6.5	0.87	8.3	0.89	10.1	0.84	10.2	0.98	13.0	0.66
5.5	0.86	7.6	0.89	9.0	0.79	8.1	0.95	10.4	0.78
4.8	0.86	6.4	0.87	7.8	0.75	6.9	0.91	9.1	070
3.9	0.84	5.7	0.86	6.6	0.74	6.1	0.89	7.8	0.66
3.2	0.80	4.5	0.79	5.8	0.70	5.3	0.81	6.5	0.58
2.6	0.44	3.8	0.67	4.7	0.58	4.5	0.62	5.2	0.55
1.6	0.34	3.0	0.39	3.9	0.36	4.1	0.59	3.2	0.58
1.0	0.08	1.9	0.19	2.7	0.04	3.3	0.47	1.9	0.08
0	0.00	1.1	0.07	1.9	0.02	2.4	0.14	0	0.00
		0	0.00	0	0.00	1.6	0.09		
						0	0.00		

PU17+0.82%							
Ar		Air		He		H$_2$	
u$_g$ (cm/s)	ΔP (-)	u$_g$ (cm/s)	ΔP (-)	u$_g$ (cm/s)	ΔP (-)	u$_g$ (cm/s)	ΔP (-)
4.7	0.99	5.5	0.96	5.7	0.97	6.8	1.02
4.1	0.99	4.6	0.96	4.9	0.95	5.9	1.01
3.5	0.99	3.7	0.96	4.1	0.96	4.9	1.00
2.8	0.99	2.8	0.97	3.3	0.95	4.1	1.00
2.4	1.00	2.0	0.96	2.4	0.96	3.2	0.99
1.9	1.00	1.5	0.94	1.9	0.95	2.7	0.98
1.6	0.99	1.1	0.93	1.6	0.94	2.2	0.97
1.3	0.97	0.9	0.92	1.3	0.94	1.6	0.96
1.1	0.96	0.7	0.88	1.0	0.89	1.4	0.97
0.9	0.94	0.6	0.79	0.8	0.88	0.9	0.92
0.8	0.93	0	0	0.6	0.88	0.7	0.89
0.6	0.97			0.4	0.82	0	0.00
0.5	0.72			0	0.00		
0	0.00						

PU22+0.82%							
Ar		Air		He		H$_2$	
u$_g$ (cm/s)	ΔP (-)	u$_g$ (cm/s)	ΔP (-)	u$_g$ (cm/s)	ΔP (-)	u$_g$ (cm/s)	ΔP (-)
4.7	0.97	5.5	0.99	5.7	0.99	6.8	0.89
4.1	0.97	4.6	0.98	4.9	0.99	5.7	0.92
3.5	0.97	3.7	0.99	4.1	0.98	4.6	0.94
2.8	0.98	2.8	0.99	3.3	0.98	3.5	0.94
2.4	0.97	2.0	0.99	2.6	0.97	2.7	0.95
1.9	0.98	1.5	0.99	2.0	0.97	1.9	0.98
1.6	0.97	1.1	0.98	1.5	0.98	1.4	0.98
1.3	0.98	0.9	0.97	1.1	0.99	0.9	0.93
0.9	0.97	0.7	0.95	0.9	0.98	0.7	0.91
0.8	0.96	0.5	0.85	0.8	0.98	0	0
0.6	0.93	0	0	0.6	0.95		
0.5	0.88			0	0		
0	0						

Minimum fluidization velocity and BER at 10cm/s

PU17								
	Ar		Air		He		H$_2$	
Nano%	u$_{mf}$ (cm/s)	BER (-)	u$_{mf}$ (cm/s)	BER (-)	u$_{mf}$ (cm/s)	BER (-)	u$_{mf}$ (cm/s)	BER (-)
0.27	0.70	2.60	0.80	2.35	0.75	2.20	0.85	1.63
0.44	0.60	2.74	0.80	2.50	0.65	2.30	0.70	1.64
0.82	0.60	2.63	0.65	2.45	0.50	2.36	0.70	1.81
PU22								
	Ar		Air		He		H$_2$	
Nano%	u$_{mf}$ (cm/s)	BER (-)	u$_{mf}$ (cm/s)	BER (-)	u$_{mf}$ (cm/s)	BER (-)	u$_{mf}$ (cm/s)	BER (-)
0.27	0.90	2.3	1.10	2.23	1.05	2.08	1.00	1.59
0.44	0.50	2.64	0.80	2.30	0.60	2.26	0.85	1.72
0.82	0.50	2.7	0.60	2.40	0.55	2.35	0.70	1.82

Bed expansion ratio

GB10+0.82%									
Ar		Air		N$_2$		He		H$_2$	
u$_g$ (cm/s)	BER (-)	u$_g$ (cm/s)	BER (-)	u$_g$ (cm/s)	BER (-)	u$_g$ (cm/s)	BER (-)	u$_g$ (cm/s)	BER (-)
0	1.00	0	1.00	0	1.00	0	1.00	0	1.00
0.9	1.04	1.1	1.00	1.2	1.02	2.0	1.14	3.2	1.05
1.6	1.17	1.9	1.02	1.9	1.02	3.2	1.24	5.2	1.05
2.6	1.48	3.0	1.28	3.1	1.07	4.1	1.33	6.5	1.05
3.2	1.52	4.2	1.41	3.9	1.22	5.3	1.52	8.4	1.19
4.2	1.74	5.7	1.64	4.7	1.38	6.1	1.57	9.7	1.28
4.8	1.78	6.8	1.73	5.8	1.53	7.3	1.67	11.7	1.33
5.8	1.83	7.9	1.81	7.0	1.58	8.1	1.71	13.0	1.38
6.8	1.87	9.5	1.90	7.8	1.63	9.8	1.76		
8.1	1.91	11.3	1.99	8.5	1.68	11.0	1.81		
9.7	2.00			9.7	1.73	12.2	1.85		
				10.9	1.78				
				11.7	1.84				

PU17+0.82%							
Ar		Air		He		H$_2$	
u$_g$ (cm/s)	BER (-)	u$_g$ (cm/s)	BER (-)	u$_g$ (cm/s)	BER (-)	u$_g$ (cm/s)	BER (-)
0	1.00	0	1.00	0	1.00	0	1.00
1.0	1.76	1.1	1.86	1.2	1.44	2.0	1.43
1.9	2.19	2.3	2.04	2.0	2.01	2.6	1.58
2.9	2.32	3.8	2.17	2.8	2.18	3.9	1.65
3.9	2.38	5.3	2.27	4.1	2.21	5.2	1.68
4.8	2.42	6.8	2.35	5.7	2.25	6.5	1.69
5.8	2.46	8.3	2.39	7.3	2.28	7.8	1.72
6.7	2.54	9.8	2.45	9.8	2.37	9.1	1.74
7.7	2.59	11.4	2.58	12.2	2.54	10.4	1.77
8.7	2.63					11.7	1.80
9.7	2.77					13.0	1.85

PU22+0.82%							
Ar		Air		He		H_2	
u_g (cm/s)	BER (-)	u_g (cm/s)	BER (-)	u_g (cm/s)	BER (-)	u_g (cm/s)	BER (-)
0	1.00	0	1	0	1.00	0	1.00
1.0	2.02	1.1	1.89	1.2	1.57	2.0	1.66
1.9	2.12	2.3	1.93	2.4	1.82	3.9	1.69
3.2	2.18	3.8	1.97	4.1	1.91	5.8	1.72
4.5	2.27	5.3	2.04	5.7	1.99	7.8	1.75
5.8	2.41	6.8	2.13	7.3	2.09	9.7	1.82
7.1	2.47	8.3	2.27	9.0	2.24	11.7	1.89
8.4	2.56	9.8	2.40	10.6	2.36	13.0	1.96
9.7	2.70	11.3	2.51	12.2	2.51		

Bed collapse test at 8.14cm/s (H_0=10cm)

	PU17+0.27%			PU17+0.44%			PU17+0.82%		
Gas	H_t (cm)	H_d (cm)	ε_d (-)	H_t (cm)	H_d (cm)	ε_d (-)	H_t (cm)	H_d (cm)	ε_d (-)
Ar	25	20.1	0.68	26	20.8	0.69	25.6	19.6	0.67
Air	22.5	18.0	0.64	23.6	18.2	0.65	22.7	18.4	0.65
He	20.0	17.2	0.63	20.8	17.2	0.63	22.6	18.4	0.65
H_2	15.6	13.5	0.53	16	14.0	0.54	16.4	14.2	0.55

	PU22+0.27%			PU22+0.44%			PU22+0.82%		
Gas	H_t (cm)	H_d (cm)	ε_d (-)	H_t (cm)	H_d (cm)	ε_d (-)	H_t (cm)	H_d (cm)	ε_d (-)
Ar	21.5	15.7	0.61	24.0	18.0	0.66	26.7	20.0	0.70
Air	20.1	15.8	0.61	21.8	16.4	0.63	22.7	17.7	0.66
He	19.5	14.4	0.58	21.0	17.2	0.65	22.0	16.7	0.63
H_2	15.5	12.5	0.51	15.9	13.2	0.54	16.7	13.5	0.55

GB10+0.82%			
Gas	H_t (cm)	H_d (cm)	ε_d (-)
Ar	18.3	16.8	0.78
Air	18.3	16.4	0.77
N_2	17.0	15.7	0.76
He	15.7	14.8	0.75
H_2	13.0	12.2	0.70

Mixed gases as the fluidizing gas (PU22+0.82%)

Mixed gas-1		Mixed gas-2		He	
u_g (cm/s)	BER (-)	u_g (cm/s)	BER (-)	u_g (cm/s)	BER (-)
0	1.00	0	1.00	0	1.00
1.3	1.67	0.7	1.11	1.2	1.57
2.7	1.70	1.4	1.74	2.4	1.82
4.7	1.76	2.7	1.85	4.1	1.91
6.7	1.82	4.0	1.97	5.7	1.99
9.3	1.91	5.4	2.08	7.3	2.09
12.0	2.01	6.7	2.18	9.0	2.24
13.3	2.09	8.0	2.31	10.6	2.36
		10.1	2.38	12.2	2.51

Bed collapse test at 8.14 cm/s (H_0=10cm)

Gas	H_t (cm)	H_d (cm)	ε_d (-)
Mixed gas-1	18.0	13.6	0.55
Mixed gas-2	22.1	17.4	0.65
He	22.0	16.4	0.63

Raw data for chapter 6

Bubble diameter distribution along the bed height at u_g-u_{mf} = 12 cm/s (H_0=26cm)

FCC8.5+			
Height (cm)	D10 (cm)	D50 (cm)	D90 (cm)
7.5	0.74	1.52	2.59
14.8	0.87	1.59	2.73
25.2	0.70	1.51	2.05
34.6	0.77	1.74	2.47
44.9	0.69	1.48	2.21
53.2	0.60	2.02	2.30
63.0	0.65	1.04	1.39

GB10+			
Height (cm)	D10 (cm)	D50 (cm)	D90 (cm)
43.5	0.81	1.65	3.29
38.3	0.76	2.06	4.31
32.4	0.85	1.58	2.59
26.7	0.76	1.23	2.28
20.0	0.61	1.02	1.52
15.0	0.66	1.14	2.15
10.2	0.70	1.45	1.79

FCC76			
Height (cm)	D10 (cm)	D50 (cm)	D90 (cm)
8.4	0.58	0.78	1.42
12.5	0.71	2.11	2.26
17.6	1.02	2.22	3.63
22.9	0.96	2.91	4.68
27.6	1.18	3.45	4.92
31.0	0.82	1.85	2.99

D50 vs. u_g-u_{mf}

u_g-u_{mf} (cm/s)	FCC8.5+	GB10+	FCC76
25.0			4.17
21.5			3.30
18.5			3.52
15.5	1.58	1.44	2.99
12.0	1.60	1.64	2.68
9.0	1.30	1.70	2.10
6.0	1.37	1.95	1.84

u_g-u_{mf} (cm/s)	FCC8.5+			GB10+			FCC76		
	Top	Middle	Bottom	Top	Middle	Bottom	Top	Middle	Bottom
25.0							6.95	4.70	2.43
21.5							5.57	5.60	2.40
18.5							4.42	4.21	2.50
15.5	2.84	3.24	2.80	2.21	2.20	1.90	4.90	3.80	1.50
12.0	2.08	2.34	2.71	3.85	2.28	1.88	3.80	2.50	0.85
9.0	1.63	2.47	1.62	2.91	2.83	1.64	3.40	2.73	1.10
6.0	2.74	1.80	2.02	3.56	3.10	1.20	6.95	4.70	2.43

Bubble rise velocity (H_0=26cm)

FCC8.5+							
u_g-u_{mf} =6.0cm/s		u_g-u_{mf} =9.0cm/s		u_g-u_{mf} =12.0cm/s		u_g-u_{mf} =15.5cm/s	
Height (cm)	u_b (m/s)	Height (cm)	u_b (m/s)	Height (cm)	u_b (m/s)	Height (cm)	u_b (m/s)
17.5	0.33	6.1	0.21	9.2	0.34	8.1	0.38
25.9	0.24	17.6	0.28	16.22	0.35	18.2	0.51
34.1	0.29	33.6	0.30	32.2	0.28	34.0	0.60
		44.2	0.27	45.8	0.33	50.0	0.47

GB10+							
u_g-u_{mf} =6.0cm/s		u_g-u_{mf} =9.0cm/s		u_g-u_{mf} =12.0cm/s		u_g-u_{mf} =15.5cm/s	
Height (cm)	u_b (m/s)	Height (cm)	u_b (m/s)	Height (cm)	u_b (m/s)	Height (cm)	u_b (m/s)
9.6	0.28	8.0	0.29	10.5	0.23	19.1	0.26
18.9	0.37	20.6	0.38	19.5	0.39	34.5	0.39
31.7	0.54	32.4	0.46	32.7	0.44	45.1	0.38
		41.3	0.37	42.8	0.43		

u$_g$-u$_{mf}$ =15.5cm/s					
FCC8.5+		GB10+		FCC76	
Height (cm)	u$_b$ (m/s)	Height (cm)	u$_b$ (m/s)	Height (cm)	u$_b$ (m/s)
8.1	0.38	19.1	0.26	15.9	0.50
18.2	0.51	34.5	0.39	22.6	0.60
34.0	0.60	45.1	0.38	28.8	0.47
50.0	0.47				

u$_g$-u$_{mf}$ =9.0cm/s					
FCC8.5+		GB10+		FCC76	
Height (cm)	u$_b$ (m/s)	Height (cm)	u$_b$ (m/s)	Height (cm)	u$_b$ (m/s)
6.1	0.21	8.0	0.29	11.7	0.28
17.6	0.28	20.5	0.38	15.6	0.35
33.6	0.30	32.4	0.46	22.4	0.39
44.2	0.27	41.3	0.37	27.6	0.43

u$_g$-u$_{mf}$ =15.5cm/s					
FCC8.5+		GB10+		FCC76	
d$_b$ (cm)	u$_b$ (m/s)	d$_b$ (cm)	u$_b$ (m/s)	d$_b$ (cm)	u$_b$ (m/s)
0.72	0.29	0.84	0.22	0.79	0.24
0.88	0.29	1.28	0.32	1.25	0.25
1.13	0.45	1.72	0.34	1.79	0.36
1.39	0.49	2.23	0.50	2.24	0.58
1.61	0.49	2.80	0.49	2.77	0.48
1.82	0.50	3.68	0.53	3.22	0.67
2.05	0.48			3.75	0.63
2.38	0.59			4.30	0.62
				4.69	0.65
				5.03	0.72
				6.23	0.52
u$_g$-u$_{mf}$ =12.0cm/s					
FCC8.5+		GB10+		FCC76	
d$_b$ (cm)	u$_b$ (m/s)	d$_b$ (cm)	u$_b$ (m/s)	d$_b$ (cm)	u$_b$ (m/s)
0.97	0.25	1.36	0.32	1.27	0.45
1.30	0.22	1.73	0.37	1.72	0.47
1.68	0.38	2.25	0.43	2.17	0.45
2.22	0.34	2.76	0.63	2.87	0.51
2.82	0.59	3.20	0.53	3.68	0.55
4.60	0.61	3.77	0.62	4.13	0.54
				5.25	0.78

u $_g$-u$_{mf}$ =9.0cm/s					
FCC8.5+		GB10+		FCC76	
d$_b$ (cm)	u$_b$ (m/s)	d$_b$ (cm)	u$_b$ (m/s)	d$_b$ (cm)	u$_b$ (m/s)
0.86	0.15	0.82	0.20	0.90	0.32
1.27	0.25	1.29	0.35	1.25	0.42
1.67	0.29	1.70	0.41	1.70	0.24
2.21	0.26	2.21	0.49	2.17	0.36
2.76	0.34	2.65	0.42	2.71	0.33
3.79	0.52	3.25	0.59	3.33	0.49
		3.91	0.62	3.64	0.59
u $_g$-u$_{mf}$ =6.0cm/s					
FCC8.5+		GB10+		FCC76	
d$_b$ (cm)	u$_b$ (m/s)	d$_b$ (cm)	u$_b$ (m/s)	d$_b$ (cm)	u$_b$ (m/s)
0.84	0.20	0.81	0.21	1.31	0.20
1.24	0.22	1.25	0.34	1.76	0.31
1.77	0.31	1.77	0.44	2.20	0.37
2.25	0.31	2.28	0.52	2.75	0.31
2.60	0.35	2.76	0.53	4.15	0.49
3.33	0.39	3.22	0.61		
		3.59	0.64		

Raw data for chapter 7

Bubble rise velocity vs. bed height (H₀=26cm)

FCC8.5+							
u g-umf =6.0cm/s		u g-umf =9.0cm/s		u g-umf =12.0cm/s		u g-umf =15.5cm/s	
Height (cm)	u_b (m/s)	Height (cm)	u_b (m/s)	Height (cm)	u_b (m/s)	Height (cm)	u_b (m/s)
17.5	0.33	6.1	0.21	9.2	0.34	8.1	0.38
25.9	0.24	17.6	0.28	16.22	0.35	18.2	0.51
34.1	0.29	33.6	0.30	32.2	0.28	34.0	0.60
		44.2	0.27	45.8	0.33	50.0	0.47
GB10+							
u g-umf =6.0cm/s		u g-umf =9.0cm/s		u g-umf =12.0cm/s		u g-umf =15.5cm/s	
Height (cm)	u_b (m/s)	Height (cm)	u_b (m/s)	Height (cm)	u_b (m/s)	Height (cm)	u_b (m/s)
9.6	0.28	8.0	0.29	10.5	0.23	19.1	0.26
18.9	0.37	20.6	0.38	19.5	0.39	34.5	0.39
31.7	0.54	32.4	0.46	32.7	0.44	45.1	0.38
		41.3	0.37	42.8	0.43		
FCC76							
u g-umf =6.0cm/s		u g-umf =9.0cm/s		u g-umf =12.0cm/s		u g-umf =15.5cm/s	
Height (cm)	u_b (m/s)	Height (cm)	u_b (m/s)	Height (cm)	u_b (m/s)	Height (cm)	u_b (m/s)
11.1	0.29	11.7	0.28	11.6	0.38	15.9	0.50
16.7	0.32	15.6	0.35	16.8	0.49	22.6	0.60
22.9	0.35	22.4	0.39	23.5	0.53	28.8	0.53
		27.6	0.42	28.9	0.55		

FCC76					
u g-umf =18.5cm/s		u g-umf =21.5cm/s		u g-umf =25.0cm/s	
Height (cm)	u_b (m/s)	Height (cm)	u_b (m/s)	Height (cm)	u_b (m/s)
10.3	0.40	8.5	0.41	9.7	0.49
18.0	0.53	16.6	0.48	16.3	0.56
22.9	0.53	23.0	0.52	23.2	0.66
28.6	0.50	29.3	0.51	29.3	0.57
				33.6	0.52

Bed height distribution (H₀=26cm)

u_g-u_{mf}	FCC8.5+ H_t (cm)	H_d (cm)	ε_d (-)	GB10+ H_t (cm)	H_d (cm)	ε_d (-)	FCC76 H_t (cm)	H_d (cm)	ε_d (-)
6.0	45.5	38	0.80	45	39.5	0.76	29	26.8	0.554
9.0	61	48	0.84	50	42	0.78	31.5	28.2	0.557
12.0	64	50	0.85	51.5	41	0.77	33	27.8	0.554
15.5	70	54	0.86	53.5	42.5	0.78	34	28.6	0.554
18.5							36	28.6	0.541
21.5							37.2	28.8	0.547
25.0							38	28.6	0.524

Y corrector

u_g-u_{mf} (cm/s)	FCC8.5+ Y	GB10+ Y	FCC76 Y
6.0	0.76	0.79	0.71
9.0	0.62	0.64	0.69
12.0	0.59	0.59	0.67
15.5	0.59	0.59	0.74
18.5			0.70
21.5			0.62
25.0			0.64

Raw data for chapter 8

Dense phase voidage vs. gas velocity

FCC8.5+0.27%		FCC8.5+0.44%		FCC8.5+0.82%	
u_d (cm/s)	ε_d (-)	u_d (cm/s)	ε_d (-)	u_d (cm/s)	ε_d (-)
10.1	0.82	9.9	0.84	8.6	0.83
9.7	0.82	9.4	0.83	8.1	0.84
9.2	0.80	8.8	0.82	7.5	0.84
8.6	0.77	8.3	0.74	7.0	0.81
8.0	0.74			6.3	0.73
GB10+0.27%		GB10+0.44%		GB10+0.82%	
u_d (cm/s)	ε_d (-)	u_d (cm/s)	ε_d (-)	u_d (cm/s)	ε_d (-)
10.7	0.75	10.0	0.78	8.2	0.79
10.4	0.73	9.5	0.78	7.8	0.80
10.0	0.74	9.1	0.71	7.0	0.78
9.8	0.66	8.7	0.71	6.7	0.79
		8.4	0.68	6.4	0.67
PU10+0.27%		PU10+0.44%		PU10+0.82%	
u_d (cm/s)	ε_d (-)	u_d (cm/s)	ε_d (-)	u_d (cm/s)	ε_d (-)
8.1	0.76	6.7	0.77	5.5	0.78
7.7	0.75	6.3	0.78	5.1	0.75
7.3	0.73	5.5	0.75	4.4	0.75
6.6	0.68	5.3	0.75	4.1	0.73
6.3	0.65	4.8	0.75	3.7	0.74
5.9	0.63	4.4	0.74	3.2	0.65
5.7	0.60	4.1	0.59	2.3	0.58
PU18+0.27%		PU18+0.44%		PU18+0.82%	
u_d (cm/s)	ε_d (-)	u_d (cm/s)	ε_d (-)	u_d (cm/s)	ε_d (-)
6.5	0.68	5.8	0.68	6.1	0.69
6.1	0.68	5.4	0.68	5.7	0.70
5.3	0.67	4.7	0.67	5.0	0.65
5.1	0.65	4.4	0.67	4.7	0.66
4.6	0.63	4.0	0.66	4.2	0.64
4.2	0.60	3.5	0.60	3.8	0.61
3.9	0.58	2.8	0.51	3.5	0.61
3.8	0.51			3.2	0.51
PU36+0.27%		PU36+0.44%		PU36+0.82%	
u_d (cm/s)	ε_d (-)	u_d (cm/s)	ε_d (-)	u_d (cm/s)	ε_d (-)
4.5	0.59	4.4	0.62	4.6	0.62
4.1	0.59	4.0	0.61	4.2	0.61
3.4	0.57	3.3	0.61	3.5	0.60
3.1	0.58	3.0	0.60	3.2	0.61
2.7	0.57	2.6	0.59	2.7	0.59
2.2	0.57	2.1	0.58	2.3	0.59
2.0	0.52	1.8	0.59	2.0	0.57

1.7	0.55	1.5	0.59	1.7	0.56
1.4	0.52	1.3	0.57	1.5	0.52
0.8	0.47	0.6	0.47	0.9	0.47

n and k_f

Cohesion (kPa)	n (-)	k_f (-)
0.93	0.20	42.0
0.92	0.80	25.0
0.85	0.35	50.0
0.47	1.93	9.0
0.56	0.64	20.9
0.41	0.91	17.5
0.60	1.33	10.0
0.35	0.29	24.0
0.35	2.03	8.0
0.38	0.62	19.0
0.23	1.40	10.7
0.35	0.66	20.0
0.06	4.64	17.4
0.001	3.64	35.0
0.001	3.57	23.8

Raw data for chapter 9

Fluidization behaviors

FCC8.5		FCC8.5+0.27%		FCC8.5+0.44%		FCC8.5+0.82%	
u_g (cm/s)	ΔP (-)	u_g (cm/s)	ΔP (-)	u_g (cm/s)	ΔP (-)	u_g (cm/s)	ΔP (-)
20.0	0.86	19.2	0.81	20.8	0.83	20.8	0.94
16.7	0.80	16.7	0.74	16.7	0.82	16.7	0.91
15.1	0.75	14.3	0.68	15.1	0.83	15.1	0.87
12.7	0.71	12.7	0.70	12.7	0.67	12.7	0.84
10.2	0.67	11.0	0.67	11.0	0.71	11.0	0.84
8.6	0.63	9.0	0.44	8.6	0.20	9.4	0.72
7.0	0.06	7.0	0.05	7.0	0.05	7.8	0.05
4.5	0.04	4.5	0.06	4.5	0.05	6.1	0.03
2.9	0.02	2.9	0.05	2.9	0.02	4.5	0.04
0	0.01	0	0	0	0	2.9	0.02
						0	0

FCC8.5		FCC8.5+0.27%		FCC8.5+0.44%		FCC8.5+0.82%	
u_g (cm/s)	BER (-)	u_g (cm/s)	BER (-)	u_g (cm/s)	BER (-)	u_g (cm/s)	BER (-)
0	1.00	0	1.00	0	1.00	0	1.00
2.9	1.03	2.9	1.01	2.9	1.00	2.9	1.00
4.5	1.03	4.5	1.01	5.3	1.02	4.5	1.04
7.0	1.07	7.0	1.01	7.8	1.04	6.1	1.04
8.6	1.17	8.6	1.01	10.2	1.36	8.6	1.63
11.0	1.62	11.0	1.06	12.7	1.56	10.2	1.67
12.7	1.72	12.7	1.11	15.1	1.68	12.7	1.85
15.1	1.83	14.3	1.76	16.7	1.88	15.1	1.96
16.7	1.93	16.7	1.93	20.8	2.12	16.7	2.22
20.8	2.10	20.8	2.22	24.9	2.44	20.8	2.40
24.9	2.17	24.9	2.37			24.9	2.59

FCC20		FCC20+0.27%		FCC20+0.44%		FCC20+0.82%	
u_g (cm/s)	ΔP (-)	u_g (cm/s)	ΔP (-)	u_g (cm/s)	ΔP (-)	u_g (cm/s)	ΔP (-)
24.9	0.93	24.9	0.96	24.9	1.00	24.9	0.97
20.8	0.85	20.8	0.96	20.8	0.99	20.8	0.96
16.7	0.79	16.7	0.94	16.7	0.80	16.7	0.94
14.3	0.76	14.3	0.92	14.3	0.79	14.3	0.92
12.7	0.76	12.7	0.93	12.7	0.80	12.7	0.95
11.0	0.75	11.0	0.92	11.4	0.81	11.0	0.92
8.6	0.73	8.6	0.90	8.6	0.82	8.6	0.92
6.1	0.72	6.1	0.84	6.1	0.83	6.1	0.78
4.5	0.66	4.5	0.63	4.5	0.62	4.5	0.59
2.9	0.52	2.9	0.57	2.9	0.28	2.9	0.08
0	0	0	0	0	0	0	0

FCC20		FCC20+0.27%		FCC20+0.44%		FCC20+0.82%	
u_g (cm/s)	BER (-)	u_g (cm/s)	BER (-)	u_g (cm/s)	BER (-)	u_g (cm/s)	BER (-)
0	1.00	0	1.00	0	1.00	0	1.00
2.9	1.21	2.9	1.04	2.9	1.24	2.9	1.04
4.5	1.41	4.5	1.32	4.5	1.56	4.5	1.54
6.1	1.58	6.1	1.60	6.1	1.72	6.1	1.75
8.6	1.75	8.6	1.80	8.6	1.84	8.6	1.88
11.0	1.88	11.0	1.94	11.0	1.94	11.0	2.00
12.7	1.97	12.7	2.00	12.7	2.04	12.7	2.08
15.1	2.05	15.1	2.08	15.1	2.12	15.1	2.12
16.7	2.18	16.7	2.12	16.7	2.24	16.7	2.21
20.8	2.35	20.8	2.36	20.8	2.44	20.8	2.45
24.9	2.52	24.9	2.56	24.9	2.68	24.9	2.71

FCC76				FCC76+0.82%			
u_g (cm/s)	ΔP (-)	u_g (cm/s)	BER (-)	u_g (cm/s)	ΔP (-)	u_g (cm/s)	BER (-)
20.8	0.89	0	1.00	24.9	0.74	0	1.00
17.6	0.92	2.9	1.12	20.8	0.76	2.9	1.09
15.1	0.93	4.5	1.14	16.7	0.79	4.5	1.12
13.5	0.95	7.0	1.20	15.1	0.78	6.1	1.15
11.8	0.95	8.6	1.24	12.7	0.80	8.6	1.19
9.4	0.95	10.2	1.27	11.0	0.80	11.0	1.21
7.8	0.96	12.7	1.30	8.6	0.76	12.7	1.22
6.1	0.95	15.1	1.32	6.1	0.75	15.1	1.23
4.5	0.95	16.7	1.32	4.5	0.74	16.7	1.25
2.9	0.95	20.8	1.36	2.9	0.73	20.8	1.27
2.1	0.93	24.9	1.39	2.1	0.65	24.9	1.29
1.2	0.91			1.2	0.66		
1.0	0.91			1.0	0.63		
0	0			0	0		

Nano%	FCC8.5		FCC20		FCC76	
	u_{mf} (cm/s)	ε_b (-)	u_{mf} (cm/s)	ε_b (-)	u_{mf} (cm/s)	ε_b (-)
0	9.0	0.86	6.0	0.86	0.8	0.64
0.27	12.0	0.87	6.0	0.85	--	--
0.44	12.5	0.89	6.5	0.86	--	--
0.82	9.5	0.90	6.5	0.87	1.2	0.58

u_g (cm/s)	FCC8.5	FCC8.5+0.27%	FCC8.5+0.44%	FCC8.5+0.82%
	ε_d (-)	ε_d (-)	ε_d (-)	ε_d (-)
13	0.81	0.75	0.75	0.86
17	0.82	0.82	0.84	0.86
21	0.83	0.84	0.83	0.86
25	0.82	0.84	0.85	0.86
u_g (cm/s)	FCC20	FCC20+0.27%	FCC20+0.44%	FCC20+0.82%
	ε_d (-)	ε_d (-)	ε_d (-)	ε_d (-)
13	0.75	0.77	0.78	0.79
17	0.77	0.77	0.78	0.79
21	0.77	0.77	0.79	0.80
25	0.77	0.80	0.79	0.80
u_g (cm/s)	FCC76			FCC76+0.82%
	ε_d (-)			ε_d (-)
13	0.519			0.524
17	0.532			0.522
21	0.533			0.523
25	0.534			0.524

Reaction conversion

u_g (cm/s)	FCC8.5	FCC8.5+0.27%	FCC8.5+0.44%	FCC8.5+0.82%
	Conversion (%)	Conversion (%)	Conversion (%)	Conversion (%)
13	13.8	21.5	24.3	40.0
17	27.2	32.6	41.5	57.3
21	39.8	43.2	51.3	63.4
25	38.7	46.2	53.6	61.0
u_g (cm/s)	FCC20	FCC20+0.27%	FCC20+0.44%	FCC20+0.82%
	Conversion (%)	Conversion (%)	Conversion (%)	Conversion (%)
13	20.8	26.1	22.2	25.7
17	17.5	25.0	19.9	24.8
21	16.6	26.2	19.7	26.4
25	18.0	26.1	20.5	27.2
u_g (cm/s)	FCC76			FCC76+0.82%
	Conversion (%)			Conversion (%)
13	19.6			23.7
17	19.5			20.7
21	20.7			20.2
25	22.3			20.7

Total contact efficiency ($α_t$)

u_g (cm/s)	FCC8.5	FCC8.5+0.27%	FCC8.5+0.44%	FCC8.5+0.82%
	$α_t$ (%)	$α_t$ (%)	$α_t$ (%)	$α_t$ (%)
13	6.4	9.2	11.6	19.7
17	15.7	18.2	24.7	39.1
21	28.1	30.0	36.4	54.2
25	31.7	37.9	44.8	57.5
u_g (cm/s)	FCC20	FCC20+0.27%	FCC20+0.44%	FCC20+0.82%
	$α_t$ (%)	$α_t$ (%)	$α_t$ (%)	$α_t$ (%)
13	9.3	11.4	8.6	10.0
17	9.5	13.2	9.5	11.7
21	10.9	16.1	11.1	14.4
25	13.7	18.3	13.2	17.1
u_g (cm/s)	FCC76			FCC76+0.82%
	$α_t$ (%)			$α_t$ (%)
13	12.7			18.2
17	16.0			19.4
21	20.8			22.6
25	27.0			26.6

Contact efficiency due to A_p (α_p)

u_g (cm/s)	FCC8.5	FCC8.5+0.27%	FCC8.5+0.44%	FCC8.5+0.82%
	α_p (%)	α_p (%)	α_p (%)	α_p (%)
13	6.4	9.2	11.6	19.7
17	15.6	18.2	24.7	39.1
21	28.1	30.0	36.4	54.2
25	31.7	37.9	44.8	57.5
u_g (cm/s)	FCC20	FCC20+0.27%	FCC20+0.44%	FCC20+0.82%
	α_p (%)	α_p (%)	α_p (%)	α_p (%)
13	9.3	11.4	8.6	10.0
17	9.5	13.2	9.5	11.7
21	10.9	16.1	11.1	14.4
25	13.7	18.3	13.2	17.1
u_g (cm/s)	FCC76			FCC76+0.82%
	α_p (%)			α_p (%)
13	12.7			18.2
17	16.0			19.4
21	20.8			22.6
25	27.0			26.6

Contact efficiency due to τ (α_f)

u_g (cm/s)	FCC8.5	FCC8.5+0.27%	FCC8.5+0.44%	FCC8.5+0.82%
	α_f (%)	α_f (%)	α_f (%)	α_f (%)
13	4.6	8.7	8.9	18.1
17	15.0	20.0	27.3	43.2
21	32.6	37.6	49.8	66.0
25	38.0	50.3	64.6	76.5
u_g (cm/s)	FCC20	FCC20+0.27%	FCC20+0.44%	FCC20+0.82%
	α_f (%)	α_f (%)	α_f (%)	α_f (%)
13	7.5	10.3	9.4	11.4
17	8.6	13.9	11.4	15.1
21	10.2	19.2	14.4	21.2
25	13.7	23.5	18.5	26.9
u_g (cm/s)	FCC76			FCC76+0.82%
	α_f (%)			α_f (%)
13	3.0			1.2
17	4.3			2.4
21	6.1			3.6
25	7.9			5.4

Appendix G: Other related publications

1. Han M, **Zhou Y**, Zhu J*. Improvement on flowability and fluidization of group C particles after nanoparticle modification. **Powder Technology**. 2020; 365:208-14.

2. Zhang Y, **Zhou Y**, Liu J, Shao Y*, Zhu J*. Performance Enhancement of Fluidized Bed Catalytic Reactors by Going to Finer Particles. **Industrial & Engineering Chemistry Research**. 2019;58(43):20173-8.

3. Zhang X, **Zhou Y**, Zhu J*. Enhanced Fluidization of Group A Particles Modulated by Group C Powder. **Powder Technology (under review)**. 2020

4. Du H, **Zhou Y**, Zhao D, Shao Y, Zhu J*. Fluidization Stability vs Powder History of Geldart Group C$^+$ Particles. **A version ready to submit.** 2020

ARTICLE IN PRESS

Contents lists available at ScienceDirect

Powder Technology

Improvement on flowability and fluidization of Group C particles after nanoparticle modification

Mengqi Han, Yandaizi Zhou, Jesse Zhu *

Department of Chemical and Biochemical Engineering, The University of Western Ontario, London, Ontario N6A 3K7, Canada

ARTICLE INFO

ABSTRACT

Group C particles have gradually become more desirable in the industry in recent years because of their special characteristics such as large specific surface area and small size. However, their poor flowability is the biggest challenge in applications. Nanoparticles, as flow additives, could significantly improve flowability of Group C particles. In this project, powder flowability was measured using three different techniques: FT4 test (cohesion), Avalanche angle (AVA) and Angle of repose (AOR). After nanoparticle modification, Group C particles present much smaller values of cohesion, AVA and AOR, indicating better flowability. In addition, fluidization behaviors such as pressure drop and minimum fluidization velocity were investigated. After nanoparticle modification, Group C particles exhibit good fluidization similar to Group A particles, thus achieving full fluidization with small minimum fluidization velocity.

© 2019 Elsevier B.V. All rights reserved.

1. Introduction

Particles are widely used in many industries, including advanced materials, paints and pigments, foods, cosmetics, ceramics, pharmaceuticals and catalysts, etc. [1–5]. Approximately, >50% of all products in chemical industrials in the world are in the form of particles [6,7]. Generally, the processing of particles involves a wide range of operations such as grinding, mixing, compaction, storage, fluidization and pneumatic transportation. The flowability of particles is related to the efficiency of these processes and can affect the final product quality. Poor flowability will cause a series of problems including the blocking of discharge openings, channeling and agglomeration in fluidization, which brings technological challenges. As a result, powder flowability is an important characteristic and is often required for design and operation of many processes.

Several measuring techniques have been developed to predict powder flowability such as shear test, compression test, angle of repose, avalanching, consolidation test, fluidization test, etc. [8,9]. However, the flow behavior of particles is complicated and relies on their general features such as the intrinsic physical properties including particle size, density and roughness, the bulk properties including size distribution and bulk density, the external conditions and processing environment [8–12]. Since powder flowability is not an inherent characteristic, no single characterization technique is able to completely understand the flow behaviors of particles [8]. The measuring techniques should match the application and the processing environment, which are classified into three groups including dynamic, dynamic-static and static according to the powder state during characterization [8–10]. As a result, different characterization techniques are required to fully understand powder flow behaviors in different operations.

Fluidization is an important and popular operation in processing particles which has many advantages, for instance high mass/heat transfer rate, the flexibility in handling particles and low pressure drop, etc. [13–15]. Apart from powder flowability, fluidization behavior is also critical for industrial applications of particles. According to Geldart's classification for fluidity in a fluidized bed [16], particles are divided into 4 groups of A, B, C and D based on particle size and density. Group A particles are regarded as possessing good fluidization properties without channeling or slugging, which are widely used as catalysts for fluidized bed reactors in the industry. Group B is bubbling particles which exhibit typical characteristics of bubbling fluidization, while Group D is spoutable particles which are much larger and denser. Group C particles are those cohesive particles <20–80 μm depending on particle density. Recently, Group C particles have attracted an increasing interest in industry because of their small particle size, high specific surface area and other specific characteristics. Consequently, Group C particles are favorable in some industries such as powder coating, pharmaceutical processes and production of heterogeneous catalysts, etc. [17–20].

Table 1
Physical properties of experimental particles.

Powder name	Particle size (µm)			Material	Shape	Particle density (kg/m³)	Bulk density (kg/m³)	Geldart type
	D_{10}	D_{50}	D_{90}					
GB10	1.6	10	29	Glass beads	Spherical	2500	916	C
Talc18	4	18	52	Hydrous magnesium silicate	Irregular	2750	713	C
PU22	6	22	59	Polyurethane	Irregular	1200	689	C
GB39	15	39	85	Glass beads	Spherical	2500	1301	A
GB65	30	65	139	Glass beads	Spherical	2500	1254	A

However, Group C particles are not flowable and not fluidizable due to their strong cohesiveness, which limits their applications. It has been accepted that the cohesiveness of Group C particles is attributed to the strong Van der Waals forces which becomes dominant when compared with gravitational and/or hydrodynamic forces [21,22]. Zhu and Zhang [23,24] found that blending flow additives into Group C particles could control their flow properties and developed a series of criteria of choosing flow additives. As flow additives, nanoparticles have been widely used to control the flowability of Group C particles which are suggested to reduce the Van der Waals force by increasing the distance between Group C particles [25–27].

In this study, three nanoparticle concentrations were adopted to investigate the nanoparticle effect on the flow and fluidization of Group C particles. These Group C particles include organic and inorganic
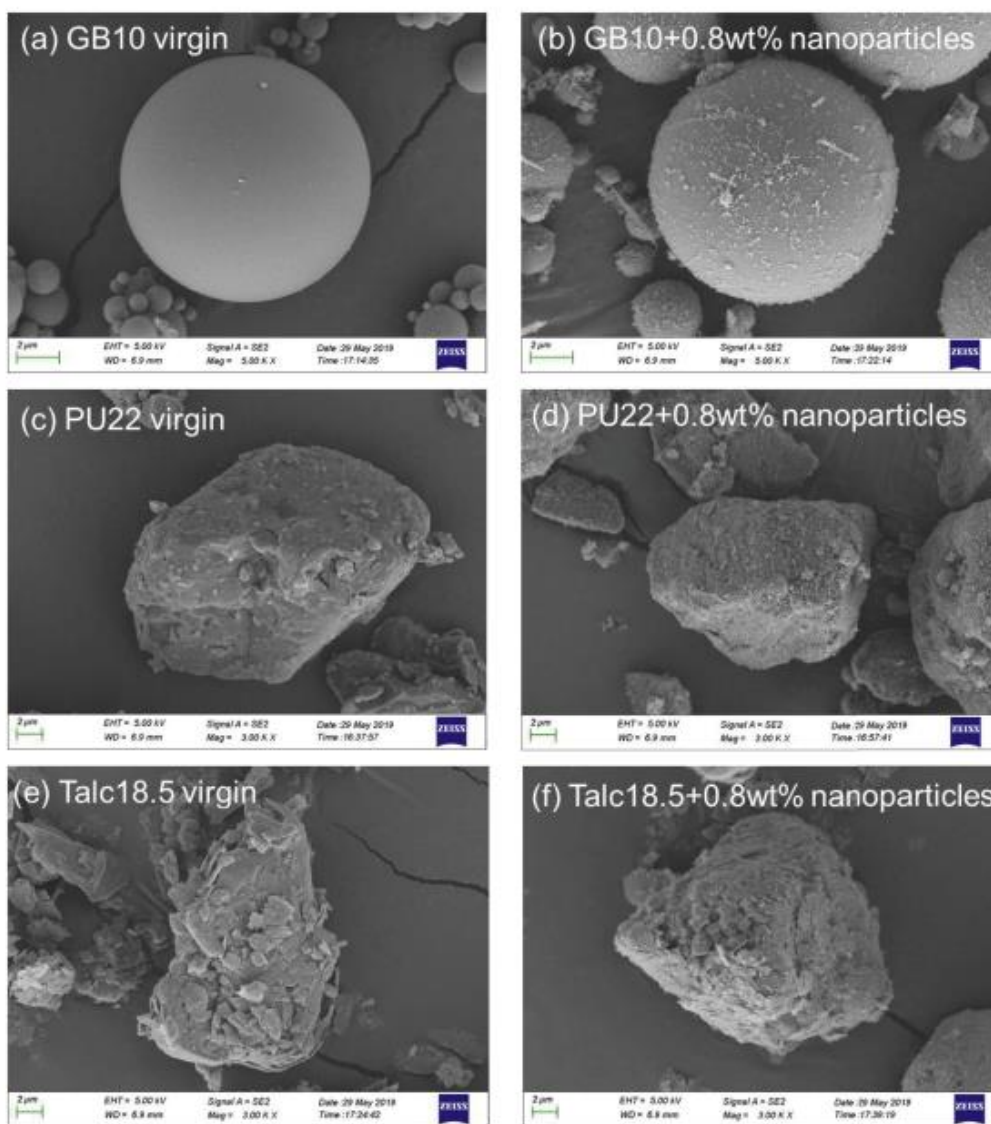

Fig. 1. SEM images of Group C particles before and after nanoparticle modification.

Fig. 2. Cohesion measurement using a FT4 powder Rheometer.

Table 2
Classification of powder flowability by AOR [34].

AOR	Flowability
$25° < \theta < 30°$	Very free-flowing
$30° < \theta < 38°$	Free-flowing
$38° < \theta < 45°$	Fair to passable flow
$45° < \theta < 55°$	Cohesive
$55° < \theta < 70°$	Very cohesive

(18.5 μm) and polyurethane (22 μm), and two Group A particles, which were glass beads with particle size of 39 μm and 65 μm. Glass beads were purchased form Potters Industries Inc., talcum powder was purchased from Powder Technology Inc. and polyurethane powder was manufactured by our research group. Their properties are listed in Table 1. Nanoparticles of SiO_2 (R972 by Evonik) with a spherical shape and a reported diameter of 16 nm are used as guest particles. In the experiments, three mass percentages of nanoparticles, that were 0.5%, 0.8% and 1.5%, were blended into the host particles by sieving method as described in a published patent by Zhu and Zhang [24]. The powder samples were sieved twice by using an ultrasonic vibrating screen with mesh of 325.

Scanning electron microscopy (S-2600 N Scanning Electron Microscope, Hitachi Ltd., JP) was applied to observe the surface morphology of the host particles before and after nanoparticle modification, as shown in Fig. 1. Clearly, the surfaces of Group C particles are rougher after nanoparticle modification. Nanoparticles adhered on Group C particle surface as asperities [25].

2.2. Experimental methods

Flowability of powder samples was characterized by cohesion test (FT4), angle of repose (AOR) and avalanche angle (AVA). A fluidized bed was used to evaluate the fluidization behaviors of powder samples, including pressure drop and minimum fluidization velocity.

2.2.1. Cohesion

The cohesion was tested by a FT4 Powder Rheometer manufactured by Freeman Technology, representing powder flowability under static state. A schematic of cohesion measurement is illustrated in Fig. 2. In a typical test, a powder sample was first conditioned to a homogeneous state in a 50 mm diameter cylindrical vessel. Then, following a standard process established by Jenike [30–32], the powder sample was compressed under a specific normal stress of 9 kPa by using a vented piston. Afterwards, the powder was pre-sheared by a shear cell under the same normal stress. The shear cell rotated until the powder sample achieved a critical state so the sample preparation for each test was consistent. Normal stress was then reduced to 7, 6, 5, 4 and 3 kPa, respectively, and the yield shear strengths were measured at different normal stresses. Finally, a yield locus was obtained and could be extrapolated to 0 kPa normal stress to obtain the cohesion value. For each sample, 2–3 measurements were repeated and the average value was used to ensure accuracy.

2.2.2. Angle of repose

Ange of repose (AOR) is the largest angle at which powders can pile up, considered as powder flowability under semi-static state. It is related to the cohesiveness and internal friction of particles. Angle of repose was measured using a PT-N Hosokawa Powder Characteristic Tester, following a standard test [33]. As shown in Fig. 3, AOR is the largest angle between the surface of the powder heap and the plate surface. Firstly, a powder sample was loaded onto a screen with a vibrator, and by adjusting the vibration intensity, the powder sample then fell down through the funnel in a slow and consistent rate. The powder would pile up on a plate and when the plate was fully covered, and no more powder could be accumulated onto the powder heal, the angle

particles, which are widely used in industrial applications, including cosmetics [28], environmental-friendly powder coating [18] and production of catalysts [29]. A variety of characterization techniques were used to evaluate the flowability of these modified Group C particles under different powder states, ranging from dynamic to static. In addition, fluidization of these modified Group C particles was also investigated. This project aims to systematically study the flow and fluidization behaviors of the modified Group C particles and create a comparison with Group A particles.

2. Experiments

2.1. Experimental materials

Five host particles were used in the experiments, including three Group C particles, which were glass beads (10 μm), talcum powder
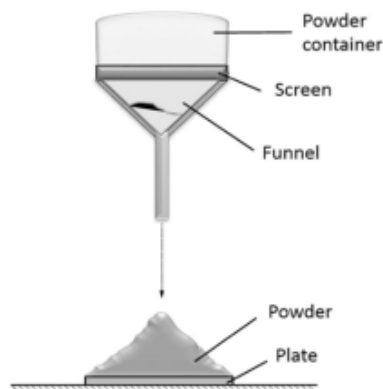

Fig. 3. Angle of repose measurement using a Hosokawa powder tester.

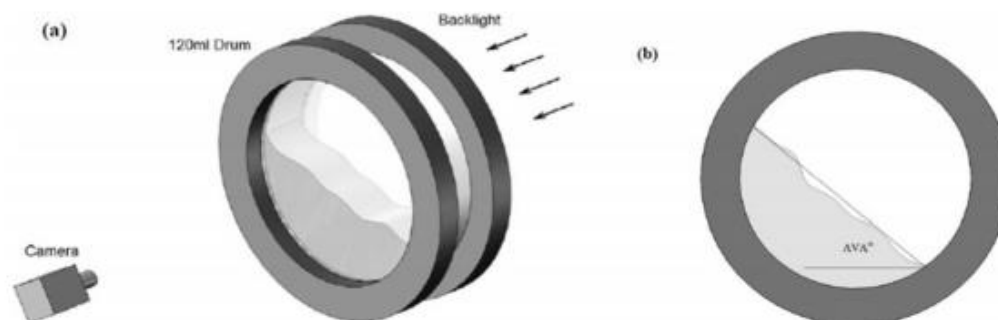4   *M. Han et al. / Powder Technology xxx (2019) xxx*
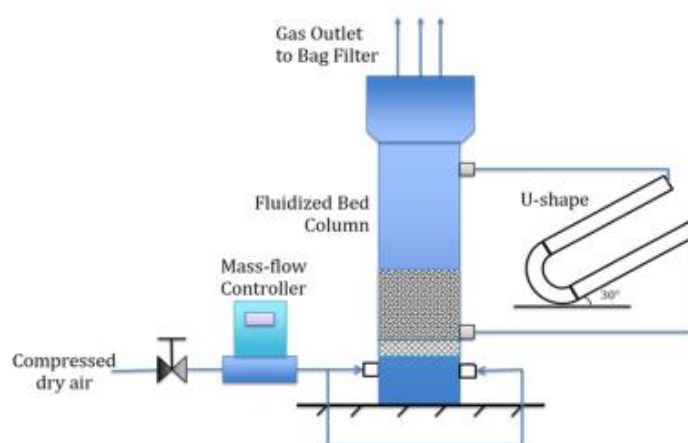

Fig. 4. AVA measurement.

Fig. 5. Fluidized bed system.

of repose was measured. This measurement was repeated 3–6 times for each powder sample and the average of three data with difference smaller than 0.6 was used. In general, smaller AOR indicates better flowability. Table 2 lists the flow properties of powders classified by AOR values.

2.2.3. Avalanche angle

Avalanche angle (AVA) is the maximum angle where the avalanche occurs at a low rotating speed, as shown in Fig. 4. AVA is referred as powder flowability under a semi-dynamic state, measured by a powder analyzer (Revolution Powder Analyzer, Mercury Scientific Inc., US). For
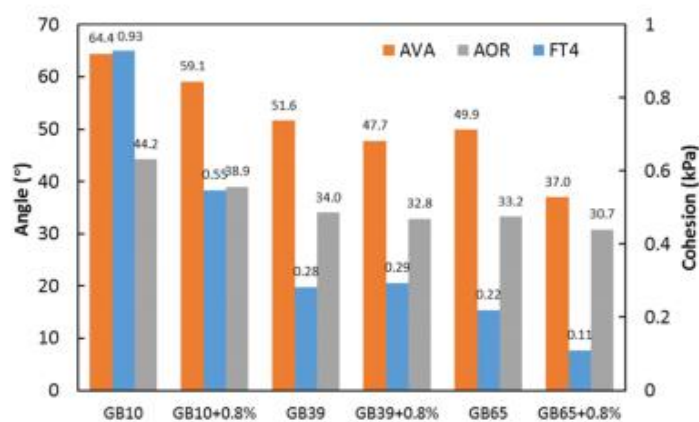

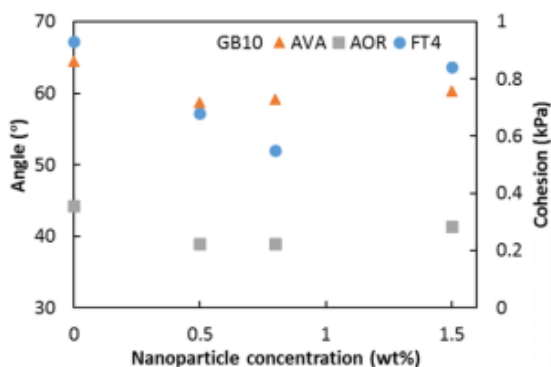**Fig. 6.** FT4, AOR and AVA of different glass beads particles.

Fig. 7. Effect of nanoparticle concentration on flowability of Group C particles.
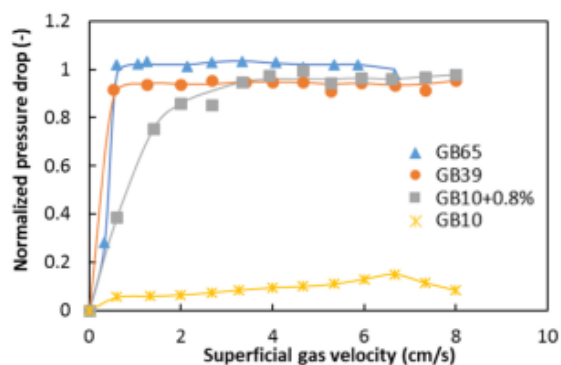

Fig. 9. Pressure drop of Group C and Group A particles.

each test, a powder sample was loaded into a 120 ml metal cup and was weighed. The powder sample was then placed into a cylindrical drum with two sides of glass which was 11.0 cm in diameter and 3.5 cm in thickness. The drum was rotated at 0.6 rpm and a digital camera

connected to a computer was used to monitor the flow behaviors of the powder sample. When the drum was rotated a certain angle, the powder would collapse or avalanche. The camera would record the maximum angle before the avalanche occurred. The drum was continuously rotated until 200 times of avalanche occurred and the average avalanche angle was used.
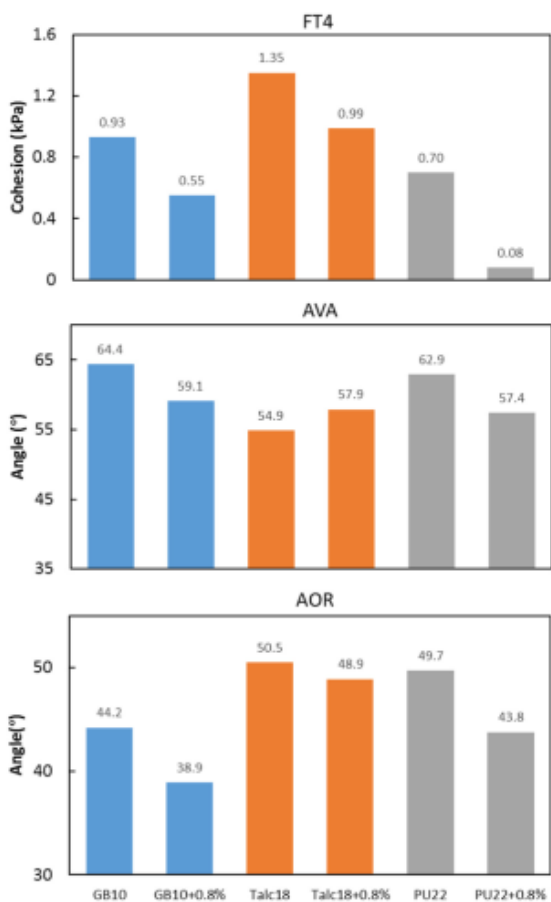
2.2.4. Fluidization

A fluidized bed was used to evaluate the pressure drop and minimum fluidization velocity of particles, as shown in Fig. 5. The minimum fluidization velocity also indicates flowability under a dynamic state. The fluidized bed was made up of Plexiglas with 5.08 cm in diameter and 45.72 cm in height. Air flowed through PVC tubing into a wind box, passed through a distributor and then contacted with the particles. The wind box was 5.08 cm in diameter and 12.7 cm in height. The distributer was a plate with 66 holes of 3 mm in diameter, whose opening area ratio was 23%. Two layers of 625 mesh screen were covered on the distributor. The pressure drop was measured by a slant U-shape manometer with the angle of 30°. The pressure drop curves were plotted by decreasing the superficial gas velocity. The minimum fluidization velocity was determined by intersecting the line of fixed bed region and the line of fluidized bed region. The normalized pressure drop was adopted in this project which is defined as the ratio of measured pressure drop (ΔP) to the particle weight per cross-sectional area (W/A).
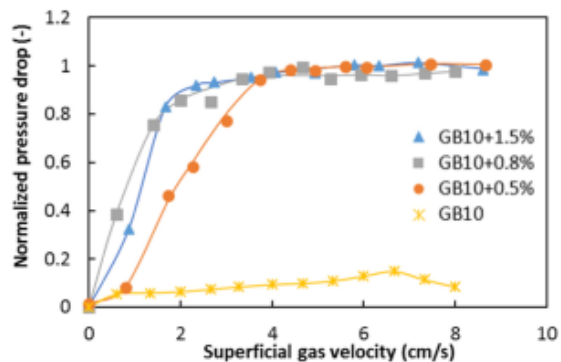

Fig. 8. Flowability of different Group C particles.

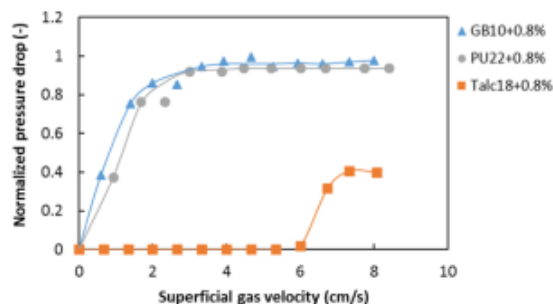Fig. 10. Effect of nanoparticle concentration on pressure drop of Group C particles.

Fig. 11. Pressure drop of different Group C particles.

3. Results and discussion

3.1. Powder flowability

Fig. 6 shows the FT4, AVA and AOR values of different glass beads particles. For GB10 particles, which is a typical type of Group C particles, the values of cohesion, AVA and AOR are very high, indicating strong cohesiveness. After modification by 0.8 wt% nanoparticles, all the values decrease significantly, for example, the cohesion value decreased from 0.93 kpa to 0.55 kpa, AVA reduced from 64.4° to 59.1° and AOR decreased from 44.2° to 38.9°, suggesting better flowability. For GB39 and GB65, which are typical Group A particles, they possess good flowability with low cohesion, AVA and AOR values. After modification by nanoparticles, the values do not decrease much, for example, AOR values of GB39 and GB65 changed from 34° to 32.8° and 33.2° to 30.7°, respectively, implying that Group A particles with or without nanoparticles are free-flowing. It is suggested that nanoparticles do not have much effect on flowability of Group A particles.

Group C particles (GB10) have much higher values of cohesion, AVA and AOR than Group A particles (GB39 and GB65), meaning that they are cohesive and not flowable, while nanoparticles could significantly reduce the cohesiveness and improve their flowability. However, after modification by nanoparticles, GB10 + 0.8% particles still have higher cohesion, AVA and AOR than GB39 and GB65 particles, signifying that flowability of GB10 + 0.8% is still poorer than that of GB39 and GB65. Ultimately, nanoparticles can significantly improve the flowability of Group C particles and turn them from cohesive to free-flowing. However, they could not make Group C particles possess the same good flowability as Group A particles.

Fig. 7 displays effect of nanoparticle concentration on the flowability of Group C particles. After the addition of 0.5 wt% nanoparticles, the values of cohesion, AVA and AOR decrease dramatically. As nanoparticle concentration increases from 0.5 wt% to 0.8 wt%, the values of AVA and AOR remain stable while the FT4 value continues decreasing. However, when nanoparticle concentration increases to 1.5 wt%, all the values show an increasing trend. It is suggested that the optimum nanoparticle concentration could be around 0.5-1 wt%, which is consistent with the previous studies [25,35–37].

Fig. 8 shows the cohesion, AVA and AOR values of different Group C particles. Among the three particles, PU22 displays the lowest cohesion values, and the sequence of cohesion values is Talc18 > GB10 > PU22. AVA values of the three particles show little difference, and Talc18 shows relatively lower values than the other two, the sequence of AVA values is GB10 > PU22 > Talc18. GB10 displays the lowest AOR values among the three particles, and the sequence of AOR values is Talc18 > PU22 > GB10. The three different measurements describe the flowability of particles under different states, so it cannot reliably evaluate powder flowability using only one index. Combing the three characterizations, Talc18 shows inferior flowability when compared to the other two, and PU22 exhibits better flowability than GB10, the sequence of powder flowability is PU22 > GB10 > Talc18. PU22 has the largest particle size which contributes to better flowability. Although Talc18 has larger particle size than GB10, it has some special physical properties such as sheet structure and extreme softness [38], leading to poor flowability.

In general, nanoparticles could almost reduce the cohesion, AVA and AOR of the three Group C particles (GB10, Talc18 and PU22) and improve flowability, except for the AVA value of Talc 18. After the addition of nanoparticles, Talc18 shows a small increase in the AVA value. In addition, nanoparticles have lesser effects on flowability of Talc18, maybe due to its sheet structure and extreme softness which make them harder to flow, while nanoparticles could significantly improve the flowability of GB10 and PU22. As shown in Fig. 1, after nanoparticle modulation, nanoparticles adhere on the surface of Group C particles to increase the surface roughness and the particle separation distance, reducing Van der Waals forces [23,25] and thus improving flowability.

3.2. Fluidization behaviors

In this part, the fluidization behaviors of Group A and Group C particles have been discussed, including pressure drop and minimum fluidization velocity. These characteristics could not only evaluate fluidization quality but also describe powder flowability under dynamic state.

Fig. 9 shows pressure drop of Group C and Group A particles. For Group A particles (GB39 and GB65), they could be fully fluidized under small superficial gas velocities. However, for Group C particles (GB10), the pressure drop across the entire bed keeps low as superficial gas velocity increases. The low pressure drop indicates that the bed was partially fluidized or even not fluidized ascribed from channeling. After the addition of nanoparticles, GB10 + 0.8% could be well fluidized under a small gas velocity. At high superficial gas velocities, the pressure drop of GB10 + 0.8% could reach around 1, the same as that of GB39 and GB65.

Fig. 10 illustrates effect of nanoparticle concentration on pressure drop of Group C particles. Obviously, nanoparticles could make Group C particles fluidized. As nanoparticle concentration increases from 0.5 wt% to 0.8 wt%, GB10 + 0.8% could reach full fluidization state (normalized pressure drop close to 1) much quicker than GB10 + 0.5%. When nanoparticle concentration continues increasing to 1.5 wt%, the line of GB10 + 1.5% does not change much compared with that of GB10 + 0.8%. It is suggested that the optimum nanoparticle concentration could be around 0.8 wt%.

Fig. 11 illustrates pressure drop of different Group C particles after modification by 0.8% nanoparticles. GB10 + 0.8% and PU22 + 0.8% could be well fluidized at around 2 cm/s, and their normalized pressure
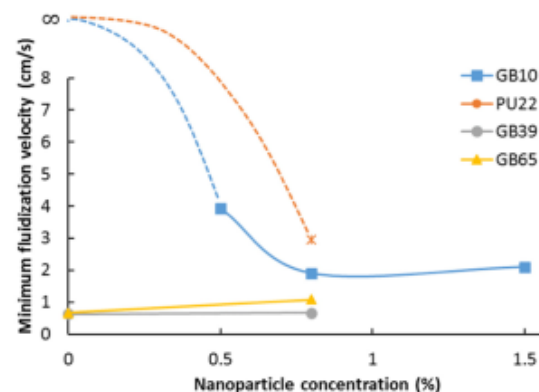

Fig. 12. Minimum fluidization velocities of different particles.

drops could reach around 1, indicating full fluidization. However, Talc18 + 0.8% is still hard to be fluidized. As shown in Fig. 11, at low gas velocities, Talc18 + 0.8% was totally de-fluidized, and when gas velocity increased to 7-8 cm/s, the normalized pressure drop only reached around 0.4, signifying partial fluidization. As a result, nanoparticles have significant effects on fluidization of GB10 and PU22, whereas little effects on that of Talc18.

Normalized pressure drop is an index which can also be used to present powder flowability under dynamic state [25]. Fig. 11 shows that GB10 and PU22 present good fluidization after nanoparticle modification, indicating good flowability under dynamic state, while Talc18 still shows poorer fluidization after nanoparticle modification. The results are consistent with that using other measurements like FT4, AVA and AOR in Fig. 8.

Fig. 12 shows minimum fluidization velocities of different particles before and after nanoparticle modification. A smaller minimum fluidization velocity usually signifies that particles could be fully fluidized at low gas velocities, which is desirable in fluidization operation [13]. For Group A particles, like GB39 and GB65, they could be fully fluidized at low gas velocities, so nanoparticles do not have much effect on their minimum fluidization velocities. For Group C particles, like GB10 and PU22, their minimum fluidization velocities could be significantly reduced after the addition of nanoparticles. As nanoparticle concentration increases, the minimum fluidization velocities of GB10 particles initially decrease and then show a little increase. The effect of nanoparticle concentration on minimum fluidization velocity is similar with that of powder flowability. It is suggested that minimum fluidization velocity is a characteristic which could not only describe fluidization quality but also present powder flowability. The flow and fluidization of a powder are closely related to powder cohesiveness. A higher powder cohesion results in poorer flowability and fluidization. As demonstrated in previous studies [25,39], the value of minimum fluidization velocity was strongly affected by powder cohesiveness, and a smaller minimum fluidization velocity was obtained by reducing powder cohesiveness. Therefore, the minimum fluidization velocity could be a useful index to predict powder cohesiveness and therefore estimate the fluidizability and flowability of fine particles.

4. Summary and conclusions

Powder flowability, as an important index in powder application, was measured using three different techniques such as FT4, AVA, AOR. Group C particles present much higher values of cohesion, AVA and AOR than Group A particles, indicating stronger cohesiveness and poorer flowability. The addition of nanoparticles could significantly decrease the values of cohesion, AVA and AOR of Group C particles, improving their flowability. There clearly exists an optimum nanoparticle concentration of around 0.5-1 wt%.

Fluidization is a popular operation in processing particles in industry, and fluidization behaviors like pressure drop and minimum fluidization velocity were also studied in this project. Group A particles exhibit good fluidization with normalized pressure drop close to 1 and small minimum fluidization velocities. However, Group C particles could not be fluidized due to strong cohesiveness and poor flowability. After nanoparticle modification, Group C particles could be well fluidized like Group A particles.

References

[1] Harry G. Brittain, Polymorphism in Pharmaceutical Solids, CRC Press, 2016.

[2] Valsesia P, Distefano G, Pirovano C, et al. Alkoxy-silanes compounds and related condensation products as cosmetic raw materials and for coating cosmetic powders: U.S. Patent Application.15/573,586. 17 May, 2018.

[3] L.K. Prasad, J.W. McGinity, R.O. Williams III, Electrostatic powder coating: principles and pharmaceutical applications, Int. J. Pharm. 505 (1–2) (2016) 289–302.

[4] G.B. Celli, A. Ghanem, M.S.L. Brooks, Bioactive encapsulated powders for functional foods—a review of methods and current limitations[J], Food Bioprocess Technol. 8 (9) (2015) 1825–1837.

[5] A. Fihri, C. Len, R.S. Varma, et al., Hydroxyapatite: a review of syntheses, structure and applications in heterogeneous catalysis, Coord. Chem. Rev. 347 (2017) 48–76.

[6] R.M. Nedderman, Statics and Kinematics of Granular Materials, Cambridge University Press, 2005.

[7] D. Schulze, Powders and bulk solids, Behaviour, Characterization, Storage and Flow, Springer 2008, pp. 35–74.

[8] J.K. Prescott, R.A. Barnum, On powder flowability, Pharm. Technol. 24 (10) (2000) 60–85.

[9] J. Schwedes, Review on testers for measuring flow properties of bulk solids, Granul. Matter 5 (1) (2003) 1–43.

[10] M. Krantz, H. Zhang, J. Zhu, Characterization of powder flow: static and dynamic testing, Powder Technol. 194 (3) (2009) 239–245.

[11] D.A. Ploof, J.W. Carson, Quality control tester to measure relative flowability of powders, Bulk. Solids Handl. 14 (1994) (127–127).

[12] M. Rios, Developments in powder flow testing, Pharm. Technol. 30 (2) (2006).

[13] D. Kunii, O. Levenspiel, Fluidization Engineering, Elsevier, 2013.

[14] R. Sivakumar, R. Saravanan, A.E. Perumal, et al., Fluidized bed drying of some agro products—a review, Renew. Sust. Energ. Rev. 61 (2016) 280–301.

[15] H.M. Abdelmotalib, M.A.M. Youssef, A.A. Hassan, et al., Heat transfer process in gas-solid fluidized bed combustors: a review, Int. J. Heat Mass Transf. 89 (2015) 567–575.

[16] D. Geldart, Types of gas fluidization, Powder Technol. 7 (5) (1973) 285–292.

[17] L. Chen, T. Okuda, X.Y. Lu, et al., Amorphous powders for inhalation drug delivery, Adv. Drug Deliv. Rev. 100 (2016) 102–115.

[18] Q. Huang, H. Zhang, J. Zhu, Flow properties of fine powders in powder coating, Particuology 8 (1) (2010) 19–27.

[19] J. Zhu, Flow properties of fine powders in powder coating, Particuology (1) (2010) 005.

[20] C. Bock, C. Paquet, M. Couillard, et al., Size-selected synthesis of Pt Ru nano-catalysts: reaction and size control mechanism, J. Am. Chem. Soc. 126 (25) (2004) 8028–8037.

[21] H.C. Hamaker, The London–van der Waals attraction between spherical particles, Physica 4 (10) (1937) 1058–1072.

[22] J. Visser, Van der Waals and other cohesive forces affecting powder fluidization, Powder Technol. 58 (1) (1989) 1–10.

[23] Zhu J, Zhang H. Fluidization dditives to ine owders: U.S. Patent 6,833,185. 21 Dec, 2004.

[24] J. Zhu, H. Zhang, Powder blending methods for uniformly dispensing additive particles to fine powders, US. Patent filed 2006.

[25] C. Xu, Q. Huang, H. Zhang, et al., Improving Fluidizability of Cohesive Particles by Surface Coating with Flow Conditioners, The Fifth World Congress on Particle Technology, Orlando, FL, United States, 2006.

[26] P. Lettieri, D. Macri, Effect of process conditions on fluidization, KONA Powder Part. J. (2016) 2016017.

[27] J.M. Valverde, Fluidization of Fine Powders: Cohesive Versus Dynamic Aggregation, Springer, 2013.

[28] K. Timm, C. Myant, H.A. Spikes, et al., Particulate lubricants in cosmetic applications, Tribol. Int. 44 (12) (2011) 1695–1703.

[29] M. Karches, M. Morstein, P.R. Von Rohr, et al., Plasma–CVD-coated glass beads as photocatalyst for water decontamination, Catal. Today 72 (3–4) (2002) 267–279.

[30] A. Standard, D6128: Standard Test Method for Shear Testing of Bulk Solids Using the Jenike Shear Cell, ASTM International, 2015.

[31] R. Freeman, Measuring the flow properties of consolidated, conditioned and aerated powders—a comparative study using a powder rheometer and a rotational shear cell, Powder Technol. 174 (2007) 25–33.

[32] M. Krantz, H. Zhang, J. Zhu, Characterization of powder flow: static and dynamic testing, Powder Technol. 194 (3) (2009) 239–245.

[33] American Society for Testing and Materials, Committee D18 on Soil and Rock. Standard Test Method for Bulk Solids Characterization by Carr Indices, ASTM International, 2008.

[34] R.L. Carr, Classifying flow properties of solids, Chem. Eng. 1 (1965) 69–72.

[35] Q. Huang, H. Zhang, J. Zhu, Flow properties of fine powders in powder coating, Particuology 8 (1) (2010) 19–27.

[36] Zhu J, Zhang H. Fluidization dditives to ine owders: U.S. Patent 6,833,185. 21 Dec, 2004.

[37] Y. Chen, J. Yang, R.N. Dave, et al., Fluidization of coated group C powders, AICHE J. 54 (1) (2008) 104–121.

[38] K. Terada, E. Yonemochi, Physicochemical properties and surface free energy of ground talc, Solid State Ionics 172 (1–4) (2004) 459–462.

[39] C. Xu, J. Zhu, Experimental and theoretical study on the agglomeration arising from fluidization of cohesive particles—effects of mechanical vibration, Chem. Eng. Sci. 60 (23) (2005) 6529–6541.

Performance Enhancement of Fluidized Bed Catalytic Reactors by Going to Finer Particles

Yuqi Zhang,[†,§] Yandaizi Zhou,[‡,§] Jiangshan Liu,[‡] Yuanyuan Shao,*[†] and Jesse Zhu*[†,‡]

[†]Collaborative Innovation Center of Chemical Science and Engineering (Tianjin), School of Chemical Engineering and Technology, Tianjin University, Tianjin 300072, China

[‡]Department of Chemical and Biochemical Engineering, The University of Western Ontario, London, Ontario N6A 5B9, Canada

ABSTRACT: Fluidization is an important operation for multiphase reactions, especially for gas-phase catalytic reactions because it provides a large solid surface area for improved gas−solid contact efficiency. Although fine particles with small particle size (<45 μm) could be more desirable in providing larger interfacial area, their strong interparticle forces lead to poor or even no fluidization. In this project, a "nanomodification" technique has been adopted to reduce the interparticle forces so as to release the potential of fine particles in multiphase reactions. As a first attempt, "nanomodified" fine catalysts (32 μm) were used in the ozone decomposition reaction and displayed better reaction performance than regular catalysts due to larger interfacial area and more gas holdup in the bed, indicating better gas−solid contact. The reaction conversion and contact efficiency using the nanomodified fine fluid cracking catalytic (FCC) catalysts significantly increased compared to that of using regular FCC catalysts (100 μm).
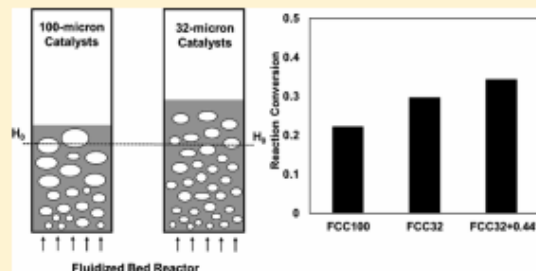
1. INTRODUCTION

The technique of gas−solid fluidization was first industrially applied in the Winkler process for gasification of coal in the early 1920s, and it has been used for gas-phase catalytic and gas−solid reactions for nearly 100 years. The applications of fluidized bed technology are numerous and can be found in most industrial processes.[1] The most important advantage of the fluidized bed is that the solid particles are in continuous motion and are very well mixed,[2] resulting in high mass/heat transfer and uniform temperature and particularly providing a large solid surface area and thus excellent gas−solid contact. In many applications, especially for gas−solid reactions and gas-phase catalytic reactions, the performance of fluidized bed reactors mainly depends on the solid surface area available for the gas reactant. As the technique of gas−solid fluidization develops from the initial Winkler process to the modern day mature FCC (fluid cracking catalytic) technology, the particle size of the solids used in the fluidized bed reactors become increasingly smaller, from several millimeters to less than 100 μm.[3] Therefore, it is more promising if finer particles with larger specific surface area could be applied in these processes.

Geldart[4] classified fine particles with a particle size of less than 45 μm and a particle density less than 1500 kg/m^3 as cohesive particles, which are difficult to fluidize because of their cohesiveness arising from strong interparticle forces.[4−8] These fine particles tend to form agglomerates and channeling, resulting in poor fluidization or complete defluidization. There are many methods employed to improve the fluidization of fine particles, such as mechanical vibration, acoustic vibration,

magnetic or electrical fields, and so forth. These methods can break the agglomerates and improve the fluidization quality by introducing external energy into the system to overcome the strong interparticle forces among fine particles. However, these methods are difficult to apply in practice as they are scale-dependent.

In previous studies of the group,[9,10] ultrafine nanoparticles were added into fine particles to improve the fluidization quality, which is proposed as the "nanomodification" technique in this project. The nanomodification technique is easily implemented and scale-independent. It is widely accepted that the van der Waals force is the dominant interparticle force in most dry systems,[11,12] and nanoparticles could adhere on the fine particles as asperities to increase the distance between fine particles and significantly reduce the van der Waals force and thus improve fluidization quality.[9] According to the previous studies,[9,10] the nanomodification technique could significantly improve fine particle fluidization, especially by increasing the bed expansion and dense phase voidage, implying that more gas contained in the dense phase is having direct contact with solid particles.

From the point view of a chemical reaction, the degree of gas−solid contact is considerable. Nanomodified fine particle fluidization is expected to improve the reaction performance by

20173

Industrial & Engineering Chemistry Research   Article

Table 1. Physical Properties of FCC Catalysts Used in the Experiments

| | | particle size (μm) | | | | | |
powder name	material	D_{10}	D_{50}	D_{90}	apparent density (kg/m³)	bulk density (kg/m³)	powder type
FCC100	impregnated FCC	45	100	173	1780	953	regular
FCC32	impregnated FCC	11	32	66	1780	921	fine
FCC32 + 0.44%	impregnated FCC with 0.44% vol R972	11	32	66	1780	912	fine

providing a large solid surface area and more gas in the dense phase. Many research studies have only studied fine particle fluidization without any reactions[13,14] and/or the fluidized bed reactors using typical Group A particles that only contain a small fraction of fine particle (<45 μm),[15-17] although the study with real reactions using fine catalysts is significantly important. Therefore, reaction performance using fine catalysts with and without nanomodification has been studied in this project, compared with using regular catalysts. A correlation on the fluidization characteristics and the reaction performance has been proposed.

2. EXPERIMENTAL SECTION

2.1. Catalyst Particles. Fresh FCC catalysts were purchased from Albemarle Catalyst LLC as based particles, which underwent an impregnation process to possess the reaction activity for ozone decomposition, as detailed in the literature.[18,19] The impregnated FCC catalysts were mixed with the fresh FCC catalysts to obtain the desired catalyst reactivity. The measurement of catalyst reactivity is described in detail in Section 2.3. Then, the mixed FCC catalysts were sieved into two groups using a 45 μm sieve: one is marked as FCC100 with a D_{50} of 100 μm and another is FCC32 with a D_{50} of 32 μm. The particle size distribution was measured by a BT-9300S laser particle size analyzer. Nanoparticles used in this experiment were SiO$_2$ with a particle size of 16 nm, commercially marketed as R972, and 0.44% by volume fraction of nanoparticles was added into FCC32, marked as FCC32 + 0.44%, based on previous studies.[10] The physical properties of these catalysts used in the experiments are shown in Table 1.

2.2. Fluidized Bed. The first part of the experiments is studying the fluidization behaviors of FCC100, FCC32, and FCC32 + 0.44%, including bed pressure drop, minimum fluidization velocity, bed expansion, and dense phase voidage. The second part is investigating the reaction performance of ozone decomposition using FCC100, FCC32, and FCC32 + 0.44%.

A schematic diagram of the fluidized bed system adopted in this study is shown in Figure 1. The fluidization column, which was made of plexiglas, was 5.08 cm in i.d. and 45.7 cm in height with a gas distributor between the fluidization column and the windbox below. The windbox was 5.08 cm in i.d. and 12.7 cm in height. The distributor was a plate with 66 holes that were 3 mm in diameter. The opening area ratio is 23%. Two layers of 625 mesh screen were covered on the distributor to ensure uniform air distribution. There were two pressure taps along the fluidization column, one was at the bottom just above the distributor and the other one was near the top, which were used to measure the total bed pressure drop by a slant U-tube manometer with an angle of 30°. Normalized pressure drop is defined as the ratio of the pressure drop to the particle weight per cross-sectional area, reaching a unit after full fluidization. One sample tap near the top of the fluidized bed was connected to the ozone sampling system and was used to measure ozone concentration. A measuring tape along the
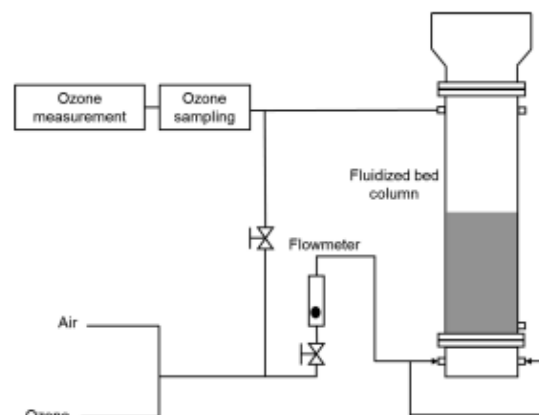

Figure 1. Schematic diagram of fluidized bed system.

fluidization column was used to measure the bed height. Bed expansion ratio (BER) is the ratio of the bed height at operating conditions to the initial fixed bed height (H_0). The operating superficial gas velocity (u_g) was in the range of 0 to 11 cm/s, typically at 4.1, 6.2 and 8.2 cm/s. The experiments were conducted at air humility less than 25% and at ambient pressure and temperature. Each experiment was conducted three times, and the mean deviation is smaller than 5%.

2.3. Reaction Rate Constant and Reaction Conversion. In this experiment, ozone decomposition is a first-order reaction, and the reaction rate constant can be measured by the fixed bed reactor and calculated using the following equation[20]

$$k_r = (F\rho_p/m) \ln(C_0/C_1) \tag{1}$$

where k_r is the reaction rate constant based on the catalyst volume (s⁻¹), F is the volumetric flowrate (m³/s), ρ_p is the particle density(kg/m³), m is the mass of catalysts in the fixed bed reactor (kg), and C_0 and C_1 are the inlet and outlet ozone concentrations, respectively (ppm).

The catalysts that were used in the experiments had identical catalytic reactivity. In other words, their reaction rate constants were the same. The conversion of the ozone decomposition reaction can be calculated based on the following equation

$$X = (C_0 - C_1)/C_0 \tag{2}$$

3. RESULTS AND DISCUSSION

3.1. Fluidization Behaviors. Figure 2 shows the pressure drop for FCC100, FCC32, and FCC32 + 0.44%. FCC100 could fluidize quickly at a low gas velocity and achieve a high normalized pressure drop close to 1, which is typical of Group A particles. FCC32 is not properly fluidized at low gas velocities, and the pressure drop in the bed is low, indicating that most particles are not fluidized. Its minimum fluidization velocity is higher and is not clear to be identified, which is
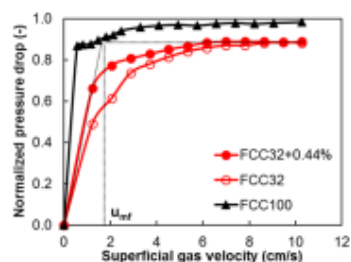
Figure 2. Pressure drop over the fluidized beds of the three types of FCC catalysts.

consistent with others' results.[9,10,21−23] After nanomodification, FCC32 + 0.44% becomes easier to fluidize with a lower minimum fluidization velocity than FCC32, and its minimum fluidization velocity is clear to identified. The order of minimum fluidization velocities of the three types of particles follows the sequence FCC100 < FCC32 + 0.44% < FCC32, which are 0.6, 1.9, and 3.4 cm/s, respectively. The value of minimum fluidization velocity depends on the particle cohesiveness, and a lower minimum fluidization velocity is obtained by reducing the cohesiveness.[9,10] As a result, nanomodification effectively reduces the cohesion of fine particles and makes them easier to fluidize.

Figure 3 shows the bed expansion for FCC100, FCC32, and FCC32 + 0.44%. In the experiments, the particle bed of
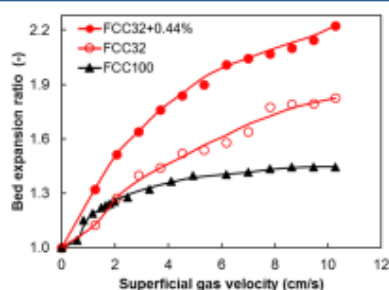

Figure 3. Bed expansion for the three types of FCC catalysts.

FCC100 shows typical bed expansion in bubbling fluidization. Although the bed of FCC32 expands higher than that of FCC100, the bed expansion at low gas velocities is poorer due to stronger interparticle forces. As gas velocity increases, the bed of FCC32 expands higher because its interparticle forces are partially overcome. After nanomodification, the bed of FCC32 + 0.44% quickly and dramatically expands and shows much higher bed expansion than the beds of FCC100 and FCC32 since the interparticle forces are essentially overcome. In Figure 5, FCC32 + 0.44% achieved the highest bed expansion, reaching up to 2.2 among the three particles, which means that the gas holdup in the bed of FCC32 + 0.44% is almost 80% more than that in the bed of FCC100. The order of bed expansion ratio of the three particles follows the sequence FCC32 + 0.44% > FCC32 > FCC100 at u_g > 3 cm/s. A high bed expansion signifies more gas in the fluidized bed and a higher chance of contact with particles, which is a key parameter for evaluating the fluidization quality and affecting the reaction performance. Conclusively, nanomodification could significantly improve the fluidization quality of fine

catalysts, especially in increasing the bed expansion, which is important for a chemical reaction and provides the potential to improve gas−solid contact.

3.2. Dense Phase Properties. The bubbling fluidized bed contains a bubble phase and a dense phase. Although the bed expansion could provide gas holdup in the fluidized bed, the gas holdup in the dense phase is more critical in providing gas−solid contact. The dense phase properties can be best characterized by the bed collapse test.[24] This test is carried out by first fully fluidizing the bed, followed by suddenly shutting off the gas supply and then tracking the bed surface level as it collapses. The collapse curve can be distinguished by three regions: the bubble escape stage, the sedimentation stage, and the consolidation stage. This can be used to evaluate the total bubble volume and the dense phase volume in the fluidized bed. The sedimentation stage yields a linear region, which is used to extrapolate the line back to time 0 to obtain the dense phase height (H_d) and therefore the dense phase voidage.

Figure 4 shows the bed collapse curves of the three types of particles under three different gas velocities (H_t is the total bed
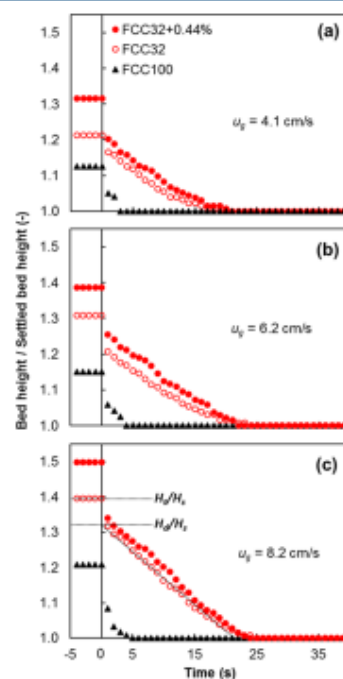

Figure 4. Bed collapse curves under different gas velocities for the three types of FCC particles: (a) at 4.1, (b) 6.2, and (c) at 8.2 cm/s.

height at the operating gas velocity and H_s is the settled bed height). FCC100 had a short collapse time while FCC32 and FCC32 + 0.44% showed much longer ones, indicating a better ability to hold gas in interparticle interstices. FCC32 and FCC32 + 0.44% had much higher dense phase height when compared with FCC100. The dense phase volume and the collapse time of the three catalysts follow the sequence FCC32 + 0.44% > FCC32 > FCC100. The increased dense phase volume and longer collapse time imply more gas in the dense phase and longer time required for gas−solid contact, which are extremely beneficial for gas-phase catalytic reactions.

The dense phase voidage (ε_d) can be calculated from the bed collapse curves using the following

$$\varepsilon_d = 1 - (1 - \varepsilon_s) H_s / H_d \tag{3}$$

where ε_s is the settled bed voidage.

Figure 5 shows the dense phase voidage for the three types of particles under different gas velocities. The dense phase
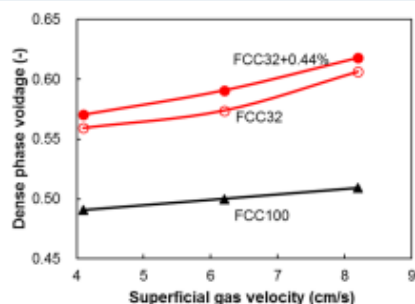
Figure 5. Dense phase voidage for the three types of FCC catalysts.

voidage in the bed of FCC 100 only reaches 0.51 at $u_g = 8.2$ cm/s, while that in the bed of FCC32 could achieve 0.61 at $u_g = 8.2$ cm/s. After nanomodification, the dense phase voidage in the bed of FCC32 + 0.44% goes even larger and reaches 0.625, which indicates more gas holdup in the dense phase to contact with particles, benefiting the contact efficiency in a reaction.

Figure 6 shows the gas holdup increase in the fluidized bed for the three types of particles under different gas velocities.
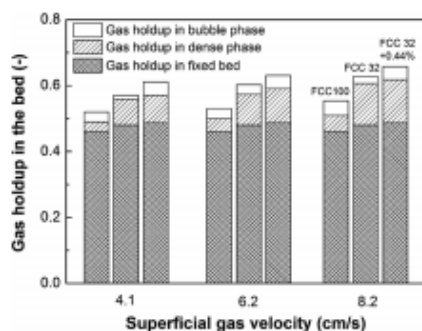
Figure 6. Influence of particle size and nanomodification on gas holdup in the dense phase.

For FCC100, the gas holdup in the dense phase shows a slight increase as gas velocity increases, while more gas goes to the bubble phase and passes through the bed as bubbles. In the bed of FCC32, the gas holdup in the dense phase dramatically increases when compared to that in the bed of FCC100, and the gas holdup in the bubble phase is almost the same or even less than that in the bed of FCC100. After nanomodification, the gas holdup in the dense phase for FCC32 + 0.44% further increases, and the gas holdup in the bubble phase is less than that in the bed of FCC100. Evidently, fine particles have the ability to hold more gas in the dense phase. Nanomodification can help fine particles fluidize even better and achieve higher gas holdup in the dense phase, which is much desirable in a reaction.

3.3. Reaction Conversion. Figure 7 shows the reaction conversion of ozone decomposition using the three types of
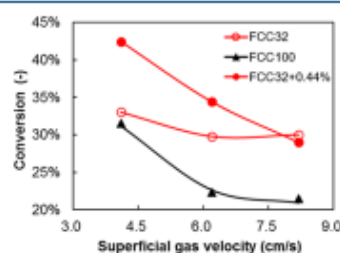
Figure 7. Reaction conversions of the fluidized bed reactors using the three types of catalysts.

catalysts. With the increase in specific surface area of catalysts and larger gas holdup in the dense phase, the fluidized bed reactor is expected to become more effective in promoting reaction performance. Indeed, the reaction conversion using FCC32 and FCC32 + 0.44% increases significantly compared with FCC100 (Figure 7). The large specific surface area of fine catalysts and the higher gas holdup in the dense phase contribute to better gas–solid contact and thus higher reaction conversion. The reaction conversion using the three types of catalysts shows the following sequence: FCC32 + 0.44% > FCC32 > FCC100. The reaction conversion decreasing with increasing gas velocity may be due to the reduced residence time of the gas reactant and more bubbles in the bed.

The increase in reaction conversion using FCC32 and FCC32 + 0.44% compared with that using FCC100 is listed below (see Table 2 for details). The reaction conversion is clearly improved by decreasing the particle size of the catalysts. For example, at 6.2 cm/s, the reaction conversion of FCC32 increases by 33.6% compared to that of FCC100, while that of FCC32 + 0.44% increases by 54.3%.

4. CONTACT EFFICIENCY

To better understand the improvement of the gas holdup in the dense phase on the reaction conversion, contact efficiency is proposed to correlate the factors. For a first-order reaction based on an ideal plug-flow model[25]

$$C_1/C_0 = \exp[-k_s A_p H / u_g] \tag{4}$$

where k_s is the reaction rate constant based on the catalyst surface (s^{-1}) (m^2/m^3), A_p is the specific surface area of the catalyst (m^2/m^3), H is the bed height of the catalyst in the reactor (m), and u_g is the operating gas velocity (m/s).

For a fluidized bed, contact efficiency (α) is defined based on the ideal plug-flow model, where the external surface area of catalysts is fully utilized and available for the gas reactant

$$C_1/C_0 = \exp[-\alpha k_s A_p H / u_g] \tag{5}$$

where H is the bed height of the fluidized bed at the operating gas velocity (m).

Based on the equation, a larger A_p and higher H both contribute to higher reaction conversion under the same operating gas velocity and catalyst reactivity. Indeed, it is the larger A_p and higher H that make the fluidization of fine particles desirable and attractive in gas-phase catalytic reactions. Therefore, the increase in contact efficiency is ascribed from the larger catalyst surface area and the higher gas

`Article`

Table 2. Details and the Increase in Reaction Conversion Based on FCC100

| | u_g = 4.1 cm/s | | u_g = 6.2 cm/s | | u_g = 8.2 cm/s | |
particles	X	X*[a]	X	X*	X	X*
FCC100	31.5%		22.3%		21.5%	
FCC32	33.0%	4.8%	29.8%	33.6%	30.1%	40.0%
FCC32 + 0.44%	42.5%	34.9%	34.4%	54.3%	29.2%	35.8%

[a]$X^* = (X_{FCC32 \text{ or } FCC32+0.44\%} - X_{FCC100})/X_{FCC100}$.

holdup in the dense phase that is available to be in contact with the particles. In this project, the total contact efficiency due to both the higher interfacial area and more gas reactant is defined as α_t

$$C_1/C_0 = \exp[-\alpha_t k_s A_{p100} H/u_g] \quad (6)$$

where A_{p100} is the specific surface area of FCC100 when calculating α_t for the three types of catalysts. α_t being calculated represents the contact efficiency relative to that using FCC100 in the reaction.

To specifically examine the relative contribution of the two factors, A_p and H, another parameter, α_g is defined as the contact efficiency only due to the amount of gas reactant available for catalysts, and the difference between α_t and α_f represents the contact efficiency due to the specific surface area of catalysts, α_p. α_f is calculated as the following

$$C_1/C_0 = \exp[-\alpha_f k_s A_{p100,32} H/u_g] \quad (7)$$

where $A_{p100,32}$ is the specific surface area of FCC100 when calculating α_f of FCC100 and is the specific surface area of FCC32 when calculating α_f of FCC32 and FCC32 + 0.44%.

A lower contact efficiency represents a poor reactor performance. Figure 8 shows the various types of contact efficiencies for the three types of FCC catalysts. It is found that the total contact efficiency (α_t) for FCC32 is much higher than that for FCC100, and FCC32 + 0.44% achieves an even higher contact efficiency, especially at low gas velocities. The contact efficiency due to gas holdup in the bed (α_f) using fine catalysts shows little improvement over that of using FCC100. The contact efficiency due to the specific surface area of catalysts, α_p, significantly increases for the finer particles. Evidently, the specific surface area of catalysts plays a more important role in improving gas–solid contact. In addition, FCC32 + 0.44% exhibits higher contact efficiency than FCC32 mainly due to the released surface area by nanomodification. The nanomodification technique could reduce the interparticle forces of fine particles and thus reduce the agglomeration in the fluidized bed, contributing to better fluidization quality and more surface area for gas reactants.

In summary, nanomodified fine catalysts show much higher contact efficiency than regular catalysts, signifying better gas–solid contacting and better reactor performance. In other words, it is the higher availability of the interfacial area between the gas and particles that contributes to enhancing the reaction performance of the fluidized bed reactor, when using particles of smaller sizes after nanomodification.

5. CONCLUSIONS

Nanomodified fine particles exhibited better fluidization quality than regular particles, including higher bed expansion and larger dense phase voidage. The reaction conversion of ozone decomposition using nanomodified fine catalysts was significantly improved over that of the same particles and over
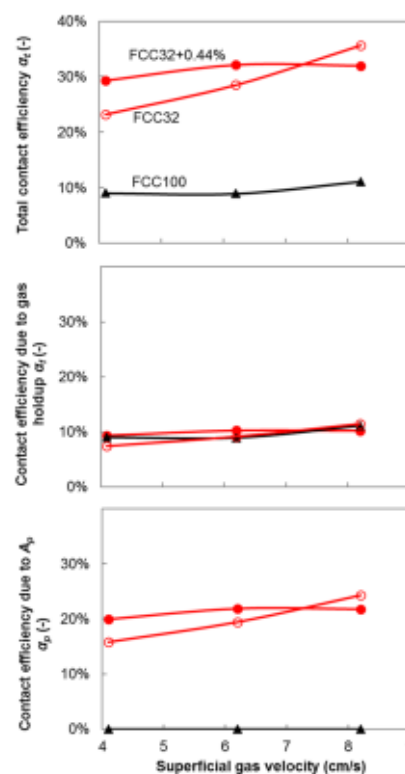

Figure 8. Contact efficiencies of the fluidized bed reactors using the three types of catalysts.

that of larger particles. In addition, the contact efficiency of fine catalysts dramatically increases and is 2 times more than that of regular catalysts. Conclusively, the fluidization of nanomodified fine catalysts is beneficial to gas-phase catalytic reactions due to the large gas–solid interfacial area and higher dense phase expansion both of which lead to better gas–solid contact. The nanomodified fine catalysts have a good prospect in further industrial applications.

■ AUTHOR INFORMATION

Corresponding Authors
*E-mail: yshao@tju.edu.cn (Y.S.).
*E-mail: jzhu@uwo.ca (J.Z.).

ORCID ⊙
Yuanyuan Shao: 0000-0002-1415-9253
Jesse Zhu: 0000-0001-7749-8917

Author Contributions
§Yuqi Z. and Yandaizi Z. contributed equally to the research work.

Notes

The authors declare no competing financial interest.

■ REFERENCES

(1) Grace, J. R.; Leckner, B.; Zhu, J.; Cheng, Y. Fluidized beds. In *Multiphase Flow Handbook*. CRC Press: 2006, 5–1.

(2) Yates, J. G. *Fundamentals of Fluidized-Bed Chemical Processes: Butterworths Monographs in Chemical Engineering*. Butterworth-Heinemann: 2013.

(3) Kunii, D.; Levenspiel, O. *Fluidization Engineering*. Elsevier: 2013.

(4) Geldart, D. Types of gas fluidization. *Powder Technol.* **1973**, 7, 285–292.

(5) Sugihara, K.; Ono, S. Galvanomagnetic properties of graphite at low Temperatures. *J. Phys. Soc. Jpn.* **1966**, 21, 631–637.

(6) Baerns, M. Effect of interparticle adhesive forces on fluidization of fine particles. *Ind. & Eng. Chem. Fund.* **1966**, 5, 508–516.

(7) Geldart, D. The effect of particle size and size distribution on the behaviour of gas-fluidised beds. *Powder Technol.* **1972**, 6, 201–215.

(8) Geldart, D.; Wong, A.C.Y. Fluidization of powders showing degrees of cohesiveness I: bed expansion. *Chem. Eng. Sci.* **1984**, 39, 1481–1488.

(9) Xu, C. C.; Zhang, H.; Zhu, J. Improving flowability of cohesive particles by partial coating on the surfaces. *Can. J. Chem. Eng.* **2009**, 87, 403–414.

(10) Han, M. *Characterization of fine particle fluidization*; The University of Western Ontario: London 2015

(11) Visser, J. van der Waals and other cohesive forces affecting powder fluidization. *Powder Technol.* **1989**, 58, 1–10.

(12) Krupp, H; Sperling, G. Theory of adhesion of small particles. *J. Appl. Phys.* **1966**, 37, 4176–4180.

(13) Chen, Y.; Yang, J.; Dave, R. N.; et al. Fluidization of coated group C powders. *AIChE J.* **2008**, 54, 104–121.

(14) Geldart, D.; Harnby, N.; Wong, A. C. Fluidization of cohesive powders. *Powder Technol.* **1984**, 37, 25–37.

(15) Yates, J. G.; Newton, D. Fine particle effects in a fluidized-bed reactor. *Chem. Eng. Sci.* **1986**, 41, 801–806.

(16) Grace, J. R.; Sun, G. Influence of particle size distribution on the performance of fluidized bed reactors. *Can. J. Chem. Eng.* **1991**, 69, 1126–1134.

(17) Sun, G.; Grace, J. R. The effect of particle size distribution on the performance of a catalytic fluidized bed reactor. *Chem. Eng. Sci.* **1990**, 45, 2187–2194.

(18) Li, D. *Investigation of circulating fluidized bed riser and downer reactor performance for catalytic ozone decomposition*; The University of Western Ontario: London, 2010.

(19) Li, D.; Zhu, J.; Ray, M. B.; Ray, A. K. Catalytic reaction in a circulating fluidized bed downer: ozone decomposition. *Chem. Eng. Sci.* **2011**, 66, 4615–4623.

(20) Wang, C. *High density gas-solids circulating fluidized bed riser and downer reactors*; The University of Western Ontario: London, 2013.

(21) Xu, C.; Cheng, Y.; Zhu, J. Fluidization of fine particles in a sound field and identification of group C/A particles using acoustic waves. *Powder Technol.* **2006**, 161, 227–234.

(22) Xu, C.; Zhu, J. Experimental and theoretical study on the agglomeration arising from fluidization of cohesive particles—effects of mechanical vibration. *Chem. Eng. Sci.* **2005**, 60, 6529–6541.

(23) Wang, Z.; Kwauk, M.; Li, H. Fluidization of fine particles. *Chem. Eng. Sci.* **1998**, 53, 377–395.

(24) Rietema, K. Application of mechanical stress theory to fluidization. *Int. Symp. on Fluidization.* **1967**, 154–163.

(25) Levenspiel, O. Chemical reaction engineering. *Ind. Eng. Chem. Res.* **1999**, 38, 4140–4143.

Enhanced Fluidization of Group A Particles Modulated by Group C powder

Xiaowei Zhang, Yandaizi Zhou, Jesse Zhu*
Department of Chemical and Biochemical Engineering, The University of Western Ontario, London, Ontario, N6A 5B9, Canada
*Corresponding authors: Jesse Zhu. E-mail address: jzhu@uwo.ca

Abstract

Geldart Group A powders are widely utilized in various industrial processes because of their good fluidization quality, which is closely related to the fine content ($\leq 45\mu m$). This work systematically investigated the effect of different types of fine powders ($\leq 20\mu m$) as additives on the fluidization quality of Group A powders. Three types of additives, Coal-15, GB-6, and SiO_2-5 were added into the base powder FCC-76 (Group A) in various volume fractions. Among the three types of additives, the addition of SiO_2-5 showed a significant improvement on the fluidization quality of Group A power, exhibiting lower minimum fluidization velocity and higher bed expansion, while the addition of Coal-15 slightly improved the fluidization quality. The addition of high-volume fraction of GB-6 would turn Group A powder into Group C/A, exhibiting some fluidization characteristics of Group C particles. Overall, the advancement of the fine contents on the fluidization quality of Group A powders has advantages for various industrial processes, especially for the gas-phase catalytic reactions.

Keywords: Geldart Group A powder; Group C powder; Fine content; Gas-solid fluidization; Fluidization quality; Bed expansion.

1. Introduction

Fluidization is a technology that utilizes a vertical flowing gas or liquid to suspend solid particles, giving the solid particles many properties of a real fluid [1-5]. Fluidization technology has achieved many applications in food processing [6-7], waste-water treatment [8], solids handling [9], coating [10], etc., because of the great extent of gas-solid contact, the excellent heat/mass transfer, and the ability to handle abundant particles continuously [11-13].

Based on the different fluidization characteristics of different particles, Geldart classified particles into four groups, Group A, B, C, and D [14]. Geldart Group B are bubble-ready particles with average particle size of 100-800μm, which directly go to bubbling fluidization after the gas velocity reaches the minimum fluidization velocity [15-17]. Group C particles are cohesive powders with small average particle size below 30μm, which have high surface area and can be utilized in gas-solid catalytic reactions [3,15,20,21]. Group D particles are spoutable with imperfect fluidization ability and are usually larger than 800μm [22-24]. Geldart Group A are aeratable powders and have the typical average particle size of 30-100μm. Group A powders possess great benefits in fluidization, including a low minimum fluidization velocity (U_{mf}), a degree of particulate bed expansion, small and more uniform bubble size, etc. [18-19]. Because of the outstanding fluidization performance, Group A powders have been employed widely in various industrial applications, such as fluid catalytic cracking (FCC) processes in petroleum refineries and many other catalytic reactions. Figure 1 shows typical bed expansion curves for Group A powders [3].
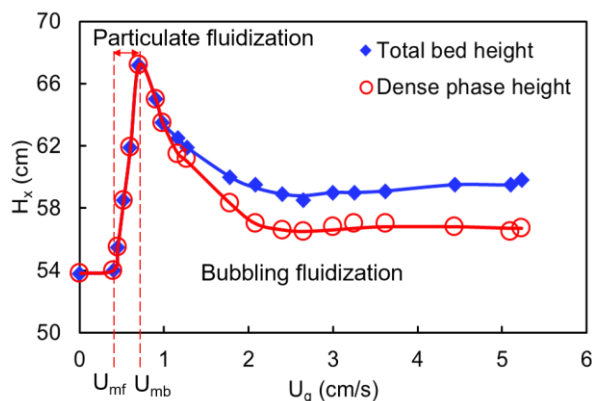

Figure 3:Typical expansion curves for Group A powder [3]

As shown in Figure 1, Group A powder starts to fluidize at the minimum fluidization velocity (U_{mf}), and the bubbles forms at the minimum bubbling velocity (U_{mb}). The fluidized bed of Group A powder expands when the superficial gas velocity is between U_{mf} and U_{mb}, reaching a peak at U_{mb}. This range of operation between U_{mf} and U_{mb} is the particulate (quiescent) fluidization regime, which is bubble-free and unique for Group A powders [14]. During the particulate fluidization, the gas has an intimate contact with the solids, and the bed can be treated as a homogeneous system [25-26]. Furthermore，The dense phase voidage in the fluidized bed of Group A powders can reach 0.60 to 0.65 at particulate fluidization [27]. When the superficial gas velocity exceeds U_{mb}, the bed height then gradually decreases because of the appearance of bubbles [3]. At high superficial gas velocities, the bed height remains relatively unchanged.

Some researchers [28-29] have found that fine contents (<45μm) played an important role in the fluidization quality of Group A powders. The increase of the fine content is shown to enhance the fluidization qualify by increasing the bed expansion and the gas holdup in the dense phase, improving the reaction conversion. For example, Sun and Grace [30] found that the change in the particle size distribution towards an increase of finer particles contributed to the improvement on the reaction efficiency. Bruni et al. [31] believed that the benefits of increasing fine content (<45μm) were ascribed to the introduction of interparticle forces. However, these earlier works almost focused on the effect of fine contents with particle size of 30-45μm, which may be Group C/A particles. This work aimed to investigate the effect of even finer particles with particle size of 5-20μm (clearly Group C particles) on the fluidization quality of Group A particles, inspired by our previous studies about the improvement on the fluidizaction quality of Group C particles with the addition of nanoparticles [32-35]. More specifically, the integration of nanoparticles, using a so-called nano-modification technology, was shown to significantly increase the fluidizability of Group C powder by decreasing the strong powder cohesion. In other words, the addition of finer particles (nanoparticles) was able to make cohesive Group C powders exhibiting great bed expansion ability. Following this trend, it would therefore be attractive to research on the effect of the addition of Group C particles on the fluidization behaviors of Group A particles.

This present work seeks to have a systematic study on the feasibility of improving the fluidization quality of Group A powders by integrating a fraction of Group C powders (≤ 20μm) as additives. A typical type of FCC particles (FCC76, Group A) was used as the base powder with the addition of three types of Group C additives, SiO_2-5, Coal-15, and GB-6, as well as fine FCC particles (FCC-20 as self-additives). The effects of the types and the volume concentration of Group C additives on the fluidization behaviors of Group A, as well as Groups B and C/A particles, were tested by evaluating three key parameters: the minimum fluidization velocity (U_{mf}), the bed expansion ratio (BER), and the dense phase expansion ratio (DER).

2. Experiments
2.1 Particulate materials

The first part was to study the effects of particle size distribution on the fluidization quality for Group A powders. FCC-Full was sieved by ultrasonic sieves into different fractions with different particle size distributions (PSDs) as shown in Figure 2.
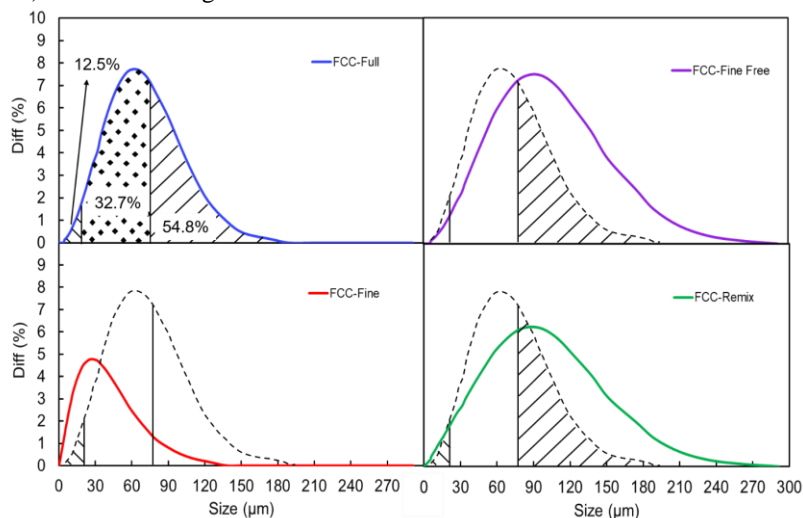

Figure 4: Particle size distribution of FCC powders

The properties of the various FCC powders with different PSD is illustrated in Table 1. The original FCC particles, termed as "FCC-Full", with an average size of 51μm, were separated into three components as shown in Table 1. FCC-Remix was made by mixing FCC-Fine Free (Coarse) and FCC-Fine portions without the middle portion (32.7% volume fraction in FCC-Full). FCC-Fine Free only contained coarse portion, which accounted for 54.8% volume fraction in FCC-Full.

Table 1: Components of FCC powders with different sizes

Name	Particulate component		
	Fine	Middle	Coarse
FCC-Full	12.5%	32.7%	54.8%
FCC-Fine Free	0%	0%	100%
FCC-Remix	18.7%	0%	81.3%

The second part was to systematically study the effect of the volume concentration of FCC-Fine (FCC-20) on the fluidization quality of the base Group A powder: FCC-Fine Free (FCC-76). Four different volume fractions of FCC-20 were added into FCC-76: 4%, 8.5%, 13.5%, and 22.6%.

The third part was to study the effects of different types of Group C additives on the fluidization quality of the bas Group A particles (FCC76): 15μm coal particles sieved out from coal particles used for combustion; 5μm silica particles of very low bulk density; and 6μm glass beads of cohesive nature. The properties of Group C additives used in the experiments are shown in Table 2.

Table 2: Additives used in the experiment

Additives	D_{50} (μm)	Powder type	Shape	Material Density (kg/m^3)	Bulk Density (kg/m^3)
SiO$_2$-5	4.94	C	Flake	2200	101
Coal-15	15.08	C	Irregular	1400	398
GB-6	6.10	C	Spherical	2500	704

The fourth part was to investigate the effects of Group C additive (GB-6) on different base powders, including Group C/A powder (GB-39), Group A powder (FCC-76), and Group B powder (Sand-156). Table 3 shows all powders used in the experiments.

Table 3: Powders used in the experiment

Base	D_{50}	Powder Type	Material Density (kg/m^3)	Additive	The Volume Fraction of Additive (%)
FCC-Full (FCC-51)	51	A	1780	None	0
FCC-Remix (FCC-65)	65	A	1780	None	0
FCC-Fine Free (FCC-76)	76	A	1780	None	0
		A		FCC-20	4, 8.5, 13.5, 22.6
		A		SiO$_2$-5	4, 8.5, 13.5, 22.6
		A		Coal-15	3, 6.2, 10
		A		GB-6	4, 8.5, 13.5
Sand-156	156	B	2600	GB-6	0, 5, 10, 15
GB-39	39	C/A	2500	GB-6*	0, 5, 10, 15

The additives with "*" can be considered as self-additives because their materials are the same as the base powders.

2.2 Experimental apparatus

Figure 3 shows a schematic diagram of the experimental apparatus. The cylindrical column with a height of 45.7cm was made by clear plexiglass. The diameter of the column was 5.08cm and the cross-sectional area was 20.3cm^2. The distributor was made by sintered plate fixed between the column and wind box, with an opening area rate of 2.5%. Three rotameters in different ranges were used, including 25-250mL/min, 0.3-3.0L/min, and 5-15L/min to measure the gas flowrate into the fluidized bed. A differential pressure transducer produced by National Instruments was used to test the pressure drop across the entire bed. A filter bag covered the outlet of the column to reduce the loss of fine powder.
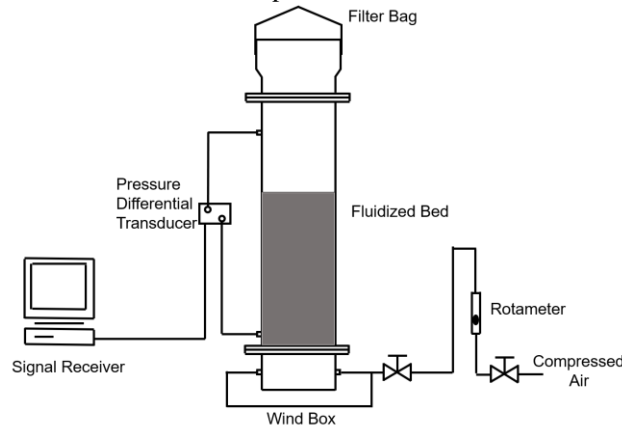
Figure 5 Schematic diagram of experimental apparatus

2.3 Experimental methodologies
Minimum fluidization velocity

The data of the pressure drop across the entire bed was obtained using the pressure transducer by decreasing the superficial gas velocity. Normalized pressure drop was defined as the ratio of the tested pressure drop P_{test} to the weight of the bed per unit cross area, as illustrated in Equation 1.

$$\text{Normalized pressure drop} = \frac{P_{test}}{P_{theory}} = \frac{P_{test}}{W/A} \qquad (1)$$

Theoretically, the value of the normalized pressure drop is close to 1 when almost all particles are fluidized in the bed. The minimum fluidization velocity (U_{mf}) was identified by plotting the normalized pressure drop as a function of the superficial gas velocity, as shown in Figure 4.
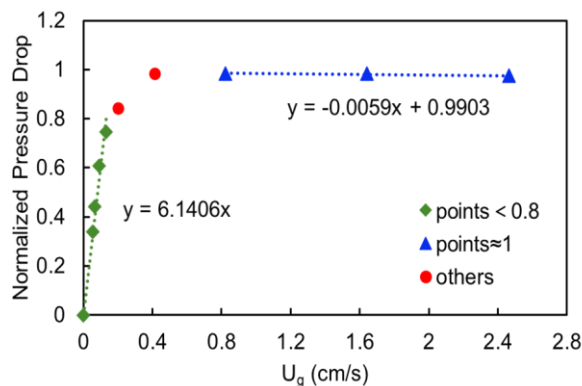
Figure 6 The method to identify minimum fluidization velocity

The points of the normalized pressure drop less than 0.8 showed a good linear relationship with the gas velocity. The points of the normalized pressure drop were unchanged after full fluidization. The x-coordinate of the intersection of two trendlines was the minimum fluidization velocity.

Bed Expansion and Bed Collapse Test

The bed expansion ratio (BER) was the fluidized bed height at operating gas velocities over the initial fixed bed height:

$$BER = \frac{H_f}{H_o} \qquad (2)$$

The initial bed heights (H_o) were 15.5 ± 1 cm.

Bed collapse technology is an effective method to determine the height of the dense phase at the fluidized bed. For Group A powders, when gas supply is suddenly shut off, the fluidized bed will experience three stages: the bubble escape stage, the hindered sedimentation stage, and the consolidation stage [33], as shown in Figure 5.
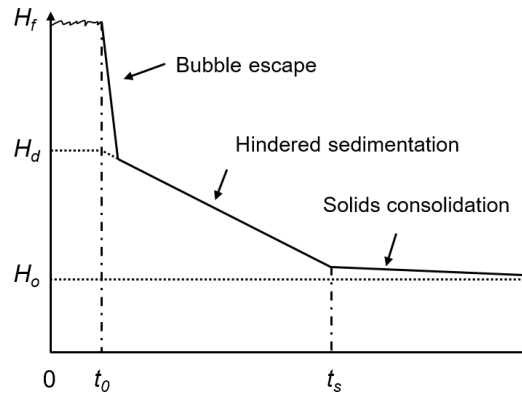
Figure 7 Typical bed collapse curve for Group A powders [36]

When the gas is suddenly shut off (t_0), the bubble escape stage is a quick collapse and takes a very short time since the density of bubbles is low and can leave rapidly. In the stage of the hindered sedimentation, the gas from the dense phase leaves slowly but uniformly.

During the bed collapse test, the bed height was recorded by a digital camera. The bed height as function of the time was utilized to obtain the dense phase height (H_d). The sedimentation stage showed a great linear relationship with the time, and H_d was obtained by extrapolating the line of the hindered sedimentation back to time t_0 [33]. The ratio of the dense phase height at operation conditions to the initial fixed bed height was the dense phase expansion ratio (DER):

$$DER = \frac{H_d}{H_o} \qquad (3)$$

Avalanche Angle

Avalanche angle (AVA) is defined as the largest angle before an avalanche of bulk powder occurs when the powder is rotated inside a cylindrical drum, as shown in Figure 6. It is one of the parameters that reflect powder cohesion, and usually, powder with higher avalanche angle leads to higher cohesion and stronger interparticle forces.
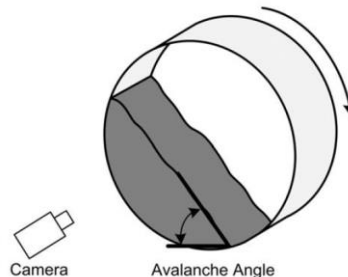

Figure 6 The schematic diagram of AVA tester (Krantz et al., 2009) [37]

3. Results and discussions

3.1 Effects of PSD

Particle size distribution (PSD) plays an important role in the operation and performance of the fluidized bed reactors [30]. Three different mixes of FCC powders with different PSD, FCC-Full (FCC-51), FCC-Remix (FCC-65), and FCC-Fine Free (FCC-76), were studied to investigate the effects of PSD on the fluidization quality.

Figure 7 shows the effects of PSD and the volume fraction of FCC-20 on the minimum fluidization velocity. FCC-Fine Free with the largest particle size without fine contents showed the highest U_{mf}. Although the particle size of FCC-Remix was slightly larger than that of FCC-Full, FCC-Remix had a similar and actually slightly lower U_{mf}, due to its higher volume fraction of fine particles, especially particles smaller than 20μm. As the volume fraction of FCC-20 increased, the values of U_{mf} decreased, indicating that the fraction of fines had a strong effect on fluidization, as have been observed before [28-30].
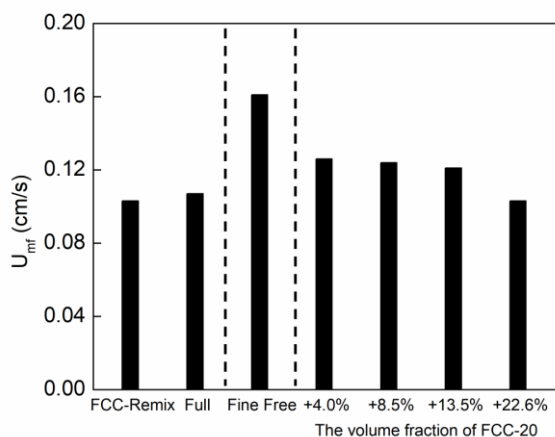
Figure 7 Effects of PSD and fine content on minimum fluidization velocity

The effects of PSD on the fluidization quality are also reflected in bed expansion, including the total bed expansion and the dense phase expansion, as shown in Figure 8. Without the fines, FCC-Fine Free with narrower PSD had the poorest expansion ability, exhibiting the lowest bed expansion and dense phase expansion. For example, when compared with FCC-Full, BER and DER of FCC-Fine Free at the peak decreased by 10.4% and 12.8%, respectively, and decreased by 13.3% and 9.64% in average at the plateau. After re-mixing the fine contents into the FCC-Fine Free, FCC-Remix had a good bed expansion ability similar with FCC-Full.

As the superficial gas velocity increased, the trend of the bed expansion curves remained the same for the three powders with different PSDs. At low superficial gas velocity, the bed and the dense phase expanded rapidly with the increase of the superficial gas velocity, and then reached the maximum values. After that, BER and DER gradually decreased and then reached a plateau with the increase of the superficial gas velocity. In addition, the three types of powders with different PSDs reached the peak at the same superficial gas velocity of 0.90cm/s, suggesting that they had the similar minimum bubbling velocity (U_{mb}).
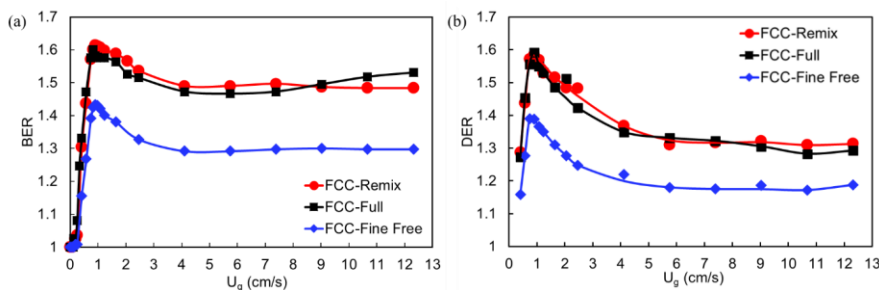
Figure 8 Effects of PSD on BER and DER

3.2 Effects of fine contents

To further investigate the effect of fine contents, different volume fractions of FCC-Fine (FCC-20) were added into the base powder: FCC-Fine Free (FCC-76). The increase of the volume fraction of FCC-20 gradually decreased the minimum fluidization velocity, as shown in Figure 7. For example, when compared with the base powder (FCC76), the addition of 4.0% and 22.6% of FCC-20 reduced the minimum fluidization velocity by 21.7% and 36.0%, respectively.

Figure 9 shows the bed expansions and the dense phase expansion of FCC-76 before and after the addition of FCC-20. It is evident that the total bed expansion tended to increase as the FCC-20 fraction increased. For example, the average bed expansion ratio for FCC-76 base powder reached a plateau of 1.30, while it reached 1.49 after adding 22.6% of FCC-20. Generally, a higher bed expansion indicates more gas holdup in the bed, allowing more gas to contact with particles, which is very important for gas-solid catalytic reactions [32-33].

For the dense phase expansion, in general, it exhibited a similar trend with the total bed expansion, that DER increased with the increase of FCC-20 content. However, when the volume fraction of FCC-20 further increased from 8.5% to 22.6%, the effect on DER was insignificant. For example, the average dense phase expansion ratios with the addition of 8.5%, 13.5% and 22.6% were almost the same, reaching a plateau of 1.32. In summary, the fluidization quality of Group A powder could be improved by the addition of fine contents.
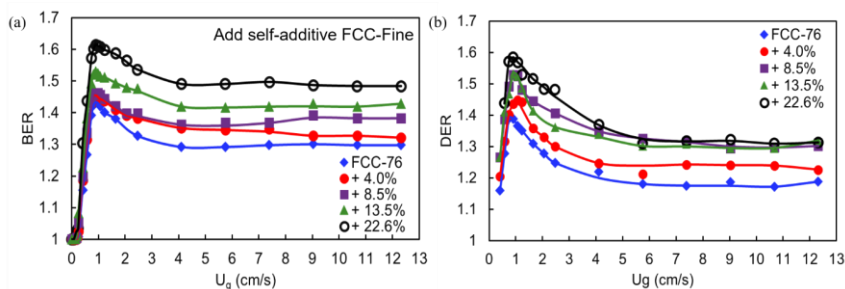

Figure 9 Effects of fine content on BER and DER

3.3 Effects of additives

Using the same FCC-76 as a base powder, the effects of different types of Group C additives on the fluidization quality of Group A powder were also studied by adding different volume fractions of three types of Group C additives, SiO_2-5, Coal-15, and GB-6.

Figure 10 shows the effects of different types of additives on the minimum fluidization velocity as a function of the additive content. The addition of SiO_2-5 and Coal-15 decreased U_{mf}, while the addition of GB-6 significantly increased U_{mf}. As shown, the minimum fluidization velocity greatly decreased as SiO_2-5 content and Coal-15 content increased, while significantly increased as GB-6 content increased. For example, when compared with FCC-76 base powder (0% additive content), the minimum fluidization velocity reduced by 28.8% and 36.6% with the addition of 13.5% and 22.6% of SiO_2-5, respectively. When compared with SiO_2-5, the effects of Coal-15 content on decreasing the minimum fluidization velocity were limited. For GB-6, when compared with the base powder, the minimum fluidization velocity of FCC-76 with 13.5% of GB-6 increased by 8.69 times, which was attributed to the increase of the powder cohesion.
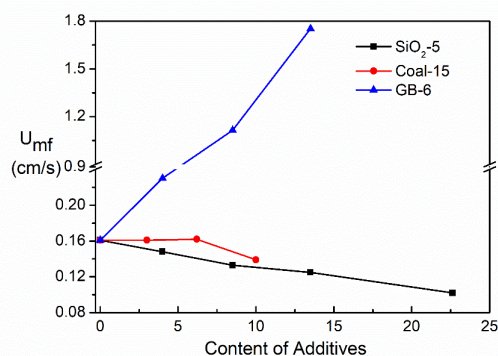
**Figure 10 Effects of additives on minimum fluidization velocity**

The effects of different types of Group C additives on the bed expansion are shown in Figure 11 (a). The increase of SiO_2-5 content significantly increased the bed expansion, and the volume fraction of 22.6% contributed to the highest BER. The addition of Coal-15 had less effect on BER. For GB-6 as Group C additives, BER with the addition of a small volume fraction (4%) showed a similar curve with the addition of SiO2-5 and Coal-15, and significantly increased when compared with that of the base powder. However, when GB-6 content increased to 8.5% and further to 13.5%, BER still increased but showed different curves, especially at low gas velocities, with the disappearance of the maximum BER values. That is, BER continued increasing with the increase of the superficial gas velocity. High GB-6 content would make the mixtures more difficult to fluidize because of the strong powder cohesion of GB-6, leading to channeling and agglomeration at low superficial gas velocities. Although the trend of BER curves changed, the high content of GB-6 still increased the bed expansion at high superficial gas velocities.

The dense phase expansions of the base powder with the addition of different types of Group C additives are shown in Figure 11 (b). The dense phase expansion showed similar trends with BER curves, and increased with the increase of Group C additive content. Specially, for GB-6, higher content led to lower DER at low superficial gas velocities, due to the stronger powder cohesion which resulted in more difficulty in the fluidization.
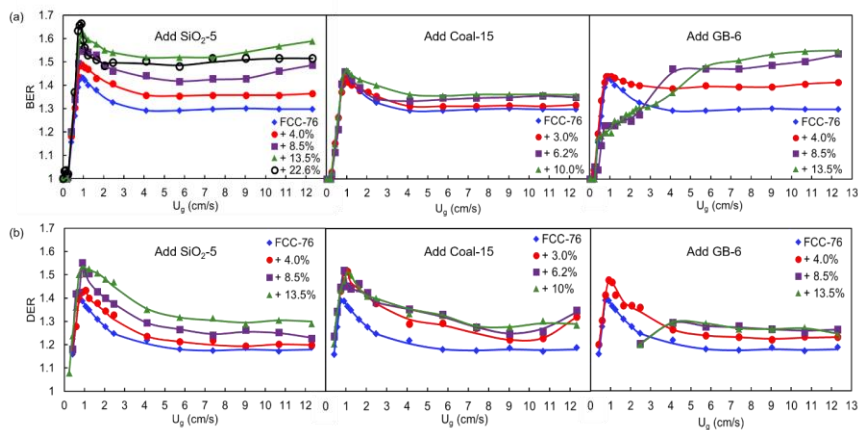

Figure 11 Effects of additives on BER and DER

Considering FCC-20 as a self-additive, Figure 12 compares the effects of FCC-20 and SiO_2-5 on the total bed expansion. When compared with FCC-20, SiO_2-5 with the volume fractions of 4.0%, 8.5%, and 13.5% contributed to higher bed expansion, while SiO_2-5 with the volume fraction of 22.6% showed a similar BER with FCC-20. For SiO_2-5 additive, the volume fraction of 22.6% was almost reached the limitation that could further improve the fluidization quality of Group A powder. Overall, SiO_2-5 could be recognized as the best one among the four types of Group C additives (including FCC-20 as self-additives) to improve the fluidization quality of Group A particles.
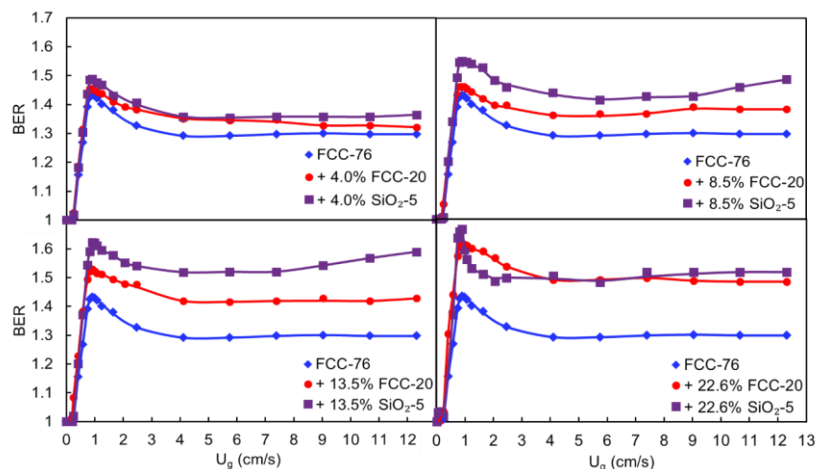
**Figure 82 Comparison of total bed expansion between FCC-76 with SiO₂-5 and FCC-20**

3.4 Effects of powder cohesion and bulk density

The Avalanche angles (AVA) of the tested powders with different types and volume fractions of Group C additives are shown in Figure 13. It is clearly shown that AVA values increased with the increase of the fine content, indicating the decrease of the powder flowability which could be ascribed to the increase of the powder cohesion.
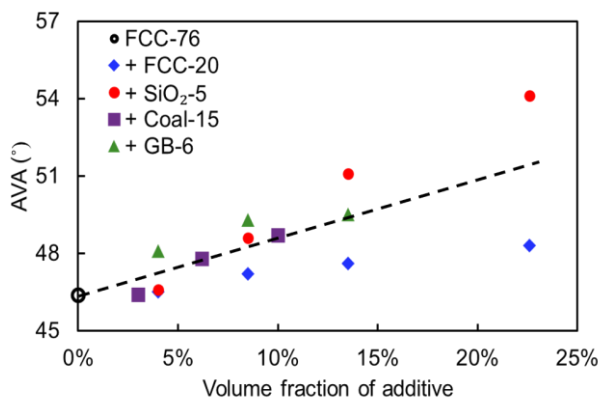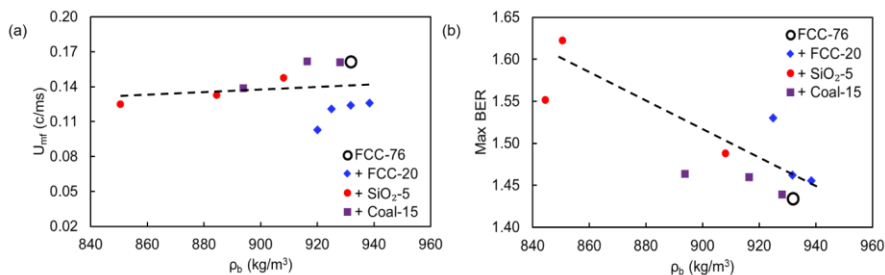

Figure 13 The relationship between volume faction of additives and avalanche angle

Figure 14 shows the relationship between the fluidization quality and the avalanche angle for FCC base powders (FCC-76) with additives. For the base powder with different types of additives, the minimum fluidization velocity tended to decrease and the maximum BER increased, as the avalanche angle increased. The addition of Group C additive could increase the powder cohesion and therefore the interparticle forces of the mixtures, which, as has been suggested by Bruni et al. [31], benefited the fluidization of Group A powders. However, the cohesion of the mixture should be controlled to a certain range to obtain the optimal fluidization quality. That is, a too strong cohesion would bring in difficulty in the fluidization and worsen the fluidization quality of Group A powders, such as the addition of a high fraction of GB-6 (as shown in Figures 10 and 11).
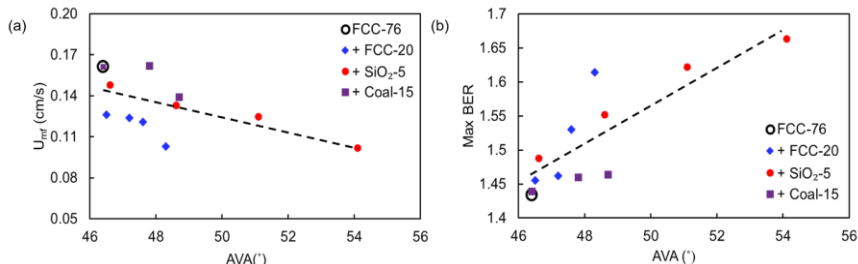
Figure 14 The relationship between fluidization quality and avalanche angle, at various additive concentrations with FCC-76 as base powder

The bulk density of the powder mixture is another factor that affects the fluidization quality, as particles with a lower bulk density would require a lower drag force to be suspended so that easier fluidization. As indicated in Figure 15, the powder mixtures with lower bulk densities (more additives) indeed tended to have lower U_{mf} and higher maximum BER.

Figure 15 The relationship between fluidization quality and powder bulk density, at various additive concentrations with FCC-76 as base powder

3.5 Effects of fine contents on Groups B and C/A powders

While the fluidization quality of Group A particles is clearly affected by the addition of fine content, the same may or may not be true for larger Group B particles. To investigate the effects of additives on the different types of the base particles, GB-6 was used as the additive and was applied to Group C/A (GB-39), Group A (FCC76), and Group B powders (Sand-156). Figure 16 shows the effects of GB-6 content on the minimum fluidization velocity of those three types of base particles (GB-39, FCC-76, and Sand-156).
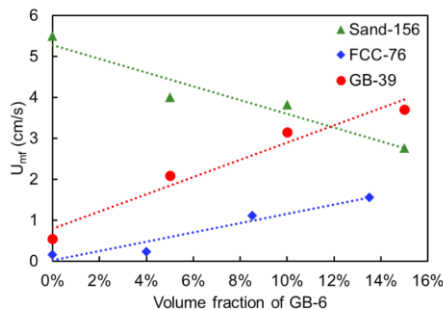
Figure 16 Effects of base powders with GB-6 on U_{mf}

Clearly, while the the minimum fluidization velocity for Group A and Group C/A particles increased with the addition of GB-6 additive, the minimum fluidization velocity for the Group B (Sand-156) particles were reduced by the addition of GB-6 additive. For example, when compared with Sand-156 virgin, the addition of 15% of GB-6 greatly decreased the minimum fluidization velocity by 50%. On the other hand,

higher content of GB-6 additive increased U_{mf} of Group C/A and Group A particles, making them more difficult to fluidize.

Figure 17 shows the bed expansion with the increase of the superficial gas velocity, for GB-39 and Sand-156 with and without Group C additives. Both types of particles expanded more significantly with the addition of fine content, however, the expansion ability of these two was clearly different.

Sand-156, a typical type of Group B powder, was more difficult to expand and could not expand as high as Group A powder. The addition of GB-6 slightly increased the bed expandability, but the effect was insignificant. For example, the bed expansion ratio only reached 1.20 for Sand-156 with 15% of GB-6 at high gas velocities. Although the effect was limited, the improvement of GB-6 on the bed expansion for Sand-156 indicated that fine powder additives nonetheless does also change the expandability of Group B particles. The lesser extent of Group C additives on the improvement of the fluidization of Group B particles is probably due to the nonuniformity. Group B particles are much larger than Group C additives, resulting in that Group C additives tend to agglomerate in the interstitial space between the large Group B particles, which leads to the nonuniformity of the mixture and also the less homogeneous fluidization.

For GB-39, at the high superficial gas velocity, GB-6 additive had a positive effect on the bed expansion. As the superficial gas velocity increased, BER slowly but monotonically increased, and reached very high values at high superficial gas velocities.
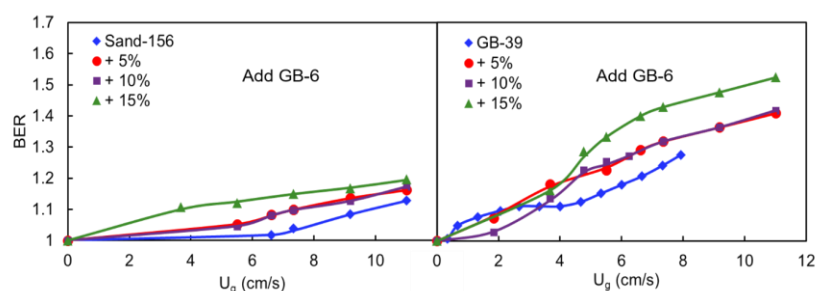

Figure 17 Effects of base powders with GB-6 on BER

4. Conclusions

Particle size distribution could affect the fluidization quality of Group A powders, especially the portion of particles smaller than 20μm. The minimum fluidization velocity would increase and bed expansion ability would decrease if there lack particles in the 20μm minus range. On the other hand, missing particles in the range of 20-45μm had less effects on the fluidization quality.

The fluidization quality of Group A powders was significantly enhanced by the addition of Group C additives and/or the "self-additive". Effective Group C additives, such as SiO_2-5 and FCC-20, could appropriately increase cohesion of the mixture, which introduces interparticle forces. As the content of additives increases, the minimum fluidization velocity of mixtures gradually decreased and bed expansion ability increased. However, too strong cohesion introduced by additive could make fluidization quality worse, such as with high content of GB-6.

Reference
[1]   H. LI, M. KWAUK, Review and prospect of fluidization science and technology [J], CIESC Journal 1 (2013).
[2]   X. Zhu, Q. Zhang, Y. Wang, F. Wei, Review on the nanoparticle fluidization science and technology, Chinese Journal of Chemical Engineering 24(1) (2016) 9-22.
[3]   D. Geldart, Gas fluidization technology, (1986).
[4]   D. Kunii, O. Levenspiel, Fluidization engineering, Elsevier, (2013).
[5]   J.R. Grace, Introduction, History, and Applications, Essentials of Fluidization Technology (2020) 1-9.
[6]   N. Shilton, K. Niranjan, Fluidization and its applications to food processing, Food structure 12(2) (1993) 8.
[7]   K. Dewettinck, A. Huyghebaert, Fluidized bed coating in food technology, Trends in Food Science & Technology 10(4-5) (1999) 163-168.

[8]   J. Heijnen, A. Mulder, W. Enger, F. Hoeks, Review on the application of anaerobic fluidized bed reactors in waste-water treatment, The Chemical Engineering Journal 41(3) (1989) B37-B50.

[9]   W.-C. Yang, Fluidization, Solids Handling, and Processing: Industrial Applications, Elsevier1998.

[10] T.P. Anh, H.P.T. Thanh, Application of Fluidized Power Coating for Propellers, CIGOS 2019, Innovation for Sustainable Infrastructure, Springer2020, pp. 355-360.

[11] R. Cocco, S.R. Karri, T. Knowlton, Introduction to fluidization, Chem. Eng. Prog 110(11) (2014) 21-29.

[12] J. Yates, Fundamentals of fluidized-Bed chemical processes: Butterworths monographs in chemical engineering, Butterworth-Heinemann2013.

[13] J.R. Grace, X. Bi, N. Ellis, Essentials of Fluidization Technology, Wiley Online Library2020.

[14] D. Geldart, Types of gas fluidization, Powder Technology 7(5) (1973) 285-292.

[15] J.-R. Lee, K.-S. Lee, N. Hasolli, Y.-O. Park, K.-Y. Lee, Y.-H. Kim, Fluidization and mixing behaviors of Geldart groups A, B and C particles assisted by vertical vibration in fluidized bed, Chemical Engineering and Processing-Process Intensification 149 (2020) 107856.

[16] J.R. Grace, Hydrodynamics of Bubbling Fluidization, Essentials of Fluidization Technology (2020) 131-152.

[17] E.R. Monazam, R.W. Breault, L.J. Shadle, J.M. Weber, Analysis of solids flow rate through nonmechanical L-valve in an industrial-scale circulating fluidized bed using group B particles, Industrial & Engineering Chemistry Research 57(33) (2018) 11439-11451.

[18] H.-Y. Xie, D. Geldart, Fluidization of FCC powders in the bubble-free regime: effect of types of gases and temperature, Powder technology 82(3) (1995) 269-277.

[19] P. Lettieri, D. Newton, J. Yates, Homogeneous bed expansion of FCC catalysts, influence of temperature on the parameters of the Richardson–Zaki equation, Powder Technology 123(2-3) (2002) 221-231.

[20] Y. Chen, J. Yang, R.N. Dave, R. Pfeffer, Fluidization of coated group C powders, AIChE journal 54(1) (2008) 104-121.

[21] Q. Zhu, H. Li, Study on magnetic fluidization of group C powders, Powder Technology 86(2) (1996) 179-185.

[22] D. Dimattia, P. Amyotte, F. Hamdullahpur, Slugging characteristics of group D particles in fluidized beds, The Canadian Journal of Chemical Engineering 75(2) (1997) 452-459.

[23] C.L. Law, S.M. Tasirin, W.R.W. Daud, D. Geldart, Effect of vertical baffles on particle mixing and drying in fluidized beds of group D particles, China Particuology 1(3) (2003) 115-118.

[24] F. Duan, S. Cong, Shannon entropy analysis of dynamic behavior of Geldart group B and Geldart group D particles in a fluidized bed, Chemical Engineering Communications 200(4) (2013) 575-586.

[25] W. Ge, J. Li, Physical mapping of fluidization regimes—the EMMS approach, Chemical Engineering Science 57(18) (2002) 3993-4004.

[26] E. Ghadirian, H. Arastoopour, CFD simulation of a fluidized bed using the EMMS approach for the gas-solid drag force, Powder Technology 288 (2016) 35-44.

[27] G. Donsi, L. Massimilla, Bubble‐free expansion of gas‐fluidized beds of fine particles, AIChE Journal 19(6) (1973) 1104-1110.

[28] G. Barreto, J. Yates, P. Rowe, The effect of pressure on the flow of gas in fluidized beds of fine particles, Chemical engineering science 38(12) (1983) 1935-1945.

[29] J. Yates, D. Newton, Fine particle effects in a fluidized-bed reactor, Chemical engineering science 41(4) (1986) 801-806.

[30] G. Sun, J.R. Grace, The effect of particle size distribution on the performance of a catalytic fluidized bed reactor, Chemical Engineering Science 45(8) (1990) 2187-2194.

[31] G. Bruni, P. Lettieri, D. Newton, D. Barletta, An investigation of the effect of the interparticle forces on the fluidization behaviour of fine powders linked with rheological studies, Chemical Engineering Science 62(1-2) (2007) 387-396.

[32] Y. Zhou, J. Zhu, Group C+ particles: Enhanced flow and fluidization of fine powders with nano-modulation, Chemical Engineering Science 207 (2019) 653-662.

[33] Y. Zhang, Y. Zhou, J. Liu, Y. Shao, J. Zhu, Performance Enhancement of Fluidized Bed Catalytic Reactors by Going to Finer Particles, Industrial & Engineering Chemistry Research 58(43) (2019) 20173-20178.

[34] Y. Zhou, J. Zhu, Group C+ particles: Extraordinary dense phase expansion during fluidization through nano-modulation, Chemical Engineering Science 214 (2020) 115420.

[35] M. Han, Y. Zhou, J. Zhu, Improvement on flowability and fluidization of Group C particles after nanoparticle modification, Powder Technology 365 (2020) 208-214.

[36] G. Bruni, P. Lettieri, D. Newton, J. Yates, The influence of fines size distribution on the behaviour of gas fluidized beds at high temperature, Powder technology 163(1-2) (2006) 88-97.

[37] M. Krantz, H. Zhang, J. Zhu, Characterization of powder flow: Static and dynamic testing, Powder Technology 194(3) (2009) 239-245.

Fluidization Stability vs. Powder History of Geldart Group C[+] Particles

Huaiming Du[1,2], Yandaizi Zhou[1], Dongqi Zhao[3], Yuanyuan Shao[3], Jesse Zhu[1]*

[1] Department of Chemical and Biochemical Engineering, The University of Western Ontario, London, Ontario, N6A 5B9, Canada

[2] College of Materials and Chemical Engineering, Sichuan University of Science & Engineering, Zigong, Sichuan, 643000, China

[3] Collaborative Innovation Center of Chemical Science and Engineering (Tianjin), School of Chemical Engineering and Technology, Tianjin University, Tianjin, 300072, China

*Corresponding authors: Jesse Zhu. E-mail address: jzhu@uwo.ca

Abstract

Geldart Group C particles with the addition of nanoparticles (Group C[+]) show a better flowability and fluidization quality. The stability of these Group C[+] particles with different nanoparticle concentrations were systematically examined in this work, including the flow properties, the particle size distribution (PSD), and the fluidization behaviors with the fluidizing time. Although the flowability, PSD, and fluidization behaviors for Group C[+] particles fluctuated with the fluidizing time, those became more stable after fluidizing for 1-2 hours. The increase of the nanoparticle concentration significantly improved the stability of these behaviors for Group C[+] particles. Group A particles showed more stable behaviors with the fluidizing time than Group C[+] particles, and nanoparticles had a little effect on the stability. In addition, Group C[+] particles exhibited much better fluidization behaviors, including higher bed expansion and higher dense phase expansion, than Group A particles, contributing to better gas-solid contact.

Keywords: Flowability; Fluidization; Group C particles; Nanoparticles; Powder history

1 Introduction

Fine powders are widely used in modern industries such as chemical, pharmaceutical, cosmetic, and food industry etc. [1-4], because of their small particle size. For example, the powder coating technology [5] employs fine powders (<30μm) in order to improve the aesthetics of coating film. In addition, the large specific surface area of fine particles is another key characteristic that is preferred by multi-phase processes, such as gas adsorption and gas-phase catalytic reactions [6,7].

According to Geldart classification [8], Group C particles which are smaller than 30-45μm are generally referred as cohesive powder, and are difficult to flow and fluidize due to their strong interparticle forces caused by the small particle size. The fluidization of Group C particles is often characterized by slugging, channeling, and agglomeration [9]. The poor flowability and partial or even none fluidizability of Group C particles hinder their application in industrial processes. Considering the increasing importance of Group C particles, many researches have been done on the improvement of the flowability and the fluidizability of Group C powders. All the techniques can be classified into two groups: the introduction of external energy to overcome the interparticle forces and the addition of finer or coarser particles to reduce the interparticle forces [10]. These techniques belonging to the first group, such as mechanical vibration/stirring [11,12], acoustic vibration [13], and electrical/magnetic field disturbance [14,15], are effective but are scale-dependent. On the other hand, the addition of finer or coarser particles can effectively improve the flowability and fluidizability of Group C particles and is scale-independent and easier to implement [16,17].

Nanoparticle modulation technique is one way to reduce the interparticle forces of Group C particles by dry coating a small amount of nanoparticles onto the surface of Group C cohesive particles [18,19]. A series of earlier works have been done in our research group on the fluidization quality of these Group C particles using the nanoparticle modulation technique, referred to as Group C[+] particles [20-25]. These Group C[+] particles exhibited good flowability similar as Group A particles, and much better fluidization quality than Group A particles, such as extremely higher bed expansion [21], larger dense phase voidage [22,25], smaller and less bubbles [24], and more gas flowing through the dense phase [24], contributing to better gas-solid contact. The reactor performance of the fluidized bed using Group C[+] catalysts was also improved significantly, showing higher reaction conversion and contact efficiency than that using Group A catalysts [7, 23].

The industrial employment of fluidized bed technology involves processes that are not only dependent on the fluidization quality, but also have a requirement for the particle stability [26], such as the change of the particle size distribution, particle flowability, and fluidization behaviors after a long run. Group C[+] particles are verified to have good fluidization quality, especially good gas-solid contact which is favored by

many gas-phase catalytic reactions [23]. However, the stability of Group C[+] particles has not been well investigated. Some researches doubted the stability of fine particles during the fluidization because of their small particle size which may easily result in particle entrainment and the loss pf particles in the fluidized beds [26-28]. Therefore, the stability of Group C[+] particles, as one of the important factors in industrial applications, was investigated in this work from three aspects: the powder flowability, the particle size distribution, and the fluidization behaviors.

In this work, the fluidization stability vs. powder history of Group C[+] particles with different medium particle size and different nanoparticle concentrations was studied and compared with typical Group A particles. The stability of these experimental particles was characterized using a variety of techniques under different powder states ranging from static to dynamic, including powder flowability and fluidization behaviors as a function of time.

2 Experiments
2.1 Experimental materials

Glass beads of three different medium particle sizes were employed in the experiment: 6.1μm, 9.7μm, and 39μm, as listed in Table 1. The particle size distributions of the three types of glass beads measured by a particle size distribution analyzer (BT-9300S Laser Particle Size Analyzer System, TSI 3603) during experiments. Nanoparticles used in this work were Aerosil R972 which is a type of hydrophobic SiO_2 nano-powder with a material density of $2200kg/m^3$ and a medium size of 16nm. Nanoparticles (R972) were dry coated onto glass beads using a high-intensity mixing method as described in Zhu and Zhang's patents [18,19]. Nanoparticle concentrations were 0.27%, 0.44%, and 0.82% in volume fraction, corresponding 0.24%, 0.39%, and 0.72% in weight fraction. The flow and fluidization behaviors of each sample were tracked with fluidizing time from 1h to 5h.

Table 1 Physical properties of the experimental powders

| Sample	Diameter (μm)			Density (kg/m³)		Shape	Geldart group
	D_{10}	D_{50}	D_{90}	Apparent	Bulk		
GB6	1.1	6	19	2500	874	Spherical	C
GB10	1.6	10	29	2500	916	Spherical	C
GB39	15	39	85	2500	1275	Spherical	A

2.2. Flow properties
2.2.1. Powder cohesion

Powder cohesion was measured using a FT4 Powder Rheometer (Freeman Technology Ltd) as illustrated in Figure 1. In a typical test, a powder sample was first conditioned to reach a homogenized state, as shown in Figure 1(a), and the powder was then compressed under a specified normal stress of 9kPa following a standard process established by Jenike (ASTM Standard D6128- 06, 2006), as shown in Figure 1(b). After that, as shown in Figure 1(c), the shear strength was measured at different normal stresses of 7, 6, 5, 4, and 3kPa, respectively. The yield locus was then extrapolated to the normal stress of 0kPa, as shown in Figure 1(d), and this extrapolated shear strength was referred to as powder cohesion and employed to characterize the powder flowability. For each sample, 3 measurements were repeated with deviation smaller than 10%, and the average was used in this work.
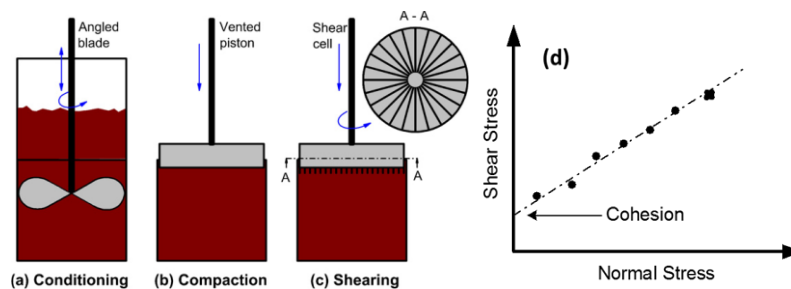
Figure 1: Measurement Powder cohesion using the FT4 Powder Rheometer

2.2.2. Angle of repose

Angle of repose (AOR) is the largest angle at which powders can pile up, which is widely used to characterize the powder flowability. Measurement of AOR was carried out using a PT-N Hosokawa Powder Characteristic Tester, following the standardized testing procedures of ASTM D6369-08 (ASTM Standard D6369-08, 1999). For each test, a powder sample was first loaded on a screen mounted with a vibrator, and then fell through the funnel onto a plate in a slow and consistent rate by adjusting the vibration intensity. The largest angle between the powder pile surface and the horizontal plane was the angle of repose, as shown in Figure 2. For each powder sample, 3–5 measurements were repeated with the difference within 1°, and the average was used. Table 2 lists the powder flowability classified by AOR values.
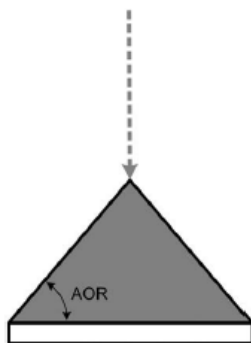

Figure 2: Measurement of Angle of repose

Table 2: Classification of powder flowability by AOR.

AOR	Flowability
25°< θ <30°	Very free-flowing
30°< θ <38°	Free-flowing
38°< θ <45°	Fair to passable flow
45°< θ <55°	Cohesive
55°< θ <70°	Very cohesive

2.2.3 Avalanche angle

Avalanche angle (AVA) was measured using a Revolution Powder Analyzer (Mercury Scientific Inc., Sandy Hook, CT). In this test, a tapped volume of 120mL of powder was placed into a cylindrical drum of 11.0cm in diameter and 3.5cm in width with transparent glass sides, and the drum was rotated at 0.6rpm. A digital camera connected to a computer was used to monitor the flow behavior of the powder inside and record the maximum angle that would occur before an avalanche, as shown in Figure 3. The drum was continuously rotated until 200 avalanches occurred and the average avalanche angle was provided.
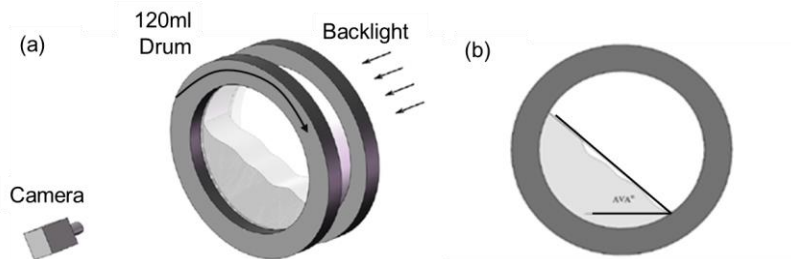

Figure 3: Measurement of Avalanche angle

2.3 Fluidization behaviors

Fluidization behaviors of the powder samples were measured in a fluidized bed as schematically shown in Figure 4. The fluidized bed column was made up of Plexiglas with 5.1cm in diameter and 45.7cm in height. Air in ambient condition flowed through PVC tubing into a wind box, passed through a gas distributor plate and then contacted with the particles. The wind box was 5.1cm in diameter and 12.7cm in height. The distributor plate had 66 holes of 3mm in diameter and was covered by two layers of filter paper with 625

mesh to prevent fine powder drooping into the wind box. A scale along the column was used to measure the bed height.
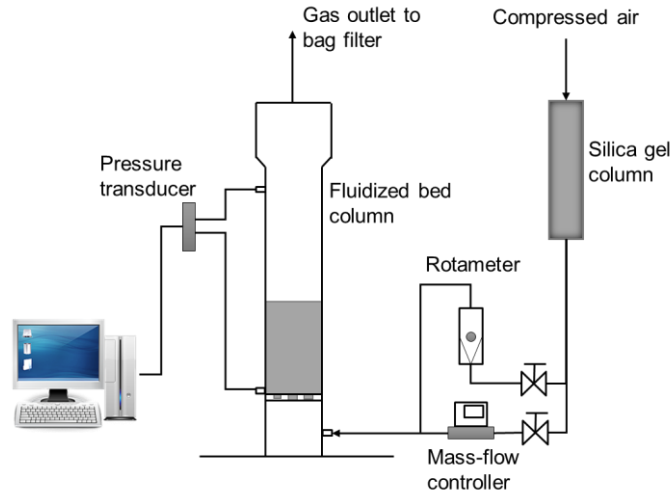

Figure 4: Schematic diagram of the fluidized bed

2.3.1 Minimum fluidization velocity and bed expansion

Approximately 350g of a powder was loaded into the column and fluidized at a high gas velocity until the powder reached a steady state. The gas velocity then gradually decreased, and the pressure drop through the entire bed and the bed height were measured ay each gas velocity. The pressure drop curves and the determination of the minimum fluidization velocity (u_{mf}) are shown in Figure 5. The bed expansion ratio (BER) was:

$BER = H_t / H_0$
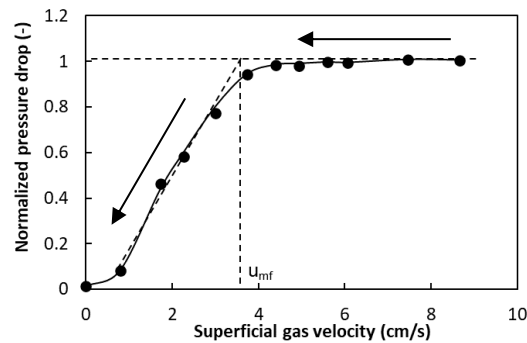
Figure 5: A typical pressure drop curves and u_{mf} of a type of Group C$^+$ particles [20]

2.3.2 Bed collapse test

Particles were loaded into the column to give a static bed height of 15cm, and fluidized at a high superficial velocity until reaching a steady state. The air supply was suddenly cut off, and the bed height started to collapse as a function of time. The whole process was recorded using a camera (). The bed collapse can be divided into three stages: the bubble escape stage, the hindered sedimentation stage, and the consolidation stage, as shown in Figure 6. From the bed collapse curves, the dense phase height can be obtained and used to calculate the dense phase voidage:
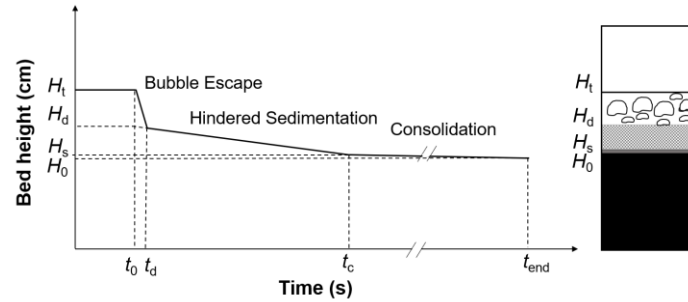
$\varepsilon_d = 1 - (H_0 / H_d) (1 - \varepsilon_0)$

**Figure 6: A typical bed collapse curve**

3 Results and discussion
3.1 Powder flowability with time

Powder flowability under different states from static to dynamic can be effectively characterized by cohesion, angle of repose (AOR), and avalanche angle (AVA). Generally, Group C particles have high cohesion, AOR, and AVA, showing poor flowability [29]. Nanoparticles play a significant role in improving the flowability of Group C particles [30,31]. Figure 7 shows the effect of nanoparticle concentration on the flowability of both Group C and Group A particles. Group C powder (GB6 and GB10) with and without nanoparticles exhibited much higher cohesion, AOR, and AVA than Group A powder (GB39). As nanoparticle concentration increased, the cohesion, AOR, and AVA for both GB6 and GB10 decreased, indicating better flowability. However, for Group A (GB39) powder, the cohesion, AOR, and AVA showed a slight increase with the increase of the nanoparticle concentration, reducing powder flowability. Group A particles themselves are free-flowing and have low cohesion, AOR, and AVA. The addition of nanoparticles, especially of a high concentration, may sometimes play a negative effect on Group A particles because of the strong interparticle forces of nanoparticles. As a result, nanoparticles could effectively improve the powder flowability of Group C particles, but show little or even reverse effect on that of Group A particles.
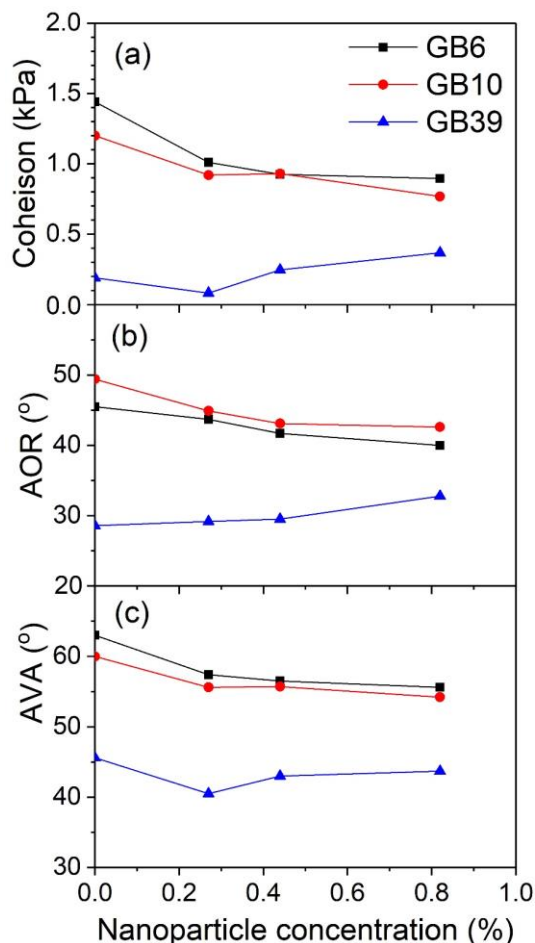
**Figure 7: Effect of nanoparticle concentration on cohesion, AOR, and AVA
for Group C and Group A particles**

The change of cohesion, AOR, and AVA for Group C and Group A particles with fluidizing time are shown in Figure 8. As the fluidizing time increased, the cohesion for GB6 with different nanoparticle concentrations (Group C[+] powder) showed a trend of decrease, while AOR fluctuated but showed an insignificant change. For GB10 with different nanoparticle concentrations (Group C[+] powder), the cohesion, AOR, and AVA all showed an even smaller fluctuation and a more insignificant change than GB 6 particles with the increase of the fluidizing time. For GB36 (Group A powder), the cohesion fluctuated more significantly than Group C[+] particles as the fluidizing time increased, while became more stable after fluidizing for 4h. AOR and AVA for GB39 were more stable than the cohesion, showing a small change with the fluidizing time. In summary, the powder flowability changed slightly with the fluidizing time for both Group C[+] and Group A/A[+] particles, especially the dynamic flowability (AOR and AVA), indicating a good stability of powder flow properties during the fluidization.
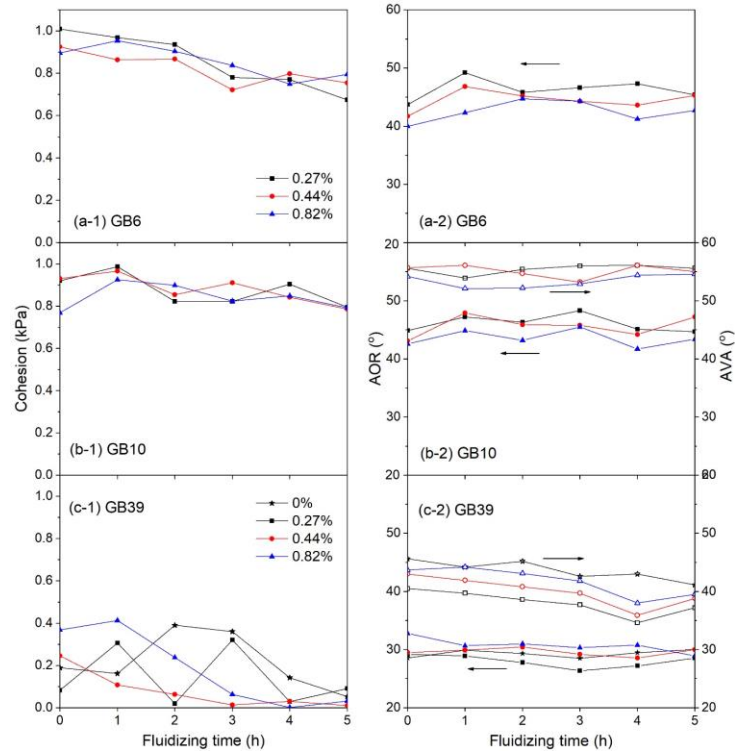
Figure 8: Cohesion, AOR, and AVA with fluidizing time for Group C and Group A particles

3.2 Particle size distribution with time

Particle size distribution (PSD) is one important parameter affecting the fluidization quality. Many researches [32-34] focused on the effect of the particle size distribution on the fluidization behaviors of fine particles. For example, Sun and Grace [35] found that Group A particles with a narrow PSD with the removal of fine contents (<45μm) exhibited poorer fluidization quality than the wide one which contained the fine contents. Considering the importance of the particle size distribution in the fluidized bed, the stability of PSD with the fluidizing time are shown in Figure 9. For GB10 with different nanoparticle concentrations (Group C+), D10 and D50 were more stable than D90 with the fluidizing time. D90 fluctuated significantly for GB10+0.27%, while the fluctuation became minor with the increase of the nanoparticle concentration, such as GB10+0.44% and GB10+0.82%. Nanoparticles, therefore, could improve the stability of the particle size distribution for Group C+ particles during the fluidization. For Group A particles (GB39), D10, D50, and D90 all were more stable and changed slightly with the fluidizing time when compared with Group C+ particles. In addition, nanoparticles played an insignificant effect on the stability of PSD for Group A particles.
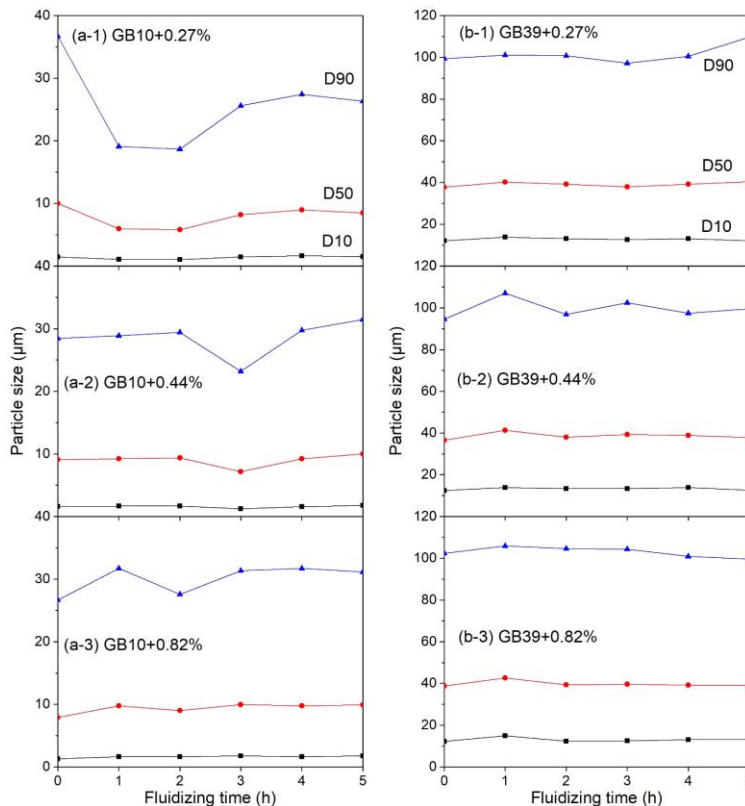
Figure 9: Particle size distribution with fluidizing time for Group C and A particles
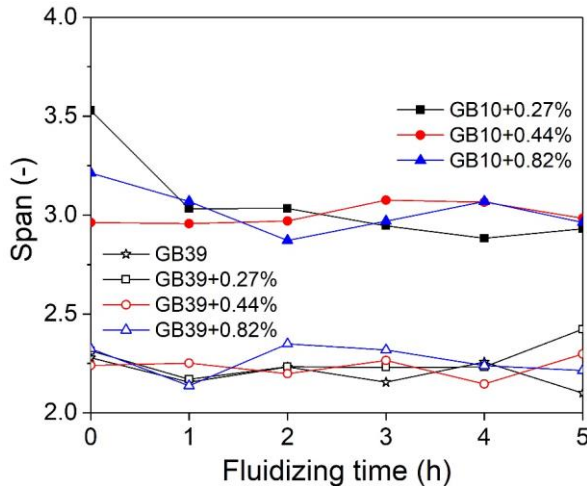

Figure 10: Span with fluidizing time for Group C and A particles

Span is used to describe the width of the particle size distribution, and is calculated using the following equation:

Span = (D90-D10) / D50

Generally, a larger span indicates a wider particle size distribution. The span for Group C and Group A particles with the fluidizing time is shown in Figure 10. The span for Group C^+ particles was much larger than that for Group A and A^+, signifying a wider particle size distribution for Group C^+ particles. For Group C^+ particles, the span kept stable after fluidizing for 1h, and the increase of the nanoparticle concentration also improved the stability of the span during fluidization. For Group A and A^+ particles, the span showed a small change before and after fluidization, exhibiting a good stability. The addition of nanoparticles slightly affected the stability of PSD for Group A particles.

In summary, Group A and A$^+$ particles showed more stable PSD and span than Group C$^+$ particles during fluidization. Group C$^+$ particle could reach stable after fluidizing for 1-2h, and nanoparticle concentration affected the particle size stability.

3.3 Fluidization behaviors with time

The industrial employment of fluidized bed technology involves processes that are strongly dependent on the fluidization qualities, such as minimum fluidization velocity (u_{mf}) and bed expansion. The stability of these fluidization characteristics is also important in the industrial processes. The minimum fluidization velocity for Group C and A particles with the fluidizing time is shown in Figure 11. U_{mf} for GB6 and GB10 particles fluctuated with the fluidizing time. The increase of the nanoparticle concentration reduced the fluctuation and improved the stability of u_{mf} for both GB6 and GB10, and also decreased u_{mf} for Group C$^+$ particles. However, Group A particles showed a much more stable u_{mf} with the fluidizing time than Group C$^+$ particles. Because Group A particles had a low u_{mf}, the addition of nanoparticles had little effect on u_{mf}.
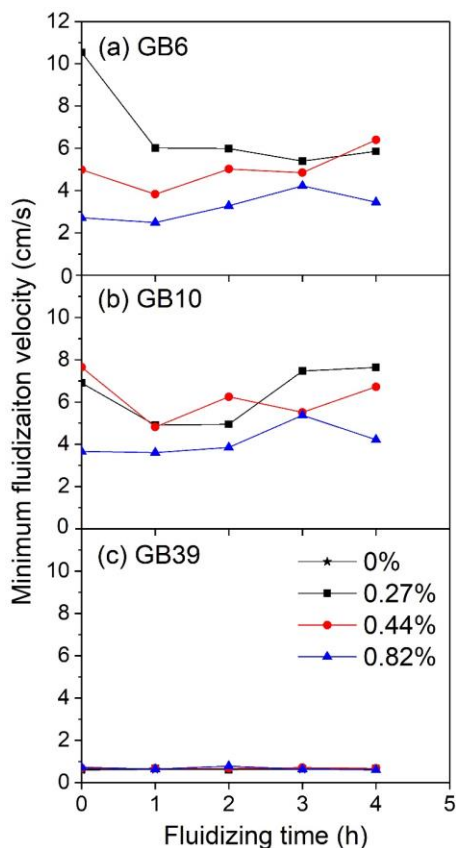
Figure 11: Minimum fluidization velocity with fluidizing time for Group C and A particles

Bed expansion is another important parameter to describe the fluidization quality. The bed expansion ratios for Group C$^+$ particles (GB6 and GB10) were much higher than Group A particles (GB39), as shown in Figure 12, indicating more gas holdup in the fluidized bed and contributing to better gas-solid contact. As nanoparticle concentration increased, the bed expansion ratios for Group C$^+$ particles increased, while that for Group A particles remained unchanged. As a result, nanoparticles significantly improved the fluidization quality for Group C$^+$ particles, but showed little effect on that for Group A particles.
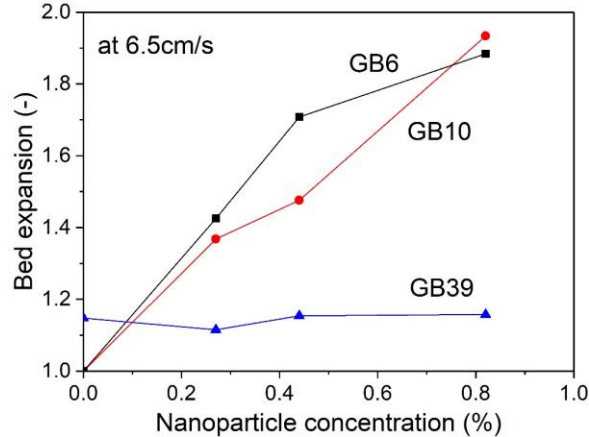
Figure 12: Effect of nanoparticle concentration on bed expansion for Group C and A particles (zero time)

The stability of the bed expansion for Group C[+] and Group A particle is shown in Figure 13 (left). The bed expansion ratios for GB6 showed larger fluctuations with the fluidizing time, but became more stable with the increase of the nanoparticle concentration. For GB10 particles, the bed expansion ratios slightly increased with the fluidizing time at nanoparticle concentrations of 0.27% and 0.44%. When the nanoparticle concentration increased to 0.82%, the bed expansion ratio kept almost unchanged with the fluidizing time. For GB39 particles, the bed expansion ratios were stable with the fluidizing time, and were not affected by the nanoparticle concentration.

The bed expansion is ascribed to both the bubble phase and the dense phase, while the dense phase is more important because of the close contact between the gas and particles. The dense phase expansion ratios for Group C[+] and Group A particles were shown in Figure 13 (right). Group C[+] particles (GB6 and GB10) exhibited much higher dense phase expansion than Group A particles (GB39), indicating more gas holdup in the dense phase and better gas-solid contact. The dense phase expansion ratios showed a similar stability as the bed expansion ratios for both Group C[+] and Group A particles. For GB6, the dense phase expansion ratios fluctuated with the fluidizing time, but the fluctuation became smaller with the increase of the nanoparticle concentration. GB10 showed a more stable dense phase expansion ratios with the fluidizing time than GB6. The dense phase expansion ratios for GB39 were almost not affected by both the fluidizing time and the nanoparticle concentration.

In summary, the fluidization behaviors for Group C[+] particles were more affected by the fluidizing time than those for Group A particles. The increase of the nanoparticle concentration could obviously improve the stability of the fluidization behaviors for Group C[+] particles, including u_{mf}, bed expansion ratio, and dense phase expansion ratio, but had little effect on that for Group A particles.
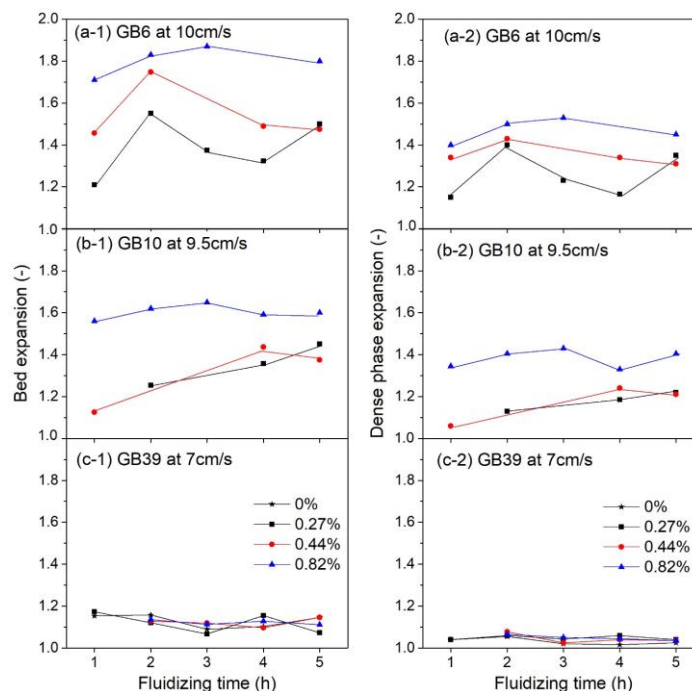
Figure 13: Bed expansion and dense phase expansion with fluidizing time for Group C and Group A particles

4. Conclusions

Two types of Group C particles were modulated by nanoparticles to modify their flow and fluidization behaviors, in comparison with Group A particles. The flow and fluidization properties were improved for Group C particles with nanoparticles, while an insignificant effect was observed for Group A particles with nanoparticles, consistent with our previous results [20-23].

The fluidization stability of Group C$^+$ and Group A particles with the fluidizing time was investigated in terms of the flow properties, the particle size distribution (PSD), and the fluidization behaviors. The flow properties (cohesion, AOR, and AVA) for both Group C$^+$ and Group A particles fluctuated with the fluidizing time, but overall changed only slightly, especially the dynamic flowability (AOR and AVA), indicating a good stability of powder flow properties. In terms of the particle size distribution, PSD for Group C$^+$ particle was variable initially and stabilized after fluidizing for 1-2 hours, while that for Group A particles was more stable.

The fluidization behaviors for Group C$^+$ particles were more affected by the fluidizing time than Group A particles, including the minimum fluidization velocity (u_{mf}), the bed expansion ratio, and the dense phase expansion ratio. The increase of the nanoparticle concentration could improve the stability of Group C$^+$ particles, especially for the PSD and the fluidization behaviors, but only slightly affected that of Group A particles. In overall, the properties of Group C$^+$ particles were stable with the fluidizing time, especially after fluidizing for 1-2 hours. The good fluidization stability of Group C$^+$ particles is favorable and makes them more promising in future industrial applications.

References

[1] Dhakshinamoorthy A, Opanasenko M, Čejka J, and Garcia H. Metal organic frameworks as heterogeneous catalysts for the production of fine chemicals. Catalysis Science & Technology. 2013; 3(10):2509-40.

[2] Zhou QT, Denman JA, Gengenbach T, Das S, Qu L, Zhang H, Larson I, Stewart PJ, and Morton DA. Characterization of the surface properties of a model pharmaceutical fine powder modified with a pharmaceutical lubricant to improve flow via a mechanical dry coating approach. Journal of pharmaceutical sciences. 2011; 100(8):3421-30.

[3] Su CY, Tang HZ, Chu K, and Lin CK. Cosmetic properties of TiO$_2$/mica-BN composite powder prepared by spray drying. Ceramics International. 2014; 40(5):6903-11.

[4]   Xiao W, Zhang Y, Fan C, and Han L. A method for producing superfine black tea powder with enhanced infusion and dispersion property. Food chemistry. 2017; 214:242-7.

[5]   Fu J, Zhang H, and Zhu J. Improvement on the first pass transfer efficiency of fine polymer coating powders for corona spraying process. Advanced Powder Technology. 2013; 24(6):1054-62.

[6]   Ammendola P, Raganati F, and Chirone R. CO_2 adsorption on a fine activated carbon in a sound assisted fluidized bed: Thermodynamics and kinetics. Chemical Engineering Journal. 2017; 322:302-13.

[7]   Zhang Y, Zhou Y, Liu J, Shao Y, and Zhu J. Performance Enhancement of Fluidized Bed Catalytic Reactors by Going to Finer Particles. Industrial & Engineering Chemistry Research. 2019; 58(43):20173-8.

[8]   Geldart D. Types of gas fluidization. Powder technology. 1973; 7(5):285-92.

[9]   Chaouki J, Chavarie C, Klvana D, and Pajonk G. Effect of interparticle forces on the hydrodynamic behaviour of fluidized aerogels. Powder Technology. 1985; 43(2):117-25.

[10]   Visser J. Van der Waals and other cohesive forces affecting powder fluidization. Powder Technology. 1989; 58(1):1-0.

[11]   Xu C and Zhu J. Experimental and theoretical study on the agglomeration arising from fluidization of cohesive particles—effects of mechanical vibration. Chemical Engineering Science. 2005; 60(23):6529-41.

[12]   Kuipers NJ, Stamhuis EJ, and Beenackers AA. Fluidization of potato starch in a stirred vibrating fluidized bed. Chemical Engineering Science. 1996; 51(11):2727-32.

[13]   Xu C, Cheng Y, and Zhu J. Fluidization of fine particles in a sound field and identification of group C/A particles using acoustic waves. Powder technology. 2006; 161(3):227-34.

[14]   van Willigen FK, Demirbas B, Deen NG, Kuipers JA, and Van Ommen JR. Discrete particle simulations of an electric-field enhanced fluidized bed. Powder technology. 2008; 183(2):196-206.

[15]   Sobral YD and Cunha FR. A stability analysis of a magnetic fluidized bed. Journal of magnetism and magnetic materials. 2003; 258:464-7.

[16]   Chen Y, Yang J, Dave RN, and Pfeffer R. Fluidization of coated group C powders. AIChE journal. 2008; 54(1):104-21.

[17]   Alavi S and Caussat B. Experimental study on fluidization of micronic powders. Powder technology. 2005; 157(1-3):114-20.

[18]   Zhu, J. and H. Zhang. Fluidization Additives to Fine Powders. U.S. Patent 6833185. December 21, 2004.

[19]   Zhu, J.-X. and H. Zhang. Method and Apparatus for Uniformly Dispensing Additive Particles in Fine Powders. U.S. Patent 7240861, 2007.

[20]   Han M, Zhou Y, and Zhu J. Improvement on flowability and fluidization of group C particles after nanoparticle modification. Powder Technology. 2020; 365:208-14.

[21]   Zhou Y and Zhu J. Group C$^+$ particles: Enhanced flow and fluidization of fine powders with nano-modulation. Chemical Engineering Science. 2019; 207:653-62.

[22]   Zhou Y and Zhu J. Group C$^+$ particles: Extraordinary dense phase expansion during fluidization through nano-modulation. Chemical Engineering Science. 2020; 214:115420.

[23]   Zhou Y, Zhao Z, Zhu J, and Bao X. Group C$^+$ particles: Efficiency augmentation of fluidized bed reactor through nano-modulation. AIChE Journal. 2020; 66(4):e16870.

[24]   Zhou Y and Zhu J. On the Two-phase Theory of Group C$^+$ and Geldart Group A Particles. Industrial & Engineering Chemistry Research. 2020.

[25]   Zhou Y and Zhu J. Prediction of Dense Phase Voidage for Group C$^+$ Fluidized Bed Reactor. Chemical Engineering Journal. 2020:126217.

[26]   Cocco R, Karri SR, and Knowlton T. Introduction to fluidization. Chem. Eng. Prog. 2014; 110(11):21-9.

[27]   Dutta A and Dullea LV. Effects of external vibration and the addition of fibers on the fluidization of a fine powder. InAIChE Symp. Ser 1991: 87(281):38-46.

[28]   Briens CL, Bergougnou MA, Inculet II, Baron T, and Hazlett JD. Size distribution of particles entrained from fluidized beds: electrostatic effects. Powder Technology. 1992; 70(1):57-62.

[29]   Huang Q, Zhang H, and Zhu J. Flow properties of fine powders in powder coating. Particuology. 2010; 8(1):19-27.

[30]   Yang J, Sliva A, Banerjee A, Dave RN, and Pfeffer R. Dry particle coating for improving the flowability of cohesive powders. Powder technology. 2005; 158(1-3):21-33.

[31] Xu CC, Zhang H, and Zhu J. Improving flowability of cohesive particles by partial coating on the surfaces. The Canadian Journal of Chemical Engineering. 2009; 87(3):403-14.

[32] Geldart D. The effect of particle size and size distribution on the behaviour of gas-fluidised beds. Powder Technology. 1972; 6(4):201-15.

[33] Abrahamsen AR and Geldart D. Behaviour of gas-fluidized beds of fine powders part I. Homogeneous expansion. Powder technology. 1980; 26(1):35-46.

[34] Abrahamsen AR and Geldart D. Behaviour of gas-fluidized beds of fine powders part II. Voidage of the dense phase in bubbling beds. Powder Technology. 1980; 26(1):47-55.

[35] Grace JR and Sun G. Influence of particle size distribution on the performance of fluidized bed reactors. The Canadian Journal of Chemical Engineering. 1991; 69(5):1126-34.

Curriculum Vitae

Name: Yandaizi Zhou

Post-secondary Education and Degrees:
China University of Petroleum (Beijing)
Beijing, China
2009-2013 B.Eng.

China University of Petroleum (Beijing)
Beijing, China
2013-2016 M.E.

The University of Western Ontario
London, Ontario, Canada
2015-2016 M.E.Sc

The University of Western Ontario
London, Ontario, Canada
2016-2020 Ph.D.

Honours and Awards:
China Scholarship Council (CSC) Full-time Scholarship
2016-2020

Related Work Experience
Teaching Assistant
The University of Western Ontario
2015-2020

Research Assistant
Particle Technology Research Center
The University of Western Ontario
2015-2020

Publications:

[1] **Zhou Y**, Zhu J. Group C^+ particles: Enhanced flow and fluidization of fine powders with nano-modulation. *Chemical Engineering Science*. 2019; 207:653-62.

[2] **Zhou Y**, Zhu J. Group C^+ particles: Extraordinary dense phase expansion during fluidization through nano-modulation. *Chemical Engineering Science*. 2020; 214:115420.

[3] **Zhou Y**, Ding H, Zhu J, Shao Y. The Effect of Gas Properties on Group C^+ Fluidized Bed Reactor. *Chemical Engineering Journal*. 2020:125039.

[4] **Zhou Y**, Zhao Z, Zhu J, Bao X. Group C^+ particles: Efficiency augmentation of fluidized bed reactor through nano-modulation. *AIChE Journal*. 2020;66(4):e16870.

[5] **<u>Zhou Y</u>**, Xu J, Zhu J. Different bubble behaviors in gas-solid fluidized bed of Geldart Group A and Group C$^+$ particles. ***AIChE Journal***. 2020. (***Positive reviews received and responded***)

[6] **<u>Zhou Y</u>**, Zhu J. On the Two-phase Theory of Group C$^+$ and Geldart Group A Particles. ***Industrial & Engineering Chemistry Research***. 2020.

[7] **<u>Zhou Y</u>**, Zhu J. Prediction of Dense Phase Voidage for Group C$^+$ Fluidized Bed Reactor. ***Chemical Engineering Journal***. 2020.

[8] Han M, **<u>Zhou Y</u>**, Zhu J. Improvement on flowability and fluidization of Group C particles after nanoparticle modification. ***Powder Technology***. 2019.

[9] Zhang Y, **<u>Zhou Y</u>**, Liu J, Shao Y, Zhu J. Performance Enhancement of Fluidized Bed Catalytic Reactors by Going to Finer Particles. ***Industrial & Engineering Chemistry Research***. 2019;58(43):20173-8.

[10] Zhao Z, **<u>Zhou Y</u>**, Bao X, Zhu J, Liu H. Reaction Performance of Group C$^+$ Fluidized Bed Catalytic Reactor. Industrial & Engineering Chemistry Research. 2020. (Under Review)

[11] Zhang X, **<u>Zhou Y</u>**, Zhu J. Enhanced Fluidization of Group A Particles Modulated by Group C Powder. Powder Technology. 2020. (under review)